frontiers | Research Topics

Bioactive compounds, functional ingredients, antioxidants, and health benefits of edible plants

Edited by
Hosam O. Elansary and Eman. A. Mahmoud

Published in
Frontiers in Plant Science

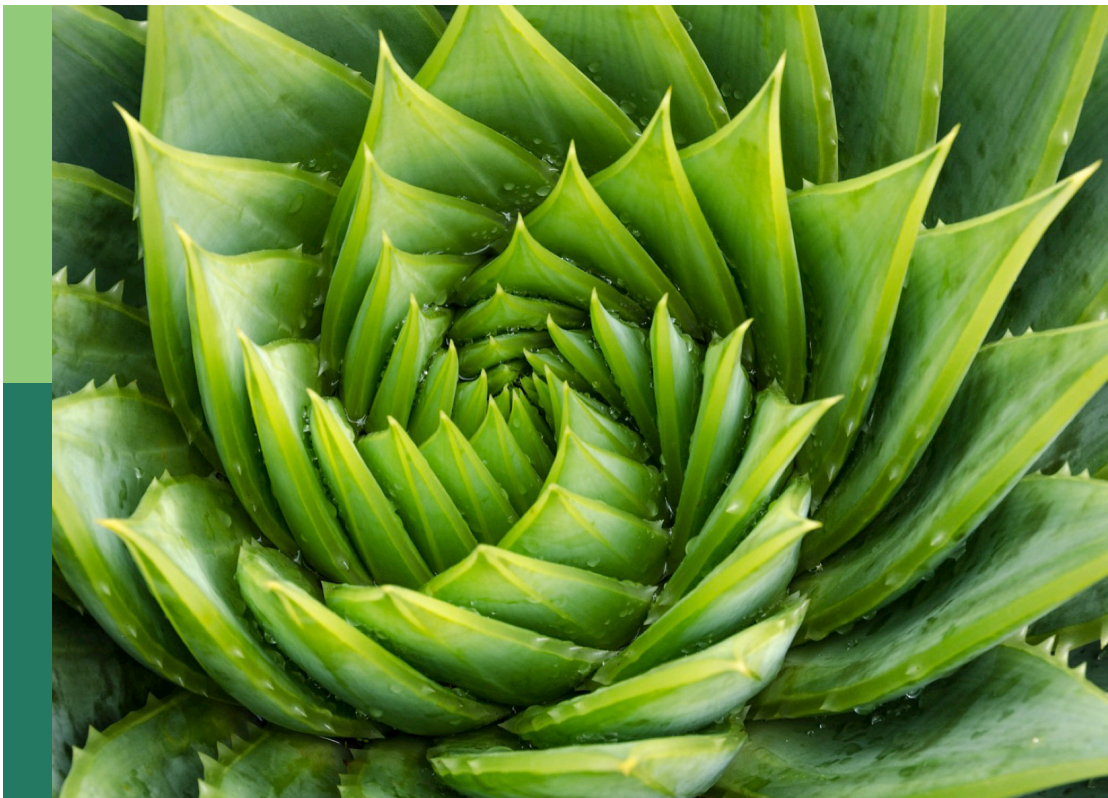

ISSN 1664-8714
ISBN 978-2-8325-4962-9
DOI 10.3389/978-2-8325-4962-9

About Frontiers

Frontiers is more than just an open access publisher of scholarly articles: it is a pioneering approach to the world of academia, radically improving the way scholarly research is managed. The grand vision of Frontiers is a world where all people have an equal opportunity to seek, share and generate knowledge. Frontiers provides immediate and permanent online open access to all its publications, but this alone is not enough to realize our grand goals.

Frontiers journal series

The Frontiers journal series is a multi-tier and interdisciplinary set of open-access, online journals, promising a paradigm shift from the current review, selection and dissemination processes in academic publishing. All Frontiers journals are driven by researchers for researchers; therefore, they constitute a service to the scholarly community. At the same time, the *Frontiers journal series* operates on a revolutionary invention, the tiered publishing system, initially addressing specific communities of scholars, and gradually climbing up to broader public understanding, thus serving the interests of the lay society, too.

Dedication to quality

Each Frontiers article is a landmark of the highest quality, thanks to genuinely collaborative interactions between authors and review editors, who include some of the world's best academicians. Research must be certified by peers before entering a stream of knowledge that may eventually reach the public - and shape society; therefore, Frontiers only applies the most rigorous and unbiased reviews. Frontiers revolutionizes research publishing by freely delivering the most outstanding research, evaluated with no bias from both the academic and social point of view. By applying the most advanced information technologies, Frontiers is catapulting scholarly publishing into a new generation.

What are Frontiers Research Topics?

Frontiers Research Topics are very popular trademarks of the *Frontiers journals series*: they are collections of at least ten articles, all centered on a particular subject. With their unique mix of varied contributions from Original Research to Review Articles, Frontiers Research Topics unify the most influential researchers, the latest key findings and historical advances in a hot research area.

Find out more on how to host your own Frontiers Research Topic or contribute to one as an author by contacting the Frontiers editorial office: frontiersin.org/about/contact

Bioactive compounds, functional ingredients, antioxidants, and health benefits of edible plants

Topic editors

Hosam O. Elansary — King Saud University, Saudi Arabia

Eman. A. Mahmoud — Damietta University, Egypt

Citation

Elansary, H. O., Mahmoud, E. A., eds. (2024). *Bioactive compounds, functional ingredients, antioxidants, and health benefits of edible plants*.

Lausanne: Frontiers Media SA. doi: 10.3389/978-2-8325-4962-9

Table of contents

frontiers | Frontiers in Plant Science

TYPE Editorial
PUBLISHED 21 May 2024
DOI 10.3389/fpls.2024.1420069

OPEN ACCESS

EDITED AND REVIEWED BY
Laigeng Li,
Chinese Academy of Sciences (CAS), China

*CORRESPONDENCE
Hosam O. Elansary
helansary@ksu.edu.sa

RECEIVED 19 April 2024
ACCEPTED 02 May 2024
PUBLISHED 21 May 2024

CITATION
Mahmoud EA and Elansary HO (2024) Editorial: Bioactive compounds, functional ingredients, antioxidants, and health benefits of edible plants. *Front. Plant Sci.* 15:1420069. doi: 10.3389/fpls.2024.1420069

Editorial: Bioactive compounds, functional ingredients, antioxidants, and health benefits of edible plants

Eman A. Mahmoud[1] and Hosam O. Elansary[2]*

[1]Department of Food Science, Faculty of Agriculture, Damietta University, Damietta, Egypt, [2]Department of Plant Production, College of Food & Agriculture Sciences, King Saud University, Riyadh, Saudi Arabia

KEYWORDS

natural products, antioxidants, biological activities, flavonoids, edible plants

Editorial on the Research Topic
Bioactive compounds, functional ingredients, antioxidants, and health benefits of edible plants

Edible plants are rich in bioactive compounds that have physiological effects such as anticancer, antioxidant, anti-inflammatory, and antimicrobial activities. Natural plant extracts are frequently used to prolong the shelf life of fresh and processed foods, thereby preserving their quality and safety. Phytochemical studies of extracts and the biological activities of various plant organs are also important in the food and human nutrition industries. They have the potential to pave the way for the commercialization of other plants by developing new applications for the food sector. Plant bioactive compounds represent a promising research objective for plant breeders, producers, and food processing industries. The study of the relationship between health and food has increased steadily and exponentially in recent years. The variety of bioactive compounds contained in edible plants, in addition to the different mechanisms of action involved in human nutrition, make this subject widely debated and the focus of this Research Topic. Furthermore, recent advances in extraction techniques, analytical approaches, and bioactivity assays have allowed scientists to explore minor dietary components and metabolites with high bioactivity and their pathways. The development of novel technological approaches for the manufacturing and processing of edible plants is of great interest to the agricultural and food industries worldwide, whose objectives include increasing the production of secondary metabolites (e.g., polyphenols) and developing novel applications. The use of bioreactors in tissue culture is strongly associated with the production of specific secondary metabolites that have important applications.

The work of Yang et al. explored the regulatory mechanisms of flavonoid synthesis in *Populus* × *euramericana* 'Zhonghuahongye' by analyzing flavonoids, polyphenols, and anthocyanins in the red and green leaves. The researchers identified 273 flavonoid metabolites (114 flavones, 41 flavonols, 34 flavonoids, 25 flavanones, 21 anthocyanins, 18 polyphenols, 15 isoflavones, and 5 proanthocyanidins). Higher levels of flavonoids were found in the red leaves and specific flavonoids were responsible for the red color of the

leaves. The coloration of the leaves was strongly associated with the *CHS*, *FLS*, *ANS*, and *LAR* genes. Biru et al. have conducted a comprehensive investigation on the effects of Si supplementation and herbivory by *Helicoverpa armigera* on the activities of antioxidant enzymes (CAT, SOD, and APX) in *Festuca arundinacea* under reduced and Anthropocene levels of CO2. They revealed that increasing CO_2 concentrations have positive effects on plant mass and foliar carbon. The researchers also found a correlation between Si supplementation and the activity of APX and SOD enzymes in plants grown under different CO_2 regimes. They suggested that *Festuca arundinacea* may be more susceptible to herbivory when subjected to specific CO_2 concentrations.

Irchad et al. found that lipidomic profiling of *Ficus carica* L. (Fig.) seed cultivars can reveal phenotypic diversity and associated nutritional benefits. The study used FTIR-ATR spectroscopy and chemometric techniques to investigate 22 fig genotypes and to explore their nutritional properties (antioxidant properties, nutritious source of lipids, minerals, and proteins), genetic relationships (Lipochemical-based fingerprinting), and potential applications as a genetic pool for future breeding programs for oil production. The findings of this study are highly relevant to the food industry. Cerulli et al. studied the metabolomics of lipids and phenols in hazelnut (*Corylus avellana* L., Betulaceae) of *n*-butanol extracts by LC-ESI/HRMS in the polar fraction of fresh and roasted kernels. The radical scavenging activity of the isolated compounds was determined using TEAC and TBARS assays. They identified phenolic compounds, polar lipids, flavonoids, and diarylheptanoid derivatives. The majority of the identified compounds showed strong antioxidant activities. The results of this are also highly relevant to the food industry. Zhang et al. conducted a comparative study on two pomegranate (*Punica granatum* L.) cultivars, 'Tunisia' and 'Qingpi', to elucidate the phenolic composition and antioxidant activities in different plant parts including fruits, flowers, and leaves. They revealed significant differences in the phenolic composition of plant organs, with petals showing the highest polyphenol and total anthocyanin compositions. The flavonoids and punicalagin were at the highest levels in the placenta, while the flavanols were at the highest levels in the peel. The highest antioxidant activity was found in fruits, followed by flowers and leaves; and was positively associated with total polyphenols. The study revealed that the placenta is the main source of punicalagin. The results of this are highly relevant to the pharmaceutical and food industries. Xu et al. revealed the nutritional value, antioxidant activity, and volatile compounds in three cultivars of jaboticaba berry (Sabara, Argentina, and Fukuoka). The authors found that the Sabara cultivar was rich in volatiles, had a suitable acid-sugar ratio, had low antioxidant capacity, and was recommended for fresh consumption. The Argentina cultivar had the most volatile compounds and was suitable for dry products. Finally, the Fukuoka cultivar had the largest fruit, with juicy flesh, and was suitable for juice processing. Similarly, Raza et al. studied different tomato (*Solanum lycopersicum* L.) genotypes to reveal the diversity in fruit nutritional composition, antioxidant, and biochemical profiles. They found that specific cultivars were rich in chlorophylls, lycopene, carotenoids, total antioxidant capacity, protease, alpha-amylase, and flavonoids, while other cultivars were rich in total soluble sugars, reducing sugars, malondialdehyde, ascorbic acid, esterase, peroxidase, and superoxide dismutase.

Abidizadegan et al. in their work presented an in-depth analysis of the impact of iron application on phycoerythrin, extracellular polymeric substances, and phenolic compounds isolated from *C. pyrenoidifera* and *Cryptomonas* sp. and their antioxidant activities. The application of iron increased the growth rates of the cryptophytes, and influenced the composition of phycoerythrin and phenolic compounds and consequently the antioxidant activities. Liu et al. investigated the anti-inflammatory compounds of *Capparis spinosa* fruits using metabolome and transcriptome analyses. They found strong anti-inflammatory effects in the fruits and identified 15 compounds exhibiting anti-inflammatory activity, with phenolic compounds being the major anti-inflammatory components in *C. spinosa*. Jiang et al. studied the chemical composition and aroma changes during the processing of Jujube tea using LC-MS-based metabolomics and GC-IMS analysis. They identified 468 non-volatile metabolites and 52 and 24 volatile metabolites. They found that lipids and lipid-like molecules, organic acids, amino acids, and flavonoids increased in composition following processing. Wang et al. found that the variability in the bioactive compound composition of *Swertia mussotii* in wild distant geographical populations of China is associated with environmental conditions including altitude, aspect, soil TK content, Fe content, and C/N and N/P ratios. Finally, Liu et al. revealed the mechanism of action of the traditional Chinese medicine YU-Pingfeng San in alleviating inflammatory allergic rhinitis. They identified 30 active ingredients in three effective herbs associated with the treatment of symptoms of nasal congestion and allergic rhinitis.

Author contributions

EM: Conceptualization, Data curation, Formal analysis, Funding acquisition, Investigation, Methodology, Project administration, Resources, Software, Supervision, Validation, Visualization, Writing – original draft, Writing – review & editing. HE: Conceptualization, Data curation, Formal analysis, Funding acquisition, Investigation, Methodology, Project administration, Resources, Software, Supervision, Validation, Visualization, Writing – original draft, Writing – review & editing.

Conflict of interest

The authors declare that the research was conducted in the absence of any commercial or financial relationships that could be construed as a potential conflict of interest.

Publisher's note

frontiers | Frontiers in Plant Science

TYPE Original Research
PUBLISHED 09 August 2022
DOI 10.3389/fpls.2022.934130

OPEN ACCESS

EDITED BY
Hosam O. Elansary,
King Saud University, Saudi Arabia

REVIEWED BY
Qintai Yang,
Sun Yat-sen University, China
Muhammad Ishtiaq,
Mirpur University of Science and Technology, Pakistan

*CORRESPONDENCE
Yumei Li
myheart1263@163.com
Yujuan Yang
yangyujuanyyj@163.com

†These authors have contributed equally to this work

SPECIALTY SECTION
This article was submitted to Plant Metabolism and Chemodiversity, a section of the journal Frontiers in Plant Science

RECEIVED 02 May 2022
ACCEPTED 13 July 2022
PUBLISHED 09 August 2022

CITATION
Liu Z, Sun Q, Liu X, Song Z, Song F, Lu C, Zhang Y, Song X, Yang Y and Li Y (2022) Network pharmacology analysis and experimental verification reveal the mechanism of the traditional Chinese medicine YU-Pingfeng San alleviating allergic rhinitis inflammatory responses.
Front. Plant Sci. 13:934130.
doi: 10.3389/fpls.2022.934130

Network pharmacology analysis and experimental verification reveal the mechanism of the traditional Chinese medicine YU-Pingfeng San alleviating allergic rhinitis inflammatory responses

Zhen Liu[1,2†], Qi Sun[1,2†], Xinyue Liu[1,2†], Zheying Song[1,2,3], Fei Song[1,2,4], Congxian Lu[1,2], Yu Zhang[1,2], Xicheng Song[1,2], Yujuan Yang[1,2*] and Yumei Li[1,2*]

[1]Department of Otorhinolaryngology, Head and Neck Surgery, Yantai Yuhuangding Hospital, Qingdao University, Yantai, China, [2]Shandong Provincial Clinical Research Center for Otorhinolaryngologic Diseases, Yantai, China, [3]Clinical Medicine College, Weifang Medical University, Weifang, China, [4]Second Clinical Medicine College, Binzhou Medical University, Yantai, China

YU-Pingfeng San (YPFS) can regulate inflammatory response to alleviate the symptoms of nasal congestion and runny rose in allergic rhinitis (AR). However, the mechanism of action remains unclear. In this study, 30 active ingredients of three effective herbs included in YPFS and 140 AR/YPFS-related genes were identified by database analysis. Gene ontology (GO) and Kyoto Encyclopedia of Genes and Genomes (KEGG) enrichment analysis showed that the targets were mainly enriched in immune inflammatory-related biological processes and pathways. Finally, three hub gene targeting epidermal growth factor receptor (EGFR), mitogen-activated protein kinase 1 (MAPK1), and protein kinase B1 (AKT1) related to YPFS and AR were identified by network pharmacology analysis. YPFS treatment decreased the expression of EGFR, MAPK1, and AKT1 in ovalbumin (OVA)-induced AR mice and impaired the production of inflammatory factors interleukin (IL)-4, IL-5, and IL-13, thus alleviating immunoglobulin E (IgE) production and the symptoms of scratching nose in AR. Through molecular docking analysis, we found that the active ingredients decursin, anomalin, and wogonin of YPFS could bind to EGFR, MAPK1, and AKT1 proteins. Moreover, decursin treatment impaired the expression of IL-4 and IL-5 in human PBMCs. These results suggested that YPFS could alleviate the AR inflammatory responses by targeting EGFR, MAPK1, and AKT1, showing the mechanism of action of YPFS in AR treatment.

KEYWORDS

YPFS, hub genes, decursin, network pharmacology analysis, allergic rhinitis

Introduction

Allergic rhinitis (AR) is an allergic disease of the nasal mucosa caused by a variety of factors. Clinical manifestations are characterized by nasal itching, sneezing, hypersecretion, and nasal mucosal swelling (Bousquet et al., 2020). AR is one of the most prevalent allergic diseases, with an estimated prevalence of 10–40% (Yan et al., 2021). AR affects the quality of life of patients and leads to increased personal and social medical costs. Currently, the treatment of AR mainly includes avoidance of exposure to allergens, drugs, surgery, and immunotherapy (Santos et al., 2015). Helper T cells (Th) 2 inflammation in the airway is characterized by induction of Th2 cytokines including interleukin (IL)-4, IL-5, and IL-13, leading to the production of immunoglobulin E (IgE) and inflammatory cell infiltration, which plays an important role in AR (Karta et al., 2016). In the pathological state of AR, the proportion of Th2 cells increases, causing an abnormal immune response, and reducing the Th2 response can reduce the inflammatory response of AR (Kappen et al., 2017). Many traditional Chinese medicines (TCMs) are used to treat AR, such as Shenqi and artemisia annua, which have a good therapeutic effect (Shao et al., 2017). In addition, it has been reported that YU-Pingfeng San (YPFS) is used frequently to treat allergic diseases, such as AR, asthma, and urticaria in modern medicine (Shen et al., 2014). However, the mechanism of action of YPFS in the treatment of AR is unclear.

YPFS, a TCM prescription, originated from The Danxi Heart Method written by Zhu Zhenheng in the Yuan Dynasty. YPFS is composed of *Astragali Radix* (Huangqi, HQ), *Atractylodis Macrocephalae Rhizoma* (Baizhu, BZ), and *Saposhnikoviae Radix* (Fangfeng, FF), at a content ratio of 3:1:1 (Xue et al., 2021). YPFS is recommended for the management of AR by the Chinese medicine clinical practice guideline (Luo et al., 2017). Chan et al. have reported that YPFS can reduce AR symptoms and enhance the quality of life (Chan and Chien, 2014). And Luo et al. reviewed 22 randomized controlled trials which showed that YPFS had an obvious effect on AR, and YPFS's combination treatment seemed more beneficial (Luo et al., 2017). In addition, these 22 Randomized controlled trials also indicated that YPFS was well-tolerated for treating adult AR (Luo et al., 2017). All these studies suggested that YPFS is effective and safe for AR treatment in clinical. Many anti-rhinitis substances and their potential targets have been found in YPFS (Nikles et al., 2017); however, which active ingredients in them mainly function for AR treatment are not clear. Network pharmacology analysis is a new strategy to analyze the molecular regulation mechanisms of TCM active ingredients (Zhang et al., 2021). We aimed to explore the active ingredients of YPFS and their targets for the treatment of AR through network pharmacology analysis and *in vitro* and *in vivo* experiments to reveal the mechanism of YPFS against AR and provide potential targets for AR treatment.

Abbreviations: YPFS, YU-Pingfeng San; AR, allergic rhinitis; EGFR, epidermal growth factor receptor; MAPK1, mitogen-activated protein kinase 1; AKT1, protein kinase B1; TCMs, traditional Chinese medicines; HQ, *Astragali Radix*; BZ, *Atractylodis Macrocephalae Rhizoma*; FF, *Saposhnikoviae Radix*; GO, Gene ontology; KEGG, Kyoto Encyclopedia of Genes and Genomes; OVA, ovalbumin; IL, interleukin; IgE, immunoglobulin E; IFN-γ, interferon-gamma; PBMCs, peripheral blood mononuclear cells.

Materials and methods

Screening of active ingredients in YU-Pingfeng San

The active ingredients of YPFS were predicted in the TCM System Pharmacological Database and Analysis Platform (TCMSP[1]). Those chemical compounds of YPFS with identifiable properties of absorption, distribution, metabolism, and excretion (ADME) and druggable properties, were selected as active components for further target prediction, with a cutoff of oral bioavailability of 30% and drug-likeness (DL) of 0.18 (Zhou et al., 2021).

Searching for the targets of the active ingredients of YU-Pingfeng San

The three-dimensional structures of the identified compounds were obtained from the PubChem Database[2] (Bahadur Gurung et al., 2022), the largest chemical compound information database in the world (Islam et al., 2021). The database of Swiss Target Prediction[3] was used to predict the potential protein targets of the bioactive ingredients of YPFS, according to the three-dimensional structure of the compounds (Yang et al., 2020; Fan et al., 2021). All targets were combined for further study.

Identification and functional analysis of the intersecting allergic rhinitis/YU-Pingfeng San-related genes

AR-associated genes were selected and combined from the Drug Bank Database[4] the Gene Card Database[5] and

1 https://www.tcmsp-e.com/
2 https://pubchem.ncbi.nlm.nih.gov/
3 http://www.swisstargetprediction.ch/
4 https://www.drugbank.com/datasets
5 https://www.genecards.org/

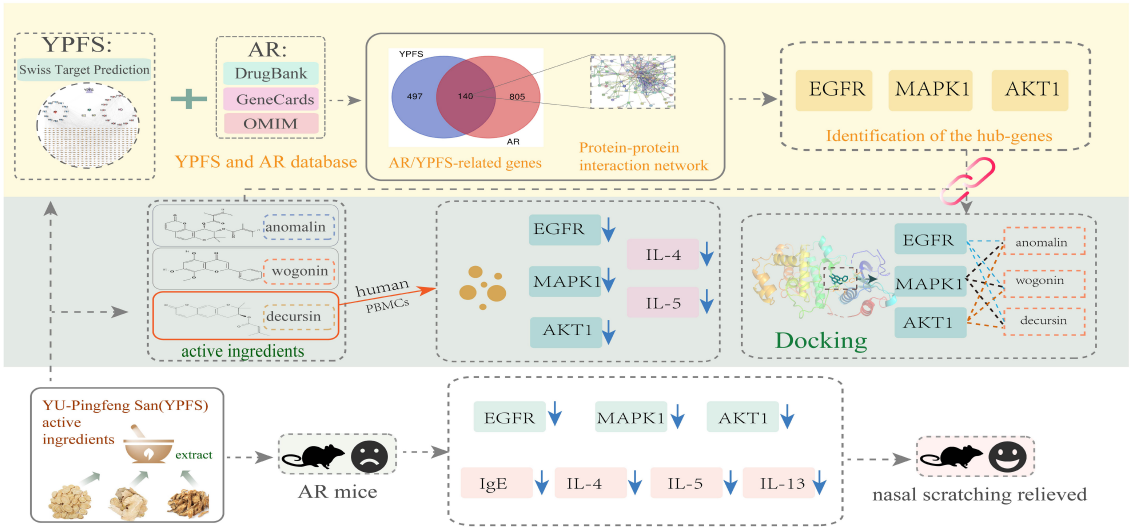

FIGURE 1
A workflow chart for treatment of allergic rhinitis with YU-Pingfeng San based on network pharmacology analysis and experimental verification.

the Human Mendelian Genetics Online Database (OMIM[6]; Tekin et al., 2016). AR/YPFS-related genes were obtained by selecting the overlapping genes between AR-associated genes and the targets of active ingredients of YPFS using a Venn diagram.[7]

Gene ontology and Kyoto Encyclopedia of Genes and Genomes pathway analysis

Gene ontology (GO) and Kyoto Encyclopedia of Genes and Genomes (KEGG) pathway enrichment analysis of AR/YPFS-related genes was performed to identify genes in the biological processes (BP), cellular components (CC), molecular functions (MF) categories, and pathways using the ClusterProfiler R Package (Wang et al., 2022). The data obtained were visualized by using bioinformatics[8] (Ding et al., 2021).

Protein–protein interaction network analysis and identification of the hub genes

The AR/YPFS-related genes were input into the String database[9] a protein interaction functional enrichment analysis website, to construct the Protein–protein interaction (PPI) network with a cutoff of high confidence of 0.7 (Silva et al., 2020). The top three genes were screened out as the hub genes by evaluating the interaction strength of each node and the average degree value (Hu et al., 2019).

Ovalbumin-induced allergic rhinitis mice

Male BALB/C mice aged 6–8 weeks were purchased from Jinan Pengyue Experimental Animal Breeding Co., Ltd. (Shandong, China; License Number: SYXK(Lu) 2014-0007). All mice were raised in a specific pathogen-free level environment in the Research Building of Yuhuangding Hospital, Yantai. All experimental animals were fed with standardized sterile feed and water, which was sterilized by high-pressure steam and cooled to room temperature. All experimental animals were dissected after fasting for 12 h. All animal experiments were conducted in accordance with the National Institutes of Health Guide for the Care and Use of Laboratory Animals and approved by the Yantai Yuhuangding Animal Ethics Committee.

Ovalbumin-induced AR mice were induced through two stages: The basic sensitization stage and the stimulation stage. In the basic sensitization stage, 200 μl of a mixture comprising 40 μg OVA (Solarbio, Beijing, China) and 2 mg aluminum hydroxide (Thermo Scientific, Waltham, MA, United States) gel were injected intraperitoneally into the OVA-induced AR group seven times on days 1, 3, 5, 7, 9, 11, and 13. In the stimulation stage, mice received nasal drops comprising 20 μl of 5% OVA solution following atomization with 5% ovalbumin

6 https://omim.org/
7 http://bioinformatics.psb.ugent.be/webtools/Venn/
8 http://www.bioinformatics.com.cn/
9 https://cn.string-db.org/

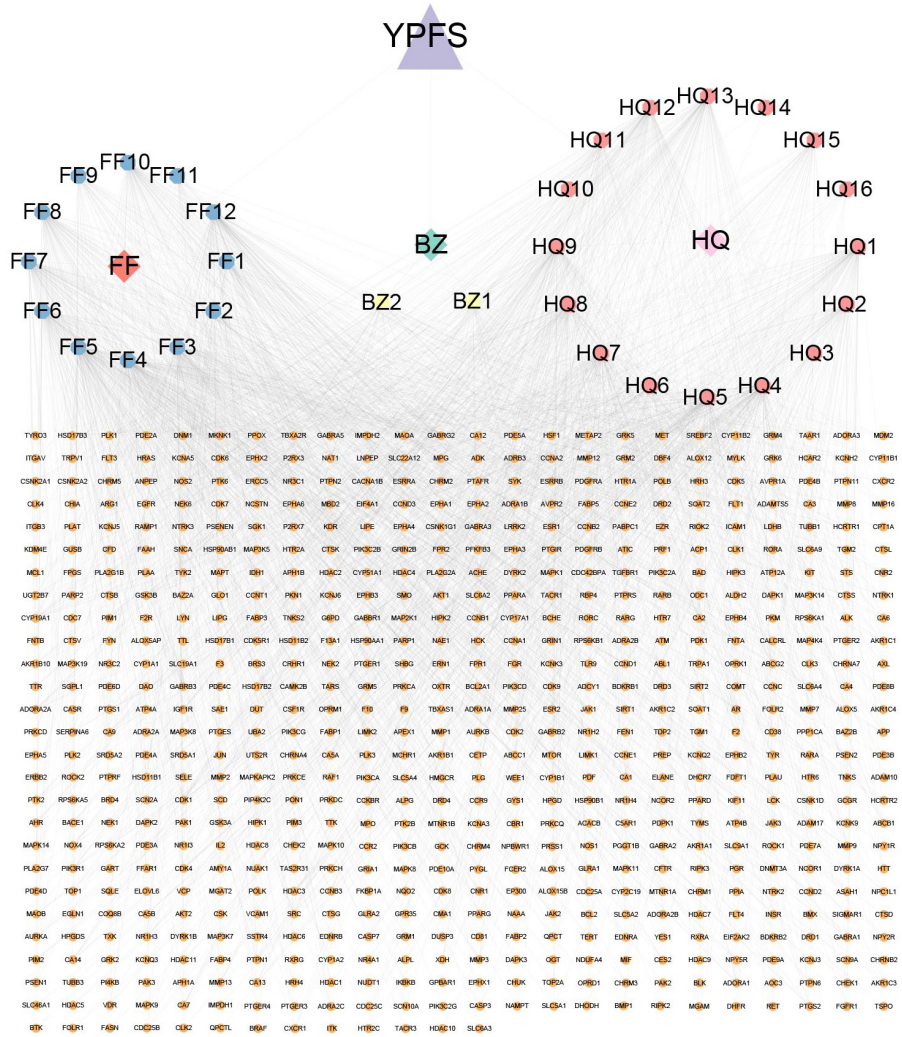

FIGURE 2
A network diagram was constructed with 3 active components, 30 active ingredients, and 637 target genes of these active ingredients using Cytoscape. The blue, yellow, and pink octagons represent the active ingredients of the three herbs in YPFS. FF1-12 are active ingredients of *Saposhnikoviae Radix* (Fangfeng, FF), BZ1-2 are active ingredients of *Atractylodis Macrocephalae Rhizoma* (Baizhu, BZ), and HQ1-16 are active ingredients of *Astragali Radix* (Huangqi, HQ). The full names of the corresponding active ingredients are listed in **Supplementary Table 7**. The orange circles represent YPFS-related genes, and the edges represent the interactions between the ingredients and the target genes. YPFS, YU-Pingfeng San.

saline solution in a homemade simple atomizer for 30 min, from days 21 to 27 (Sun et al., 2012). The mice in the control group were treated with 0.9% sterilized normal saline in the same way. Nasal symptoms were assessed immediately after the last OVA stimulation for 30 min as the scratching nose frequency and the times of scratching nose per session (Zhang et al., 2020).

YU-Pingfeng San decoction preparation and treatment

YPFS comprises three kinds of herbs, HQ (lot:20200617, Beijing Materia Medica Fangyuan Pharmaceutical Technology Co. Ltd., China), BZ (lot:20602, Haozhou City, Jing Wan Chinese medicine yinpian factory, China), and FF (lot:201001, Beijing Materia Medica Fangyuan Pharmaceutical Technology Co. Ltd., China) at a content ratio of 3:1:1. The three herbs were mixed, soaked in water for 1 h, and then decocted two times using an automatic decocting machine for 1.5 h each time. The decoctions (extracted by Beijing Tongrentang Co., Ltd., China) were filtered through double gauze to concentrate the filtrate to the final concentration of 1 g/ml and stored at 4°C until use (Bao et al., 2019).

YPFS was intragastrically administered to the AR mice in the YPFS group at a dose of 130 mg/20 g body weight for 14 days continuously (Wang et al., 2019). The same amount of saline

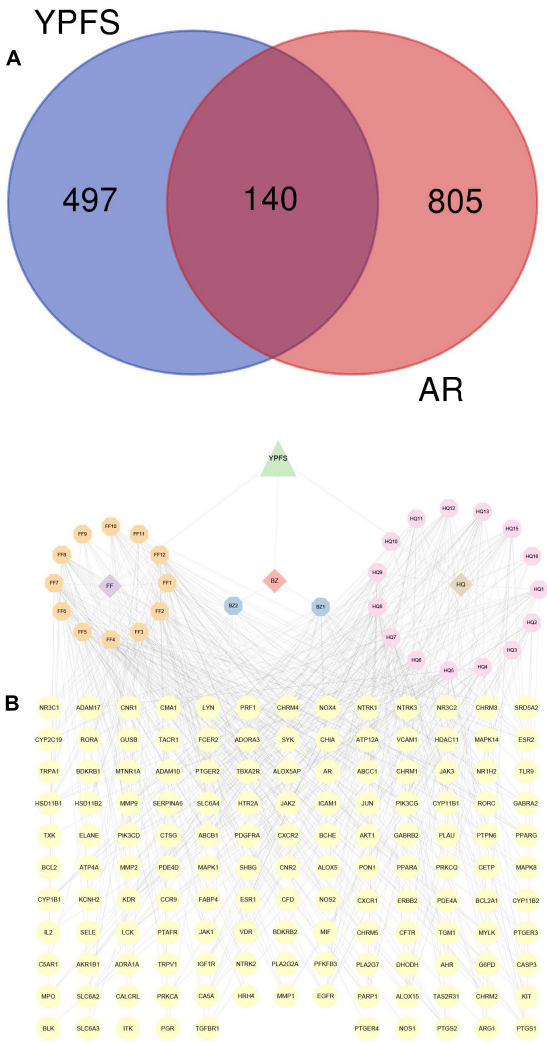

FIGURE 3
Screening for AR/YPFS-related genes. **(A)** Venn analysis of the common targets of YPFS and AR-associated genes. **(B)** The interaction network is constructed using ingredients and targets genes. The orange, blue, and pink octagons represent the active ingredients of the three herbs in YPFS. FF1-12 are active ingredients of *Saposhnikoviae Radix* (Fangfeng, FF), BZ1-2 are active ingredients of *Atractylodis Macrocephalae Rhizoma* (Baizhu, BZ), and HQ1-16 are active ingredients of *Astragali Radix* (Huangqi, HQ). The full names of the corresponding active ingredients are listed in **Supplementary Table 7**. The yellow circles represent the common targets of YPFS and AR-related genes, and the edges represent the interactions between the ingredients and the targets. YPFS, YU-Pingfeng San; AR, allergic rhinitis.

was intragastrically administrated into mice in the OVA-induced AR group. On days 3, 6, 9, and 12, 5% OVA was dropped into the nasal cavity to maintain intranasal stimulation. After the last administration, the blood and nasal mucosa of the mice were obtained by dissection under a microscope (Möller-Wedel, Wedel, Germany).

Enzyme-linked immunosorbent assay

The serum was separated from the upper layer of the blood after centrifugation for 20 min at 900 g. The concentrations of immunoglobulin E (IgE), interleukin (IL)-4, IL-5, IL-13, and interferon-gamma (IFN-γ) in mouse serum were detected using an Enzyme-linked immunosorbent assay (ELISA) kit (Jingmei Biotechnology, Guangzhou, China) according to the manufacturer's instructions.

Quantitative real-time reverse transcription PCR

Total RNA was extracted from mouse nasal mucosa and human peripheral blood mononuclear cells (PBMCs) using the Trizol reagent (SparkJade, Qingdao, China) and reverse transcribed into cDNA using a reverse transcription kit (Accurate Bio, Changsha, China). The qPCR step was performed using an SYBR Green qPCR Mix kit (SparkJade) in a StepOnePlus fluorescence quantitative PCR instrument (Applied Biosystems, Foster City, CA, United States). The expression levels of the genes encoding IL-4, IL-5, epidermal growth factor receptor (EGFR), mitogen-activated protein kinase 1 (MAPK1), and protein kinase B1 (AKT1) were detected. The relative expression level was calculated using the $2^{-\Delta\Delta CT}$ method (Livak and Schmittgen, 2001). The primers for mouse *Egfr*, *Mapk1*, and *Akt1* and human IL4, IL5, EGFR, MAPK1, and AKT1 are listed in **Supplementary Table 1**.

Molecular docking analysis

The interactions between active ingredients and the AR/YPFS-related genes were analyzed using Cytoscape.[10] Ingredients involved in regulating immune inflammation were selected for molecular docking with the three hub genes decursin (Yang et al., 2009; Shehzad et al., 2018), anomalin (Khan et al., 2016, 2019), and wogonin (Kim et al., 2018). The three-dimensional chemical structures of candidate compounds were retrieved from PubChem (see text footnote 2) and the crystal structures of the target proteins were retrieved from the RCSB Protein Data Bank (RCSB PDB[11]). The eutectic ligands isolated from the receptor and the active pocket of each target were identified using AutodockTools-1.5.6 (Caliceti et al., 2019). Autodock Vina-1.1.2 software (Algethami et al., 2021) was used to dock the active ingredients with the putative target molecules and determine their free binding energy. PyMOL software was used to visually analyze the interaction and binding patterns of active ingredients (Agnew et al., 2021).

10 https://cytoscape.org/
11 https://www.rcsb.org/

Human peripheral blood mononuclear cells culture and decursin treatment

Ficoll (Solarbio) was used to isolate Human PBMCs according to the manufacturer's instructions. The Human PBMCs were cultured in 10% fetal bovine serum and 90% Roswell Park Memorial Institute-1640 medium for 48 h. Then, decursin (MCE, Macau, China) was added to PBMCs at concentrations of 0, 5, and 10 μM, respectively, and incubated for 48 h.

Statistical analysis

The experimental data were analyzed using GraphPad Prism 8 (GraphPad Inc., La Jolla, CA, United States) using unpaired *t*-tests, and p-value < 0.05 was considered statistically significant. The results are shown as the mean and standard deviation.

Results

Active components of YU-Pingfeng San and prediction of their targets

The workflow chart for network pharmacology analysis and experimental verification is shown in **Figure 1**. Totally 20 active ingredients for HQ, 7 for BZ, and 18 for FF in YPFS were identified in the TCMSP. These 45 active ingredients of YPFS are shown in **Supplementary Table 2**. Among them, 30 active ingredients were predicted to have target proteins by Swiss target prediction, including 16 components for HQ, 2 for BZ, and 12 for FF. We found 637 potential drug targets for the 30 active ingredients (**Supplementary Table 3**). The interaction network among the three herbs, 30 active ingredients, and 637 target genes is shown in **Figure 2**.

Screening of allergic rhinitis/YU-Pingfeng San-related genes

A total of 49 AR-associated target genes were obtained from the DrugBank database, 1,311 AR-associated target genes were obtained from the Genecards database, and 214 AR-associated target genes were obtained from the OMIM database. After combining the related target genes from the three databases and the removal of duplicates, a total of 945 AR-associated target genes were obtained (**Supplementary Table 4**). About 140 AR/YPFS-related genes (**Supplementary Table 5**) overlapped between the 945 AR-associated genes and the 637 YPFS target genes (**Figure 3A**). The interaction network among the three herbs, 29 active ingredients, and 140 AR/YPFS-related genes is shown in **Figure 3B**.

Functional enrichment and pathway analysis

Functional enrichment analysis was performed on the 140 AR/YPFS-related genes using GO, which showed that these genes were mainly enriched in processes involved in immune regulation, such as regulation of inflammatory response, leukocyte migration and chemotaxis, regulation of leukocyte migration, lymphocyte differentiation, and T cell activation (**Figure 4A**). KEGG pathway enrichment analysis showed that these genes were enriched in certain immune and inflammatory-related pathways, such as the phosphatidylinositol-4,5-bisphosphate 3-kinase (PI3K)-AKT signaling pathway, the T cell receptor signaling pathway, the MAPK signaling pathway, the Janus kinase (Jak)-signal transducer and activator of transcription (STAT) signaling pathway, and the Ras signaling pathway (**Figure 4B**).

Identification of the hub genes from among the allergic rhinitis/YU-Pingfeng San-related genes

To understand the interaction regulation of the 140 AR/YPFS-related genes, we uploaded them to the String database to obtain a PPI network diagram (**Figure 5**). Using Cytoscape's degree score analysis, we screened out three hub targets: EGFR, MAPK1, and AKT1 which had the strongest interaction scores of 32, 27, and 24, respectively. The degrees between target nodes are shown in **Supplementary Table 6**.

YU-Pingfeng San relieved inflammatory reactions of ovalbumin-induced allergic rhinitis

Compared with those in the control group, serum IgE, IL-4, IL-5, and IL-13 levels were significantly higher in the OVA-induced AR group (**Figures 6A–D**). The IFNγ level was significantly lower in the OVA-induced AR group than in the control group (**Figure 6E**). Through YPFS treatment, serum IL-5 and IL-13 levels decreased significantly (**Figures 6A–D**), and IFNγ levels increased significantly compared with those in the OVA-induced AR group (**Figure 6E**). Meanwhile, IgE, IL-4, IL-5, IL-13, and IFNγ showed no obvious change between the YPFS treatment group and the control group, which showed that YPFS treatment could rescue the levels of IgE, IL-4, IL-5, IL-13, and IFNγ to their normal levels. Compared with the control group, OVA modeling and YPFS treatment had no effect on the body weight of mice (**Supplementary Figure 1**).

Compared with those in the control group, the frequency and times of nasal scratching in the OVA-induced AR group mice increased significantly (**Figure 6F**), whereas the frequency

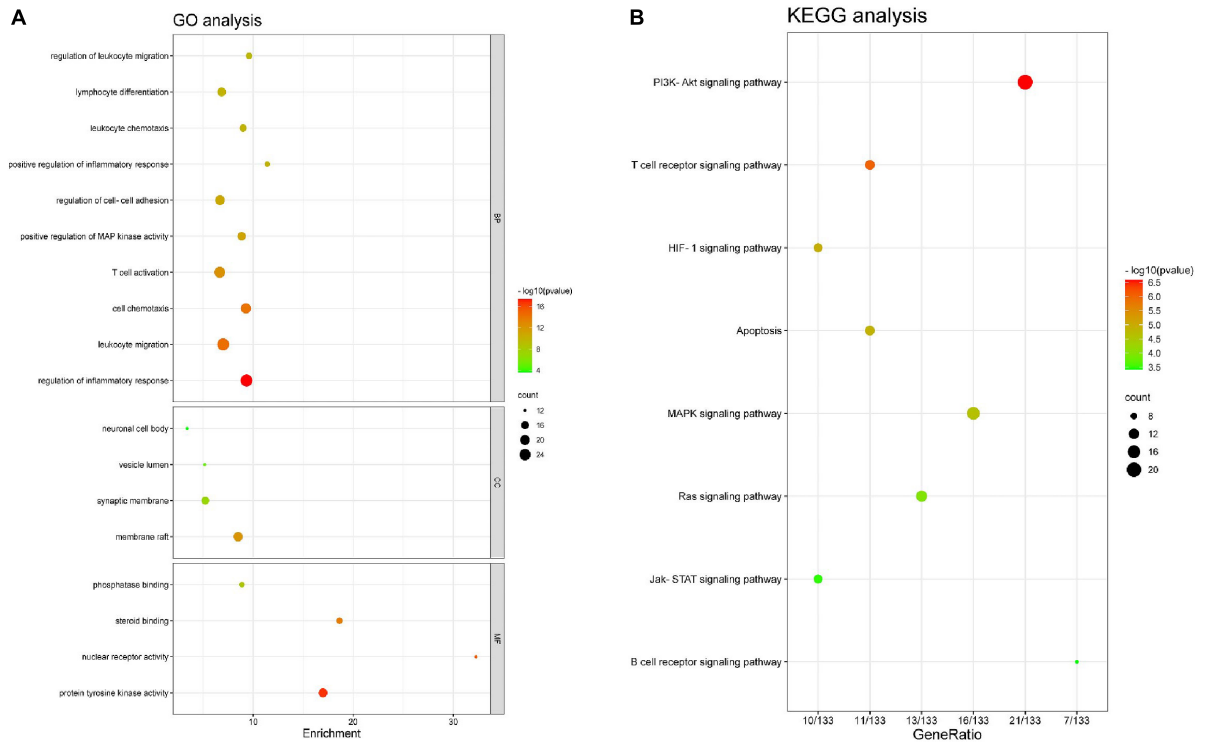

FIGURE 4
Enrichment analysis. **(A)** Gene ontology (GO) functional enrichment analysis. **(B)** Kyoto Encyclopedia of Genes and Genomes (KEGG) pathway enrichment analysis.

and times of nasal scratching were reduced in the YPFS group (Figure 6G), showing that the AR symptoms were significantly relieved after YPFS treatment.

YU-Pingfeng San reduced the expression of the hub genes in the nasal mucosa of ovalbumin-induced allergic rhinitis mice

Compared with the control group, the expression levels of the hub genes *Egfr, Mapk1,* and *Akt1* in the nasal mucosa of the OVA-induced AR group were significantly increased, and no significant expression differences were found between the YPFS treatment group and the control group (Figures 7A–C). These results indicated that YPFS treatment could reduce the expression of the hub genes *Egfr, Mapk1,* and *Akt1* to their normal level.

Identifying the docking sites between active ingredients and hub genes

Through the correlation analysis between active ingredients and the 140 AR/YPFS-related genes (Supplementary Table 7), three active ingredients, decursin, anomalin, and wogonin, were selected for molecular docking with EGFR, MAPK1, and AKT1. The results showed that decursin could bind to EGFR at Tyr998 (Figure 8A); to MAPK1 at Tyr36 and Lys54 (Figure 8A'); and to AKT1 at Ala50, Pro51, and Leu52 (Figure 8A"). Anomalin was identified to bind to EGFR at Glu967 (Figure 8B); to MAPK1 at Asn201 and His180 (Figure 8B'); and to AKT1 at Arg15 and Trp22 (Figure 8B"). Meanwhile, wogonin was identified to bind to EGFR at Lys842, Lys846, and Gln791 (Figure 8C); to MAPK1 at Tyr36 and Arg67 (Figure 8C'); and to AKT1 at Arg48 (Figure 8C"). These results showed that YPFS could target the hub proteins EGFR, MAPK1, and AKT1 via the active ingredients decursin, anomalin, and wogonin.

Decursin decreased the expression of inflammatory factors in human peripheral blood mononuclear cells

Compared with those in the control group, the expression levels of IL-4 and IL-5 in Human PBMCs after decursin treatment were decreased in a dose-dependent manner (Figures 9A,B). Similarly, the expression levels of EGFR, MAPK1, and AKT1 in Human PBMCs decreased after decursin

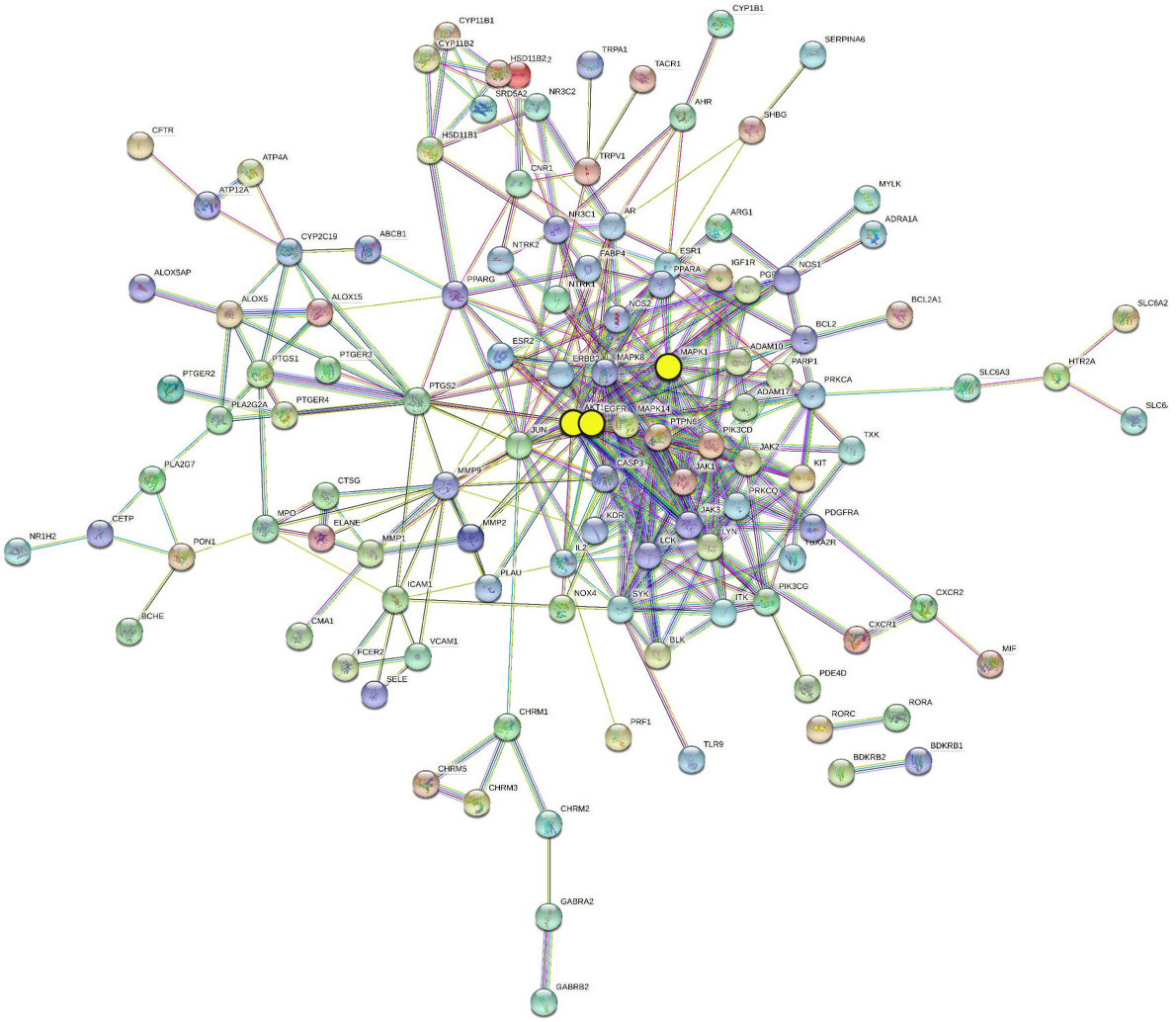

FIGURE 5
Protein–protein interaction (PPI) network of 140 AR/YPFS-related genes. The three yellow circles represent the selected genes: EGFR, MAPK1, and AKT1.

treatment (Figures 9C–E). These results showed that decursin could relieve the inflammatory reaction in AR by affecting EGFR, MAPK1, and AKT1 expression in Human PBMCs.

Discussion

TCM formulations composed of multiple ingredients can affect multiple targets and pathways via complex mechanisms. YPFS is often used to treat AR in the clinic; however, its mechanism of action remains unclear. In this study, using network pharmacology analysis and experimental verification, the active ingredients and target genes of YPFS were identified for AR treatment. Based on the network pharmacology analysis, 30 active ingredients and 140 AR/YPFS-associated genes were screened from network databases. Through PPI network analysis of the 140 targets, three hub gene targets with the strongest interactions were found: AKT1, MAPK1, and EGFR, which are enriched in T-helper 1 (Th1) and 2 types (Th2) immune responses and T cell cytokine production. Through *in vivo* experiments, YPFS treatment was observed to relieve AR symptoms, reduce the expression levels of Th2 cytokines IL-4, IL-5, and IL-13, and increase the expression level of the Th1 cytokine IFNγ in serum. Meanwhile, the expression levels of MAPK1, EGFR, and AKT1 were reduced by YPFS treatment. Through a molecular docking approach of ingredients and targets and *in vitro* cell experiments, decursin was found to have the most potential as the bioactive ingredient in YPFS to relieve the Th2 inflammatory response of AR by decreasing the expression of the hub genes MAPK1, EGFR, and AKT1.

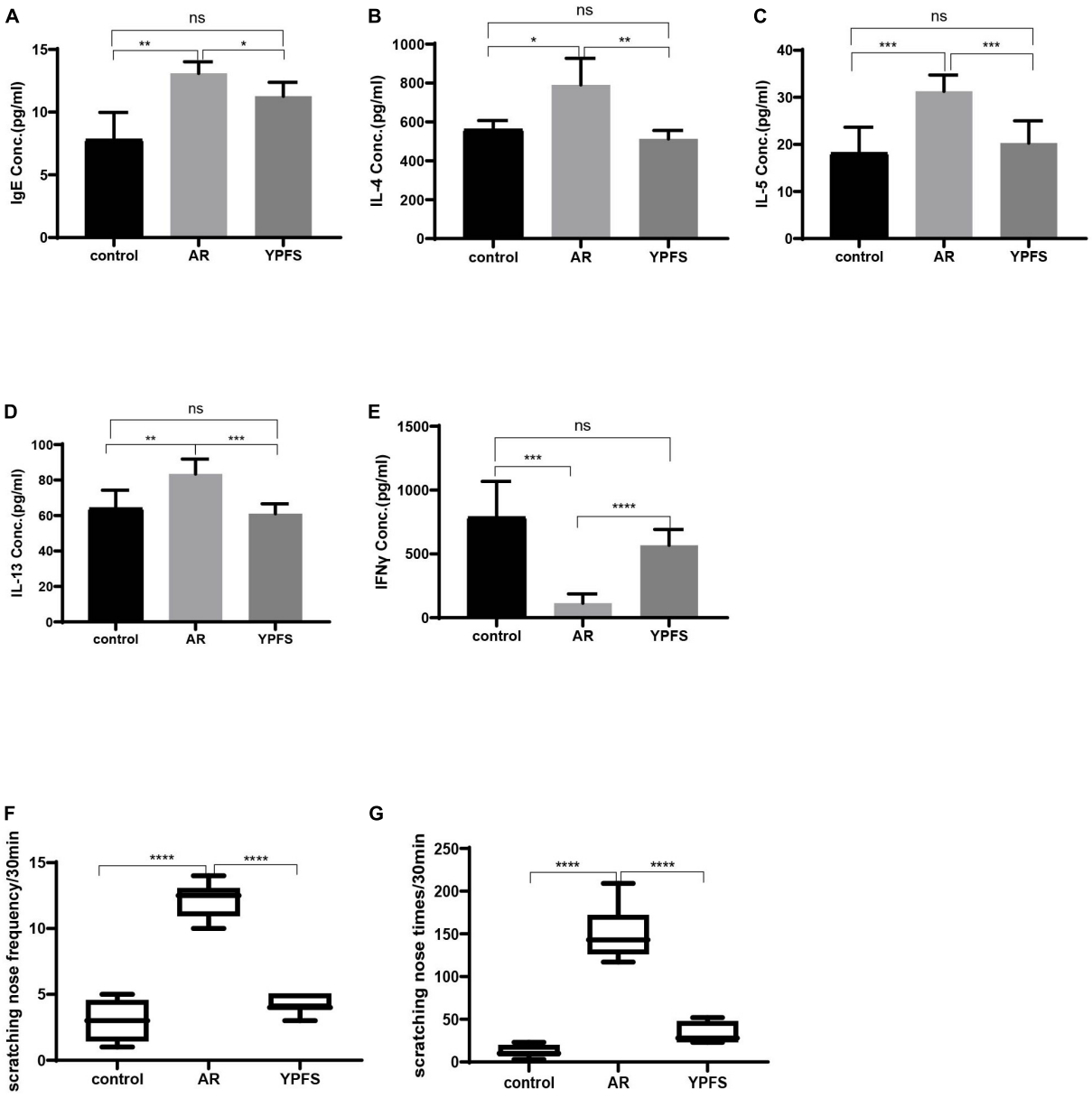

FIGURE 6
YPFS relieved inflammatory reactions of ovalbumin (OVA)-induced AR. Comparisons of IgE **(A)**, IL-4 **(B)**, IL-5 **(C)**, IL-13 **(D)**, and IFNγ **(E)** concentrations (Conc.) in the serum of mice. The frequency **(F)** and times **(G)** of nasal scratching scores in mice for 30 min in the control group, OVA-induced AR group, and YPFS group. *$P < 0.05$, **$P < 0.01$, ***$P < 0.001$, ****$P < 0.0001$; $n = 6$. YPFS, YU-Pingfeng San; AR, allergic rhinitis.

In AR, allergens stimulate nasal epithelial cells to secrete inflammatory factors acting on innate lymphoid cells type 2 (ILC2) to produce the type 2 cytokines IL-5 and IL-13 and also acting on dendritic cells (DCs). DCs present antigens to resident lymph nodes to activate $CD4^+$ T cell differentiation to Th2 cells, which produce the cytokines IL-4, IL-5, and IL-13, thus inducing a classical type 2 inflammatory response (Peng et al., 2020). In our study, the 140 AR/YPFS-related genes were enriched in those biological processes regulating AR pathogenesis such as lymphocyte chemotaxis, differentiation and migration, and T cell activation, further showing that these genes could play important roles in AR regulation through mediating lymphocyte activities.

AR is an allergic disease of the nasal mucosa caused by the imbalance of differentiation of T cells. YPFS is recommended for the management of AR by the Chinese medicine clinical practice guidelines and can relieve the clinical symptoms of AR. However, how YPFS functions is still not clear. YPFS could impair the inflammatory response by reducing thymic stromal lymphopoietin (TSLP), tumor necrosis factor-alpha

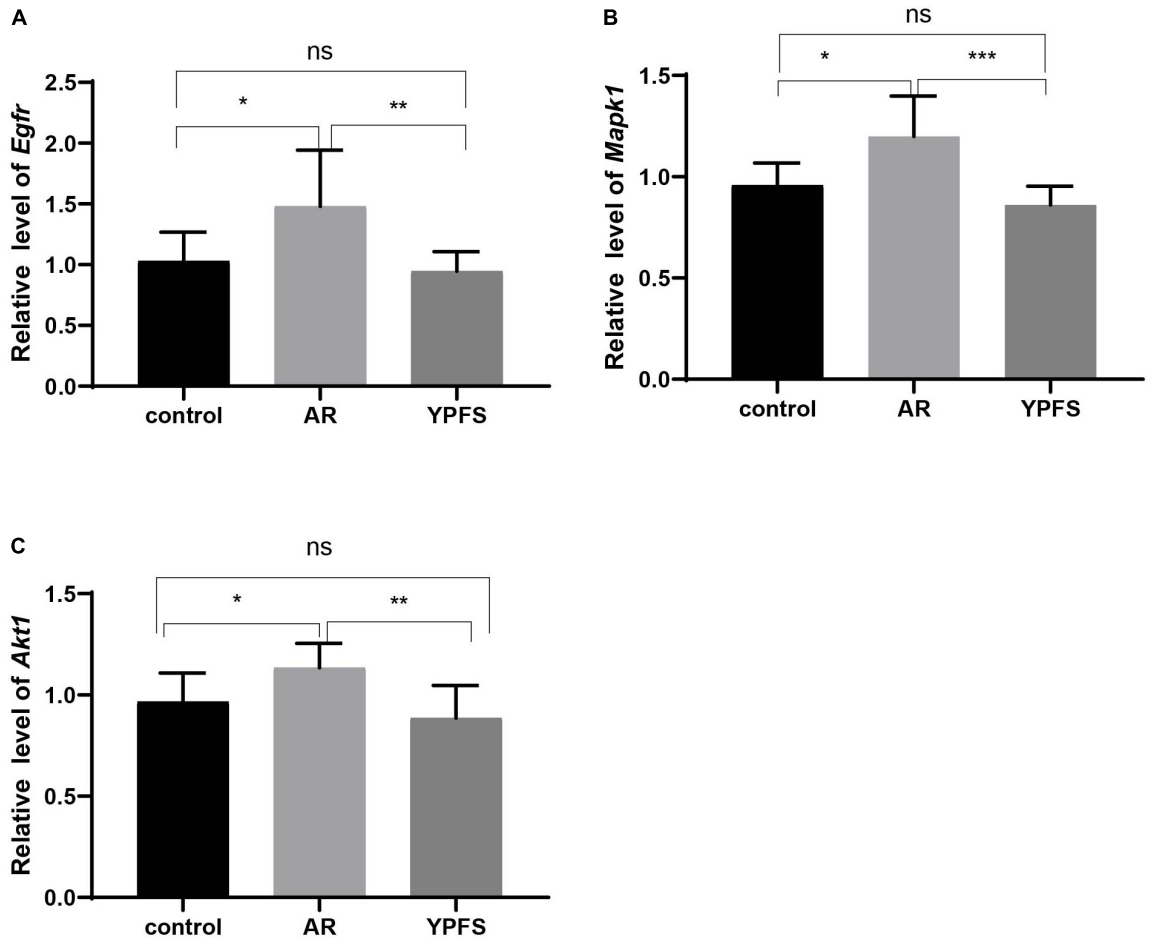

FIGURE 7
Relative expression levels of *Egfr* **(A)**, *Mapk1* **(B)**, and *Akt1* **(C)** in the nasal mucosa of mice in the control group, ovalbumin (OVA)-induced AR group, and YPFS group. $^{*}P < 0.05$, $^{**}P < 0.01$, $^{***}P < 0.001$; $n = 6$. YPFS, YU-Pingfeng San; AR, allergic rhinitis.

(TNFα), and IL-6 production (Shen et al., 2014; Liu et al., 2017). YPFS also decreased eosinophils and the IgE content in serum and reduced IL-4 and IFNγ in lung tissue in OVA-induced allergic asthmatic mice (Chen et al., 2021). Moreover, YPFS has been reported to impair the inflammatory response by regulating inflammatory factor production (Shen et al., 2014), tight junctions (Zheng et al., 2019), and epithelial-mesenchymal transition (Yao et al., 2019) in epithelial cells. However, little is known about how YPFS regulates the Th2 cell response and Th2-type inflammatory factor production in AR. In the present study, the levels of Th2-type inflammatory factors IL-4, IL-5, and IL-13 were markedly reduced by YPFS treatment in OVA-induced AR mice, suggesting that YPFS could relieve AR symptoms by inhibiting the Th2 cell response. Meanwhile, we also found that IFNγ production was increased by YPFS. These results indicated that YPFS preferentially increases the Th1 cell response and decreases the Th2 cell response.

KEGG pathway enrichment analysis showed that 140 AR/YPFS-related genes were enriched in pathways involved in regulating AR, such as the PI3K/AKT pathway, the hypoxia-inducible factor 1 alpha (HIF1α) signaling pathway, and the MAPK, RAS, and JAK/STAT signaling pathways. The PI3K/AKT signaling pathway is involved in a variety of AR inflammatory responses, including Th2-mediated inflammation (Zeng et al., 2018), the percentage of regulatory T cells (Tregs), and IL-10 and TGF-β1 expression (Zeng et al., 2019), the expression of ILC2 cell transcription factors and type II cytokines (Zeng et al., 2020); mast cell activity suppression (Lin et al., 2015); and vascular endothelial growth factor (VEGF) and fibroblast growth factor 2 (FGF-2) expression in nasal epithelial cells (Chen et al., 2016). The level of HIF-1α is increased in patients with AR, and HIF-1α accumulation is critical for sustaining human allergic effector cell survival and function (Cheng et al., 2016; Kou et al., 2018). HIF-1α deficiency decreased inflammatory responses and symptoms caused by AR (Niu et al., 2020). HIF-1α inhibitors or antagonists could induce antiallergic effects by decreasing both local and systemic Th2 cytokine (IL-4 and IL-5) production, IgE production,

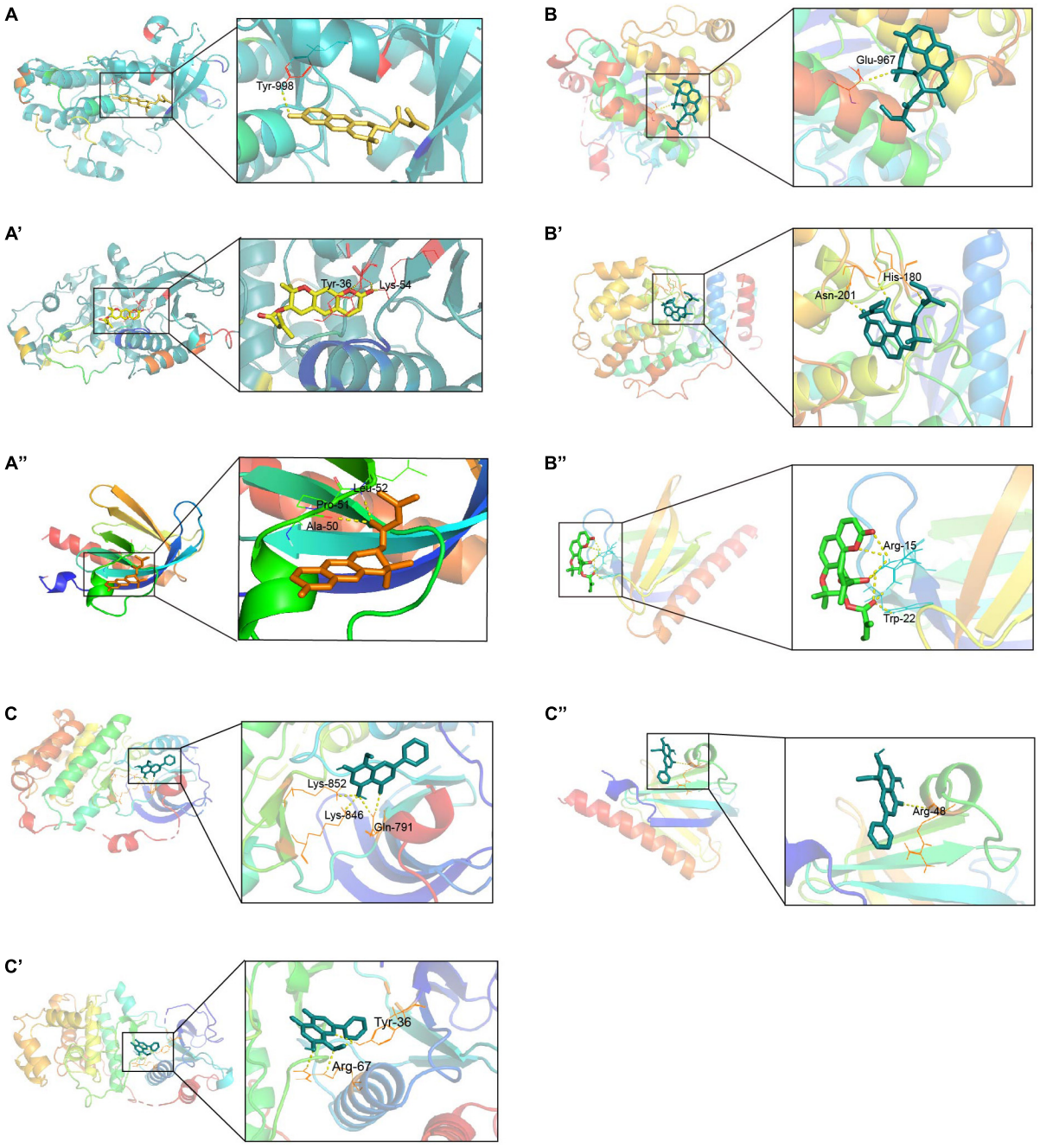

FIGURE 8
Docking sites of YPFS ingredients with target proteins. **(A)** Docking sites of EGFR and decursin. **(A')** Docking sites of MAPK1 and decursin. **(A")** Docking sites of AKT1 and decursin. **(B)** Docking sites of EGFR and anomalin. **(B')** Docking sites of MAPK1 and anomalin. **(B")** Docking sites of AKT1 and anomalin. **(C)** Docking sites of EGFR and wogonin. **(C')** Docking sites of MAPK1 and wogonin. **(C")** Docking sites of AKT1 and wogonin. EGFR PDB ID: 1XKK. MAPK1 PDB ID: 1PME. AKT1 PDB ID: 1H10.

and eosinophil infiltration into the nasal mucosa in an AR model (Mo et al., 2014; Wang et al., 2016). MAPK and JAK/STAT signaling pathways play key roles in the proliferation, differentiation, and production of inflammatory cells and are involved in the activation of AR (Yang et al., 2021). After blocking the MAPK or JAK/STAT signaling pathways, the symptoms of rhinitis in AR mice were reduced, and the aggregation of inflammatory cells in the epithelial cells of the nasal mucosa and vascular area was decreased (Howell et al., 2018; Paiva Ferreira et al., 2021). These observations show that the pathways play important roles in AR regulation, and indicate the reliability of the 140 selected AR/YPFS-related genes.

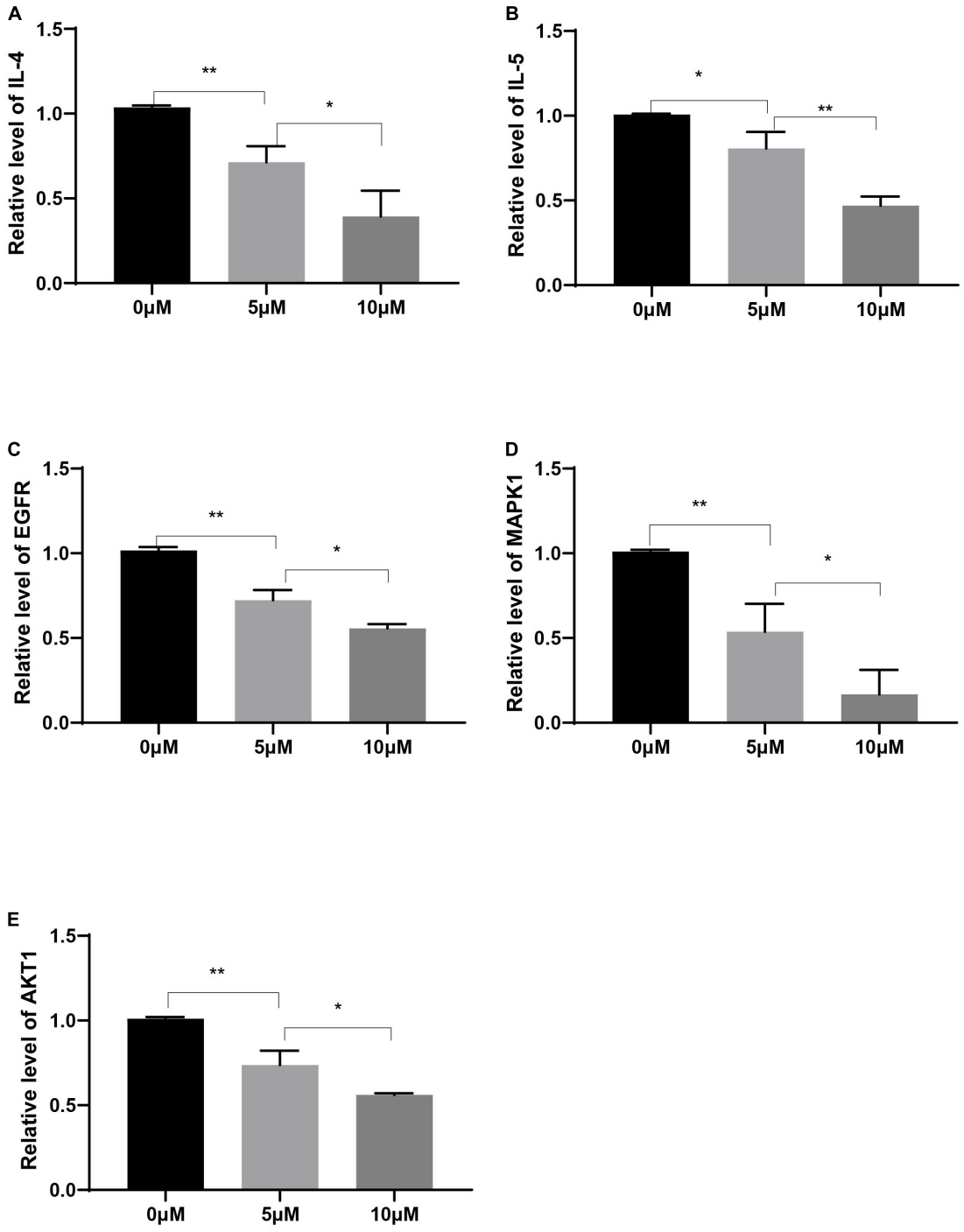

FIGURE 9
Relative expression levels of IL-4 **(A)**, IL-5 **(B)**, EGFR **(C)**, MAPK1 **(D)**, and AKT1 **(E)** in Human PBMCs treated with decursin at 0, 5, and 10 μM. $^{*}P < 0.05$, $^{**}P < 0.01$; $n = 3$.

Three hub genes, EGFR, MAPK1, and AKT1, were identified through PPI analysis and Cytoscape analysis. Accumulating studies have shown that EGFR, MAPK1, and AKT1 participate in AR regulation. EGFR was significantly elevated in patients with AR (Matovinovic et al., 2003), and the activation of EGFR was likely to drive airway inflammation and epithelial cytokine production (Daines et al., 2020). EGFR inhibitors have been shown to inhibit OVA-induced metaplasia, mucus production, and eosinophilic/neutrophil infiltration in rat nasal epithelial goblet cells, and inhibition of the EGF signaling pathway

activity alleviates nasal mucosal injury (Shimizu et al., 2018). The results of the present study confirmed that after YPFS treatment of AR mice and EGFR reduction, the expression of inflammatory factors in the OVA-induced AR group decreased, and rhinitis symptoms were alleviated, suggesting that EGFR reduction benefits AR treatment. MAPK1 and AKT1 participate in AR regulation via the MAPK and PI3K/AKT signaling pathways, respectively. MAPK1 was also identified as the core gene of YPFS targets in a study by Yang et al. based on network pharmacology (Yang et al., 2021). In our study, the elevated expression of MAPK1 and AKT1 were reversed by YPFS treatment in the AR mice. Thus, YPFS could alleviate the AR inflammatory response and symptoms by reducing the expression levels of EGFR, MAPK1, and AKT1. Gene enrichment analysis showed that EGFR, MAPK1, and AKT1 are involved in the HIF-1α pathway, indicating that YPFS could also alleviate AR responses by regulating the HIF-1α pathway.

The compounds decursin, anomalin, and wogonin, screened from YPFS, can potentially bind to EGFR, MAPK, and AKT and inhibit their expression. Decursin has been reported to be associated with inflammatory immunity (Shehzad et al., 2018). A novel (S)-(+)-decursin derivative reduced ovalbumin-specific immunoglobulin E (IgE) levels in an OVA-induced mouse model of asthma and alleviated lung inflammation in mice, and thus might be an effective therapeutic agent for allergic airway diseases (Yang et al., 2009). Studies have found that decursinol angelate inhibits the expression of pro-inflammatory cytokines, such as IL-1β and IL-6, NADPH oxidase (NOX), and inducible nitric oxide synthase (iNOS) in cells. It has the potential to inhibit macrophage polarization and inflammation by blocking the activation of pro-inflammatory signals (Islam et al., 2018). Decursin analogs also inhibit inflammation by downregulating nuclear factor kappa B (NF-κB) and STAT1 (Lee et al., 2021). Anomalin significantly inhibited the production of pro-inflammatory mediators and significantly reduced the activation of MAPK and AKT proteins in macrophages (Khan et al., 2019). Studies have shown that anomalin inhibits the levels of inflammatory cytokines through the inactivation of NF-κB, nuclear factor erythroid 2-related factor 2 (Nrf2), and MAPK signaling pathways (Khan et al., 2016). Wogonin produced an antiallergic effect in AR mouse models by reducing eosinophil infiltration and the Th2 cytokines IL-4, IL-5, and IL-13 in the serum and nasal mucosa (Shin et al., 2014; Kim et al., 2018). Wogonin can also reduce allergic airway inflammation *in vivo* by reducing the number of eosinophils, increasing eosinophil apoptosis, reducing airway mucus production, and reducing airway hyperresponsiveness. Studies have shown that wogonin might play a role in the treatment of allergic diseases by regulating Th1/Th2 cytokine imbalance and histamine release in mast cells (Bui et al., 2017). These studies support our results that decursin, anomalin, and wogonin might be the key active ingredients in YPFS for AR treatment.

Conclusion

In summary, we identified the active ingredients in YPFS and 140 AR/YPFS-related genes through network pharmacology analysis. *In vivo* experiments showed that YPFS reduced the IgE level in serum, decreased the production of Th2-type cytokines, and relieved AR symptoms. Meanwhile, EGFR, MAPK1, and AKT1 were found to be downregulated by YPFS in OVA-induced AR mice, and be targeted by active ingredients decursin, anomalin, and wogonin from YPFS through molecular docking prediction. These results showed that YPFS could relieve the AR inflammatory response and symptoms mainly via active ingredients decursin, anomalin, and wogonin targeting and inhibiting EGFR, MAPK1, and AKT1, which may provide novel ingredients for AR treatment. However, these results should be further verified using more detailed molecular mechanism studies, contributing to the *in-depth* research and application of traditional Chinese medicines.

Data availability statement

The original contributions presented in this study are included in the article/**Supplementary material**, further inquiries can be directed to the corresponding authors.

Ethics statement

The studies involving human participants were reviewed and approved by Yantai Yuhuangding Animal Ethics Committee. The patients/participants provided their written informed consent to participate in this study. The animal study was reviewed and approved by Yantai Yuhuangding Animal Ethics Committee.

Author contributions

YY and YL designed and directed the study. ZL and QS organized the public data and wrote the manuscript. ZL, XL, XS, QS, and ZS performed the experimental work and analyzed the data. FS, CL, and QS took charge of data visualization. XS, YZ, and YL revised the manuscript. All authors contributed to the article and approved the submitted version.

Funding

This work was supported by the National Natural Science Foundation of China (82071021); Key Technology research and development program of Shandong (2020CXGC011302).

Conflict of interest

The authors declare that the research was conducted in the absence of any commercial or financial relationships that could be construed as a potential conflict of interest.

Publisher's note

All claims expressed in this article are solely those of the authors and do not necessarily represent those of their affiliated organizations, or those of the publisher, the editors and the reviewers. Any product that may be evaluated in this article, or claim that may be made by its manufacturer, is not guaranteed or endorsed by the publisher.

Supplementary material

The Supplementary Material for this article can be found online at: https://www.frontiersin.org/articles/10.3389/fpls.2022.934130/full#supplementary-material

References

Agnew, C., Ayaz, P., Kashima, R., Loving, H. S., Ghatpande, P., Kung, J. E., et al. (2021). Structural basis for ALK2/BMPR2 receptor complex signaling through kinase domain oligomerization. *Nat. Commun.* 12:4950. doi: 10.1038/s41467-021-25248-5

Algethami, F. K., Saidi, I., Abdelhamid, H. N., Elamin, M. R., Abdulkhair, B. Y., Chrouda, A., et al. (2021). Trifluoromethylated flavonoid-based isoxazoles as antidiabetic and anti-obesity agents: Synthesis, in vitro α-amylase inhibitory activity, molecular docking and structure-activity relationship analysis. *Molecules* 26:5214. doi: 10.3390/molecules26175214

Bahadur Gurung, A., Ajmal Ali, M., Al-Hemaid, F., El-Zaidy, M., and Lee, J. (2022). *In silico* analyses of major active constituents of fingerroot (*Boesenbergia rotunda*) unveils inhibitory activities against SARS-CoV-2 main protease enzyme. *Saudi J. Biol. Sci.* 29, 65–74. doi: 10.1016/j.sjbs.2021.11.053

Bao, K., Yuan, W., Zhou, Y., Chen, Y., Yu, X., Wang, X., et al. (2019). A Chinese prescription Yu-Ping-Feng-San administered in remission restores bronchial epithelial barrier to inhibit house dust mite-induced asthma recurrence. *Front. Pharmacol.* 10:1698. doi: 10.3389/fphar.2019.01698

Bousquet, J., Anto, J. M., Bachert, C., Baiardini, I., Bosnic-Anticevich, S., Walter Canonica, G., et al. (2020). Allergic rhinitis. *Nat. Rev. Dis. Primers* 6:95. doi: 10.1038/s41572-020-00227-0

Bui, T. T., Piao, C. H., Song, C. H., Lee, C. H., Shin, H. S., and Chai, O. H. (2017). Baicalein, wogonin, and *Scutellaria baicalensis* ethanol extract alleviate ovalbumin-induced allergic airway inflammation and mast cell-mediated anaphylactic shock by regulation of Th1/Th2 imbalance and histamine release. *Anat. Cell Biol.* 50, 124–134. doi: 10.5115/acb.2017.50.2.124

Caliceti, C., Capriotti, A. L., Calabria, D., Bonvicini, F., Zenezini Chiozzi, R., Montone, C. M., et al. (2019). Peptides from cauliflower by-products, obtained by an efficient, ecosustainable, and semi-industrial method, exert protective effects on endothelial function. *Oxid. Med. Cell. Longev.* 2019:1046504. doi: 10.1155/2019/1046504

Chan, R. Y., and Chien, W. T. (2014). The effects of two Chinese herbal medicinal formulae vs. placebo controls for treatment of allergic rhinitis: A randomised controlled trial. *Trials* 15:261. doi: 10.1186/1745-6215-15-261

Chen, H., Feng, W., Lu, Y., Yang, Y., Xin, Z. H., Li, M., et al. (2021). Effects and mechanism of Chinese medicine Jiawei Yupingfeng in a mouse model of allergic rhinitis. *J. Integr. Med.* 19, 354–361. doi: 10.1016/j.joim.2021.01.012

Chen, X., Li, Y. Y., Zhang, W. Q., Zhang, W. M., and Zhou, H. (2016). House dust mite extract induces growth factor expression in nasal mucosa by activating the PI3K/Akt/HIF-1α pathway. *Biochem. Biophys. Res. Commun.* 469, 1055–1061. doi: 10.1016/j.bbrc.2015.12.110

Cheng, K. J., Bao, Y. Y., and Zhou, S. H. (2016). The role of hypoxia inducible factor in nasal inflammations. *Eur. Rev. Med. Pharmacol. Sci.* 20, 5067–5076.

Daines, M., Zhu, L., Pereira, R., Zhou, X., Bondy, C., Pryor, B. M., et al. (2020). Alternaria induces airway epithelial cytokine expression independent of protease-activated receptor. *Respirology* 25, 502–510. doi: 10.1111/resp.13675

Ding, Z., Xu, F., Sun, Q., Li, B., Liang, N., Chen, J., et al. (2021). Exploring the mechanism of action of herbal medicine (Gan-Mai-Da-Zao decoction) for poststroke depression based on network pharmacology and molecular docking. *Evid. Based Complement. Alternat. Med.* 2021:2126967. doi: 10.1155/2021/2126967

Fan, X., Guo, X., Li, Y., and Xu, M. (2021). Utilizing network pharmacology to explore the possible mechanism of coptidis rhizoma in Kawasaki disease. *Front. Pediatr.* 9:708553. doi: 10.3389/fped.2021.708553

Howell, M. D., Fitzsimons, C., and Smith, P. A. (2018). JAK/STAT inhibitors and other small molecule cytokine antagonists for the treatment of allergic disease. *Ann. Allergy Asthma Immunol.* 120, 367–375. doi: 10.1016/j.anai.2018.02.012

Hu, S., Liao, Y., Zheng, J., Gou, L., Regmi, A., Zafar, M. I., et al. (2019). In silico integration approach reveals key MicroRNAs and their target genes in follicular thyroid carcinoma. *Biomed Res. Int.* 2019:2725192. doi: 10.1155/2019/2725192

Islam, M. A., Rallabandi, V. P. S., Mohammed, S., Srinivasan, S., Natarajan, S., Dudekula, D. B., et al. (2021). Screening of β1- and β2-adrenergic receptor modulators through advanced pharmacoinformatics and machine learning approaches. *Int. J. Mol. Sci.* 22:11191. doi: 10.3390/ijms222011191

Islam, S. U., Lee, J. H., Shehzad, A., Ahn, E. M., Lee, Y. M., and Lee, Y. S. (2018). Decursinol angelate inhibits LPS-induced macrophage polarization through modulation of the NFκB and MAPK signaling pathways. *Molecules* 23:1880. doi: 10.3390/molecules23081880

Kappen, J. H., Durham, S. R., Veen, H. I., and Shamji, M. H. (2017). Applications and mechanisms of immunotherapy in allergic rhinitis and asthma. *Ther. Adv. Respir. Dis.* 11, 73–86. doi: 10.1177/1753465816669662

Karta, M. R., Broide, D. H., and Doherty, T. A. (2016). Insights into group 2 innate lymphoid cells in human airway disease. *Curr. Allergy Asthma Rep.* 16:8. doi: 10.1007/s11882-015-0581-6

Khan, A., Khan, S., Ali, H., Shah, K. U., Ali, H., Shehzad, O., et al. (2019). Anomalin attenuates LPS-induced acute lungs injury through inhibition of AP-1 signaling. *Int. Immunopharmacol.* 73, 451–460. doi: 10.1016/j.intimp.2019.05.032

Khan, S., Choi, R. J., Lee, J., and Kim, Y. S. (2016). Attenuation of neuropathic pain and neuroinflammatory responses by a pyranocoumarin derivative, anomalin in animal and cellular models. *Eur. J. Pharmacol.* 774, 95–104. doi: 10.1016/j.ejphar.2016.02.008

Kim, K. A., Jung, J. H., Choi, Y. S., Kang, G., and Kim, S. T. (2018). Anti-inflammatory effect of wogonin on allergic responses in ovalbumin-induced allergic rhinitis in the mouse. *Allergy Rhinol.* 9:2152656718764145. doi: 10.1177/2152656718764145

Kou, W., Li, X., Yao, H., Zhang, C., and Wei, P. (2018). Hypoxia disrupts aryl hydrocarbon receptor signaling and the Th17 response in allergic rhinitis patients. *Mol. Immunol.* 101, 364–369. doi: 10.1016/j.molimm.2018.07.025

Lee, W., Sim, H., Choi, Y. J., Seo, J. Y., Yun, M. Y., Song, G. Y., et al. (2021). The decursin analog, CYJ-27, suppresses inflammation via the downregulation of NF-κB and STAT-1. *J. Med. Food* 24, 852–859. doi: 10.1089/jmf.2021.K.0027

Lin, H., Zheng, C., Li, J., Yang, C., and Hu, L. (2015). Lentiviral shRNA against KCa3.1 inhibits allergic response in allergic rhinitis and suppresses mast cell activity via PI3K/AKT signaling pathway. *Sci. Rep.* 5:13127. doi: 10.1038/srep13127

Liu, X., Shen, J., Fan, D., Qiu, X., Guo, Q., Zheng, K., et al. (2017). Yupingfeng san inhibits NLRP3 inflammasome to attenuate the inflammatory response in asthma mice. *Front. Pharmacol.* 8:944. doi: 10.3389/fphar.2017.00944

Livak, K. J., and Schmittgen, T. D. (2001). Analysis of relative gene expression data using real-time quantitative PCR and the 2(-Delta Delta C(T)) method. *Methods* 25, 402–408. doi: 10.1006/meth.2001.1262

Luo, Q., Zhang, C. S., Yang, L., Zhang, A. L., Guo, X., Xue, C. C., et al. (2017). Potential effectiveness of Chinese herbal medicine Yu ping feng san for adult allergic rhinitis: A systematic review and meta-analysis of randomized controlled trials. *BMC Complement. Altern. Med.* 17:485. doi: 10.1186/s12906-017-1988-5

Matovinovic, E., Solberg, O., and Shusterman, D. (2003). Epidermal growth factor receptor – but not histamine receptor – is upregulated in seasonal allergic rhinitis. *Allergy* 58, 472–475. doi: 10.1034/j.1398-9995.2003.00156.x

Mo, J. H., Kim, J. H., Lim, D. J., and Kim, E. H. (2014). The role of hypoxia-inducible factor 1α in allergic rhinitis. *Am. J. Rhinol. Allergy* 28, e100–e106. doi: 10.2500/ajra.2014.28.4025

Nikles, S., Monschein, M., Zou, H., Liu, Y., He, X., Fan, D., et al. (2017). Metabolic profiling of the traditional Chinese medicine formulation Yu Ping Feng San for the identification of constituents relevant for effects on expression of TNF-α, IFN-γ, IL-1β and IL-4 in U937 cells. *J. Pharm. Biomed. Anal.* 145, 219–229. doi: 10.1016/j.jpba.2017.03.049

Niu, Y., Wang, J., Li, Z., Yao, K., Wang, L., and Song, J. (2020). HIF1α deficiency in dendritic cells attenuates symptoms and inflammatory indicators of allergic rhinitis in a SIRT1-dependent manner. *Int. Arch. Allergy Immunol.* 181, 585–593. doi: 10.1159/000506862

Paiva Ferreira, L. K. D., Paiva Ferreira, L. A. M., Bezerra Barros, G. C., Mozzini Monteiro, T., de Araújo Silva, L. A., Pereira, R. A., et al. (2021). MHTP, a synthetic alkaloid, attenuates combined allergic rhinitis and asthma syndrome through downregulation of the p38/ERK1/2 MAPK signaling pathway in mice. *Int. Immunopharmacol.* 96:107590. doi: 10.1016/j.intimp.2021.107590

Peng, Y. Q., Qin, Z. L., Fang, S. B., Xu, Z. B., Zhang, H. Y., Chen, D., et al. (2020). Effects of myeloid and plasmacytoid dendritic cells on ILC2s in patients with allergic rhinitis. *J. Allergy Clin. Immunol.* 145, 855–867.e8. doi: 10.1016/j.jaci.2019.11.029

Santos, A. F., Borrego, L. M., Rotiroti, G., Scadding, G., and Roberts, G. (2015). The need for patient-focused therapy for children and teenagers with allergic rhinitis: A case-based review of current European practice. *Clin. Transl. Allergy* 5:2. doi: 10.1186/s13601-014-0044-5

Shao, Y. Y., Zhou, Y. M., Hu, M., Li, J. Z., Chen, C. J., Wang, Y. J., et al. (2017). The anti-allergic rhinitis effect of traditional Chinese medicine of shenqi by regulating mast cell degranulation and Th1/Th2 cytokine balance. *Molecules* 22:504. doi: 10.3390/molecules22030504

Shehzad, A., Parveen, S., Qureshi, M., Subhan, F., and Lee, Y. S. (2018). Decursin and decursinol angelate: Molecular mechanism and therapeutic potential in inflammatory diseases. *Inflamm. Res.* 67, 209–218. doi: 10.1007/s00011-017-1114-7

Shen, D., Xie, X., Zhu, Z., Yu, X., Liu, H., Wang, H., et al. (2014). Screening active components from Yu-ping-Feng-san for regulating initiative key factors in allergic sensitization. *PLoS One* 9:e107279. doi: 10.1371/journal.pone.0107279

Shimizu, S., Takezawa-Yasuoka, K., Ogawa, T., Tojima, I., Kouzaki, H., and Shimizu, T. (2018). The epidermal growth factor receptor inhibitor AG1478 inhibits eosinophilic inflammation in upper airways. *Clin. Immunol.* 188, 1–6. doi: 10.1016/j.clim.2017.11.010

Shin, H. S., Bae, M. J., Choi, D. W., and Shon, D. H. (2014). Skullcap (*Scutellaria baicalensis*) extract and its active compound, wogonin, inhibit ovalbumin-induced Th2-mediated response. *Molecules* 19, 2536–2545. doi: 10.3390/molecules19022536

Silva, L. C. F., Lima, H. S., Mendes, T. A. O., Sartoratto, A., Sousa, M. P., de Souza, R. S., et al. (2020). Physicochemical characterization of *Pseudomonas stutzeri* UFV5 and analysis of its transcriptome under heterotrophic nitrification/aerobic denitrification pathway induction condition. *Sci. Rep.* 10:2215. doi: 10.1038/s41598-020-59279-7

Sun, Y. Q., Deng, M. X., He, J., Zeng, Q. X., Wen, W., Wong, D. S., et al. (2012). Human pluripotent stem cell-derived mesenchymal stem cells prevent allergic airway inflammation in mice. *Stem Cells* 30, 2692–2699. doi: 10.1002/stem.1241

Tekin, D., Yan, D., Bademci, G., Feng, Y., Guo, S., Foster, J. II, et al. (2016). A next-generation sequencing gene panel (MiamiOtoGenes) for comprehensive analysis of deafness genes. *Hear. Res.* 333, 179–184. doi: 10.1016/j.heares.2016.01.018

Wang, B., Liu, W., Li, J. J., Chai, S., Xing, D., Yu, H., et al. (2022). A low dose cell therapy system for treating osteoarthritis: In vivo study and in vitro mechanistic investigations. *Bioact. Mater.* 7, 478–490. doi: 10.1016/j.bioactmat.2021.05.029

Wang, L., Wu, W., Zhu, X., Ng, W., Gong, C., Yao, C., et al. (2019). The ancient Chinese decoction Yu-Ping-Feng suppresses orthotopic lewis lung cancer tumor growth through increasing M1 macrophage polarization and CD4(+) T cell cytotoxicity. *Front. Pharmacol.* 10:1333. doi: 10.3389/fphar.2019.01333

Wang, X., Liu, C., Wu, L., and Zhu, S. (2016). Potent ameliorating effect of hypoxia-inducible factor 1α (HIF-1α) antagonist YC-1 on combined allergic rhinitis and asthma syndrome (CARAS) in Rats. *Eur. J. Pharmacol.* 788, 343–350. doi: 10.1016/j.ejphar.2016.07.040

Xue, L., Li, C., Ge, G., Zhang, S., Tian, L., Wang, Y., et al. (2021). Jia-Wei-Yu-Ping-Feng-San attenuates group 2 innate lymphoid cell-mediated airway inflammation in allergic asthma. *Front. Pharmacol.* 12:703724. doi: 10.3389/fphar.2021.703724

Yan, Z., Liu, L., Yuan, J., Jiao, L., Zhou, M., Liu, J., et al. (2021). Yiqi Jiemin decoction alleviates allergic rhinitis in a guinea pig model by suppressing inflammation, restoring Th1/Th2 balance, and improving cellular metabolism. *Aging* 13, 18423–18441. doi: 10.18632/aging.203292

Yang, E. J., Song, G. Y., Lee, J. S., Yun, C. Y., and Kim, I. S. (2009). A novel (S)-(+)-decursin derivative, (S)-(+)-3-(3,4-dihydroxy-phenyl)-acrylic acid 2,2-dimethyl-8-oxo-3,4-dihydro-2H,8H-pyrano[3,2-g]chromen-3-yl-ester, inhibits ovalbumin-induced lung inflammation in a mouse model of asthma. *Biol. Pharm. Bull.* 32, 444–449. doi: 10.1248/bpb.32.444

Yang, R., Liu, H., Bai, C., Wang, Y., Zhang, X., Guo, R., et al. (2020). Chemical composition and pharmacological mechanism of qingfei paidu decoction and ma xing shi gan decoction against coronavirus disease 2019 (COVID-19): In silico and experimental study. *Pharmacol. Res.* 157:104820. doi: 10.1016/j.phrs.2020.104820

Yang, S., Fu, Q., Deng, H., Liu, Z., Zhong, J., Zhu, X., et al. (2021). Mechanisms and molecular targets of the Yu-Ping-Feng powder for allergic rhinitis, based on network pharmacology. *Medicine* 100:e26929. doi: 10.1097/md.0000000000026929

Yao, L., Wang, S., Wei, P., Bao, K., Yuan, W., Wang, X., et al. (2019). Huangqi-Fangfeng protects against allergic airway remodeling through inhibiting epithelial-mesenchymal transition process in mice via regulating epithelial derived TGF-β1. *Phytomedicine* 64:153076. doi: 10.1016/j.phymed.2019.153076

Zeng, Q., Liu, W., Luo, R., and Lu, G. (2019). MicroRNA-181a and microRNA-155 are involved in the regulation of the differentiation and function of regulatory T cells in allergic rhinitis children. *Pediatr. Allergy Immunol.* 30, 434–442. doi: 10.1111/pai.13038

Zeng, Q., Luo, X., Han, M., Liu, W., and Li, H. (2018). Leptin/Osteopontin axis regulated type 2T helper cell response in allergic rhinitis with obesity. *EBioMedicine* 32, 43–49. doi: 10.1016/j.ebiom.2018.05.037

Zeng, Q., Luo, X., Tang, Y., Liu, W., and Luo, R. (2020). Leptin regulated ILC2 Cell through the PI3K/AKT pathway in allergic rhinitis. *Mediators Inflamm.* 2020:4176082. doi: 10.1155/2020/4176082

Zhang, J., Zhou, Y., and Ma, Z. (2021). Multi-target mechanism of *Tripteryguim wilfordii* Hook for treatment of ankylosing spondylitis based on network pharmacology and molecular docking. *Ann. Med.* 53, 1090–1098. doi: 10.1080/07853890.2021.1918345

Zhang, W., Tang, R., Ba, G., Li, M., and Lin, H. (2020). Anti-allergic and anti-inflammatory effects of resveratrol via inhibiting TXNIP-oxidative stress pathway in a mouse model of allergic rhinitis. *World Allergy Organ. J.* 13:100473. doi: 10.1016/j.waojou.2020.100473

Zheng, J., Wang, X., Tao, Y., Wang, Y., Yu, X., Liu, H., et al. (2019). Yu-Ping-Feng-San ameliorates recurrent allergic inflammation of atopic dermatitis by repairing tight junction defects of the epithelial barrier. *Phytomedicine* 54, 214–223. doi: 10.1016/j.phymed.2018.09.190

Zhou, W., Sha, Y., Zeng, J., Zhang, X., Zhang, A., and Ge, X. (2021). Computational systems pharmacology, molecular docking and experiments reveal the protective mechanism of Li-Da-Qian mixture in the treatment of glomerulonephritis. *J. Inflamm. Res.* 14, 6939–6958. doi: 10.2147/jir.S338055

frontiers | Frontiers in Plant Science

TYPE Original Research
PUBLISHED 13 October 2022
DOI 10.3389/fpls.2022.1035163

OPEN ACCESS

EDITED BY
Sezai Ercisli,
Atatürk University, Turkey

REVIEWED BY
Gülçe Ilhan,
Atatürk University, Turkey
Mehmet Ramazan Bozhuyuk,
Iğdır Üniversitesi, Turkey

*CORRESPONDENCE
Amjad Hameed
amjad46pk@yahoo.com

SPECIALTY SECTION
This article was submitted to Plant Metabolism and Chemodiversity, a section of the journal Frontiers in Plant Science

RECEIVED 02 September 2022
ACCEPTED 28 September 2022
PUBLISHED 13 October 2022

CITATION
Raza B, Hameed A and Saleem MY (2022) Fruit nutritional composition, antioxidant and biochemical profiling of diverse tomato *(Solanum lycopersicum L.)* genetic resource. *Front. Plant Sci.* 13:1035163. doi: 10.3389/fpls.2022.1035163

Fruit nutritional composition, antioxidant and biochemical profiling of diverse tomato *(Solanum lycopersicum L.)* genetic resource

Bushra Raza, Amjad Hameed* and Muhammad Yussouf Saleem

Nuclear Institute for Agriculture and Biology College, Pakistan Institute of Engineering and Applied Sciences (NIAB-C, PIEAS), Faisalabad, Pakistan

Tomato is the second most important vegetable crop consumed globally, by the virtue of its antioxidant-rich phytochemicals and bioactive compounds. Identifying genotypes with high antioxidant capacities and nutritionally rich phytochemicals is imperative for improving human health. The present study aimed to analyze 21 antioxidant and nutritional compounds in 93 geographically diverse, high yielding, better quality, stress tolerant tomato genotypes (hybrids, parental lines, inbred lines, and advanced lines). Significant variation ($p < 0.05$) was detected for investigated traits among the tested genotypes. Principal component analysis revealed the hybrids NIAB-Jauhar, Iron-lady F1, NBH-258, Ahmar F1, NIAB-Gohar, the parents H-24, B-25, AVTO1080, Astra and AVTO1003, as well as the lines LBR-17, AVTO1315, AVTO1311 and Lyp-1 revealed superior performance for the traits such as chlorophylls, lycopene, total carotenoids, total antioxidant capacity, total oxidant status, protease, alpha-amylase and total flavonoid content. Whereas the hybrids Surkhail F1, NBH-204, NBH-229, NBH-151, NBH-196, NBH-152, NBH-261, NBH-228, NIAB-Jauhar, NBH-256 and NBH-255, the lines 21354, AVTO1315, Newcherry, LA4097, AVTO1311 and UAF-1 together with the parents Naqeeb, NCEBR-5, M-82 and LBR-10 exhibited significant contribution to the traits such as total soluble sugars, reducing sugars, malondialdehyde, ascorbic acid, esterase, peroxidase and superoxide dismutase. Moreover, the semi-determinate and determinate tomato genotypes together with the categories parent and line with positive factor scores of 3.184, 0.015, 0.325 and 0.186 in PC- I, exhibited better performance for the trait such as total chlorophylls, lycopene, total carotenoids, total oxidant status, protease, alpha-amylase, total antioxidant capacity, esterase and total flavonoid content. Whereas again the semi-determinate and indeterminate tomato genotypes along with the category hybrid with positive factor scores of 2.619, 0.252 and 0.114 in PC- II, exhibited better performance for the traits such as total soluble sugars, reducing sugars, chlorophyll b, malondialdehyde content, ascorbic acid, superoxide dismutase and peroxidase. Hybrid vigor was observed in the hybrids for investigated traits. The aforementioned tomato

genotypes showing outstanding performance in the respective traits can be exploited in the breeding programs to improve nutritional quality of tomato that can further improve human health.

KEYWORDS

tomato, antioxidants, bioactive compounds, nutritional quality, determinate, indeterminate

Introduction

Horticultural plants including tomato *(Solanum lycopersicum L.)* have gained more popularity in recent years. They contain high amount of bioactive compounds such as flavonoids, phenolics, anthocyanins, phenolic acids as well as important nutritive compounds such as sugars, essential oils, carotenoids, vitamins, and minerals. Horticulture plants have a distinct flavor, taste, together with excellent medicinal value and health care functions (Dogan et al., 2014; Grygorieva et al., 2021; Saran et al., 2021). Tomato, which is an essential part of the Mediterranean diet, plays a pivotal role in human nutrition. It has been known as a potential source of bioactive compounds, exhibiting antimicrobial, anti-mutagenic, anti-inflammatory and anti-carcinogenic properties (García-Hernández et al., 2018; Navarro-González et al., 2018; Uçan and Uğur, 2021). Its effects are correlated to antioxidant activity of carotenoids (lycopene and β carotene) and various phenolic compounds (flavonoids and phenolic acids) (Coyago-Cruz et al., 2019). In human nutrition tomato plays a significant role because of its health-promoting benefits (Salehi et al., 2019). Tomato fruit is a reservoir of minerals, proteins, vitamins, essential amino acids, monounsaturated fatty acids and phytosterols (Elbadrawy and Sello, 2016). Lycopene is considered a major compound contributing 80-90% of the total carotenoid content (Nguyen and Schwartz, 1999), while β-carotene contributes about 7-10% to the total carotenoids content in tomato fruit (Frusciante et al., 2007). Lycopene exhibits a maximum singlet oxygen quenching rate and has strong antioxidant properties (Di Mascio et al., 1989). However, β-carotene is associated with provitamin A activity (Sies, 1991). Tomato fruit is a healthy source of bioactive molecules, including ascorbic acid and tocopherol (Beecher, 1998; Raffo et al., 2002). More than two billion people around the world are presently reported to be influenced by "hidden hunger" (lack of minerals and vitamins). Tomatoes along with oranges are a major source of vitamin C in many countries of the world (Proteggente et al., 2002).

The human body needs an appropriate balance between antioxidants and free radicals to maintain homeostasis. Free radicals are naturally produced in the body by various exogenous and endogenous sources, resulting in oxidative damage to the molecules (Khalid and Hameed, 2017). There are several endogenous sources of oxidants including mitochondrial respiratory chain, immune reaction and enzymes such as nitric oxide synthase and xanthine oxidase. Inadequate amount of nutrients intake in daily diet may also result in oxidative stress, damaging cellular defense mechanism. Macromolecules particularly protein, lipids and DNA are the natural target of oxidative stress. Antioxidant properties of tomato fruit are attributed to enzymes that can inhibit the multiplication of free radicals, resulting in a positive impact on a human diet (Borguini and Ferraz Da Silva Torres, 2009; Ulewicz-Magulska and Wesolowski, 2019). In plants enzymatic and non-enzymatic antioxidants overcome oxidative stresses. Enzymatic antioxidants particularly superoxide dismutase, catalase, ascorbate peroxidase and peroxidase have the ability to eliminate hydrogen peroxide and free radicals in the mitochondria as well as the chloroplast (Lee et al., 2007). Non-enzymatic antioxidants include two classes i.e., antioxidant related with the membrane that is lipid-soluble like beta carotene and alpha-tocopherol and the second class include water-soluble reducer such as phenolics, ascorbate and glutathione (Jaleel et al., 2009).

The antioxidant molecules involve in the living organism defense system works at different level. These levels may include prevention, radical scavenging and radical induced damage repair. Based on the line of defense, these antioxidants are grouped into three different levels. The enzymes superoxide dismutase, catalase, glutathione peroxidase, ascorbate peroxidase and peroxidase are considered the first line of defense against reactive oxygen species. These enzymes dismutate superoxide radical, breakdown hydroperoxides and hydrogen peroxides H_2O_2 to harmless molecules (alcohol/water and O_2). They have a preventive role (prevents free radical formation). The second line defense antioxidants such as ascorbic acid and alpha tocopherol are involve in scavenging active radical to control chain propagation reaction by producing lesser damaging molecules in human body. The

antioxidants included in the third line defense group works when free radical damage has already occurred. These enzymes repair DNA, lipids and proteins. They identify the damaged oxidized DNA, protein and lipids and prevent their accumulation to protect toxic effects in the human body. This group includes proteolytic enzymes (proteases) and DNA repair enzyme systems (glycosylases polymerases and nucleases) (Ighodaro and Akinloye, 2018). Whereas, malondialdehyde level in human body is commonly used as a marker of oxidative stress (Gaweł et al., 2004). Moreover, Superoxide dismutase (SODs) serves as an excellent therapeutic and anti-inflammatory agent against diseases caused by reactive oxygen species (Noor et al., 2002; Yasui and Baba, 2006; Younus, 2018).

Nutritional quality and flavor have been adversely affected during the period of domestication and progress of the cultivated tomato, *Solanum lycopersicum* (Aono et al., 2021). The nutritional and physiochemical properties of tomato differ on the bases of its cultivar and prevailing environmental conditions (Anza et al., 2006; Ali et al., 2021). Moreover, many crop species have been modified genetically to enhance productivity, quality and resistance to intrinsic and extrinsic damages (Asensio et al., 2019). As a result, crop varieties differ in their secondary metabolites profile, which is responsible for biological defense mechanism and stage differentiation. They are important aspects to be taken into account in the determination of the role of crops in human nutrition and health (Huang et al., 2005). Moreover, different varieties of tomato are not considered in the present nutritional databases. Although it is most likely that different varieties of tomato might exhibit important differences in their nutritional qualities and bioactive compounds (Anza et al., 2006). Significant efforts are required to explore the nutritional potential of important crops (Vats et al., 2020). Recent years has proved to enhance awareness of the significance of antioxidant in daily intake. As a result, the development of crop varieties with better nutritional value and antioxidant properties has now become the main concern.

The present study aimed to identify nutritional, antioxidant and biochemical composition of diverse tomato germplasm including hybrids, parental lines, inbred lines and advanced lines. The study aided to identify the tomato genotypes with superior nutritional, antioxidant and bioactive properties, that can be further utilized in tomato breeding program(s) aimed to improve these human health promoting traits in tomato fruit.

Materials and methods

A diverse set of tomato germplasm with different genetic makeup including hybrids, parental lines and other lines were used for the estimation of bioactive pigments, antioxidant activities and nutritional parameters (Table 1). Different enzymatic and non-enzymatic antioxidants such as ascorbic acid (AsA), total flavonoids content (TFC), total phenolic content (TPC), ascorbate peroxidase (APX), superoxidase dismutase (SOD), catalase (CAT), peroxidase (POD), together with hydrolytic enzymes like alpha-amylase, protease and esterase activities were estimated. Important bioactive compounds like lycopene and total carotenoids, total chlorophyll, chlorophyll a, chlorophyll b and other biochemical parameter including Malondialdehyde (MDA) content, total soluble sugar (TSS), reducing sugars (RS), non-reducing sugars (NRS), total antioxidant capacity (TAC) and total antioxidant status (TOS) were also evaluated.

For fruit sample collection, field experiment was conducted during year 2018-2019 growing season, at Nuclear Institute for Agriculture and Biology (NIAB), Faisalabad, Pakistan. All standard agronomic practices were followed to keep tomato crop in good condition. Fully matured tomato fruits from each genotype were collected from the field in triplicates (May 2019) and stored at -80°C until further evaluation. The fruit compositional analysis was conducted at Plant Breeding and Genetic Division, Marker Assisted Breeding Lab-1, NIAB, Faisalabad.

Estimation of antioxidant activities

Tomato fruit sample extraction

Fruit sample (pericarp) weight (0.2 g) was taken out in 2 ml (50 mM) potassium phosphate buffer (pH 7.4). The supernatant was separated after centrifugation of 10 min at 14462 x g and 4° C. The extracted supernatant was used for the estimation of enzymatic and non-enzymatic (ascorbic acid, total flavonoid content, total phenolic compounds activities) by using different methods (Khalid and Hameed, 2017). A triplicated data of each genotype was collected for further investigations.

Pigment estimation

The levels of pigments including lycopene, carotenoids, total chlorophyll, chlorophyll a and chlorophyll b, were estimated by a previously described method (Lichtenthaler and Wellburn, 1983). Tomato fruit sample weight 0.2 g was extracted in 80% acetone at -4°C centrifuged for 5 min at 10,000 × g using Sigma (Micro 1-14) centrifuge. The absorbance of chlorophyll a 663 nm, chlorophyll b 645 nm, lycopene, total carotenoids (480 nm) and total chlorophyll was measured at 663, 645, 505, 453 and 470 nm wavelength respectively using a spectrophotometer (SPH-003, HITACHI U-2800).

TABLE 1 Tomato genotypes used in the study.

Sr.#	Genotypes/ accession #	Type	Origin/source	Other description/pedigree		Traits of importance
1.	NBH-149	D	NIAB, Pakistan	Hybrid	NCEBR-5 x AVTO1219	–
2.	NBH-150	D	NIAB, Pakistan	Hybrid	NCEBR-5 x AVTO1005	–
3.	NBH-151	D	NIAB, Pakistan	Hybrid	Naqeeb x AVTO1219	–
4.	NBH-152	D	NIAB, Pakistan	Hybrid	Naqeeb x AVTO1005	–
5.	NBH-154	D	NIAB, Pakistan	Hybrid	B-L-35 x AVTO1005	–
6.	NBH-182	D	NIAB, Pakistan	Hybrid	(Roma x LBR-7) x Flora-Dade	–
7.	NBH-188	D	NIAB, Pakistan	Hybrid	(Roma x LBR-10) x Flora-Dade	–
8.	NBH-190	D	NIAB, Pakistan	Hybrid	(Roma x LBR-17) x Flora-Dade	–
9.	NBH-196	D	NIAB, Pakistan	Hybrid	Canda-25 × AVTO1219	–
10.	NBH-200	D	NIAB, Pakistan	Hybrid	NCEBR-6 x AVTO1219	–
11.	NBH-204	D	NIAB, Pakistan	Hybrid	Galia x AVTO1219	–
12.	NBH-227	D	NIAB, Pakistan	Hybrid	B25 x AVTO1080	–
13.	NBH-228	D	NIAB, Pakistan	Hybrid	NCEBR-5 x AVTO1080	–
14.	NBH-229	D	NIAB, Pakistan	Hybrid	Naqeeb x AVTO1080	–
15.	NBH-235	D	NIAB, Pakistan	Hybrid	NCEBR-5 x B-31	–
16.	NBH-255	ID	NIAB, Pakistan	Hybrid	PRN x AVTO1003	–
17.	NBH-256	ID	NIAB, Pakistan	Hybrid	PRN x AVTO1005	–
18.	NBH-257	ID	NIAB, Pakistan	Hybrid	PRN x AVTO1080	–
19.	NBH-258	D	NIAB, Pakistan	Hybrid	B23 x AVTO1003	–
20.	NBH-259	D	NIAB, Pakistan	Hybrid	B23 x AVTO1005	–
21.	NBH-260	D	NIAB, Pakistan	Hybrid	B23 x AVTO1005	–
22.	NBH-261	D	NIAB, Pakistan	Hybrid	B24 x AVTO1003	–
23.	NBH-263	D	NIAB, Pakistan	Hybrid	B24 x AVTO1080	–
24.	NBH-265	D	NIAB, Pakistan	Hybrid	NCEBR-5 x AVTO1003	–
25.	NBH-266	D	NIAB, Pakistan	Hybrid	Galia x AVTO1003	–
26.	NBH-267	D	NIAB, Pakistan	Hybrid	Galia x AVTO1005	–
27.	NBH-268	D	NIAB, Pakistan	Hybrid	Riogrande x AVTO1003	–
28.	NBH-281	D	NIAB, Pakistan	Hybrid	Naqeeb x AVTO 1003	–
29.	NBH-282	D	NIAB, Pakistan	Hybrid	Naqeeb x H 24	–
30.	NBH-5	D	NIAB, Pakistan	Hybrid	B25 x NCEBR-6	–
31.	NBH-78	D	NIAB, Pakistan	Hybrid	Astra x Naqeeb	–
32.	NBH-95	D	NIAB, Pakistan	Hybrid	M-82 x Naqeeb	–
33.	Sundar F1	ID	ARRI, Pakistan	Hybrid	–	Tolerance against disease and temperature, tunnel crop, approved variety
34.	NIAB-Gohar	D	NIAB, Pakistan	Hybrid	(LBR-7 × Nagina)	High fruit firmness and yield, moderate disease tolerance, approved variety
35.	NIAB-Jauhar	D	NIAB, Pakistan	Hybrid	(Roma × LBR-10)	High fruit firmness and yield, moderate disease tolerance, approved variety
36.	Sahel F1	ID	Syngenta	Hybrid	–	Disease resistance, plum type
37.	T-1359 F1	D	Syngenta	Hybrid	–	Highly susceptible to blight
38.	Surkhail F1	ID	ARRI, Pakistan	Hybrid	–	High yield, fruit quality
39.	Iron-Lady F1	D	–	Hybrid	–	Disease resistance and fruit quality
40.	Ahmar F1	D	ARRI, Pakistan	Hybrid	–	Tolerance against disease and temperature, tunnel crop, approved variety
Parent genotypes						
Sr.#	Genotypes/Accession #	Type	Origin/Source	Other description/pedigree		Traits of importance
41.	AVTO1219 /CLN3241H-27	SD	AVRDC, Taiwan	Inbred line	Pedigree: CLN3241F1-34-28-2-20-5-28-27	Fair heat tolerance, disease resistance: late blight, tomato yellow leaf curl virus

(Continued)

TABLE 1 Continued

Sr.#	Genotypes/ accession #	Type	Origin/source	Other description/pedigree		Traits of importance
42.	AVTO1003 /CLN3125L	D	AVRDC, Taiwan	Inbred line	-	Fair heat tolerance, resistance to diseases: tomato mosaic virus, tomato yellow leaf curl virus
43.	AVTO1005 /CLN3125P	D	AVRDC, Taiwan	Inbred line	Pedigree: CLN3125F2-21-4-13-1-0	Tomato yellow leaf curl resistance (TYLCD), Ty-1/Ty-3 and Ty-2
44.	AVTO1080/ CLN3022E (ck)	D	AVRDC, Taiwan	Inbred line	Pedigree: CLN3022F2-154-4-2-30-0	Tomato mosaic virus resistance (TMV), tomato yellow leaf curl virus susceptible
45.	B-31/Berika	D	Bulgaria			High yield
46.	B-23/Jaklin	D	Bulgaria			High yield
47.	B-24/Unkown line	D	Bulgaria			High yield
48.	B-25/Unknown line	D	Bulgaria			High yield
49.	Canada-25	D	EFUP			Fruit firmness, fruit quality and fruit size
50.	Flora-Dade/LA3242	D	University of Florida (1976)	OPV	*Solanum lycopersicum*	Heat tolerance, high yield, susceptible to early blight
51.	Galia	D	Gujranwala/ Pakistan	OPV	*Solanum lycopersicum*	High yield, fruit quality
52.	H-24	D	ARRI, Pakistan	OPV	*Solanum lycopersicum*	High yield, fruit quality
53.	LBR-10/LB4	D	AVRDC, Taiwan		*Solanum lycopersicum*	Moderate early blight resistance,
54.	LBR-7/LB2	D	AVRDC, Taiwan		*Solanum lycopersicum*	Late/Early blight resistance, fruit size, fruit quality
55.	NCEBR-5 /LA3845	D	North Carolina, USA	Inbred line	*Solanum lycopersicum* Barksdale and Stoner (1977)	Late/Early blight resistance
56.	NCEBR-6 /LA3846	D	USA	Inbred line	*Solanum lycopersicum* Barksdale and Stoner (1978)	Early blight resistance
57.	M-82 /LA3475	D	TRGC, UC	Inbred line	*Solanum lycopersicum*	Cultivated tomato, fruit quality
58.	Nagina	D	Faisalabad, Pakistan	OPV	*Solanum lycopersicum*	High yield, fruit quality, disease resistance
59.	Naqeeb	D	Faisalabad, Pakistan	OPV	*Solanum lycopersicum*	High yield, good fruit size, excellent shelf life tolerant salinity and nickel stress
60.	PRN-28-10	ID	NIAB, Pakistan		*Solanum lycopersicum*	Fruit firmness
61.	Roma	D	USA, Mexico	OPV	*Solanum lycopersicum*	Plum shaped tomato, fruit quality and high yield
62.	Riogrande	D	USA/ARRI, Faisalabad	OPV	*Solanum lycopersicum*	Disease resistance: Fusarium 1 & 2, Verticillium wilt
63.	LA4157 /TA2893	D	TGRC, UC	BRIL	Solanum Lycopersicum × *Solanum Pimpinellifolium*	moderate resistance to early blight, fruit quality
64.	Astra	D	EFUP	OPV		
Lines						
Sr.#	Genotypes/ Accession #	Type	Origin/Source	Other description/pedigree		Traits of importance
65.	17253	ID	ARRI, Pakistan	OPV		High yield, cherry tomato, disease resistance
66.	21354	D	Mexico			Fruit quality
67.	21396	D	Guatemala		*Solanum lycopersicum*	Disease resistance, high yield
68.	V-48 /PAK0010576	D	PGR N. Korea			
69.	AVTO 1009 /CLN3078G	D	AVRDC	Inbred line	Pedigree: CLN3078F1-12-6-25-8-4-0	Moderate heat tolerance, Disease resistance: Bacterial wilt, tomato mosaic virus (Tm22)
70.	AVTO 1010 /CLN3070J	D	AVRDC, Taiwan	Inbred line	—	
71.	AVTO 1311 /CLN3241R	SD	AVRDC, Taiwan	Inbred line	—	Moderate heat susceptible, Disease resistance: Late blight, bacterial wilt, fusarium wilt (R1 R2)
72.	AVTO 1315 /CLN3241Q	SD	AVRDC, Taiwan	Inbred line	Pedigree: CLN3241F1-34-28-2-20-10-17-27-25	Moderate heat susceptible, Disease resistance

(Continued)

TABLE 1 Continued

Sr.#	Genotypes/ accession #	Type	Origin/source	Other description/pedigree		Traits of importance
73.	CLN2768A/LA1035	D	Ecuador/AVRDC	Wild type	*Solanum cheesmaniae*	Moderate resistance to late blight
74.	LA4097 /I.L. 12-1	D	Israel/TGRC, UC	IL	*Solanum Lycopersicum* × *Solanum Pennellie*	Drought tolerance, fruit quality
75.	LA4141 /TA2876	D	TGRC, UC	BRIL	*Solanum Lycopersicum* × *Solanum Pimpinellifolium*	Fruit quality, biotic and abiotic stress tolerance
76.	B-L-35/ LA4347	D	TRGC, UC	Inbred line	*Solanum lycopersicum*	Disease resistance, fruit quality
77.	LBR-17	D	AVRDC, Taiwan		*Solanum lycopersicum*	
78.	Lukullus/ LA0534	ID	Germany/TGRC	OPV	*Solanum lycopersicum*	Rabbit Resistant (roots and leaves are poisonous)
79.	Money maker/ LA2706	ID	Bristol/ARRI, Pakistan	OPV	*Solanum lycopersicum*	Inexpensive compared to hybrid tomato, Blight prone, cold sensitive
80.	New cherry	ID	ARRI, Pakistan	Wild type		High yield, cherry type
81.	NI-Cherry	ID	ARRI, Pakistan	Wild type		High yield, cherry type
82.	V-83/011856	D				
83.	Pakit	ID	ARRI, Pakistan			Resistance to tomato fruit borer, high number of fruits per cluster
84.	Vendor/ LA3122	ID	TGRC, UC	OPV	*Solanum lycopersicum*	Tomato mosaic virus resistance
85.	West Virginia -63	ID	TGRC, UC	OPV	*Solanum lycopersicum*	Mild sweet flavor, late blight resistance (race T-0 and some resistance to T-1)
86.	UAF-1	ID	ARRI, Pakistan		Wild type	High yield, Cherry type
87.	LYP-1	D	ARRI, Pakistan		—	Fruit quality, high yield
88.	Nadir	D	ARRI, Pakistan	OPV	*Solanum lycopersicum*	High yield, good fruit size, excellent shelf life, sensitive to salinity and Nickel stress
Advance lines						
89.	CKD-6-15 F6	D	NIAB, Pakistan	AD		High fruit firmness
90.	CKD-8-15 F6	D	NIAB, Pakistan	AD		High fruit firmness
91.	MIL-10 (F4)	D	NIAB, Pakistan	AD	Riogrande x NCEBR-6	High fruit firmness
92.	MIL-13 (F4)	D	NIAB, Pakistan	AD	Naqeeb x NCEBR-6	High yielding line, high fruit firmness
93.	T-1359-6-15F6	D	NIAB, Pakistan	AD		High fruit firmness

NIAB, Nuclear Institute for Agriculture and Biology, Pakistan; AARI, Ayub Agricultural Research Institute, Faisalabad, Pakistan; NARC, National Agricultural Research Council, Pakistan; PARC, Pakistan Agricultural Research Council; TGRC, Tomato Genetic Resources Centre, United States of America; AVRDC, Asian Vegetable Research and Development Centre, Taiwan; EFUP, Establishment of facilitation unit for participatory vegetable seed and nursery production programme, Pakistan; PGR N. Korea, Plant Genetic Resource Center, North Korea; D, determinate; ID, Indeterminate; SD, Semi-determinate; OPV, Open Pollinated Variety; AD, Advance line; BRIL, Backcross Recombinant inbred; IL, Introgression Lines.

Non-enzymatic antioxidants

Ascorbic acid

A previously defined 2,6- dichloroindophenol (DCIP) method (Hameed et al., 2005) was followed to measure reduction in ascorbic acid (AsA) concentration. The reaction mixture contained 110 µl of DCIP (0.2 mg DCIP per ml of distilled water), 110 µl of 0.1% meta phosphoric acid, 100 µl sample extract and 900 µl distilled water. The absorbance of the reaction mixture was then measured at 520 nm using a spectrophotometer. Briefly, each molecule of ascorbic acid converts a molecule of DICP into $DCIPH_2$ molecule. This conversion can be determined as a decline in absorbance at 520 nm by a spectrophotometer. A series of known ascorbic acid concentrations were used to prepare a standard curve. A simple regression equation was utilized to measure ascorbate concentrations in unspecified samples.

Total flavonoid content

An aluminum chloride colorimetric method (Lin and Tang, 2007) was exploited to determine total flavonoid content (TFC). A reaction mixture containing tomato fruit sample (400 µl + 1.6 ml distilled water), 1 M potassium acetate (0.1 ml), 10%

aluminum chloride hexahydrate (0.1 ml) and deionized water (2.8 ml) was prepared. The reaction mixture was then subjected to incubation at room temperature for 40-minutes, followed by measuring absorbance at 415 nm using a spectrophotometer. The standard curve was plotted using various known concentrations (0.005 to 0.1 mg/ml) of Rutin. The TFC was expressed as microgram per ml of the sample.

Total phenolic contents

Total phenolic content (TPC) for each tomato genotype was determined by micro colorimetric technique (Ainsworth and Gillespie, 2007). Briefly, Folin-Ciocalteu (F-C) reagent was used for determining TPC in tomato fruit extract. For the purpose, 0.5 g of fruit sample was homogenized in 500 µl 95% methanol (ice-cold) using an ice-cold mortar and pestle. The samples were then incubated at room temperature in dark for 48 hours. When the incubation was completed, sample were centrifuged at 14,462 × g for 5 minutes at room temperature. The supernatant was removed and used for the measurement of TPC. The 100 µl of the supernatant was added with 100 ml of 10% (v/v) F-C reagent, vortex thoroughly, finally 800 µl of 700 mM Na2CO3 was added. Samples were then subjected to incubation at room temperature for an hour. Blank corrected absorbance of samples was measured at 765 nm. A standard curve was established using various known concentrations of gallic acid concentrations (300, 400, 500, 600, 700, and 800 mM/100 mL). The phenolic contents (gallic acid equivalents) of tomato samples were estimated using a linear regression equation.

Enzymatic antioxidants

Ascorbate peroxidase activity

Ascorbate peroxidase (APX) activity was estimated by homogenizing tomato fruit sample in 50 mM potassium phosphate buffer (pH 7), by exploiting previously established method (Dixit et al., 2001). By adding 200 mM potassium phosphate (pH 7.0), 0.5 M ethylenediamine tetra acetic acid (EDTA) and 10 mM ascorbic acid, an assay buffer was prepared. The buffer was then combined with 1 ml of H_2O_2 and 50 µl of supernatant. For estimation of APX activity, absorbance was recorded at 290 nm with 30 seconds interval. The decrease in absorbance indicated an ascorbic acid oxidation rate (Chen and Asada, 1989).

Superoxide dismutase activity

Superoxide dismutase (SOD) activity was estimated by homogenizing tomato fruit samples in a medium consisting of 50 mM potassium phosphate buffer (pH 7.0), 0.1 mM EDTA, and 1 mM dithiothreitol (DTT) following previously reported method (Dixit et al., 2001). The SOD activity was determined by its ability to inhibit the photochemical reduction of nitro blue tetrazolium (NBT) following a previously described protocol (Giannopolitis and Ries, 1977). One unit of SOD activity was defined as the amount of enzyme that caused 50% inhibition of photochemical reduction of NBT.

Catalase activity

Catalase (CAT) activity was determined by homogenizing fruit samples in a medium containing 50 mM potassium phosphate buffer (pH 7.0) and 1 mM dithiothreitol (DTT). CAT activity was determined by a previously defined method (Beers and Sizer, 1952). Estimation of CAT activity was carried out by preparing an assay buffer containing 50 mM phosphate buffer (pH 7.0), 59 mM H_2O_2 and 0.1 ml enzyme extract. At a wavelength of 240 nm the decline in absorbance of the reaction mixture was recorded after every 20 seconds for one min. One unit of CAT activity was defined as an absorbance change of 0.01 min^{-1}. Enzyme activity was expressed on the bases of fruit weight.

Peroxidase activity

Peroxidase (POD) activity was determined by homogenizing the fruit sample in a medium containing 50 mM potassium phosphate buffer (pH 7.0), 0.1 M EDTA, and 1 mM DTT. A previously described method (Chance and Maehly, 1957) with some modifications was used to measure POD activity. The assay solution for POD activity determination contained distilled water (535 µl), 250 µl of 200 mM phosphate buffer (pH 7.0), 100 µl of 200 mM guaiacol, 100 µl of 400 mM H_2O_2. Enzyme extract (15 µl) was added to initiate the reaction. After every 20 second the change in the absorbance was recorded at 470 nm for one min. An absorbance change of 0.01 min^{-1} was defined as one unit of POD activity. Enzyme activity was expressed on fruit weight bases.

Hydrolytic enzymes

Alpha-amylase activity

For the determination of fruit alpha-amylase activity, a previously defined method (Varavinit et al., 2002). Two reagents 3,5-dinitrosalicyclic acid (DNS) and 1% starch solution were used for the estimation of alpha-amylase activity. DNS reagent used for the assay was prepared by adding 96 mM DNS (1 g DNS in 50 ml of distilled water),

30 g of sodium potassium tartrate, 20 ml of 2 N NaOH and the final volume was made to 100 ml using distilled water. After mixing 0.2 ml sample + 1.8 ml distilled water and 1 ml of 1% starch solution, the reaction mixture was incubated for 3 min, then 1 ml of DNS reagent was added in each tube and placed in water bath for 15 min at 100°C. The boiled samples were then cooled at room temperature and finally 9 ml of distilled water was added. Absorption was observed at 540 nm using spectrophotometer.

Protease activity

Fruit samples were extracted in 50 mM potassium phosphate buffer (pH 7.8) for protease activity estimation using Casein digestion assay (Drapeau, 1976). A reaction mixture containing 2 ml of 1% casein solution, 100 µl of enzyme extract and 2 ml of 10% TCA was prepared. The prepared reaction mixture was then filtered with a filter paper and absorbance was measured at 280 nm using spectrophotometer. For preparing 1% Casein solution, 1 g of casein, 50 ml of 0.01 N NaOH, 5 ml of 1 M Tris-base and 40 ml of distilled water was used, whereas the pH of the solution was maintained at 7.8 using phosphoric acid and final volume was made up to 100 ml. In this method, one unit is the quantity of an enzyme which delivers acid-soluble fragments equivalent to 0.001 A_{280} per min at 37°C with pH 7.8. Enzyme activity was expressed on a fruit weight basis.

Esterase activity

A previously described method (Van Asperen, 1962) was exploited to determine α-esterases and β-esterases activity by using α-naphthyl acetate and β-naphthyl acetate substrates, respectively. The reaction mixture was composed of substrate solution (0.04 M phosphate buffer (pH 7), 1% acetone, and 30 mM α or β-naphthyl acetate) along with the enzyme extract. The mixture was incubated in dark for exactly 15 min at 27°C. A staining solution (1% Fast blue BB and 5% SDS combined in a ratio of 2:5) was mixed with the above-mentioned reaction mixture and incubated for another 20 min in dark at 27°C. The quantity of α- and β-naphthol produced was estimated by measuring the absorbance at 590 nm. Enzyme activity was α or β naphthol produced in µM min^{-1} per g fruit weight, using a standard curve.

Other biochemical assays

Total soluble sugars

The phenol–sulphuric acid reagent method (Dubois et al., 1951) was exploited for the estimation of total sugar content. The reaction mixture contained sample extract, reagent 1 (5% phenol solution) and reagent 2 (96% sulphuric acid). After adding 250 µl of reagent 1, 1.25 ml of reagent 2 and 500 µl of sample extract, the reaction mixture was placed in a water bath for 20 minutes at 30°C, later absorbance of the reaction mixture was measured at 490 nm using a spectrophotometer.

Reducing sugars

For the determination of fruit reducing sugars content dinitrosalicylic acid (DNS) method (Miller 1959) was used. The assay mixture was composed of 200 µl of sample extract, 1 ml of DNS reagent and 1.8 ml of distilled water. After adding the above-mentioned reagents with sample extract, the reaction mixture was heated in water bath for 15 minutes at 100°C, then the boiled reaction mixture was allowed to cool at room temperature and 9 ml of distilled water was added in each test tube. The absorbance of the reaction mixture was finally measured at 540 nm by using a spectrophotometer. DNS reagent used for the assay was prepared by adding 96 mM DNS (1 g DNS in 50 ml of distilled water), 30 g of sodium potassium tartrate, 20 ml of 2 N NaOH and the final volume was made to 100 ml using distilled water. Non-reducing sugars were estimated by the difference in total soluble sugars and reducing sugars.

Malondialdehyde content

Malondialdehyde (MDA), a byproduct of lipid peroxidation was estimated by the thiobarbituric acid (TBA) reaction method (Heath and Packer, 1968), with minor changes (Dhindsa et al., 1981; Zhang and Kirkham, 1994). A fruit sample weight of 0.25 g was homogenized in 5ml TCA (0.1%). The homogenate was then centrifuged for about 5 min at 10,000 × g. In 1 ml of aliquot of supernatant, 4 ml TCA (20%) containing 0.5% TBA were added. The mixture was then heated for 30 min at 95°C and then immediately cooled in an ice bath. A centrifugation of 10,000 × g for 10 min was done. The absorbance of the supernatant at 532nm was measured and the value for non-specific absorption at 600nm was subtracted. MDA content was measured by using extinction coefficient of 155 mM^{-1} cm^{-1}.

Total oxidant status

For the estimation of total oxidant status (TOS) a previously used method (Erel, 2005) based upon the oxidation of ferrous ion to ferric ion by oxidants present in the sample in an acidic medium and the measurement of ferric ion by xylenol orange (Harma et al., 2005) was used. The assay mixture contained reagent one (R1), reagent two (R2), along with the sample

extract. The reagent R1 was the stock xylene orange solution containing 75 µl xylenol orange dye (0.38 g xylenol orange in 500 µl of 25 mM H_2SO_4), 0.409 g of NaCl, 500 µl of glycerol and final volume was made up to 50 ml with 25 mM H_2SO_4. The reagent 2 (R2) contained 0.0317 g of o-dianisidine and 0.0196 g of ferrous ammonium sulfate in 10 ml of 25 mM H_2SO_4. After adding 900 µl of reagent 1, 140 µl of sample and 44 µl of reagent 2 and the reaction mixture was incubated for 5 minutes. Then the absorbance of the reaction mixture was measured at 560 nm by using a spectrophotometer. A standard curve was formed using known concentrations of H_2O_2. The results were explained in µ M H_2O_2 equivalent per L.

Total antioxidant capacity

Total antioxidant capacity was estimated by a previously reported method (Erel, 2004). The 2,2-Azinobis-3-ethylbenzthiazolin-6-sulfonic acid (ABTS) assay exhibits a decline of 2,2-azino-bis (3 ethylbenzothiazoline-6- sulfonate) radical cation ABTS+ (blue green in colour) into the actual ABTS (colorless compound), representing the presence of antioxidant in the tested sample. The antioxidant content present in the sample decolorizes the ABTS+ radical cation. The reaction mixture for TAC estimation contained sample extract, reagent R1 and reagent R2. Reagent 1 contained 94 ml of 0.4 M sodium acetate and 6 ml of 0.4 M glacial acetic acid, the pH of reagent 1 was maintained at 5.8. The reagent 2 contained 0.75 ml of 30 mM sodium acetate and 9.25 ml of glacial acetic acid. Then, 3.52 µl was taken out from R2 and 3.52 µl of 35% of hydrogen peroxide solution was added in R2. Finally, 10 mM 2,2-Azinobis-3-ethylbenzthiazolin-6-sulfonic acid (ABTS) (0.549 g in 10 ml H_2O_2) was added in in above-mentioned solution. Assay was performed by adding 1ml of reagent 1, 25 µl sample extract and 100 µl reagent 2 incubated for 5 minutes and absorbance was measured at 660 nm using spectrophotometer. Ascorbic acid was used as a standard to develop standard curves. The range of concentrations for ascorbic acid was between 0.075 and 2.0 mM/L. The amount of antioxidant present in the sample was expressed as µM of AsA equivalent to 1 g.

Statistical analysis

For Statistical analysis the computer software Microsoft Excel along with XLSTAT (Version 2021.3.01), (http://www.xlstat.com) was used. Descriptive statistics were applied to organize the data. The data was expressed in mean ± SD. Analysis of variance (ANOVA) was performed for the data using three replications. The significance level of the data was tested by analysis of variance and Tukey (HSD) test at $P < 0.05$ using software XLSTAT. Principal component analysis and Pearson correlation test was performed.

Results

Tomato genotypes including hybrids, parents and other lines were divided into three categories low, medium and high based upon the variability in their mean values for different tested parameters (Table 2). Detailed description of the results is as follows.

Pigment analysis

Lycopene content

Among forty hybrid tomato genotypes tested for their fruit lycopene content, fourteen exhibited low mean values ranging from 1.74 to 2.45 mg/100 g FW (Figure 1). For determinate tomato genotype, a local hybrid tomato NBH-282 showed the lowest mean value (1.74 mg/100 g FW) for fruit lycopene content. Twenty-one hybrids exhibited intermediate values for fruit lycopene content ranging from 2.53 to 4.17 mg/100 g FW. Five hybrids were grouped in the high category for fruit lycopene content with the mean values ranging from 5.58 to 7.96 mg/100 g FW. The highest value for determinate tomato genotype was observed in a local hybrid variety NIAB-Gohar (7.96 mg/100 g FW).

Out of twenty-four tomato parent genotypes tested for fruit lycopene content, seven were grouped into low category with their mean values ranging from 1.90 to 2.37 mg/100 g FW. The lowest value for determinate tomato parent genotype was observed in NCEBR-5 (1.90 mg/100 g FW). Fifteen parents showed intermediate fruit lycopene mean values ranging from 2.56 to 4.82 mg/100 g FW. Only two parent tomato genotypes were grouped into the high category for fruit lycopene content, with the highest value observed in a determinate parent line H-24 (7.23 mg/100 g FW).

Total twenty-four tomato lines tested for fruit lycopene content, eight were categorized into low category with their mean values ranging from 1.93 to 2.49 mg/100 g FW. The lowest value was detected in a determinate tomato line V-83 (1.93 mg/100 g FW). Fifteen tomato lines were placed in the medium category for fruit lycopene content ranging from 2.53 to 4.95 (mg/100 g FW). The highest value for fruit lycopene content was observed in determinate tomato line, LBR-17 (7.02 mg/100 g FW).

Total five tomato advance lines tested for fruit lycopene content, two were grouped into a low category with the lowest value detected in an advance line, MIL-13-F4 (2.29 mg/100 g

10.3389/fpls.2022.1035163

TABLE 2 Scale for categorization of tomato genotypes having low, medium, and high values of different biochemical parameters.

Parameters		Range of values		Number of genotypes per category			
				Hybrids (Total 40)	Parents (Total 24)	Lines (Total 24)	Advance lines (Total 5)
1. Pigments	a. Lycopene	Low	1.5-2.5 (mg/100g FW)	14	7	8	2
		Medium	2.5-5.5 (mg/100g FW)	21	15	15	3
		High	5.5-7.9 (mg/100g FW)	5	2	1	–
	b. Total carotenoids	Low	2-5 (mg/100g FW)	12	3	3	1
		Medium	5-10 (mg/100g FW)	23	18	19	4
		High	10-18 (mg/100g FW)	5	3	2	–
	c. Total chlorophyll	Low	60-100 (µg/100g FW)	26	14	16	2
		Medium	100-160 (µg/100g FW)	11	8	7	3
		High	160-215 (µg/100g FW)	3	2	1	–
	d. Chlorophyll a	Low	24-40 (µg/100g FW)	15	8	4	–
		Medium	40-70 (µg/100g FW)	20	10	15	2
		High	70-100 (µg/100g FW)	5	6	5	3
	e. Chlorophyll b	Low	10-40 (µg/100g FW)	14	5	8	2
		Medium	40-70 (µg/100g FW)	20	15	14	3
		High	70-120 (µg/100g FW)	6	4	2	–
2. Non enzymatic antioxidants	a. Ascorbic acid	Low	100-350 (µg/g FW)	7	5	6	2
		Medium	350-380 (µg/g FW)	27	17	15	1
		High	380-450 (µg/g FW)	6	2	3	2
	b. Total flavonoid content	Low	1,000-1,500 (µg/100g FW)	27	17	14	3
		Medium	1,500-3,000 (µg/100g FW)	7	5	5	2
		High	3000-5,000 (µg/100g FW)	6	2	5	–
	c. Total phenolic compounds	Low	300-1000 (µM/g FW)	4	4	–	–
		Medium	1000-10,000 (µM/g FW)	35	19	19	5
		High	10,000-14,650 (µM/g FW)	1	1	5	–
3. Enzymatic antioxidants	a. Ascorbate peroxidase	Low	200-600 (U/g FW)	17	7	12	2
		Medium	600-1,000 (U/g FW)	15	14	10	3
		High	1000-2,000 (U/g FW)	8	3	2	–
	b. Superoxide dismutase	Low	20-150 (U/g FW)	20	12	10	3
		Medium	150-250 (U/g FW)	18	11	11	2
		High	250-350 (U/g FW)	2	1	3	–
	c. Catalase	Low	100-300 (U/g FW)	2	2	–	–
		Medium	300-700 (U/g FW)	29	16	15	4
		High	700-1,200 (U/g FW)	9	6	9	1
	d. Peroxidase	Low	150-1,000 (U/g FW)	24	13	15	4

(Continued)

TABLE 2 Continued

Parameters		Range of values		Number of genotypes per category			
				Hybrids (Total 40)	Parents (Total 24)	Lines (Total 24)	Advance lines (Total 5)
		Medium	1,000-5,000 (U/g FW)	14	7	8	1
		High	5,000-8,000 (U/g FW)	2	4	1	–
4. Hydrolytic enzymes	a. Alpha-amylase	Low	16-100 (mg/g FW)	9	6	6	–
		Medium	100-200 (mg/g FW)	26	14	12	5
		High	200-245 (mg/g FW)	5	4	6	–
	b. Protease	Low	5,000-6,500 (U/g FW)	22	12	11	1
		Medium	6,500-7,500 (U/g FW)	16	10	12	4
		High	7,500-8,500 (U/g FW)	2	2	1	–
	c. Esterase	Low	10-25 (μM/min/g FW)	17	8	7	1
		Medium	25-35 (μM/min/g FW)	14	13	11	2
		High	35-50 (μM/min/g FW)	9	3	6	2
5. Sugars	a. Total soluble sugars	Low	20-35 (mg/g FW)	5	4	7	–
		Medium	35-60 (mg/g FW)	26	16	10	4
		High	60-80 (mg/g FW)	9	4	7	1
	b. Reducing sugars	Low	21-40 (mg/g FW)	27	17	14	3
		Medium	40-60 (mg/g FW)	7	5	5	2
		High	60-71 (mg/g FW)	6	2	5	–
	c. Non-reducing sugar	Low	1-5 (mg/g FW)	12	8	6	
		Medium	5-14.4 (mg/g FW)	18	11	15	3
		High	14.4-20 (mg/g FW)	10	5	3	2
6. Other biochemical parameter	a. Malondialdehyde content	Low	20-80 (μM/g FW)	24	12	14	2
		Medium	80-150 (μM/g FW)	10	11	5	3
		High	150-270 (μM/g FW)	6	1	5	–
	b. Total oxidant status	Low	200-3,000 (μM/g FW)	19	9	7	4
		Medium	3,000-10,000 (μM/g FW)	11	8	8	–
		High	10,000-17,000 (μM/g FW)	10	7	9	1
	c. Total antioxidant capacity	Low	1-7 (μM/g FW)	14	–	4	2
		Medium	7-11 (μM/g FW)	23	17	17	3
		High	11-12 (μM/g FW)	3	7	3	–

FW). Three advance lines exhibited medium values for fruit lycopene content ranging from 2.85 to 3.57 (mg/100 g FW).

Total sixteen indeterminate tomato genotypes were tested for fruit lycopene content, with the lowest mean value observed in a local hybrid Sundar F1 (2.13 mg/100 g FW), and the highest mean value observed in an indeterminate variety Moneymaker (4.43 mg/100 g FW). Two semi-determinate tomato lines under study, exhibited intermediate values for fruit lycopene content. Semi-determinate line, AVTO1311 showed a mean value of 3.92 mg/100 g FW, and semi-determinate line AVTO1315 showed a value of 4.95 mg/100 g FW respectively.

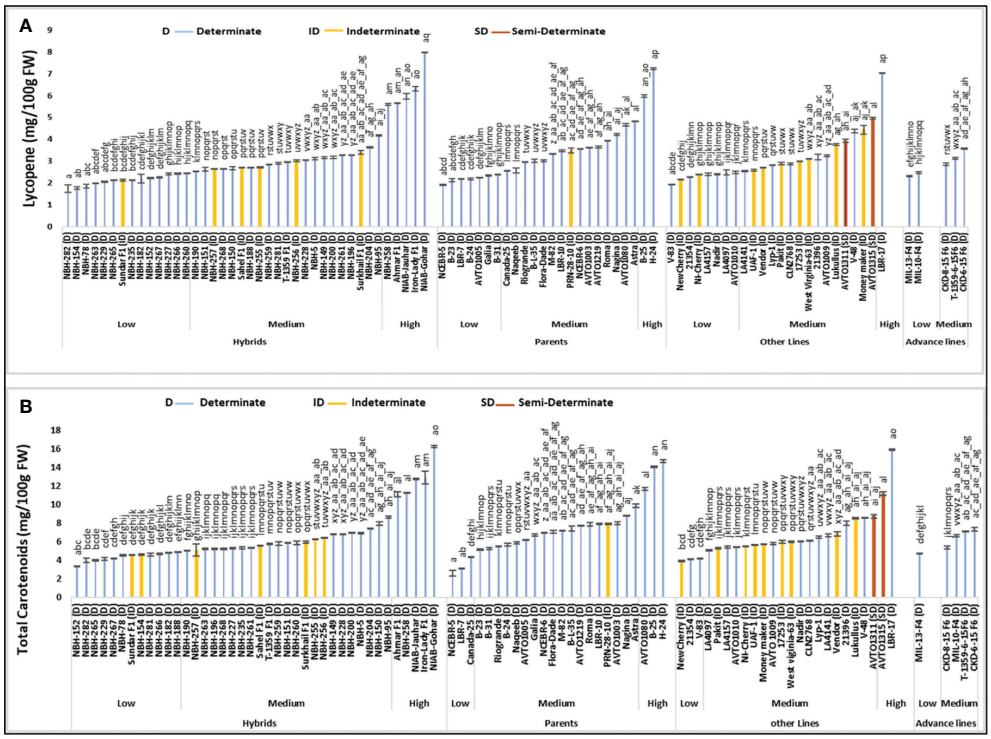

FIGURE 1
Comparison of fruit **(A)** lycopene and **(B)** total carotenoids content in different tomato genotypes (mean value ± SD). Mean value with varying alphabet differs significantly ($p < 0.05$, Tukey's HSD).

Total carotenoids

The data of mean values for tomato fruit total carotenoid content showed that twelve hybrids out of a total twenty-four fall under the low category with a mean value ranging from 3.35 to 4.86 mg/100 g FW (Figure 1). The lowest mean value for determinate tomato type was observed in a local hybrid, NBH-152 (3.35 mg/100 g FW). In the intermediate category, twenty-three tomato hybrids were grouped with the total fruit carotenoids content ranging from 5.02 to 8.62 mg/100 g FW. Five tomato hybrids were placed in the high category for fruit total carotenoid content with their mean values ranging from 11.07 to 16.23 mg/100 g FW. The highest mean value for determinate tomato genotypes was observed in a local hybrid variety, NIAB-Gohar (16.23 mg/100 g FW).

Among twenty-four parent tomato genotypes, three were grouped into the low category for fruit total carotenoid content ranging from 2.56 to 4.35 mg/100g FW. The lowest value for determinate tomato genotype was observed in a parent, NCEBR-5 (2.56 mg/100 g FW). Eighteen parent tomato genotypes were categorized in medium category with their mean values varying from 5.11 to 9.82 mg/100 g FW. In the high category for fruit total carotenoid content, three parent tomato genotypes were grouped with the mean values ranging from 11.65 to 14.63 mg/100 g FW, while the highest mean value for determinate tomato genotype was observed in a parent, H-24 (14.6 mg/100 g FW).

Twenty-four tomato lines were tested for fruit total carotenoid content, three were grouped into low category ranging from 3.90 to 4.19 mg/100 g FW. The lowest value for determinate tomatoes was observed in an exotic line 21354 (4.12 mg/100 g FW). In the intermediate category nineteen lines were grouped with their fruit total carotenoid content ranging from 5.06 to 8.69 mg/100 g FW. Two lines were included in the high category for fruit total carotenoids content, the highest value was observed in a determinate line LBR-17 (15.88 mg/100 g FW).

Tomato advance lines showed low and medium values for fruit total carotenoids content. The lowest value was observed in a determinate advance line MIL-13-F4 (4.68 mg/100 g FW). Four advance lines were placed in an intermediate category for fruit total carotenoids content ranging from 5.35 to 7.31 mg/100 g FW, respectively.

Among sixteen indeterminate genotypes tested, the lowest value for fruit total carotenoid content was observed in an indeterminate cherry tomato NewCherry (3.90 mg/100g FW), while the highest mean value was observed in an indeterminate German variety Lukullus (8.48 mg/100 g FW). The two semi-determinate inbred lines AVTO1311 and AVTO1315 showed a mean value of 8.69 and 11.14 mg/100 g FW for fruit total carotenoid content.

10.3389/fpls.2022.1035163

Total chlorophyll content

Among forty tomato hybrid genotypes, total twenty-six were placed in the low category for fruit total chlorophyll content, with their mean values ranging from 60.09 to 98.35 µg/100 g FW (Figure 2). The lowest value for determinate tomato genotype was observed in a hybrid NBH-150 (60.09 µg/100 g FW). In the intermediate category, eleven tomato hybrids were placed with their mean values ranging from 100.40 to 151.67 (µg/100 g FW). Whereas in the high category for fruit total chlorophyll content three hybrids were placed with their mean values ranging from 174.28 to 194.74 µg/100 g FW. While the highest value for determinate tomato was observed in a local hybrid, NIAB-Jauhar (194.74 µg/100 g FW).

Tomato parent genotypes evaluated for their fruit total chlorophyll content showed significant variation in the mean values. Fourteen parent genotypes out of a total twenty-four were categorized into low category with their mean values ranging from 65.73 to 99.67 (µg/100 g FW). The lowest value for determinate tomatoes was observed in a parent line, LBR-7

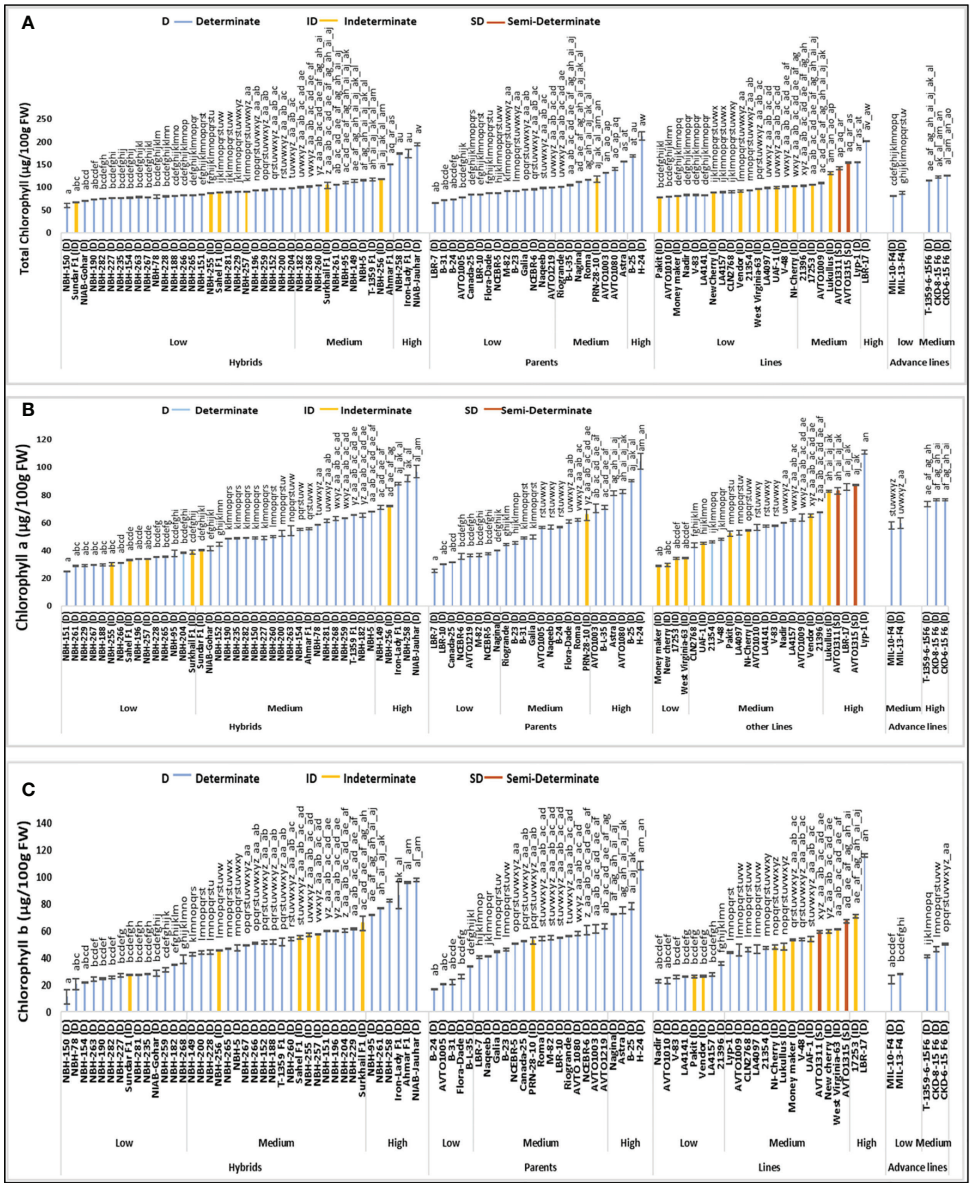

FIGURE 2
Comparison of fruit **(A)** total chlorophyll content, **(B)** chlorophyll a and **(C)** chlorophyll b in different tomato genotypes (mean value ± SD). Mean value with varying alphabet differs significantly ($p < 0.05$, Tukey's HSD).

(65.73 μg/100 g FW). In the intermediate category eight parents were grouped with their mean values ranging from 100.59 to 156.64 (μg/100 g FW). The high category for tomato fruit total chlorophyll content contained two determinate parent genotypes, B-25 (168.76 μg/100 g FW) and H-24 (212.67 μg/100 g FW).

Tomato lines tested for their fruit total chlorophyll content showed significant variation. Sixteen out of total twenty-four lines were grouped into low category for fruit total chlorophyll content with their mean values ranging from 78.22 to 102.38 (μg/100 g FW). The lowest value of total chlorophyll content for determinate tomato lines was observe in an exotic line, AVTO1010 (79.59 μg/100 g FW). Seven lines were grouped into the medium category for total chlorophyll content in fruit, with a range of 103.39 to 155.26 μg/100 g FW. In the high category only one line (LBR-17) was placed with a mean value of 201.82 μg/100 g FW, respectively.

Tomato advance lines were grouped into the low and medium category for fruit total chlorophyll content, based upon the observed variation in the mean value. In the low category two tomato advance lines were placed with the lowest value observed in MIL-10-F4 (81.98 μg/100 g FW). Three tomato advance lines were placed in the medium category for fruit total chlorophyll content with their mean value ranging from 114.52 to 126.77 μg/100 g FW, respectively.

Among sixteen indeterminate tomato genotypes, the lowest fruit total chlorophyl content was observed in a local hybrid, Sundar F1 (67.85 μg/100 g FW). While the highest mean value for total chlorophyll content was observed in an indeterminate variety, Lukullus (131.20 μg/100 g FW), respectively. The two semi-determinate lines tested showed medium mean values for fruit total chlorophyll content, AVTO1311 showed a value of 142.39 μg/100 g FW, while AVTO1315 exhibited a value of 154.21 μg/100 g FW, respectively.

Chlorophyll a content

Based upon the variation in the mean values for fruit chlorophyll a content, out of a total of twenty-four hybrid tomato genotypes fifteen hybrids were categorized into low category with their mean values ranging from 24.79 to 38.71 μg/100 g FW (Figure 2). The lowest value for determinate tomatoes was observed in a local hybrid, NBH-151 (24.79 μg/100 g FW). In the intermediate category for chlorophyll a content twenty hybrid tomatoes were grouped, with their mean values ranging from 40.21 to 67.96 μg/100 g FW. Category with the highest value for chlorophyll a content contained five tomato hybrids, with their mean values varying from 71.22 to 96.93 μg/100g FW. The highest chlorophyll a content for determinate tomatoes was observed in a local hybrid variety, NIAB Jauhar (96.93 μg/100 g FW).

Among twenty-four tomato parents, eight were grouped in the low category for fruit chlorophyll a content, with their mean values ranging from 25.31 to 39.87 μg/100g FW. The lowest value for determinate tomatoes was observed in a parent line, LBR-7 (25.31 μg/100 g FW). In the medium category ten parents were placed, with the values ranging from 44.26 to 65.70 μg/100 g FW. Six tested parent genotypes were included in the high category for chlorophyll a content ranging from 70.35 to 104.19 μg/100 g FW. The highest chlorophyll a content of 104.19 μg/100 g FW was observed in a determinate parent tomato, H-24 respectively.

Out of twenty-four tomato lines tested, four fall under the low category for fruit chlorophyll a content ranging from 28.79 to 34.17 μg/100 g FW. In the intermediate category fifteen lines were grouped with mean values ranging from 43.83 to 67.75 μg/100 g FW. In high category for chlorophyll a content, five tested lines were categorized with mean value ranging from 82.77 to 111.10 μg/100 g FW. The highest value for determinate tomatoes was observed in a local line Lyp-1 (111.10 μg/100 g FW).

Tomato advance lines showed medium and high values for fruit chlorophyll a content. Based upon the detected variation two advance lines MIL-10-F4 and MIL-13-F4 were grouped into an intermediate category with the mean values of 58.12 and 59.68 (μg/100g FW) for fruit chlorophyll a content. The remaining tomato advance lines showed high values for fruit chlorophyll a content, ranging from 73.43 to 76.53 μg/100g FW, respectively.

Among sixteen indeterminate tomato genotypes tested for fruit chlorophyll a content, the lowest value was observed in an indeterminate genotype Moneymaker (28.79 μg/100 g FW), while the highest value of chlorophyll a content was observed in an exotic indeterminate variety, Lukullus (82.77 μg/100 g FW). Semi-determinate inbred lines AVTO1311 and AVTO1315 were grouped in high category for fruit chlorophyll a content, with the mean values of 83.09 and 87.06 (μg/100g FW), respectively.

Chlorophyll b content

Total forty tomato hybrids tested for fruit chlorophyll b content, fourteen were placed in the low category ranging from 11.13 to 38.86 μg/100 g FW (Figure 2). The lowest value for determinate tomato was observed in local hybrid, NBH-150 (11.13 μg/100 g FW). In the intermediate category twenty tomato hybrids were grouped with the mean values ranging from 42.94 to 65.63 μg/100 g FW. Six hybrid tomatoes were grouped into high category, with their mean value ranging from 72.07 to 97.80 μg/100 g FW. The highest value for determinate tomato was observed in a local hybrid NBH-Jauhar (97.80 μg/100 g FW).

Twenty-four tomato parent genotypes tested showed significant variation in their fruit chlorophyll b content. In the low category five

tomato parents were placed, ranging from 16.92 to 34.03 μg/100 g FW. The lowest value for determinate tomato was observed in parent line B-24 (16.92 μg/100 g FW). In the intermediate category for fruit chlorophyll b content fifteen parents were grouped, with their mean values ranging from 40.41 to 63.41 μg/100 g FW. The category with the highest mean values for chlorophyll b content consisted of four parents ranging from 72.93 to 108.47 μg/100 g FW. The highest value for determinate tomato was observed in a parent, H-24 (108.47 μg/100g FW).

Tomato lines exhibited significant variation for fruit chlorophyll b content. Out of a total twenty-four lines tested, eight lines were categorized into low category, with their mean values ranging from 22.91 to 35.64 (μg/100 g FW). The lowest value for determinate tomato was observed in a line, Nadir (22.91 μg/100 g FW). In the intermediate category for fruit chlorophyll b content fourteen lines were grouped, with their mean values ranging from 44.16 to 67.15 (μg/100 g FW). In the high category two tomato lines were placed with their mean values ranging from 70.91 to 116.07 (μg/100 g FW). Highest chlorophyll b content for determinate tomato was observed in a line LBR-17 (116.07 μg/100 g FW).

Total five tomato advance lines were tested for fruit chlorophyll b content; low and medium values were detected among these lines. In the low category two advance lines were placed, the lowest value was observed in an advance line MIL-10-F4 (23.86 μg/100 g FW). In the medium category three advance lines were grouped, with their mean values ranging from 41.08 to 50.24 μg/100 g FW.

Among the indeterminate tomato genotypes lowest value for fruit chlorophyll b content was observed in Pakit (26.18 μg/100 g FW), while the highest value was observed in an indeterminate genotype, 17253 (70.91 μg/100 g FW). The two semi-determinate lines showed a medium value for chlorophyll b content, with the mean values of 59.30 μg/100 g FW (AVTO1311) and 67.15 μg/100 g FW, (AVTO1315) respectively.

Non-enzymatic antioxidants

Ascorbic acid

Total forty tomato hybrids tested for fruit ascorbic acid (AsA) content showed significant variation. Seven tomato hybrids were grouped into low category with their mean values ranging from 298.00 to 349.25 μg/g FW (Figure 3). The lowest fruit ascorbic acid content for determinate tomato was detected in an exotic hybrid, Iron Lady F1 (298.00 μg/g FW). In the intermediate category, twenty-seven hybrids were grouped with the mean values varying between 361.50 to 379.50 μg/g FW. Total six tomato hybrids were grouped into high category, with their values ranging from 381.25 to 400.75 μg/g FW. The highest value for determinate tomato was observed in hybrid, NBH-152 (400.75 μg/g FW) respectively.

Tomato parents showed significant variation in the mean values for fruit ascorbic acid content. Five out of total twenty-four parents were grouped into the low category, with the mean values ranging from 329.50 to 345.00 μg/g FW. The lowest value for determinate tomato was observed in an AVRDC line, AVTO1080 (329.50 μg/g FW). In the medium category seventeen parents were placed with their mean values ranging from 350.00 to 379.25 μg/g FW. Two determinate tomato parents, NCEBR-6 (386.00 μg/g FW) and B-25 (394.25 μg/g FW) showed high values for fruit ascorbic acid content.

Out of twenty-four tomato lines tested, six exhibited comparatively low values for fruit ascorbic acid content. The mean values for tomato lines placed in low category varied between 321.75 to 349.50 μg/g FW. While the lowest value for determinate tomato was observed in a line, V-48 (321.00 μg/g FW). In the intermediate category fifteen lines were grouped with the mean values varying from 355.00 to 376.50 μg/g FW. Three lines exhibited high values for fruit ascorbic acidic content, ranging from 396.76 to 435.25 μg/g FW. The highest value for determinate tomato was observed in a line 21396 (435.25 μg/g FW) respectively.

Comparative analysis of the advance lines exhibited low, medium and high values for fruit ascorbic acidic content. Two advance lines showed low values while the lowest was observed in an advance line, T-1359-6-15 F6 (332.75 μg/g FW). MIL-10-F4 showed a medium value for ascorbic acid content (363.75 μg/g FW), while MIL-13-F4 (381.25 μg/g FW) and CDK-6-15 F6 (394.50 μg/g FW) showed high value for fruit ascorbic acid content.

A total of sixteen indeterminate tomato lines were tested, the lowest value for ascorbic acid was observed in an indeterminate line, Vendor (334.00 μg/g FW). The highest value was observed in indeterminate hybrid tomato, Surkhail F1 (383.75 μg/g FW). The two semi-determinate lines showed low and high values for fruit ascorbic acid content. AVTO1311 (339.25 μg/g FW) was placed in the low category whereas, AVTO1315 (429.25 μg/g FW) was placed in high category.

Total flavonoid content

Significant variation was observed among forty tested tomato hybrids for fruit total flavonoid content (TFC). Twenty-seven hybrids were categorized in low category, ranging from 1295.33 to 2466.74 μg/100 g FW (Figure 3). The lowest value for determinate tomato was observed in a hybrid, NBH-227 (1295.335 μg/100 g FW). Seven hybrids were placed in the medium category with their mean values ranging from 2525.05 to 2858.98 μg/100 g FW. In the high category for total flavonoid content six hybrids were grouped, with their mean values varying between 2986.19 to 3972.08 (μg/100 g FW) and the highest value for determinate tomato was observed in a hybrid, Iron lady F1 (3972.08 μg/100 g FW).

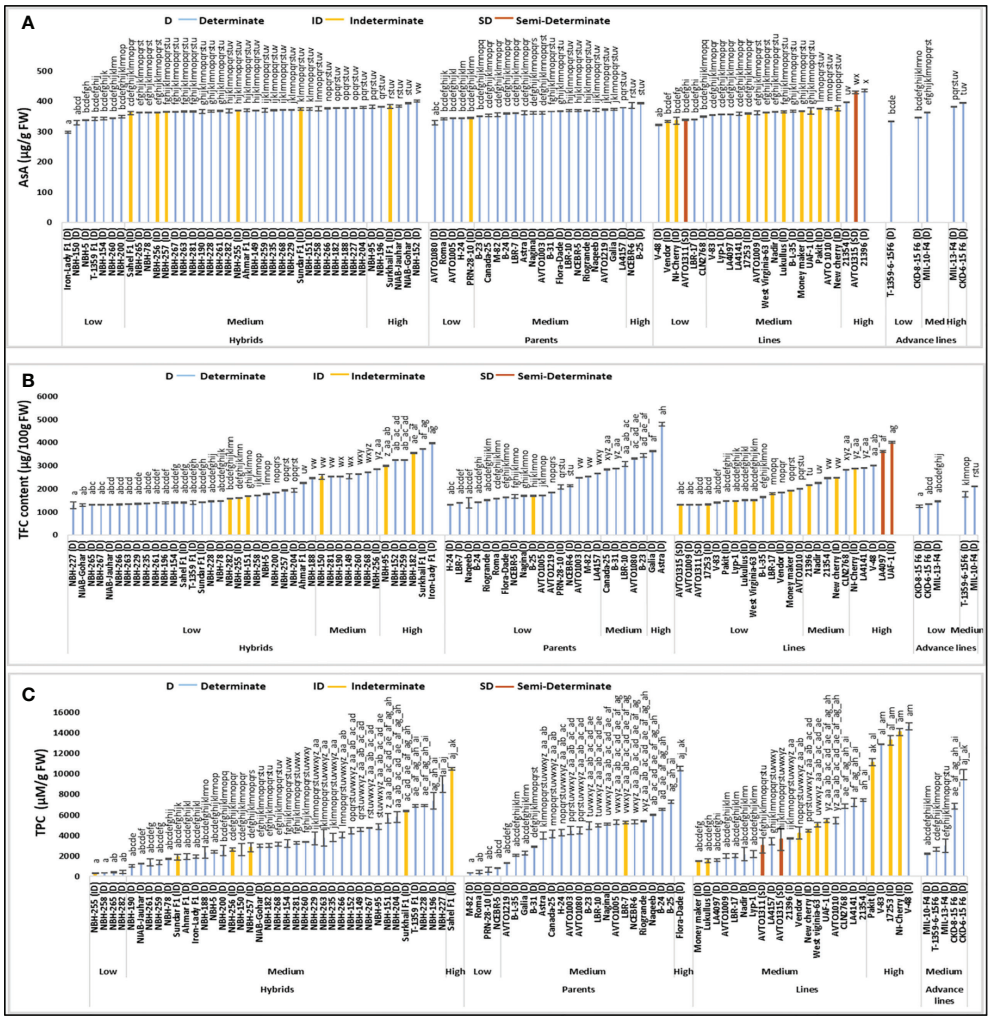

FIGURE 3
Comparison of fruit ascorbic acid (AsA) **(A)**, total flavonoid content (TFC) **(B)** and total phenolic compounds (TPC) **(C)** in different tomato genotypes (mean value ± SD). Mean value with varying alphabet differs significantly ($p < 0.05$, Tukey's HSD).

Twenty-four tomato parents tested for fruit total flavonoid content exhibited significant variation. Seventeen parents were placed in the low category with their mean values ranging from 1321.83 to 2662.86 µg/100 g FW. For determinate tomato lowest value was observed in a parent, H-24 (1321.83 µg/100 g FW). Five parents were placed in the medium category for fruit total flavonoid content, ranging from 2837.78 to 3447.33 (µg/100 g FW). In the high category, two determinate tomatoes, Galia (3643.45 µg/100 g FW) and Astra (4793.66 µg/100 g FW) were placed.

Twenty-four tomato lines evaluated for the fruit total flavonoid content varied significantly, while fourteen lines were placed in a low category, ranging from 1321.83 to 2000.30 µg/100 g FW. The lowest value for determinate tomato was observed in a line, AVTO1009 (1321.83 µg/100 g FW). Five tested lines showed intermediate value for total flavonoid content, ranging from 2164.61 to 2832.48 µg/100 g FW. Another five lines showed high mean values for total flavonoid content, ranging from 2885.48 to 4009.19 µg/100 g FW. The highest value for determinate tomato was observed in an exotic line, LA4097 (3627.55 µg/100 g FW).

Tomato advance lines showed low and medium value for fruit total flavonoid content. Three advance lines were included in the low category, ranging from 1242.33 to 1459.65 µg/100 g FW. The lowest value was observed in an advance line, CKD-8-15-F6 (1242.33 µg/100 g FW). Two tested tomato advance lines

were placed in the medium category, T-1359-6-15 F6 (1767.08 µg/100 g FW) and MIL-10-F4 (2106.31 µg/100 g FW).

Among the indeterminate tomato genotypes, the lowest value for total fruit flavonoid content was observed in 17253 (1332.43 µg/100 g FW) and the highest value was observed in an indeterminate line, UAF-1 (4009.19 µg/100 g FW) respectively. The two semi-determinate tomato lines tested showed low values for fruit total flavonoid content, whereas lowest mean was observed in AVTO1315 (1321.83 µg/100 g FW) followed by AVTO1311 (1332.43 µg/100 g FW).

Total phenolic compounds

Significant variation was observed for fruit total phenolic compounds (TPC) among forty tested tomato hybrids. In the low category four hybrids were placed with their mean values ranging from 325 to 450 µM/g FW (Figure 3). The lowest value for determinate tomato was observed in a hybrid, NBH-258 (350 µM/g FW). In the intermediate category thirty-five tested hybrids were grouped, with their mean values ranging from 1025 to 9000 µM/g FW, respectively. Sahel F1 was the only hybrid tomato grouped in the high category for fruit total phenolic compounds with the mean values 10500 µM/g FW.

Twenty-four tomato parents tested for fruit total phenolic compound showed significant variation. In the low category four parent genotypes were categorized ranging from 350 to 800 µM/g FW, with the lowest mean value for determinate tomato observed in a parent, M-82 (350 µM/g FW). In the intermediate category for fruit total phenolic compounds, nineteen parents were categorized, with the mean values ranging from 1300 to 7300 µM/g FW. The highest value of fruit total phenolic compound for determinate tomato was observed in the parent, Flora-Dade (10525 µM/g FW) respectively.

Twenty-four tomato lines evaluated for fruit total phenolic compound were categorized into medium and high category. In the intermediate category nineteen lines were placed with their mean values ranging from 1475 to 7475 µM/g FW. In the high category five lines were placed, ranging from 11150 to 14650 µM/g FW. The highest value for determinate tomato was observed in V-48 (14650 µM/g FW). Tomato advance lines tested for the fruit total phenolic compound exhibited medium value ranging from 2200 to 9950 µM/g FW, respectively.

Among the indeterminate tomato lines the lowest value for fruit total phenolic compound was observed in a hybrid, NBH-255 (325 µM/g FW). While the highest value was observed in an indeterminate cherry tomato, NI-cherry (14100 µM/g FW). The two semi-determinate tomato lines showed intermediate values for fruit total phenolic compound, AVTO1311 showed a value of 3025 µM/g FW and AVTO1315 showed a value of 3625 µM/g FW, respectively.

Enzymatic antioxidants

Ascorbate peroxidase activity

Significant variation was observed for fruit ascorbate peroxidase (APX) activity among forty tomato hybrids tested. In the low category seventeen tested hybrids were placed with their mean values ranging from 280 to 580 U/g FW (Figure 4). The lowest value for determinate tomato was observed in a hybrid, T-1359 F1 (280 U/g FW). In the intermediate category fifteen hybrids were placed ranging from 600 to 960 U/g FW. Eight hybrids were included in the high category with their mean values ranging from 1020 to 1520 U/g FW respectively. The highest value for determinate tomato was observed in hybrid, NBH-149 (1520 U/g FW).

Twenty-four tomato parents were tested for fruit ascorbate per oxidase (APX) activity. Seven parent genotypes showed low values ranging from 320 to 500 U/g FW. The lowest value for determinate tomato was observed in a parent, M-82 (320 U/g FW). In the intermediate category, fourteen tomato parents were placed with their mean values ranging from 660 to 960 U/g FW. Three tomato parent genotypes were placed in high category for fruit ascorbate peroxidase activity, with their mean values ranging from 1120 to 1480 U/g. The highest value for determinate tomato was observed in a parent line, AVTO1080 (1480 U/g FW).

Among twenty-four tested tomato lines, twelve lines were categorized in low category for fruit ascorbate peroxidase (APX) activity. Lowest value for determinate tomato was observed in an inbred line, AVTO1009 (380 U/g FW). The overall range for the lines placed in low category was between 280 to 580 U/g FW. In the intermediate category ten lines were placed with their mean value ranging from 600 to 920 U/g FW. In the high category, only two lines were grouped including a local determinate tomato line, Lyp-1 (1180 U/g FW) and an exotic determinate tomato line, B-L-35 (1860 U/g FW).

Tomato advance lines tested exhibited low and medium values for fruit ascorbate peroxidase (APX) activity. Two advance lines were placed in low category. The lowest value was observed in T-1359-6-15F6, (240 U/g FW), remaining advance lines were placed in medium category ranging from 640 to 940 U/g FW, respectively.

Among sixteen indeterminate tomato lines tested, the lowest value for fruit ascorbate peroxidase (APX) activity was observed in a hybrid Sahel F1 (300 U/g FW) and the highest value was observed in a hybrid Sundar F1 (1180 U/g FW). The two semi-determinate tomato lines showed a low value for fruit ascorbate oxidase activity, with the lowest value observed in a line AVTO1311 (280 U/g FW) followed by a line AVTO1315 (360 U/g FW), respectively.

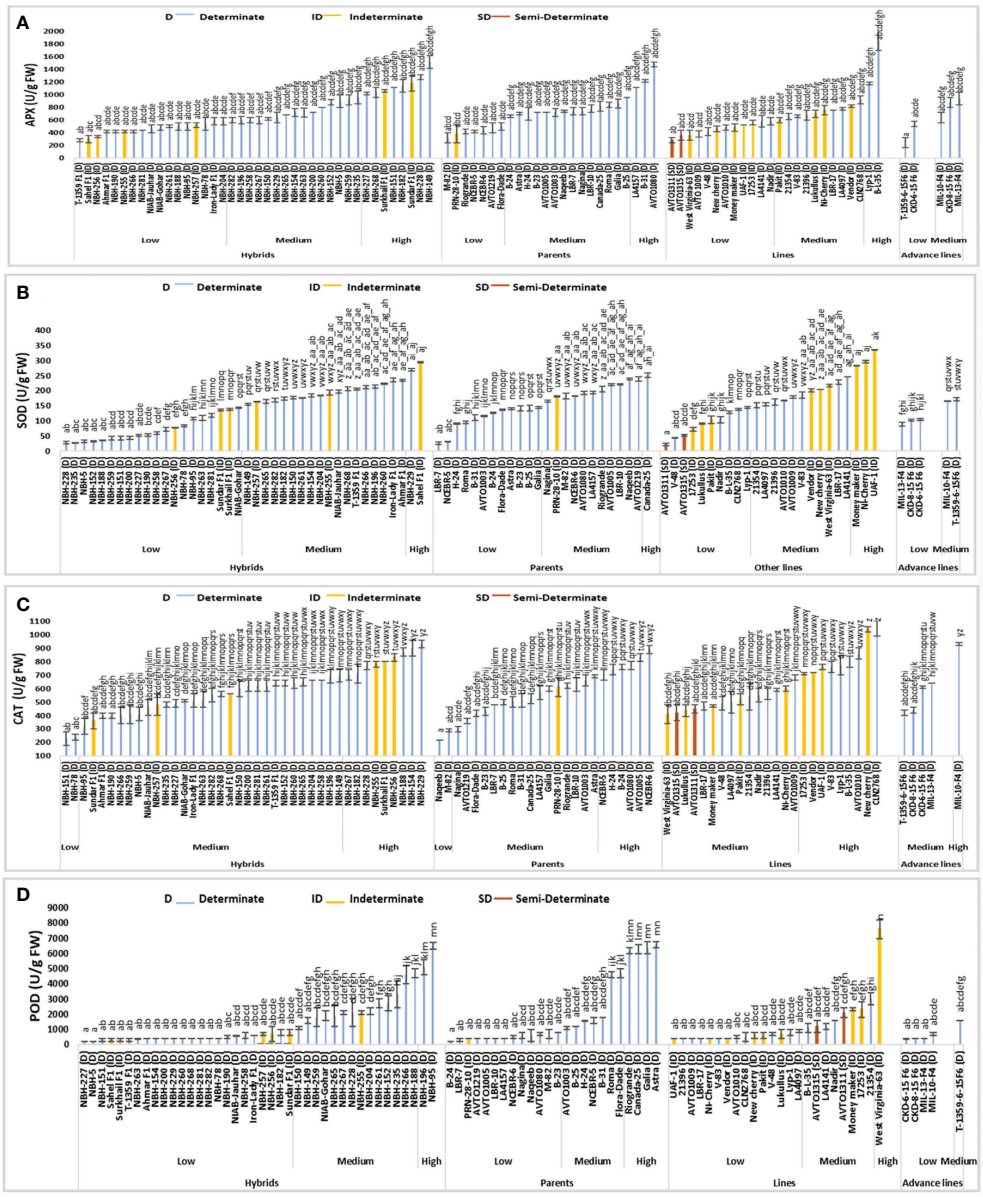

FIGURE 4
Comparison of fruit **(A)** ascorbate peroxidase (APX), **(B)** superoxide dismutase (SOD), **(C)** catalase (CAT) and **(D)** peroxidase (POD) activities in different tomato genotypes (mean value ± SD). Mean value with varying alphabet differs significantly ($p < 0.05$, Tukey's HSD).

Superoxide dismutase activity

Among forty tomato hybrids, twenty showed low values for fruit superoxide dismutase (SOD) activity ranging from 28.02 to 143.34 U/g FW (Figure 4). The lowest SOD activity for determinate tomato was observed in a hybrid, NBH-228 (28.02 U/g FW). Eighteen hybrid tomatoes showed intermediate value for fruit SOD activity, ranging from 155.73 to 235.11 U/g FW. For determinate tomatoes highest SOD activity was observed in the hybrid, NBH-229 (269.90 U/g FW).

SOD activity for twelve tomato parents exhibited low values ranging from 25.26 to 144.04 U/g FW. The lowest SOD activity for determinate tomato was observed in a parent line, LBR-7 (25.26 U/g FW). Eleven tomato parents were grouped in the intermediate category for SOD activity with their mean value ranging from 165.27 to 239.21 U/g FW. Canada-25, a determinate tomato parent genotype showed the highest value (251.30 U/g FW) for SOD activity.

Among twenty-four tested tomato lines, ten showed the lowest fruit SOD activity ranging from 21.52 to 144.79 U/g FW.

The lowest SOD activity for determinate tomato was observed in a line V-48 (43.21 U/g FW). Eleven lines were grouped in the medium category for SOD activity ranging from 151.06 to 245.50 U/g FW. Three lines were grouped into high category.

Low and medium values were observed for SOD activity among five tested advance lines. Total three exhibited low values ranging from 88.88 to 104.92 U/g FW. While the lowest SOD activity was detected in an advance line, MIL-13 -F4 (88.88 U/g FW). In the medium category two advance lines were grouped.

For sixteen indeterminate tomato genotypes the lowest SOD activity was observed in a line, 17253 (72.28 U/g FW) and the highest was observed in a local line UAF-1 (335.54 U/g FW). The two semi-determinate inbred lines exhibited low SOD activities. An inbred line AVTO1311 showed a value of 21.52 U/g FW. While the semi-determinate inbred line AVTO1315 exhibited an SOD activity of 52.67 U/g FW, respectively.

Catalase activity

Significant variation was observed for fruit catalase (CAT) activity in the forty tested tomato hybrids (Figure 4). In low category two hybrids NBH-151 (230 U/g FW) and NBH-78 (240 U/g FW) were placed. In the medium category twenty-nine hybrids were grouped ranging from 320 to 695 U/g FW. Nine genotypes were grouped into high category for CAT activity ranging from 700 to 930 U/g FW. The highest value for determinate tomato was observed in a local hybrid, NBH-229 (930 U/g FW).

Out of twenty-four tomato parent lines tested for fruit CAT activity, two parents were categorized in low category. The lowest value for determinate tomato was observed in a parent genotype, Naqeeb (220 U/g FW). In the intermediate category sixteen parent their mean values ranging from 300 to 690 U/g FW. Six parents were grouped in the high category, ranging from 700 to 890 (U/g FW). The highest value for determinate tomato was observed in a parent, NCEBR-6 (890 U/g FW).

Tomato lines tested for fruit CAT activity showed medium and high mean values. Out of twenty-four tomato lines tested, fifteen were grouped into medium category ranging from 410 to 680 U/g FW. In the high category for fruit CAT activity nine lines were grouped ranging from 710 to1045 U/g FW and the highest value was observed in CLN2768 (1045 U/g FW).

Among five tomato advance lines tested for fruit CAT activity, four were grouped into medium category ranging from 420 to 640 U/g FW. An advance line MIL-10-F4 was categorized in the high category with the mean value of 930 U/g FW.

Among the indeterminate tomato genotypes, lowest value for fruit CAT activity was observed in a local hybrid Sundar F1 (360 U/g). While the highest mean value was exhibited by a local indeterminate cherry tomato NewCherry (1040 U/g FW). The two semi-determinate lines tested for CAT activity exhibited medium values, whereas AVTO1315 showed a mean value of 420 U/g FW, and AVTO1311 showed mean value of 450 U/g FW, respectively.

Peroxidase activity

Significant variation was observed among forty tested tomato hybrids for fruit peroxidase (POD) activity (Figure 4). In the low category twenty-four genotypes were grouped ranging from 199.80 to 799.20 U/g FW. The lowest value for determinate tomato was observed in a hybrid, NBH-227 (199.80 U/g FW). In the intermediate category fourteen hybrids were placed ranging from 1098.90 to 4695.30 U/g FW. Two tested determinate hybrids NBH-196 (5094.94 U/g FW) and NBH-95 (6496.50 U/g FW) were placed in the high category for fruit POD activity.

The parent genotypes tested for their fruit POD activity exhibited significant differences. In the low category thirteen out of twenty-four genotypes were grouped ranging from 199.80 to 799.20 (U/g FW). Whereas the lowest value for determinate tomato was observed in a parent line, B-24 (199.80 U/g FW). Seven parent genotypes were placed in an intermediate category ranging from 1098.00 to 4695.30 U/g FW. In the high category four parents were grouped ranging from 6193.80 to 6593.40 U/g FW. The highest value for determinate tomato was observed in a parent line, Astra (6593.40 U/g FW).

Out of twenty-four tomato lines tested for fruit POD activity fifteen were categorized into low category ranging from 399.60 to 899.10 (U/g FW). The lowest value for determinate tomato was observed in a line 21396 (399.60 U/g FW). Eight lines were grouped into medium category ranging from 1098.90 to 2997.00 U/g FW. Only one line West Virginia-63 (7592.4 U/g FW) was included in high category.

Total five tomato advance lines tested for POD activity showed low and medium category for POD activity, four of them were grouped into low category ranging from 399.10 to 699.30 (U/g FW). The lowest value was observed in an advance line CKD-6-15 F6 (399.1 U/g FW). In the intermediate category only one advance line T-1359-6-15F6 (1598.40 U/g FW) was placed.

Among the indeterminate tomato lines lowest value for POD activity was observed in a hybrid Sahel F1 (299.70 U/g FW). The highest value for POD activity was observed in an indeterminate line West Virginia-63 (7592.40 U/g FW). The two tested semi-determinate tomato lines AVTO1315 (1198.80 U/g FW) and AVTO1311 (2097.90 U/g FW) were placed in the medium category.

Hydrolytic enzymes

Alpha-amylase activity

Total forty tomato hybrids evaluated for their fruit alpha-amylase activity exhibited significant variations (Figure 5). In the

low category nine tested hybrids were placed with their mean values ranging from 16.79 to 86.60 mg/g FW, respectively. The lowest value for determinate tomatoes was observed in a local hybrid, NBH-228 (16.79 mg/g FW). In the intermediate category twenty-six hybrids were categorized with their mean values ranging from 100.00 to 194.52 mg/g FW. Five tested hybrids were categorized in high category with their mean values ranging from 204.90 to 238.11 mg/g FW, respectively. The highest value for determinate tomato was observed in a local hybrid, NBH-268 (238.11 mg/g FW).

Among twenty-four tomato parents tested for alpha-amylase activity six showed low mean values ranging from 50.56 to 96.98 mg/g FW. Lowest value for determinate tomato was observed in a parent line, NCEBR-5 (50.56 mg/g FW). In the intermediate category fourteen parents were placed with the mean values ranging from 101.32 to 187.35 mg/g FW. Four parent tomatoes were placed in high category with the mean values ranging from 210.75 to 243.01 (mg/g FW). Highest value for determinate tomato was observed in a parent, PRN-28-10 (243.01 mg/g FW).

The tomato lines evaluated for fruit alpha-amylase activity exhibited significant variation. In the low category six lines were grouped with their mean values ranging from 48.86 to 88.86 mg/g FW, respectively. The lowest value for determinate tomato was observed in a line V-83 (48.86 mg/g FW). In the intermediate category twelve lines were placed with the mean values ranging from 103.58 to 210.00 (mg/g FW). Six tomato lines were grouped into high category with the mean value ranging from 210.56 to 237.73 mg/g FW. The highest value for determinate tomato was observed in a line Nadir (237.73 mg/g FW).

Five tomato advance lines tested for fruit alpha-amylase activity showed medium value ranging from 102.07 to 180.37 mg/g FW. Among the indeterminate tomato lines lowest value was observed in a hybrid Surkhail F1 (27.73 mg/g FW) whereas, the highest value was observed in a parent genotype PRN-28-10 (243.01 mg/g FW). The two semi-determinate line AVTO1311 (133.20 mg/g FW) and AVTO1315 (161.69 mg/g FW) were grouped in the medium category for fruit alpha-amylase activity.

Protease activity

Hybrids under study exhibited significant variation in the mean value for fruit protease activity (Figure 5). In the low category out of a total forty hybrids twenty-two were grouped ranging from 5560 to 6415 U/g FW. The lowest value for determinate tomato was observed in a hybrid, NBH-182 (5560 U/g FW). In the intermediate category sixteen hybrids were grouped ranging from 6535 to 7335 (U/g FW). Two hybrids, Sahel F1(7660 U/g FW) and NBH-150 (8525 U/g FW) were grouped in the high category.

In the low category for fruit protease activity, twelve out of a total twenty-four parents were grouped with their mean value ranging from 5285 to 6400 (U/g FW). The lowest value was observed in a parent Riogrande (5285 U/g FW). In the medium category ten parent genotypes were grouped ranging from 6540 to 7385 (U/g FW). Two parent genotypes were grouped in high category for fruit protease activity including an AVRDC inbred line, AVTO1003 (8070 U/g FW) followed by a line, AVTO1080 (8525 U/g FW).

Among twenty-four tomato lines evaluated for protease activity, eleven showed low values ranging from 5745 to 6490 U/g FW. The lowest value for determinate tomato was observed in a line V-83 (5760 U/g FW). In the intermediate category twelve lines were grouped with their mean values ranging from 6550 to 7430 (U/g FW). The highest value of 7730 U/g FW for protease activity was observed in a line AVTO-1311.

Five tomato advance lines tested for fruit protease activity showed low and medium mean values. The lowest value was observed in a line CKD-8-15 F6 (5910 U/g FW). In the intermediate category four advance lines were grouped with their mean values ranging from 6830 to 7455 (U/g FW).

Among the sixteen indeterminate tomato lines the lowest value was observed in a hybrid Sundar F1 (5575 U/g FW). While the highest value was observed in an indeterminate hybrid Sahel F1 (7660 U/g FW). The semi-determinate line AVTO1315 showed a medium mean value (6550 U/g FW) for protease activity, while the semi-determinate line AVTO1311 (7730 U/g FW) was placed in high category for fruit protease activity.

Esterase activity

Among forty tomato hybrids tested for fruit esterase activity, seventeen showed low values ranging from 18.85 to 24.87 μM/min/g FW, respectively (Figure 5). The lowest value for determinate tomato was observed in a local hybrid, NBH-196 (20.87 μM/min/g FW). In the medium category fourteen hybrids were placed, with their values varying between 25.41 to 34.40 μM/min/g FW. In the high category nine hybrids were grouped with their mean values ranging from 35.70 to 50.15 μM/min/g FW. The highest value for determinate tomato was observed in a hybrid, NBH-154 (50.15 μM/min/g FW).

Tomato parents tested for fruit esterase activity exhibited significant variation. Eight genotypes were grouped into low category with their mean value ranging from 18.85 to 24.64 μM/min/g FW. The lowest value was observed in a parent M-82 (18.85 μM/min/g FW). In the intermediate category thirteen parents were grouped ranging from 26.58 to 34.44 μM/min/g FW. Three genotypes were categorized in high category ranging from 37.50 to 38.13 μM/min/g FW with the highest value observed in Nagina (38.13 μM/min/g FW).

Tomato lines evaluated for fruit esterase activity exhibited significant variation. Out of twenty-four lines total seven were grouped in the low category with the mean value ranging from 20.24 to 24.91 μM/min/g FW. The lowest value was observed in an exotic line LA4097 (20.24 μM/min/g FW). In the intermediate

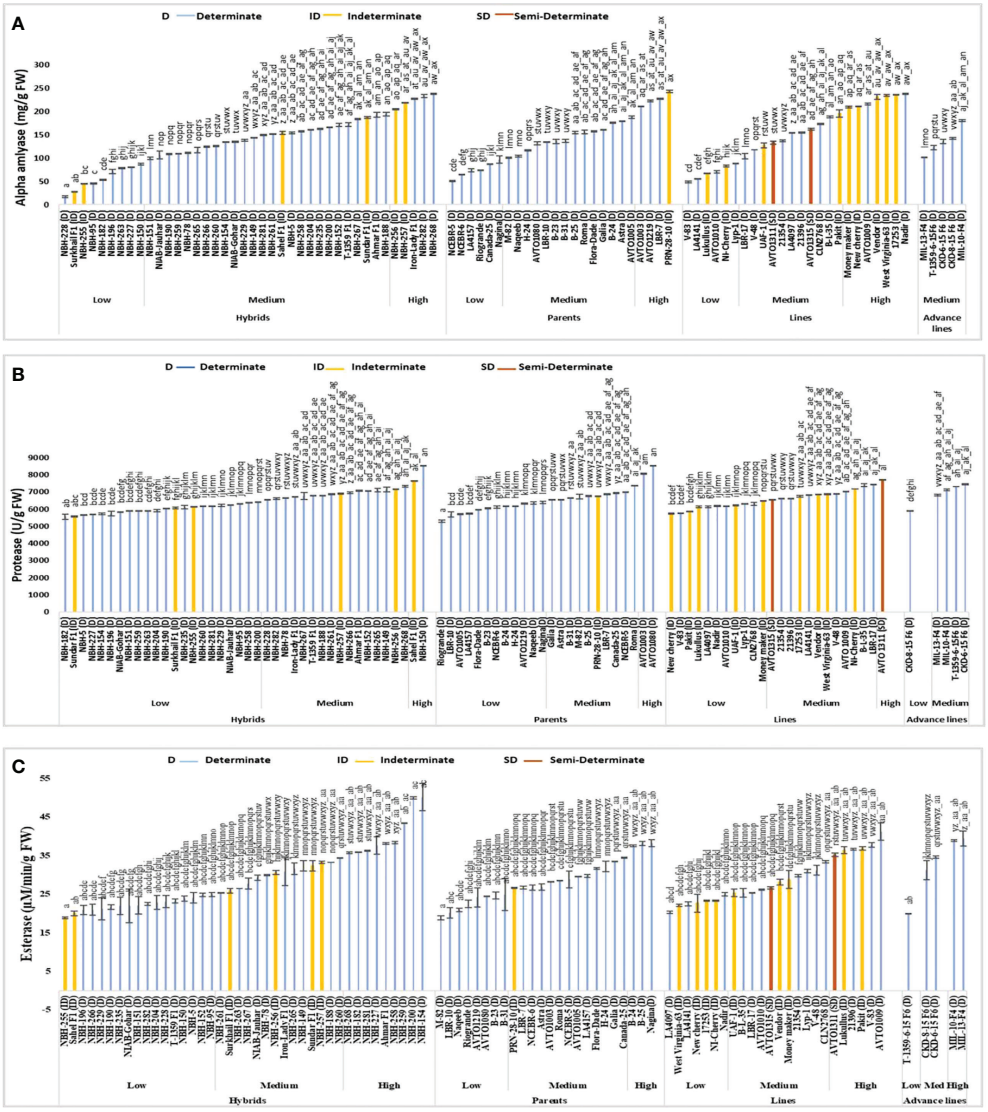

FIGURE 5
Comparison of fruit **(A)** alpha-amylase, **(B)** protease, and **(C)** esterase activities in different tomato genotypes (mean value ± SD). Mean value with varying alphabet differs significantly ($p < 0.05$, Tukey's HSD).

category eleven lines were grouped with their mean values ranging from 25.32 to 33.32 µM/min/g FW. In high category six tomato lines were placed with their mean value ranging from 35.25 to 41.19 µM/min/g FW. The highest value was observed in an AVRDC developed inbred line AVTO1009 (41.19 µM/min/g FW).

Tomato advance lines tested for fruit esterase activity exhibited significant variation. In the low category an advance line T-1359-6-15 F6 (19.92 µM/min/g FW) was placed. Two advance lines CKD-8-15 F6 (31.21 µM/min/g FW) and CKD-6-15 F6 (34.62 µM/min/g FW) showed medium values, while the remaining two were grouped in the high category with the highest value observed in MIL-13-F4 (39.43 µM/min/g FW).

Among sixteen indeterminate lines tested for fruit esterase activity, the lowest value was observed in an indeterminate hybrid, NBH-255 (18.85 µM/min/g FW), while the highest value was observed in a genotype, Pakit (36.83 µM/min/g FW). The two semi-determinate lines showed medium and high values for fruit esterase activity i.e., AVTO1315 showed a value of 26.58 µM/min/g FW, while AVTO1311 exhibited a value of 35.25 µM/min/g FW, respectively.

Other biochemical assays

Total soluble sugars

Tomato hybrids tested for fruit total soluble sugar (TSS) showed significant variation (Figure 6). In the low category five genotypes were grouped ranging from 28.01 to 33.89 mg/g FW. The lowest value for determinate tomato was observed in a local hybrid, NBH-200 (28.10 mg/g FW). In the intermediate category twenty-six hybrids were grouped ranging from 36.20 to 59.40 mg/g FW. Total nine hybrids were included in high category with their mean values ranging from 61.55 to 73.00 mg/g FW. The highest value for determinate tomato was observed in a hybrid, NBH-229 (73 mg/g FW).

Among twenty-four tomato parents tested for fruit total soluble sugar, four showed low values ranging from 29.00 to 34.55 mg/g FW. The lowest value was observed in a parent line, B-24 (29.00 mg/g FW). In the medium category sixteen parents

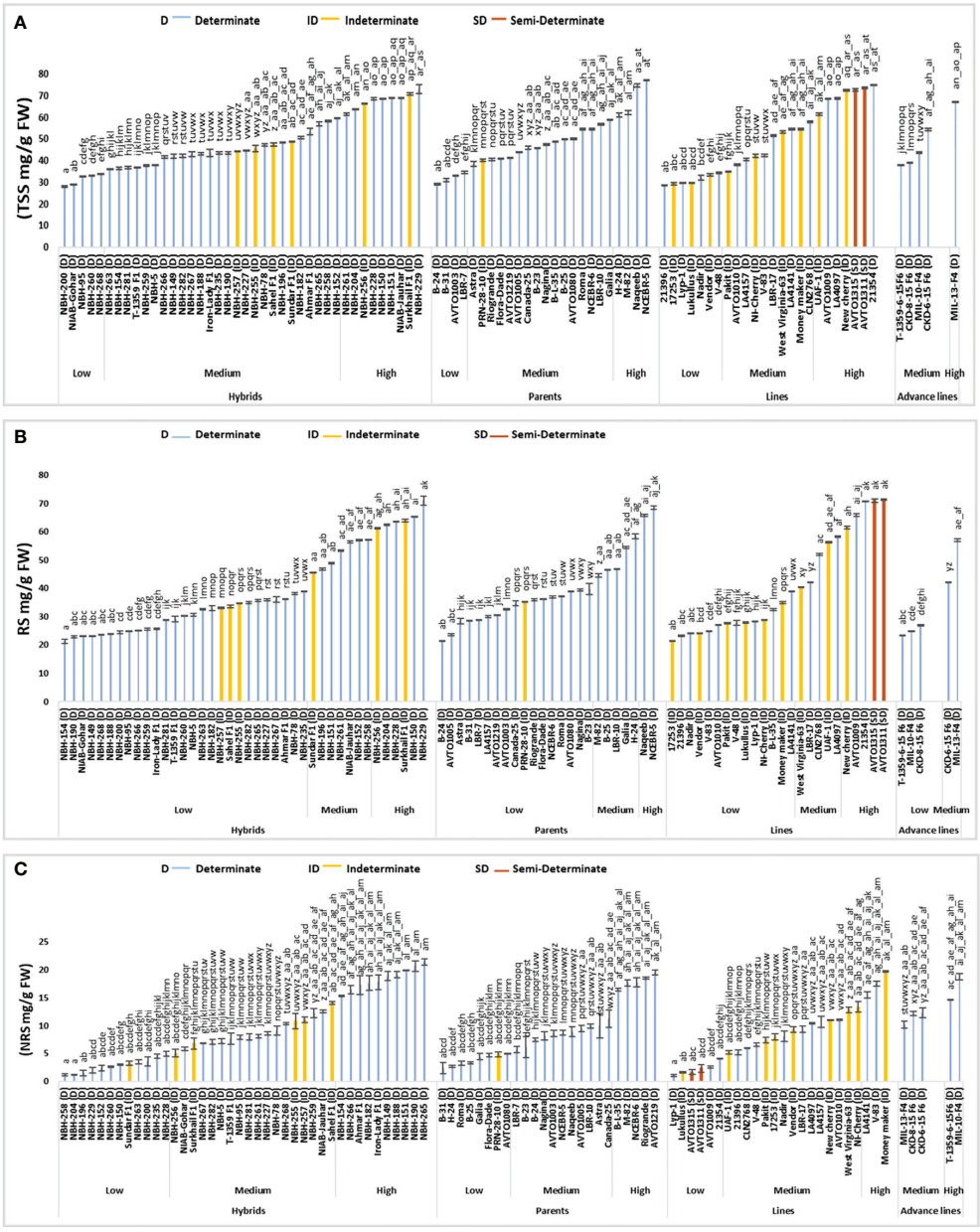

FIGURE 6
Comparison of fruit **(A)** total soluble sugars (TSS), **(B)** reducing sugars (RS) and **(C)** non-reducing sugars (NRS) in different tomato genotypes (mean value ± SD). Mean value with varying alphabet differs significantly ($p < 0.05$, Tukey's HSD).

were grouped ranging from 38.45 to 58.85 (mg/g FW). Four parents were grouped in high category ranging from 61.10 to 77.15 mg/g FW, with the highest value observed in a parent line, NCEBR-5 (77.15 mg/g FW).

Tomato lines tested for fruit total soluble sugars showed significant variation. Seven lines were grouped in the low category with their mean values ranging from 28.51 to 34.40 mg/g FW. The lowest value was observed in a line 21396 (28.51 mg/g FW). In the medium category ten lines were grouped with their mean values ranging from 35.05 to 57.90 mg/g FW. Seven lines were grouped in high category ranging from 61.45 to 74.90 mg/g FW, whereas the highest value was observed in a line 21354 (74.90 mg/g FW).

Tomato advance lines exhibited medium and high value for fruit total soluble sugar. In the medium category four advance lines were grouped ranging from 37.95 to 67.15 mg/g FW. Highest value was observed in an advance line MIL-13-F4 (67.15 mg/g FW).

Among the indeterminate tomato genotypes lowest value was observed in a line, 17253 (29.35 mg/g FW), whereas the highest value for total soluble sugars was observed in a hybrid Surkhail F1 (70.75 mg/g FW). The two semi-determinate lines showed a high value for fruit total soluble sugar AVTO1315 showed a value of 72.65 mg/g FW followed by AVTO1311 (73.60 mg/g FW), respectively.

Reducing sugar

Among forty tomato hybrids tested for fruit reducing sugars (RS) twenty-seven showed low values ranging from 21.30 to 38.97 mg/g FW (Figure 6). The lowest value for determinate tomato was observed in a hybrid, NBH-154 (21.30 mg/g FW). In the intermediate category seven hybrids were grouped with their mean values ranging from 45.57 to 57.15 mg/g FW. Six hybrids were grouped in high category ranging from 61.22 to 70.98 mg/g FW. The highest value for determinate tomato was observed in a hybrid, NBH-229 (70.98 mg/g FW).

Twenty-four tomato parents tested for fruit reducing sugars showed significant variation. In the low category seventeen parents were grouped with the mean values ranging from 21.54 to 39.84 mg/g FW. The lowest value for determinate tomato was observed in a parent line, B-24 (21.54 mg/g FW). In the medium category five parents were grouped with the mean value ranging from 44.58 to 58.41 mg/g FW. Two determinate parents, Naqeeb (65.81 mg/g FW) and NCEBR-5 (68.45 mg/g FW) were grouped in the high category for fruit reducing sugars.

Tomato lines evaluated for their fruit reducing sugars exhibited significant variations. Fourteen lines were grouped in low category with their mean values ranging from 21.42 to 39.05 mg/g FW. The lowest value for the determinate line was observed in 21396 (23.24 mg/g FW). In the intermediate category five lines were grouped ranging from 40.39 to 58.22 mg/g FW. Five tomato lines were categorized in high category with their mean values ranging from 61.50 to 71.26 mg/g FW. The highest value was observed in a determinate line21354 (70.79 mg/g FW).

Out of five advance lines tested for fruit reducing sugars, total three were categorized in low category ranging from 23.35 to 26.95 mg/g FW. While the lowest value was observed in T-1359-6-15 F6 (23.35 mg/g FW). Two advance lines CKD-6-15 F6 (42.09 mg/g FW) and MIL-13-F4 (56.99 mg/g FW) were grouped into the medium category.

The lowest value of fruit reducing sugar for the indeterminate tomato was observed in a line, 17253 (21.42 mg/g FW). While the highest value was observed in a hybrid, Surkhail F1 (63.99 mg/g FW). The two semi-determinate lines AVTO1315 and AVTO 1311 showed high values of 71.00 mg/g FW and 71.26 mg/g FW, respectively.

Non-reducing sugars

Forty tomato hybrids tested for fruit non reducing sugars (NRS) exhibited significant variation (Figure 6). In the low category twelve hybrids were grouped ranging from 1.19 to 4.93 mg/g FW. The lowest value for determinate tomato was observed in a local hybrid, NBH-258 (1.19 mg/g FW). In the intermediate category, eighteen hybrids were placed ranging from 5.07 to 14.03 mg/g FW. Whereas in the high category ten hybrids were grouped, ranging from 15.24 to 21.38 mg/g FW. The highest value of fruit non reducing sugars for determinate hybrids was observed in NBH-265 (21.38 mg/g FW).

The tomato parents tested for their fruit non reducing sugars exhibited significant variation. Out of twenty-four parents tested eight were included in low category ranging from 2.34 to 4.94 mg/g FW. The lowest value for determinate tomato was observed in a parent genotype, B-31 (2.34 mg/g FW). Eleven parents were grouped in the medium category ranging from 5.69 to 11.24 mg/g FW. In the high category five parent lines were grouped ranging from 16.40 to 19.47 mg/g FW. The highest value for determinate tomato was observed in a parent line, AVTO1219 (19.47 mg/g FW).

The tomato lines tested for the fruit non reducing sugars showed significant variation. In the low category six out of a total twenty- four lines were grouped ranging from 1.10 to 4.10 mg/g FW. The lowest value for determinate tomato was observed in a local line Lyp-1 (1.10 mg/g FW). In the medium category fifteen lines were grouped ranging from 5.24 to 13.30 mg/g FW. Three lines showed high values for fruit non reducing sugars ranging from 15.44 to 19.65 (mg/g FW). The highest value for the determinate line was observed in V-83 (17.48 mg/g FW).

Tomato advance lines showed medium and high values for fruit non reducing sugar. In the medium category three advance

lines were grouped ranging from 10.15 to 12.25 mg/g FW. Two advance lines were grouped in the high category with the highest value observed in MIL-10-F4 (18.77 mg/g FW).

Sixteen indeterminate tomato lines were tested for fruit non reducing sugar, the lowest value was observed in line Lukullus (1.62 mg/g FW). Whereas, the highest value was observed in an indeterminate variety, Moneymaker (19.65 mg/g FW). The two semi-determinate lines, AVTO1315 (1.65 mg/g FW) and AVTO1311 (2.33 mg/g FW) showed low values for fruit non reducing sugars.

Malondialdehyde content

Forty hybrid tomatoes tested for malondialdehyde (MDA) content exhibited significant variation (Figure 7). In the low category twenty-four hybrids were grouped ranging from 22.45 to 78.96 μM/g FW, with the lowest value for determinate tomato observed in NBH-228 (22.45 μM/g FW). In the intermediate category ten hybrids were placed ranging from 82.06 to 145.54 μM/g FW. Total Six hybrids were grouped in the high category for fruit MDA content ranging from 153.29 to 267.87 μM/g FW.

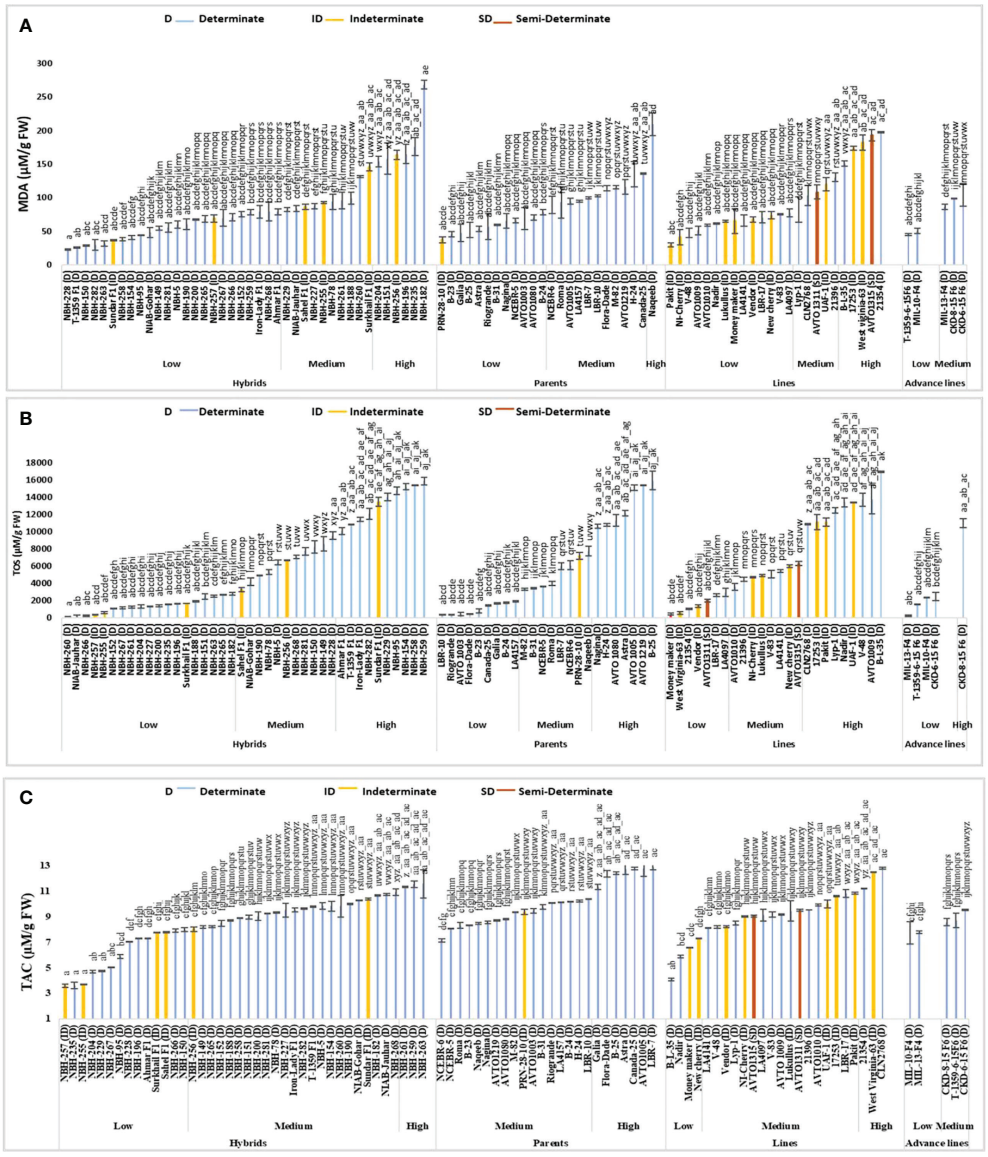

FIGURE 7
Comparison of fruit **(A)** malondialdehyde (MDA) content, **(B)** total oxidant status (TOS), and **(C)** total antioxidant capacity (TAC) in different tomato genotypes (mean value ± SD). Mean value with varying alphabet differs significantly ($p < 0.05$, Tukey's HSD).

The highest value for determinate tomato was observed in a hybrid, NBH-182 (267.87 μM/g FW).

Tomato parents tested for MDA content exhibited significant variation. Out of twenty-four tested tomato parents twelve were grouped in low category ranging from 37.16 to 78.19 μM/g FW. The lowest value for determinate tomato was observed in a parent, B-23 (45.67 μM/g FW). In the medium category eleven parents were grouped, ranging from 89.03 to 135.48 μM/g FW. Only a single determinate tomato parent Naqeeb (209.03 μM/g FW) showed a high value for MDA content.

Tomato lines showed significant variation for fruit MDA content. In the low category fourteen lines were grouped ranging from 29.41 to 77.41 μM/g FW. The lowest value for determinate tomato was observed in a line V-48 (47.22 μM/g FW). In the medium category five lines were grouped ranging from 82.06 to 130.06 μM/g FW. Five lines were placed in the high category for fruit MDA content ranging from 150.96 to 197.41 μM/g FW, respectively. The highest value for determinate tomato was observed in a line 21354 (197.41μM/g FW).

Tomato advance lines showed low and high values for fruit MDA content. In the low category two advance lines were grouped with the lowest value observed in an advance line T-1359-6-15 F6 (44.90 μM/g FW). Whereas, in medium category three advance lines were grouped ranging from 85.93 to 103.74 μM/g FW, respectively.

Among sixteen indeterminate tomato lines tested for fruit MDA content, the lowest value was observed in Pakit (29.41 μM/g FW). Whereas the highest value was observed in an indeterminate line, West Virginia-63 (181.93 μM/g FW). The two semi-determinate line tested showed medium and high values for tomato fruit MDA content, AVTO1311 showed a value of 108.38 μM/g FW, whereas AVTO1315 exhibited a value of 192.77 μM/g FW, respectively.

Total oxidant status

Out of forty tomato hybrids tested for fruit total oxidant status (TOS) nineteen were classified into a low category with the mean values ranging from 100 to 2775 μM/g FW respectively (Figure 7). The lowest value for determinate tomato was observed in a local hybrid, NBH-260 (100 μM/g FW). In the intermediate category eleven hybrids were grouped with their mean values ranging from 3250 to 9525 μM/g FW. Ten tested hybrids were categorized in high category with their mean values ranging from 10050 to 15875 μM/g FW. The highest value of TOS for determinate tomato was observed in a local hybrid, NBH-259 (15875 μM/g FW).

Twenty-four tomato parents involved in the study showed significant variation for fruit TOS. In the low category for fruit TOS nine parents were grouped with their mean values ranging from 325 to 1875 μM/g FW. The lowest value for determinate tomato was observed in the parent line, LBR-10 (325 μM/g FW). In the medium category, eight parents were grouped with their mean values ranging from 3300 to 7750 μM/g FW. In the high category, seven parents were grouped with their mean values ranging from 10600 to 15925 μM/g FW. The highest value for fruit TOS among determinate tomatoes was observed in a parent line, B-25 (15925 μM/g FW).

Twenty-four tomato lines tested for fruit TOS, seven were categorized in the low category with the mean values ranging from 375 to 2950 μM/g FW. Among the determinate tomato lines lowest value for TOS was observed in a line 21354 (1000 μM/g FW). In the medium category for fruit TOS eight tomato lines were grouped with the mean value ranging from 3600 to 6300 μM/g FW. In the high category for tomato fruit TOS nine tomato lines were grouped with their mean values ranging from 10875 to 16950 μM/g FW. The highest value for determinate tomato was observed in a line B-L-35 (16950 μM/g FW).

Tomato advance lines showed low and high values for fruit TOS. In the low category four tomato advance lines were placed ranging from 225 to 2475 μM/g FW. The lowest value was observed in MIL-13-F4 (225 μM/g FW). The highest value of 10975 μM/g FW was observed in the advance line CKD-8-15 -F6, respectively.

Among the indeterminate tomatoes, the lowest value of TOS was observed in a local hybrid, NBH-257 (325 μM/g FW). While the highest value for indeterminate tomato was observed in a local hybrid Sundar F1 (13450 μM/g FW). The semi-determinate lines showed low and medium values for fruit TOS. Semi-determinate line AVTO1311 showed a low value of 1975 μM/g FW, whereas AVTO1315 showed a low value of 6300 μM/g FW, respectively.

Total antioxidant capacity

Forty tomato hybrids evaluated for their fruit total antioxidant capacity (TAC) values showed significant variation. Fourteen hybrids showed low TAC values ranging from 3.57 to 7.98 μM/g FW (Figure 7). The lowest value for determinate tomato was observed in NBH-235 (3.62μM/g FW). In the medium category twenty-three hybrids were grouped ranging from 8.03 to 10.94 μM/g FW. Total three hybrids were grouped into high category ranging from 11.35 to 11.59 μM/g FW. The highest mean value for determinate tomato was observed in a local determinate hybrid, NBH-263 (11.59 μM/g FW).

Tomato parent genotypes showed medium and high values for fruit TAC. In the medium category seventeen out a of total twenty-four parents were grouped with their mean values ranging from 7.14 to 10.37 μM/g FW. The remaining seven tomato parents were placed in the high category ranging from 11.35 to 12.90 μM/g FW. The highest mean value of TAC for determinate tomato was observed in a parent tomato line, LBR-7 (12.90 μM/g FW).

Tomato lines showed significant variation for fruit TAC values. In the low category four out of twenty-four lines were grouped with their mean values ranging from 4.06 to 7.31 µM/g FW. The lowest value for determinate tomato was observed in an exotic line B-L-35 (4.06 µM/g FW). Seventeen lines were grouped in medium category ranging from 8.12 to10.84 µM/g FW. In the high category three lines were grouped with their fruit TAC values ranging from 11.21 to 12.80 µM/g FW. The highest value for determinate tomato was observed in an exotic line CLN2768 (12.80 µM/g FW) respectively.

Tomato advance lines tested for fruit TAC exhibited low and medium values. In the low category, two advance lines were grouped with the lowest value observed in MIL-10-F4 (7.74 µM/g FW). Three advance lines were grouped in medium category ranging from 8.57 to 9.54 µM/g FW.

Among indeterminate tomatoes genotypes tested for fruit TAC, the lowest value was observed in NBH-257 (3.57 µM/g FW), whereas the highest TAC value was observed in an exotic indeterminate line, West Virginia-63 (12.48 µM/g FW). The semi-determinate tomato lines tested for their fruit TAC showed medium values i.e., AVTO1315 showed a value of 9.06 µM/g FW, whereas AVTO1311 showed a value of 9.50 µM/g FW.

Principal component analysis

Principal component analysis was performed to minimize the dimensionality of datasets in an interpretable manner while preserving all the possible variability among the tested genotypes for studied parameters. The eigenvalue determines an important principal component for further investigation. The principal component with eigen value more than 1 represents about 10% of the total variation (Brejda et al., 2000). Data was subjected to principal component analysis (PCA). Eigen value >1 was the best indicator of the system traits in principal components (Kumar et al., 2019). Scree plot (Figure 8) exhibited that, out of total 21 principal components eight (PC-I, PC-II, PC-III, PC-IV, PC-V, PC-VI, and PC-VII) had Eigenvalues > 1 and carried 69.81% of the total cumulative variability. PC-I and PC-II together with cumulative variability of 31.13%, were the largest contributors to the total cumulative variability in the genetic resource. PC-I, PC-II, PC-III, PC-IV, PC-V contributed 50% to the total cumulative variability and PC-I was the major component which explained maximum variation (18.56%) (Table S1).

By plotting the PC-I scores (x-axis) against PC-II scores (y-axis), a genotype by trait (G-T) biplot was generated for all the genotypes and their traits (Figure 9). A multiple traits visual comparison among the genotypes and the interrelationship between the traits was effectively revealed in the genotype by trait (G-T) biplot. Important information was extracted from the angles between the vectors and the distance of the variables from the origin of the biplot. The angle of the vector with principal component axis determined its contribution to that PC. The more parallel is a vector to the principal component axis the more it contributed to that specific PC. In the correlation circle, vector length represented the representativeness quality in the investigated PCA dimensions. Correlation between the two traits was considered positive, if the angle between these traits was less than 90, whereas correlation was considered negative if the angle between the two vector traits was greater than 90. The right angle between the traits represented that the traits were independent of each other *(*Shah et al., 2020*)*. Considering the angle between the vectors and principal component axis a positive correlation was observed between total chlorophyll, lycopene, total carotenoids, chlorophyll b and chlorophyll a. Moreover, total chlorophyll, total carotenoids, lycopene, chlorophyll b and chlorophyll a exhibited positive factor loading 0.477, 0.450, 0.450, 0.380, 0.351 with positive contribution to PC-I (Table S1). Whereas TSS, RS, MDA, ascorbic acid, chlorophyll b and POD with factor loading 0.512, 0.504, 0.311, 0.253, 0.208 and 0.153 showed positive correlation and had greater contribution to PC-II. NRS, SOD, POD and chlorophyll b with factor loading 0.415, 0.412, 0.241 and 0.207 showed positive contribution to PC-III. Among the individual category of tomato genotypes (hybrids,

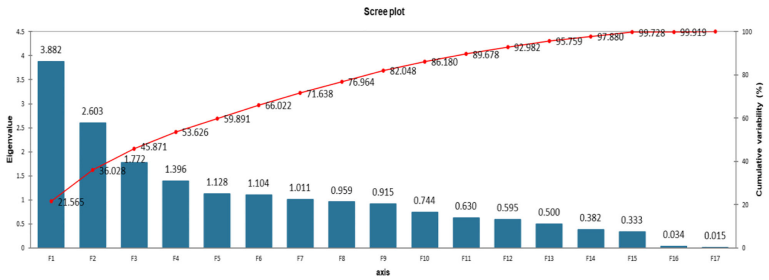

FIGURE 8
Scree plot **(A)** representing eigenvalue and cumulative variability for parameter under investigation.

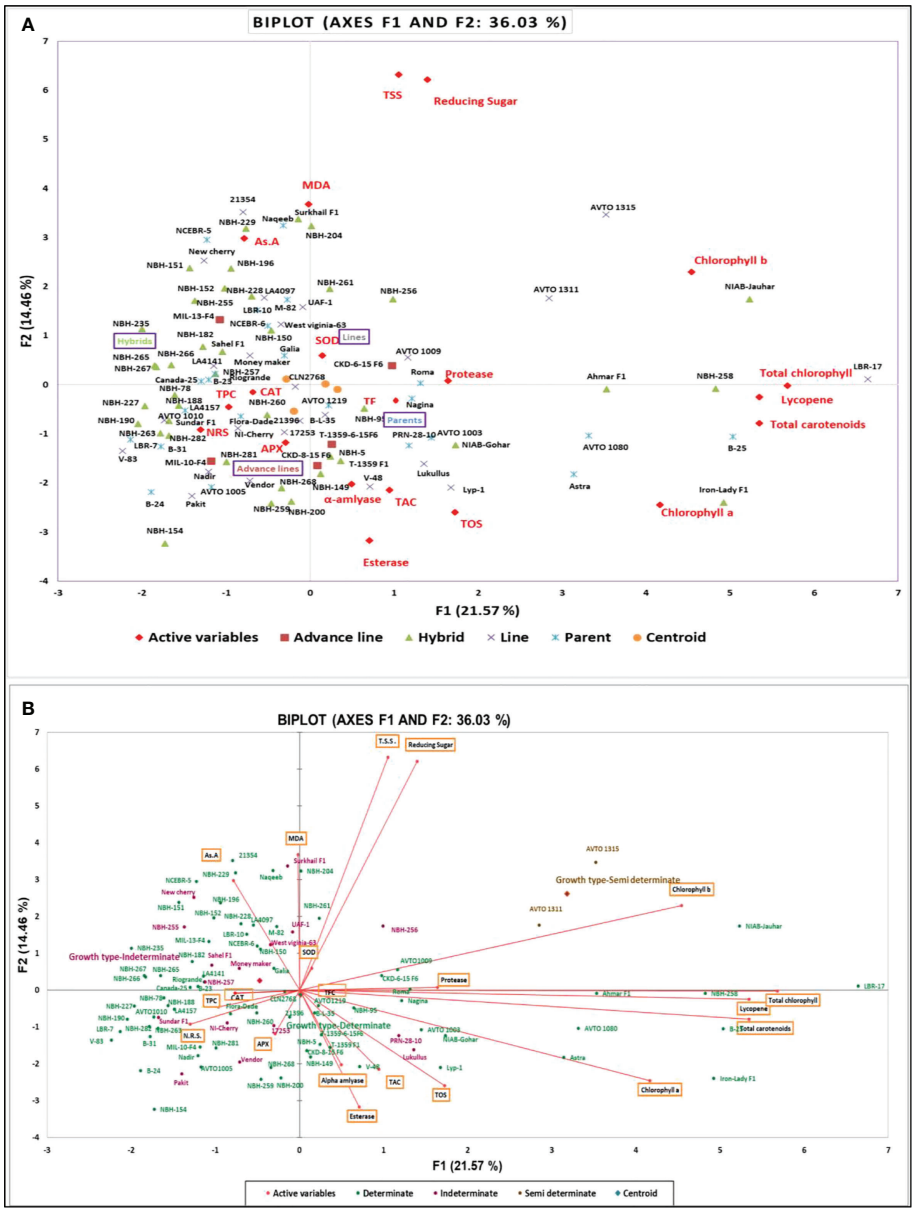

FIGURE 9
Biplot of the tomato genotypes for first two principal components **(A)** representing centroids of categories hybrid, parents, lines and advance line, and **(B)** representing centroids for growth habit determinate, indeterminate and semi-determinate.

parents, lines and advance lines), the parents and the lines had factor scores 0.325 and 0.186 in PC-I, whereas the hybrids had factor score 0.114 in PC-II. Moreover, categories of tomato genotypes based on the growth habit revealed that semi-determinate and determinate tomato genotypes had the factor scores 3.184 and 0.015, whereas semi-determinate and indeterminate tomato with factor scores 0.252 and 2.612 exhibited greater influence on the traits having significant contribution in PC-II respectively.

Correlation analysis

Correlation (Pearson test) for all investigated biochemical traits was performed with 95% confidence interval. Lycopene showed a significant positive correlation with chlorophyll a, chlorophyll b, total carotenoids and total chlorophyll (Table S3). Whereas chlorophyll a showed a significant positive correlation with Total antioxidant capacity (TAC), esterase, total oxidant status (TOS), total chlorophyll and total

carotenoids and significant negative correlation with non-reducing sugars. Chlorophyll b showed a significant positive correlation with total chlorophyll, total carotenoids, reducing sugar and total soluble sugars. Whereas the total carotenoids exhibited significant positive correlation with total chlorophyll and TOS. A significant positive correlation was observed between total chlorophyll, protease, and TOS. Total soluble sugars (TSS), ascorbic acid (ASA) and malondialdehyde (MDA) showed a significant positive correlation with reducing sugars and significant negative correlation with non-reducing sugars. TSS exhibited significant positive correlation with MDA. Moreover, non-reducing sugars represented significant positive correlation with the superoxide dismutase (SOD). Alpha-amylase showed a significant positive correlation with protease. Whereas AsA showed significant positive correlation with MDA and significant negative correlation with protease. MDA showed a significant negative correlation with TOS. Esterase exhibited a significant positive correlation with TAC and significant negative correlation with SOD respectively.

Discussion

Tomato (*Solanum lycopersicum* L.) is a rich source of nutrients, antioxidants and bioactive compounds (Salehi et al., 2019; Ali et al., 2021). These nutrients helps accomplish numerous body functions such as lipid profile maintenance, blood circulation stimulation and detoxification of bone structure (Campestrini et al., 2019; Vats et al., 2020). A direct relationship was found between tomato fruit intake and its anticancer activity (Wargovich, 2000). The presence of high concentrations of natural antioxidant in tomato fruit plays significant role in inhibiting reactive oxygen species (ROS) by free radicals scavenging, prevents cellular proliferation and apoptosis, plays role in enzymatic activities modulation and signal transduction pathways (Agarwal and Rao, 2000; Hossen et al., 2017; Navarro-González et al., 2018). The present study aims to evaluate the comprehensive nutritional and antioxidant potential of the tomato fruit. Different biochemical assays were performed to find nutritionally rich genotypes that can be further manipulated in crop improvement programs.

Tomato offers a key dietary source of carotenoids including lycopene and β-carotene (Manoharan et al., 2017). Lycopene is considered a strong lipophilic antioxidant in tomatoes. It is the most important free radical scavenger of all carotenoids (Shi and Maguer, 2000). It has been reported to enhance glutathione levels and the overall activities of antioxidant enzymes. The antioxidant activity of lycopene can protect lipids, DNA and other macromolecules from damage (Anlar and Bacanli, 2020). Lycopene accounts for 80 to 95% of the total carotenoid content in tomatoes (Karniel et al., 2020). In the present study, comparatively 13% of the forty tomato hybrids and 6% of the other fifty-three genotypes showed high fruit lycopene content. Previously reported lycopene content in fresh tomato fruit ranged between 1.86–14.62 mg/100g which was in accordance with the present findings (Frusciante et al., 2007). In general, the highest lycopene content was found in a local developed determinate hybrid NIAB-Gohar. The increased lycopene content in the hybrid NIAB-Gohar compared with the parents (LBR-7 and Nagina) may be attributed to heterosis. Whereas heterosis is a commonly used natural biological phenomena in which heterozygotes with different genetic bases are produced between two or more parents by hybridization. Hybrids are superior to parents related to growth rate, yield, quality, viability and disease resistance (Hochholdinger and Hoecker, 2007). Heterosis is commonly utilized in plants including vegetables to enhance yield, stress tolerance, quality and nutritional properties (Wang et al., 2021; Yu et al., 2021; Zhang et al., 2021).

Carotenoids are a chief dietary reservoir of vitamin A, which is obtained from bioconversion of β-carotene retinol into pro-vitamin A (Tang, 2010). For total carotenoid content 13% of the forty hybrids and 9% of the remaining fifty-three genotypes exhibited high values. Generally, the maximum total carotenoid was observed in the hybrid local NIAB-Gohar exhibiting heterosis compared with the parents (Nagina and LBR-7). In a previous report the total carotenoid content in fresh tomato fruit varied between 3.87-18 mg/100 g which was in accordance the present study (Frusciante et al., 2007; Alda et al., 2009; Pal et al., 2018; Górecka et al., 2020). Notably present finding validates that the local hybrid NIAB-Gohar could be a potential source for improving tomato fruit lycopene and total carotenoid contents.

Carotenoids as a precursor of aroma compounds indirectly affect flavor, whereas chlorophylls play role in the production of sugar through photosynthesis. Carotenoid accumulation during ripening determines chlorophyll degradation together with the fruit color (Aono et al., 2021). Both these traits have been and will continue to be of great importance in plant breeding efforts (Manoharan et al., 2017). In the present investigation 8% of the hybrids and 6% of the remaining genotypes exhibited high total chlorophyll content. Among hybrids, NIAB-Jauhar showed the highest total chlorophyll content (194.74 μg/100g FW) which was higher than the better parents, (LBR-10, 84.71 μg/100g FW and Roma, 116.28 μg/100g FW) indicating hybrid vigor. The activities of domestication and improvement in the cultivated tomato has jeopardized flavor and nutritional quality parameters in tomato fruit. Recent emphasis on breeding strategies aims on flavor associated chemicals like acids, sugar and aroma compounds (Aono et al., 2021).

Ascorbic acid (AsA) is an important non-enzymatic antioxidant. It functions as an antioxidant by scavenging reactive oxygen species (Jameel et al., 2021). The high concentration of AsA content in tomatoes plays a fundamental role in different aspects related to plant life and human health (Di Matteo et al., 2010). Moreover, AsA also acts as plant growth modulator *via* hormone signaling (Khalid and Hameed, 2017). The human body is unable to make AsA by its own because its

biosynthesis is prevented at the final stage. Consequently, food crops containing a high level of AsA content are essential for human health (Davuluri et al., 2005; Hancock and Viola, 2005). In the present investigation AsA content was found higher in 15% of the forty tomato hybrids and 13% of the remaining fifty-three genotypes. The highest AsA content was found in a line 21396 (435.25 μg/g FW), which was in accordance with the previously reported AsA content in fresh tomato fruit i.e., 122 to 475 μg/g FW (Frusciante et al., 2007; Di Matteo et al., 2010; Pal et al., 2018). Whereas, among hybrids the highest AsA was observed in a local determinate hybrid NBH-152 (400.75 μg/g FW), which was higher than both the parents AVTO1005 and Naqeeb (343.75 and 371.25 μg/g FW) showing heterosis. Currently, in different crops hybrids are cultivated globally owing to their superior performances and adaptability to various environments compared with inbred. Heterosis can be exploited to improve fruit nutritional composition in tomato (Fortuny et al., 2021).

Flavonoids are the major naturally occurring phenols (Evans, 2009). In the present investigation, generally 15% of the forty hybrids and 13% of the other fifty-three genotypes showed high total flavonoid content (TFC). Notably in the case of two local indeterminate cherry tomato UAF-1 (4009.19 μg/100 g FW) and NI-Cherry (2487.94 μg/100 g FW) TFC was found maximum. In the previous study, TFC in fresh tomato fruit was reported to vary between 1150 to 8160 μg/100 g FW (Dewanto et al., 2002; Martínez-Valverde et al., 2002; Raffo et al., 2002; Dumas et al., 2003; Raffo et al., 2006; Frusciante et al., 2007) which validates the present finding. Generally, the Total phenolic compounds (TPC) in 3% of the hybrids and 11% of the remaining genotypes was found higher. Notably again the two cherry tomatoes NI-Cherry (14100 μM/g FW) and 17253 (13275 μM/g FW) were included in high category for TPC (George et al., 2004). In a previous study it was found that the TPC in the pulp of three cherry tomato cultivars to be higher than other larger fruit tomato varieties (George et al., 2004). Moreover, another finding explained that the higher amount of TPC in cherry tomatoes compared to cultivars with larger fruits is mainly due to the higher skin to volume ratio of cherry varieties, which could improve their phenolic content especially flavonols, as these compounds occur inside the skin of the fruit (Stewart et al., 2000). In a previous report, TPC in tomato fruit varied between 37 to 86 mg GAE 100/g FW (Delgado-Vargas et al., 2018), whereas in another report the TPC of tomatoes was estimated between 267.18 and 775.04 mg GAE/kg FW (Park et al., 2020). Although various studies have described the phenolic content in tomatoes however comparison of findings is not feasible in most of the cases because of diverse methods of extraction as well as various solvents and evaluating techniques have been used.

Plant develops several ROS-scavenging mechanism to counter adverse impacts of ROS accumlation and to establish appropriate ROS homeostasis. Antioxidant enzymes such as superoxide dismutase (SOD), peroxidase (POD), ascorbate peroxidase (APX) and catalase (CAT) plays a vital role in ROS scavenging and maintain homestasis in fruit and plants (Apel and Hirt, 2004; Vall-Llaura et al., 2022). ROS apart from being considered a toxic by-product, also plays significant role as a signaling molecule in various biological processes including fruit development, ripening and responses to various abiotic and biotic stresses (Fichman and Mittler, 2020). Superoxide dismutase (SOD) is a vital primary enzyme that removes superoxide radicles, transforming them into hydrogen peroxide and dioxygen. In the present study, comparatively 2% of the forty hybrid tomatoes and 8% of the other fifty-three genotypes divulged high SOD activity. Generally the highest activity was observed in a cherry tomatoes UAF-1 (335.54 U/g FW) and among hybrids the highest value was observed in Sahel F1 (294.46 U/g FW) which was in accordance with the previously reported SOD activity in tomato fruit (Gautier et al., 2010). Ascorbate peroxidase (APX) reduces hydrogen peroxide by using ascorbate as the electron donor and regulates the accumulation of toxic level of hydrogen peroxide under stress conditions (Salandanan et al., 2009). In the present investigation, comparatively 23% of the forty tomato hybrids and 9% of the other fifty-three genotypes showed high APX activity. In general, maximum APX activity was detected in a local determinate line, B-L-35 (1860 U/g FW) and among hybrids, NBH-149 showed the maximum activity (1520 U/g FW) which was found to be greater than both the parents NCEBR-5 and AVTO1219 (420 and 480 U/g FW), that could be attributed to heterosis. The APX activity at the red ripe stage of tomato fruit was reported between 200 to 1200 (μmol min-1 g-1 FW) respectively (Gautier et al., 2010). Catalase (CAT) catalyzes hydrogen peroxide dismutation in oxygen and water (Rani et al., 2004; Ortega-Ortiz et al., 2007). In the present research, comparatively 23% of the forty tomato hybrids and 30% of the remaining genotypes showed high CAT activity, whereas maximum activity was observed for a line CLN2768 (1045 U/g FW) and again hybrid vigor was observed in the hybrid NBH-229 (930 U/g FW) for CAT activity compared with the better parents (Naqeeb 220 U/g FW and AVTO1080 770 U/g FW). In a previous report, a medicinal plant *Peganum harmala* used in the treatment of various diseases such as diabetes, depression, cough, and some other human ailment divulged lower catalase activity (555 U/g) (Ahmed et al., 2020) compared with the present finding. Peroxidase (POD) contributes to phenol oxidation, hormone catabolism, lignin polymerization, cell wall, proteins and polysaccharides intercrossing, defense against pathogens and fruit ripening. In fruit ripening, and mainly during climacterium POD is increased along with the cellulase enzymes and polygalacturonase (Robinson and Eskin, 1991; Ortega-Ortiz et al., 2007). In the present study, comparatively 5% of the hybrid tomatoes and 9% of the remaining fifty-three genotypes exhibited high POD activity. In general, the highest POD activity was observed for an indeterminate exotic line West Virginia-63 (7592.40 U/g FW),

and a local determinate hybrid NBH-95 (6496.50 U/g FW) respectively. The high value of POD activity for hybrid NBH-95 compared with the parent Naqeeb and M-82 (and 599.40 and 699.30 U/g FW) could be attributed to heterosis.

Different enzymes present in the tomato pulp, plays a significant part in the nutrient turnover in tomato pulp at various maturity stages. Previously it has been reported that hydrolytic and proteolytic enzymes perform some physiological functions during maturation and fruit senescence (Desai and Deshpande, 1978; Hashinaga et al., 1983). Hydrolytic enzymes such as alpha-amylase, esterase and protease in living organisms specifically break up larger molecules into smaller molecule by the process of hydrolysis, a water molecule is added to a substance during the process (Wong et al., 2020). Hydrolytic enzymes also behave as a secondary source of antioxidant by utilizing damaged molecules and repairing DNA (Pradedova et al., 2011). Amylase enzyme hydrolysis starch to obtain monomeric carbohydrates. Starch degradation occurs during cereal seed germination. Hydrolytic enzymes are responsible for the breakdown, it is generally believed that phosphorylases are not involved in this activity, whereas α-amylase performs a significant role during the breakdown of local starch granules (Perata et al., 1992). Alpha-amylase help catalyzes hydrolysis of 4-glycosidic linkages, together with internal a-1 in starch to obtain products such as maltose and glucose. The enzyme can be obtained from plants, animals, and microorganisms (Sundarram and Murthy, 2014). In general, 13% of the tomato hybrids and 21% of the remaining genotypes explicated high alpha-amylase activity. The maximum alpha-amylase activity was observed in an indeterminate parent PRN-28-10 (243.01 mg/g FW), which was relatively higher than the alpha-amylase activity (164.90 mg/g dry wt.) found in a medicinal plant, T. simplex (Ahmed et al., 2020), and fairly lower than the alpha-amylase activity (292.70 mg/g s. wt.) of wheat flour (Khalid and Hameed, 2017). Among hybrid NBH-268 (238.11 mg/g FW) showed maximum alpha-amylase activity, which was higher than better parents (Riogrande, 74.52 mg/g FW and AVTO1003, 210.75 mg/g FW) that can be ascribed to hybrid vigor. To utilize carbon and energy present in the starch polymer it must be degraded to smaller digestible sugars prior to its conversion into individual glucose unit (Alam et al., 2006). In different stages of plant life cycle, proteases play a vital role in the overall procedure of protein turnover (Rani et al., 2012). Proteases being a protein hydrolytic enzymes, act upon proteinaceous substance present in the cell wall delivering amides and amino acids (Alam et al., 2006). In the present study 5% of the tomato hybrids and 6% of the remaining genotypes revealed high protease activity. Generally, the highest activity was observed in a local hybrid NBH-150 and determinate line AVTO1080 (8525 U/g FW) respectively. Hybrid NBH-150 showed protease activity higher than the better parent NCEBR-5 (7005 U/g FW) that could be accredited to hybrid vigor. According to previous studies, during ripening protease activity increases in kiwi and tomato fruit (Hashinaga et al., 1983; Alam et al., 2006). Increased protease activity during maturation has also been detected in passion fruit juice (Hashinaga et al., 1978). High protease activity in the ripening stage may be ascribed to protein catabolism which is connected to leaf senescence (Dilley, 1970). The present investigation validates higher protease activity in tomato fruit at the red ripe stage. Esterases are found in a variety of living organisms and have the capacity to catalyze the synthesis of ester bond and their hydrolysis from different substrates (Zhong et al., 2020). In the present study, 23% of the tomato hybrids and 21% of the remaining genotypes showed maximum esterase activity. In general, the highest activity was observed in a local hybrid NBH-154 (50.15 μM/min/g FW) respectively which was relatively higher than the previously reported esterase activity of 14.30 mg/g in a medicinal plant, *Zygophyllum fabago* (Ahmed et al., 2020).

Sugars accounts for an essential component of tomato fruit, as they regulate sweetness and flavor. High sugars are needed for the best flavor. Tomato fruit contains mainly glucose and fructose, whereas sucrose is present in the trace amount (Tadesse et al., 2012). Fructose and glucose accounts for about 65% of total soluble solid in tomato fruit (Turhan and Şeniz, 2009). Different genotypes under investigation showed significant variation in their sugar content. In general, 25% of the hybrid tomatoes and 23% of the remaining genotypes showed high Total soluble sugars (TSS). The highest TSS content was observed for a determinate parent NCEBR-5 (77.15 mg/g FW) and among hybrids NBH-229 (73.00 mg/g FW) showed highest total TSS. Previously reported TSS content in fresh tomato fruit ranged between 1.7% to 4.7% (17 to 47 mg/g FW) respectively (Melkamu et al., 2008; Turhan and Şeniz, 2009; Tadesse et al., 2012), which was fairly lower than the TSS content in the highest category of the present investigation. The low and medium categories of the present finding were in accordance with the previously reported TSS content of 1.4 to 5% (14 – 50 g/g FW) in tomato fruit (Dai et al., 2016) respectively.

Reducing sugars (RS) in tomato contributes to the sweet taste, whereas total sugars exhibits a significant fraction of fruit dry weight and are influenced by seasons and variety (Tadesse et al., 2012). Present investigation explicated that comparatively 15% of the forty tomato hybrids and 13% of the remaining genotypes showed high RS content, whereas the highest RS content was observed for a semi-determinate AVRDC line AVTO1311 (71.26 mg/g) and among hybrids NBH-299 (70.98 mg/g FW) showed hybrid vigor compared with parents (AVTO1080, 39.05 mg/g FW and Naqeeb, 65.81 mg/g FW). Reducing sugars (RS) content in fresh tomato fruit was reported to be 1.1 to 4.1% (11-41 mg/g) which was relatively lower than the RS content in the highest category (60 to 72 mg/g FW) of the present investigation, while RS content in the low and medium category (20- 59 mg/g FW) of the present study validates the previous report (Ereifej et al., 1997; Tadesse et al., 2012). In

general, 25% of the forty tomato hybrids and 19% of the remaining fifty three genotypes showed high values for non reducing sugars (NRS) content. The highest value was observed for a determinate hybrid NBH 265 (21.39 mg/g) showed a value greater than the better parent (AVTO1003, 8.59 mg/g FW and NCEBR-5, 8.69 mg/g FW). The NRS content in low and medium categories (1.1 to 14.4 mg/g FW) of the present study confirmed the previous findings whereas non reducing sugar (NRS) content for tomato fruit was detected to vary between 0.11 to 14 mg/g respectively (Ereifej et al., 1997; Tadesse et al., 2012).

Malondialdehyde (MDA) content is usually used as a lipid peroxidation marker and is mainly utilized as a sign of damage to the plant membranes (Morales and Munné-Bosch, 2019). In general, 15% of the tomato hybrids and 11% of the remaining genotypes showed high MDA content. The highest MDA content was in the local determinate hybrid NBH-182 (267.87 μM/g FW), and this high value could be ascribed to heterosis. MDA can play a significant positive role in the acclimation process rather than damage by activation of regulatory genes associated with the plant defense system (Tounekti et al., 2011).

The total antioxidant status (TAS) is used to estimate the overall antioxidant capacity in an organism (Sevindik, 2018), whereas the total oxidant status (TOS) is used to estimate the overall oxidation state of the living organism (Vaiserman et al., 2020). According to the present investigation 25% of the tomato hybrids and 32% of the remaining genotypes showed high total oxidant status (TOS). In general, the highest TOS was observed in a determinate line B-L-35 (16950 μM/g FW) and determinate hybrid NBH-259 (15875 μM/g FW). The hybrid showed TOS higher than both parents B-23 and AVTO1005 (775 and 15100 μM/g FW). The TOS level of tomato genotypes was higher than the TOS reported in Asteraceae (3020 μM/L) and Lamiaceae (5260 mM/L) families (Caf et al., 2018). According to a previous report there was a progressive enhancement in oxidative stresses throughout fruit development. Moreover, during the early period of fruit ripening, the antioxidant system is efficient to protect tomato fruit from progressive oxidative damages. But at later stages the ROS scavenging system is not effective enough to manage the production system resulting in ROS accumulation (Mondal et al., 2004). The high TOS value for the tomato fruit could be because of its red ripe stage. In the present study, the free radical scavenging activity was divulged in the form of inhibition of free radical ABTS. Comparatively 8% of the hybrid tomatoes and 19% of the other fifty-three genotypes showed maximum TAC. Generally, the maximum TAC was observed in a parent line LBR-7 (12.90 μM/g FW) and among hybrids in NBH-263 (11.59 μM/g FW), which was higher than the parents AVTO1080 and B-24 (8.81 and 10.17 μM/g FW) that could be attributed to heterosis. The TAC of the tomato genotypes in the present investigation was found to be relatively lower than the previously reported tomato fruit TAC (14-27 μmol g−1) (Sahlin et al., 2004). However it was quite higher than the TAC (0.48 -1.18 μmol/g−1 and 0.054 – 0.209 μmol 100 g−1) of tomato fruit reported in another study (Zhou and Yu, 2006; Erge and Karadeniz, 2011).

To simplify the explanation of a larger amount of data and to obtain significant information from the data set, a multivariant statistical method called Principal Component Analysis (PCA) is applied (Rathinavel, 2018). PCA explained the significance of the main contributor to the total variation at the differentiation axis. Eigenvalues helps in interpreting the important factor which can be taken. The numerical closer to unity in PC- I having the largest absolute value influence the grouping considerably more, in contrast to the ones with smaller absolute values that are closer to zero (Bhanupriya et al., 2014; Mishra et al., 2015). In the present study, PCA was launched for all variables to understand the pattern of variation. Out of twenty-one principal components, total eight principal components with eigenvalues >1 elucidated 69.81% of the total variation. PC-I, PCII, PC-III, PC-IV, PC-V, PC-VI, and PC-VII revealed 18.56, 12.58, 8.74, 7.46, 6.54, 5.61, 5.33, and 4.99% variability, respectively (Table S1). The traits like total chlorophyll, lycopene, total carotenoids, chlorophyll a, chlorophyll b, α amylase, TAC, protease, esterase, TOS, SOD and TFC showed considerable positive contribution in PC- I with positive factor loadings. On the basis of individual loading, a single variable is normally selected from these recognized groups (Mishra et al., 2015). Total chlorophyll showed the highest factor loading (0.941), followed by total carotenoids (0.889), and lycopene (0.888). Total chlorophyll could be the finest choice with the highest contribution in PC-I, whereas Chlorophyll b, total chlorophyll, RS, TSS, AsA, MDA, protease, SOD, POD exhibited considerable positive contribution in PC- II. So, PC- II was related to diversity among genotypes due to TSS (0.832) and RS (0.819) with their positive influence (Figure 9). Distance of the genotype from biplot origin estimated genotypic differences relating to the grand mean, thus distances of the genotypes from the origin can be a good indicator of genotypes with superior and inferior performance in the environment. The genotypes found away from the biplot's origin can be a good performers (Hagos and Abay, 2013) and the genotypes nearer to a particular trait show best performance related to the corresponding trait. The correlation analysis further confirmed the PCA results by exhibiting strong positive and strong negative association between the traits that are closer and far from each other in the PC axis (Table S3). In general parents and lines showed a positive contribution in PC- I and the hybrids showed positive contribution in PC- II with positive factor scores (Table S2). Therefore, parents and lines could be a potential source for traits like lycopene, chlorophylls, total carotenoids, alpha-amylase, TAC, protease, esterase, TOS and TFC, whereas hybrids could be a potential source for the traits such as total soluble sugars, reducing sugars, MDA, ascorbic acid, chlorophyll b, POD and SOD, respectively. Moreover, semi-determinate and determinate tomato genotypes showed positive factor score in PC-I, thus the

genotypes with semi-determinate and determinate growth habits could be a potential source for the above-mentioned traits with greater influence in PC-I, while the semi-determinate and indeterminate tomato genotypes showed significant contribution to the trait performing superior in PC- II. More specifically the hybrids NIAB-Jauhar, Iron-lady F1, NBH-258, Ahmar F1 and NIAB-Gohar, the parents H-24, B-25, AVTO1080, and Astra as well as the lines LBR-17, AVTO1315, AVTO1311 and Lyp-1 found far away from biplot origin with positive factor score in PC-I. Consequently, these genotypes could be a potential source for the traits with better performance in PC-I (Table S2). Whereas the hybrids Surkhail F1, NBH-204, NBH-229, NBH-151, NBH-196, NBH-152, NBH-261, NBH-228, NIAB-Jauhar, NBH-256, NBH-255, the lines 21354, AVTO1315, Newcherry, LA4097, AVTO1311 and UAF-1 together with the parents Naqeeb, NCEBR-5, M-82 and LBR-10 were found far away from biplot origin with positive factor score in PC- II. Hence, the above-mentioned genotypes could be a finest choice for the traits with positive influence in PC- II, respectively. Present results demonstrates that principal component analysis along with genetic resource characterization help indicate traits of interest for scheming breeding strategies.

Conclusion

The present finding concludes that tomato genotypes including hybrids, parents and lines have prominent antioxidant potential and bioactive compounds. For the investigated traits including pigment, hydrolytic enzymes, TOS, TAC and TFC it was found that determinate and semi-determinate tomatoes, category parents and lines and the following genotypes NIAB-Jauhar, Iron-lady F1, NBH-258, H-24, B-25, AVTO1080, Astra, LBR-17, AVTO1315, AVTO1311 and Lyp-1 showed an excellent potential. Moreover for the traits including sugars, AsA, MDA, POD and SOD the indeterminate and semi-determinate tomatoes, category hybrids and the following genotypes Surkhail F1, NBH-204, NBH-229, NBH-151, NBH-196, 21354, AVTO1315, Newcherry, LA4097, AVTO1311, UAF-1, Naqeeb, NCEBR-5, M-82 and LBR-10 exhibited an outstanding performance. Hybrids exhibited superior performance for the investigated traits compared with the parent. The identified growth types, categories and genotypes with superior activity for investigated traits, can be utilized in breeding programs to establish specific breeding strategies and to improve the desirable traits in tomatoes. Moreover, the identified genotypes with higher antioxidant potential and nutritionally rich bioactive compounds can be utilized as a source to improve human health and prevent various chronic degenerative diseases. Moreover, tomato genotypes can also be consumed directly as a natural source of antioxidants to improve endogenous immune system.

Data availability statement

The original contributions presented in the study are included in the article/Supplementary Material. Further inquiries can be directed to the corresponding author.

Author contributions

BR conducted the overall experiment, analytical work, data collection, data organization, result compilation, write-up, and revision of the manuscript. AH contributed to designing, and finalization of basic idea related to the experiment, overall supervision during wet lab work, data analysis using statistical software, revisions, and finalization of the manuscript. MS aided in providing the tomato germplasm and technical advice. All authors have significant contributions in improving the submitted article. All authors contributed to the article and approved the submitted version.

Funding

The research work was conducted by the support provided by Nuclear Institute for Agriculture and Biology, Jhang Road, Faisalabad Pakistan.

Conflict of interest

The authors declare that the research was conducted in the absence of any commercial or financial relationships that could be construed as a potential conflict of interest.

Publisher's note

Supplementary material

The Supplementary Material for this article can be found online at: https://www.frontiersin.org/articles/10.3389/fpls.2022.1035163/full#supplementary-material

References

Agarwal, S., and Rao, A. V. (2000). Tomato lycopene and its role in human health and chronic diseases. *Cmaj* 15, e0231612. doi: 10.1371/journal.pone.0231612

Ahmed, A., Hameed, A., and Saeed, S. (2020). Biochemical profile and bioactive potential of wild folk medicinal plants of zygophyllaceae from balochistan, Pakistan. *bioRxiv*. doi: 10.1101/2020.03.30.016212

Ainsworth, E. A., and Gillespie, K. M. (2007). Estimation of total phenolic content and other oxidation substrates in plant tissues using folin–ciocalteu reagent. *Nat. Protoc.* 2, 875–877. doi: 10.1038/nprot.2007.102

Alam, M., Rahman, M. H., Mamun, M., Ahmad, I., and Islam, K. (2006). Enzyme activities in relation to sugar accumulation in tomato. *Proceedings Pakistan Acad. Sci.* 43, 241.

Alda, L. M., Gogoasa, I., Bordean, D.-M., Gergen, I., Alda, S., Moldovan, C., et al. (2009). Lycopene content of tomatoes and tomato products. *J. Agroaliment. Processes Technol.* 15, 540–542.

Ali, M. Y., Sina, A., Khandker, S. S., Neesa, L., Tanvir, E., Kabir, A., et al. (2021). Nutritional composition and bioactive compounds in tomatoes and their impact on human health and disease: A review. *Foods* 10, 45. doi: 10.3390/foods10010045

Anlar, H. G., and Bacanli, M. (2020). "Lycopene as an antioxidant in human health and diseases,". *Pathology*, 247–254. doi: 10.1016/B978-0-12-815972-9.00024-X

Anza, M., Riga, P., and Garbisu, C. (2006). Effects of variety and growth season on the organoleptic and nutritional quality of hydroponically grown tomato. *J. Food Qual.* 29, 16–37. doi: 10.1111/j.1745-4557.2006.00053.x

Aono, Y., Asikin, Y., Wang, N., Tieman, D., Klee, H., and Kusano, M. (2021). High-throughput chlorophyll and carotenoid profiling reveals positive associations with sugar and apocarotenoid volatile content in fruits of tomato varieties in modern and wild accessions. *Metabolites* 11, 398. doi: 10.3390/metabo11060398

Apel, K., and Hirt, H. (2004). Reactive oxygen species: metabolism, oxidative stress, and signal transduction. *Annu. Rev. Plant Biol.* 55, 373–399. doi: 10.1146/annurev.arplant.55.031903.141701

Asensio, E., Sanvicente, I., Mallor, C., and Menal-Puey, S. (2019). Spanish Traditional tomato. effects of genotype, location and agronomic conditions on the nutritional quality and evaluation of consumer preferences. *Food Chem.* 270, 452–458. doi: 10.1016/j.foodchem.2018.07.131

Beecher, G. R. (1998). Nutrient content of tomatoes and tomato products. *Proc. Soc. Exp. Biol. Med.* 218, 98–100. doi: 10.3181/00379727-218-44282a

Beers, R. F., and Sizer, I. W. (1952). A spectrophotometric method for measuring the breakdown of hydrogen peroxide by catalase. *J. Biol. Chem.* 195, 133–140. doi: 10.1016/S0021-9258(19)50881-X

Bhanupriya, B., Satyanarayana, N., Mukherjee, S., and Sarkar, K. (2014). Genetic diversity of wheat genotypes based on principal component analysis in gangetic alluvial soil of West Bengal. *J. Crop Weed* 10, 104–107.

Borguini, R. G., and Ferraz Da Silva Torres, E. A. (2009). Tomatoes and tomato products as dietary sources of antioxidants. *Food Rev. Int.* 25, 313–325. doi: 10.1080/87559120903155859

Brejda, J. J., Moorman, T. B., Karlen, D. L., and Dao, T. H. (2000). Identification of regional soil quality factors and indicators i. central and southern high plains. *Soil Sci. Soc. America J.* 64, 2115–2124. doi: 10.2136/sssaj2000.6462115x

Caf, F., Kiliç, Ö., and Algül, S. (2018). Evaluation of total antioxidant status, total oxidant status and oxidative stress index of some economically important plants from Turkey. *Prog. IN Nutr.* 20, 145–152. doi: 10.23751/pn.v20i1-S.6125

Campestrini, L. H., Melo, P. S., Peres, L. E., Calhelha, R. C., Ferreira, I. C., and Alencar, S. M. (2019). A new variety of purple tomato as a rich source of bioactive carotenoids and its potential health benefits. *Heliyon* 5, e02831. doi: 10.1016/j.heliyon.2019.e02831

Chance, B., and Maehly, A. (1957). *Methods in enzymol* Vol. 4. Eds. S. P. Colowick and N. O. Kaplan (New York: Academic Press, Inc.), 273.

Chen, G.-X., and Asada, K. (1989). Ascorbate peroxidase in tea leaves: occurrence of two isozymes and the differences in their enzymatic and molecular properties. *Plant Cell Physiol.* 30, 987–998. doi: 10.1093/oxfordjournals.pcp.a077844

Coyago-Cruz, E., Corell, M., Moriana, A., Mapelli-Brahm, P., Hernanz, D., Stinco, C. M., et al. (2019). Study of commercial quality parameters, sugars, phenolics, carotenoids and plastids in different tomato varieties. *Food Chem.* 277, 480–489. doi: 10.1016/j.foodchem.2018.10.139

Dai, Z., Wu, H., Baldazzi, V., Van Leeuwen, C., Bertin, N., Gautier, H., et al. (2016). Inter-species comparative analysis of components of soluble sugar concentration in fleshy fruits. *Front. Plant Sci.* 7, 649. doi: 10.3389/fpls.2016.00649

Davuluri, G. R., Van Tuinen, A., Fraser, P. D., Manfredonia, A., Newman, R., Burgess, D., et al. (2005). Fruit-specific RNAi-mediated suppression of DET1 enhances carotenoid and flavonoid content in tomatoes. *Nat. Biotechnol.* 23, 890–895. doi: 10.1038/nbt1108

Delgado-Vargas, F., Sicairos-Medina, L. Y., Luna-Mandujan, A. G., López-Angulo, G., Salazar-Salas, N. Y., Vega-García, M. O., et al. (2018). Phenolic profiles, antioxidant and antimutagenic activities of solanum lycopersicum var. cerasiforme accessions from Mexico. *CyTA Journal Food* 16, 715–722. doi: 10.1080/19476337.2018.1481146

Desai, B., and Deshpande, P. (1978). Effects of stage of maturity on some physical and biochemical constituents and enzyme activities of banana (Musa paradisiaca linn.) fruits. *Mysore J. Agric. Sci* 12, 193–201.

Dewanto, V., Wu, X., Adom, K. K., and Liu, R. H. (2002). Thermal processing enhances the nutritional value of tomatoes by increasing total antioxidant activity. *J. Agric. Food Chem.* 50, 3010–3014. doi: 10.1021/jf0115589

Dhindsa, R. S., Plumb-Dhindsa, P., and Thorpe, T. A. (1981). Leaf senescence: correlated with increased levels of membrane permeability and lipid peroxidation, and decreased levels of superoxide dismutase and catalase. *J. Exp. Bot.* 32, 93–101. doi: 10.1093/jxb/32.1.93

Dilley, D. (1970). Enzymes.(In) the biochemistry of fruits and their products. *Acad. Press London* 179, 179–207.

Di Mascio, P., Kaiser, S., and Sies, H. (1989). Lycopene as the most efficient biological carotenoid singlet oxygen quencher. *Arch. Biochem. Biophys.* 274, 532–538. doi: 10.1016/0003-9861(89)90467-0

Di Matteo, A., Sacco, A., Anacleria, M., Pezzotti, M., Delledonne, M., Ferrarini, A., et al. (2010). The ascorbic acid content of tomato fruits is associated with the expression of genes involved in pectin degradation. *BMC Plant Biol.* 10, 1–11. doi: 10.1186/1471-2229-10-163

Dixit, V., Pandey, V., and Shyam, R. (2001). Differential antioxidative responses to cadmium in roots and leaves of pea (Pisum sativum l. cv. azad). *J. Exp. Bot.* 52, 1101–1109. doi: 10.1093/jexbot/52.358.1101

Dogan, H., ErcİşlÎ, S., Temim, E., Hadziabulic, A., Tosun, M., Yilmaz, S., et al. (2014). Diversity of chemical content and biological activity in flower buds of a wide number of wild grown caper (Capparis ovata desf.) genotypes from Turkey. *Comptes Rendus L Academie Bulgare Des. Sci.* 67, 1593–1600.

Drapeau, G. R. (1976). "[38] protease from staphyloccus aureus," in *Methods in enzymology* (New York:Academic Press), 469–475.

Dubois, M., Gilles, K., Hamilton, J., Rebers, P., and Smith, F. (1951). A colorimetric method for the determination of sugars. *Nature* 168, 167–167. doi: 10.1038/168167a0

Dumas, Y., Dadomo, M., Di Lucca, G., and Grolier, P. (2003). Effects of environmental factors and agricultural techniques on antioxidantcontent of tomatoes. *J. Sci. Food Agric.* 83, 369–382. doi: 10.1002/jsfa.1370

Elbadrawy, E., and Sello, A. (2016). Evaluation of nutritional value and antioxidant activity of tomato peel extracts. *Arabian J. Chem.* 9, S1010–S1018. doi: 10.1016/j.arabjc.2011.11.011

Ereifej, K., Shibli, R., Ajlouni, M., and Hussain, A. (1997). Physico-chemical characteristics and processing quality of newly introduced seven tomato cultivars into Jordan in comparison with local variety. *J. Food Sci. Technol.* 34, 171–174.

Erel, O. (2004). A novel automated direct measurement method for total antioxidant capacity using a new generation, more stable ABTS radical cation. *Clin. Biochem.* 37, 277–285. doi: 10.1016/j.clinbiochem.2003.11.015

Erel, O. (2005). A new automated colorimetric method for measuring total oxidant status. *Clin. Biochem.* 38, 1103–1111. doi: 10.1016/j.clinbiochem.2005.08.008

Erge, H. S., and Karadeniz, F. (2011). Bioactive compounds and antioxidant activity of tomato cultivars. *Int. J. Food Properties* 14, 968–977. doi: 10.1080/10942910903506210

Evans, W. (2009). *Treaseosy. 16th Ed* (Edinburgh, London, New York, Philadelphia, St Louis, Sydney, Toronto: Saunders/Elsevier).

Fichman, Y., and Mittler, R. (2020). Rapid systemic signaling during abiotic and biotic stresses: is the ROS wave master of all trades? *Plant J.* 102, 887–896. doi: 10.1111/tpj.14685

Fortuny, A. P., Bueno, R. A., Pereira Da Costa, J. H., Zanor, M. I., and Rodríguez, G. R. (2021). Tomato fruit quality traits and metabolite content are affected by reciprocal crosses and heterosis. *J. Exp. Bot.* 72, 5407–5425. doi: 10.1093/jxb/erab222

Frusciante, L., Carli, P., Ercolano, M. R., Pernice, R., Di Matteo, A., Fogliano, V., et al. (2007). Antioxidant nutritional quality of tomato. *Mol. Nutr. Food Res.* 51, 609–617. doi: 10.1002/mnfr.200600158

García-Hernández, J., Hernández-Pérez, M., Peinado, I., Andrés, A., and Heredia, A. (2018). Tomato-antioxidants enhance viability of l. reuteri under gastrointestinal conditions while the probiotic negatively affects bioaccessibility of lycopene and phenols. *J. Funct. Foods* 43, 1–7. doi: 10.1016/j.jff.2017.12.052

Gautier, H., Lopez-Lauri, F., Massot, C., Murshed, R., Marty, I., Grasselly, D., et al. (2010). Impact of ripening and salinity on tomato fruit ascorbate content and enzymatic activities related to ascorbate recycling. *Funct. Plant Sci. Biotechnol.* 4, 66–75.

Gaweł, S., Wardas, M., Niedworok, E., and Wardas, P. (2004). Malondialdehyde (MDA) as a lipid peroxidation marker. *Wiadomosci lekarskie (Warsaw Poland: 1960)* 57, 453–455.

George, B., Kaur, C., Khurdiya, D., and Kapoor, H. (2004). Antioxidants in tomato (Lycopersium esculentum) as a function of genotype. *Food Chem.* 84, 45–51. doi: 10.1016/S0308-8146(03)00165-1

Giannopolitis, C. N., and Ries, S. K. (1977). Superoxide dismutases: I. occurrence in higher plants. *Plant Physiol.* 59, 309–314. doi: 10.1104/pp.59.2.309

Górecka, D., Wawrzyniak, A., Jędrusek-Golińska, A., Dziedzic, K., Hamułka, J., Kowalczewski, P. Ł., et al. (2020). Lycopene in tomatoes and tomato products. *Open Chem.* 18, 752–756. doi: 10.1515/chem-2020-0050

Grygorieva, O., Klymenko, S., Kuklina, A., Vinogradova, Y., Vergun, O., Sedlackova, V. H., et al. (2021). Evaluation of lonicera caerulea l. genotypes based on morphological characteristics offruits germplasm collection. *Turkish J. Agric. Forestry* 45, 850–860. doi: 10.3906/tar-2002-14

Hagos, H. G., and Abay, F. (2013). AMMI and GGE biplot analysis of bread wheat genotypes in the northern part of Ethiopia. *J. Plant Breed. Genet.* 1, 12–18.

Hameed, A., Iqbal, N., Malik, S. A., Syed, H., and Ahsanul-Haq, M. (2005). Age and organ specific accumulation of ascorbate in wheat (Triticum aestivum l.) seedlings grown under etiolation alone and in combination with oxidative stress. *Caderno de Pesquisa série Biologia* 17, 51–63

Hancock, R. D., and Viola, R. (2005). Improving the nutritional value of crops through enhancement of l-ascorbic acid (vitamin c) content: rationale and biotechnological opportunities. *J. Agric. Food Chem.* 53, 5248–5257. doi: 10.1021/jf0503863

Harma, M., Harma, M., and Erel, O. (2005). Oxidative stress in women with preeclampsia. *Am. J. Obstet. Gynecol.* 192, 656–657. doi: 10.1016/j.ajog.2004.07.094

Hashinaga, F., Sawa, D., and Itoo, S. (1978). Protease in the juice of passion fruit (Passiflora edulis sims). *J. Japanese Soc. Hortic. Sci.* 47, 282–288. doi: 10.2503/jjshs.47.282

Hashinaga, F., Yamato, F., and Itoo, S. (1983). Partial purification and characterization of protease from passion fruit juice *Mem. Fac. Agric. Kagoshima Univ.*

Heath, R. L., and Packer, L. (1968). Photoperoxidation in isolated chloroplasts: I. kinetics and stoichiometry of fatty acid peroxidation. *Arch. Biochem. Biophys.* 125, 189–198. doi: 10.1016/0003-9861(68)90654-1

Hochholdinger, F., and Hoecker, N. (2007). Towards the molecular basis of heterosis. *Trends Plant Sci.* 12, 427–432. doi: 10.1016/j.tplants.2007.08.005

Hossen, M. S., Ali, M. Y., Jahurul, M., Abdel-Daim, M. M., Gan, S. H., and Khalil, M. I. (2017). Beneficial roles of honey polyphenols against some human degenerative diseases: A review. *Pharmacol. Rep.* 69, 1194–1205. doi: 10.1016/j.pharep.2017.07.002

Huang, D., Ou, B., and Prior, R. L. (2005). The chemistry behind antioxidant capacity assays. *J. Agric. Food Chem.* 53, 1841–1856. doi: 10.1021/jf030723c

Ighodaro, O., and Akinloye, O. (2018). First line defence antioxidants-superoxide dismutase (SOD), catalase (CAT) and glutathione peroxidase (GPX): Their fundamental role in the entire antioxidant defence grid. *Alexandria J. Med.* 54, 287–293. doi: 10.1016/j.ajme.2017.09.001

Jaleel, C. A., Riadh, K., Gopi, R., Manivannan, P., Ines, J., Al-Juburi, H. J., et al. (2009). Antioxidant defense responses: physiological plasticity in higher plants under abiotic constraints. *Acta Physiologiae Plantarum* 31, 427–436. doi: 10.1007/s11738-009-0275-6

Jameel, S., Hameed, A., and Shah, T. M. (2021). Biochemical profiling for antioxidant and therapeutic potential of Pakistani chickpea (Cicer arietinum l.) genetic resource. *Front. Plant Sci.* 12, 574. doi: 10.3389/fpls.2021.663623

Karniel, U., Koch, A., Zamir, D., and Hirschberg, J. (2020). Development of zeaxanthin-rich tomato fruit through genetic manipulations of carotenoid biosynthesis. *Plant Biotechnol. J.* 18, 2292–2303. doi: 10.1111/pbi.13387

Khalid, A., and Hameed, A. (2017). Seed biochemical analysis based profiling of diverse wheat genetic resource from Pakistan. *Front. Plant Sci.* 8, 1276. doi: 10.3389/fpls.2017.01276

Kumar, A., Kumar, A., Ranjan, R., Kumar, S., Rajani, K., and Singh, P. (2019). Principal component analysis of agro-morpho-genetic traits in desi chickpea (Cicer arietinum l.). *SP*, 362–365.

Lee, S.-H., Ahsan, N., Lee, K.-W., Kim, D.-H., Lee, D.-G., Kwak, S.-S, et al. (2007). Simultaneous overexpression of both CuZn superoxide dismutase and ascorbate peroxidase in transgenic tall fescue plants confers increased tolerance to a wide range of abiotic stresses. *J Plant Physiol* 164, 1626–1638.

Lichtenthaler, H. K., and Wellburn, A. R. (1983). *Determinations of total carotenoids and chlorophylls a and b of leaf extracts in different solvents* (United kingdom:Portland Press).

Lin, J.-Y., and Tang, C.-Y. (2007). Determination of total phenolic and flavonoid contents in selected fruits and vegetables, as well as their stimulatory effects on mouse splenocyte proliferation. *Food Chem.* 101, 140–147. doi: 10.1016/j.foodchem.2006.01.014

Manoharan, R. K., Jung, H.-J., Hwang, I., Jeong, N., Kho, K. H., Chung, M.-Y., et al. (2017). Molecular breeding of a novel orange-brown tomato fruit with enhanced beta-carotene and chlorophyll accumulation. *Hereditas* 154, 1–8. doi: 10.1186/s41065-016-0023-z

Martínez-Valverde, I., Periago, M. J., Provan, G., and Chesson, A. (2002). Phenolic compounds, lycopene and antioxidant activity in commercial varieties of tomato (Lycopersicum esculentum). *J. Sci. Food Agric.* 82, 323–330. doi: 10.1002/jsfa.1035

Melkamu, M., Seyoum, T., and Woldetsadik, K. (2008). Effects of pre-and post harvest treatments on changes in sugar content of tomato. *Afr. J. Biotechnol.* 7, 1139–1144.

Mishra, C., Tiwari, V., Satish-Kumar, V. G., Kumar, A., and Sharma, I. (2015). Genetic diversity and genotype by trait analysis for agromorphological and physiological traits of wheat (Triticum aestivum l.). *Sabrao J. Breed. Genet.* 47, 40–48.

Mondal, K., Sharma, N., Malhotra, S., Dhawan, K., and Singh, R. (2004). Antioxidant systems in ripening tomato fruits. *Biol. Plantarum* 48, 49–53. doi: 10.1023/B:BIOP.0000024274.43874.5b

Morales, M., and Munné-Bosch, S. (2019). Malondialdehyde: facts and artifacts. *Plant Physiol.* 180, 1246–1250. doi: 10.1104/pp.19.00405

Navarro-González, I., García-Alonso, J., and Periago, M. J. (2018). Bioactive compounds of tomato: Cancer chemopreventive effects and influence on the transcriptome in hepatocytes. *J. Funct. Foods* 42, 271–280. doi: 10.1016/j.jff.2018.01.003

Nguyen, M. L., and Schwartz, S. J. (1999). Lycopene: Chemical chemical and biological properties: Developing nutraceuticals for the new millenium. *Food Technol. (Chicago)* 53, 38–45.

Noor, R., Mittal, S., and Iqbal, J. (2002). Superoxide dismutase–applications and relevance to human diseases. *Med. Sci. Monit.: Int. Med. J. Exp. Clin. Res.* 8, RA210–RA215.

Ortega-Ortiz, H., Benavides-Mendoza, A., Mendoza-Villarreal, R., Ramírez-Rodríguez, H., and De Alba Romenus, K. (2007). Enzymatic activity in tomato fruits as a response to chemical elicitors. *J. Mexican Chem. Soc.* 51, 141–144.

Pal, R., Hedau, N., Kant, L., and Pattanayak, A. (2018). Functional quality and antioxidant properties of tomato genotypes for breeding better quality varieties. *Electronic J. of Plant Breed.* doi: 10.5958/0975-928X.2018.00001.7

Park, H., Kim, Y.-J., and Shin, Y. (2020). Estimation of daily intake of lycopene, antioxidant contents and activities from tomatoes, watermelons, and their processed products in Korea. *Appl. Biol. Chem.* 63, 1–11. doi: 10.1186/s13765-020-00534-w

Perata, P., Pozueta-Romero, J., Akazawa, T., and Yamaguchi, J. (1992). Effect of anoxia on starch breakdown in rice and wheat seeds. *Planta* 188, 611–618. doi: 10.1007/BF00197056

Pradedova, E., Isheeva, O., and Salyaev, R. (2011). Classification of the antioxidant defense system as the ground for reasonable organization of experimental studies of the oxidative stress in plants. *Russian J. Plant Physiol.* 58, 210–217. doi: 10.1134/S1021443711020166

Proteggente, A. R., Pannala, A. S., Paganga, G., Buren, L. V., Wagner, E., Wiseman, S., et al. (2002). The antioxidant activity of regularly consumed fruit and vegetables reflects their phenolic and vitamin c composition. *Free Radical Res.* 36, 217–233. doi: 10.1080/10715760290006484

Raffo, A., La Malfa, G., Fogliano, V., Maiani, G., and Quaglia, G. (2006). Seasonal variations in antioxidant components of cherry tomatoes (Lycopersicon esculentum cv. Naomi F1). *J. Food Composition Anal.* 19, 11–19. doi: 10.1016/j.jfca.2005.02.003

Raffo, A., Leonardi, C., Fogliano, V., Ambrosino, P., Salucci, M., Gennaro, L., et al. (2002). Nutritional value of cherry tomatoes (Lycopersicon esculentum cv. Naomi F1) harvested at different ripening stages. *J. Agric. Food Chem.* 50, 6550–6556. doi: 10.1021/jf020315t

Rani, K., Rana, R., and Datt, S. (2012). Review on latest overview of proteases. *Int. J. Curr. Life Sci.* 2, 12–18.

Rani, P., Unni, K. M., and Karthikeyan, J. (2004). Evaluation of antioxidant properties of berries. *Indian J. Clin. Biochem.* 19, 103–110. doi: 10.1007/BF02894266

Rathinavel, K. (2018). Principal component analysis with quantitative traits in extant cotton varieties (Gossypium hirsutum l.) and parental lines for diversity. *Curr. Agric. Res. J.* 6, 54. doi: 10.12944/CARJ.6.1.07

Robinson, D. S., and Eskin, N. (1991). *Oxidative enzymes in foods. sole distributor in the USA and Canada* (London: Elsevier Applied Science).

Sahlin, E., Savage, G., and Lister, C. (2004). Investigation of the antioxidant properties of tomatoes after processing. *J. Food Composition Anal.* 17, 635–647. doi: 10.1016/j.jfca.2003.10.003

Salandanan, K., Bunning, M., Stonaker, F., Külen, O., Kendall, P., and Stushnoff, C. (2009). Comparative analysis of antioxidant properties and fruit quality attributes of organically and conventionally grown melons (Cucumis melo l.). *HortScience* 44, 1825–1832. doi: 10.21273/HORTSCI.44.7.1825

Salehi, B., Sharifi-Rad, R., Sharopov, F., Namiesnik, J., Roointan, A., Kamle, M., et al. (2019). Beneficial effects and potential risks of tomato consumption for human health: An overview. *Nutrition* 62, 201–208. doi: 10.1016/j.nut.2019.01.012

Saran, P. L., Singh, S., Solanki, V., Choudhary, R., and Manivel, P. (2021). Evaluation of asparagus adscendens accessions for root yield and shatavarin IV content in India. *Turkish J. Agric. Forestry* 45, 475–483. doi: 10.3906/tar-2006-42

Sevindik, M. (2018). Investigation of oxidant and antioxidant status of edible mushroom *Clavariadelphus truncatus*. *Mantar Dergisi* 9, 165–168.

Shah, T. M., Imran, M., Atta, B. M., Ashraf, M. Y., Hameed, A., Waqar, I., et al. (2020). Selection and screening of drought tolerant high yielding chickpea genotypes based on physio-biochemical indices and multi-environmental yield trials. *BMC Plant Biol.* 20, 1–16. doi: 10.1186/s12870-020-02381-9

Shi, J., and Maguer, M. L. (2000). Lycopene in tomatoes: chemical and physical properties affected by food processing. *Crit. Rev. Food Sci. Nutr.* 40, 1–42. doi: 10.1080/10408690091189275

Sies, H. (1991). *Oxidative stress: Oxidants and antioxidants* (New York and London: Academic Press).

Stewart, A. J., Bozonnet, S., Mullen, W., Jenkins, G. I., Lean, M. E., and Crozier, A. (2000). Occurrence of flavonols in tomatoes and tomato-based products. *J. Agric. Food Chem.* 48, 2663–2669. doi: 10.1021/jf000070p

Sundarram, A., and Murthy, T. P. K. (2014). α-amylase production and applications: a review. *J. Appl. Environ. Microbiol.* 2, 166–175. doi: 10.12691/jaem-2-4-10

Tadesse, T., Workneh, T. S., and Woldetsadik, K. (2012). Effect of varieties on changes in sugar content and marketability of tomato stored under ambient conditions. *Afr. J. Agric. Res.* 7, 2024–2030. doi: 10.5897/AJAR11.1216

Tang, G. (2010). Bioconversion of dietary provitamin a carotenoids to vitamin a in humans. *Am. J. Clin. Nutr.* 91, 1468S–1473S. doi: 10.3945/ajcn.2010.28674G

Tounekti, T., Vadel, A., Oñate, M., Khmeira, H., and BOSCH, S. (2011). Salt induced oxidative stress in rosemary plants: damage or protection. *Environ. Exp. Bot.* 71 298–305. doi: 10.1016/j.envexpbot.2010.12.016

Turhan, A., and Şeniz, V. (2009). Estimation of certain chemical constituents of fruits of selected tomato genotypes grown in Turkey. *Afr. J. Agric. Res.* 4, 1086–1092.

Uçan, U., and Uğur, A. (2021). Acceleration of growth in tomato seedlings grown with growth retardant. *Turkish J. Agric. Forestry* 45, 669–679. doi: 10.3906/tar-2011-4

Ulewicz-Magulska, B., and Wesolowski, M. (2019). Total phenolic contents and antioxidant potential of herbs used for medical and culinary purposes. *Plant Foods Hum. Nutr.* 74, 61–67. doi: 10.1007/s11130-018-0699-5

Vaiserman, A., Koliada, A., Zayachkivska, A., and Lushchak, O. (2020). Nanodelivery of natural antioxidants: An anti-aging perspective. *Front. Bioeng. Biotechnol.* 447. doi: 10.3389/fbioe.2019.00447

Vall-Llaura, N., Fernández-Cancelo, P., Nativitas-Lima, I., Echeverria, G., Teixidó, N., Larrigaudière, C., et al. (2022). ROS-scavenging-associated transcriptional and biochemical shifts during nectarine fruit development and ripening. *Plant Physiol. Biochem.* 171, 38–48. doi: 10.1016/j.plaphy.2021.12.022

Van Asperen, K. (1962). A study of housefly esterases by means of a sensitive colorimetric method. *J. Insect Physiol.* 8, 401–416. doi: 10.1016/0022-1910(62)90074-4

Varavinit, S., Chaokasem, N., and Shobsngob, S. (2002). Immobilization of a thermostable alpha-amylase. *Sci. Asia* 28, 247–251. doi: 10.2306/scienceasia1513-1874.2002.28.247

Vats, S., Bansal, R., Rana, N., Kumawat, S., Bhatt, V., Jadhav, P., et al. (2020). Unexplored nutritive potential of tomato to combat global malnutrition. *Crit. Rev. Food Sci. Nutr.* 60, 1–32. doi: 10.1080/10408398.2020.1832954

Wang, D., Mu, Y., Hu, X., Ma, B., Wang, Z., Zhu, L., et al. (2021). Comparative proteomic analysis reveals that the heterosis of two maize hybrids is related to enhancement of stress response and photosynthesis respectively. *BMC Plant Biol.* 21, 1–15. doi: 10.1186/s12870-020-02806-5

Wargovich, M. J. (2000). Anticancer properties of fruits and vegetables. *HortScience* 35, 573–575. doi: 10.21273/HORTSCI.35.4.573

Wong, F.-C., Xiao, J., Wang, S., Ee, K.-Y., and Chai, T.-T. (2020). Advances on the antioxidant peptides from edible plant sources. *Trends Food Sci. Technol.* 99, 44–57. doi: 10.1016/j.tifs.2020.02.012

Yasui, K., and Baba, A. (2006). Therapeutic potential of superoxide dismutase (SOD) for resolution of inflammation. *Inflammation Res.* 55, 359–363. doi: 10.1007/s00011-006-5195-y

Younus, H. (2018). Therapeutic potentials of superoxide dismutase. *Int. J. Health Sci.* 12, 88.

Yu, D., Gu, X., Zhang, S., Dong, S., Miao, H., Gebretsadik, K., et al. (2021). Molecular basis of heterosis and related breeding strategies reveal its importance in vegetable breeding. *Horticul. Res.* 8, 120. doi: 10.1038/s41438-021-00552-9

Zhang, S., Huang, X., and Han, B. (2021). Understanding the genetic basis of rice heterosis: Advances and prospects. *Crop J.* 9, 688–692. doi: 10.1016/j.cj.2021.03.011

Zhang, J., and Kirkham, M. (1994). Drought-stress-induced changes in activities of superoxide dismutase, catalase, and peroxidase in wheat species. *Plant Cell Physiol.* 35, 785–791. doi: 10.1093/oxfordjournals.pcp.a078658

Zhong, X.-L., Tian, Y.-Z., Jia, M.-L., Liu, Y.-D., Cheng, D., and Li, G. (2020). Characterization and purification *via* nucleic acid aptamers of a novel esterase from the metagenome of paper mill wastewater sediments. *Int. J. Biol. Macromol.* 153, 441–450. doi: 10.1016/j.ijbiomac.2020.02.319

Zhou, K., and Yu, L. (2006). Total phenolic contents and antioxidant properties of commonly consumed vegetables grown in Colorado. *LWT Food Sci. Technol.* 39, 1155–1162. doi: 10.1016/j.lwt.2005.07.015

frontiers | Frontiers in Plant Science

TYPE Original Research
PUBLISHED 24 January 2023
DOI 10.3389/fpls.2023.1060242

OPEN ACCESS

EDITED BY
Hosam O. Elansary,
King Saud University, Saudi Arabia

REVIEWED BY
Yujun Liu,
Beijing Forestry University, China
Ahmed M. Abd-ElGawad,
Mansoura University, Egypt

*CORRESPONDENCE
Qiong Nie
nqiong10@163.com

SPECIALTY SECTION
This article was submitted to Plant Metabolism and Chemodiversity, a section of the journal Frontiers in Plant Science

RECEIVED 07 October 2022
ACCEPTED 02 January 2023
PUBLISHED 24 January 2023

CITATION
Luo Z, Liu L, Nie Q, Huang M, Luo C, Sun Y, Ma Y, Yu J and Du F (2023) HPLC-based metabolomics of *Dendrobium officinale* revealing its antioxidant ability. *Front. Plant Sci.* 14:1060242. doi: 10.3389/fpls.2023.1060242

HPLC-based metabolomics of *Dendrobium officinale* revealing its antioxidant ability

Zhengfei Luo[1], Lian Liu[1], Qiong Nie[1]*, Mingjin Huang[1], Chunlii Luo[1], Yedong Sun[2], Yongyan Ma[2], Jianxin Yu[3] and Fuqiang Du[3]

[1]College of Agriculture, Guizhou University, Guiyang, China, [2]Anlong County Xicheng Xiushu Agriculture and Forestry Co., Ltd, Anlong, China, [3]GuiZhou Warmen Pharmaceutical Co., Ltd, Guiyang, China

Dendrobium officinale is an orchid with medicinal and nutritional properties that has received increasing attention because of its health benefits; however, there is limited information about the metabolic basis of these properties. In this report, secondary metabolites and the antioxidant activity of *D. officinale* stem samples from three provenances were analyzed, using a UHPLC-QqQ-MS/MS-based metabolomics approach. In total, 411 metabolites were identified including 8 categories such as flavonoids and phenolic acids, 136 of which were differential metabolites. These differentially accumulated metabolites (DAMs) were mainly enriched in secondary metabolic pathways such as flavone, flavonol, tropane, piperidine, pyridine, isoquinoline alkaloid biosynthesis and tyrosine metabolism. The metabolomic profiling suggested that the quantity and content of flavonoid compounds accounted for the highest proportion of total metabolites. Hierarchical cluster analysis (HCA) showed that the marker metabolites of *D. officinale* from the three provenances were mainly flavonoids, alkaloids and phenolic acids. Correlation analysis identified that 48 differential metabolites showed a significant positive correlation with antioxidant capacity (r^3 0.8 and $p < 0.0092$), and flavonoids were the main factors affecting the different antioxidant activities. It is worth noting that quercetin-3-O-sophoroside-7-O-rhamnoside and dihydropinosylvin methyl ether might be the main compounds causing the differences in antioxidant capacity of Yunnan provenance (YN), Zhejiang provenance (ZJ), and Guizhou provenance (GZ). These finding provides valuable information for screening varieties, quality control and product development of *D. officinale*.

KEYWORDS

Dendrobium officinale, metabolic profiling, differential metabolites, flavonoid, antioxidant activity

1 Introduction

Dendrobium officinale Kimura & Migo, a perennial herb and belongs to the genus *Dendrobium* in the family *Orchidaceae* is a well-known perennial herb used as a medicinal and food homologous product, has been utilized for the treatment of yin-deficiency diseases for decades. *D. officinale* is rich in alkaloids, polysaccharides, flavonoids, terpenoids, stilbenes, phenols and lignins (Lam et al., 2015; Zhang et al., 2018; Cai and Peng, 2021), with potential pharmacological activity against cataracts (Huang et al., 2019), acts as a neuroprotective (Liu et al., 2020), controls diabetes, and displays antioxidant (Hostetler et al., 2017), antibacterial, immune regulatory (Xie et al., 2018; Sun et al., 2020; Xi et al., 2020), antitumor and antimutation effects (Li et al., 2019; He et al., 2020). In traditional Chinese medicine, the fresh or dry stem of *D. officinale* has been linked to generating fluid and benefiting the stomach, nourishing yin and clearing heat, protecting the liver and eyesight, relieving coughing and moistening the lungs (Meng et al., 2017; Yue et al., 2020), and famously known as one of the nine immortal herbs (Zhang et al., 2016).

Wild *D. officinale* grows mainly on damp trunks or limestone, and mainly distributed in tropical and subtropical areas between 15° 31' north latitude and 25° 12' south latitude, e.g., Myanmar, Vietnam and China's Anhui, Zhejiang, Yunnan and Guizhou Provinces (Shiau et al., 2005; Pan et al., 2022).Wild *D. officinale* is scarce because it requires a peculiar growth environment and takes a long time to grow. Moreover, wild *D. officinale* has been exploited excessively due to the large demand from the market (Tang et al., 2017). In order to satisfy market demand, researchers tried to plant *D. officinale* by means of artificial cultivation (Si et al., 2013; Fan et al., 2015). Recently, the artificial planting technology of *D. officinale* has made breakthroughs, with the production quality increasing (Zeng et al., 2012; Mala et al., 2017). The cultivation method of *D. officinale* mainly include imitating wild cultivation (attached to trees and stones) and greenhouse cultivation. The contents of *Dendrobium* polysaccharides, polyphenols and flavonoids cultivated with imitation wild cultivation under a forest are higher than those in greenhouse cultivation (Si et al., 2013). However, the harvest of *D. officinale* using greenhouse cultivation is higher than that achieved by imitation wild cultivation (Huang et al., 2022). Artificial cultivation of *D. officinale* has expanded from the traditional Zhejiang and Yunnan Provinces to Guangxi, Guangdong, Anhui, Hunan and Guizhou Provinces. The forest coverage rate in Guizhou Province is as much as 60%, and planting *D. officinale*-attached trees or cultivating this orchid in three-dimensional planting under a forest has significant economic and ecological advantages. In 2020, the planting area of *D. officinale* in Guizhou was 4,522.26 ha, the largest of the country's original ecological cultivation area. However, most of the *D. officinale* cultivated in Guizhou Province came from Zhejiang and Yunnan provenance, and the native provenances are less cultivated.

Chinese herbal medicine pays particular attention to authenticity. Specific provenances and climatic conditions have a specific effect on the growth and effect of medicinal herbs. There are obvious differences between the metabolites of *Dendrobium* from different origins, and the epiphytic cultivation mode of living trees under a forest can improve the biosynthesis levels of flavonoids and flavonoid compounds (Li et al., 2022; Fan et al., 2022). Several studies reported a close relationship between *D. officinale* from different regions and its physiological activities, especially the antioxidant activity (Xu et al., 2013; Zhang et al., 2019). Plant secondary metabolites are a arise from the interaction between plants and biological and abiotic factors during evolution. The active ingredients of Chinese medicinal herb are mostly the secondary metabolites, and the evaluation of quality and effectiveness of medicinal materials are based on the types and content of secondary metabolism. Metabolomics is a new omics technology after genomics and proteomics (Monteiro et al., 2013). Metabolomics have been widely used in the analysis of herbal composition (Li et al., 2022; Gao et al., 2022) and the mechanism of efficacy based on high-throughput detect the content of metabolites in samples qualitatively, quantitatively and with high coverage (Wei et al., 2010).

Currently, the planting *D. officinale*-attached trees area under forests in Guizhou is nearly 3,335 ha. The seedling sources are mainly from Zhejiang, Yunnan and Guizhou. The products have sold well in China and abroad, but there are only a few reports on their yield and quality characteristics. Anlong County, Guizhou Province, is one of the origins of *D. officinale*, which has had the advantage of wild *Dendrobium* growth since ancient times. The objectives of the present study were to: 1) detected the components and contents of secondary metabolites of *D. officinale* from three provenances planted in Anlong County, 2) measured the antioxidant activity of *D. officinale in vitro*, to analyze the correlation between metabolites and antioxidant activity, 3) comprehensive analysis of the composition and quality of *D. officinale* can provide reference for the selection and cultivation of excellent varieties, and making better use of local provenance. Our overall aim was that used the morphology, metabolomics and HPLC technology to analyses the phenotype, secondary metabolite composition and antioxidant activity of fresh stems of *D. officinale* from three provenances planted in Anlong County, to understand the correlation between the different metabolites and antioxidant activities.

2 Materials and methods

2.1 Experimental materials and preparation of samples

Three *D. officinale* from Yunnan provenance (YN), Zhejiang provenance (ZJ) and Guizhou Anlong native provenance (GZ) were cultivated in Anlong County Zhegui village, GZ Province, and it is cultivated by attaching trees (Figure 1A). YN and ZJ materials were introduced and cultivated from Guangnan County of Yunnan Province and Yandang Mountain of Zhejiang Province in March and August 2016, respectively. In August of the same year, Anlong native species (GZ) were planted in the nearby forest land, with an area of 6.67 ha each. The same management mode of wild imitating cultivation is adopted. In December 2021, the "5-point sampling method" was adopted to take 2–3-year-old stems of *D. officinale* as experimental samples. A total of 200 stems were collected from each

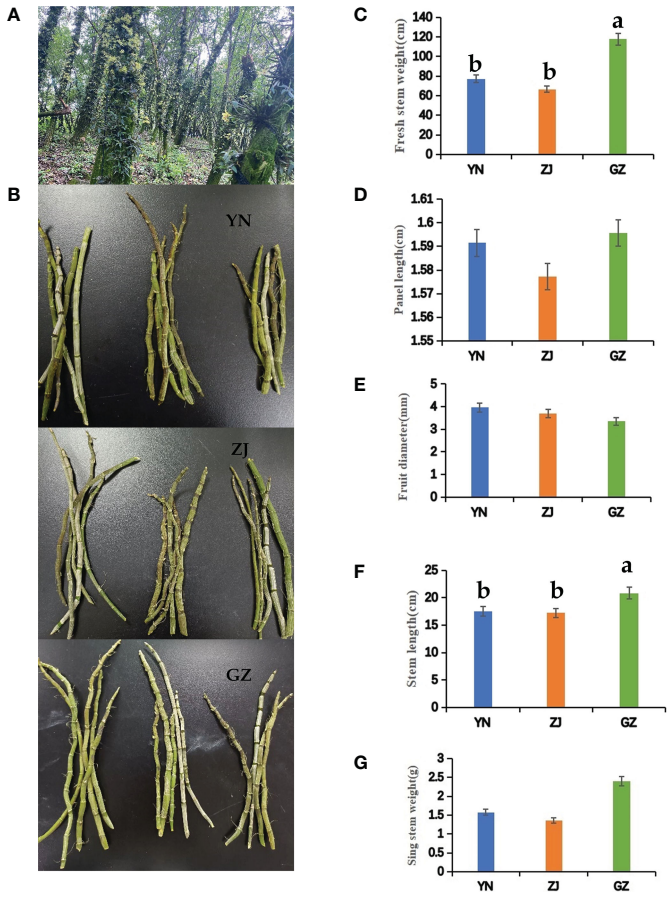

FIGURE 1
Agronomic traits of *Dendrobium officinale* from different provenances. **(A)** Attached to the tree planting. **(B)** Photographs showing *Dendrobium officinale* from different provenances, YN; ZJ; GZ. **(C)** fresh stem weight; **(D)** panel length; **(E)** fruit diameter; **(F)** stem length; **(G)** single stem weight. Different lowercase letters represent significant differences.

variety for mixing, and the stem phenotypes of 49 *D. officinale* were randomly determined. All stems were sliced and evenly mixed, and three pieces were randomly taken as a sample. Three biological replicates were conducted. Nine samples were treated with liquid nitrogen and stored at –80°C for metabolome analysis. The remaining materials were dried, ground and passed through a No. 3 sieve for antioxidant analysis and flavonoid determination.

2.2 Determination of antioxidant activity

An alcohol extraction approach was used for the antioxidant analysis of *D. officinale*. Two grams of *D. officinale* powder was weighed into a 50 mL centrifuge tube. Fifty milliliters of 70% (v/v) ethanol were added, the extract ultrasonicated in a 50°C water bath for 1.5 h, centrifuged (5000 r/min, 2 min) and filtered, and the filtered residue was extracted by the same method for 1 h. The filtrate was combined and transferred to a 100 mL volumetric flask and 70% (v/v) ethanol added to a volume that yielded a 20 mg/mL sample, which was stored at –20°C until use. Three antioxidant methods, DPPH, ABTS and FRAP, were used to examine the antioxidant properties of samples using the instructions in each kit (A153-1-1, A015-2-1, A015-3-1, NanJing JianCheng Bioengineering Institute) and a microplate reader (Multiskan GO, Thermo Scientific, Massachusetts, USA).

2.3 Flavonoid content determination

2.3.1 Chromatographic conditions

A Z0RBAX SB-C18 column (4.6 mm x 250 mm, 5 mm) was used. The gradient elution conditions were: 0 to 10 min, 10% to 11% solvent A, where solvent A was tetrahydrofuran: acetonitrile: methanol (10:22:5) and solvent B was 0.05% aqueous phosphate; 10–25 min, 11%–11.5% solvent A; 25–32 min, 11.5%–12% solvent A; 32–42 min, 2%–12.5% solvent A; 42–52 min, 12.5%–13.5% solvent A; 52–75 min, 13.5%–14% solvent A; and 75–85 min, 14%–20% solvent A. The flow rate was 1 mL min^{-1}, the detection wavelength was 340 nm to determine the five flavonoid components (C1–C5), the column temperature was 30°C, and effects of inject ion volume was 10 μL.

2.3.2 Preparation of control solutions

Reference materials vicenin-2, schaftoside, isoschaftoside, isoviolanthin and violanthin (C1–C5) were accurately weighed and methanol was added to dissolve each reference. A single component control stock solution was then mixed and shaken well. The

appropriate amount of the abovementioned control stock solution was taken, and methanol was added to make a mixed control solution. The mixed control solution prepared above was further diluted into five control solutions of different mass concentrations. The injection mass concentration X (mg L^{-1}) and the chromatographic peak area Y were taken to obtain the regression equation (C1 vicenin-2: y = 5.8944x + 9.9518, R^2 = 0.9985; C2 schaftoside: y = 25.762x – 23.996, R^2 = 0.9945; C3 isoschaftoside: y = 9.2539x + 10.91, R^2 = 0.9959; C4 isoviolanthin: y = 9.7296x + 59.31, R^2 = 0.9968; C5 violanthin: y = 10.567x + 18.353, R^2 = 0.998).

2.3.3 Preparation of sample solutions for testing

Dendrobium powder (through a no. 3 sieve) was taken and dried to a constant weight of ~4 g. The precise weight was measured, and 200 mL 80% (v/v) methanol was added. The sample was heat refluxed for 2 h and cooled to room temperature. The sample was filtered, the filter residue was washed with an appropriate amount of 80% (v/v) methanol, the filtrates combined, the solvent evaporated, and 80% (v/v) methanol was added to dissolve the material. Ten milliliters were added to a measuring bottle, and 80% (v/v) methanol was added. The sample was shaken well and filtered with a 0.45 μm microporous filter membrane to obtain the desired product.

2.3.4 Determination of flavonoids

The content of flavonoid carbonoside was determined by HPLC (Agilent 1260), refer to the literature (Tang Y et al., 2021). In brief, the precision absorption control solution and the test solution were 10 μL. Sample injection and analysis were carried out according to instructions. Flavonoid amounts were determined using the standard curve equations (2.3.2).

2.4 Secondary metabolites detection by UPLC-MS/MS

2.4.1 Sample preparation and extraction

Biological samples were lyophilized using a vacuum freeze-dryer (Scientz-100F) and crushed using a mixer mill (MM 400, Retsch) with a zirconia bead for 1.5 min at 30 Hz. The lyophilized powder (100 mg) was dissolved in 1.2 mL, 70% methanol, mixed for 30 s every 30 min six times and placed at 4°C overnight. Following centrifugation at 12000 rpm for 10 min, the extracts were filtered (SCAA-104, 0.22 μm pore size; ANPEL, Shanghai, China) and analyzed by UPLC-MS/MS.

2.4.2 UPLC conditions, ESI-Q TRAP-MS/MS and qualitative and quantitative analysis of metabolites

UPLC conditions and ESI-Q TRAP-MS/MS parameters reported in reference [Tang et al., 2021] were used. Based on the local metabolic database, the metabolites of the sample were qualitatively quantified by MS. The multi-reaction monitoring mode (MRM) and metabolite detection multimodal diagram were used to identify the substances detected in the sample. The characteristic ions of each substance were screened by the triple four-stage rod, and the signal strength (CPS) of the characteristic ions was obtained using the detector. The sample data were analyzed with MultiQuant, and the integration and correction of the MS peaks were carried out. The peak area of each MS peak represents the relative content of the corresponding substance, and all MS peak integration data was exported for preservation.

2.4.3 Treatment of data

Logarithmic transformations were performed on the abundant original metabolites to normalize the data and achieve homogeneity of variances. Principal component analysis (PCA) and quadrature partial least squares discriminant analysis (OPLS-DA) were performed using R (www.r-project.org/). Hotelling's T-squared ellipse method was used to determine the sample repeatability and confidence interval. Heat maps were drawn using the R ComplexHeatmap package, and Pearson correlation coefficients were calculated using the built-in cor function of R. Metabolites satisfying the following two criteria were selected as differential metabolites between two prov (YN vs. ZJ, YN vs. GZ, ZJ vs. GZ): (i) high confidence (VIP ≥ 1) in pairwise comparisons; (ii) a minimum of a two-fold change or a maximum of 0.5-fold change (fold change ≥ 2 and fold change ≤ 0.5). Differential metabolites were annotated and classified using the Kyoto Encyclopedia of Genes and Genomes (KEGG) database (http://www.kegg.jp/kegg/pathway.html). Significantly enriched pathways in which the metabolites in a module were involved were compared with the background and defined by both a hypergeometric test and a threshold p-value < 0.05.

Microsoft Office Excel 2019 was used for the initial collation of data, and analysis of variance (ANOVA) was used with PASS 27.0.1. The results were expressed as mean ± standard deviation (SD). The significance of the sample-to-sample difference was determined using one-way ANOVA and Duncan's Multiple Range Test with a significance level of 0.05. For secondary metabolome data, significantly regulated metabolites between groups were determined by Variable Importance in Projection (VIP) ≥ 1 and absolute log2FC (fold change) ≥ 1. VIP values were extracted from the OPLS-DA results, which also contained score plots and permutation plots and were generated using the R package MetaboAnalystR. The data were log-transformed (log2) and mean-centered before OPLS-DA. To avoid overfitting, a permutation test (200 permutations) was performed. The functions of differentially accumulated metabolites (DAMs) were annotated based on the KEGG compound database to determine the metabolic pathways.

3 Results

3.1 Stem morphology of *D. officinale* from different provenances

The shape and size of fresh stems of *D. officinale* were the main factors determining the yield. The stem length of *D. officinale* from different provenances varies significantly. The stem lengths of samples taken from GZ are significantly longer than those from YN and ZJ, and the internode length was the longest among samples taken from the three provenances. The phenotype of the internode and stem lengths was the same, with YN samples measured as the second. GZ fresh and single stem weights were heavier than the corresponding weights from YN and ZJ samples. In contrast, the stem diameter of GZ samples was smaller than ZJ and YN but not significant (Figures 1B–G).

3.2 Antioxidant activity analysis of *D. officinale* from different provenances

DPPH radical scavenging activities, radical cation ABTS+ scavenging activities and ferric reducing antioxidant power (FRAP) are listed in (Table 1). The antioxidant capacity of the two extraction methods (alcohol extraction and water extraction) showed the same trend in *D. officinale* from three different Provenances, indicating the reliability of the antioxidant activity value. The DPPH value of GZ was significantly higher than that of YN. The ABTS radical cation scavenging activities of *D. officinale* from the three provenances ranged between 0.2126 and 0.7758 mmol/L. The ABTS values from YN were significantly lower when compared with fractions from GZ and ZJ, and the GZ fractions displayed the highest ABTS values among the fractions from the three provenances. The FRAP values of GZ fractions were the highest, followed by fractions from ZJ. A comparison of all DPPH, ABTS and FRAP values among the stem samples taken from the three provenances showed that GZ fractions had the highest antioxidant activities and YN fractions had the lowest.

3.3 Flavonoid carbonoside components and contents analysis of *D. officinale* from different provenances

The content of flavonoid carbonoside in *D. officinale* fractions from the three provenances is shown in Table 2. The contents of vicenin-2 (C1), isoschaftoside (C3) and isoviolanthin (C4) in *D. officinale* fractions from GZ were significantly greater than those from ZJ and YN, and the contents of vicenin-2 (C1) and isoschaftoside (C3) in *D. officinale* fractions from ZJ were significantly higher than those from YN. However, there was no significant difference in the content of C4 from *D. officinale* fractions derived from ZJ and YN. Schaftoside (C2) and violanthin (C5) were not detected in *D. officinale* fractions from GZ, and violanthin (C5) was not detected in *D. officinale* fractions from ZJ. The total flavonoid carbonoside was higher in GZ than in ZJ and YN, indicating that the content of flavonoid carbonoside and antioxidant capacity of *D. officinale* from different provenances had the same trend.

3.4 Qualitative metabolic profiling of *D. officinale* stems

UPLC-MS/MS was used to analyze differences in metabolic components among *D. officinale* stems taken from GZ, ZJ and YN provenances. Based on the local metabolite database (metware database), qualitative and quantitative MS analyses were conducted on the metabolites in the samples. Four hundred eleven metabolites were identified and divided into eight known first-order categories according to their structure. These metabolites included 143 flavonoids, 128 phenolic acids, 68 alkaloids, 28 lignans and coumarins, 12 quinones, 6 terpenoids, 3 tannins and 23 other metabolites (Table 3). The 143 flavonoid metabolites included 42 flavonols, 39 flavones, 33 flavonoid carbonosides, 15 flavanones, 7 chalcones, 5 flavanols and 2 flavanonols. The 68 alkaloids metabolites included 28 alkaloids, 17 phenolamine, 10 plumerane, 6 pyridine alkaloids, 5 piperidine alkaloids, 1 benzylphenylethylamine alkaloid and 1 sesquiterpene alkaloid.

TABLE 1 Antioxidant activities of *D. officinale* from different provenances.

Materials	AE			WE		
	(DPPH μg/mL)	(ABTS mmol/L)	(FRAP mmol/L)	(DPPH μg/mL)	(ABTS mmol/L)	(FRAP mmol/L)
GZ	2737.75 ± 16.24 a	0.7758 ± 0.04 a	4.7239 ± 0.34 a	2426.93 ± 17.86 a	0.6414 ± 0.01 a	4.3851 ± 0.05 a
ZJ	2711.95 ± 0.78 ab	0.6193 ± 0.01 b	3.9651 ± 0.21 b	2279.65 ± 4.29 b	0.4900 ± 0.01 b	3.5519 ± 0.01 b
YN	2703.06 ± 7.06 b	0.5184 ± 0.04 c	3.4909 ± 0.09 b	2108.06 ± 21.59 c	0.2126 ± 0.02 c	2.7547 ± 0.03 c

AE are alcohol extraction methods; WE are water extration methods. DPPH, 2,2-diphenyl-1-picrylhydrazyl radical scavenging ability; ABTS, 2,2'-Azinobis- (3-ethylbenzthiazoline-6-sulphonate; FRAP, ferric reducing antioxidant power. If the value of ABTS and FRAP from the extract is 1mM, the antioxidant capacity is equivalent to 1mM Trolox. Different letters followed the numbers indicate statistically significant differences ($p < 0.05$). Values are expressed as the mean ± SD, on a dry basis.

TABLE 2 Total flavonoid carbonoside and reference substance content of *D. officinale* from different provenances(C1-C5).

Materials	C1	C2	C3	C4	C5	Total flavonoid carbonoside
	μg/g	μg/g	μg/g	μg/g	μg/g	μg/g
GZ	68.44 ± 0.33a	0	51.31 ± 0.22a	29.48 ± 0.36a	0	149.22 ± 0.67a
ZJ	54.38 ± 0.08b	6.31 ± 0.09	43.31 ± 0.33b	12.66 ± 0.22b	0	116.66 ± 1.02b
YN	41.37 ± 0.63c	6.69 ± 0.10	40.76 ± 0.06c	12.91 ± 0.21b	14.98 ± 1.13	116.71 ± 0.36b

C1: vicenin-2; C2: schaftoside; C3: isoschaftoside; C4: isoviolanthin; C5: violanthin. Different letters followed the numbers indicate statistically significant differences ($p < 0.05$). Values are expressed as the mean ± SD, on a dry basis.

TABLE 3 Number of differential metabolites in the leaves of *Dendrobium officinale* from different provenances.

Group Class	YN vs ZJ		YN vs GZ		ZJ vs GZ	
	Up	Down	Up	Down	Up	Down
Flavonoids	17	8	35	10	10	10
Alkaloids	16	0	10	2	2	4
Phenolic acids	13	2	9	3	8	10
Lignans and Coumarins	2	1	1	2	1	3
Tannins	0	0	1	1	0	1
Quinones	1	1	0	0	0	5
Terpenoids	2	0	0	0		
Others	3	2	5	1	4	0
Total	68		80		58	

3.5 Principal component analysis and orthogonal projections to latent structures-discriminant analysis for stems of *D. officinale* from the three provenances

The differences among the three *D. officinale* provenances were distinguishable and verified by 2D PCA (Figure 2A). In the PCA score plot, two principal components (PC1 and PC2) were extracted to be 28.93% and 24.42%, respectively. The results showed that the three *D. officinale* provenances were clearly separated, and three biological replicates of each variety were compactly gathered together, indicating that the experiment was reproducible and reliable. This comparison indicated significant differences between the three provenances, with all samples falling within the 95% confidence intervals. In addition, the cluster heatmap and class heatmap of the metabolites clearly showed the similarity of components among biological repeats and the difference of components among different species (Figure 2B). These results suggest that the provenance strongly influences the metabolite profiles of different *D. officinale*. Venn diagram analysis of the substances contained in the different species showed that 403 compounds were

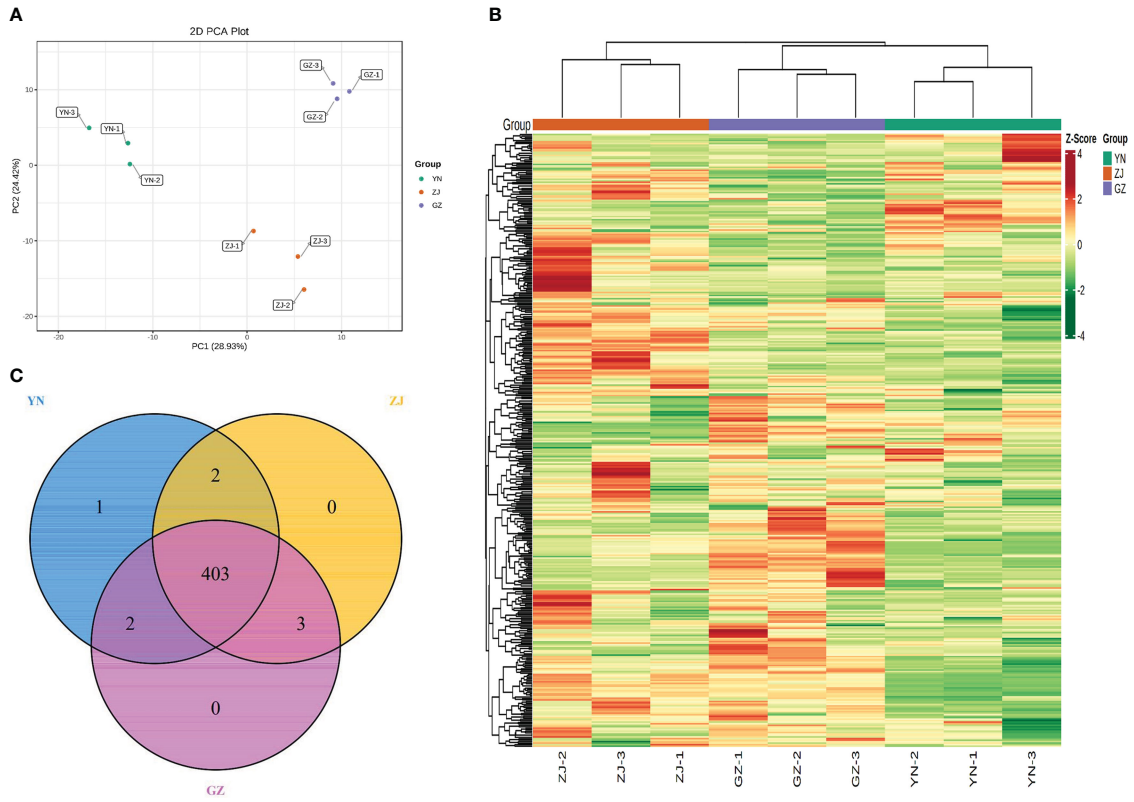

FIGURE 2
Overview of metabolites analysis detected in three *Dendrobium officinale* provenances. **(A)** Principal component analysis of the relative of metabolites for YN, ZJ and GZ: **(B)** Cluster heatmap of metabolite content in different samples. **(C)** Venn diagram of metabolite distribution in different materials.

common to all three provenances, with only one specific metabolite (4-acetoxy-3-ethoxybenzaldehyde) found in *D. officinale* from the YN provenance and three metabolites (luteolin, 1-O-Feruloyl-β-D-glucose and 6-O-Feruloyl-β-D-glucose) were only present in extracts of ZJ and GZ. Two metabolites (2,4,6,6-Tetramethyl-3(6H)-pyridinone and vitexin-7-O-rutinoside) were only present in extracts of YN and ZJ, and two metabolites (fraxetin and 3-Hydroxy-4-methoxybenzoic acid) were only present in extracts of YN and GZ (Figure 2C).

Difference analysis was performed for the substances detected in all samples, and compounds with fold-change (FC) ≥ 2 or FC ≤ 0.5 and OPLS-DA VIP values ≥ 1 were defined as DAMs. In this study, the OPLS-DA model compared metabolite contents of the provenances in pairs to evaluate the differences between YN and ZJ ($R^2X = 0.409$, $R^2Y = 0.997$, $Q^2 = 0.839$), YN and GZ ($R^2X = 0.448$, $R^2Y = 0.994$, $Q^2 = 0.877$), and ZJ and GZ ($R^2X = 0.389$, $R^2Y = 0.994$, $Q^2 = 0.842$) (Figures 3A–C). The Q^2 values of all comparison groups exceeded 0.8, demonstrating that these models were stable. OPLS-DA score plots showed that the three provenances were well-separated in pairs, suggesting significant differences in metabolic phenotypes (Figures 3A–F).

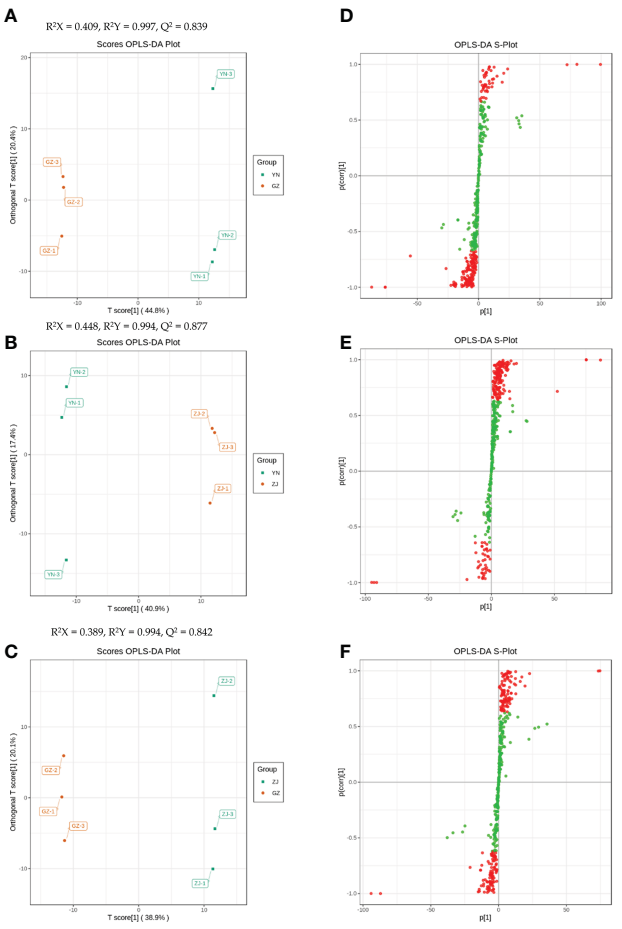

FIGURE 3
Orthogonal partial least squares-discriminant Analysis (OPLS – DA) scores. Scores of the OPLS – DA model with **(A)** YN vs GZ; **(B)** YN vs ZJ; **(C)** ZJ vs GZ. OPLS – DA s-plot model with **(D)** YN vs GZ; **(E)** YN vs ZJ; **(F)** ZJ vs GZ. R2Yscores and Q2values represent the interpretation rate of the model to the Y matrix and the prediction When Q2> 0.5, the model can be considered an effective model, And Q2> 0.9 is an excellent model.

3.6 Differential metabolite screening, functional annotation, and enrichment analysis among the three *D. officinale* provenances

Based on fold change ≥ 2 or ≤ 0.5 and VIP ≥ 1, the number of up- and downregulated compounds resulting from pairwise comparison of tested species is shown in (Figures 4A–C) and (Table 3). The smallest number of differential metabolites was found in the ZJ vs. GZ group, with 58 (25 were upregulated and 33 were downregulated). Moreover, there were 80 significantly different metabolites between YN and GZ (61 upregulated, 19 downregulated) and 68 between YN and ZJ (54 upregulated, 14 downregulated). After taking the intersection of each comparison group in a Venn diagram (Figure 4D), no metabolites were shared among the comparison groups (YN vs. ZJ/GZ, ZJ vs. GZ). Moreover, there were 33, 12 and 25 differentially expressed metabolites between YN vs. ZJ and YN vs. GZ, YN vs. ZJ and ZJ vs. GZ, and YN vs. GZ and ZJ vs. GZ, respectively. These results showed that the metabolites that caused the differences between YN and ZJ, GZ were noticeably different. Among the differential metabolites, the contents of dihydropinosylvin methyl ether, quercetin-3-O-sophoroside-7-O-rhamnoside, quercetin-3-O-(4”-O-glucosyl)rhamnoside, quercetin-3-O-glucoside-7-O-rhamnoside, orientin-7-O-glucoside and quercetin-7-O-rutinosider were relatively high in the three provenances, and the DAMs were relatively large. Noteworthy, phenolic acids (dihydropinosylvin methyl ether) in GZ provenance were 22.60-fold and 13.67-fold higher than in YN provenance and ZJ provenance, respectively, and phenolic acids in ZJ provenance were 1.65-fol higher than in YN provenance.

To explore the metabolite information in YN, ZJ and GZ provenances, we used the KEGG database to annotate and enrich the differential metabolites. In YN vs. ZJ, YN vs. GZ and ZJ vs. GZ groups, 16, 17 and 10 DAMs were annotated by KEGG and showed significant differences, respectively. The major pathways are presented in bubble plots (Figures 5A–C). Most noteworthy, in the YN vs. GZ comparison group, the DAMs were mainly enriched in “flavone and flavonol biosynthesis” and “tropane, piperidine and pyridine alkaloid biosynthesis” metabolic pathways (p-value < 0.05). In the YN vs. ZJ comparison group, the DAMs were mainly enriched in the “pyridine alkaloid biosynthesis” metabolic pathway (p-value < 0.05). In the ZJ vs. GZ comparison group, the DAMs were primarily enriched in “isoquinoline alkaloid biosynthesis” and “tyrosine metabolism” metabolic pathways (p-value < 0.05).

To more comprehensively and visually show the relationship between samples and screen marker metabolites, we performed hierarchical clustering of samples across groups using the expression levels of significant differential metabolites. Hierarchical cluster analysis (HCA) showed that the marker metabolites of *D. officinale* from the three provenances were mainly flavonoids, alkaloids and phenolic acids. The contents of l-tyramine (MWSmce584), sinapic acid (mws4085), 4-hydroxy-3-methoxyamygdaloic acid (pmb2497) and kaempferol-3-O-rutinoside (MWSHY0050) in GZ were significantly higher than those in YN and ZJ. Moreover, the contents of 2-phenylethylamine (MWSslk106), L-pipecolic acid (MWS0811), tryptamine (mws0005) and 5,7,3’,4’-tetrahydroxyflavone (MWSHY0058) in YN were significantly lower than those in GZ and ZJ (Figures 5D–F).

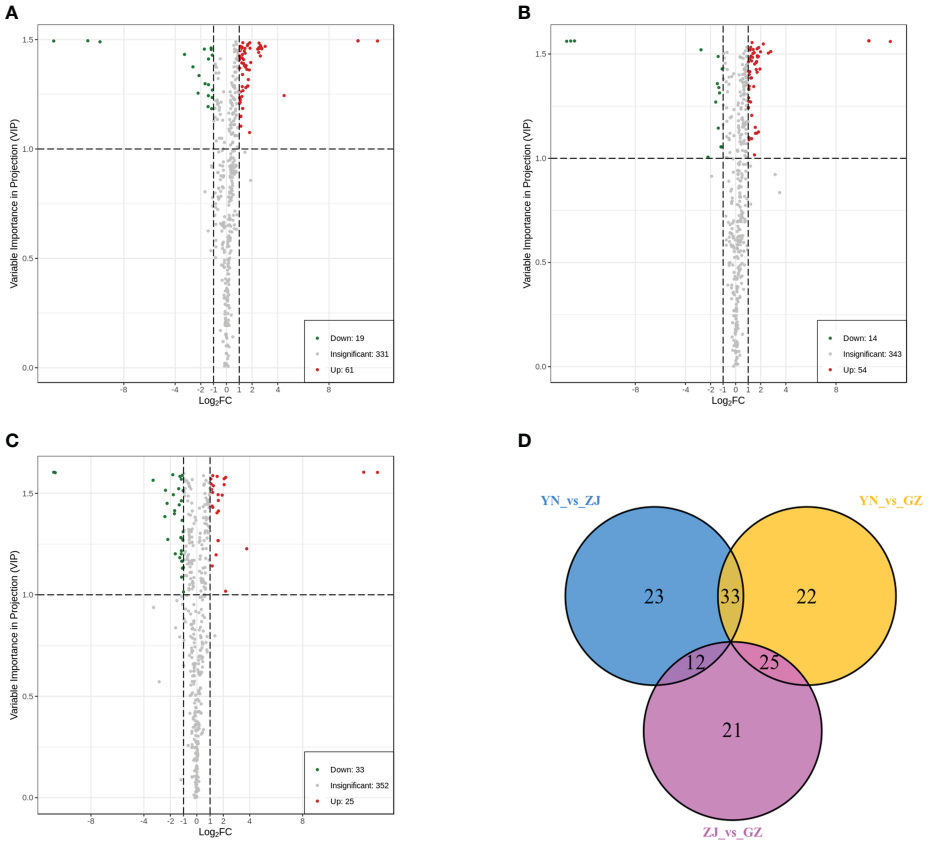

FIGURE 4
Volcano maps and venn diagram analysis of differential metabolites for three comparison groups (YN vs. GZ, YN vs. ZJ, ZJ vs. GZ). Differential metabolite analysis of *Dendrobium officinale* from different provenances. **(A–C)** Volcano maps of differential metabolites in different pairwise comparisons: **(A)** YN vs GZJ; **(B)** YN vs ZJ; **(C)** ZJ vs GZ. **(D)** Venn diagram shows the overlapping and unique metabolites amongst the comparison groups.

3.7 Correlation analysis of the secondary metabolites in *D. officinale* and their antioxidant activity

We performed correlation analysis for all flavonoids, phenolic acids and alkaloids detected in the three materials because these compounds are the major antioxidants in plants (Zhang et al., 2017) and account for the largest proportion of *D. officinale* constituents. The total flavonoid content (TFC) from GZ provenance *D. officinale* fractions was significantly higher than that from ZJ provenance, and TFC from ZJ provenance *D. officinale* fractions was significantly higher than that from YN provenance. Measured total alkaloid content (TAC) revealed that extracts from GZ and ZJ provenances had significantly higher levels than the *D. officinale* stem extract from YN provenance. In contrast, total phenolic acid content (TPC) in extracts had no significant difference among the three provenances (Figure 6). The results showed that TFC may be closely related to the antioxidant activity of the three species of *D. officinale*.

We examined the correlation (Spearman correlation coefficient) between all the different metabolites detected and antioxidant activities (ABTS, DPPH, FRAP) to gain further insight into the ingredients of antioxidants present in *D. officinale* and identified 48 metabolites that displayed a significant positive correlation ($r \geq 0.8$, $p < 0.0092$) with antioxidant activity. Here, 30 flavonoids, 9 alkaloids, 4 phenolic acids, 2 stilbenes, 1 sesquiterpenoid, 1 coumarin and 1 other substance displayed a significant positive correlation with at least one antioxidant activity, suggesting that in addition to flavonoids, alkaloids and phenolic acids, some stilbenes and other substances in *D. officinale* may also be important antioxidants (Figure 7). Moreover, flavonols (quercetin-3-O-neohesperidoside, quercetin-3-O-(4”-O-glucosyl)rhamnoside, quercetin-7-O-rutinoside, quercetin-3-O-rutinoside (Rutin) and quercetin-3-O-sophoroside-7-O-rhamnoside) levels in GZ extracts were 3.92- and 1.84-fold, 4.65- and 1.93-fold, 4.55- and 1.91-fold, 5.71- and 1.83-fold, 6.64- and 4.56-fold higher than in YN and ZJ extracts, respectively. alkaloids (1-methoxy-indole-3-acetamide, 3-amino-2-naphthoic acid and 3-Indoleacrylic acid) levels in GZ extracts were 1.40- and 1.13-fold, 1.48- and 1.16-fold, 1.50- and 1.20-fold higher than in YN and ZJ extracts, respectively. phenolic acids (1-O-Gentisoyl-β-D-glucoside, glucosyringic acid and dihydropinosylvin methyl ether) levels in GZ extracts were 1.59- and 1.42-fold, 1.94- and 1.76-fold, 71.06- and 13.67-fold higher than in YN and ZJ extracts, respectively (Table S1). Among them, the correlation coefficient between flavonols (quercetin-3-O-neohesperidoside, quercetin-3-O-(4’’-O-glucosyl)rhamnoside, quercetin-7-O-rutinoside, quercetin-3-O-rutinoside (Rutin) and quercetin-3-O-sophoroside-7-O-rhamnoside) and antioxidant index was 0.867, 0.867, 0.867, 0.900 and 0.833 for ABTS, respectively. The correlation coefficients of alkaloids (1-methoxy-indole-3-acetamide, 3-amino-2-naphthoic acid and 3-Indoleacrylic acid) were 0.954, 0.867 and 0.950 for FRAP, respectively. The correlation coefficients between 1-O-Gentisoyl-β-D-glucoside and the antioxidant indexes were 0.883 for

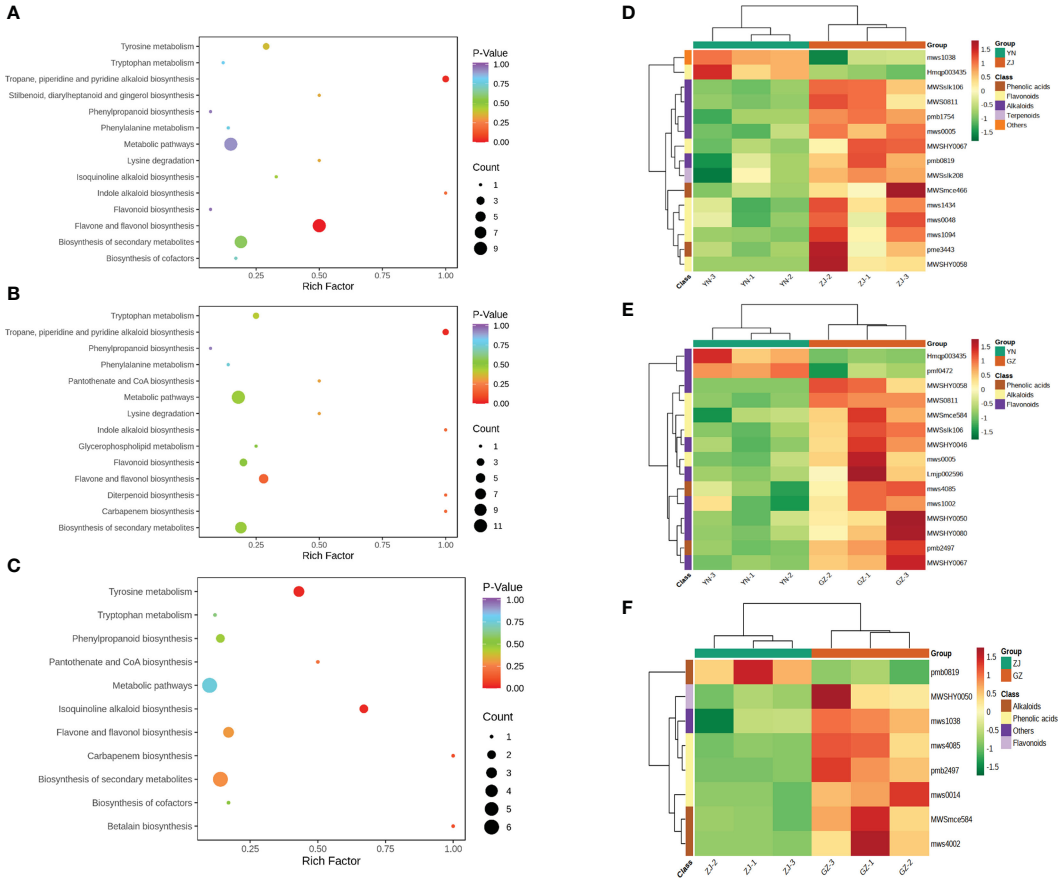

FIGURE 5
KEGG enrichment maps and heatmaps analysis of differential metabolites for three comparison groups (YN vs. GZ, YN vs. ZJ, ZJ vs. GZ). **(A–C)**, KEGG enrichment maps of differential metabolites in different pairwise comparisons: **(A)** YN vs. ZJ; **(B)** YN vs. GZ; **(C)** ZJ vs. GZ. D-F, Heatmaps of hierarchical cluster analysis (HCA): **(D)** YN vs ZJ; **(E)** YN vs GZ; **(F)** ZJ vs GZ. **(A–C)** The abscissa represents the enrichment factor of the pathway and the ordinate shows the names of pathways. The color of the dot represents the p-value, and the deeper the red of the dot, the stronger the enrichment effects. The size of points represents the number of metabolites enriched in the pathways. **(D–F)** The abscissa is used to display the names of samples, and the ordinate on the right is used to display the names of differential metabolites. The deeper the red color, the higher the content of the metabolites; the deeper the green color, the lower the content of the metabolites. The abscissa is the name of the sample and the ordinate is the differential metabolite. Different colors in the heat map represent the relative content of the differential metabolite. The value obtained after normalization reflects the relative content (red represents high content and green represents low content).

ABTS; The correlation coefficients between glucosyringic acid and the antioxidant indexes were 0.812 for DPPH; The correlation coefficients between dihydropinosylvin methyl ether and the antioxidant indexes were 0.837 for DPPH (Table S2). According to the multiple and correlation coefficient, we infer thatwe infer that content of quercetin-3-O-sophoroside-7-O-rhamnoside and dihydropinosylvin methyl ether might be the underlying causes of the differences in antioxidant capacity and pharmacological effects of YN, ZJ, and GZ.

4 Discussion

4.1 The secondary metabolites of *D. officinale* from different provenances were significantly different

The provenance is the regional adaptive varieties derived from different natural distribution areas or formed from geographical

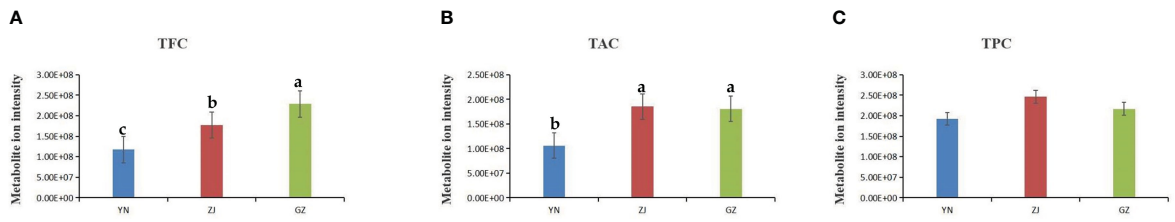

FIGURE 6
Comparison of the total ion intensity of various class of metabolites among stems from YN, ZJ and GZ. **(A)** TFC, total flavonoid content, **(B)** TAC, total alkaloid content, **(C)** TPC, total phenolic acid content. Different lowercase letters represent significant differences.

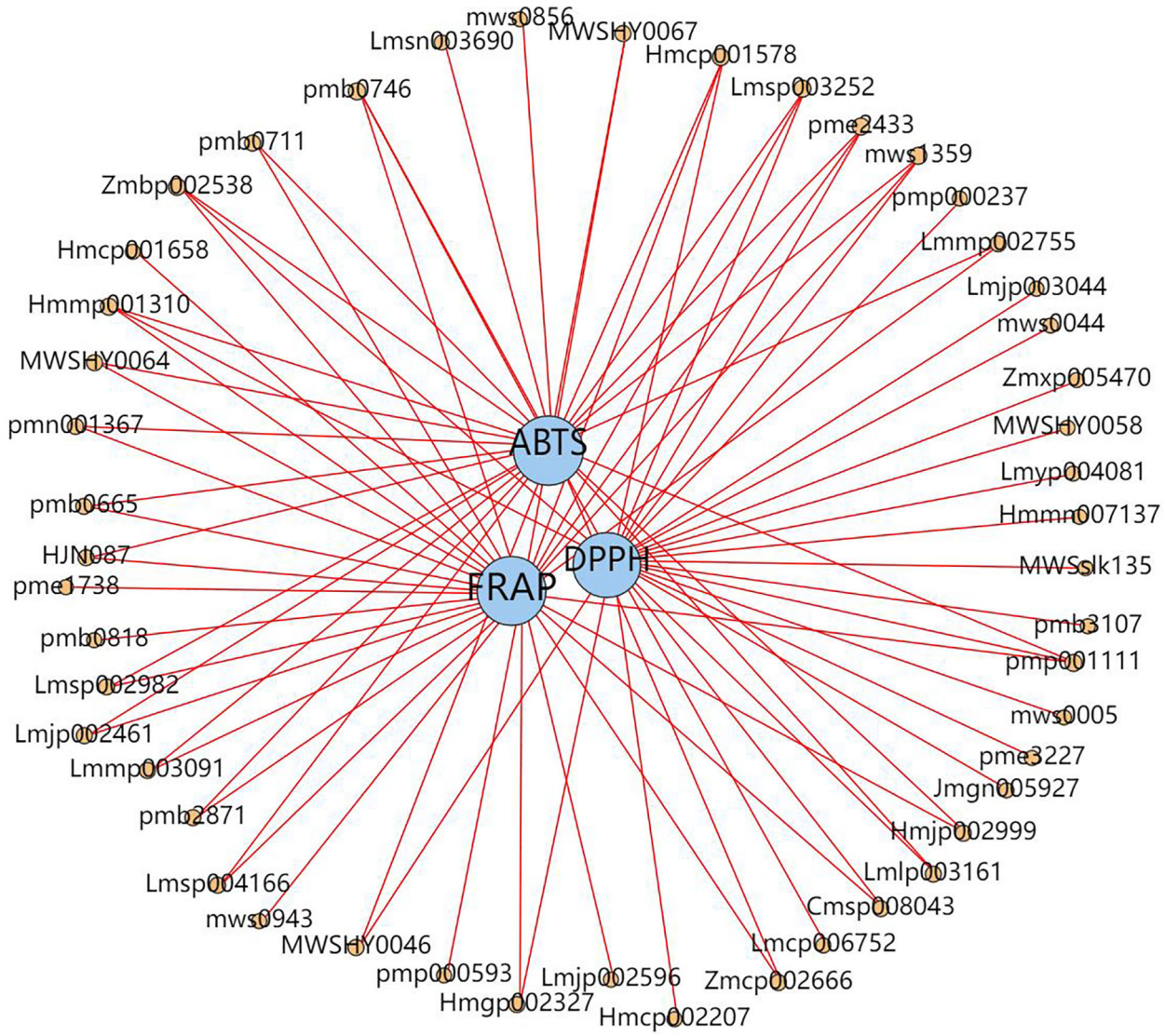

FIGURE 7
Network diagram between antioxidant capacity and metabolites. Blue circles indicate different antioxidant capacity (DPPH, 2,2-diphenyl-1-picrylhydrazyl radical scavenging ability; ABTS, 2,2'-Azinobis- (3-ethylbenzthiazoline-6-sulphonate; FRAP, ferric reducing antioxidant power.), orange circles indicate different metabolites (The number above the circle indicates the component ID of Metware), and the line connecting the two circles represents the correlation ($r \geq 0.8$, $p < 0.0092$).

isolation through artificial cultivation and domestication. There may be great differences in the growth, development and quality of different provenances, which is the basis for the selection and cultivation of excellent varieties.

Lan et al., indicated that a total of 442 metabolites were identified in three different origins from Guangxi Province (GP), Guangdong Province (RS) and Zhejiang Province (ZJ), and were divided into 16 major categories, among including 244 differential metabolites Lan et al. (2022). In our study, 411 metabolites were identified including 8 categories, among 136 differential metabolites were identified in the three comparison groups from YN, ZJ, and GZ. Compared with previous studies, the metabolites, categories, differential metabolites have decreased, it may be that our three provenance materials are cultivated in the same place, which excludes the influence of growth environment on metabolites. By comparing the species and content of different metabolites between YN, ZJ provenances and GZ native provenances, the difference is mainly reflected in flavonoids, alkaloids and phenolic acid metabolites. Besides, the content of quercetin-3-O-rutinoside noticeably different, while the *in vivo* radiation protection effect of quercetin-3-o-rutinoside has been evaluated (Bansal et al., 2012) and may represent a quality evaluation index. Similarly, the content of l-pipecolic acid significantly different, while previous study indicated that Pipecolic acid (Pip) biosynthesis and hydroxylated modification pathways play a critical role in drought tolerance through the antioxidant system in tomato (Wang et al., 2021). Thus, these compound may also be used as a quality evaluation index. In this study, the content of l-tyramine was observed to be noticeably different, and previous study showed that l-tyramine also serves as a precursor of numerous specialized metabolites that have diverse physiological roles as antioxidants and defense compounds in plant (Schenck and Maeda, 2018). Furthermore, vicenin-2 was detected in *D. officinale* from the three different provenances, and

the abundance of this compound is relatively large, which is consistent with a previous study (Xu et al., 2013). Besides, the *D. officinale* also contains a variety of flavonoid carbonosides with apigenin as an aglycone (Chen et al., 2021). Thus, these metabolites can be used to evaluate the quality of *D. officinale*.

The growing environment of plants affects the changes in metabolites in plants. Important factors affecting the accumulation of secondary metabolites in plants include different altitude, temperature, and Light. It has been observed that the production of polysaccharides *D. officinale* decreases gradually, with the increase in altitude and decrease in temperature (He et al., 2022). Light-treatment affected the accumulation of primary and secondary metabolites in *D. officinale*, especially the biosynthesis of flavonoids, which the components of flavonoid glycosides were significantly upregulated (Jia et al., 2022). Zuo et al., (2020) conducted a comparative analysis of the metabolomics of *D. officinale* under different cultivation substrates, and they found that only three shared metabolites differed significantly among the different comparisons. Lan et al. (2022) conducted a comparative analysis of the metabolomics of *D. officinale* under different region, and found that were 22 significantly different metabolites shared among the three comparison groups. Nevertheless, in our study, there weren't significantly different metabolites shared among the three comparison groups. This difference indicates that provenance is the main factor affecting the differential metabolites of *D. officinale*, while the growing environment has more lesser. In summary, YN and ZJ provenances were introduced to Guizhou Province for cultivation, which the homogeneity of the cultivation environment in the later period may lead to the decrease of some differential metabolites.

4.2 Relationship between composition and content of secondary metabolites of *D. officinale* and antioxidant capacity

We identified 48 different metabolites that displayed a significant positive correlation with antioxidant activity in *D. officinale*. Among them, the quantity and content of flavonoids were the most abundant. Flavonoids are important secondary metabolites, and flavonoids in medicinal plants have been shown to have various biological and pharmacological activities such as anti-diabetic, anti-cancer and antioxidant (Mo et al., 1992; Wang et al., 2006; Wang et al., 2019). Huang et al. (2022) showed that the contents of polyphenols and flavonoids in alcohol extracts were positively correlated with the *in vitro* antioxidant capacity of *D. officinale*. While, in this study, we found that flavonoid compounds accounted for the highest proportion of total metabolites, meanwhile the total flavonoids content and total alkaloids content had significant positive correlation with antioxidant activity, which is consistented with previous studies. However, the total phenolic acid content hadn't significant positive correlation with antioxidant activity, inconsistent with previous studies (Huang et al., 2022). This indicates that phenolic acids have little effect on the antioxidant activity of the three provenances. Flavonols (quercetin-3-O-glucoside-7-O-rhamnoside, quercetin-3-O-neohesperidoside, quercetin-3-O-(4''-O-glucosyl)rhamnoside, quercetin-7-O-rutinoside and rutin) were significantly and positively correlated with the antioxidant capacity of *D. officinale*, and the content of metabolites was relatively high. This observation is consistent with previous reports that flavonols are important antioxidants (Jonathon and Bozzo, 2015). Equally, the antioxidant activity of stems from *D. officinale* showed a positive correlation with alkaloids (1-methoxy-indole-3-acetamide, 3-amino-2-naphthoic acid and 3-Indoleacrylic acid), which is consistent with a previous study [Tang et al., 2021]. In addition, previous studies have shown that many phenolic acid compounds in plants also have antioxidant activity, we found that phenolic acids (1-O-Gentisoyl-β-D-glucoside, glucosyringic acid and dihydropinosylvin methyl ether) were significantly and positively correlated with the antioxidant capacity of *D. officinale*, which is consistent with previous studies (Pradeep and Sreerama, 2018). Therefore, these metabolites can be used as quality evaluation indicators for screening high-quality provenances of *D. officinale*, which has certain reference significance for industrial planting and promotion of *D. officinale*. We found that the contents of quercetin-3-O-sophoroside-7-O-rhamnoside and dihydropinosylvin methyl ether in three different provenances were the most different. Whereas, in the previous studies quercetin-3-O-sophoroside-7-O-rhamnoside and dihydropinosylvin methyl ether has not been reported in *D. officinale*. It can be further studied on the separation, purification and function of these landmark metabolites.

5 Conclusions

The secondary metabolic composition and antioxidant capacity in *D. officinale* from three different provenances (GZ, ZJ, YN), were systematically studied for the first time. In total, 411 metabolites were identified including 8 categories such as flavonoids and phenolic acids, 136 of which were differential metabolites. These differentially accumulated metabolites (DAMs) were enriched in secondary metabolic pathways such as "flavone and flavonol biosynthesis", "tropane, piperidine and pyridine alkaloid biosynthesis", "isoquinoline alkaloid biosynthesis" and "tryptophan metabolism". The metabolites among the three *D. officinale* showed significant differences, mainly differences in accumulated quantity. GZ has the highest TFC and the highest antioxidant activity, followed by ZJ. Correlation analysis identified that 48 differential metabolites showed a significant positive correlation with antioxidant capacity, and flavonoids were the main factors affecting the different antioxidant activities. Quercetin-3-O-sophoroside-7-O-rhamnoside and dihydropinosylvin methyl ether might be the underlying causes of the differences in antioxidant capacity of three *D. officinale*. This study provided reference for the breeding, quality control and product development of *D. officinale*.

Data availability statement

The original contributions presented in the study are included in the article/Supplementary Material. Further inquiries can be directed to the corresponding author.

Author contributions

Conception and design: QN and LL. Analysis and interpretation: ZL. Data collection: ZL, LL, MH, CL, JY and FD. Provide the materials: YS and YM. Writing the article: ZL and QN. Final approval of the article: QN. All authors have read and agreed to the published version of the manuscript. All authors contributed to the article and approved the submitted version.

Funding

This research was funded by the Science and Technology Project of Guizhou Province ([2020]4Y071), and the Traditional Chinese Medicine Industry Development Project of Guizhou Provincial Department of Agriculture and Rural Affairs ([2020]101), and the Science and Technology Project of Guiyang City ([2020]-19-12-3), and the Science and Technology Project of Qiannan Prefecture ([2022] 15).

Acknowledgments

The authors would like to acknowledge Wuhan Metware Biotechnology Co., Ltd. (www.metware.cn (assessed on 21 April 2021)) for their support during detection, and quantitative analysis of metabolites. We thank Liwen Bianji (Edanz) (www.liwenbianji.cn) for editing the English text of a draft of this manuscript.

Conflict of interest

Authors YS, and YM were employed by Anlong County Xicheng Xiushu Agriculture and Forestry Co., Ltd. Authors JY, and FD were employed by GuiZhou Warmen Pharmaceutical Co., Ltd.

The remaining authors declare that the research was conducted in the absence of any commercial or financial relationships that could be construed as a potential conflict of interest.

Publisher's note

Supplementary material

The Supplementary Material for this article can be found online at: https://www.frontiersin.org/articles/10.3389/fpls.2023.1060242/full#supplementary-material

References

Bansal, P., Paul, P., Kunwar, A., Jayakumar, S., Nayak, P. G., Priyadarsini, K. I., et al. (2012). Radioprotection by quercetin-3-O-rutinoside, a flavonoid glycoside – a cellular and mechanistic approach. *J. Funct. Foods* 44, 924–932. doi: 10.1016/j.jff.2012.06.010

Cai, L., and Peng, P. (2021). A brief introduction on the chemical constituents and pharmacological action of rare Chinese medicine *Dendrobium officinale*. *Anhui Chem. Industry* 47 (01), 24–25. doi: 10.3969/j.issn.1008-553X.2021.01.008

Chen, D., Li, J., Xu, H., Yang, Q., Yang, L., Li, S., et al. (2021). Identification of dendrobium officinale from different provenances by HPLC and TLC. *West China J. Pharm. Sci.* 36 (06), 691–695. doi: 10.13375/j.cnki.wcjps.2021.06.020

Fan, L., Chuan-Gao, J., Xian-Ying, R., Xuan, F., Qi, Z., Xiao-Jun, P., et al. (2022). UPLC-MS/MS metabonomics technology revealing difference of flavonoids in *Dendrobium officinale* under different planting modes. *Chin. Traditional Herbal Drugs* 53 (04), 1156–1162. doi: 10.7501/j.issn.0253-2670.2022.04.024

Fan, O., Lin, Z., Dong, W. B., and Wang, C. Z. (2015). Research progress on the rapid propagation of *Dendrobium officinale*. *J. Food Saf. Qual.* 11, 4378–4383. doi: 10.19812/j.cnki.jfsq11-5956/ts.2015.11.022

Gao, M., Cao, X., Wei, S., Huang, X., Ouyang, H., Chang, Y., et al. (2022). Quantitative comparison and chemical profile of different botanical parts of *Panax notoginseng* from different regions. *Front. Nutr.* 9, 841541. doi: 10.3389/fnut.2022.841541

He, Q., Lu, A., Qin, L., Zhang, Q., Lu, Y., Yang, Z., et al. (2022). An UPLC-Q-TOF/MS-Based analysis of the differential composition of *Dendrobium officinale* in different regions. *J. Anal. Methods Chem.* 2022, 8026410. doi: 10.1155/2022/8026410

He, L., Su, Q., Bai, L., Li, M., Liu, J., Liu, X., et al. (2020). Recent research progress on natural small molecule bibenzyls and its derivatives in dendrobium species. *Eur. J. Med. Chem.* 204, 112530. doi: 10.1016/j.ejmech.2020.112530

Hostetler, G. L., Ralston, R. A., and Schwartz, S. J. (2017). Flavones: Food sources, bioavailability, metabolism, and bioactivity. *Adv. Nutr.* 8, 423–435. doi: 10.3945/an.116.012948

Huang, J., Huang, N., Zhang, M., Nie, J., Xu, Y., and Wu, Q. (2019). Decrease aβ by regulating α- and β-secretases in hippocampal neurons of SD rats. *Peer J.* 7, e7627. doi: 10.7717/peerj.7627

Huang, B., Liu, W.-J., Li, W., and Wu, J.-H. (2022). Comparative analysis of active constituents and antioxidant activities of *Dendrobium officinale* in different artificial cultivation models. *J. Food Saf. Qual.* 13 (08), 2665–2671. doi: 10.19812/j.cnki.jfsq11-5956/ts.2022.08.033

Jia, Y., Liu, J., Xu, M., Chen, G., Tan, M., and Xiang, Z. (2022). Light and potassium improve the quality of *Dendrobium officinale* through optimizing transcriptomic and metabolomic alteration. *Molecules* 27 (15), 4866. doi: 10.3390/molecules27154866

Jonathon, R., and Bozzo, G. G. (2015). Arabidopsis thaliana β-glucosidase BGLU15 attacks flavonol 3-O-β-glucoside-7-O-α-rhamnosides. *Phytochemistry* 109, 14–24. doi: 10.1016/j.phytochem.2014.10.028

Lam, Y., Ng, T. B., Yao, R. M., Shi, J., Xu, K., Sze, S. C., et al. (2015). Evaluation of chemical constituents and important mechanism of pharmacological biology in dendrobium plants. *Evid Based Complement Alternat Med.* 2015, 841752. doi: 10.1155/2015/841752

Lan, Q., Liu, C., Wu, Z., Ni, C., Li, J., Huang, C, et al. (2022). Does the metabolome of wild-like *Dendrobium officinale* of different origins have regional differences? *Molecules* 27 (20), 7024. doi: 10.3390/molecules27207024

Li, Y.-Y., Lyu, C.-H., Wu, G., Zheng, Z.-B., Luo, Y.-B., and Qin, Si. (2019). Research progress on molecular mechanism of *Dendrobium officinale* and its active components to metabolic syndrome. *China J. Chin. Materia Med.* 44 (23), 5102–5108. doi: 10.19540/j.cnki.cjcmm.20190813.402

Liu, D., Dong, Z., Xiang, F., Liu, H., Wang, Y., Wang, Q., et al. (2020). Dendrobium alkaloids promote neural function after cerebral ischemia-reperfusion injury through inhibiting pyroptosis induced neuronal death in both in vivo and *In vitro* models. *Neurochem. Res.* 45 (2), 437–454. doi: 10.1007/s11064-019-02935-w

Li, Y., Zhao, G., Zhang, R., Wei, Y., Yao, Z., Su, S., et al. (2022). Using untargeted metabolomics to profile the differences of the fruits of *Lycium barbarum* in different geographical origins. *Anal. Sci.* 38 (8), 1083–1093. doi: 10.1007/s44211-022-00137-z

Mala, B., Kuegkong, K., Sa-ngiaemsri, N., and Nontachaiyapoom, S. (2017). Effect of germination media on *in vitro* symbiotic seed germination of three *Dendrobium orchids* s. *Afr. J. Bot.* 112, 521–526. doi: 10.1016/j.sajb.2017.05.008

Meng, C. W., He, Y. L., Peng, C., Ding, X. J., Guo, L., and Xiong, L. (2017). Picrotoxane sesquiterpenoids from the stems of *Dendrobium nobile* and their absolute configurations and angiogenesis effect. *Fitoterapia* 121, 206–211. doi: 10.1016/j.fitote.2017.07.017

Mo, Y., Nagel, C., and Taylor, L. P. (1992). Biochemical complementation of chalcone synthase mutants defines a role for flavonols in functional pollen. *Proc. Natl. Acad. Sci. U S A.* 89 (15), 7213–7217. doi: 10.1073/pnas.89.15.7213

Monteiro, M. S., Carvalho, M., Bastos, M. L., and Guedes de Pinho, P. (2013). Metabolomics analysis for biomarker discovery: Advances and challenges. *Curr. Medicinal Chem.* 20 (2), 257–271. doi: 10.2174/092986713804806621

Pan, C., Chen, S., Chen, Z., Li, Y., Liu, Y., Zhang, Z., et al. (2022). Assessing the geographical distribution of 76 *Dendrobium* species and impacts of climate change on their potential suitable distribution area in China. *Environ. Sci. pollut. Res. Int.* 29 (14), 20571–20592. doi: 10.1007/s11356-021-15788-0

Pradeep, P. M., and Sreerama, Y. N. (2018). Termprotein removing of foxtail and little millet and their inhibitory effects on α-amylase and α-glucosidase activities. *Food Chem.* 247, 46–55. doi: 10.1016/j.foodchem.2017.11.103

Schenck, C. A., and Maeda, H. A. (2018). Tyrosine biosynthesis, metabolism, and catabolism in plants. *Phytochemistry* 149, 82–102. doi: 10.1016/j.phytochem.2018.02.003

Shiau, Y. J., Nalawade, S. M., Hsia, C. N., Mulabagal, V., and Tsay, H. S. (2005). *In vitro* propagation of the chinese medicinal plant, *Dendrobium candidum* wall. ex lindl., from axenic nodal segments. *In Vitro Cell.Dev.Biol.-Plant* 41, 666–670. doi: 10.1079/IVP2005685

Si, J. P., Yu, Q. X., Song, X. S., and Shao, W. J. (2013). Artificial cultivation modes for *Dendrobium officinale*. *China J. Chin. Mater. Med.* 38, 481–484.

Sun, Le, Chen, X.-M., Wu, C.-M., and Guo, S.-X. (2020). Advances and prospects of pharmacological activities of *Dendrobium officinale* kimura et migo polysaccharides. *Acta Pharm. Sin.* 55 (10), 2322–2329. doi: 10.16438/j.0513-4870.2020-0126

Tang, Y. C., Liu, Y. J., He, G. R., Cao, Y. W., Bi, M. M., Song, M., et al. (2021). Comprehensive analysis of secondary metabolites in the extracts from different *Lily bulbs* and their antioxidant ability. *Antioxid. (Basel).* 10 (10), 1634. doi: 10.3390/antiox10101634

Tang, W.-W., Xia, J.-L., and Cheng, Y. (2021). Analysis of functional composition, antioxidant activity and their correlation in stem, leaf and flower from *Dendrobium officinale*. *Food Machinery* 37 (07), 45–50. doi: 10.13652/j.issn.1003-5788.2021.07.007

Tang, H., Zhao, T., Sheng, Y., Zheng, T., Fu, L., and Zhang, Y. (2017). *Dendrobium officinale* kimura et migo: A review on its ethnopharmacology, phytochemistry, pharmacology, and industrialization. *Evid. Based Complementary Altern. Med.*, 7436259. doi: 10.1155/2017/7436259

Wang, S., Alseekh, S., Fernie, A. R., and Luo, J. (2019). The structure and function of major plant metabolite modifications. *Mol. Plant* 12, 899–919. doi: 10.1016/j.molp.2019.06.001

Wang, P., Luo, Q., Yang, W., Ahammed, G. J., Ding, S., Chen, X., et al. (2021). Shi k. a novel role of pipecolic acid biosynthetic pathway in drought tolerance through the antioxidant system in *Tomato*. *Antioxidants* 10 (12), 1923. doi: 10.3390/antiox10121923

Wang, L., Tu, Y. C., Lian, T. W., Hung, J. T., Yen, J. H., and Wu, M. J. (2006). Distinctive antioxidant and antiinflammatory effects of flavonols. *J. Agric. Food Chem.* 54 (26), 9798–9804. doi: 10.1021/jf0620719

Wei, R., Li, G., and Seymour, A. B. (2010). High-throughput and multiplexed LC/MS/MRM method for targeted metabolomics. *Anal. Chem.* 82 (13), 5527–5533. doi: 10.1021/ac100331b

Xie, T., Chen, J., and Li, Y. (2018). Study on Anti-fatigue effect of aqueous extracts from *Dendrobium candidum* in different producing areas. *Yunnan J. Traditional Chin. Med.* 39 (08), 66–67. doi: 10.16254/j.cnki.53-1120/r.2018.08.030

Xi, H.-X., Liu, C., Liu, J.-J., Zhang, X.-F., Si, J.-P., and Zhang, L. (2020). Chemical components and pharmacological action for *Dendrobium officinale* and its prediction analysis on q-marker. *Chin. Traditional Herbal Drugs* 51 (11), 3097–3109. doi: 10.7501/j.issn.0253-2670.2020.11.030

Xu, J., Han, Q. B., Li, S. L., Chen, X. J., Wang, X. N., Zhao, Z. Z, et al. (2013). Chemistry, bioactivity and quality control of *Dendrobium*, a commonly used tonic herb in traditional Chinese medicine. *Phytochem. Rev.* 12, 341–367. doi: 10.1007/s11101-013-9310-8

Yue, H., Zeng, H., and Ding, K. (2020). A review of isolation methods, structure features and bioactivities of polysaccharides from dendrobium species. *Chin. J. Nat. Med.* 18 (1), 1–27. doi: 10.1016/S1875-5364(20)30001-7

Zeng, W. Y., Li, J. H., Wang, Z., Yang, Y. W., and Hu., Q. (2012). Research on the condition of aseptic germination and plantlet rapid propagation of *Dendrobium officinale* kimura et migo. *J. Wuhan. Polytech. Univ.* 31 (3), 10–13. doi: 10.3969j. issn.1009-4881.2012.03.003

Zhang, G. Q., Xu, Q., Bian, C., Tsai, W. C., Yeh, C. M., Liu, K. W., et al. (2016). The *Dendrobium catenatum* lindl. genome sequence provides insights into polysaccharide synthase, floral development and adaptive evolution. *Sci. Rep.* 6, 19029. doi: 10.1038/srep19029

Zhang, Y., Zhang, L., Liu, J., Liang, J., Si, J., and Wu, S. (2017). *Dendrobium officinale* leaves as a new antioxidant source. *J. Funct. Foods* 37, 400–415. doi: 10.1016/j.jff.2017.08.006

Zhang, X.-Q., Zhao, T.-M., Liu, J., Zhao, R.-X., Zheng, S.-G., Chun, Ze, et al. (2018). Advances in chemical compounds and pharmacological effects of dendrobii caulis. *Chin. Traditional Herbal Drugs* 49 (13), 3174–3182. doi: 10.7501/j.issn.0253-2670.2018.13.033

Zhang, X.-F., Zhuo, C.-H., Zhang, L.-K., Jiang, M., Xie, Z.-S., Yuan, Y., et al. (2019). Isolation and identification of main flavonoid glycosides of *Dendrobium officinale* from danxia species and yunnan guangnan species. *Chin. J. Exp. Traditional Med. Formulae* 25 (01), 29–34. doi: 10.13422/j.cnki.syfjx.20182417

Zuo, S. M., Yu, H. D., Zhang, W., Zhong, Q., Chen, W., Chen, W., et al. (2020). Comparative metabolomic analysis of dendrobium officinale under different cultivation substrates. *Metabolites* 10 (8), 325. doi: 10.3390/metabo10080325

frontiers | Frontiers in Plant Science

TYPE Original Research
PUBLISHED 17 May 2023
DOI 10.3389/fpls.2023.1179553

OPEN ACCESS

EDITED BY
Hosam O. Elansary,
King Saud University, Saudi Arabia

REVIEWED BY
Xiumin Fu,
South China Botanical Garden (CAS), China
Gang Jin,
Ningxia University, China

*CORRESPONDENCE
Zhihui Zhao
lyzhihuizhao@126.com
Mengjun Liu
lmj1234567@aliyun.com

†These authors share first authorship

RECEIVED 04 March 2023
ACCEPTED 17 April 2023
PUBLISHED 17 May 2023

CITATION
Jiang N, Hou S, Liu Y, Ren P, Xie N, Yuan Y, Hao Q, Liu M and Zhao Z (2023) Combined LC-MS-based metabolomics and GC-IMS analysis reveal changes in chemical components and aroma components of Jujube leaf tea during processing.
Front. Plant Sci. 14:1179553.
doi: 10.3389/fpls.2023.1179553

Combined LC-MS-based metabolomics and GC-IMS analysis reveal changes in chemical components and aroma components of Jujube leaf tea during processing

Nan Jiang[1,2†], Shujuan Hou[1†], Yuye Liu[1], Peixing Ren[1], Nuoyu Xie[1], Ye Yuan[1], Qing Hao[3], Mengjun Liu[1,2*] and Zhihui Zhao[1,2,3*]

[1]College of Horticulture, Hebei Agricultural University, Baoding, Hebei, China, [2]Research Center of Chinese Jujube, Hebei Agricultural University, Baoding, Hebei, China, [3]Institute of Horticultural Crops, Xinjiang Academy of Agricultural Sciences, Urumqi, Xinjiang, China

Making tea from jujube leaves changed the chemical composition and aroma composition of jujube leaves. Here, Through LC-MS, GC-IMS, and GC-MS technology, we have revealed the effect of jujube leaf processing changes on metabolites. LC-MS identified 468 non-volatile metabolites, while GC-IMS and GC-MS detected 52 and 24 volatile metabolites, respectively. 109 non-volatile metabolites exhibiting more pronounced differences were screened. Most lipids and lipid-like molecules, organic acids, amino acids, and flavonoids increased significantly after processing. GC-IMS and GC-MS analysis revealed that the contents of aldehydes and ketones were significantly increased, while esters and partial alcohols were decreased after processing into jujube leaf tea. The main flavor substances of fresh jujube leaf and jujube leaf tea were eugenol and (E) - 2-Hexenal, respectively. Furthermore, amino acids and lipids were closely linked to the formation of volatile metabolites. Our study provided new insights into the changes in metabolites of jujube leaves processed into jujube leaf tea, and had great potential for industrial application. It laid a foundation for further research on fruit tree leaf tea.

KEYWORDS

jujube leaf, jujube leaf tea, metabolite, aroma components, amino acids, lipids

Highlights

- Analysis of metabolites by LC-MS, GC-IMS, and GC-MS.
- LC-MS identified 468 non-volatile metabolites, while GC-IMS and GC-MS detected 52 and 24 volatile metabolites, respectively.
- Glycerophospholipid, tryptophan, and linoleic acid metabolism pathways were significantly enriched.
- Significant changes in metabolites during the processing of jujube leaves.
- Amino acids and lipids are closely related to the formation of volatile metabolites.

1 Introduction

Jujube (*Ziziphus jujuba* Mill.) is China's economically significant fruit tree. It has an enormous cultivation scale and the highest economic and ecological value among the species of the Rhamnaceae family worldwide. Jujube has been domesticated and cultivated in China for more than 7000 years. It is mainly distributed in the Northwest (Xinjiang, Gansu), the Yellow River Basin (Ningxia, Shaanxi, Shanxi), and the eastern region (Shandong, Hebei, Henan) (Liu et al., 2020). Research has shown that jujube leaves are rich in flavonoids, polysaccharides, amino acids, vitamins, and other nutrients (Zhao et al., 2008; Zhang et al., 2018). It has antioxidant, anti-aging, sedative, and hypnotic activities (Zemouri-Alioui et al., 2019; Hua et al., 2022). Jujube leaves have yet to be adequately commercially exploited in the production and health industry. They are usually used as livestock feed or for natural degradation, a massive waste of jujube leaf resources. One innovative technique for utilizing jujube leaves is to make tea. And some green teas have made from fruit tree leaves with important health-promoting properties such as sea buckthorn leaf tea, mulberry leaf tea, guava leaf tea, and persimmon leaf tea. (Sakanaka et al., 2005, Deguchi and Miyazaki, 2010, Lee et al., 2011; Wilson and Islam, 2015).

Tea is the second largest beverage consumed in the world after water, with much higher consumption than coffee, beer, and wine (Rietveld and Wiseman, 2003). Green tea is one of the most popular tea beverages in China. Due to its green leaves, clear soup, aroma, fresh taste, and other unique sensory qualities, green tea is increasingly favored by consumers. The functional properties of green tea are mainly determined by non-volatile metabolites, while volatile metabolites mainly determine the aroma. Regarding tea soup freshness, amino acids are the essential compounds underlying it. On the other hand, flavone glycosides and catechins give bitterness (Scharbert and Hofmann, 2005; Zhang, 2016), soluble sugars give sweetness (Das et al., 2019), organic acids contribute significantly to acidity and fruitiness, and lipids are conducive to shape of the tea. Jujube leaves do not contain caffeine, theophylline, and other stimulating compounds but are rich in flavonoids and other substances with sedative and hypnotic effects (Zhang et al., 2014). Therefore, jujube leaf tea soup consumption at night may improve sleep quality probably.

Extensive targeted metabolomic analysis can simultaneously quantify hundreds of known and 1000 known and unknown metabolites when combined techniques are combined (Sawada et al., 2009). It has applications in multiple fields due to its high throughput, high sensitivity, wide-coverage, and other advantages (Wang et al., 2018, Zhang et al., 2018). Currently, widely targeted metabolomics has been used to identify and analyze metabolite biosynthesis (Albinsky et al., 2010; Zou et al., 2020). Metabolite changes during tea making, such as white tea, green tea, black tea, and oolong tea, are also commonly used in metabonomics (Dai et al., 2017; Cheng et al., 2020; Wu et al., 2020; Xu et al., 2021). Our study aimed to detect the non-volatile and volatile metabolites in jujube leaves and jujube leaf tea through extensively targeted metabolomics, GC-IMS and GC-MS technology. Orthogonal partial least squares discriminant analysis (OPLS-DA), heat map, and other statistical analysis approaches were used to evaluate metabolite changes before and after jujube leaf processing and to explore the relationship between non-volatile metabolites and volatile metabolites. Our results provide essential leads for developing jujube leaf tea and improving the quality and efficiency of the jujube industry.

2 Materials and methods

2.1 Experimental materials

Leaves from the *Ziziphus jujuba* Mill. cv. Dongzao were used, and the picking standard is two leaves and one bud on the fruit-bearing shoot (Figure 1C). The leaves were collected in June 2022 in Baoding (115° 47'E; 38° 87'N) (Hebei Province, China). Liquid chromatography grade solvents methanol and acetonitrile were purchased from Fisher Chemical, 2-propanol from Merck, formal acid from CNW, and 2-Chloro-L-phenylalanine (≥98%) from Adamas-beta. Alanine, arginine, asparagine, aspartic acid, cystine, glutamine, glutamic acid, glycine, histidine, isoleucine, L-cysteine, leucine, L-hydroxyproline, L-tryptophan, lysine, methionine, phenylalanine, proline, serine, threonine, tyrosine, valine, and 1,3-dichlorobenzene were all analytically pure and purchased from Beijing Solarbio Science&Technology Co., Ltd.

2.2 Jujube leaf green tea processing

2.2.1 Harvesting

Select intact leaves with fresh, bright color and no disease spots and pests on the fruit-bearing shoot (D1). Avoid picking weeds or petioles.

2.2.2 Cleaning

Wash the jujube leaves with clean water to remove the dust from the leaf surface.

2.2.3 Spreading

Spread the leaves at room temperature (26 °) for 10-12h until they lose luster and their water content drops to 70%. When the leaves are pinched, they feel soft, and their grass smell is weakened.

2.2.4 Fixing

Fixing leaves should be done to expose aroma, reduce the grass smell, and change the color from fresh green to dark green. The leaves are pinched tightly into clusters and become slightly sticky.

FIGURE 1
(A) D1, Fresh jujube leaves; **(B)** D2, jujube leaf tea; **(C)** Jujube leaves used in green tea processing (Left: the fruit bearing shoots, Right: the leaves used in green tea processing).

The pot fixation method was used in this study. The parameters were as follows: a pan was placed on an induction cooker, the temperature was adjusted to 120 °, and the pan was preheated for 3min. Then the leaves were placed in the pan and fixed for the 60s by grasping, throwing, and shaking.

2.2.5 Rolling

Spread the sticky jujube leaves on the chopping board. After the leaf temperature is reduced, they are rolled into strips using both hands while they are kneaded clockwise. If too much strength is used, it is easy to crush the tea. After rolling for a few minutes, they are spread and continue kneaded into strips. Kneading is in the order of "light heavy light." The total kneading time is about 0.5h. Kneading should be done until the leaves can loosen naturally, and their color becomes dark green and bright.

2.2.6 Drying

Return the rolled jujube leaves to the pan at about 90 ° until they are dried. To ensure that the dry tea leaves remain in tight and curly strips, it is necessary to knead, break up, shake and stir continuously when drying. At the same time, the pan temperature is gradually reduced with the evaporation of water from the leaves. Finally, it is stabilized at about 40 °, and the tea aroma gradually increased. This is the jujube leaf tea product (D2). D1, D2, and fruit-bearing shoots are shown in Figure 1.

2.3 Analysis of non-volatile metabolites of jujube leaf tea before and after processing

2.3.1 Sample preparation and extraction

Grinding jujube leaves with liquid nitrogen, 50mg dry samples of jujube leaves before and after processing were accurately weighed and placed into a 1.5ml centrifuge tube, adding a 6 mm diameter grinding bead. 400 μl of extract (methanol: water =4:1 (v:v)) was added, containing 0.02 mg/ml of internal standard (l-2-chlorophenyl alanine). The frozen tissue samples were ground for 6 minutes (-10 °, 50 Hz). A low-temperature ultrasonic extraction was performed for 30 minutes (5 °, 40KHz), and then the samples were let to stand at -20 ° for 30 minutes. They were then centrifuged for 15min (13000g, 4 °), and the supernatant was transferred t to the injection vial with internal intubation for the analysis. In addition, 20 μl supernatant was taken from each sample and was mixed to be used as a quality control sample. It was used to monitor deviations in the analysis results and identify potential errors caused by the analytical instrument.

2.3.2 LC-MC conditions

The LC-MS instrument platform used was the HPLC-Q executive HF-X system (Thermo Scientific). The chromatographic conditions were as follows: the chromatographic column used was the ACQUITY UPLC HSS T3 (100 mm × 2.1 mm i.d., 1.8 μm; Waters, Milford, USA); mobile phase A was 95% water +5% acetonitrile (containing 0.1% formic acid); mobile phase B was 47.5% acetonitrile +47.5% isopropanol +5% water (containing 0.1% formic acid); the injection volume was 2 μL. The column temperature was 40 °. Elution procedure: 0min, 100% of phase A; 3.5min, 75.5% of phase A; 5min, phase A 35%; 5.5min, phase A 0%; 7.4min, phase A 0%; 7.6min, phase A 48.5%; 7.8min, 100% of phase A; 19min, phase A 100%.

Mass spectral analysis conditions: electrospray spray ion source (ESI) was used to collect mass spectrum signals through positive and negative ion scanning modes. The scan type was 70~1050 m/z, the sheath gas flow rate was 50 arb, the aux gas flow rate was 13 arb, the heater temperature was 425 °, and the capillary temperature was 325 °. The spray voltage was 3500 v and -3500 v in positive and negative ion modes, respectively.

2.3.3 Quantitative analysis of amino acids

Mixed 50mg of dry sample with 750μL of acetonitrile, sonicated for 30 minutes, then centrifuged the extract at 13000 rpm for 5 minutes, repeat once, and took the supernatant for LC-MS/MS detection. The LC-MS/MS system consisted of ultra-high performance liquid chromatography(ExionLC AD system) and mass spectrometry(AB SCIEX QTRAP 6500+), using a liquid chromatography column maintained at 35 °(Waters BEH Amide,100*2.1 mm,1.7 μm). The mobile solutions were water with 0.4% formic acid (A) and acetonitrile containing 0.4% formic acid (B). The chromatographic gradient table was shown in Table 1, the mass spectrometry condition adopted positive mode detection, with Curtain Gas of 35 psi and Collision Gas was Medium, the ionspray voltage was set to 5500 V, the source temperature was set to 350°, the nebulizer and heater gases were maintained at 70 psi.

2.4 GC-IMS analysis

GC-IMS analysis of volatile compounds in jujube leaves before and after processing was performed according to the method of Wang et al. (Wang et al., 2021). The FlavorSpec ® Flavor analyzer was used to measure the volatile headspace components in the samples. The fresh jujube leaves were cut, and the jujube leaf tea was ground; 1 g was accurately weighed from each and placed into a 20ml headspace bottle and on the machine after sealing. The headspace incubation temperature was 80 °, the incubation time was 15min, and the incubation speed was 500 rpm. The injection volume was 200ul, and the injection needle temperature was set at 85 °. Gas phase ion migration conditions were: MXT-WAX column, 30 meters, 0.53 mm ID, 1.0 μm df (RESTEK company, USA), column temperature 80 °, IMS temperature 45 °, analysis time 30min; The carrier gas was high-purity nitrogen (purity ≥ 99.999%), rate of 150 mL/min, and used the following programmed flow: 2 mL/min for 2 min,10 mL/min for 8 min, and raised to 100 mL/min within 10 min, and then held for 10 min.

TABLE 1 Chromatographic gradient table.

Time(min)	Velocity of flow(mL/min)	A%	B%
0	1	100	0
1	1	90	10
2.6	1	85	15
3.5	1	70	30
4	1	70	30
4.1	1	100	0
6	1	100	0

2.5 GC-MS analysis

Placed a dry sample (1g) and 1,3-dichlorobenzene (50mL, 0.5mg/mL) as the internal standard into an extraction bottle, equilibrated in a 100 ° water bath for 10 minutes, exposed the SPME fiber in the top space of the sample, performed volatile absorption for 45 minutes at 60 °, and then immediately inserted it into the GC(Agilent, USA) injection port (250 °) for desorption for 5 minutes. The heating procedure was as follows: maintained at 50 ° for 3 minutes, raised to 120 ° at 4 °/min, maintained for 8 minutes, then raised to 200 ° at 4 °/min, maintained for 3 minutes, and finally raised to 250 ° at 10 °/min, maintained for 3 minutes. Helium is used as the carrier gas, with a flow rate of 1.0mL/min and a split ratio of 1:60. The MS ion source temperature was maintained at 230 °. The GC-MS data detection results were retrieved and identified through the NIST14.0 spectral library. The concentration of each volatile substance was calculated according to equation (1) based on the peak area of the internal standard substance, and the OAV value of the volatile substance was calculated according to equation (2).

$$C_i(\mathrm{mg/L}) = \frac{A0}{Ais} * C_{is} \quad (1)$$

C_i was the concentration of the compound, C_{is} *was* the final concentration of the internal standard in the sample, A_0 was the peak area of the compound, and A_{is} was the peak area of the internal standard.

$$\mathrm{OAV(\mu g/L)} = \frac{Ci}{OTi} \quad (2)$$

C_i was the concentration of the compound, OT_i was the aroma threshold of the compound.

2.6 Statistical analysis

The experiments were repeated independently three times, and the results from each experiment were the average of three replicates. The raw data were imported into the metabonomics processing software ProgenesisQI (Waters Corporation, Milford,

USA) for baseline filtering, peak recognition, integration, retention time correction, and peak alignment. Finally, a data matrix containing information such as retention time, mass charge ratio, peak intensity, etc., was obtained. The software identified the characteristic peak library, and the MS and MS/MS mass spectrometry information was matched with the respective metabolic database. The MS mass error was set to less than 10 ppm, and the metabolites were identified according to their secondary mass spectrometry matching score. Multivariate statistical analysis will be conducted for the planned metabolite data set. The hypergeometric distribution algorithm was used to obtain the pathway of metabolite significant enrichment in the metabolic data set, and the BH method was used to correct the P value. When the corrected P value was<0.05, the pathway was considered to have significant enrichment.

The Vocal volatile component analysis software was used to view spectra and data's qualitative and quantitative analysis. The built-in NIST database and IMS database can carry out qualitative analyses of the compounds. The Reporter plug-in was used to directly compare the spectrum differences between samples (three-dimensional spectrum, two-dimensional top view, and difference spectrum). The Gallery plot plug-in was used for fingerprint comparison and quantitative comparison of volatile organic compounds between different samples.

3 Results and discussion

3.1 Non-volatile metabolite analysis of jujube leaf tea before and after processing

3.1.1 LC-MS non-targeted metabolome analysis of jujube leaf tea before and after processing

In this study, we analyzed and compared the metabolome of fresh jujube leaf and jujube leaf tea. We detected 761 peaks and identified 468 metabolites (Supplementary Materials Table S1), including 245 lipids and lipid-like molecules and 68 organic acids and their derivatives. Furthermore, 53 organic heterocyclic compounds were identified, such as furan, indole, and pyridine, as well as 28 carbohydrates and alcohols, 10 phenols and phenolic ethers, 9 flavonoids, 8 cinnamic acids, 8 coumarins, 7 nucleosides and nucleotides, 5 alkaloids, and their derivatives, and 27 other metabolites. The changes in classified non-volatile metabolites before and after processing were observed. As shown in Figure 2A, the total amount of non-volatile metabolites shows the following trend: D2>D1. The highest expression amounts are lipids and lipid-like molecules, organic acids and their derivatives, organic heterocyclic compounds, carbohydrates, and alcohols. After processing, the expression of 11 metabolites (except organic heterocyclic compounds and others) in jujube leaves increased to varying degrees, indicating that the nutritional value of jujube leaf tea was higher than that of jujube leaves.

The samples were comprehensively analyzed using unsupervised PCA statistical tools (including the quality control (QC) samples). As shown from the PCA score chart (Figure 2B), principal component 1 contributed 68.60% of the total variation, and principal component 2 contributed 20.00%, respectively, with all samples within the 95% confidence interval. QC samples, fresh jujube leaf, and jujube leaf tea samples were clustered into three groups. Therefore significant differences between the groups require further study. To quickly and accurately analyze the differences between groups, the OPLS-DA model with supervision function was used for analysis. The OPLS-DA scoring chart results (Figure 2C) showed that fresh jujube leaves and jujube leave tea samples were distributed on the left and right sides of the 95% confidence interval. The discrimination effect was obvious, indicating that the composition of the two samples was significantly different, attributed to differentially accumulated metabolites. The model parameters were two principal components, and its cumulative prediction rate was Q2 = 1, R2X=0.95, and R2Y=1, the regression lines of R2 and Q2 showed a downward trend as the replacement retention decreases(Figure 2D), indicating that the replacement test had passed and the model was reliable.

We brought the metabolites into KEGG database for classification and analysis of related pathways. The results showed that most metabolites were classified into "metabolism" which we expected (Figure 2E). The main metabolic pathways were lipid metabolism and amino acid metabolism. Subsequently, we conducted KEGG pathway enrichment analysis to identify differences in metabolic pathways between D1 and D2. As shown in Figure 2F, there were significant differences ($p<0.05$) in 11 metabolic pathways between D1 and D, and the top three were glycerophospholipid metabolism, tryptophan metabolism, and linoleic acid metabolism.

3.1.2 Dynamic changes in non-volatile metabolites of Jujube leaf tea before and after processing

Different metabolites were screened through a t-test, based on the parameters VIP > 1, $p<0.05$, fold change ≥ 1.5 or ≤ 0.5, to clarify the specific differences in chemical components of jujube leaves before and after processing. A total of 107 compounds with significant differences between groups were screened (Supplementary Materials Table S2), including 94 up-regulated and 13 down-regulated (Figure 3A). 107 differentially accumulated metabolites were identified, including 26 organic acids and derivatives, 18 amino acids and their derivatives, 17 lipids and lipid-like molecules, 11 furan, indole, pyridine, and other organic heterocyclic compounds, 8 carbohydrates and other organic oxygen compounds, 6 flavonoids, 5 phenol, and phenyl ether, 3 coumarins and derivatives, and 15 other metabolites (Figure 3B). To investigate the changes between the different metabolites more intuitively, a heat map of the 109 differentially accumulated metabolites was constructed (Figure 3C), the metabolites of D1 and D2 showed significant difference. Four important metabolites were selected for specific analysis, as shown in Figure 3D. Compared with D1, D2 has significantly increased the content of organic acids and their derivatives, lipids, and lipid-like molecules, and the difference becomes more significant, while the content of amino acids and their derivatives, flavonoids has little difference, almost no difference. The results are described below.

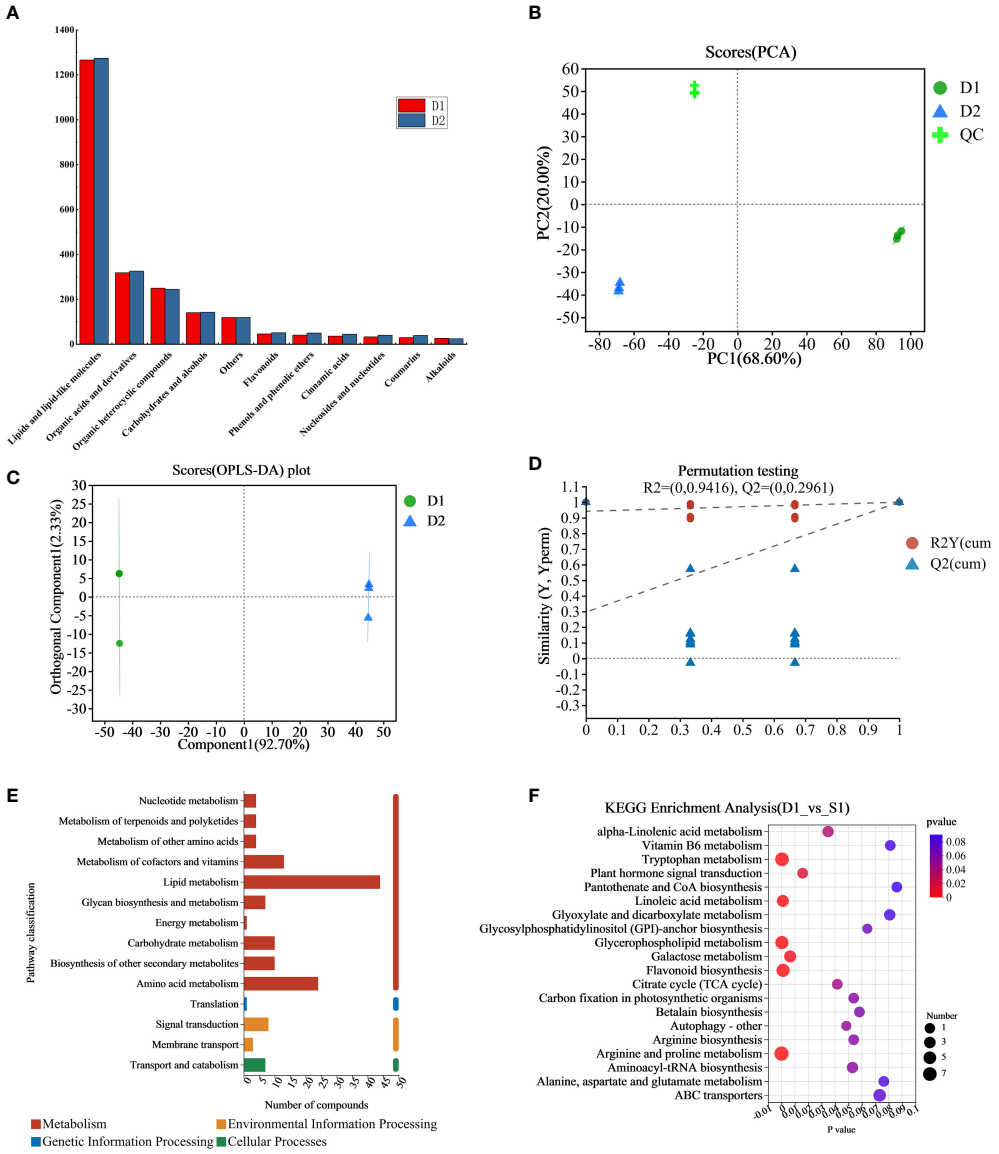

FIGURE 2
(A) Expression map of 11 metabolites in D1 and D2, **(B)** The PCA scores plot of the D1 group, the D2 group and the QC group, **(C)** OPLS-DA score plots of the D1 group versus the D2 group. **(D)** Displacement check diagram for D1 and D2. **(E)** D1 and D2 classification diagram of KEGG metabolic pathway, the ordinate is the second classification of KEGG metabolic pathway, and the abscissa is the number of metabolites annotated to this pathway. **(F)** D1 and D2 KEGG enrichment analysis bubble diagram, the abscissa is the enrichment significance p-value, and the ordinate is the KEGG pathway. The bubble size in the figure represents the number of metabolites enriched in the pathway. D1, Fresh jujube leaves; D2, Jujube leaf tea; QC, the quality control samples.

3.1.2.1 Organic acids

Organic acids can inhibit bitter and sour tastes and give fruity tastes and flavors. They are critical intermediate products of carbohydrate catabolism (HE and SUN, 2015). After jujube leaves are processed into tea, the organic acid content generally increases. Among them, hydroxyoctanoic acid and chorismic acid content changed more prominently, increasing by about 50%. Chorismic acid is an intermediate of aromatic amino acids biosynthesis in plants. It is a compound produced at a key metabolic bifurcation point, significantly contributing to the formation of tryptophan (Gibson and Gibson, 1964). As a result, the tryptophan content in D2 increased significantly.

3.1.2.2 Lipids and lipid-like molecules

Lipids are hydrophobic metabolites related to tea flavor quality (Li et al., 2021). Various lipid metabolites detected in our study include fatty acyl, glycerol lipids, glycerol phospholipids, and pregnenolone lipids. Lipid metabolism plays a significant role in D1 and D2, and the glycerophospholipid metabolic pathway is the most prominent. Except for methyl helianthenoate-a glucoside and neoacrimarine F, most lipid metabolites were higher in D2 than in D1 (D1 is fresh jujube leaf, D2 is jujube leaf tea). PC (16:0/18:3 (9Z, 12Z, 15Z)), PG(18:1(11Z)/18:3(9Z,12Z,15Z)), PG (20:4 (5Z,8Z,11Z,14Z)/22:6 (4Z,7Z,10Z,13Z,16Z,19Z)), and 1,2-Di-O-palmitoyl-3-O - (6-sulfoquinovopyranosyl) glycerol increased

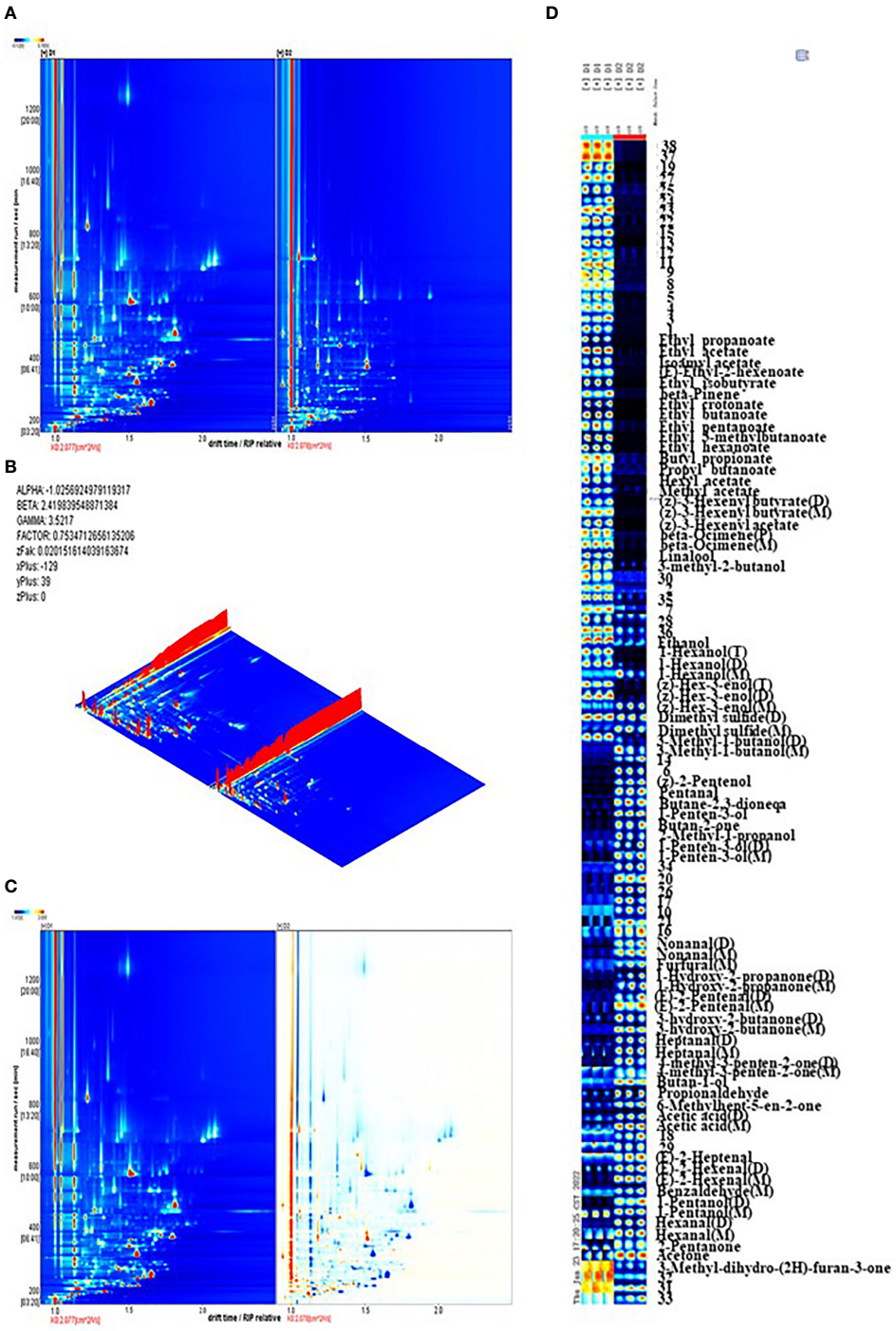

FIGURE 3
(A) Volcanic map of differential metabolites in D1 and D2, **(B)** Pie chart of the number of different types of 107 specific non-volatile metabolites in D1 vs D2, **(C)** and Heat maps of 107 different nonvolatile metabolites of jujube leaf tea before and after processing. D1, Fresh jujube leaves; D2, Jujube leaf tea. Each contains three repeats. **(D)** Thermogram of four types of non-volatile components in jujube leaf tea before and after processing. D1, Fresh jujube leaves; D2, Jujube leaf tea. Each contains three repeats.

most significantly. This might be due to the high processing temperature promoting lipid transformation. Previous research identified that during green tea production, Phosphatidylcholine, Phosphatidylglycerol, and Phosphatidylethanolamine showed an increasing trend after a long high-temperature exposure (Li et al., 2021), which is consistent with our results.

3.1.2.3 Amino acids and their derivatives

Amino acids play an essential role in tea soup and aroma (Yao et al., 2006) as shown in Table 2. In D2, L-(-)-threonine, L-phenylalanine, L-tryptophan, L-asparagine anhydrous, L-(-)-tyrosine, L-serine, L-asparticacid, L-(+)-arginine, L-alanine, L- glutamic acid increased significantly, potentially resulting

TABLE 2 Changes in amino acid content of jujube leaves before and after processing.

Amino acid	Concentration (ng/mg)		Significance
	D1	D2	
L-Alanine	0.7595 ± 0.0468	8.4164 ± 0.6122	**
L-(+)-Arginine	10.8746 ± 0.3730	34.3396 ± 0.9493	**
L-Asparagine Anhydrous	1.5223 ± 0.0398	10.5983 ± 0.5759	**
L-AsparticAcid	3.4421 ± 0.0718	9.9193 ± 0.0355	**
L-Glutamine	0.7001 ± 0.0220	2.9210 ± 0.1266	*
L-GlutamicAcid	0.0193 ± 0.0046	8.3479 ± 0.2546	**
Glycine	0.4184 ± 0.0699	0.6455 ± 0.1350	
L-Histidine	2.8057 ± 0.1341	4.7529 ± 0.1839	*
L-Isoleucine	4.9850 ± 0.8250	3.8939 ± 0.2091	*
L-Leucine	1.2892 ± 0.0548	1.9906 ± 0.0423	
L-Hydroxyproline	0.3454 ± 0.0060	1.4673 ± 0.1389	*
L-Tryptophan	1.1112 ± 0.1065	3.2294 ± 0.0540	*
L-(+)-Lysine	1.1182 ± 0.0036	1.4048 ± 0.0163	
L-Methionine	0.0516 ± 0.0025	0.7330 ± 0.0226	
L-Phenylalanine	0.8322 ± 0.0278	3.0297 ± 0.1093	*
L-Proline	1.1221 ± 0.0162	2.9393 ± 0.0395	
L-Serine	1.3104 ± 0.0373	6.3473 ± 0.1883	**
L-(-)-Threonine	0.5849 ± 0.0494	3.8235 ± 0.4293	*
L-(-)-Tyrosine	1.7618 ± 0.0773	3.2459 ± 0.0734	*
L-Valine	0.6081 ± 0.0114	1.6812 ± 0.0311	

*P<0.05, **P<0.01.

from protein decomposition (Fraser et al., 2014; Liu et al., 2018) and oxidation of amino acids such as L-asparagine anhydrous, L-(+)-lysine, L-Phenylalanine, and L-asparticacid (Nathanael and Wille, 2019). The increase in tryptophan was probably due to the promotion of chorismic acid, a biosynthetic intermediate (Gibson and Gibson, 1964). This was related to the significant enrichment of the tryptophan metabolism pathway. Amino acids had flavor characteristics. The content of sweet amino acids (serine, threonine, alanine), fresh amino acids (aspartic acid, glutamic acid), and aromatic amino acids (arginine, tyrosine, phenylalanine) increased after processing into D2, while the content of bitter amino acids (isoleucine) decreased, bringing a fresh and sweet taste to jujube leaf tea (Scharbert and Hofmann, 2005; Yu et al., 2014; Dai et al., 2015; Yu and Yang, 2020).

3.1.2.4 Flavonoids

Flavonoids are essential active ingredients in both fresh jujube leaves and processed tea. We found that the contents of proanthocyanidin A5', dihydrobrinetin, 3,3'-digalloylprocyanidin B2, epiafzelechin- (4b->8) -epicatechin 3,3'-digallate and epigallocatechin 3-o- (4-hydroxybenzoate) increased in jujube leaves after tea processing. Notably, the concentration of 6-hydrohydraidzein 4'-glucoside increased fivefold after processing compared to the fresh jujube leaves due to the hydrothermal hydrolysis of flavonoid glycosides. Aglycones and glycosomes are also produced during processing. Glycoside flavonoids can significantly enhance pentobarbital-induced sleep (Wang et al., 2008). This may make jujube leaf tea have the function of helping sleep. Previous studies have shown that flavonoid aglycones are absorbed by the body relatively quickly, which enhances their functional activity.

3.2 Volatile metabolites analysis in jujube leaf tea before and after processing

3.2.1 GC-IMS determination of volatile metabolites in jujube leaves before and after processing

To identify the presence and changes in aromatic compounds in jujube leaf tea processing, we carried out GC-IMS to obtain global IMS information. The topographic map obtained from the GC-IMS analysis is shown in Figure 4A. The three-dimensional spectra of jujube leaf tea volatile components before and after processing are presented in Figure 4B. There was a significant difference between volatile organic compounds between D1 and D2. To evaluate these

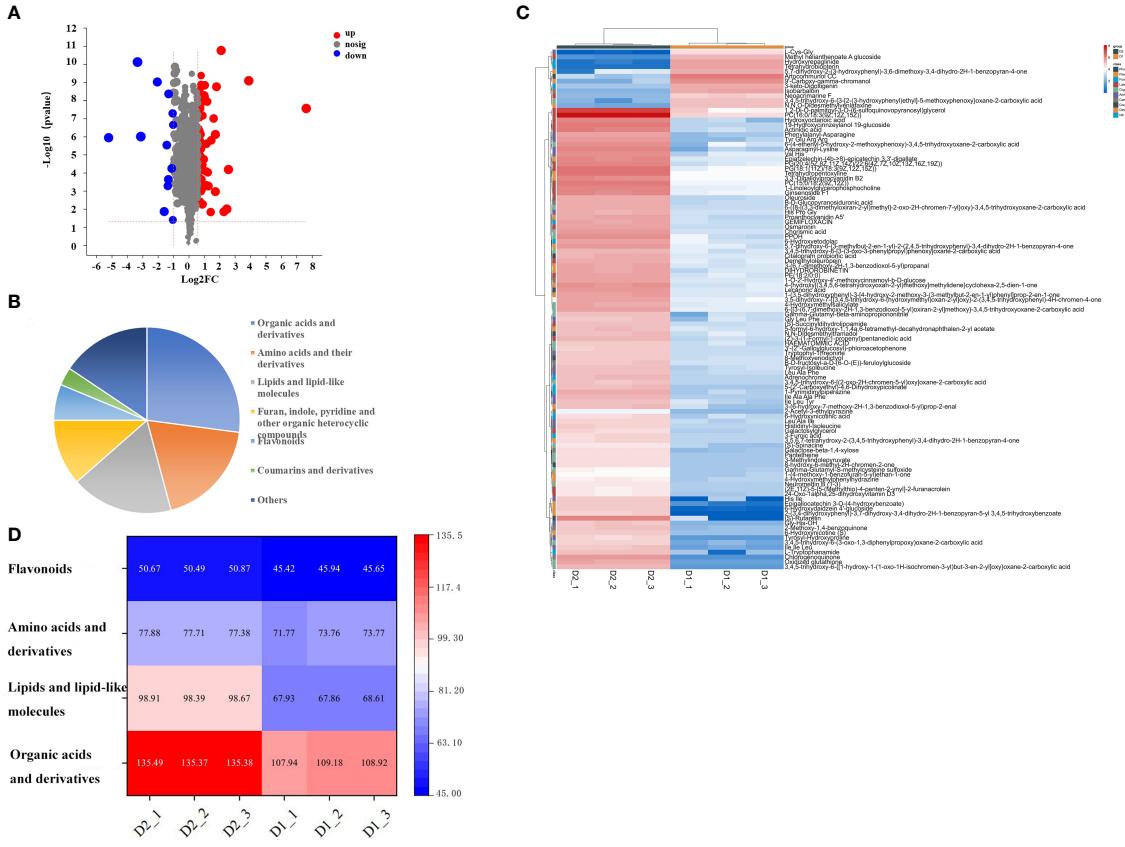

FIGURE 4
(A) The topographic plot of D1 and D2 based on GC-IMS, The ordinate represents the retention time of gas chromatography, and the abscissa represents the ion migration time. Each point on both sides of the rip peak(the horizontal red line) represents a volatile organic compound. The compound concentration is represented by different colors, with white corresponding to low concentration and red corresponding to high concentration. The darker the color, the greater the concentration. **(B)** The three-dimensional topographic map of D1 and D2, **(C)** Difference comparison plots of D1 and D2, **(D)** Dynamic fingerprints of jujube leaves before and after processing, generated by Gallery Plot. Each row represents the sample signal peak, while each column represents each volatile compound in the different samples. The color represents the volatile compound concentration. The brighter the color, the higher the concentration.

differences more in-depth, the difference comparison mode was adopted: the spectrum of D1 was selected as the reference, and the spectrum of D2 was deducted from the reference. Suppose two volatile organic compounds have the same concentration in D1 and D2. In that case, the background after deduction is white (Figure 4C). At the same time, red represents that the target compound concentration is higher than the reference, and blue is lower, respectively. As shown in Figure 4C, most signals appear in the retention time range of 200 to 600 seconds and the drift time range of 1.0 to 1.8 seconds. There are obvious red points representing a higher compound concentration and blue spots representing a lower concentration at this location in the D2 map. This indicates that compared with D1, the volatile compound composition of D2 has changed significantly. The dynamic changes of these volatile components form the unique flavor characteristics of jujube leaf tea.

A total of 112 peaks were observed through qualitative analysis of volatile compounds. Compared with the GC - IMS library, 74 peaks of 52 compounds were identified, including 17 esters, 11 alcohols, 10 aldehydes, 10 ketones, 2 olefins, 1 acid, and 1 sulfide (Supplementary Materials Table S3). Among them, 38 peaks could not be annotated. Certain volatile compounds may produce numerous signals due to high proton affinity or signals that allow ions to form dimers and trimers when moving in the drift tank, such as (z) -3-hexenyl butyrate, hexyl 2-methyl butanoate, 1-hexanol, nonanal, 1-hydro-2-propanone. The visualization of characteristic fingerprints was carried out to observe the signal difference of volatile compounds before and after processing (Figure 4D).

After jujube leaf processing, esters (ethyl acetate, propyl butyrate, ethyl isobutyrate, ethyl crotonate, ethyl 3-methyl butyrate, folic alcohol acetate, Etc.), partial alcohols (linalool, 3-methyl-2-butanol, ethanol, 1-hexanol, Z-3-hexen-1-alcohol, 3-methyl butanol), olefins(β- Pinene, β- Ocimene) and methyl sulfide were significantly reduced (Figure 4D, red box), which reduced grass and fruit flavors (Colonges et al., 2022; Li et al., 2022). Aldehyde content (glutaraldehyde, nonanal, furfural, (E)-2-hexenal, (E)-2-pentenoaldehyde, heptanaldehyde, etc.), ketones (2,3-butanedione, 2-butanone, 1-penten-3-one, hydroxyacetone, etc.), some alcohols (Z-2-pentenol, 1-penten-3-alcohol, isobutanol) and acetic acid increased significantly (Figure 4D, yellow box), providing the aromas of almond oil, cream, and fragrance (Kfoury et al., 2018; Huang et al., 2022). Ethyl 3-

methylbutyrate and ethyl crotonate accounted for 19.32% of the volatile metabolites in D1, occupying a dominant position. (E)-2-hexenal (dimer) in D2 accounts for 11% of the volatile substances, accounting for the highest proportion, and emits a unique green leaf smell(Liu, Liu et al., 2022). It is also the main active aroma compound in jujube fruit, thus giving jujube leaf tea the aroma of the jujube fruit (Song et al., 2019).

3.2.2 GC-MS determination of volatile metabolites in jujube leaves before and after processing

To study the changes in the content of volatile metabolites in jujube leaves before and after processing, and to supplement the determination of metabolites by GC-IMS, solid-phase microextraction technology was used to extract volatile substances, and the extracts were analyzed using gas chromatography-mass spectrometry. A total of 24 volatile compounds were identified by GC-MS, and it was found that there was a significant increase in Hexanal, 1-Penten-3-ol, (E) -2-Hexanal, 6-Methyl-5-hepten-2-one, and Acetic acid in D2, while there was a significant decrease in 2-ethyl-Furan, (Z) -3-Hexenyl acetate, (Z) -3-Hexen-1-ol, Oxime, methoxy-phenyl -, and Eugenol. Allyl ethyl ether, D-limonene, Benzene,4-ethyl-1,2-dimethyl-, (Z)-Hex-3-enyl2-methylbutyrate, 3,5-Octadien-2-one, Hexanoic acid, 1,3-cis,5-cis-Octatriene, these substances grew from scratch during the processing of jujube leaf tea, giving it a unique aroma.

OAV is used to evaluate the contribution of volatile compounds to the aroma of tea. It is generally believed that volatile metabolites with OAV≥1 contribute significantly to the overall aroma, while volatile metabolites with OAV≥10 are identified as important aroma components (Tan et al., 2022). From the Supplementary Materials Table S4, it can be concluded that there are 9 substances with OAV≥1 in D1 and 8 in D2. 2-pentyl-Furan, (E) -2-Hexanal, 1-Pentanol, 6-Methyl-5-hepten-2-one were common and important aroma components in D1 and D2. Eugenol was the volatile compound with the highest OAV value in D1, which can be considered to be the characteristic flavor substance in jujube leaves. Eugenol, as a natural compound, has various pharmacological effects, such as antioxidant, anticancer, hypoglycemic, antibacterial, etc (Pramod et al., 2010). Natural food flavor (E)-2-Hexanal is a potential antifungal compound with high content in D2 (Ma et al., 2019), which was the key flavor active substance in D2. By combining the identified volatile flavor compounds with their aroma thresholds, we further understood the specific contribution of each substance to the overall flavor formation.

3.3 Discussion

Extensively targeted metabonomics has been successfully applied to large-scale metabolite analysis and comparative metabonomics of many essential plant species (Mattivi et al., 2006; Wang et al., 2016; Cebulj et al., 2017; Price et al., 2020). In jujube, previous studies focused more on the metabolites of jujube fruits including the nutrient components, active components, the color in different maturity (Feng et al., 2020; Shen et al., 2022; Shi et al., 2022). Comprehensive research on LC-MS-based metabolomics, GC-IMS and GC-MS analysis has not yet to be carried out on the jujube leaves before and after tea processing. In this study, we found that there were 107 different metabolites in fresh jujube leaves and leaf tea. Therefore, this study provided insights into the changes of metabolites in jujube leaves before and after processing into tea.

The aroma and taste of tea are important attributes (Ho et al., 2015; Han et al., 2016; Chen et al., 2020). Based on the volatile metabolites in jujube leaf tea, we can predict that jujube leaf tea has the scent of soft leaves, fruit, cream and fat. Among all metabolites, (E)-2-Hexenal was the most volatile metabolite, providing a solid aroma of green leaves and fruits (Buttery et al., 1987). 2-pentyl-furan provided a roasted aroma, often presented in white tea (Lin et al., 2021). 6-Methyl-5-hepten-2-one had a fresh fruity aroma and citrus like aroma, making it an intermediate in the synthesis of linalool (Baldwin et al., 2000). In our laboratory we carried out the sensorial evaluation of the jujube tea leaf. It was concluded that the jujube leaf tea had a clear soup color, a delightful taste and frangrance of roses, oranges and tender leaves, which was consistent with our prediction.

Fresh leaves contain various ester compounds. After processing into jujube leaf tea, their contents decreased significantly, while aldehydes, ketones, and olefins increased significantly. This may be due to the high temperature during the fixation processing procedure, which leads to a large amount of volatilization of alcohols and aldehydes with low boiling points, isomerization and oxidation reaction, and the formation of high boiling point volatile compounds with special flavor (Coxon et al., 1970). The increase of ketones such as 6-methyl-5-hepten-2-one is caused by the thermal degradation of carotenoids. Volatile substances such as Hexanal, Pentanal, Nonanal, 1-Penten-3-ol, (E) - 2-Hexanal, (E) - 2-Hexen-1-ol are formed with the assistance of lipoxygenase. Lipids are oxidized by lipoxygenase to form lipid hydroperoxide, which is then cracked by hydroperoxide lyase to form six carbon aliphatic aromatic compounds, such as (Z) - 3-hexenal and n-hexanal. Subsequently, these aldehydes can be further reduced to alcohols directly through alcohol dehydrogenase, or isomerized to trans isomers, and then reduced to alcohols (Ho et al., 2015).The Strecker synthesis of amino acids, glucosides, and glycosides also generates alcohols, ketones, aldehydes, alkenes, and aromatic hydrocarbons at high temperatures (Ho et al., 2015; Feng et al., 2019, Li C. et al., 2019, Li P. et al., 2019). It has been previously shown that drying can promote the glycerol phospholipids conversion to unsaturated fatty acids (Wang et al., 2022). These eventually form the unique volatile compound profile of jujube leaf green tea. In other words, jujube leaf processing can modify the amino acids and lipids content affecting the flavor and intensity of jujube leaf tea. Therefore, temperature, rolling, and other vital parameters affect the degree of the formation/transformation of non-volatile compounds in jujube leaves. These can be adjusted and fine-tuned to obtain jujube leaf tea products with different flavor characteristics.

It is reported that flavonoids have the effect of sedation and hypnosis (Jiang et al., 2007; San et al., 2013; Shi et al., 2016). There are many kinds of flavonoids in jujube leaves. After processing into

jujube leaf tea, the content of flavonoids increased. Flavanol is one of the most typical and plentiful metabolites of tea (Scharbert and Hofmann, 2005). After processing fresh leaves into leaf tea, the content of Epicatechin Ent - (4alpha ->6) - ent Epicatechin, (+/-) - Catechin, and Epigallocatechin augmented. In this study, no exciting chemical components, such as caffeine and ephedrine, were found in jujube leaf tea. As flavonoids have sedating and hypnotic effects, we predict that jujube leaf tea will have hypnotic effects. This necessitates further study.

4 Conclusion

Jujube leaf tea metabolomic analysis combined with GC-IMS and GC-MS showed that jujube leaves' non-volatile and volatile metabolites changed significantly before and after processing. A total of 468 non-volatile were identified, and 109 non-volatile metabolites were differentially accumulated and further evaluated. We found that the rapid transformation of lipids, organic acids, amino acids, and flavonoids was the main factor regulating the jujube leaf tea sensory quality. The pathway enrichment analysis revealed that glycerophospholipid metabolism, tryptophan metabolism, and linoleic acid metabolism had the most significant impact. 52 and 24 volatile metabolites were identified by GC-IMS and GC-MS, respectively. Eugenol was the main flavor substances in fresh jujube leaves, and (E) - 2-Hexenal was the fundamental volatile substance of jujube leaf tea. Besides the changes in volatile metabolites, amino acids and lipids play an essential role in aromatic compound formation. This study provides novel insights into metabolic profile changes before and after jujube leaf processing and how they affect its sensory and health-promoting properties. It provides technical insights for improving the quality and efficiency of the jujube processing industry.

Data availability statement

The original contributions presented in the study are included in the article/Supplementary Material. Further inquiries can be directed to the corresponding authors.

Author contributions

All authors listed have made a substantial, direct, and intellectual contribution to the work and approved it for publication.

Funding

This research was financially supported by the Key R&D Projects of Ministry of Science and Technology of the People's Republic of China (2021YFD1000404), Funding Project for Introducing Overseas Students in Hebei Province (C20210362), Project of Intelligent Horticulture Discipline Group of Hebei Agricultural University.

Conflict of interest

The authors declare that the research was conducted in the absence of any commercial or financial relationships that could be construed as a potential conflict of interest.

Publisher's note

All claims expressed in this article are solely those of the authors and do not necessarily represent those of their affiliated organizations, or those of the publisher, the editors and the reviewers. Any product that may be evaluated in this article, or claim that may be made by its manufacturer, is not guaranteed or endorsed by the publisher.

Supplementary material

The Supplementary Material for this article can be found online at: https://www.frontiersin.org/articles/10.3389/fpls.2023.1179553/full#supplementary-material

References

Albinsky, D., Sawada, Y., Kuwahara, A., Nagano, M., Hirai, A., Saito, K., et al. (2010). Widely targeted metabolomics and coexpression analysis as tools to identify genes involved in the side-chain elongation steps of aliphatic glucosinolate biosynthesis. *Amino Acids* 39 (4), 1067–1075. doi: 10.1007/s00726-010-0681-5

Baldwin, E. A., Scott, J. W., Shewmaker, C. K., and Schuch, W. (2000). Flavor trivia and tomato aroma: biochemistry and possible mechanisms for control of important aroma components. *HortScience* 35 (6), 1013–1021. doi: 10.21273/HORTSCI.35.6.1013

Buttery, R. G., Ling, L. C., and Light, D. M. (1987). Tomato leaf volatile aroma components. *J. Agric. Food Chem.* 35 (6), 1039–1042. doi: 10.1021/jf00078a043

Cebulj, A., Cunja, V., Mikulic-Petkovsek, M., and Veberic, R. (2017). Importance of metabolite distribution in apple fruit. *Scientia Hortic.* 214, 214–220. doi: 10.1016/j.scienta.2016.11.048

Chen, S., Liu, H., Zhao, X., Li, X., Shan, W., Wang, X., et al. (2020). Non-targeted metabolomics analysis reveals dynamic changes of volatile and non-volatile metabolites during oolong tea manufacture. *Food Res. Int.* 128, 108778. doi: 10.1016/j.foodres.2019.108778

Cheng, L., Yang, Q., Chen, Z., Zhang, J., Chen, Q., Wang, Y., et al. (2020). Distinct changes of metabolic profile and sensory quality during qingzhuan tea processing revealed by LC-MS-based metabolomics. *J. Agric. Food Chem.* 68 (17), 4955–4965. doi: 10.1021/acs.jafc.0c00581

Colonges, K., Jimenez, J.-C., Saltos, A., Seguine, E., Solorzano, R. G. L., Fouet, O., et al. (2022). Integration of GWAS, metabolomics, and sensorial analyses to reveal novel metabolic pathways involved in cocoa fruity aroma GWAS of fruity aroma in theobroma cacao. *Plant Physiol. Biochem.* 171, 213–225. doi: 10.1016/j.plaphy.2021.11.006

Coxon, D., Holmes, A., and Ollis, W. (1970). Isotheaflavin. a new black tea pigment. *Tetrahedron Lett.* 11 (60), 5241–5246. doi: 10.1016/S0040-4039(00)99984-2

Dai, W., Qi, D., Yang, T., Lv, H., Guo, L., Zhang, Y., et al. (2015). Nontargeted analysis using ultraperformance liquid chromatography–quadrupole time-of-flight mass spectrometry uncovers the effects of harvest season on the metabolites and taste quality of tea (Camellia sinensis l.). *J. Agric. Food Chem.* 63 (44), 9869–9878. doi: 10.1021/acs.jafc.5b03967

Dai, W., Xie, D., Lu, M., Li, P., Lv, H., Yang, C., et al. (2017). Characterization of white tea metabolome: comparison against green and black tea by a nontargeted metabolomics approach. *Food Chem.* 96, 40–45. doi: 10.1016/j.foodres.2017.03.028

Das, P. R., Kim, Y., Hong, S.-J., and Eun, J.-B. (2019). Profiling of volatile and non-phenolic metabolites–amino acids, organic acids, and sugars of green tea extracts obtained by different extraction techniques. *Food Chem.* 296, 69–77. doi: 10.1016/j.foodchem.2019.05.194

Deguchi, Y., and Miyazaki, K. J. N. (2010). Anti-hyperglycemic and anti-hyperlipidemic effects of guava leaf extract. *Nutr. Metabol.* 7 (1) 1–10. doi: 10.1186/1743-7075-7-9

Feng, Z., Gao, Z., Jiao, X., Shi, J., and Wang, R. (2020). Widely targeted metabolomic analysis of active compounds at different maturity stages of 'Hupingzao'jujube. *J. Food Composition Anal.* 88, 103417. doi: 10.1016/j.jfca.2020.103417

Feng, Z., Li, Y., Li, M., Wang, Y., Zhang, L., Wan, X., et al. (2019). Tea aroma formation from six model manufacturing processes. *Food Chem.* 285, 347–354. doi: 10.1016/j.foodchem.2019.01.174

Fraser, K., Lane, G. A., Otter, D. E., Harrison, S. J., Quek, S.-Y., Hemar, Y., et al. (2014). Non-targeted analysis by LC–MS of major metabolite changes during the oolong tea manufacturing in new Zealand. *Food Chem.* 151, 394–403. doi: 10.1016/j.foodchem.2013.11.054

Gibson, M. I., and Gibson, F. (1964). Preliminary studies on the isolation and metabolism of an intermediate in aromatic biosynthesis: chorismic acid. *Biochem. J.* 90 (2), 248. doi: 10.1042/bj0900248

Han, Z.-X., Rana, M. M., Liu, G.-F., Gao, M.-J., Li, D.-X., Wu, F.-G., et al. (2016). Green tea flavour determinants and their changes over manufacturing processes. *Food Chem.* 212, 739–748. doi: 10.1016/j.foodchem.2016.06.049

HE, S. P. G., and SUN, Y. (2015). Research progress of organic acids in tea. *Subtropical Agric. Res.* 11 (1), 63–67. doi: 10.13321/j.cnki.subtrop.agric.res.2015.01.013

Ho, C.-T., Zheng, X., and Li, S. (2015). Tea aroma formation. *Food Sci. Hum. wellness* 4 (1), 9–27. doi: 10.1016/j.fshw.2015.04.001

Hua, Y., Xu, X.-x., Guo, S., Xie, H., Yan, H., Ma, X.-f., et al. (2022). Wild jujube (Ziziphus jujuba var. spinosa): a review of its phytonutrients, health benefits, metabolism, and applications. *J. Agric. Food Chem.* 70 (26), 7871–7886.

Huang, W., Fang, S., Wang, J., Zhuo, C., Luo, Y., Yu, Y., et al. (2022). Sensomics analysis of the effect of the withering method on the aroma components of keemun black tea. *Food Chem.* 395, 133549. doi: 10.1016/j.foodchem.2022.133549

Jiang, J.-G., Huang, X.-J., Chen, J., and Lin, Q.-S. (2007). Comparison of the sedative and hypnotic effects of flavonoids, saponins, and polysaccharides extracted from semen ziziphus jujube. *Natural Product Res.* 21 (4), 310–320. doi: 10.1080/14786410701192827

Kfoury, N., Baydakov, E., Gankin, Y., and Robbat, A.Jr (2018). Differentiation of key biomarkers in tea infusions using a target/nontarget gas chromatography/mass spectrometry workflow. *Food Res. Int.* 113, 414–423. doi: 10.1016/j.foodres.2018.07.028

Lee, H.-I., Kim, M.-S., Lee, K.-M., Park, S.-K., Seo, K.-I., Kim, H.-J., et al. (2011). Anti-visceral obesity and antioxidant effects of powdered sea buckthorn (Hippophae rhamnoides l.) leaf tea in diet-induced obese mice. *Food Chem. Toxicol.* 49 (9), 2370–2376.

Li, J., Hao, C., Jia, H., Zhang, J., Wu, H., Ning, J., et al. (2022). "Aroma characterization and their changes during the processing of black teas from the cultivar, camellia sinensis (L.) o. kuntze cv. jinmudan. *J. Food Composition And Anal.* 108, 104449. doi: 10.1016/j.jfca.2022.104449

Li, J., Hua, J., Yuan, H., Deng, Y., Zhou, Q., Yang, Y., et al. (2021). Investigation on green tea lipids and their metabolic variations during manufacturing by nontargeted lipidomics. *Food Chem.* 339, 128114. doi: 10.1016/j.foodchem.2020.128114

Li, C., YuLong, Y., ChunYan, W., JingNa, Y., and HuaRong, T. (2019). Research progress on carotenoid aroma precursors in tea. *Food Fermentation Industries* 45 (5), 266–273.

Li, P., Zhu, Y., Lu, M., Yang, C., Xie, D., Tan, J., et al. (2019). Variation patterns in the content of glycosides during green tea manufacturing by a modification-specific metabolomics approach: enzymatic reaction promoting an increase in the glycosidically bound volatiles at the pan firing stage. *Food Chem.* 279, 80–87. doi: 10.1016/j.foodchem.2018.11.148

Lin, Q., Ni, H., Wu, L., Weng, S. Y., Li, L., and Chen, F. (2021). Analysis of aroma-active volatiles in an SDE extract of white tea. *Food Sci. Nutr.* 9 (2), 605–615. doi: 10.1002/fsn3.1954

Liu, H.-Y., Liu, Y., Li, M.-Y., Mai, Y.-H., Guo, H., Wadood, S. A., et al. (2022). The chemical, sensory, and volatile characteristics of instant sweet tea (Lithocarpus litseifolius [Hance] chun) using electronic nose and GC-MS-based metabolomics analysis. *LWT* 163, 113518. doi: 10.1016/j.lwt.2022.113518

Liu, M., Wang, J., Wang, L., Liu, P., Zhao, J., Zhao, Z., et al. (2020). The historical and current research progress on jujube–a superfruit for the future. *Horticulture Res.* 7. doi: 10.1038/s41438-020-00346-5

Liu, P.-P., Yin, J.-F., Chen, G.-S., Wang, F., and Xu, Y.-Q. (2018). Flavor characteristics and chemical compositions of oolong tea processed using different semi-fermentation times. *J. Food Sci. Technol.* 55 (3), 1185–1195. doi: 10.1007/s13197-018-3034-0

Ma, W., Zhao, L., Zhao, W., and Xie, Y. (2019). "(E)-2-Hexenal, as a potential natural antifungal compound, inhibits aspergillus flavus spore germination by disrupting mitochondrial energy metabolism. *J. Agric. Food Chem.* 67 (4), 1138–1145. doi: 10.1021/acs.jafc.8b06367

Mattivi, F., Guzzon, R., Vrhovsek, U., Stefanini, M., and Velasco, R. (2006). Metabolite profiling of grape: flavonols and anthocyanins. *J. Agric. Food Chem.* 54 (20), 7692–7702. doi: 10.1021/jf061538c

Nathanael, J. G., and Wille, U. (2019). Oxidative damage in aliphatic amino acids and di-and tripeptides by the environmental free radical oxidant NO3•: the role of the amide bond revealed by kinetic and computational studies. *J. Organic Chem.* 84 (6), 3405–3418. doi: 10.1021/acs.joc.8b03224

Pramod, K., Ansari, S. H., and Ali, J. (2010). Eugenol: a natural compound with versatile pharmacological actions. *Natural product Commun.* 5 (12), 1934578X1000501236. doi: 10.1177/1934578X1000501236

Price, E. J., Drapal, M., Perez-Fons, L., Amah, D., Bhattacharjee, R., Heider, B., et al. (2020). Metabolite database for root, tuber, and banana crops to facilitate modern breeding in understudied crops. *Plant J.* 101 (6), 1258–1268. doi: 10.1111/tpj.14649

Rietveld, A., and Wiseman, S. (2003). Antioxidant effects of tea: evidence from human clinical trials. *J. Nutr.* 133 (10), 3285S–3292S. doi: 10.1093/jn/133.10.3285S

Sakanaka, S., Tachibana, Y., and Okada, Y. (2005). Preparation and antioxidant properties of extracts of Japanese persimmon leaf tea (kakinoha-cha). *Food Chem.* 89 (4), 569–575. doi: 10.1016/j.foodchem.2004.03.013

San, A. M. M., Thongpraditchote, S., Sithisarn, P., and Gritsanapan, W. (2013). Total phenolics and total flavonoids contents and hypnotic effect in mice of ziziphus mauritiana lam. seed extract. *Evidence-Based complementary Altern. Med.* 2013.

Sawada, Y., Akiyama, K., Sakata, A., Kuwahara, A., Otsuki, H., Sakurai, T., et al. (2009). Widely targeted metabolomics based on large-scale MS/MS data for elucidating metabolite accumulation patterns in plants. *Plant Cell Physiol.* 50 (1), 37–47. doi: 10.1093/pcp/pcn183

Scharbert, S., and Hofmann, T. (2005). Molecular definition of black tea taste by means of quantitative studies, taste reconstitution, and omission experiments. *J. Agric. Food Chem.* 53 (13), 5377–5384. doi: 10.1021/jf050294d

Shen, B., Zhang, Z., Shi, Q., Du, J., Xue, Q., and Li, X. (2022). Active compound analysis of ziziphus jujuba cv. jinsixiaozao in different developmental stages using metabolomic and transcriptomic approaches. *Plant Physiol. Biochem.* 189, 14–23. doi: 10.1016/j.plaphy.2022.08.015

Shi, Q., Han, G., Liu, Y., Jiang, J., Jia, Y., and Li, X. (2022). Nutrient composition and quality traits of dried jujube fruits in seven producing areas based on metabolomics analysis. *Food Chem.* 385, 132627. doi: 10.1016/j.foodchem.2022.132627

Shi, M.-M., Piao, J.-H., Xu, X.-L., Zhu, L., Yang, L., Lin, F.-L., et al. (2016). Chinese Medicines with sedative–hypnotic effects and their active components. *Sleep Med. Rev.* 29, 108–118. doi: 10.1016/j.smrv.2015.10.001

Song, J., Bi, J., Chen, Q., Wu, X., Lyu, Y., and Meng, X. (2019). Assessment of sugar content, fatty acids, free amino acids, and volatile profiles in jujube fruits at different ripening stages. *Food Chem.* 270, 344–352.

Tan, F., Wang, P., Zhan, P., and Tian, H. (2022). Characterization of key aroma compounds in flat peach juice based on gas chromatography-mass spectrometry-olfactometry (GC-MS-O), odor activity value (OAV), aroma recombination, and omission experiments. *Food Chem.* 366, 130604.

Wang, L.-E., Bai, Y.-J., Shi, X.-R., Cui, X.-Y., Cui, S.-Y., Zhang, F., et al. (2008). Spinosin, a c-glycoside flavonoid from semen zizhiphi spinozae, potentiated pentobarbital-induced sleep via the serotonergic system. *Biochem. Behav.* 90 (3), 399–403.

Wang, S., Tu, H., Wan, J., Chen, W., Liu, X., Luo, J., et al. (2016). Spatio-temporal distribution and natural variation of metabolites in citrus fruits. *Food Chem.* 199, 8–17.

Wang, X., Yang, H., Tian, R., Mo, Y., Dong, L., Shen, C., et al. (2021). Effect of the joint fermentation of pyracantha powder and glutinous rice on the physicochemical characterization and functional evaluation of rice wine. *Food Sci. Nutr.* 9 (11), 6099–6108.

Wang, D., Zhang, L., Huang, X., Wang, X., Yang, R., Mao, J., et al. (2018). Identification of nutritional components in black sesame determined by widely targeted metabolomics and traditional Chinese medicines. *Molecules* 23 (5), 1180.

Wang, P., Zhong, L., Yang, H., Zhang, J., Hou, X., Wu, C., et al. (2022). Comprehensive comparative analysis of lipid profile in dried and fresh walnut kernels by UHPLC-Q-Exactive Orbitrap/MS. *Food Chem.* 386, 132706.

Wilson, R. D., and Islam, S. (2015). Effects of white mulberry (Morus alba) leaf tea investigated in a type 2 diabetes model of rats. *Acta Pol. Pharm.* 72, 1, 153–160.

Wu, L., Huang, X., Liu, S., Liu, J., Guo, Y., Sun, Y., et al. (2020). Understanding the formation mechanism of oolong tea characteristic non-volatile chemical constitutes during manufacturing processes by using integrated widely-targeted metabolome and DIA proteome analysis. *Food Chem.* 310, 125941.

Xu, C., Liang, L., Yang, T., Feng, L., Mao, X., and Wang, Y. (2021). In-vitro bioactivity evaluation and non-targeted metabolomic analysis of green tea processed from different tea shoot maturity. *LWT* 152, 112234.

Yao, L., Liu, X., Jiang, Y., Caffin, N., D'Arcy, B., Singanusong, R., et al. (2006). Compositional analysis of teas from Australian supermarkets. *Food Chem.* 94 (1), 115–122. doi: 10.1016/j.foodchem.2004.11.009

Yu, Z., and Yang, Z. (2020). Understanding different regulatory mechanisms of proteinaceous and non-proteinaceous amino acid formation in tea (Camellia sinensis) provides new insights into the safe and effective alteration of tea flavor and function. *Crit. Rev. Food Sci. Nutr.* 60 (5), 844–858. doi: 10.1080/10408398.2018.1552245

Yu, P., Yeo, A. S.-L., Low, M.-Y., and Zhou, W. (2014). Identifying key non-volatile compounds in ready-to-drink green tea and their impact on taste profile. *Food Chem.* 155, 9–16. doi: 10.1016/j.foodchem.2014.01.046

Zemouri-Alioui, S., Kurt, B. Z., Sonmez, F., and Louaileche, H. (2019). Optimization of ultrasound-assisted extraction of total phenolic contents and antioxidant activity using response surface methodology from jujube leaves (Ziziphus jujuba) and evaluation of anticholinesterase inhibitory activity. *J. Food Measurement Characterization* 13 (1), 321–329. doi: 10.1007/s11694-018-9947-5

Zhang, Y. (2016). Study on the taste characteristics of the main catechins on green tea infusion. *Chin. Acad. Agric. Sci.* 31–93.

Zhang, R., Chen, J., Shi, Q., Li, Z., Peng, Z., Zheng, L., et al. (2014). Phytochemical analysis of Chinese commercial ziziphus jujube leaf tea using high performance liquid chromatography–electrospray ionization-time of flight mass spectrometry. *Food Res. Int.* 56, 47–54. doi: 10.1016/j.foodres.2013.12.019

Zhang, L., Liu, P., Li, L., Huang, Y., Pu, Y., Hou, X., et al. (2018). Identification and antioxidant activity of flavonoids extracted from xinjiang jujube (Ziziphus jujube mill.) leaves with ultra-high pressure extraction technology. *Molecules* 24 (1), 122.

Zhao, Z., Liu, M., and Tu, P. (2008). Characterization of water soluble polysaccharides from organs of Chinese jujube (Ziziphus jujuba mill. cv. dongzao). *Eur. Food Res. Technol.* 226 (5), 985–989. doi: 10.1007/s00217-007-0620-1

Zou, S., Wu, J., Shahid, M. Q., He, Y., Lin, S., Liu, Z., et al. (2020). Identification of key taste components in loquat using widely targeted metabolomics. *Food Chem.* 323, 126822. doi: 10.1016/j.foodchem.2020.126822

frontiers | Frontiers in Plant Science

TYPE Original Research
PUBLISHED 28 June 2023
DOI 10.3389/fpls.2023.1112164

OPEN ACCESS

EDITED BY
Prof Eman. A. Mahmoud,
Damietta University, Egypt

REVIEWED BY
Ashish Rambhau Warghat,
Institute of Himalayan Bioresource Technology (CSIR), India
Xiwen Li,
China Academy of Chinese Medical Sciences, China

*CORRESPONDENCE
Xiaobo Wang
wangxiaobo@lzb.ac.cn
Yulin Li
liyulin@nwipb.cas.cn

RECEIVED 30 November 2022
ACCEPTED 07 June 2023
PUBLISHED 28 June 2023

CITATION
Wang X, Shen C, Chen T, Zhou X and Li Y (2023) Geographical equations of *Swertia mussotii* bioactivities: evidence from the western Sichuan region of China. *Front. Plant Sci.* 14:1112164. doi: 10.3389/fpls.2023.1112164

Geographical equations of *Swertia mussotii* bioactivities: evidence from the western Sichuan region of China

Xiaobo Wang[1]*, Cheng Shen[2], Tao Chen[2], Xiaodan Zhou[3] and Yulin Li[2]*

[1]Northwest Institute of Eco-Environment and Resources, Chinese Academy of Sciences (CAS), Lanzhou, China, [2]Northwest Institute of Plateau Biology, Chinese Academy of Sciences (CAS), Xining, China, [3]Department of Pharmacy, Gansu Provincial Hospital, Lanzhou, China

Swertia mussotii is the most authentic raw material used in Tibetan medicine in China for its various bioactivities. This natural medicine resource is at risk of being exhausted due to the double interference of climate change and anthropogenic over-collection. Little is known about habitat characteristics and the crucial environmental factors that influence the levels of active ingredients. The goal of this study is to understand the variability in the bioactive compound content of a wide range of wild *S. mussotii* as it adapts to changing environmental conditions. The target compound content of the whole plant material was analyzed with the environmental explanatory variables of the field sample sites using a constrained ordination method for their correlation analysis. The results show that 16.3 percent of the sampled wild *S. mussotii* populations with the highest bioactive content can be grouped into the elite type. The most prominent environmental variables affecting the content of major bioactive products include altitude, aspect, soil TK content, Fe content, and C/N and N/P ratios. Altitude and aspect put indirect effects that are mediated by plant height and density, N/P ratio puts a direct effect, while soil TK content, Fe content and C/N ratio have both direct and indirect effects on the bioactivity of *S. mussotii*. In addition to the total negative effects of altitude and C/N ratio, the remaining factors play a driving role. These findings demonstrate variation by geographical conditions across S. mussotii accessions for physiologic responses and secondary compounds in wild populations. The knowledge gained from this study can be used for environmental and plant physiology research, efficient collection of naturally active compounds, and conservation strategies for rare natural plant resources.

KEYWORDS

***Swertia mussotii* Franch, environmental factor, bioactive compounds, correspondences analysis, Western China**

1 Introduction

In nature, various plant secondary metabolites (SMs) mean that many plants containing large amounts of these bioactive compounds have long been used as important sources of traditional medicines, industrial raw materials, and spices (Li and Vederas, 2009; Piccolella et al., 2018). Offering great potential for their nutraceutical and medicinal exploitation, the extraction and purification of SMs from wild natural plants usually not only requires a complex and time-consuming process, but also obtains quite a low yield of the target product (Christensen, 2020; Tava et al., 2022). Geographical locations have an important effect on the quality of many medicinal plants because environmental abiotic factors are always regulating the formation and storage of SMs in plants (Szakiel et al., 2011). Therefore, finding reliable ways to enhance this systematic process to increase the yield of natural compounds has been a serious long-term challenge for researchers (Ashraf et al., 2018). This strategy also holds extremely important prospects for the development of improved quality and conservation of traditional Chinese medicinal plants.

To date, much research has focused on finding the most productive plant species and optimizing breeding conditions to improve the output of plant SMs (Motta et al., 2019; Huang et al., 2022). While the number of studies directly highlighting the significant correspondence between abiotic factors and wild-type plant SMs is growing, the current understanding of the different geographical factors that regulate the production of active metabolites in diverse plants is still limited. In literature, materials sampled from the South-Central U.S. has 7-fold lower mitragynine content than the Southeast Asian samples (León et al., 2009), and there is also a significant content difference between Thai origin trees and Malaysian ones (Leksungnoen et al., 2022). Even on a regional scale, the active product contents of medical materials vary enormously depending on where they come from (Lu et al., 2009; Yang et al., 2010). That means not only that abiotic stresses are interrelated, but changes at the physiological, biochemical, and molecular levels are linked, both individually and in combination (Bita and Gerats, 2013; Misra et al., 2021). Therefore, the synthesis and accumulation of phytochemical components are heavily dependent on various environmental conditions of the habitat (Hinojosa et al., 2018; Tabatabaei et al., 2022).

Different combinations of abiotic external conditions regulate the level of variation in the chemical properties of the bioactive compounds that play a decisive role in plant growth. This internal variation is also reflected to some extent in the plant heights and population densities that are directly visible from the outside, indicating a high degree of ecological plasticity. Many climate trends are commonly associated with altitude (Guevara-Terán et al., 2022), which is also an easily identified geographical factor (Sun et al., 2021). A review on the adaptation of medicinal plants to various environmental stresses in the Himalayas provides relatively comprehensive information, in which only one reference is made to the physiological differentiation caused by adaptation to solely different altitudes (Pandey et al., 2019). This means that altitude usually coordinates the influences of abiotic factors, for instance, different altitudes are associated with various annual temperatures (Ahmed et al., 2019). At different altitudes, plants accumulated different SMs levels mainly regulated by changes in temperature and solar radiation (Senica et al., 2016). The way altitude affects plants can also be directly or indirectly through reduced atmospheric pressure (Arce et al., 2021), significantly related to site characteristics such as slope (Mullin et al., 2021). Additionally, climate change that manifests as warming takes contradictory effects on the SMs production of medicinal plants (Holopainen et al., 2018).

Swertia mussotii Franch (*S. mussotii*) is a star species of the Swertia genus in the Gentianaceae family growing in the West China mountains. For thousands of years, it has been used in the treatment of liver disorders and jaundice, and has anti-inflammatory, antipyretic, and gallbladder- and diuretic-promoting functions, making it a raw material for a variety of liver and gallbladder diseases (Chen et al., 2015). The bioactive SMs of *S. mussotii* include swertiamarin, gentiopicroside, sweroside, mangiferin, and isoorientin (Tan et al., 2017), applied for dispelling heat and improving gallbladder function, dehumidifying and detoxifying, soothing the liver and strengthening the stomach, helping heart function and nourishing the blood, and are considered as important indexes to measure the material quality (Shen et al., 2021). However, in previous studies on the difference in compound content, scholars tended to make cross-regional and large-scale comparisons in order to emphasize the heterogeneity of site environmental conditions (Bazargani et al., 2021). They did not systematically design environmental variables, so only a qualitative understanding of the quality differences between different places of medicinal materials could be proposed (Lu et al., 2009; Yang et al., 2010). As a result, current knowledge of the interplay between *S. mussotii* quality and environmental variability is not sufficient to aid conservation and rational development of this valuable natural resource.

Taking the homogeneity of geographical units on the macro level into consideration, the objectives of this study include: 1) To examine the correlation between the chemical types of wild *S. mussotii* population and its growing environmental conditions; 2) To identify the classification of active SMs and the sorting of main environmental factors of *S. mussotii* under current climatic conditions; and 3) To clarify the influence mechanism of geographical factors on natural *S. mussotii* growth and its medicinal quality. In this study, we established an HPLC chromatogram of *S. mussotii* extraction to assess the content of plant active ingredients, used unconstrained ordination analysis to assess the overall differences in phytochemical types, screened environmental predictors with constrained ordination for explanation and contribution, and explored the effects and pathways of important influencing factors by regression analysis and structural equation model. This study thus endeavors to use the newly-acquired knowledge to provide a scientific reference for the conservation introduction and exploitation of *S. mussotii* to facilitate the development of appropriate sustainable management measures in future warm and humid climate scenarios.

2 Materials and methods

2.1 Plant sampling design and field collections of sample material

A total of 107 potential sites were visited with a local guide, and 98 of these sites with *S. mussotii* growth were recorded for sampling in Xiaojin County, West Sichuan, China in late August 2021. The whole sampling period lasted for 10 days and collections from each sampling site were taken at least 1.5 km apart. According to the intuitive perception on the growth density of S. mussotii found, the dense and sparse groups of study areas accounted for 39.79% and 26.53%, respectively. ArcGIS 10.2 (Esri, Redlands, California USA) was used to construct the location occurrence point map, as shown in Figure 1. Wild *S. mussotii* at each sampling site were mostly in full bloom. Flowering adults were thus selected for collection whole, until approximately 20 sample plants were collected within an area of approximately 20 m by 20 m at each sampling point. The average plant height of each collected sample was then recorded. At the same time, the topsoil was removed from the collection area according to the five-point sampling method, and 5-20cm of soil depth was excavated with a sampling shovel, mixed, and marked for preservation.

The stoichiometric analysis was carried out at the institutional center of core facilities and technologies in Northwest Institute of Plateau Biology, CAS following established methods to detect 14 soil characteristics. Among them, Ca, Fe, Mn, Zn, Na, total phosphorus (TP), and total potassium (TK) were analyzed by ICP-MS (Thermo fisher, USA); total salt content (water-soluble cation and anion), available nitrogen (AN), available phosphorus (AP), available potassium (AK), and pH by water solution method with corresponding detectors; and total nitrogen (TN) and organic carbon (C) by elemental analyzer (Elementar, Germany). Then the ratio of carbon to nitrogen (C/N) and nitrogen to phosphorus (N/P) indexes of soil samples could be calculated. The GPS and altitude information was recorded at the center of the sampling site, and the major aspects were recorded under the classification of the eight directions. These obtained data were stored in IBM SPSS 23 software for processing and analysis.

2.2 Separation and collection of bioactive products

In view of the processing and application principle of *S. mussotii*, this study focused on swertiamarine (A), gentiopicroside (B), sweroside (C), mangiferin (D), isoorientin (E), and swertioside (F). The content of these compound groups was also the main standard to measure the quality of this herbal medicine in the Chinese medicinal industry (Shen et al., 2021). All samples were naturally shade-dried and crushed, then screened by 60 mesh. Reflux extraction was used and the extraction conditions were as follows: extraction solvent, 30% ethanol; liquid-material ratio; extraction temperature, 80°C; extraction, three times; each extraction time, 90 min. The extraction was titrated to 100 mL for sample injection after filtration. On the other hand, the compounds A~F with different weights of the standard product were fully dissolved in the methanol solution and well shaken at a constant volume, so that the standard solution was configured in a ratio of 1:5:2:2:1:1. Then, 2, 4, 8, 12, and 16 µL of standard solution were injected into HPLC for testing, respectively, to draw a standard curve. The fitted peak area (y) and injection volume (x) were used as regression curves, as shown in Figure 2.

The stability, accuracy, repeatability, and addition of standard recovery of the bioactive compound separation and collection processes have been adopted to verify the compound

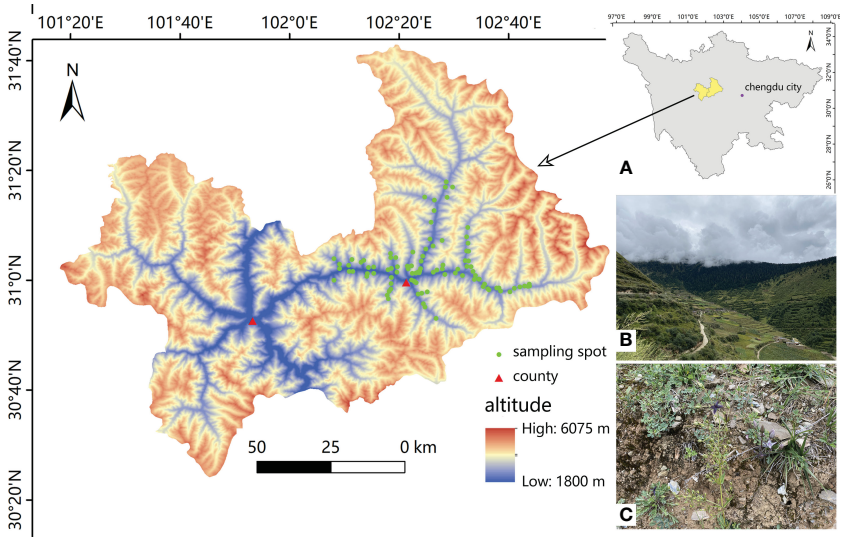

FIGURE 1
The geographic distribution of the natural population of *S. mussotii* in this study (*n*=98). **(A)** The study area in its administrative geography of western Sichuan province; **(B)** environmental conditions of *S. mussotii via* landscape; **(C)** a typical site habitat of wild *S. mussotii*. Both photos were taken on 31 August, 2021.

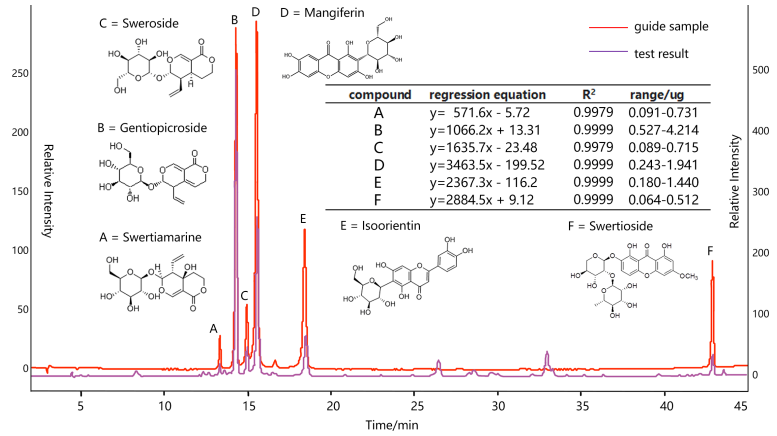

FIGURE 2
HPLC analysis of ethanol extract of *S. mussotii* conditions: column, DIKMA platisit (250×4.6mm, i.d. 5μm); column temperature, 30 °C; mobile phase, 0.1% glacial acetic acid (solvent α) and CH_3OH (solvent β); HPLC analysis, 0-45 min, linear gradient from 10% to 40% β during 0-10 min, 10-15 min 40%-42.5% β, 15-25 min 50% β, 25-35 min 60% β, 35-45 min 95% β; flow rate, 1.0 mL/min; detection wavelength, 254 nm.

determination. Specifically, measuring the same sample solution at 0,2,4,8,12 and 24 h, respectively, the results showed that the HPLC peak areas RSD of A-F are all less than 3.0%, indicating that the samples are stable at 24 h. Taking 10 μL of the mixed reference solution and sample solution to measure each peak area six times, the former RSD is less than 2.0% and the latter is less than 2.5%, meaning that the instrument and injection process is very precise. Six raw material samples are randomly taken and filled into the same solution volume, and their determinations proved to be similar, with the peak area RSD of all six compounds being less than 3%, suggesting that the method is reproducible. Finally, adding reference solutions with 80%, 100%, and 120%, respectively, corresponding compound contents into a tested sample solution, the new mixed solutions are injected into HPLC to measure the six objective recoveries (n=3) ranging from 98%-103%, with all RSD less than 3%.

2.3 Bioclimatic data and data processing

Bioclimatic variables (BIO1-BIO19) were extracted from monthly data from the World Climate Database covering 1950-2000 (www.worldclim.org) (Hijmans et al., 2005) according to the longitude and latitude coordinates of each collection locality; the spatial resolution was 30-arc second, which was robust multivariate bias corrected by meteorological data from 2001-2020 from national weather stations (Chen et al., 2022). Although the sampling sites are not less than 1.5 km from each other, some spots still fall within the same 1 km by 1 km grid as reflected in the GIS. In this case, there are 7 collection points in the same grid that are processed by averaging the data obtained at the two nearest sites.

To study the effect of other climatic conditions, altitude, slope, slope aspect, mean solar radiation intensity, water vapor pressure, and mean wind speed variables were also extracted from the climate dataset. In the assignment of aspect, 1~5 represents north, northwest or northeast, east-west, southwest or southeast, and south respectively, replacing the original 0~360° azimuth values. The altitude result showed a significant correlation with the field GPS records of the sampling points, the correlation coefficient was 0.770 ($p < 0.001$), and the correlation coefficient between the extracted aspect information and the manual records was 0.530 (($p < 0.001$). This indicats a good reliability of the extracted data.

2.4 Statistical analysis

Following the principle of parsimony, the above 41 environmental factors were input into Canoco5 software to test the arch effect of environmental predictors, and the analysis model was simplified by excluding multicollinearity and environmental variables with low contribution (ter Braak and Smilauer, 2012). A factor analysis of 41 environmental variables reveals the influence of more than 4 components, so directly casting constraint ordination method inevitably decreases the level of interpretability. Thus, 18 collinear variables have been removed in data preprocessing based on the correlation of the variables and the contribution of the control variables. The variables with less indicative values than the overall mean value were then eliminated by unconstrained ordination analysis, and the final 13 most informative variables were selected, as shown in Table 1. This stepwise analysis also assessed the differences in eigenvalues between environmental variables and bioactive compounds to determine whether erroneous variables or too many variables had been deleted from the environmental dataset.

The levels of compound content obtained from *S. mussotii* can be distinguished using the clustering method. For example, the significant classification results of K-means clustering indicate that there is a significant difference between elite and common groups in wild populations. In addition, the environmental factors affecting the active compound content can be fitted by regression models. But it is necessary to compare and check the standardized effects of different environmental factors in the structural equation model.

TABLE 1 Summary of the final environmental variable set of *S. mussotii*. population.

	max	min	mean	stand. dev.	inflation factor
Altitude(m)	3323	2434	2855	182.7	2.56
Aspect	5	1	3.48	1.198	1.86
C/N ratio	10.77	1.38	6.06	1.945	2.51
TP(g/kg)	0.97	0.27	0.57	0.129	1.84
N/P ratio	13.92	2.91	7.67	2.372	1.95
TK(g/kg)	25.7	13.3	18.35	2.371	2.48
Fe(g/kg)	34.4	23.8	29.17	2.317	2.82
Mn(g/kg)	0.91	0.29	0.54	0.084	2.16
Na(g/kg)	12.9	5.36	8.79	1.4	1.59
Zn(mg/kg)	110.3	58.3	80.3	8.371	1.85
TS(g/kg)	2.3	0.6	1.2	0.335	1.59
AK(mg/kg)	283	32.6	111.04	53.019	1.85
MTCM(°C)	-4.6	12.8	-8.26	1.604	3.28

aspect was assigned in 1 to 5 for shady to sunny orientation, respectively; all soil element contents were tested by dry weight; TK and TP refer to total K and P content in soil samples, TS means total soluble salt content, AK refers to available K; MTCM means minimum temperature of coldest month.

The structural equation model in this study was implemented by MPLUS 8 software (Muthén and Muthén, 1998–2017).

3 Result

3.1 Descriptive statistics of six bioactive compounds

According to the extraction scheme in this study, the sum of 6 active compounds in *S. mussotii* from 98 collection sites is 76.75 ± 10.14 mg/g. Compound B as the second peak in the HPLC chromatogram reached the highest content of them all, with an average ratio of over 60%. This is because the separation and collection method employed in this study have been developed to determine the amount of compound B in wild *S. mussotii* material to the greatest extent for the approval of a national standard. Compound D, which averages 17.73% in this work, is a common flavonoid with a wide range of plant sources. The other 4 active constituents each make up less than 10% of the total extracted content, as shown in Figure 3A. We put the content data into a non-metric multidimensional scaling (NMDS) analysis, with the ordination model set as 2 dimensions for fitting; the result showed that these two axes have reached 100% of explanatory power on the correlation among active constituents with its stress value returns 0.0646, showing that the model is significant. The arrow directions of different compounds in Figure 3B indicate that there is a certain correlation between several components, such as compounds A and C, and B and E. Compound B has contributed the most to the total content of all six for these two vectors in Figure 3B are similar, with a *Pearson* coefficient reaches 0.936 (p<0.001). At the same time, the compounds D and E also exceed the total content by a coefficient of 0.5, respectively.

Using the contents of the compounds A-F as variables, the 98 existing sets of samples can be grouped by K-means clustering under the iterative classification algorithm. Due to the different content of bioactive compounds, the study sample can be divided into low, middle, high, and elite groups, which contain 26, 27, 29, and 16 populations, respectively. The variance test of the cluster analysis result shows that compounds B, D, and E significant differences in high and low content among the 4 groups, revealing that these 3 compounds are the main indicators in the classification. This can also be understood from the principle of the minority subordination to majority, since the absolute concentration of the three is generally higher. Taking compound B into account, the cluster centers were 43.79mg/g for the elite group and 36.54mg/g for the high group, both greater than the sample mean of 32.26mg/g. Besides, the sequence of cluster centers of compound A and C is inconsistent, which verified the difference from these two compounds to the other in Figure 3B. Cluster analysis also suggests that there is an elite type in the wild *S. mussotii* population, which may accumulate higher SMs than other plants.

In terms of plant population and height of growth, the average plant height of *S. mussotii* is 65.7 ± 11.6 cm. The plant height is significantly affected by altitude and slope aspect, with correlation coefficients of -0.509 (p<0.001) and -0.666 (p<0.001), respectively. That is, *S. mussotii* plants grow shorter overall with increasing altitude, and shorter in the direction of the sun. At the same time, plant height is positively affected by temperature factors, but negatively by precipitation. It is also negatively correlated with the total content of extracted active ingredients with a coefficient of -0.674 (p<0.001). On the other hand, the degree of population density recorded by sampling shows a negative significant correlation with altitude to the coefficient of -0.511 (p<0.001), while a positive correlation with aspect to the coefficient of 0.348

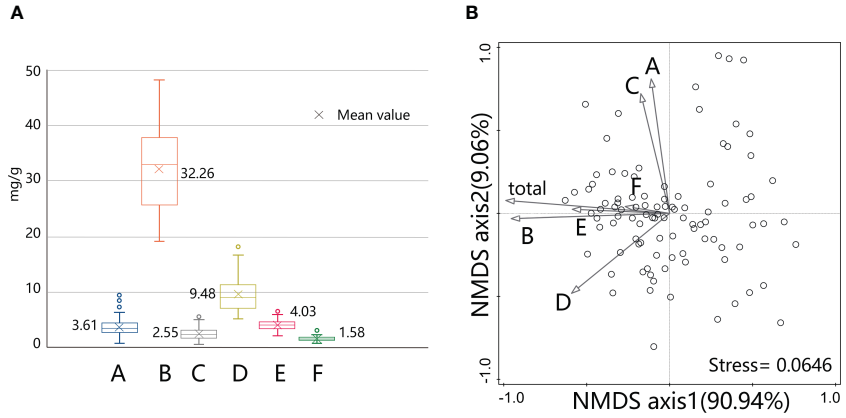

FIGURE 3
Content levels of active compounds extracted from *S. mussotii* in this study **(A)** and their clustering analysis by NMDS method **(B)**.

(p<0.001). At present, the population density also reflects the difference in bioactive compound content to some extent, and the correlation coefficient between them is 0.518 (p<0.001), showing a significant negative correlation with plant height with a coefficient of -0.208 (p=0.040).

Based on the classification results of different groups with high to low bioactive compound content, the independent sample Kruskal-Wallis test was further conducted for 13 key environmental variables extracted from the post-redundancy analysis. The result shows that significant differences occur in aspect (p<0.001), soil TK content (p<0.001), Fe (p<0.001), C/N ratio (p=0.007), minimum temperature of coldest month (p=0.007), Na (p=0.012), and N/P ratio (p=0.020), while there is no highlighted difference in soil total soluble salt content (p=0.097), AK (p=0.111), altitude (p=0.118), TP (p=0.165), Zn (p=0.530), and Mn (p=0.563). From the low to the elite group, the average altitude shows a trend of first increasing and then decreasing. Overall, the elite group consists of mostly low-altitude samples but a few high-altitude ones. It demonstrates that the composition and content of different bioactive compounds in plants are clearly regulated by various environmental conditions.

3.2 Correspondence analysis of environmental variables and active compounds

The linear combination of unconstrained ordination analysis for environmental variables has first been used to pre-process the obtained environmental predictors to account for variations in content, which facilitates the classification and contribution of each predictor. As shown in Figure 4A, the 13 environmental predictors (see Table 1) have been analyzed with the sample chemical type data of bioactive compounds content by unconstrained ordination. In the PCA plots of the two first axes, axis 1 explains 84.64% of all variables and is highly correlated with soil Fe content, aspect, and soil TK content. The direction of axis 1 is also an explanatory dimension for the content of compound B, indicating the contribution of these environmental predictors to this compound. At the same time, the MTCM and Na content present a negative relation with respect to axis 1, leading to an adverse effect. Axis 2 contributes 8.9% of the explanatory power, roughly related to the site soil predictors. Compound D is highly consistent with the direction of these factors, indicating a correlation between them. Since compounds A and C point in the negative direction of axis 2 and are negatively correlated with most environmental factors, this suggests that these two components are only positively correlated with soil Na content and MTCM in the ordination analysis.

To further analyze the correlation between environmental predictors and compound content, constrained ordination analysis has been used to calculate the explanatory variation for 13 environmental predictors. The environmental variables are selected one by one in the forward selection analysis process until the explanatory power exceeded the estimated one in the model by 55.2% and a total of 7 predictors are finally included in the redundancy analysis model. The explained variation of the explanatory variables then reached 55.6%. Axis 1 accounted for 52.91% of the explanation, while axis 2 accounted for only 2%. However, all 4 axes appear to be significant with test F-ratio of 16.126 (p=0.002), showing that the redundancy analysis model is remarkably helpful. There were significant differences in the conditional effects of environmental variables, with the soil TK content contributing the most 35.67%. Then there is the aspect, Na, Fe, and Zn content, accounting for 11.3%, 2.7%, 2%, and 1.6%, respectively. The remaining predictors do not stand out in terms of interpretation. As shown in Figure 4B, the soil Fe, total K content and aspect of wild *S. mussotii* population growth sites significantly affect the output of compound B. In other words, the more south-facing the habitat site and the higher the site soil total K, the more abundant the compound B in *S. mussotii* plants. Similarly, compounds D and E are strongly correlated with site soil N/P ratio, aspect, Zn content, and altitude. Inversely, the concentration of compounds A and C is significantly promoted by soil Na content.

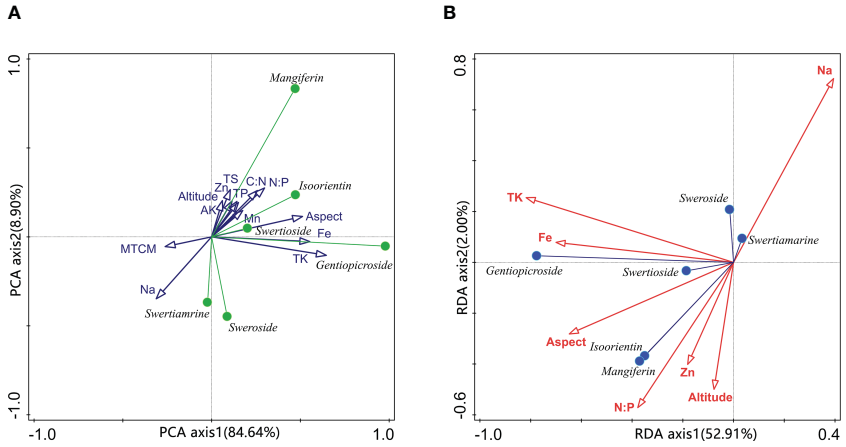

FIGURE 4
Principal component analysis of environmental variables and compounds-environmental variables biplot of redundancy analysis. TS in **(A)** means total soluble salt content; MTCM means the minimum temperature of the coldest month.

3.3 Structural equation model of bioactive compounds

Using the wild *S. mussotii* population density and plant height data recorded in the sampling as outcome variables, respectively, the confirmatory factor analysis of the structural equation model has been carried out with environmental predictors using Bootstrap analysis and maximum likelihood estimation. In each fit, the independent variables with the worst significance in the model fit results are excluded and then repeated until the best combination is obtained. With the results for plant height and population density, the different content of bioactive compounds is then incorporated into the structural model. Thus, this structural equation model contains 23 non-collinear environmental predictors as explanatory variables and each bioactive compound content as an outcome variable, mediated by the plant height and population density of *S. mussotii*, and is modified by removing one by one the predictors that did not work well. By permuting the combinations of explanatory variables, the best-fit structural equation model is finally obtained. In the case of compound B, a final set of 6 environmental predictors were used as explanatory variables, including altitude, aspect, C/N ratio, N/P ratio, TK, and Fe content in the soil samples. As Figure 5 shown, the χ^2 of the structural equation model is 13.95 with a d*f* of 7, the ratio of which two falls between 1 to 3 (p=0.0649), meeting the recommended value. The same holds for the other test values. The CFI and TLI are recommended to be greater than 0.9, while the model values are 0.979 and 0.938, respectively. RMSEA is 0.079 and SRMR is 0.031, both below the threshold value of 0.08. At the same time, a 95% confidence interval test has been performed on the model results *via* Bootstrap analysis, and the returned interval does not contain a zero value for each variable, proving that the estimated values of the explanatory variables are all significant. Briefly, plant height and population density have different negative and positive effects on its output level, respectively. This can be understood as an increase in biological mass within a plant reduces the relative content of bioactive constituents, while growth in dense areas corresponds to higher levels of the content outcome.

As site spatial factors, altitude and aspect have no direct effect on compound accumulation, but have significant indirect effects

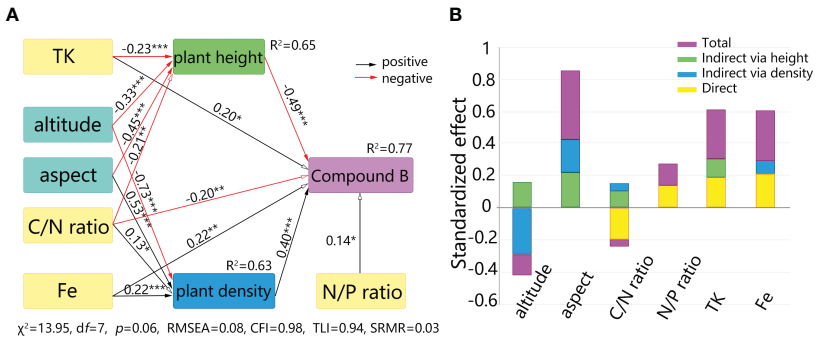

FIGURE 5
Direct and indirect effects on bioactive compounds of S. mussotii from abiotic factors. **(A)** Structural equation model between bioactive compound and geographical factors. **(B)** Standardized effects from the explanatory variables. * means p<0.05, ** means p<0.01, *** means p<0.001.

through plant height and population density, respectively. Altitude has a negative effect on both plant height and population density, followed by two negative direct effects on bioactive content through plant height and one negative indirect effect through population density. As the negative indirect effect is greater than the positive one, the final effect from altitude to compound B manifests as a significantly negative one, -0.13 (p=0.023). Likewise, the indirect effect from aspect to compound content is positive and the total standardized effect is 0.43 (p<0.001). In terms of site soil factor, the N/P ratio only has a direct effect on the compound B content, while the C/N ratio plays the most complex path of influence. The direct effect of the C/N ratio reaches -0.20(p=0.008), and a concurrently indirect effect *via* plant height and density, 0.11(p=0.023) and 0.05 (p=0.032), separately, resulting in a non-significant total effect of -0.04(p=0.601). There are both significant direct and indirect effects from soil TK and Fe on compound B output, ultimately resulting in total standardized effects of 0.31(p=0.001) and 0.30 (p<0.001), respectively.

Similarly, results for the other biologically active compounds can be obtained within the structural equation model, as shown in Table 2. These environmental factors are here simply distinguished into spatial and edaphic predictors, the former consisting mainly of altitude, aspect, temperature, and precipitation, the latter consisting mainly of soil C/N and N/P ratios, TP, TK, Fe, and Na content, etc. In order to observe the regulation mechanism of different environmental variables, the absolute and superimposed effects of the two factor groups are distinguished. Compounds A, C, D, and E are generally subject to strong spatial factor effects, but the total effect decreases after stacking. This suggests that spatial factors exert a fairly strong effect over the course of the course, but with consequences at different levels depending on the variety of bioactive compound types and combinations of environmental variables. The total effect given by the environmental variables on compounds A, C, and D turn out to be a negative result, suggesting that the same environmental factors have contradictory effects on the accumulation of different bioactive compounds in plants. In addition, compounds D and E receive a much larger absolute effect than B, while the total effect turns out to be smaller than B. This indicates that the different regulatory effects among environmental variables superimpose or counteract each other, resulting in diverse levels of influence effects.

4 Discussion

4.1 Diversity and heterogeneity of bioactive compound contents

Just as species distribution models have been used to predict where species grow within a study area based on the environmental conditions of several certain locations (Guisan and Thuiller, 2005; Dong et al., 2017), the environmental gradient analysis can also be used to predict the distribution of compound types and their contents under specific environmental conditions, or the optimal environmental conditions required to enrich the types and contents of target compounds (Isah, 2019). This study casts light on the correspondence analysis between target bioactive compounds and growing environmental conditions of wild *S. mussotii* through field sampling and experimental testing and helps to enrich the knowledge of quality improvement, conservation introduction, and equitable utilization of this valuable medicinal plant. Our results demonstrate that metabolomic expression across the geographic distribution of wild-type *S. mussotii* populations can follow a non-linear, non-restrictive, and non-monotonic relationship with environmental variables. It is thus possible to make much greater use of the ecological factors affecting plant SMs production to enhance targeted phytochemicals output (Khare et al., 2020).

Determined by the utility pattern of *S. mussotii* according to medicine application and preparation production, the current research on this medical material mainly focused on its swertiamarin, gentiopicroside, sweroside, mangiferin, and isoorientin content level (Tan et al., 2017). Represented by gentiopicroside of compound B in this study, the active components of *S. mussotii* have been analyzed not by an extensive total metabolomic analysis once samples were collected but by chromatographic separation in the scheme of target natural products (Chen et al., 2015). Research on the quality and standardization of *S. mussotii* has framed the variety of bioactive compounds (Shen et al., 2021). Consequently, the six bioactive compounds focused on in this study have been widely concerned in the existing literature (Yang et al., 2010; Chen et al., 2015; Tan et al., 2017). This study provides unique insight into the many environmental conditions in which these *S. mussotii* compounds

TABLE 2 Standardized effects of environmental predictors on *S. mussotii* compounds.

compounds	spatial		edaphic		total
	absolute	total	absolute	total	
A	1.587	-1.033[a]	0.599	0.233[a]	-0.800
B	0.555	0.303[b]	0.765	0.765	1.068
C	1.168	-0.570[a]	0.152	0.152[a]	-0.418
D	2.120	0.140	1.696	-0.542	-0.403
E	2.018	-0.043	0.366	0.100	0.057
F	0.220	0.220[a]	0.562	-0.008[a]	0.212

a superscript means direct effect, b means indirect effect, no mark means both.

are produced. Although county-scale and climatic factors can be viewed as homologous, most wild *S. mussotii* populations grow with variations in the chemical profile under different combinations of spatial and edaphic conditions.

Existing samples can thus be grouped into different levels of content by the K-means clustering method. From poor to abundant, they can be clearly identified into four groups: low, middle, high, and elite. Due to the difference in separation methods, there is no comparability between the samples analyzed in the scheme of this study and the previous results on the absolute contents of bioactive compounds. But the results obtained in this study are in a constituent proportion similar to that reported in former studies conducted in other geographical locations and have told the distinction of wild populations between different sites, like the Sichuan region and Qinghai region (Lu et al., 2009; Yang et al., 2010; Tan et al., 2017). This indicates the diversity of *S. mussotii* chemical types. Subsequent studies can determine whether the 16.3% elite group has the optimal configuration of environmental conditions by excluding the genotype effects. Moreover, if the under-sampled left side of the study region shown in Figure 1 is supplemented to increase the number of samples, a more accurate and affluent result might be obtained to delve into the details.

The bioactive product content depends on various factors such as plant genetics, harvesting time, crude extraction, and growing environment. Similarly, focusing on different bioactive compounds may yield different results for the same environmental predictor. In this study, a higher amount of compound B was observed under higher TK and Fe edaphic sites and on sunny slopes, leading to a difference between the explanatory variables obtained from its result model and those of the other compounds (see Figure 2). On the other hand, the altitude of the spatial factors has a direct and significant effect only on compounds A and C, and aspect has a direct effect on compound F, while both of them have no indirect effect on these three compounds. Altitude also puts an indirect effect *via* plant height to compound D without direct effect, while both direct effect and indirect one *via* population density on compound E. As seen in Table 2, compounds A, C, and F mainly suffer from the direct impact of spatial and edaphic factors, while D and E simultaneously impact the direct and indirect effects of environmental conditions. Only compound B stands up to the indirect effects of the spatial factors, while the integrated effects of the edaphic conditions, both of which are positive, lead to the highest level of regulation of the final total effect.

4.2 Interaction among geographical factors

With the redundancy analysis and factor analysis in this study, most of the crucial environmental variables that bring about significant changes in the bioactive compounds in wild *S. mussotii* can now be clearly identified as spatial and edaphic factors. The spatial gradients include the aspect, altitude, and minimum temperature of the coldest month, with decreasing explanations and contributions forming a relatively important group of predictors. Given that climate change largely prompts sensitive plants to change the content and composition of SMs by warming (Gérard et al., 2020), the quality and habitats of wild *S. mussotii* may vary greatly under future environmental warming in the climate-vulnerable Qinghai Tibetan plateau. Because higher altitude usually means lower temperature, larger temperature differences, and more solar radiation (Arias et al., 2022). As the overall ambient environmental temperature increases, however, the synergistic adjustment effect between altitude and temperature will gradually change or be lost. This means that existing combinations of geographic factors will adjust in a warm and humid future environmental scenario, leading to variations in bioactive compound content. Thus, there will be a large reduction in the area that can contain *S. mussotii* habitat. Therefore, researchers and related practitioners need to make greater efforts for the conservation and rational utilization of wild *S. mussotii* resources in order to cope with future climate change and human disturbances.

The edaphic factors are composed of TK, Na, TP, Fe, C/N ratio, AK, N/P ratio, Zn, total soluble salt, and Mn content, with the order of the contributions descending in turn. The involvement of so many soil factors suggests that wild *S. mussotii* is strongly dependent on a variety of environmental conditions during its lifetime for the synthesis and accumulation of SMs. However, little literature has reported the tendency of bioactive compound levels of *S. mussotii* across different soil characteristics. For example, soil organic carbon restricts plant-microbial interaction by affecting the communication between plant root flavonoid signal compounds and microbial symbionts, which leads to changes in plant physiological and ecological processes (Del Valle et al., 2020). The regulation of multiple abiotic properties of site soils may also have complex synergistic or antagonistic effects, although soil organic carbon content has been shown to have weak relationships with target compounds, and the biological factors of soil microbial communities have not been introduced in this study. For C/N and N/P ratios, which generally fit the correspondence analysis better in the competing tests, their high relative indicators such as soil organic carbon, TN, and soil pH have been removed from the study. But it is important to point out that the elite group of wild *S. mussotii* populations grows neither in the highest nor lowest soil organic carbon sites, but in the medium soil organic carbon highest TN regions, corresponding to a mid-level of C/N ratio. Besides, soil pH value is highly correlated with conductivity, salinity, and other indicators, and plays a certain role in regulating plant SMs (Kandimalla et al., 2020). The soil pH of 98 sample sites ranges from 7.8 to 9.0, with an average of 8.2, which is just the mean value of the pH index for the elite group. It also shows that the previous general situation described for the physiological demands of the wild *S. mussotii* population is extremely rough (Ji et al., 2020). If more of the growth factors associated with *S. mussotii* are put into a comprehensive and credible framework, then the vital coordination and operation of geographical conditions may be worked out.

After distinguishing the four levels of *S. mussotii* according to the amount of bioactive compounds, the dramatically significant environmental factors are the aspect, the soil TK, and the Na content. In this case, a more southerly slope direction, higher TK, and lower Na content in the soil correspond to a more abundant flora of bioactive compounds. Among them, south-facing means

more sunshine, which may be associated with the facilitation that many plants improve SMs outcome under the enhancement of light exposure or UV stress (Amarasinghe et al., 2015; Tohge et al., 2016; Hernández et al., 2022). The effects of different contents of soil total K on the regulation of SMs in plants have also been reported (Liu et al., 2020). The increase in soil Na content may be related to salt stress (Bittencourt et al., 2022). But this study with total soluble salt factor data does not provide a deeper analysis of the correlation between these two indicators but only provides a certain perspective on the plant stress process.

In contrast to the correspondence analysis and the clustering analysis, the structural equation model gives the most detailed and unambiguous correlation between the bioactive compound content and environmental predictors in wild *S. mussotii* populations. The final fitted model explains a mechanism for the influence of spatial factors, namely altitude and aspect, on the bioactive compounds in *S. mussotii* plants. This indirect effect is also consistent with plant physiological metabolism and response to external stress. Previous studies have demonstrated that plant synthesis of flavonoid compounds is synthetically influenced by temperature, light, drought, and salinity in the site habitats. However, this process is not simply expected to improve production by introducing UV radiation or drought stress, but there are highly complex and organized mechanisms related to specific metabolic pathways and enzyme catalysis (Bo et al., 2016; Prinsloo and Nogemane, 2018). There are geographical variations in flavonoids and terpenoids in plant metabolism for altitude conditions that significantly affect the contents of these two compounds and the effects on them are not completely mutually exclusive (Sun et al., 2021). Therefore, an attempt to directly establish a linear or monotonous relationship between different plant populations of *S. mussotii* and altitude conditions may not clearly be obtained (Yang et al., 2010). This study provides a perspective that relationships between the environment and SMs can be mediated by plant physiological and ecological processes, such as plant height and population density. Still, it is undeniable that the indirect effect of plant density from altitude and aspect on the synthesis of bioactive compounds may be mediated by the other factors that also significantly affect population density but were not observed in this study also mediate this indirect effect.

Although the soil C/N ratio does not show a significant total effect or significant results in correspondence analysis, it has a statistically quantifiable indirect effect on the bioactive compound content of the *S. mussotii* plant. Since the C/N ratio of available samples is relatively low, the correspondence analysis model does not identify the arched effect on the SMs content of *S. mussotii* caused by superfluous nutrition, that is, the process of first increasing and then decreasing with the increase of total carbon and nitrogen contents (Scogings, 2018). In fact, long-term nitrogen and phosphorus addition changes the carbon distribution of plants to carbon-based defense compounds, showing a close correlation between SMs content and plant carbon, nitrogen, and phosphorus stoichiometry (Shan et al., 2018). Thus, the present results can only demonstrate the plasticity of the bioactive output in *S. mussotii* plant growing in poor conditions of soil carbon and nutrient content. Further relation needs to be supplemented with data under diverse nutritional conditions.

In the end, correlation and significance in statistics do not imply causal links in reality, as the knowledge available to correlate environmental variables of *S. mussotii* with changes in bioactive compounds is based on ordination analysis and regression models. Attributes such as soil types, thickness, and granularity size compositions, as well as *in situ* control tests, all need to be checked before large-scale conservation introductions could be formally undertaken (Yun et al., 2018). While the spatial factors which have a distinct effect on the quality of raw *S. mussotii* material cannot be neglected. Thus, human intervention and habitat conservation may remain the most appropriate coping strategies at this stage. As one local guide put it, the demand for wild plant resources has increased in recent years, but the awareness and adaptation measures for their sustainable use have not kept pace. The one act of ability which he deemed meaningful and mindful of his duty was to sow the seeds of these ripening herbs in the places where they had been growing. This is also the purpose and motivation for this study.

5 Conclusion

This study has analyzed the correlation between the amount of bioactive compounds and environmental variables for wild *S. mussotii* populations. The content of biologically active compounds varies with different environmental conditions, and a change in an individual factor may alter the SMs content. We report on the variability of the main bioactive compounds in *S. mussotii* material sampled from Xiaojin County in western China and demonstrate the existence of an elite group with the optimal combinations of geographical conditions and the highest bioactive compound content. Key factors associated with the high quality of wild *S. mussotii* populations include the altitude, aspect, air temperature and solar radiation intensity, soil TK, Fe content, and C/N and N/P ratios. The standardized effects and the final stacking result differ significantly between the two sets of abiotic factors, so the regulation of plant SMs by environmental variables should be analyzed in terms of the combination of target compounds and geographical predictors.

In view of the fact that spatial factors have a non-negligible effect on herb quality, it is necessary to consider similar habitats in the practice of remote introduction. This knowledge provides an explanatory basis for further laboratory and field control experiments to identify the underlying environmental factors that enhance the quality of this valuable medicinal plant. There may be many more other factors that affect the bioactive ingredient content, such as endogenous genetic and exogenous abiotic and biotic factors, as well as the collection, vegetation, and storage of plant material itself. In addition to examining the genetic differences among *S.*

mussotii populations at different sample sites, future studies need to systematically design a more comprehensive framework for plant SMs formation and accumulation and various combinations of environmental conditions, as well as plant-environment interactions, to finally confirm the optimal configuration of environmental conditions to improve medicinal quality.

Data availability statement

The datasets generated for this study are available on request to the corresponding authors.

Author contributions

XW and CS contributed equally to this work. XW and YL: conceptualization. XW, CS, XZ and YL: validation. XW, TC and CS: investigation. XZ, TC and CS: experiment and analysis. XW and CS: writing-original draft preparation. CS, TC, XZ and YL: writing-review and editing. XW, TC and YL: funding acquisition. All authors contributed to the article and approved the submitted version.

Funding

This work was supported by Youth Science and Technology Fund Program of Gansu Province (No. 20JR5RA542); National Natural Science Foundation of China (No. 82174052); Youth Innovation Promotion Association of CAS (No. 2020425).

Conflict of interest

The authors declare that the research was conducted in the absence of any commercial or financial relationships that could be construed as a potential conflict of interest.

Publisher's note

References

Ahmed, S., Griffin, T. S., Kraner, D., Schaffner, M. K., Sharma, D., Hazel, M., et al. (2019). Environmental factors variably impact tea secondary metabolites in the context of climate change. *Front. Plant Sci.* 10, 939. doi: 10.3389/fpls.2019.00939

Amarasinghe, R., Poldy, J., Matsuba, Y., Barrow, R. A., Hemmi, J. M., Pichersky, E., et al. (2015). UV-B light contributes directly to the synthesis of chiloglottone floral volatiles. *Ann. Bot.* 115, 693–703. doi: 10.1093/aob/mcu262

Arce, C. C. M., Bont, Z., Machado, R. A. R., Cristaldo, P. F., and Erb, M. (2021). Adaptations and responses of the common dandelion to low atmospheric pressure in high-altitude environments. *J. Ecol.* 109 (10), 3487–3501. doi: 10.1111/1365-2745.13736

Arias, L. A., Berli, F., Fontana, A., Bottini, R., and Piccoli, P. (2022). Climate change effects on grapevine physiology and biochemistry: benefits and challenges of high altitude as an adaptation strategy. *Front. Plant Sci.* 13, 835425. doi: 10.3389/fpls.2022.835425

Ashraf, M., Iqbal, M., Rasheed, R., Hussain, I., Riaz, M., and Arif, M. S. (2018). "Chapter 8 - environmental stress and secondary metabolites in plants: an overview," in *Plant metabolites and regulation under environmental stress*. Ed. P. Ahmad, et al (Academic Press of Elsevier Inc).

Bazargani, M. M., Falahati-Anbaran, M., and Rohloff, J. (2021). Comparative analyses of phytochemical variation within and between congeneric species of willow herb, epilobium hirsutum and e. parviflorum: contribution of environmental factors. *Front. Plant Sci.* 11, 595190. doi: 10.3389/fpls.2020.595190

Bita, C., and Gerats, T. (2013). Plant tolerance to high temperature in a changing environment: scientific fundamentals and production of heat stress-tolerant crops. *Front. Plant Sci.* 4, 00273. doi: 10.3389/fpls.2013.00273

Bittencourt, C. B., da Silva, T. L. C., Neto, J. C. R., Vieira, L. R., Leao, A. P., Ribeiro, J. A. D., et al. (2022). Insights from a multi-omics integration (MOI) study in oil palm (Elaeis guineensis jacq.) response to abiotic stresses: part one-salinity. *Plants-Basel* 11 (13), 1755. doi: 10.3390/plants11131755

Chen, C., Chen, T., Liu, Y. L., Zou, D. L., You, J. M., and Li, Y. L. (2015). Rapid screening, identification, separation, and purification of four bioactive compounds from *Swertia mussotii* franch. *Separation Sci. Technol.* 50 (4), 604–610. doi: 10.1080/01496395.2014.957316

Chen, L., Shen, Y. R., Yang, W. J., Pan, Q. M., Li, C., Sun, Q. G., et al. (2022). Hydrological response to future climate change in a mountainous watershed in the northeast of Tibetan plateau. *J. Hydrol.* 44, 101256. doi: 10.1016/j.ejrh.2022.101256

Christensen, L. P. (2020). Bioactive C17 and C18 acetylenic oxylipins from terrestrial plants as potential lead compounds for anticancer drug development. *Molecules* 25 (11), 2568. doi: 10.3390/molecules25112568

Del Valle, I., Webster, T. M., Cheng, H. Y., Thies, J. E., Kessler, A., Miller, M. K., et al. (2020). Soil organic matter attenuates the efficacy of flavonoid-based plant-microbe communication. *Sci. Adv.* 6 (5), eaax8254. doi: 10.1126/sciadv.aax8254

Dong, Y. B., Luo, Y., Zhu, C., Peng, W. F., Xu, X. L., and Fang, Q. M. (2017). Application of remote sensing and GIS in study of suitability distribution of *Swertia mussotii*, a Tibetan medicine in sichuan province. *China J. Chin. Mater. Med.* 42 (22), 4387–4394. doi: 10.19540/j.cnki.cjcmm.2017.0189

Fu, B., Ji, X. M., Zhao, M. Q., He, F., Wang, X. L., Wang, Y. D., et al. (2016). The influence of light quality on the accumulation of flavonoids in tobacco (Nicotiana tabacunm l.) leaves. *J. Photochem. Photobiol. B: Biol.* 162, 544–549. doi: 10.1016/j.jphotobiol.2016.07.016

Gérard, M., Vanderplanck, M., Wood, T., and Michez, D. (2020). Global warming and plant–pollinator mismatches. *Emerg. Topics Life Sci.* 4, 77–86. doi: 10.1042/ETLS20190139

Guevara-Terán, M., Gonzalez-Paramás, A. M., Beltrán-Noboa, A., Giampieri, F., Battino, M., Tejera, E., et al. (2022). influence of altitude on the physicochemical composition and antioxidant capacity of strawberry: a preliminary systematic review and meta-analysis. *Phytochem. Rev.* doi: 10.1007/s11101-022-09834-z

Guisan, A., and Thuiller, W. (2005). Predicting species distribution: offering more than simple habitat models. *Ecol. Letter* 8, 993–1009. doi: 10.1111/j.1461-0248.2005.00792.x

Hernández, K. V., Moreno-Romero, J., de la Torre, M. H., Manriquez, C. P., Leal, D. R., and Martinez-Garcia, J. F. (2022). Effect of light intensity on steviol glycosides production in leaves of stevia rebaudiana plants. *Phytochemistry* 194, 113027. doi: 10.1016/j.phytochem.2021.113027

Hijmans, R. J., Cameron, S. E., Parra, J. L., Jones, P. G., and Jarvis, A. (2005). Very high resolution interpolated climate surfaces for global land areas int. *J. Climatol.* 25, 1965–1978. doi: 10.1002/joc.1276

Hinojosa, L., González, J. A., Barrios-Masias, F. H., Fuentes, F., and Murphy, K. M. (2018). Quinoa abiotic stress responses: A review. *Plants* 7 (4), 106.

Holopainen, J. K., Virjamo, V., Ghimire, R. P., Blande, J. D., Julkunen-Tiitto, R., and Kivimaenpaa, M. (2018). Climate change effects on secondary compounds of forest trees in the northern hemisphere. *Front. Plant Sci.* 9, 1445. doi: 10.3389/fpls.2018.01445

Huang, W. J., Yang, G. Z., Liu, D. D., Li, Q., Zheng, L. P., and Ma, J. (2022). Metabolomics and transcriptomics analysis of vitro growth in pitaya plantlets with different LED light spectra treatment. *Industrial Crops Prod.* 186, 115237. doi: 10.1016/j.indcrop.2022.115237

Isah, T. (2019). Stress and defense responses in plant secondary metabolites production. *Biol. Res.* 52, 39. doi: 10.1186/s40659-019-0246-3

Ji, S., Liang, X. P., Zhang, M., and Xie, H. C. (2020). Effect of site factors on drug efficacy of *Swertia mussotii*. *Ahhui Agric. Sci. Bull.* 26 (23), 33–34. doi: 10.16377/j.cnki.issn1007-7731.2020.23.012

Kandimalla, R., Das, M., Barge, S. R., Sarma, P. P., Koiri, D. J., Devi, A., et al. (2020). Variation in biosynthesis of an effective anticancer secondary metabolite, mahanine in murraya koenigii, conditional on soil physicochemistry and weather suitability. *Sci. Rep.* 10, 20096. doi: 10.1038/s41598-020-77113-y

Khare, S., Singh, N. B., Singh, A., Hussain, I., Niharika, K., Yadav, V., et al. (2020). Plant secondary metabolites synthesis and their regulations under biotic and abiotic constraints. *J. Plant Biol.* 63, 203–216. doi: 10.1007/s12374-020-09245-7

Leksungnoen, N., Andriyas, T., Ngernsaengsaruay, C., Uthairatsamee, S., Racharak, P., Sonjaroon, W., et al. (2022). Variations in mitragynine content in the naturally growing kratom (Mitragyna speciosa) population of Thailand. *Front. Plant Sci.* 13, 1028547.

León, F., Habib, E., Adkins, J. E., Furr, E. B., McCurdy, C. R., and Cutler, S. J. (2009). Phytochemical characterization of the leaves of mitragyna speciosa grown in U.S.A. *Nat. Prod. Commun.* 4, 907–910.

Li, J. W. H., and Vederas, J. C. (2009). Drug discovery and natural products: end of an era or an endless frontier? *Science* 325 (5937), 161–165. doi: 10.1126/science.1168243

Liu, Y., Li, Y. M., Luo, W., Liu, S., Chen, W. M., Chen, C., et al. (2020). Soil potassium is correlated with root secondary metabolites and root-associated core bacteria in licorice of different ages. *Plant Soil* 456, 61–79. doi: 10.1007/s11104-020-04692-0

Lu, Y. C., Lin, P. C., and Li, L. L. (2009). Determination of active constituents in *Swertia mussotii* from different regions of qinghai province by HPLC. *Chineses Trandition. Patent Med.* 31 (10), 1558–1559.

Misra, A., Mishra, P., Kumar, B., Shukla, P. K., Kumar, M., Singh, S. P., et al. (2021). Chemodiversity and molecular variability in the natural populations (India) of gloriosa superba (L.) and correlation with eco- geographical factors for the identification of elite chemotype(s). *Fitoterapia* 150, 104831. doi: 1016/j.fitote.2021.104831

Motta, E. V. S., Sampaio, B. L., Costa, J. C., Teixeira, S. P., and Bastos, J. K. (2019). Quantitative analysis of phenolic metabolites in copaifera langsdorffii leaves from plants of different geographic origins cultivated under the same environmental conditions. *Phytochem. Anal.* 30 (3), 364–372. doi: 10.1002/pca.2819

Mullin, M., Klutsch, J. G., Cale, J. A., Hussain, A., Zhao, S., Whitehouse, C., et al. (2021). Primary and secondary metabolite profiles of lodgepole pine trees change with elevation, but not with latitude. *J. Chem. Ecol.* 47, 280–293. doi: 10.1007/s10886-021-01249-y

Muthén, L. K., and Muthén, B. (2017). *Mplus user's guide: Statistical analysis with latent variables, user's guide* (Los Angeles, CA: Muthén & Muthén).

Pandey, V., Bhatt, I. D., and Nandi, S. K. (2019). Environmental stresses in Himalayan medicinal plants: research needs and future priorities. *Biodivers. Conserv.* 28, 2431–2455. doi: 10.1007/s10531-019-01776-x

Piccolella, S., Crescente, G., Pacifico, F., and Pacifico, S. (2018). Wild aromatic plants bioactivity: a function of their (poly)phenol seasonality? A case study from Mediterranean area. *Phytochem. Rev.* 17, 785–799.

Prinsloo, G., and Nogemane, N. (2018). The effects of season and water availability on chemical composition, secondary metabolites and biological activity in plants. *Phytochem. Rev.* 17, 889–902. doi: 10.1007/s11101-018-9567-z

Scogings, P. F. (2018). Foliar flavonol concentration in sclerocarya birrea saplings responds to nutrient fertilisation according to growth-differentiation balance hypothesis. *Phytochem. Lett.* 23, 180–184. doi: 10.1016/j.phytol.2017.12.010

Senica, M., Stampar, F., Veberic, R., and Mikulic-Petkovsek, M. (2016). The higher the better? differences in phenolics and cyanogenic glycosides in sambucus nigra leaves, flowers and berries from different altitudes. *Sci. Food Agric.* 97 (8), 2623–2632. doi: 10.1016/j.fitote.2021.104831

Shan, L. P., Song, C. C., Zhang, X. H., and Ren, J. S. (2018). Effects of long-term nitrogen and phosphorus addition on plant defence compounds in a freshwater wetland. *Ecol. Indic.* 94 (1), 1–6.

Shen, C., Chen, T., Wang, D. J., Chen, C., Zhao, J. Y., Chen, J. L., et al. (2020). Research and development of certified reference material of swertioside. *China J. Chin. Mater. Med.* 45 (04), 955–960. doi: 10.19540/j.cnki.cjcmm.20191111.202

Sun, C. W., Shan, X. L., Ding, H. F., Cao, Y. N., and Fang, S. Z. (2021). Natural variations in flavonoids and triterpenoids of cyclocarya paliurus leaves. *J. Forest. Res.* 32, 805–814. doi: 10.1007/s11676-020-01139-1

Szakiel, A., Paczkowski, C., and Henry, M. (2011). Influence of environmental abiotic factors on the content of saponins in plants. *Phytochem. Rev.* 10, 471–491. doi: 10.1007/s11101-010-9177-x

Tabatabaei, I., Alseekh, S., Shahid, M., Leniak, E., Wagner, M., Mahmoudi, H., et al. (2022). The diversity of quinoa morphological traits and seed metabolic composition. *Sci. Data* 9, 323. doi: 10.1038/s41597-022-01399-y

Tan, L., Hu, F. Z., and Dong, Q. (2017). Simultaneous determination of three iridoid glycosides and three flavonoids in *Swertia mussotii* franch. from qinghai by UPLC. *Chin. J. Pharm. Anal.* 37 (08), 1469–1475. doi: 10.16155/j.0254-1793.2017.08.16

Tava, A., Biazzi, E., Ronga, D., Pecetti, L., and Avato, P. (2022). Biologically active compounds from forage plants. *Phytochem. Rev.* 21, 471–501. doi: 10.1007/s11101-021-09779-9

ter Braak, C. J. F., and Smilauer, P. (2012). *Canoco reference manual and user's guide: software for ordination, version 5.0* Vol. 2012 (Ithaca USA: Microcomputer Power).

Tohge, T., Wendenburg, R., Ishihara, H., Nakabayashi, R., Watanabe, M., Sulpice, R., et al. (2016). Characterization of a recently evolved flavonol-phenylacyltransferase gene provides signatures of natural light selection in brassicaceae. *Nat. Communication* 7, 12399. doi: 10.1038/ncomms12399

Yang, H. X., Wei, L. X., Du, Y. Z., Xiao, Y. C., Lv, P., Wang, D. P., et al. (2010). HPLC analysis of medicinal components of *Swertia mussotii* from different elevations. *J. Chin. Med. Mater.* 33 (6), 867–869. doi: 10.13863/j.issn1001-4454.2010.06.011

Yun, D. Y., Kang, Y. G., Kim, E. H., Kim, M., Park, N. H., Choi, H. T., et al. (2018). Metabolomics approach for understanding geographical dependence of soybean leaf metabolome. *Food Res. Int.* 106, 842–852. doi: 10.1016/j.foodres.2018.01.061

frontiers | Frontiers in Plant Science

TYPE Original Research
PUBLISHED 10 July 2023
DOI 10.3389/fpls.2023.1105373

OPEN ACCESS

EDITED BY
Eman A. Mahmoud,
Damietta University, Egypt

REVIEWED BY
Mónika Alejandra Valdenegro-Espinoza,
Pontificia Universidad Católica de Valparaíso, Chile
Washington Azevêdo Da Silva,
Universidade Federal de São João del-Rei, Brazil
Marcilio Morais,
Federal University of Pampa, Brazil

*CORRESPONDENCE
Luqiang Huang
biohlq@fjnu.edu.cn

RECEIVED 22 November 2022
ACCEPTED 12 June 2023
PUBLISHED 10 July 2023

CITATION
Xu S, Pang Y, Cai X, Chen Q, Jin G, Zhang M and Huang L (2023) Comparative study of three cultivars of jaboticaba berry: nutrient, antioxidant and volatile compounds.
Front. Plant Sci. 14:1105373.
doi: 10.3389/fpls.2023.1105373

Comparative study of three cultivars of jaboticaba berry: nutrient, antioxidant and volatile compounds

Shaosi Xu[1], Yingying Pang[2], Xiaoming Cai[3], Qinchang Chen[1], Gang Jin[4], Miao Zhang[1] and Luqiang Huang[1]*

[1]College of Life Science, Fujian Normal University, Fuzhou, China, [2]School of Food Science and Engineering, South China University of Technology, Guangzhou, China, [3]Institute of Food Inspection, Fujian Institute of Product Quality Supervision and Inspection, National Center for Quality Supervision and Inspection of Processed Foods, Fuzhou, China, [4]School of Food and Wine, Ningxia University, Yinchuan, China

Jaboticaba is a tropical plant and its fruit rich in nutrients, volatile compounds, and biological activities, which considered to be an edible health benefits plant. Despite its popularity for fresh consumption, jaboticaba is rarely used in intensive processing in China. The content of nutrients and antioxidant in jaboticaba greatly impacts how it is processed healthy food. In this study, we evaluated the nutrients, antioxidant capacity, and volatile compounds of three jaboticaba cultivars including Sabara, Argentina, and Fukuoka, respectively. Our results revealed each variety has its merits. Sabara had an abundance of volatile compounds, a suitable acid-sugar ratio, and a slightly lower antioxidant capacity, making it suitable for fresh consumption. Argentina is the richest in volatile compounds in ripe fruit, but slightly lighter in taste and acid-sugar ratio, making it suitable for dry products. The large size, juicy flesh, low acid-sugar ratio, and less volatile compounds content of Fukuoka also make it suitable for juice processing. Three cultivars of jaboticaba berry exhibited different characteristics, providing reference evidence for the manufacturing and processing of jaboticaba health food.

KEYWORDS

jaboticaba, berry, nutrient, antioxidant, volatile compounds

1 Introduction

Jaboticaba (*Myrciaria cauliflora*) belongs to the Myrtle family and is native to South America, which was introduced from Taiwan in 2004 and mostly grow in southern provinces of China (Zhu, 2014; Zhu, 2017). The flower and berry of jaboticaba grow on the main trunk and branches. Due to its berry resemblance to grape, jaboticaba is commonly

known as "tree grape". The jaboticaba skin changes from green to red and then purple as it matures, with only 4 to 7 days of fruiting after ripening. Ripe berry is purple-black, and its flesh is white and semi-translucent crystal (Inada et al., 2021). Jaboticaba tastes sweet and sour, with aromas of guavas, pineapples, mangosteens, and sakas. Qiu (Qiu et al., 2021) measured the volatile components of jaboticaba at different developmental stages *via* headspace-gas chromatography/mass spectrometry and found the most predominant volatile components were monoterpenes, including α-pinene, β-pinene, and D-limonene.

Jaboticaba is also considered as an edible health benefits plant and its pulp is rich in acids, sugars, vitamins, dietary fiber, minerals, and polyphenols (Qiu et al., 2021; Correia et al., 2022; Boldori et al., 2023). There are numerous phenolic substances, including anthocyanins, ellagic acid, and tannins (Pereira et al., 2017; Albuquerque et al., 2020; Fernandes et al., 2020) in the peel, which afford various biological activities, such as antioxidation, anti-inflammatory, antibacterial, hypoglycemic, and lipid-lowering properties (Inada et al., 2018; Zhao et al., 2019; Ferreira et al., 2021; Geraldi et al., 2021; Da Silva-Maia et al., 2023). Through a randomized crossover study, Geraldi (Geraldi et al., 2021) demonstrated jaboticaba juice improved serum antioxidant capacity and plasma glucagon-like peptide-1 response after a carbohydrate meal in healthy adults. Wang (Wang et al., 2014) found that jaboticaba seed extract had anti-proliferative effects on oral cancer cells. Hsu (Hsu et al., 2016) reported an extract from jaboticaba improved diabetic nephropathy by inhibiting oxidative stress and inflammation in streptozotocin-nicotinamide mice. Nayara (Sarkar et al., 2022) have demonstrated that the phenolic compounds and sugars in jaboticaba can be used by colon microbes. Jaboticaba extract promotes the fermentation of intestinal microflora, which is beneficial to human health. As a tropical fruit, the jaboticaba is a potential source of bioactive and functional foods (Massa et al., 2022; Lima et al., 2023).

Many previous studies have proven the nutritional and unique taste of the jaboticaba, but it is the way in which it is processed that has not been well promoted because of its limited freshness and difficulty in storage (Inada et al., 2021). Jaboticaba is very popular throughout Brazil and is consumed as fresh fruit, as well as artisanal products, such as juices, jellies, vinegar, liqueurs, and wines. However, its limited shelf life has hindered the commercialization of fresh fruit. Therefore, to add value and expand its consumption, researchers have been investigating technological processes to develop products derived from jaboticaba (Appelt et al., 2015). The pleasant organoleptic properties and rich nutritional content of jaboticaba make it a functional ingredient in beverage, jams, and jellies (Asquieri et al., 2009; Oliveira et al., 2018; Qiu et al., 2018; Benvenutti et al., 2021). Thus, jaboticaba has high economic benefits due to its consumption as a high-quality natural food ingredient. However, the research on the nutritional composition and active components of the main cultivated varieties of jaboticaba berry is still insufficient. In this study, the immature and ripe fruits of Sabara, Fukuoka, and Argentina were evaluated for their morphological appearance, nutritional composition, antioxidant activity and flavor content. Based on variety of bioactive compounds contained in jaboticaba berry, this study would provide an insight and reference about breeding, preserving, processing of jaboticaba cultivars for both the producer and researcher further research and development.

2 Materials and methods

2.1 Materials

The unripe and ripe fruits of Sabara, Fukuoka, and Argentina were provided by Fujian Putian Taichuang Agricultural Development Co (Putian Fujian, China). The unripe fruit were collected at 15 days after flowering and the ripe fruit are harvested at 30 days after flowering. 2,2-Diphenyl-1-picrylhydrazyl (DPPH) was purchased from Shanghai Yuanye Biotechnology Co (Shanghai, China). Forinol was purchased from Beijing Solarbio Biotechnology Co (Beijing, China). 2,2'-azino-bis(3-ethylbenzothiazoline-6-sulfonate) (ABTS) was purchased from Sigma-Aldrich Biotechnology Co (St Louis, MO, USA). The total antioxidant capacity (T-AOC) assay kit and hydroxyl radical assay kit were purchased from Nanjing Jiancheng Institute of Biological Engineering (Nanjing Jiangsu, China). Potassium metabisulphite was purchased from LAMOTHE-ABIET, France (Bordeaux, France). Cyclohexanone (chromatographically pure) was purchased from China Pharmaceutical Group Co (Beijing, China). All other chemicals and reagents were analytically pure and purchased from China Pharmaceutical Group Co (Beijing, China).

Three cultivars of jaboticaba were cultivated on a randomly selected plot of land in the farm. During their cultivation, they were given equal amounts of water and organic fertilizer to provide nutrients. Samples were taken before and after the fruit had ripened. In sampling, fruits of the same maturity were taken from several trees of the same cultivar and mixed as samples to be tested. For testing and analysis, three different cultivars of jaboticaba were divided into ripe and unripe groups in order to assess their physicochemical properties and volatile compounds. Around 50 g of randomly selected jaboticaba were placed in 50mL centrifuge tubes to crush them and then placed in an ultrasonic extractor for 30 minutes to leach the substances from the peel and pulp into the juice. Finally, the juice was taken for assay, with three biological replicates.

2.2 Methods

2.2.1 Determination of basic chemical parameters

2.2.1.1 Mean fruit diameter and weight

Ten fruits were randomly selected from each of the two periods of the three cultivars. The weight and diameter of each fruit were measured using an electronic balance and vernier calipers, and the mean was calculated.

2.2.1.2 Total soluble solids

Total soluble solids was determined according to the method of NY/T2637-2014 Refractometric method for determination of total soluble solids in fruits and vegetables (The Ministry of Agriculture of the People's Republic of China, China).

2.2.1.3 Reducing and total sugars

Using the method published by Wu (Wu et al., 2018), with slight modification, reducing sugars in the fruit was determined. A glucose standard curve was generated using 1 mL of glucose standard solutions at concentrations of 0, 0.2, 0.4, 0.6, 0.8, and 1 mg/mL. The modified method was to pipette the solutions into 10 mL colorimetric tubes, and 2 mL 3, 5-dinitrosalicylic acid (DNS) reagents (Solarbio, China) were added. The mixture was boiled accurately in a boiling water bath for 5 min and then cooled to 25°C with tap water. Then, 9 mL of distilled water was added to each tube and mixed well. The absorbance values were measured at 540 nm. The final regression equation $y = 0.7214x + 0.041$ ($R^2 = 0.999$) was obtained.

After extracting the reducing sugars, the samples were treated in the same way as described above. The absorbance values were measured, and the reducing sugar content was calculated according to the regression equation.

Total sugars were determined by the phenol-sulfuric acid method, with reference to (Liu et al., 2011).

2.2.1.4 Total acid (as tartaric acid)

Total acid was determined according to the method of "GB 12456-2021 Determination of total acid in foods" (National Health and Family Planning Commission, China).

2.2.1.5 Total polyphenols

Total polyphenols were determined according to the method reported by Li (Li et al., 2020), with slight modification. A standard curve was generated using 1 mL of gallic acid monohydrate standard solutions at concentrations of 0, 10, 20, 30, 40, and 50 μg/mL. The modified method was to pipette the solutions into 10 mL colorimetric tubes, and 5 mL of distilled water, 1 mL of Forinol color developer, and 3 mL of 7.5% sodium carbonate solution were added. The solutions were mixed with a vortex oscillator, and the reaction was carried out at room temperature for 2 h, protected from light. The absorbance was measured at 765 nm, and the regression equation $y = 0.0075x - 0.0039$ ($R^2 = 0.9996$) was obtained. The samples were treated in the same way as described above. The absorbance values were recorded, and the total polyphenols content was calculated according to the regression equation.

2.2.1.6 Vitamins B1 and C

Vitamin C was determined by high-performance liquid chromatography (Waters, USA) according to the method of "GB5009.86-2016 Determination of Ascorbic Acid in Foods" (National Health and Family Planning Commission, China). The determination of vitamin B1 was performed by high-performance liquid chromatography (Waters Corporation, USA), according to the method of "GB 5009.84-2016 Determination of vitamin B1 in foods" (National Health and Family Planning Commission, China).

2.2.1.7 Amino acid content

The amino acids were determined according to the method of "GB5009.127-2016 Determination of amino acids in foods" (National Health and Family Planning Commission, China).

2.2.1.8 Elemental composition

Arsenic, lead, sodium, potassium, magnesium, iron, copper, zinc, calcium, manganese, and mercury were determined using inductively-coupled plasma mass spectrometry (ICP-MS 7900, Agilent, USA), according to the method of "GB5009.268-2016 Determination of Multiple Elements in Foods" (National Health and Family Planning Commission, China). Chromium and cadmium were determined according to the method of "GB5009.123-2014 Determination of Chromium in Foods" and "GB5009.15-2014Determination of Cadmium in Foods" (National Health and Family Planning Commission, China). The determination of cadmium in food was carried out using an atomic absorption spectrophotometer (PE AA 900T, PE Inc., USA). Mercury was determined *via* an atomic fluorescence photometer, according to the method of "GB5009.17-2021 Determination of Mercury in Foods" (National Health and Family Planning Commission, China) using an Atomic Fluorescence Photometer (AFS-930, Beijing Jitian Instruments Co., Ltd., China).

2.2.2 *In vitro* antioxidant assay

2.2.2.1 Total antioxidant capacity

A total antioxidant capacity (T-AOC) assay kit (A015-1-2, Nanjing Jiancheng Institute of Biological Engineering, China) was employed for the determination of antioxidant activity.

2.2.2.2 Hydroxyl radical inhibition

A hydroxyl free radical assay kit (A018-1-1, Nanjing Jiancheng Institute of Biological Engineering, China) was used to determine the hydroxyl radical inhibition.

2.2.2.3 DPPH scavenging capacity

The method of Liu (Liu et al., 2022) was referenced and modified.

The DPPH standard was accurately weighed to 7.8864 mg and fixed to 100 mL with anhydrous ethanol was added to obtain an ethanolic solution of DPPH at a concentration of 0.2 mmol/L. The solution was transferred to a brown bottle and set aside. The sample was added to the test tube according to Table 1 and mixed well. The absorbance was measured at 517 nm after 30 min reaction at room temperature, protected from light.

DPPH scavenging was calculated according to the following formula:

$$Removal\ rate(\%) = \left[1 - \frac{As - Aj}{Ao}\right] \times 100\,\% \quad (1)$$

TABLE 1 The amount of DPPH added.

Absorbance value	Amount of sample added
Ao	1mL DPPH ethanol solution + 2mL anhydrous ethanol + 1mL blank solvent
As	1mL DPPH ethanol solution + 2mL anhydrous ethanol + 1mL sample solution
Aj	3mL anhydrous ethanol + 1mL sample solution

2.2.2.4 Determination of the ability to scavenge ABTS cationic radicals

The ABTS assay was performed according to the procedures described by Tao (Tao et al., 2016; Wang et al., 2022), with some modifications. Briefly, 96 mg of ABTS was dissolved in 20 mL of deionized water, and then 5 mL of 2.45 mmol/L potassium persulfate solution was added. The mixture was left overnight (12–16 h) in the dark at room temperature before use. The obtained $ABTS^+$ radical solution was diluted 11-fold with ethanol, to achieve an absorbance of 0.70 (± 0.02) at 734 nm. In the next step, 20 μL of juice (with proper dilution in ethanol) was added to 2 mL of the aforementioned $ABTS^+$ solution. In addition, 20 μL of ethanol was added to 2 mL of the ABTS+ solution, and this sample was the blank. After incubation at 30°C in the dark for 6 min, the absorbance at 734 nm was recorded. The results are expressed as the percent $ABTS^+$ radical inhibition.

The scavenging capacity was calculated as follows:

$$Inhibition\,\% = (1 - \frac{Asample}{Ablank}) \times 100 \quad (2)$$

2.2.2.5 Inhibit superoxide anion radicals

An inhibition and generation of superoxide anion radical assay kit (A052-1-1, Nanjing Jiancheng Institute of Biological Engineering, China) was used to determine the inhibition of superoxide.

2.2.3 Volatile compounds

The volatile compounds were determined on an HS-SPME/GC–MS system (Agilent, California, USA) (Ricci et al., 2019). Briefly, 5 mL of samples and 3.6 g of NaCl were added to the headspace bottle and equilibrated at 50°C for 5 min. The extraction fiber was inserted into the sample bottle for 30 min. The oven temperature program was as follows: hold at 40°C for 3 min, increase to 60°C at a rate of 2°C/min and hold for 5 min, increase to 150°C at a rate of 3°C/min and hold for 10 min, increase to 220°C at a rate of 5°C/min and hold for 10 min. Volatile compounds were identified by comparison of the retention time and mass spectra with pure standards in the NIST 17 mass spectral and retention index libraries. Quantitative analysis was performed using cyclohexanone purchased from China Pharmaceutical Group (Beijing, China) as the internal standard.

2.3 Statistical analysis

Statistical analysis was performed using Statistical Product Service Solutions (SPSS), version 20.0 (IBM Corp., Armonk, NY, USA) and Prism, version 8.0 (GraphPad Software Inc., San Diego, CA, USA). The data are expressed as the mean ± SD of three biological replicates. The one-way analysis of variance (ANOVA) within the ripe and unripe groups followed by Tukey's test and $P< 0.05$ was considered statistically significant. PCA analysis using the R package prcomp. All analysis were visualized using Prism, version 8.0.

3 Results and discussion

By examining the differences in quality between three different cultivars of jaboticaba, we identified suitable cultivars for fresh consumption and processing. To investigate the quality of fruits upon maturity, we examined various quality parameters of the fruit at unripe and ripe stages. The three varieties of jaboticaba fruits had excellent quality at the unripe stage, and differences were found upon ripening. Generally, we consume only the ripe fruits; thus, in the following discussion and analysis, we focus on analyzing the differences of these three kinds of Jaboticaba fruits in the ripening stage, using the unripe fruits as controls.

3.1 Fundamental properties and chemical analysis

The appearance of the three different cultivars of jaboticaba is shown in Figure 1A, and the cross-sectional cut is shown in Figure 1B. From this figure we can see that the outer skin of the jaboticaba fruit is black at the ripening stage and green when unripe. Superficially, the jabotic fruits of the three cultivars have large size differences. In cross-section, the three cultivars also differ considerably in flesh color and form and seeds.

In addition, the fundamental properties and chemical composition of unripe and ripe jaboticaba fruit of three different cultivars were determined. The average diameter and weight were measured to determine the size of the fruit. The contents of amino acids, vitamin C, vitamin B1, reducing sugar, total sugar, total acid, and total polyphenols were measured to determine their nutritional and volatile compounds.

3.1.1 The average diameter and weight

The average size of the fruit is summarized in Table 2. The average diameter of the three different fruits, both in the unripe and ripe stages, was larger in Fukuoka than in Argentina and Sabara. At maturity, the average diameter of Fukuoka reached 31.10 ± 2.71 mm; Argentina was 25.61 ± 2.05 mm; Sabara was only 24.12 ± 1.17 mm. The diameter of the ripe fruit of Fukuoka was significantly different from that of Sabara and Argentina, but at the unripe stage, Sabara was significantly different from the other two cultivars. Similar to the average diameter, the average weight followed the same trend. In the

10.3389/fpls.2023.1105373

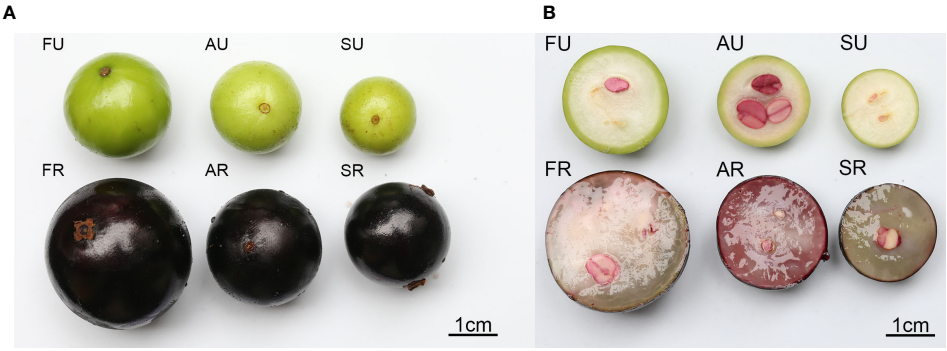

FIGURE 1
Three cultivars of jaboticaba berry. Appearance of a jaboticaba **(A)**; cross-sectional section of a jaboticaba **(B)**. SU represent Sabara unripe, AU, Argentina unripe; FU, Fukuoka unripe; SR, Sabara ripe; AR, Argentina ripe; FR, Fukuoka ripe.

TABLE 2 Average weight and diameter of jaboticaba at unripe and ripe stages.

Type	Ripe fruit			Unripe fruit		
	Sabara	Argentina	Fukuoka	Sabara	Argentina	Fukuoka
Average diameter(mm)	24.12 ± 1.17b	25.61 ± 2.05b	31.10 ± 2.71a	20.64 ± 1.30b	23.74 ± 3.07a	24.41 ± 1.98a
Average weight (g)	8.26 ± 0.7b	9.93 ± 2.54b	16.76 ± 3.63a	5.39 ± 0.77b	7.49 ± 2.45a	8.45 ± 1.78a

Different letters indicated significant differences within the ripe and unripe groups. $p<0.05$.

immature stage, Fukuoka and Argentina were significantly heavier than Sabara, and in the mature stage, Fukuoka was significantly heavier than Argentina and Sabara. In the mature stage, Fukuoka reached an average weight of 16.76 ± 3.63 g, while Argentina and Sabara were only 9.93 ± 2.54 g and 8.26 ± 0.7 g, respectively.

For each of the three jaboticaba cultivars, we measured the average weight and diameter and found that Fukuoka was the largest, followed by Argentina and Sabara. This suggests that Fukuoka is better than Argentina and Sabara, in terms of fruit size. From a consumer's point of view, when buying fruit most consumers will pick the larger ones, so in terms of weight per fruit, the Fukuoka is probably more popular for fresh eating.

3.1.2 Total soluble solids, total sugar, reducing sugar and acidity

In general, both for unripe and ripe fruit, total soluble solids content was highest in Sabara, followed by Fukuoka and Argentina (Figure 2A). In the ripe fruit, total soluble solids content reached

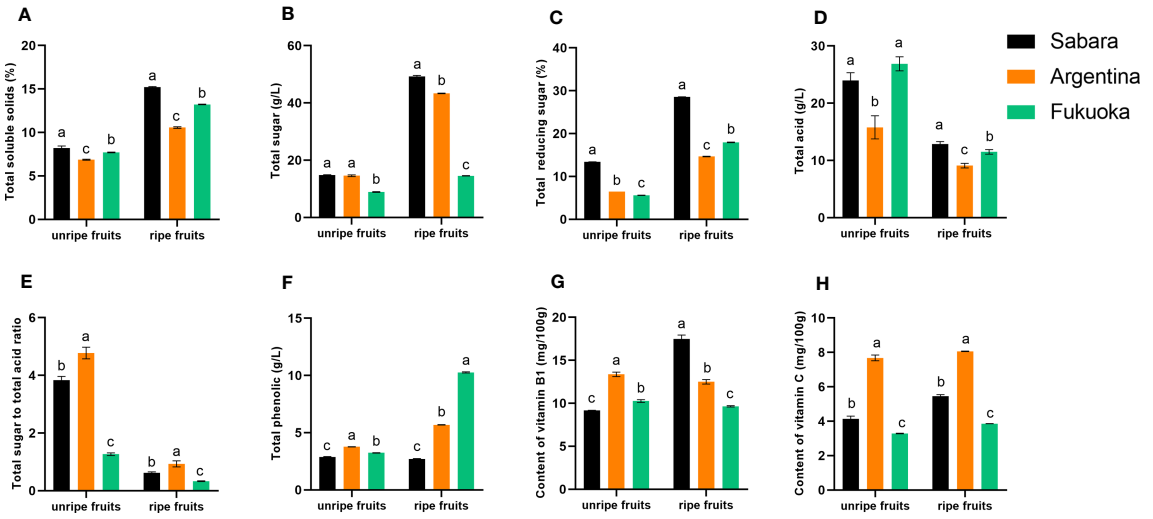

FIGURE 2
Physical and chemical characteristics of jaboticaba. **(A–H)** represent the total soluble solids, total sugar, total reducing sugar, total acid, total sugar to total acid ratio, total polyphenols, Vitamin B1 content, and Vitamin C content of different jaboticaba, respectively. Different lowercases indicate significant difference within the ripe and unripe groups. $p<0.05$.

15.22% in Sabara and 13.23% in Fukuoka, while in Argentina it was only 10.56%. Among the unripe fruits, total soluble solids content reached 8.21% in Sabara and 7.7% in Fukuoka, while in Argentina it was only 6.87%. Notably, Sabara exhibited significantly higher total soluble solids content than the other two cultivars.

In general, both for unripe and ripe fruit, the total sugar content was highest in Sabara, followed by Argentina and Fukuoka (Figure 2B). In the ripe fruit, the total sugar content reached 49.22 g/L in Sabara and 43.30 g/L in Argentina, while in Fukuoka it was only 14.54 g/L. The total sugar content of Sabara and Argentina was almost three folds that of Fukuoka. To better evaluate of the sugar content of these jaboticaba cultivars, we also determined the percentage of reducing sugar in the total sugar. The trend in the percentage of reducing sugar differed between ripe and unripe fruit (Figure 2C). Among the unripe fruits, Sabara had the highest percentage of reducing sugar, followed by Argentina and Fukuoka. Among the ripe fruits, the highest percentage of reducing sugar was found in Sabara, followed by Fukuoka and then Argentina. Notably, Sabara exhibited significantly higher total sugar content and reducing sugar percentage than the other two cultivars.

In terms of total acidity, unripe and ripe fruit have different trends (Figure 2D). The acidity of unripe fruit was highest in Fukuoka, followed by Sabara and Argentina. On the contrary, Sabara was more acidic than Fukuoka and Argentina, in the ripe fruit. In addition, the acidity decreased as the fruit matured, and ultimately, the acidity of the three fruits was not significantly different at approximately 10 g/L. The ratio of total sugar to total acidity is presented in Figure 2E.

The content and composition of acids and sugars are important quality factors that directly influence the flavor and acceptability of fruits and berries (Tang et al., 2001; Liu et al., 2010). Fruit acids promote food digestion and improve blood circulation. The acid content may also affect the stability of phenolic compounds in the fruit (Chang et al., 2006). We determined the sugar and acid concentrations separately and calculated the sugar-acid ratio. There were significant differences in the sugar-acid ratios of the three jaboticaba cultivars. In general, a high sugar-to-acid ratio means the fruit has a sweet and sour taste. From this, it can be concluded that Argentina and Sabara had more desirable flavor. Since Fukuoka had a lower sugar-to-acid ratio, it is better suited for use in processed products.

3.1.3 Total polyphenols

The total polyphenols content of the ripe fruit was higher than in unripe for all cultivars except Sabara (Figure 2F). For the unripe fruit, the difference in total polyphenols content between the three cultivars of jaboticaba was not significant, all at around 3 g/L. However, when the fruit was ripe, there were very significant differences in total polyphenols content between the cultivars. In Sabara, the total polyphenols content was only 2.69 g/L. Argentina had 5.68 g/L, and the highest was Fukuoka with 10.27 g/L, about three times that of Sabara and twice that of Argentina.

Jaboticaba fruit is a dark berry rich in phenolic compounds, particularly anthocyanins and ellagitannins (Wu et al., 2012; Inada et al., 2015; Plaza et al., 2016; Pereira et al., 2017). The phenolic content has been studied by a large number of scholars who discovered many potential uses for jaboticaba (Lee et al., 2017; Rodrigues et al., 2021; Soares et al., 2021). In this study, we obtained results that are consistent with those of previous researchers. We also found large differences between the three jaboticaba cultivars. In particular, the total polyphenols content of Fukuoka was extremely high. Phenolic compounds derived from jaboticaba could be used to treat inflammation. In South American countries, such as Brazil, people take jaboticaba directly to combat some inflammation (Brito et al., 2021). Therefore, the consumption of Fukuoka could provide good anti-inflammatory effects, and intensive processing of Fukuoka is likely.

3.1.4 Vitamin B1 and Vitamin C

The vitamin content varied slightly between the three cultivars of jaboticaba (Figures 2G, H). The vitamin B1 content in Sabara increased with fruit maturity, whereas the opposite was true for Argentine and Fukuoka. Moreover, the ripe Sabara fruit had a much higher vitamin B1 content than Argentina and Fukuoka, reaching 17.47 mg/100 g. The trend for vitamin C differed from vitamin B1. The vitamin C content was highest in Argentina, followed by Sabara and Fukuoka for unripe and ripe fruits, and the vitamin C content increased with fruit maturity. Argentina had 8.06 mg/100 g of vitamin C in ripe fruit, compared to 3.86 mg/100 g in Fukuoka, which is about two times higher. In general, jaboticaba has a slightly higher vitamin C content than grapes (Tavasolinasab et al., 2023).

Vitamin B1 has been reported to be effective in reducing the risk of depression (Nguyen et al., 2022), and vitamin C has good antiviral (Colunga Biancatelli et al., 2020) and antioxidant properties, as well as potential benefits for skin health (Pullar et al., 2017). Previously, it was verified that jaboticaba contains a wide range of vitamins. From our results, Argentina had a much higher vitamin C content than Sabara and Fukuoka, but Sabara has a much higher vitamin B1 content than Argentina and Fukuoka. It can therefore be concluded that in terms of vitamins, Sabara and Argentina are of higher quality than Fukuoka. However, vitamins can easily lose their activity at high temperatures or under other conditions. In this respect, Argentina and Sabara should be consumed fresh to maximize their vitamin absorption by the human body.

3.1.5 Amino acids

Jaboticaba has been reported to be rich in amino acids, and our findings are consistent with these reports. In our study, we detected 16 amino acids, such as aspartic acid, glutamic acid, and threonine, in different cultivars of jaboticaba, and the detailed data are shown in Table 3. Both unripe and ripe fruits contained these 16 amino acids, with differences in their content. In the case of Sabara, the most abundant amino acid was glutamic acid at 0.69 g/kg, and the least abundant was methionine at 0.03 g/kg in unripe fruit. At

TABLE 3 Concentration of amino acid (g/Kg) in jaboticaba at unripe and ripe stages.

Amino acid	Ripe fruit			Unripe fruit		
	Sabara	Argentina	Fukuoka	Sabara	Argentina	Fukuoka
Asp	0.50 ± 0.00c	0.36 ± 0.01a	0.46 ± 0.00b	0.60 ± 0.01b	0.51 ± 0.01c	0.53 ± 0.00a
Thr	0.22 ± 0.00b	0.24 ± 0.00b	0.21 ± 0.00c	0.27 ± 0.00c	0.25 ± 0.00a	0.24 ± 0.00a
Ser	0.27 ± 0.00b	0.11 ± 0.00a	0.23 ± 0.00b	0.30 ± 0.00c	0.29 ± 0.00c	0.26 ± 0.00a
Glu	0.66 ± 0.00b	0.29 ± 0.00b	0.75 ± 0.00a	0.69 ± 0.01b	0.64 ± 0.01c	0.63 ± 0.00a
Gly	0.27 ± 0.01c	0.31 ± 0.00b	0.25 ± 0.00c	0.29 ± 0.00b	0.25 ± 0.00a	0.26 ± 0.00a
Ala	0.38 ± 0.00b	0.25 ± 0.00a	0.31 ± 0.00b	0.36 ± 0.00c	0.34 ± 0.01c	0.29 ± 0.00a
Val	0.23 ± 0.00b	0.25 ± 0.00b	0.22 ± 0.00c	0.29 ± 0.00b	0.26 ± 0.00a	0.26 ± 0.00a
Met	0.04 ± 0.00a	0.02 ± 0.00a	0.03 ± 0.00b	0.03 ± 0.00b	0.03 ± 0.00c	0.03 ± 0.00a
Ile	0.17 ± 0.01b	0.03 ± 0.00a	0.16 ± 0.00a	0.22 ± 0.00b	0.20 ± 0.00b	0.20 ± 0.00a
Leu	0.32 ± 0.01b	0.39 ± 0.00b	0.31 ± 0.00b	0.41 ± 0.01b	0.38 ± 0.01a	0.38 ± 0.00a
Tyr	0.09 ± 0.00b	0.05 ± 0.00b	0.11 ± 0.00a	0.17 ± 0.00b	0.16 ± 0.00c	0.15 ± 0.00a
Phe	0.22 ± 0.00b	0.19 ± 0.00a	0.21 ± 0.00b	0.27 ± 0.00b	0.25 ± 0.00c	0.25 ± 0.00a
Lys	0.35 ± 0.01b	0.25 ± 0.00a	0.34 ± 0.01b	0.46 ± 0.00c	0.43 ± 0.01c	0.39 ± 0.00a
His	0.16 ± 0.01b	0.12 ± 0.00a	0.13 ± 0.00b	0.21 ± 0.00c	0.19 ± 0.00c	0.16 ± 0.00a
Arg	0.23 ± 0.00b	0.17 ± 0.00a	0.23 ± 0.00a	0.31 ± 0.00c	0.29 ± 0.00b	0.26 ± 0.00a
Pro	0.25 ± 0.00b	0.11 ± 0.00a	0.23 ± 0.01b	0.27 ± 0.00b	0.24 ± 0.00c	0.24 ± 0.01a

Different letters indicated significant differences within the ripe and unripe groups. $p<0.05$.

maturity, the amino acid with the highest concentration was glutamic acid at 0.66 g/kg, and the lowest was methionine at 0.04 g/kg. For Argentina, the most abundant amino acid in ripe fruit was glutamic acid at 0.64 g/kg and the least abundant was methionine at 0.03 g/kg. At unmaturity, the most abundant amino acid was leucine at 0.39 g/kg, and the least abundant was methionine at 0.02 g/kg. For Fukuoka, the most abundant amino acid was glutamic acid at 0.63 g/kg and the least abundant was methionine at 0.03 g/kg in unripe fruit. At maturity, the amino acid with the highest concentration was glutamic acid at 0.75 g/kg, and the lowest was methionine at 0.03 g/kg.

Amino acids are essential nutrients, but they cannot be synthesized by the body. They must be replenished through the consumption of foods rich in amino acids (Kurpad et al., 2006). In this work, all three varieties of jaboticaba were rich in a variety of amino acids, and the amino acid content was slightly different between cultivars. Amino acids, such as glutamic acid, arginine, aspartic acid, and cysteine, have biological activities in the treatment of several diseases and have been used in clinical applications (Ferrando et al., 2005; MacDonald et al., 2019). Our results demonstrate the contents of aspartic acid, glutamic acid, and glycine were relatively high in jaboticaba fruits, in comparison to other amino acids. In addition, for the 16 amino acids detected, Argentina generally had lower levels than Fukuoka and Sabara, with the lysine, leucine, etc. We can assume that Fukuoka and Sabara contain more amino acids than Argentina, making them excellent choices in a healthy diet.

3.1.6 Elemental analysis

Trace elements are important to human wellness; thus, we examined the trace element content of the three jaboticaba cultivars, and the data are summarized in Table 4. Significant differences in the content of each element were found. K, Ca and Mg were present in significant amounts, and Cu, Al, and Sr were present at low levels relative to the other elements. Toxic elements including As, Cr, and Cd were detected at remarkably low and almost negligible levels. Of the 25 vital elements closely associated with the human body, essential macro elements, including K, Mg, and Ca, and essential microelements, such as Zn, Fe, Cu, and Mn, play an extremely important role in the control of human diseases (Anuk et al., 2021; Budinger et al., 2021; Zeidan et al., 2021). We also found some difference in trace element content between unripe and ripe fruit, with these elements except Al, Mn, Cu, As, Sr, and Ba were slightly higher in ripe fruit than in unripe fruit. The results indicate the highest trace element content in Sabara, Argentina, and Fukuoka was K, followed by Mg. Furthermore, Argentina had slightly higher trace element content than Sabara and Fukuoka, which would suggest that Argentina contains the most beneficial trace elements. It is also worth noting that all three cultivars of jaboticaba contain Fe and Zn, which are also beneficial to human wellness.

TABLE 4 Concentration of elemental (mg/Kg) in jaboticaba at unripe and ripe stages.

Element	Ripe fruit			Unripe fruit		
	Sabara	Argentina	Fukuoka	Sabara	Argentina	Fukuoka
Na	3.00 ± 0.00a	3.00 ± 0.00a	3.00 ± 0.00a	3.00 ± 0.00a	3.00 ± 0.00a	3.00 ± 0.00a
Mg	119.06 ± 3.08b	116.97 ± 1.44a	106.67 ± 2.97b	110.61 ± 1.16c	107.73 ± 0.53a	99.66 ± 1.86b
Al	0.97 ± 0.06a	0.74 ± 0.31a	0.89 ± 0.17a	0.93 ± 0.32a	1.27 ± 0.29a	0.95 ± 0.13a
K	1746.16 ± 39.10b	1639.45 ± 8.69a	1415.36 ± 25.82c	1274.53 ± 12.44b	1528.64 ± 6.97a	1368.09 ± 33.00c
Ca	78.44 ± 0.26b	68.48 ± 3.17a	56.24 ± 3.30c	123.65 ± 1.46b	67.03 ± 1.13c	94.36 ± 6.09a
Ti	ND	ND	ND	ND	ND	ND
V	ND	ND	ND	ND	ND	ND
Cr	ND	ND	ND	ND	ND	ND
Mn	3.03 ± 0.04a	4.20 ± 0.04a	3.98 ± 0.06b	7.35 ± 0.17c	6.39 ± 0.03b	3.00 ± 0.07a
Fe	2.21 ± 0.07b	1.52 ± 0.05b	1.32 ± 0.02b	1.27 ± 0.18b	1.41 ± 0.06a	1.19 ± 0.06ab
Co	ND	ND	0.02 ± 0.00a	0.02 ± 0.00b	ND	0.00 ± 0.00a
Ni	ND	ND	ND	ND	ND	ND
Cu	0.37 ± 0.01b	0.23 ± 0.02a	0.88 ± 0.01a	0.95 ± 0.03a	0.64 ± 0.02b	0.89 ± 0.03a
Zn	3.85 ± 0.03a	3.12 ± 0.62a	2.79 ± 0.35b	4.49 ± 0.30a	3.41 ± 0.11a	3.99 ± 0.74a
As	0.01 ± 0.00b	0.01 ± 0.00b	0.01 ± 0.00b	0.02 ± 0.00a	0.01 ± 0.00c	0.02 ± 0.00b
Sr	0.13 ± 0.00c	0.14 ± 0.00a	0.29 ± 0.01a	0.53 ± 0.02b	0.12 ± 0.00c	0.26 ± 0.00a
Cd	ND	ND	ND	ND	ND	ND
Sn	ND	ND	ND	ND	ND	ND
Sb	ND	ND	ND	ND	ND	ND
Ba	0.55 ± 0.10b	0.37 ± 0.05a	0.61 ± 0.01a	0.95 ± 0.01b	0.29 ± 0.08b	0.42 ± 0.03a
Hg	ND	ND	ND	ND	ND	ND
Pb	ND	ND	ND	ND	ND	ND

Different letters indicated significant differences within the ripe and unripe groups. ND indicates not detected. $p<0.05$.

Similar to the amino acid content, trace elements must be supplemented through the external intake. In particular, trace elements, such as calcium, iron, and potassium, are beneficial and necessary to human wellness, but some elements, such as lead and mercury, are harmful (Zeidan et al., 2021; Nag and Cummins, 2022; Pierezan et al., 2022). In this study, all three cultivars of jaboticaba had some amount of beneficial trace elements, and no harmful elements were detected. This result further confirmed the consumption of jaboticaba as a nutritional food. In addition, our results showed the overall micronutrient content of Sabara was slightly higher than the other two cultivars, which means that Sabara may be more preferred by consumers.

3.2 Analysis of the capacity of antioxidants *in vitro*

The content of phenolic compounds is closely related to antioxidant capacity (Chang et al., 2019). Therefore, to better investigate the best way to consume these three cultivars of jaboticaba, we tested several *in vitro* antioxidant indicators.

3.2.1 Total antioxidant capacity

The results of the total antioxidant capacity test are shown in Figure 3A. The trend was the same for both unripe and ripe fruit, with Argentina having a higher total antioxidant capacity than Sabara and Fukuoka. Additionally, the unripe fruit had a higher total antioxidant capacity than the ripe fruit of the corresponding cultivars. The total antioxidant capacity of the three cultivars of jaboticaba differed significantly, with the highest total antioxidant capacity in Argentina being almost twice that of Sabara and three times that of Fukuoka.

3.2.2 Hydroxyl radical inhibition

The ability to the hydroxyl radical inhibiting capacity of jaboticaba was similar (Figure 3B), either between cultivars or between different stages of ripening. The hydroxyl radical inhibitory capacity of Sabara was 5023.23 U/mL in ripe fruit and

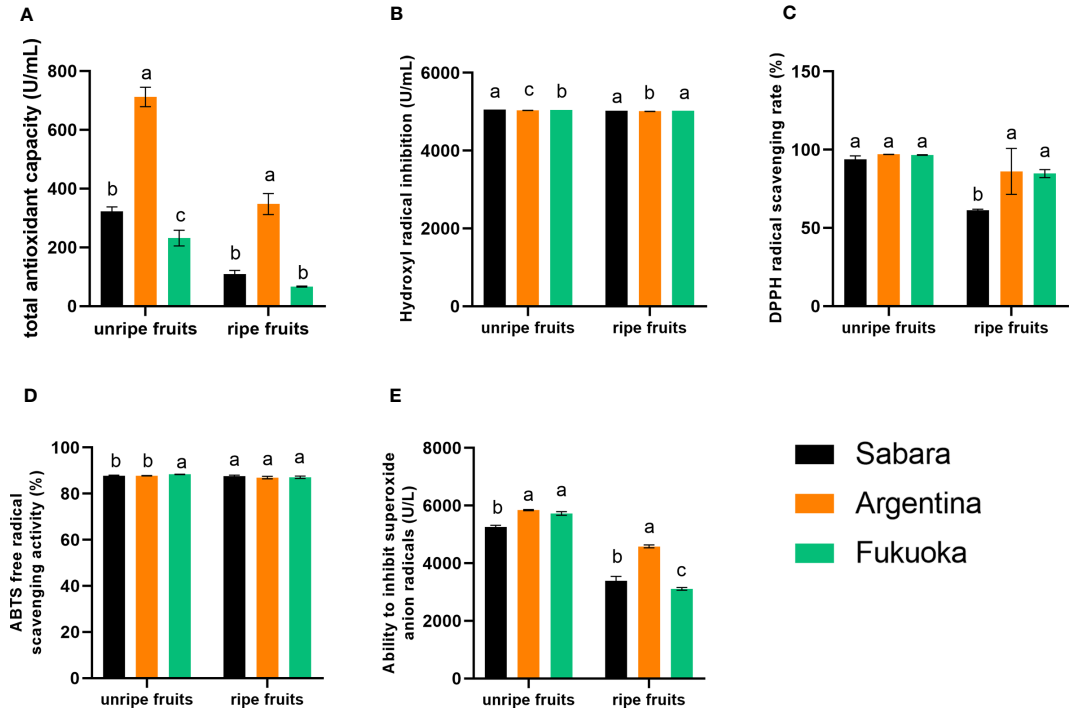

FIGURE 3
Antioxidant capacity of jaboticaba. **(A–E)** represent the antioxidant capacity, hydroxyl radical inhibition capacity, DPPH radical scavenging rate, ABTS free radical scavenging activity, and ability to inhibition superoxide anion radicals of different jaboticaba, respectively. Different lowercases indicate significant difference within the ripe and unripe groups. $p<0.05$.

5055.78 U/mL in unripe fruit, while that of Argentina was 5010.48 U/mL in ripe fruit and 5034.84 U/mL in unripe fruit. Therefore, we conclude that the hydroxyl radical inhibiting capacity of unripe fruit was slightly higher than that of ripe fruit, and the inhibiting capacity of Sabara was higher than that of Fukuoka and Argentina.

3.2.3 DPPH radical scavenging rate

The results of the DPPH radical scavenging rate are shown in Figure 3C. There was no significant difference in the DPPH radical scavenging rate between the three cultivars of unripe jaboticaba, and all samples reached more than 93.75%. The highest scavenging rate of 97.03% for DPPH radicals was found in Argentina. However, in the ripe fruit, all three cultivars of jaboticaba showed a decrease in DPPH radical scavenging, compared to the unripe fruit. In particular, Sabara fruit exhibited a significant decrease from 93.75% to 61.34%. The other two cultivars also decreased but both still had more than 80% DPPH scavenging, with 86.16% in Argentina and 84.77% in Fukuoka. In general, all three cultivars exhibited good scavenging ability for DPPH free radicals.

3.2.4 ABTS free radical scavenging activity

There were no significant differences in the ABTS free radical scavenging capacity of jaboticaba cultivars, either between unripe and ripe fruit or between cultivars (Figure 3D). Among the unripe fruits, the strongest scavenging ability was that of Fukuoka, at 88.38%, and the lowest scavenging ability was that of Argentina, at 87.80%. Among the ripe fruits, the strongest scavenging ability was found in Sabara, at 87.64%, and the lowest scavenging ability was also found in Argentina, at 86.99%. Thus, the best scavenger of ABTS free radicals was Sabara, followed by Fukuoka and Argentina; however, the differences between their scavenging abilities were very small (i.e., the values were very close).

3.2.5 Ability to inhibit superoxide anion radicals

The ability of the fruit to inhibit superoxide anion radicals is shown in Figure 3E. There were differences in the results, both between cultivars and between ripening periods. The superoxide anion radical inhibition capacity of unripe fruit was higher than that of ripe fruit, and there was a relatively large difference. The superoxide anion radical inhibition capacity of ripe Sabara fruit was 3387.26 U/L, while that of unripe fruit reached 5263.81 U/L. The superoxide anion radical inhibition capacity of ripe Argentina fruit was 4584.87 U/L, while that of unripe fruit reached 5843.70 U/L. The superoxide anion radical inhibition capacity of ripe Fukuoka fruit was 4584.87 U/L, while that of unripe fruit reached 5843.70 U/L. In summary, the superoxide anion radical inhibiting capacity of Argentina was higher than that of Sabara and Fukuoka.

Interestingly, not all of the *in vitro* antioxidants we tested were higher in one variety than in the other two, but each had its own advantages. For example, Argentina had the highest total antioxidant capacity, superoxide anion inhibition capacity, and DPPH scavenging rate among the three. Sabara had the highest hydroxyl radical inhibition capacity and ABTS cation scavenging rate among the three. Although Fukuoka was not the highest among

several indexes we tested, it still presented a high antioxidant capacity. Thus, the antioxidant capacity of all three cultivars of jaboticaba was similar, and all were considered to have strong antioxidant capacity. Combining the total polyphenols content and the *in vitro* antioxidant assay results, we believe that Argentina and Fukuoka have stronger anti-inflammatory and antioxidant properties than Sabara. In general, we believe that those with weaker antioxidant properties are not suitable for processed products and are more suitable for fresh consumption. Therefore, we concluded Argentine and Fukuoka are more suitable for processed products, and Sabara is more suitable for fresh consumption. The high polyphenol content of the three cultivars and their strength *in vitro* antioxidant capacity could contribute to anti-aging in humans. This means that all three cultivars of kapok fruit have the perspective of being able to become a medicinal food source.

3.3 Volatile compounds analysis

The data from the analysis of the volatile compounds are summarized in Table 5. The volatile compounds detected in the

TABLE 5 Concentration of volatile compounds (μg/L) in jaboticaba at unripe and ripe stages.

Volatile compounds	Ripe fruit			Unripe fruit		
	Sabara	Argentina	Fukuoka	Sabara	Argentina	Fukuoka
Terpenes:						
Copaene	288.83 ± 221.3	160.82 ± 19.73	ND	ND	867.71 ± 82.87	ND
Levo-b-elemene	273.32 ± 34.3	321.38 ± 80.81	ND	ND	2161.03 ± 171.95	596.11 ± 467.39
Caryophyllene	542.21 ± 22.48	378.73 ± 45.98	663.22 ± 205.09	186.51 ± 158.95	3127.14 ± 1.68	4195.14 ± 93.31
γ-Muurolene	ND	174.72 ± 74.2	ND	ND	1749.31 ± 996.64	ND
Viridiflorene	ND	205.81 ± 24.42	ND	ND	2813.02 ± 1740.41	494.61 ± 47.85
Germacrene D	ND	257.8 ± 45.4	ND	359.69 ± 408.56	637.07 ± 76.99	ND
(-)-α-Muurolene	ND	ND	ND	ND	1672.77 ± 948.53	ND
Alloaromadendrene	ND	243.05 ± 77.87	ND	ND	ND	ND
(+)-α.-Muurolene	ND	119.88 ± 6.25	ND	160.77 ± 133.18	ND	ND
Aromandendrene	ND	ND	ND	ND	ND	387.85 ± 123.01
(+)-b-Selinene	ND	ND	ND	ND	ND	201.56 ± 6.65
D-Limonene	397.14 ± 248.69	ND	ND	ND	ND	ND
d-Cadinene	ND	175.03 ± 43.18	ND	ND	1677.47 ± 250.47	ND
Bicyclogermacren	ND	336.17 ± 64.79	ND	ND	ND	ND
Alcohols:						
Himbaccol	ND	ND	ND	ND	344.3 ± 114.27	ND
α.-Cadinol	ND	ND	145.87 ± 35.58	ND	206.1 ± 148.46	27.51 ± 19.61
Linalool	581.9 ± 47.14	ND	ND	ND	ND	ND
α.-Terpineol	ND	68.31 ± 4.51	ND	55.42 ± 2.61	ND	ND
Phenylethyl Alcohol	ND	99.25 ± 24.99	172.88 ± 56.78	223.49 ± 88.93	ND	193.96 ± 37.13
Espatulenol	ND	82.65 ± 15.96	ND	ND	ND	89.96 ± 32.99
Eucalyptol	471 ± 153.22	ND	ND	ND	ND	273.21 ± 44.07
Ledol	ND	ND	ND	ND	ND	44.72 ± 15.27
2-((3R,3aR,3bS,4R,7R,7aS)-3,7-Dimethyloctahydro-1H-cyclopenta[1,3]cyclopropa[1,2]benzen-4-yl)propan-2-ol	ND	ND	ND	ND	ND	74.44 ± 20.69
(-)-Globulol	ND	ND	ND	ND	ND	48.29 ± 15.77
Rosifoliol	ND	ND	ND	ND	ND	28.72 ± 9.72

(Continued)

TABLE 5 Continued

Volatile compounds	Ripe fruit			Unripe fruit		
	Sabara	Argentina	Fukuoka	Sabara	Argentina	Fukuoka
3-Hexen-1-ol, (E)-	125.63 ± 38.2	ND	ND	ND	ND	ND
Esters:						
Benzoic acid methyl ester	1438.35 ± 65.47	309.89 ± 125.67	168.09 ± 62.59	132.72 ± 22.22	ND	ND
Decanoic acid ethyl ester	ND	255.78 ± 70.04	154.67 ± 40.84	ND	ND	185.02 ± 88.74
Octanoic acid ethyl ester	ND	ND	180.48 ± 60.78	ND	ND	42.13 ± 10.38
Methyl trans-cinnamate	298.27 ± 34.64	ND	ND	ND	ND	ND
Benzoic acid ethyl ester	756.82 ± 265.17	ND	ND	144.01 ± 15.55	ND	147.39 ± 64.32
Butanedioic acid diethyl ester	ND	ND	ND	ND	ND	77.55 ± 6.36
(Z)-Ethyl cinnamate	ND	ND	ND	ND	ND	173.62 ± 12.86
Diethyl Phthalate	93.76 ± 4.41	145.81 ± 25.19	ND	124.32 ± 15.44	231.07 ± 95.53	39.85 ± 3.25
Alkanes:						
Cadalin	101.34 ± 33.4	72.69 ± 20.95	ND	123.5 ± 5.13	186.11 ± 117.09	54.63 ± 4.06
trans-Calamenene	832.56 ± 114.54	508.43 ± 84.7	ND	822.76 ± 545.5	1301.58 ± 746.3	ND
(-)-g-Cadinene	ND	122.87 ± 20.35	ND	ND	1680.11 ± 620.89	ND
Ketones:						
Zonarene	ND	81.1 ± 13.23	ND	ND	ND	ND
1-(2,4,5-Trimethoxyphenyl) butan-1-one	ND	ND	ND	ND	ND	43.88 ± 0.98
Bicyclohexyliden-2-one	ND	74.24 ± 10.67	ND	ND	ND	ND
Phenols:						
Neointermedeol	ND	ND	ND	ND	ND	101.89 ± 47.65

ND indicates not detected.

three fruit cultivars were mainly alkenes and esters. In addition, for ripe fruit, a greater variety of aromatic substances was detected in Argentina and Sabara. And varieties of volatile compounds were changed as the fruit matured. In contrast, Fukuoka had 22 volatile compounds in unripe fruit but only six in ripe fruit. A total of 41 volatile compounds were identified in Sabara, Argentina, and Fukuoka by HS-SPME-GC/MS. The volatile compounds were divided into terpenes, alcohols, esters, alkanes, ketones, and phenols (Figure 4A). Among them, terpenes contributed the most (approximately 34%), followed by alcohols (29%), esters (20%), alkanes (7%) and ketones (7%).

Principal component analysis (PCA) is a technique that shows general variation between groups and variation within groups. In the results of PCA, the first principal component (PC1) explained 32.49% of the total variance. Different distributions indicated different maturity stages of the samples. The second principal component (PC2) explained 26.2% of the total variance (Figure 4B). In addition, significant differences between cultivars and periods were found.

Row standardized cluster analysis [values taken as log2 (value + 1)] was performed on the volatile compounds detected from jaboticaba, and the results are shown in the heat map (Figure 4C). It is clear that the types and contents of volatile compounds detected varied between periods and cultivars.

The composition of volatile compounds is the basis for the flavor provided by the fruit, consistent with previous studies in jaboticaba (Plagemann et al., 2012), and terpenes and alcohols were the predominant aromatic compounds in jaboticaba. However, the volatile compounds of jaboticaba is lower than that of grapes (Wu et al., 2020). There were differences in the aromatic composition of the three cultivars of jaboticaba. For ripe fruit, Sabara and Argentina had more abundant volatile compounds, which makes them more suitable for fresh consumption. In contrast, Fukuoka had a more homogeneous composition, as only six volatile compounds were

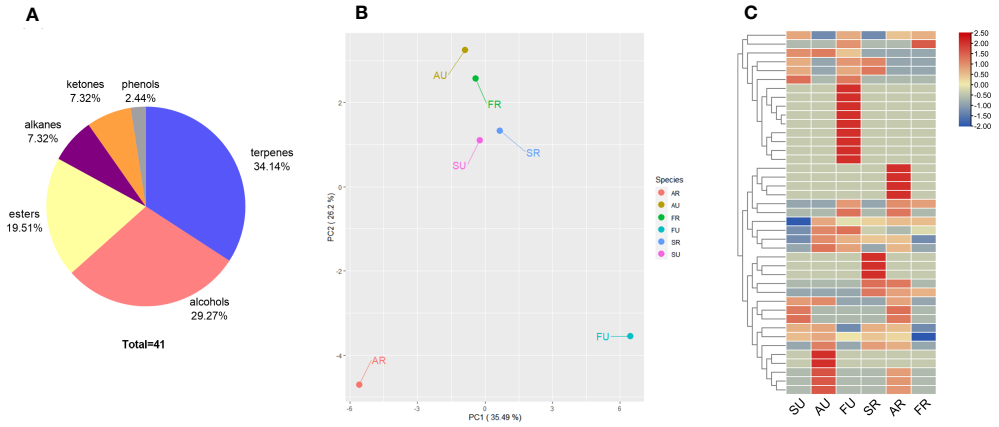

FIGURE 4
The volatile compounds of jaboticaba. Classification and proportion of total 41 volatile compounds detected in jaboticaba **(A)**; PCA among samples of jaboticaba at different stages and periods **(B)**; heat map displays the hierarchical clustering of volatile compound content in ug/L in the difference within the ripe and unripe groups, with red indicating high levels of content and blue indicating low levels. SU represent Sabara unripe, AU, Argentina unripe; FU, Fukuoka unripe; SR, Sabara ripe; AR, Argentina ripe; FR, Fukuoka ripe **(C)**.

detected, despite the fact that it detects the most volatile substances when unripe. Since the aromatic profile was limited, Fukuoka was not considered suitable for fresh consumption. As mentioned earlier, the fruit size of Fukuoka were larger, which also confirms its suitability for intensive processing.

4 Conclusion

In this study, it was found that generally, three jaboticaba cultivars berry were rich in nutrients, high in polyphenols content antioxidant capacity. However, there were significant differences in their nutrient content and volatile compounds. Sabara has a suitable acid-to-sugar ratio, superior flavor and slightly lower antioxidant capacity for fresh consumption. Argentina, although it does not taste as good as Sabara, has a high antioxidant capacity and is the richest in volatile compounds, making it suitable for development of dry products. The large size, juicy flesh and low sugar-acid content of Fukuoka also make it suitable for juice processing. The results could promote the development of the jaboticaba industry and broaden potential applications in the field of health products. Selective cultivation and processing of jaboticaba cultivars could lead to numerous health and economic benefits.

Data availability statement

The original contributions presented in the study are included in the article/supplementary material. Further inquiries can be directed to the corresponding author.

Author contributions

SX: conceptualization, methodology, validation, writing - original draft, and data curation. YP: methodology, validation, and writing - original draft. XC: methodology, validation, and data curation. QC: formal analysis and writing - original draft. GJ: conceptualization and writing - review and editing. MZ: conceptualization and writing - review and editing. LH: conceptualization, writing - original draft, writing - review and editing, methodology, and validation. All authors contributed to the article and approved the submitted version.

Funding

This work was supported by the Science and Technology Guided Project of Fujian Province (No. 2021N0010), and Xiyuanjiang River Scholarship of College of Life Sciences, Fujian Normal University (22FSSK018). We greatly appreciate the helpful suggestions and comments on the manuscript from the editor and reviewers.

Acknowledgments

We greatly appreciate the helpful suggestions and comments on the manuscript from the editor and reviewers.

Conflict of interest

The authors declare that the research was conducted in the absence of any commercial or financial relationships that could be construed as a potential conflict of interest.

Publisher's note

References

Albuquerque, B. R., Pereira, C., Calhelha, R. C., Alves, M. J., Abreu, R. M. V., Barros, L., et al. (2020). Jabuticaba residues (*Myrciaria jaboticaba* (Vell.) berg) are rich sources of valuable compounds with bioactive properties. *Food Chem.* 309, 8. doi: 10.1016/j.foodchem.2019.125735

Anuk, A. T., Polat, N., Akdas, S., Erol, S. A., Tanacan, A., Biriken, D., et al. (2021). The relation between trace element status (zinc, copper, magnesium) and clinical outcomes in COVID-19 infection during pregnancy. *Biol. Trace Element Res.* 199, 3608–3617. doi: 10.1007/s12011-020-02496-y

Appelt, P., Da Cunha, M. A. A., Guerra, A. P., Kalinke, C., and De Lima, V. A. (2015). Development and characterization of cereal bars made with flour of jabuticaba peel and okara. *Acta Scientiarum-Technol.* 37, 117–122. doi: 10.4025/actascitechnol.v37i1.21070

Asquieri, E. R., Silva, A.G.D.M.E., and Cândido, M. A. (2009). Aguardente de jabuticaba obtida da casca e borra da fabricação de fermentado de jabuticaba. *Food Sci. Technol. (Campinas)* 29, 896–904. doi: 10.1590/S0101-20612009000400030

Benvenutti, L., Zielinski, A. A. F., and Ferreira, S. R. S. (2021). Jaboticaba (*Myrtaceae cauliflora*) fruit and its by-products: alternative sources for new foods and functional components. *Trends Food Sci. Technol.* 112, 118–136. doi: 10.1016/j.tifs.2021.03.044

Boldori, J. R., Moraes, L. D., Rodrigues, C. D., Tambara, A. L., and Denardin, C. C. (2023). Involvement of the DAF-16/FOXO pathway in the antioxidant activity of the jaboticaba (*Myrciaria trunciflora*) extract against various stressors using caenorhabditis elegans. *Chem. Biodiversity* 20, e202201046. doi: 10.1002/cbdv.202201046

Brito, T., Silva, A., Cunha, R. X. D., Fonseca, C., Araújo, T., Campos, J. K. L., et al. (2021). Anti-inflammatory, hypoglycemic, hypolipidemic, and analgesic activities of *Plinia cauliflora* (Mart.) kausel (Brazilian grape) epicarp. *J. Ethnopharmacol.* 268, 113611. doi: 10.1016/j.jep.2020.113611

Budinger, D., Barral, S., Soo, A. K. S., and Kurian, M. A. (2021). The role of manganese dysregulation in neurological disease: emerging evidence. *Lancet Neurol.* 20, 956–968. doi: 10.1016/S1474-4422(21)00238-6

Chang, S. K., Alasalvar, C., and Shahidi, F. (2019). Superfruits: phytochemicals, antioxidant efficacies, and health effects - a comprehensive review. *Crit. Rev. Food Sci. Nutr.* 59, 1580–1604. doi: 10.1080/10408398.2017.1422111

Chang, Q., Zuo, Z., Chow, M. S. S., and Ho, W. K. K. (2006). Effect of storage temperature on phenolics stability in hawthorn (*Crataegus pinnatifida* var. major) fruits and a hawthorn drink. *Food Chem.* 98, 426–430. doi: 10.1016/j.foodchem.2005.06.015

Colunga Biancatelli, R. M. L., Berrill, M., and Marik, P. E. (2020). The antiviral properties of vitamin c. *Expert Rev. Anti-infective Ther.* 18, 99–101. doi: 10.1080/14787210.2020.1706483

Correia, V. T. D., Da Silva, P. R., Ribeiro, C. M. S., Ramos, A., Mazzinghy, A. C. D., Silva, V. D. M., et al. (2022). An integrative review on the main flavonoids found in some species of the myrtaceae family: phytochemical characterization, health benefits and development of products. *Plants-Basel* 11, 30. doi: 10.3390/plants11202796

Da Silva-Maia, J. K., Nagalingam, A., Cazarin, C. B. B., Marostica Junior, M. R., and Sharma, D. (2023). Jaboticaba (*Myrciaria jaboticaba*) peel extracts induce reticulum stress and apoptosis in breast cancer cells. *Food Chem.* 6, 100167. doi: 10.1016/j.fochms.2023.100167

Fernandes, F., Fonteles, T. V., Rodrigues, S., De Brito, E. S., and Tiwari, B. K. (2020). Ultrasound-assisted extraction of anthocyanins and phenolics from jabuticaba (*Myrciaria cauliflora*) peel: kinetics and mathematical modeling. *J. Food Sci. Technology-Mysore* 57, 2321–2328. doi: 10.1007/s13197-020-04270-3

Ferrando, A. A., Raj, D., and Wolfe, R. R. (2005). Amino acid control of muscle protein turnover in renal disease. *J. Renal Nutr.* 15, 34–38. doi: 10.1053/j.jrn.2004.09.014

Ferreira, P. R., Pinheiro, F. D. A., Duarte, M. D. S., Silva, W. D., Reis, N. R. D., Marques, D. B. D., et al. (2021). Effect of jaboticaba and pequi extracts on gene expression of antioxidant enzymes in C2C12 mouse muscle cells. *Res. Soc. Dev.* 10, e375101018864. doi: 10.33448/rsd-v10i10.18864

Geraldi, M. V., Cazarin, C. B. B., Cristianini, M., Vasques, A. C., Geloneze, B., and Maróstica Júnior, M. R. (2021). Jabuticaba juice improves postprandial glucagon-like peptide-1 and antioxidant status in healthy adults: a randomized crossover trial. *Br. J. Nutr.* 128, 1545–1554. doi: 10.1017/S0007114521004530

Hsu, J. D., Wu, C. C., Hung, C. N., Wang, C. J., and Huang, H. P. (2016). Myrciaria cauliflora extract improves diabetic nephropathy *via* suppression of oxidative stress and inflammation in streptozotocin-nicotinamide mice. *J. Food Drug Anal.* 24, 730–737. doi: 10.1016/j.jfda.2016.03.009

Inada, K. O. P., Duarte, P. A., Lapa, J., Miguel, M. A. L., and Monteiro, M. (2018). Jabuticaba (*Myrciaria jaboticaba*) juice obtained by steam-extraction: phenolic compound profile, antioxidant capacity, microbiological stability, and sensory acceptability. *J. Food Sci. Technol.* 55, 52–61. doi: 10.1007/s13197-017-2769-3

Inada, K. O. P., Leite, I. B., Martins, A. B. N., Fialho, E., Tomas-Barberan, F. A., Perrone, D., et al. (2021). Jaboticaba berry: a comprehensive review on its polyphenol composition, health effects, metabolism, and the development of food products. *Food Res. Int.* 147, 39. doi: 10.1016/j.foodres.2021.110518

Inada, K. O. P., Oliveira, A. A., Revoredo, T. B., Martins, A. B. N., Lacerda, E. C. Q., Freire, A. S., et al. (2015). Screening of the chemical composition and occurring antioxidants in jabuticaba (*Myrciaria jaboticaba*) and jussara (*Euterpe edulis*) fruits and their fractions. *J. Funct. Foods* 17, 422–433. doi: 10.1016/j.jff.2015.06.002

Kurpad, A. V., Regan, M. M., Raj, T., and Gnanou, J. V. (2006). Branched-chain amino acid requirements in healthy adult human subjects. *J. Nutr.* 136, 256s–263s. doi: 10.1093/jn/136.1.256S

Lee, Y. M., Yoon, Y., Yoon, H., Park, H. M., Song, S., and Yeum, K. J. (2017). Dietary anthocyanins against obesity and inflammation. *Nutrients* 9, 1089. doi: 10.3390/nu9101089

Li, J., Wang, H. R., Lin, Z. B., Huang, J. X., and Li, X. D. (2020). Effects of storage and heat treatment on polyphenols content in mulberry wine. *Food Industry* 41, 30–34.

Lima, R., Silva, M. V. T., Gomes, B. A., Macedo, E., Santana, M. N., Amaral, A. C. F., et al. (2023). Chemical profile and hematoprotective activity of artisanal jabuticaba (*Plinia jabuticaba*) wine and derived extracts. *Fermentation-Basel* 9, 17. doi: 10.3390/fermentation9020157

Liu, M., Fu, X. T., Wang, L., Xu, J. C., and Gao, X. (2022). Fermentation optimization of kelp-apple compound juice beverage and the antioxidant activity of its fermentation system. *Sci. Technol. Food Industry* 43, 214–220. doi: 10.13386/j.issn1002-0306.2021060184

Liu, P., Kallio, H., Lü, D., Zhou, C., Ou, S., and Yang, B. (2010). Acids, sugars, and sugar alcohols in Chinese hawthorn (*Crataegus* spp.) fruits. *J. Agric. Food Chem.* 58, 1012–1019. doi: 10.1021/jf902773v

Liu, Z. M., Tang, Y. J., Wu, H. Z., and Zhang, Q. R. (2011). Sample treatment for determination of total sugar content in wine by phenol-sulfuric acid method. *China Brewing*, 227:158–161.

MacDonald, A., Singh, R. H., Rocha, J. C., and Van Spronsen, F. J. (2019). Optimising amino acid absorption: essential to improve nitrogen balance and metabolic control in phenylketonuria. *Nutr. Res. Rev.* 32, 70–78. doi: 10.1017/S0954422418000173

Massa, N. M. L., De Oliveira, S. P. A., Rodrigues, N. P. A., Menezes, F., Dos Santos Lima, M., Magnani, M., et al. (2022). *In vitro* colonic fermentation and potential prebiotic properties of pre-digested jabuticaba (*Myrciaria jaboticaba* (Vell.) berg) by-products. *Food Chem.* 388, 133003. doi: 10.1016/j.foodchem.2022.133003

Nag, R., and Cummins, E. (2022). Human health risk assessment of lead (Pb) through the environmental-food pathway. *Sci. Total Environ.* 810, 151168. doi: 10.1016/j.scitotenv.2021.151168

Nguyen, H. D., Oh, H., and Kim, M. S. (2022). Mixtures modeling identifies vitamin B1 and B3 intakes associated with depression. *J. Affect. Disord.* 301, 68–80. doi: 10.1016/j.jad.2021.12.133

Oliveira, L. C., Alencar, N. M. M., and Steel, C. J. (2018). Improvement of sensorial and technological characteristics of extruded breakfast cereals enriched with whole grain wheat flour and jabuticaba (*Myrciaria cauliflora*) peel. *LWT-Food Sci. Technol.* 90, 207–214. doi: 10.1016/j.lwt.2017.12.017

Pereira, L. D., Barbosa, J. M. C., Da Silva, A. J. R., Ferri, P. H., and Santos, S. C. (2017). Polyphenol and ellagitannin constituents of jabuticaba (*Myrciaria cauliflora*) and chemical variability at different stages of fruit development. *J. Agric. Food Chem.* 65, 1209–1219. doi: 10.1021/acs.jafc.6b02929

Pierezan, M. D., Dalla Nora, F. M., and Verruck, S. (2022). Correlation between as, cd, Hg, Pb and Sn concentration in human milk and breastfeeding mothers' food consumption: a systematic review and infants' health risk assessment. *Crit. Rev. Food Sci. Nutr.*, 1–14. doi: 10.1080/10408398.2022.2056869

Plagemann, I., Krings, U., Berger, R. G., and Marostica, M. R. (2012). Volatile constituents of jabuticaba (Myrciaria jaboticaba (Vell.) o. berg) fruits. *J. Essential Oil Res.* 24, 45–51. doi: 10.1080/10412905.2012.645651

Plaza, M., Batista, A. G., Cazarin, C. B. B., Sandahl, M., Turner, C., Ostman, E., et al. (2016). Characterization of antioxidant polyphenols from *Myrciaria jaboticaba* peel and their effects on glucose metabolism and antioxidant status: a pilot clinical study. *Food Chem.* 211, 185–197. doi: 10.1016/j.foodchem.2016.04.142

Pullar, J. M., Carr, A. C., and Vissers, M. C. M. (2017). The roles of vitamin c in skin health. *Nutrients* 9, 866. doi: 10.3390/nu9080866

Qiu, S. L., Lin, B. M., Zheng, K. B., Wu, M. H., and Hong, J. M. (2021). Volatile components in flowers, fruits and leaves of jaboticaba at different developmental stage. *J. Trop. Subtropical Bot.* 30, 423–433.

Qiu, S. L., Zhang, S. P., Lin, B. M., Hong, J. M., and Zheng, K. B. (2018). Researsh progressin gargaric processing. *Fujian Agric. Sci. Technol.* 49, 67–70. doi: 10.13651/j.cnki.fjnykj.2018.08.021

Ricci, A., Cirlini, M., Maoloni, A., Del Rio, D., Calani, L., Bernini, V., et al. (2019). Use of dairy and plant-derived lactobacilli as starters for cherry juice fermentation. *Nutrients* 11, 213. doi: 10.3390/nu11020213

Rodrigues, L., Donado-Pestana, C. M., Moura, M. H. C., Rossi, E. S. R., Pessoa É, V. M., and Genovese, M. I. (2021). Phenolic compounds from jaboticaba (*Plinia jaboticaba* (Vell.) berg) ameliorate intestinal inflammation and associated endotoxemia in obesity. *Food Res. Int.* 141, 110139. doi: 10.1016/j.foodres.2021.110139

Sarkar, T., Salauddin, M., Roy, A., Sharma, N., Sharma, A., Yadav, S., et al. (2022). Minor tropical fruits as a potential source of bioactive and functional foods. *Crit. Rev. Food Sci. Nutr.*, 1–45. doi: 10.1080/10408398.2022.2033953

Soares, E., Soares, A. C., Trindade, P. L., Monteiro, E. B., Martins, F. F., Forgie, A. J., et al. (2021). Jaboticaba (*Myrciaria jaboticaba*) powder consumption improves the metabolic profile and regulates gut microbiome composition in high-fat diet-fed mice. *BioMed. Pharmacother.* 144, 112314. doi: 10.1016/j.biopha.2021.112314

Tang, X. R., Kalviainen, N., and Tuorila, H. (2001). Sensory and hedonic characteristics of juice of sea buckthorn (*Hippophae rhamnoides* l.) origins and hybrids. *Lebensmittel-Wissenschaft Und-Technologie-Food Sci. Technol.* 34, 102–110. doi: 10.1006/fstl.2000.0751

Tao, Y., Sun, D. W., Górecki, A., Błaszczak, W., Lamparski, G., Amarowicz, R., et al. (2016). A preliminary study about the influence of high hydrostatic pressure processing in parallel with oak chip maceration on the physicochemical and sensory properties of a young red wine. *Food Chem.* 194, 545–554. doi: 10.1016/j.foodchem.2015.07.041

Tavasolinasab, S., Valizadehkaji, B., and Abbasifar, A. (2023). Post-harvest application of hot water and *aloe vera* gel improves the physico-chemical properties and shelf-life of table grapes. *Erwerbs-Obstbau* 13. doi: 10.1007/s10341-023-00895-8

Wang, Z., Feng, Y., Yang, N., Jiang, T., Xu, H., and Lei, H. (2022). Fermentation of kiwifruit juice from two cultivars by probiotic bacteria: bioactive phenolics, antioxidant activities and flavor volatiles. *Food Chem.* 373, 131455. doi: 10.1016/j.foodchem.2021.131455

Wang, W. H., Tyan, Y. C., Chen, Z. S., Lin, C. G., Yang, M. H., Yuan, S. S., et al. (2014). Evaluation of the antioxidant activity and antiproliferative effect of the jaboticaba (*Myrciaria cauliflora*) seed extracts in oral carcinoma cells. *BioMed. Res. Int.* 2014, 185946. doi: 10.1155/2014/185946

Wu, S. B., Dastmalchi, K., Long, C., and Kennelly, E. J. (2012). Metabolite profiling of jaboticaba (*Myrciaria cauliflora*) and other dark-colored fruit juices. *J. Agric. Food Chem.* 60, 7513–7525. doi: 10.1021/jf301888y

Wu, Y., Xu, L., Yin, Z., Feng, H., and Huang, L. (2018). Transcription factor VmSeb1 is required for the growth, development, and virulence in *Valsa mali*. *Microbial Pathogen.* 123, 132–138. doi: 10.1016/j.micpath.2018.06.043

Wu, Y. S., Zhang, W. W., Song, S. R., Xu, W. P., Zhang, C. X., Ma, C., et al. (2020). Evolution of volatile compounds during the development of Muscat grape 'Shine muscat' (Vitis labrusca x v. vinifera). *Food Chem.* 309, 11. doi: 10.1016/j.foodchem.2019.125778

Zeidan, R. S., Han, S. M., Leeuwenburgh, C., and Xiao, R. (2021). Iron homeostasis and organismal aging. *Ageing Res. Rev.* 72, 101510. doi: 10.1016/j.arr.2021.101510

Zhao, D. K., Shi, Y. N., Petroya, V., Yue, G. G. L., Negrin, A., Wu, S. B., et al. (2019). Jaboticabin and related polyphenols from jaboticaba (*Myrciaria cauliflora*) with anti-inflammatory activity for chronic obstructive pulmonary disease. *J. Agric. Food Chem.* 67, 1513–1520. doi: 10.1021/acs.jafc.8b05814

Zhu, Z. H. (2014). Prospect and pollution-free cultivation techniques for *Myrciaria cauliflora* berg in yongchun county. *Fujian Agric. Sci. Technol.* 45, 32–34. doi: 10.13651/j.cnki.fjnykj.2014.11.014

Zhu, R. Y. (2017). *Introduction cultivation and its specialized garden planning for myrciaria cauliflora berg* (Fuzhou: Fujian Agriculture & Forestry University). Master's thesis.

frontiers | Frontiers in Plant Science

TYPE Original Research
PUBLISHED 17 July 2023
DOI 10.3389/fpls.2023.1224073

OPEN ACCESS

EDITED BY
Eman. A. Mahmoud,
Damietta University, Egypt

REVIEWED BY
Andrey Stoyanov Marchev,
Bulgarian Academy of Sciences, Bulgaria
Sophia Letsiou,
University of West Attica, Greece

*CORRESPONDENCE
Jinyao Li
ljyxju@xju.edu.cn
Xinhui Wang
wangxh@xju.edu.cn

†These authors have contributed equally to this work

RECEIVED 17 May 2023
ACCEPTED 26 June 2023
PUBLISHED 17 July 2023

CITATION
Liu X, Aimaier A, Wang W, Dong Y, Han P, He J, Mu L, Wang X and Li J (2023) Quality variation and biosynthesis of anti-inflammatory compounds for *Capparis spinosa* based on the metabolome and transcriptome analysis.
Front. Plant Sci. 14:1224073.
doi: 10.3389/fpls.2023.1224073

Quality variation and biosynthesis of anti-inflammatory compounds for *Capparis spinosa* based on the metabolome and transcriptome analysis

Xiaoying Liu[1†], Alimu Aimaier[1†], Weilan Wang[1], Yuliang Dong[1], Peng Han[1], Jiang He[2], Lihong Mu[1], Xinhui Wang[3*†] and Jinyao Li[1*†]

[1]Xinjiang Key Laboratory of Biological Resources and Genetic Engineering, College of Life Science and Technology, Xinjiang University, Urumqi, China, [2]Key Laboratory of Uygur Medicine, Xinjiang Institute of Materia Medica, Urumqi, China, [3]College of Ecology and Environment, Xinjiang University, Urumqi, China

Introduction: *Capparis spinosa* L. fruits as edible and medicinal plant, has anti-inflammatory activities. The different morphological characteristics of *C. spinosa* fruits from Ili, Turpan, and Karamay may affect their anti-inflammatory components and functions.

Methods: The anti-inflammatory activity of *C. spinosa* fruit was assessed using an LPS-induced inflammatory cell model. Furthermore, the differences in anti-inflammatory compounds were analyzed by metabolome and RNA-seq. Additionally, the anti-inflammatory mechanism was elucidated using network pharmacology.

Results: In the study, we found that the 95% ethanol extracts (CSE) obtained from the three kinds of fruits showed remarkable anti-inflammatory effects both *in vivo* and *in vitro*. However, the CSE derived from Ili fruits significantly reduced CD86 levels on DCs. As a result of metabolomic analysis, the metabolic profiles of Ili fruits differed significantly from those of the other two habitats, which were consistent with transcriptome analysis. A total of 15 compounds exhibiting anti-inflammatory activity were subjected to screening, revealing a greater accumulation of flavonoids in the Turpan and Karamay districts. Notably, phenolic compounds were identified as the principal anti-inflammatory components in *C. spinosa*.

Conclusion: There were significant differences in the morphology, metabolites, transcriptional levels, and anti-inflammatory activity of *C. spinosa* from the three districts.

KEYWORDS

Capparis spinosa, quality variation, anti-inflammation, metabolome, RNA-seq

1 Highlights

1. The three origins of *Capparis spinosa* L. fruits have anti-inflammatory effects, but the anti-inflammatory effects of *Capparis spinosa* L. vary by origin.
2. Phenolic compounds are the main anti-inflammatory substances in *Capparis spinosa* L. fruits.
3. A gene that increases ferulic acid synthesis was identified.

2 Introduction

Capparis spinosa L. (English name: Caper; Chinese name: Cishangan) belongs to the Capparidaceae family, Capparis genus. This shrub is distributed throughout the Mediterranean basin and is particularly common in the northwest region of China (Cao et al., 2010). It is also known as caper, wild watermelon in China. *C. spinosa* is extremely drought-resistant and can be found in semi-desert and desert regions as well as in gobi, sandy and gravelly slopes at low elevations (Khatib et al., 2016). *C. spinosa* is mainly distributed in the Turpan, Junggar, Tarim basins, and Ili River valleys of Xinjiang, China (Editorial Committee of Flora of Xinjiang, 1995; Editorial Committee of Flora of China and Chinese Academy of Sciences, 1999).

C. spinosa fruits and flower buds are fermented and consumed as foods or condiments (Francesca et al., 2016). Fruits have also traditionally been used for pharmacological purposes, especially for treating inflammation and arthritis through external applications. Studies showed that capers also have antidiabetic (Jalali et al., 2016), anti-hyperlipidemic (Khavasi et al., 2017), antiallergic (Trombetta et al., 2005), anti-oxidation (Tlili et al., 2015), anti-tumor (Ji and Yu, 2015), hepatoprotective (Kalantari et al., 2018) and neuroprotective effects (Mohebali et al., 2016; Rahimi et al., 2020). *C. spinosa* contains many kinds of biochemical compounds, including flavonoids, alkaloids, terpenoids, polyphenols, lipids, essential oils, and glycosides (Zhang et al., 2018).

Intraspecific variation is obvious, so traditional classification methods are difficult to accurately identify the taxonomic position of polymorphic *C. spinosa* (Fici, 2001; El Zayat et al., 2020). A genetic study based on AFLP fingerprinting confirmed this phenomenon (Inocencio et al., 2005). Our observation showed that the capers from Ili were significantly different from those from Turpan in terms of morphology. Meanwhile, through our investigation, we found that more than 60% of the capers in Xinjiang came from Turpan. It has not been studied whether such morphological and habitat differences affect the anti-inflammatory components and activity of *C. spinosa*.

The variation of habitat and morphology of traditional Chinese medicine (TCM) sometimes affects the content of active substances. The dry root and rhizome of *Salvia miltiorrhiza* Bunge (Danshen) are a TCM. Tanshinones are important active compounds, and their accumulation in the pericardium affects root color. The contents of Tanshinone IIA and Tanshinone I in the orange roots of the mutant were significantly reduced. However, the key enzyme genes involved in biosynthesis did not differ at the transcriptional level between the two kinds of *S. miltiorrhiza* (Zhan et al., 2019). *Cistanche deserticola* is an edible and medicinal plant, with phenylethanoid glycosides (PhGs) as its major active compounds. However, the content of PhGs in samples from three ecotypes grown in saline-alkali land, grassland, and sandy land was significantly different. Compared with other ecotypes, the content of PhGs was higher in saline-alkali soils, which may be due to the up-regulation of PhGs biosynthesis genes (Sun et al., 2020). Sixty samples of *glycyrrhiza uralensis* from different districts in Gansu, China, were analyzed, and the results showed significant differences in active compounds (Bai et al., 2020).

In this study, we conducted a comparative analysis of the anti-inflammatory activity, metabolites, and transcriptome data of *C. spinosa* fruits from different habitats. We identified the habitats with the strongest anti-inflammatory activity and screened the major anti-inflammatory components in *C. spinosa* fruits. Through gene-metabolic network analysis, we identified several key metabolic pathways and genes that influence the synthesis of anti-inflammatory compounds. These findings provided new insights into the further development, cultivation, and genetic modification of *C. spinosa*.

3 Results

3.1 Fruit morphology and sampling location information

C. spinosa fruits (6/habitat) were collected from three districts, including Turpan, Karamay, and Ili in Xinjiang Uygur Autonomous Region of China, which were named as groups A, B, and C. The fruits were identified by Dr. Jiang He from the Xinjiang Institute of Materia Medica. The fruits from Turpan were green and medium in size (Figure 1A), the fruits from Karamay were the smallest and

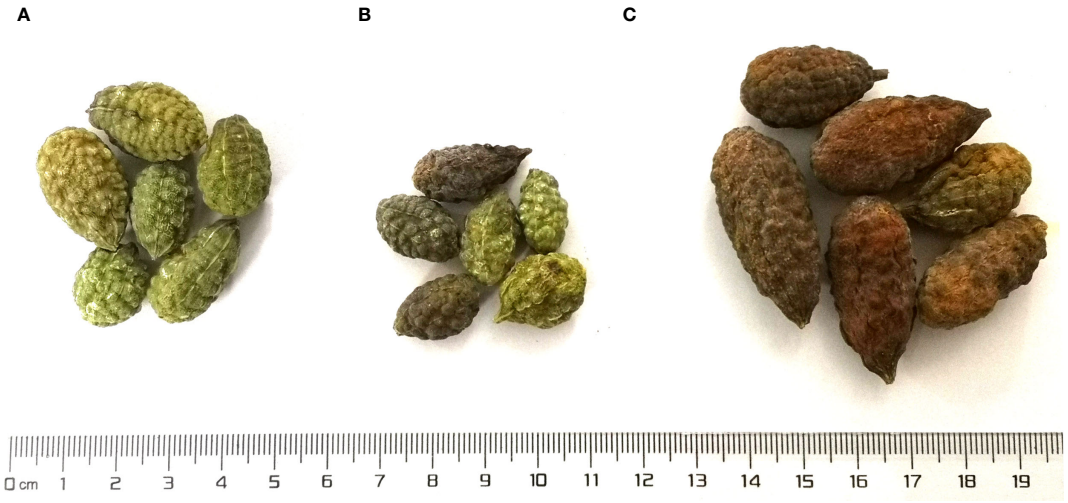

FIGURE 1
The fruits from three districts. **(A)** Turpan; **(B)** Karamay; **(C)** Ili.

bottle-green or brown (Figure 1B), and the fruits from Ili were the largest and brown (Figure 1C). The GPS coordinates and climate information of the habitats can be found in Table 1. Turpan had the least precipitation, the most arid climate, and the highest annual average temperature, while Ili had the most humid climate and the lowest annual average temperature, and Karamay had the middle climate index. The contents of N, P, and K in Ili soil were the highest.

3.2 Validation of anti-inflammatory function

C. spinosa fruits were extracted with 95% ethanol, then the extract was concentrated and lyophilized, named CSE. The yield of the extract was about 24%. CSEs prepared with *C. spinosa* fruits from Turpan, Karamay, and Ili were named CSEA, CSEB, and CSEC, respectively. To detect the anti-inflammatory effects of CSE *in vitro*, different concentrations (0.5, 1.0 and, 1.5 mg/mL) of CSEs were used to treat DCs in the presence of LPS. Results of flow cytometry showed that there was no significant change in cell proportion among all groups, suggesting that the selected doses of CSEs did not affect the viability of DCs (Figure 2A). Compared with the LPS group, CSEs did not inhibit the expression of surface molecule CD40 induced by LPS, whereas CSEC (1.5 mg/mL) significantly suppressed the expression of CD86 induced by LPS (Figure 2B). Three pro-inflammatory cytokines, including TNF-α, IL-6, and IL-12p40, were significantly decreased (Figure 2C).

In vivo, CSE treatment significantly suppressed the expression of pro-inflammatory cytokines TNF-α and IL-6 and relieved the degree of ear edema in the TPA-induced mouse ear edema model (Figure 2D).

TABLE 1 The GPS coordinates and climate information of the habitats.

Factors	Turpan	Karamay	Ili
Sample number	A(A1-A6)	B(B1-B6)	C(C1-C6)
Longitude (degree) Latitude (degree)	89.54 42.83	84.92 45.53	82.15 43.62
Altitude (m)	-61.7031	278.189	823.518
Annual average precipitation (mm)	16.4	108.9	350.2-510
Annual average evaporation (mm)	3000	2692.1	2331
Annual average temperature (°C)	13.9	8.6	5.6
Total nitrogen	0.663	0.08	1.613
Alkeline-N	61	83	126
Olsen-P	31.9	22.89	18.9
Olsen-K	171	199	332
Soil type	Saline anthropogenic alluvial soil	Gypsum ash desert soil	Gypsum gray brown desert soil

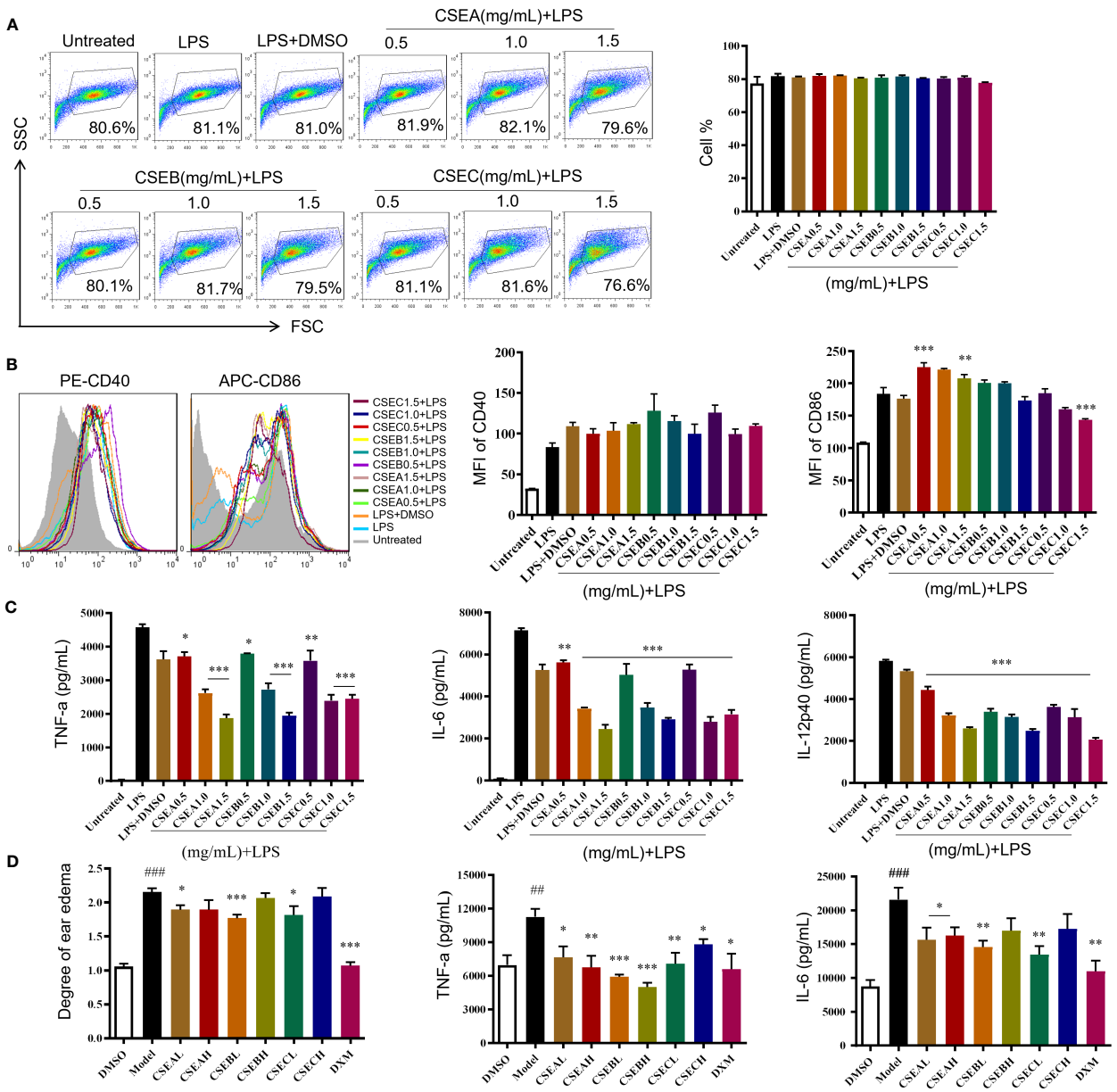

FIGURE 2
The anti-inflammatory activity of capers from different districts *in vitro* and *in vivo*. **(A–C)** The maturation and the secretion of cytokines of DCs upon CSEs treatment. **(A)** The cell proportion. **(B)** The expression of surface molecular. **(C)** The cytokine production. Data are means ± SE (n = 3). **(D)** Therapeutic effect of CSEs on mouse edema model. Data are means ± SE (n = 5). ##*P* < 0.01, ###*P* < 0.001 compared to DMSO; **P* < 0.05, ***P* < 0.01, ****P* < 0.001 compared to LPS/Model.

These results showed that *C. spinosa* from all three different districts had anti-inflammatory effects, but the effect of fruits from Ili was better than the other two groups in inhibiting DC maturation.

3.3 Qualitative and quantitative metabolites

Base peak ion chromatograms of the three groups were shown as fingerprints. There were significant differences among the samples of Ili and the other two districts (Figure 3A). A total of 82 compounds were identified, of which 47 were in positive ion mode (Tables S1, S3) and 43 were in negative ion mode (Tables S2, S4). Eight compounds were found in both modes. Principal component analysis (PCA) was performed on the 18 samples (6/habitat) (Figure 3B) or together with quality control (QC) (Figure S1). All samples were within Hotelling's T-squared ellipse, indicating that the detection system had good stability. In positive ion mode, PC1, PC2, and PC3 were 66.95%, 19.14%, and 8.98%, respectively, while in negative ion mode, PC1, PC2, and PC3 were 87.59%, 7.16% and, 1.29%, respectively (Figure 3B). The model of orthogonal partial least squares discriminant analysis (OPLS-DA)

10.3389/fpls.2023.1224073

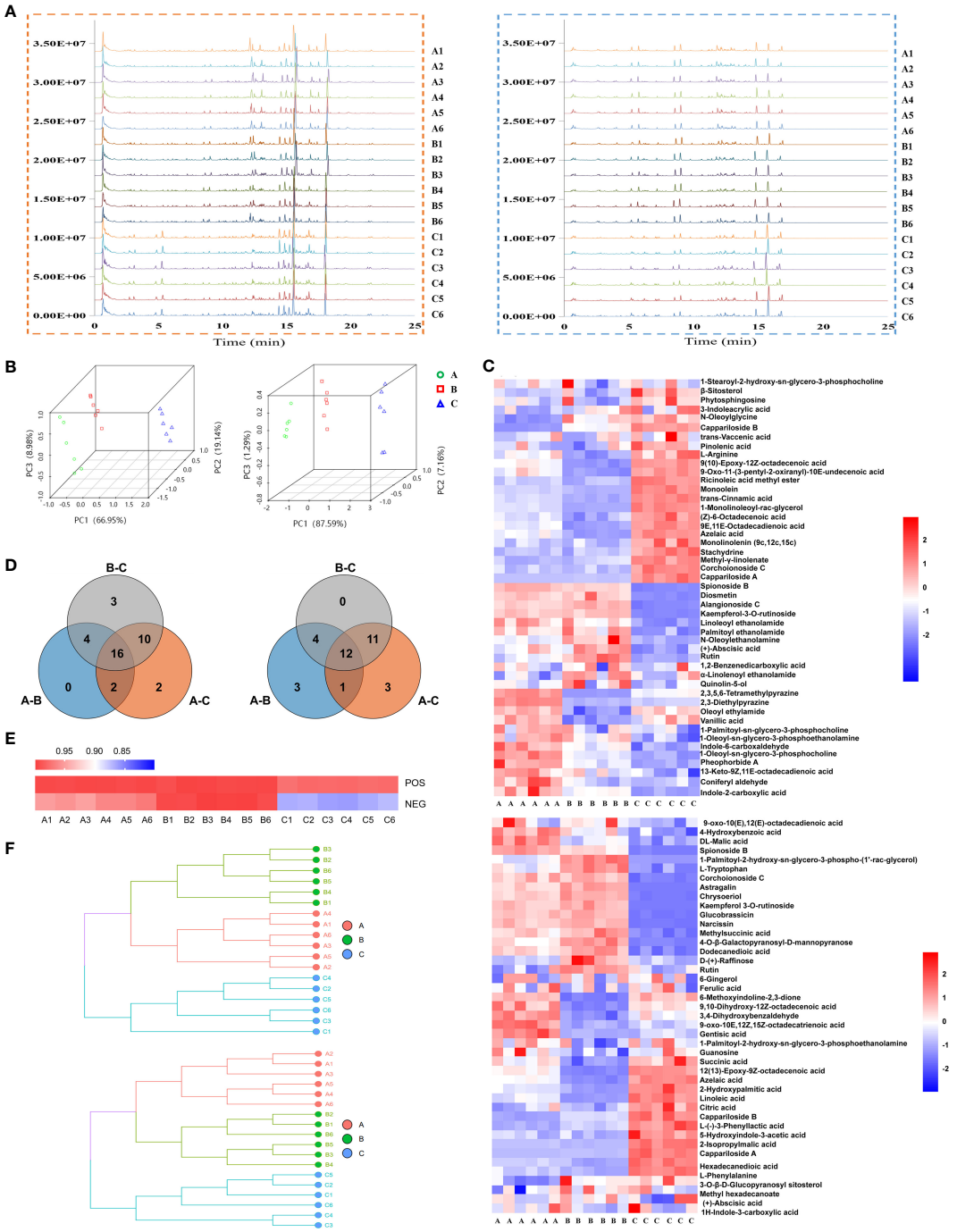

FIGURE 3
Metabolite's analysis of *C. spinosa* fruit by ultra-high-performance liquid tandem chromatography quadrupole time of flight mass spectrometry (UHPLC-QTOFMS). **(A)** Chromatographic fingerprint. **(B)** PCA score map. **(C)** HCA of all metabolites. **(D)** Venn map showing the common and differential metabolites. **(E)** Heat map showing the cosine similarity of metabolites. **(F)** Cluster dendrogram showing the cosine similarity of metabolites. In all panels, the positive ion mode was on the left/up and the negative ion mode was on the right/down.

was stable and reliable (Figure S2). The score plots of PCA and OPLS-DA exhibited an obvious separation among the samples.

The identified compounds were analyzed by hierarchical clustering analysis. The heatmap of hierarchical cluster analysis (HCA) showed that group C was separated from the other two groups (Figure 3C). Differential metabolites were screened by the Venn analysis in positive and negative modes, respectively (Figure 3D; Table S5).

Cosine similarity analysis showed a significant difference among the three groups in negative ion mode, and the similarity value in group C was 86% (Figure 3E). The clustering tree revealed that the

distance between groups A and B was close, but group C was far from the other two groups (Figure 3F).

Stachydrine, ferulic acid, and chrysoeriol were selected to be quantified, and their contents in groups A, B, and C were consistent with the metabolomics (Figure S3). These results suggested that the metabolic level of group C was considerably different from that of the other two groups. The metabolomics data were deposited in the OMIX repository, accession number OMIX004470 (https://ngdc.cncb.ac.cn/omix/preview/QoEYJ1oa).

3.4 Screening and analyzing of anti-inflammatory compounds

By retrieving the database, 15 anti-inflammatory compounds were selected. They included one alkaloid, four lipids, three flavones, four phenols, one glycoside, and two other compounds (Figure 4A).

Considering the quantitative value (Figure 4B) and log2 (fold change) value of the compound (Figure 4C), the contents of almost compounds were similar between groups A and C except for oleoyl

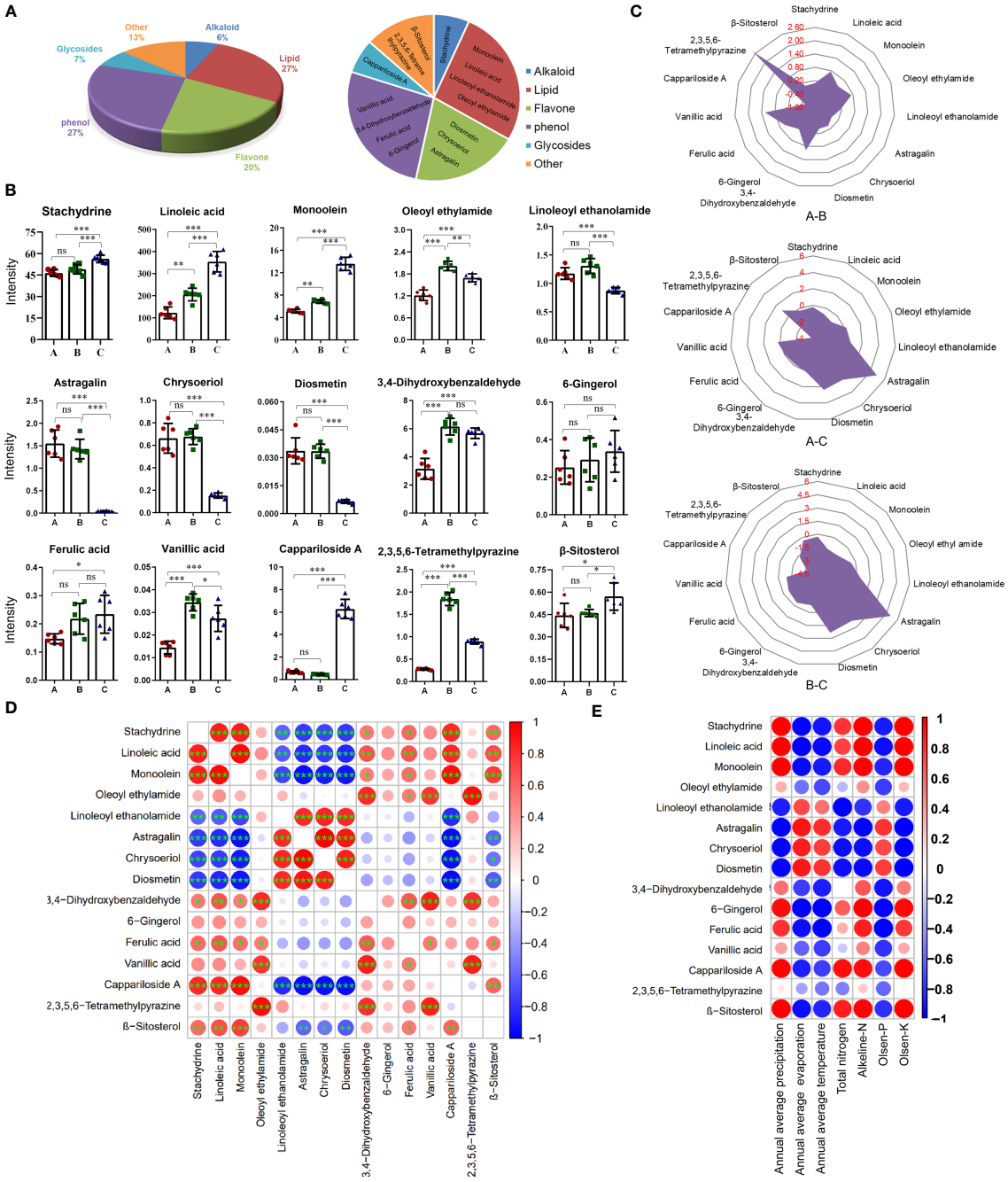

FIGURE 4
Content differences of 15 anti-inflammatory compounds from the three different districts. **(A)** The pie chart shows the classification of anti-inflammatory compounds. **(B)** Histogram of contents. Data are means ± SE (n = 6). ns: no significance, *$P < 0.05$, **$P < 0.01$, ***$P < 0.001$. **(C)** Radar chart showing the log2 (fold change) of anti-inflammatory compounds. **(D)** Bubble chart of correlation analysis for anti-inflammatory compounds. (n = 6). *$P < 0.05$, **$P < 0.01$, ***$P < 0.001$. **(E)** Bubble chart of correlation analysis between anti-inflammatory compounds and environmental factors. Data are average.

ethyl amid, 3,4-dihydroxybenzaldehyde, 2,3,5,6-tetramethylpyraz and vanillic acid, but the contents of almost compounds in group A and B were different with that in group C except for 6-gingerol and ferulic acid. The contents of three flavonoids including diosmetin, chrysoeriol, and astragalin in groups A and B were significantly higher than that in group C. The contents of linoleic acid, monoolein, and cappariloside A in group C were significantly higher than that in groups A and B, whereas the content of 2,3,5,6-tetramethylpyrazine in group B was highest. The contents of stachydrine, 6-gingerol, ferulic acid, and β-sitosterol in the three different districts showed no significant difference in the three groups.

The correlation analysis of the quantitative values of metabolites showed that three flavones had a significantly negative correlation with stachydrine, linoleic acid, monoolein, cappariloside A, and β-sitosterol. There was a significantly positive correlation between the three flavones and linoleoyl ethanolamide. Linoleoyl ethanolamide was negatively correlated with stachydrine, linoleic acid, monoolein, and cappariloside A. Stachydrine had a significantly high positive correlation with linoleic acid, monoolein, and cappariloside A. Stachydrine was significantly correlated with 3,4-dihydroxybenzaldehyde, ferulic acid and β-sitosterol. Among the four phenol compounds, ferulic acid, vanillic acid and, 3,4-dihydroxybenzaldehyde had a significant correlation, but the correlation among 6-gingerol and other compounds was weak. The contents of compounds in similar synthetic pathways existed a positive correlation (Figure 4D).

The contents of most anti-inflammatory compounds were strongly correlated with environmental factors. High evaporation, high temperature, and high Olsen-P contributed to the accumulation of the three flavones compounds. The trend of linoleoyl ethanolamide was similar to that of flavones. The trends of stachydrine, linoleic acid, monoolein, 6-gingerol, ferulic acid, cappariloside A, and β-sitosterol were opposite to that of flavone. On the other hand, 2,3,5,6-tetramethylpyrazine had a weak correlation with environmental factors (Figure 4E).

There was no difference in abscisic acid and tryptophan contents among the three groups, indicating that all the materials were in the same period of fruit development (Figure S4). Compounds with consistent response trends to environmental factors also had a strong positive correlation in their content, indicating that the quality variation of *C. spinosa* was caused mainly by environmental factors.

3.5 Prediction of anti-inflammatory mechanisms by network pharmacology

To explore the anti-inflammatory mechanism of *C. spinosa* fruit, the above 15 anti-inflammatory compounds were used for network pharmacological analysis. 564 targets of compounds were collected, and 1,196 human targets of rheumatoid arthritis (RA) were obtained. Thus, after intersection analysis, 167 common targets were acquired (Figure S5). The common targets were imputed into STRING to build the protein-protein interaction (PPI) network. Subsequently, the interaction network was constructed for illustrating the interactive relationship between compounds and targets (Figure 5A). Based on degree value, the top 20 were the core targets including MAPK1, STAT3, IL-6, TNF, VEGFA (vascular endothelial growth factor A), SRC, MMP9, and JUN (Figure 5B).

In addition, the common targets were subjected to GO and KEGG enrichment analysis, and the terms associated with RA of GO mainly focused on the regulation of interleukin-6 production, regulation of tumor necrosis factor production, regulation of interleukin-12 production, dendrite, immune receptor activity, cytokine activity, etc. (Figure 5C). KEGG pathways mainly focused on the TNF signaling pathway, NF-kappa B signaling pathway, Cytokine-cytokine receptor interaction, etc. (Figure 5D).

These results suggested that *C. spinosa* plays an anti-inflammatory role by affecting cytokine expression and lymphocyte differentiation.

3.6 Screening of anti-inflammatory compounds *in vitro*

To identify key active compounds in CSE that inhibit the maturation of LPS-induced DC, we examined the effect of stachydrine (ST), diosmetin (DIO), and 3,4-dihydroxybenzaldehyde (DHB) to treat DCs in the presence of LPS. Sachydrine and diosmetin did not inhibit the expression of costimulatory molecules (CD40 and CD86) and the secretion of pro-inflammatory cytokines IL-6 and TNF-α (Figures 6A, B). 3,4-dihydroxybenzaldehyde significantly suppressed the expression of CD40 and IL-6 induced by LPS at the concentration of 1 mM, and it significantly suppressed the expression of CD86 and TNF-α at the concentration of 0.5 mM (Figure 6C). The results showed that phenols were the main compounds that inhibited DCs maturation and secretion of pro-inflammatory cytokines in capers.

3.7 Identifying key genes in phenols biosynthetic pathway

Transcriptome data of *C. spinosa* fruits were analyzed. PCA showed PC1, PC2, and PC3 were 49.31%, 17.50%, and 9.04%, respectively, and all samples were within the Hotelling's T-squared ellipse. Group C was significantly separated from the other two groups (Figure S6A). Volcano Analysis showed that 2,432 genes were up-regulated, and 1,705 genes were down-regulated in group A and group B, 9,104 genes were up-regulated, and 4,209 genes were down-regulated in group A and group C, 4,872 genes were up-regulated, and 2.320 genes were down-regulated in group B and group C (Figure S6B). HCA and Venn's analysis showed that group C was significantly different from the other two groups (Figures S6C, D). The enrichment differential pathways were concentrated in biosynthesis and metabolism pathways between groups A and C (Figure S7). These data indicated that group C was significantly different from the other two groups at the transcriptional level. These transcript data were deposited into the NCBI database with identifier number PRJNA778809 (https://www.ncbi.nlm.nih.gov/sra/PRJNA778809).

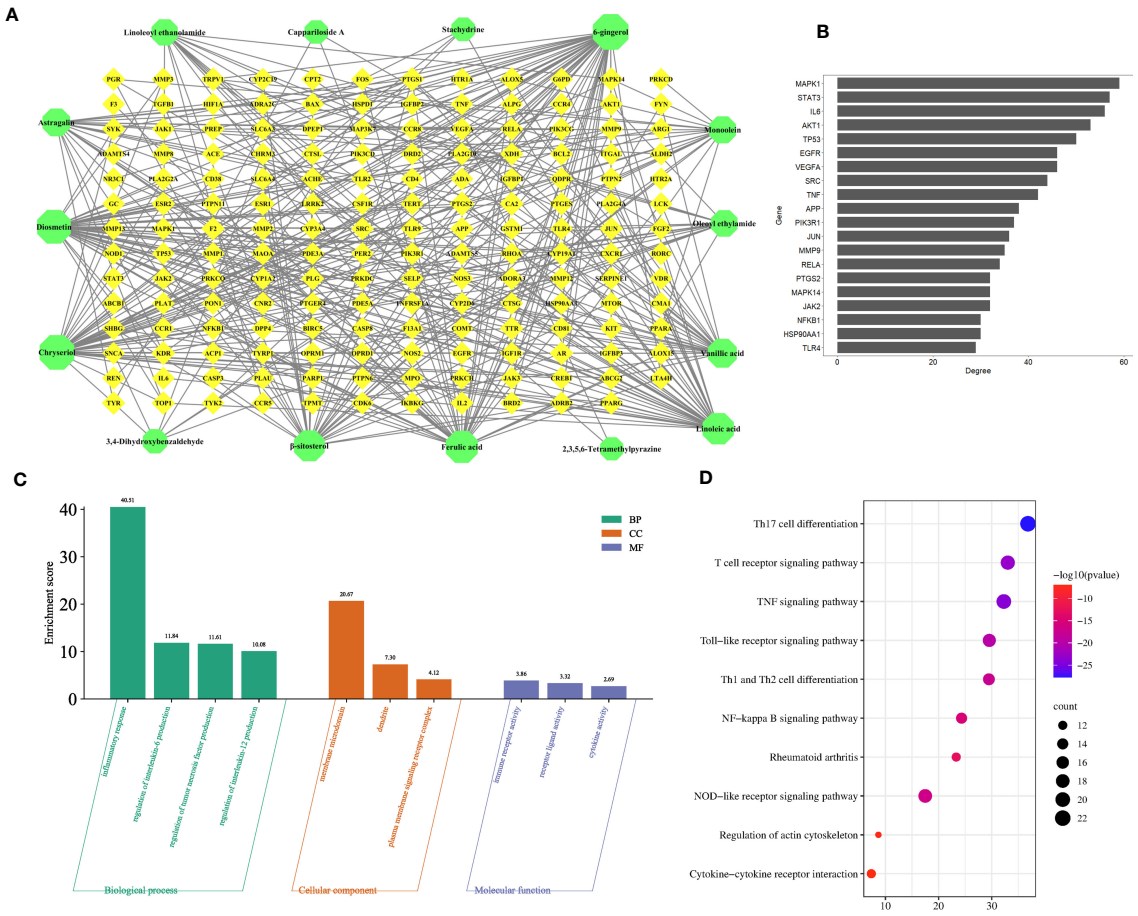

FIGURE 5
Prediction of the anti-inflammatory mechanism *via* the network pharmacological. **(A)** The compound-target network. **(B)** Core targets. **(C)** GO enrichment analysis. **(D)** KEGG enrichment analysis.

The biosynthetic pathway was constructed based on three KEGG pathways: 'Phenylpropanoid biosynthesis (Ko00940)', 'Stilbenoid, diarylheptanoid and gingerol biosynthesis (Ko00945)', 'Biosynthesis of alkaloids derived from shikimate pathway (Ko01063)' (Figure 7A).

The genes encoding PAL (Cluster-19971.0), CYP73A (Cluster-22225.2180), COMT (Cluster-22225.2209, Cluster-23341.0, Cluster-30723.0), 4CL (Cluster-22225.12442, Cluster- 22225.4017), CCR (Cluster-22225.2355) were down-regulated in group C, but the genes encoding CYP73A (Cluster-22225.4290) and REF1 (Cluster-22225.2080, Cluster-22225.7764) were up-regulated in group C (Figure 7B). The qRT–PCR results showed good consistency with the RNA-Seq data. The qRT–PCR results indicated that the expression of CYP73A (Cluster-22225.2180) in groups A and B was significantly higher than that in group C, while the expression of CYP73A (Cluster-22225.4290) in group C was significantly higher than that in the other two groups. REF1 (Cluster-22225.7764) was highly expressed in all three groups (Figure S8).

The expression level of REF1 (Cluster-22225.7764) indicated a strong positive correlation with ferulic acid content (r = 0.7667, P = 0.0214), which might be the key gene promoting ferulic acid biosynthesis in *C. spinosa* (Figure 7C). These results indicated that *C. spinosa* fruits from different districts affected the biosynthesis of secondary metabolites by regulating gene transcription.

4 Material and methods

4.1 Materials and regents

The fruits of *C. spinosa* were collected from June to July 2019 from Turpan, Karamay, and Ili in Xinjiang Uygur Autonomous Region of China. The fruits were immediately frozen in liquid nitrogen and then stored at -80°C. The identification was carried out by Dr. Jiang He of Xinjiang Institute of Materia Medica.

BALB/c mice (20 ± 5 g) aged six weeks old were obtained from the experimental animal center of the Xinjiang Medical University (Urumqi, China). Mice were allowed free access to distilled water and standard food, mice room under conditions of maintained temperature (24~26°C) and humidity (69~71%) as well as a 12:12 h light-dark cycle. All experimental animal protocols were reviewed and approved by the Ethics Committee of Xinjiang University for the use of Laboratory Animals.

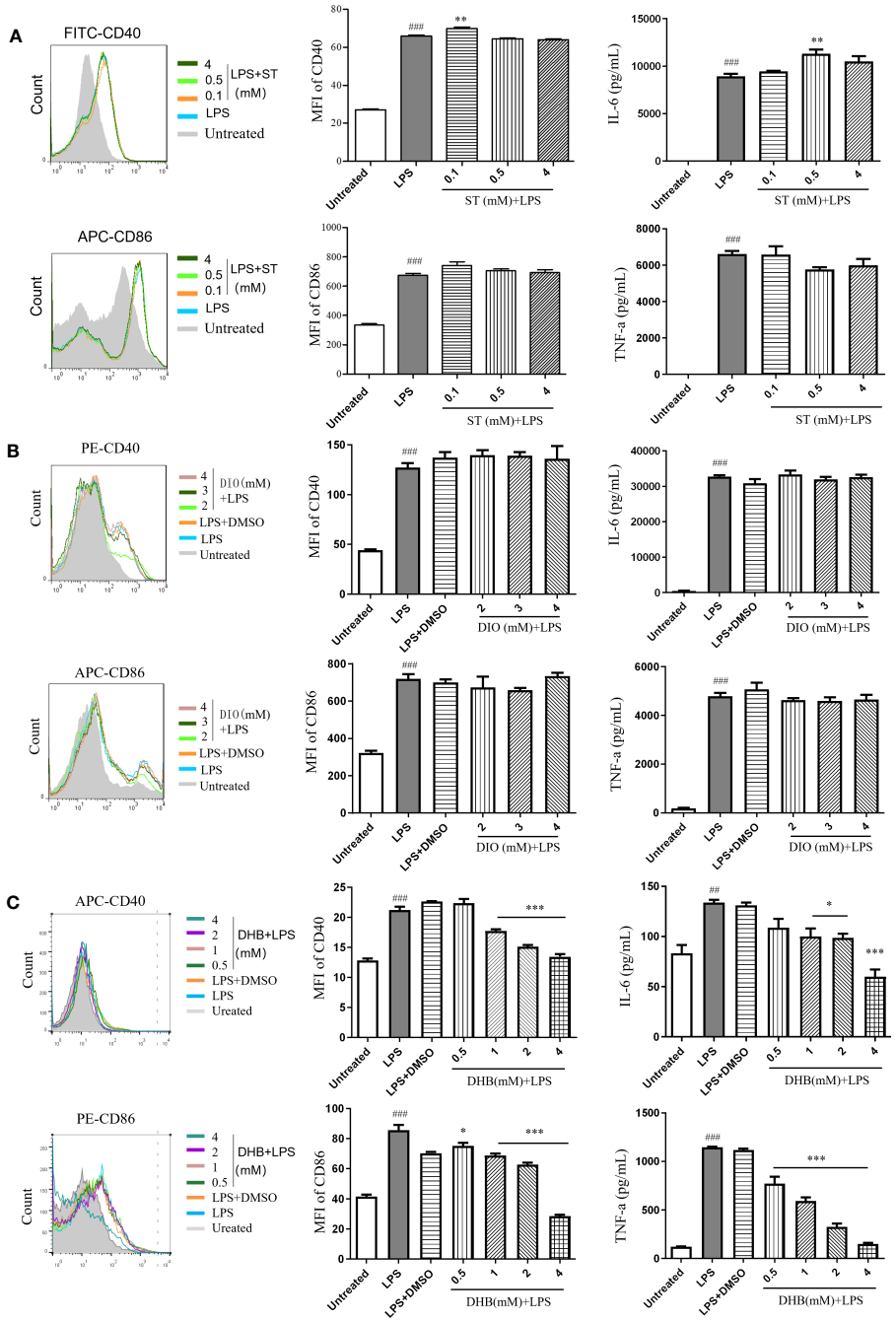

FIGURE 6
Anti-inflammatory effects of three compounds *in vitro*. **(A)** Stachydrine (ST). **(B)** Diosmetin (DIO). **(C)** 3,4-Dihydroxybenzaldehyde (DHB). Data are means ± SE (n = 3). $^{\#\#}P < 0.01$, $^{\#\#\#}P < 0.001$ compared to Untreated; $^{*}P < 0.05$, $^{**}P < 0.01$, $^{***}P < 0.001$ compared to LPS.

4.2 Preparation of *C. spinosa* fruits ethanol extracts

First, the dried fruits of *C. spinosa* were ground into a powder and passed through a 40-mesh sieve. Then, 50 g of the powder was mixed with 95% ethanol in a ratio of 1:6 (w/v). The mixture was ultra-sonicated for 20 minutes, followed by extraction for 2 hours in a water bath at 60° C. This extraction process was repeated three times, and the extracts were mixed. The extract was concentrated using rotary evaporation. Then, the extract was subjected to lyophilization and named 'CSE'.

4.3 Detection of anti-inflammatory effect *in vitro*

Immature DCs were induced from bone marrow cells of BALB/c mice by Granulocyte-macrophage colony-stimulating factor (GM-CSF, Peprotech, USA) (Aipire et al., 2017). The cells were cultured in RPMI-1640 medium containing 10% heat-inactivated fetal bovine serum (FBS), 100 units/ml penicillin-streptomycin, 50μM β-mercaptoethanol and 20 ng/ml GM-CSF. Subsequently, they were placed in a 5% CO_2, 37°C incubator. The cells were collected on the

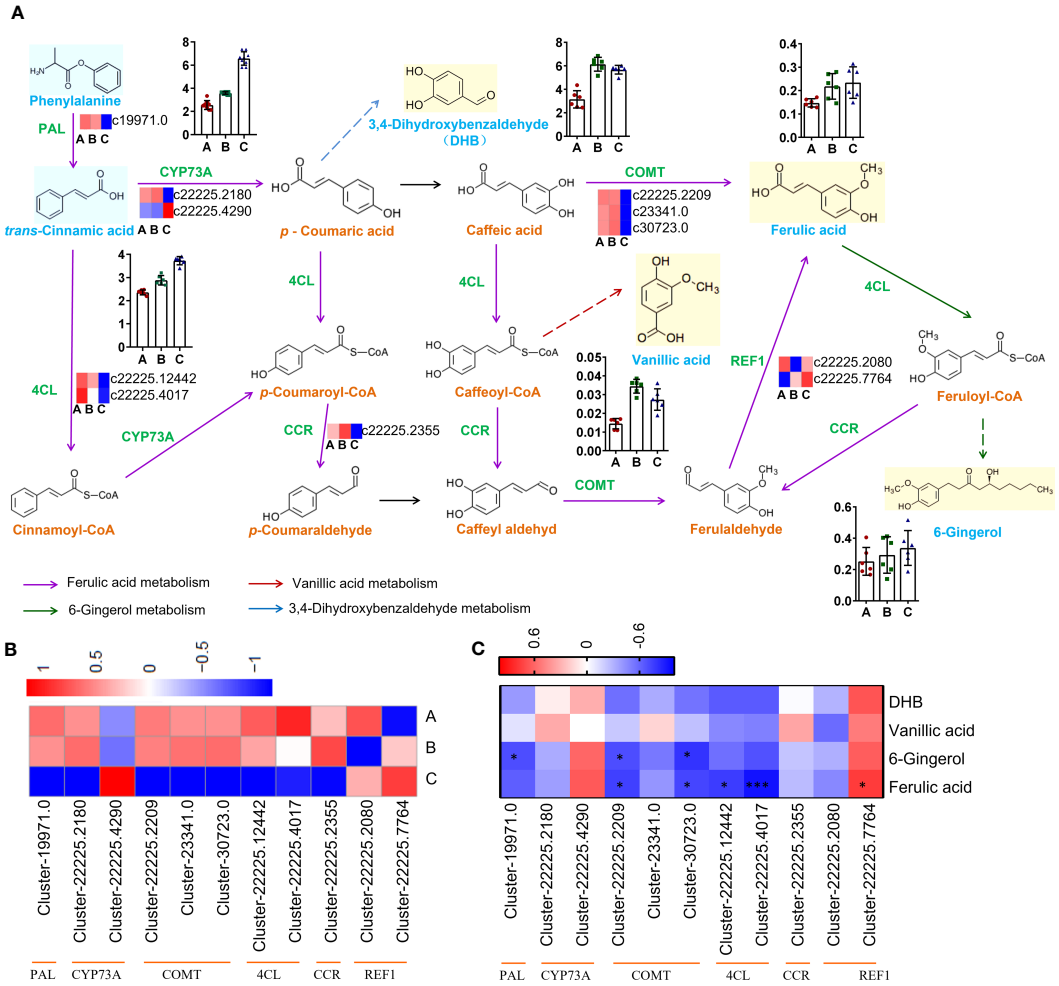

FIGURE 7
Pathways and genes involved in the biosynthesis of phenols. **(A)** Changes in gene expression and compound accumulation in the synthetic pathway. **(B)** Heatmap showing the expression profiles of genes related to phenols from three districts. **(C)** Heat map showing correlation analysis of compound content and gene expression level. *$P < 0.05$, ***$P < 0.001$.

seventh day, cultured at a concentration of 1×10^6/mL on a 24-well plate, and treated with different concentrations of CSEs or standards in the presence of 80 ng/mL LPS for 12h. The cells were collected and stained using the mAbs, including anti-mouse CD40, and anti-mouse APC-CD86. All samples were detected on FACSCalibur (BD Biosciences, USA), and the data were analyzed by the FlowJo software (v7.6). The cell supernatant was collected, and the cytokines (TNF-α, IL-6, and IL-12p40) were measured by ELISA kit. OD_{450} was measured using a microplate reader (Bio-Rad, USA).

4.4 Treatment of TPA-induced mouse ear edema model

TPA was used to induce the ear edema model in mice. The 45 mice were randomly divided into a control group (DMSO), model group (TPA, 75 μg/kg), positive control group (dexamethasone, DXM, 2.5 mg/kg), low-dose group (200 mg/kg) and high-dose group (500 mg/kg), with five mice in each group. The medicine was applied to the right ear for 6 h, ear edema degree of mice was calculated by right ear mass (mg)/left ear mass (mg), and the cytokines (TNF-α and IL-6) were measured by ELISA kit.

4.5 Metabolites extraction and LC-MS/MS analysis

A 100 mg sample was extracted with 500 μL of 80% methanol. 2-Chloro-L-phenylalanine (1000:10) was used as the internal standard. After 30 s vortex, the samples were homogenized at 45 Hz for 4 min. Then the extracts were ultra-sonicated for 1 hour in the ice bath. The extracts were left at -20°C for 1 h and centrifuged at 12000 rpm for 15 min at 4°C. The supernatant was aspirated and filtered through a 0.22 μm filter membrane and set aside.

LC-MS/MS analysis was detected on an AB SCIEX Triple TOF 5600 mass spectrometer coupled with a Shimadzu Nexera UPLC LC-30A system with a Waters UPLC BEH C18 (1.7 μm × 2.1 × 100 mm) column. The flow rate was 0.4 mL/min, and the sample injection volume was 3 μL. The mobile phases were 0.1% formic acid aqueous solution (A) and 0.1% formic acid acetonitrile solution (B). The elution gradients were: 0-3.5 min, 95-85% A; 3.5-6 min, 85-70% A; 6-6.5, 70-70% A; 6.5-12 min, 70-30% A; 12-12.5 min, 30-30% A; 12.5-18 min, 30-0% A; 18-22 min, 0% A. Data were collected using Analyst TF 1.7 software to view and process.

4.6 Differential metabolite analysis

The raw data were imported into Progenesis QI software for retention time correction, peak identification, peak extraction, peak integration, and peak alignment, and the corresponding TCM metabolic database was established. Substance identification of the unknown components was performed using the self-built mass spectrometry database. Multivariate statistical analysis, including PCA, and OPLS-DA, was performed using SIMCA software (V15.0.2, Sartorius Stedim Data Analytics AB, Umea, Sweden). Also, R software or GraphPad Prism software (V8.0, La Jolla, CA, USA) was used HCA, Venn analysis, cosine similarity analysis, radar plot, clustering tree, pie chart, histogram, and Pearson correlation analysis were performed in combination with univariate analysis for metabolite accumulation patterns between different samples.

4.7 Validation of metabolomic data by UHPLC-QTOF-MS

Metabolites were extracted according to 2.2. Stachydrine, ferulic acid, and chrysinol (HPLC ≥ 98%, Yuanye, China) were dissolved in with methanolic solution, respectively. The prepared extracts were each taken 400 μL, mixed to prepare mixed standard solutions and a series of mixed standard solutions of different concentrations were prepared by stepwise dilution with methanol. The mass spectrometer apparatus and elution conditions were the same as in 3.4.

4.8 Analysis of network pharmacology

The compounds with anti-inflammatory functions were screened from metabolites for network pharmacological analysis. The chemical targets were screened by TCMSP databases (http://lsp.nwu.edu.cn/tcmsp.php), Swiss Target Prediction Database (http://www.swisstargetprediction.ch/), SEA databases (https://sea.bkslab.org/). The disease targets were screened by GeneCards (https://www.genecards.org), and OMIM databases (https://www.omim.org/). Furthermore, the keyword 'rheumatoid arthritis' was used to retrieve all targets under the condition of 'Homo sapiens'. Venny software (v2.1.0) was used to intersect anti-inflammatory component targets and disease targets, which were named 'the common targets'. Then, the common targets of RA and active ingredients were used to construct the PPI network by the STRING database (https://string-db.org/cgi/input.pl). The results were visualized using Cytoscape software (v3.6.1). The top 20 targets with degree value in the PPI network were named 'core targets'. The R Project was used to visualize core targets. GO enrichment analysis of common targets was performed by Metascape (http://metascape.org).

4.9 Extraction RNA and analysis of transcriptomics

Total RNA was extracted using TRIzol reagent, and genomic DNA was removed using DNase I (Takara) according to the manufacturer's instructions. RNA quality and quantification were measured using a 2100 Bioanalyser (Agilent) and an ND-2000 (Nano-Drop Technologies) RNA-seq transcriptome libraries were then prepared from total RNA (1 μg) using the TruSeqTM RNA Sample Preparation Kit (Illumina, San Diego, CA, USA). The expression levels of each transcript were calculated according to the mapping reads per million exon kilobase fragment method to identify these DEGs in different samples. EdgeR (Empirical Analysis of Digital Gene Expression in R) was used for differential expression analysis and NR (NCBI non-redundant protein sequences) was used to annotate the assembled unigenes. In addition, Gene Ontology (GO) and Kyoto Encyclopedia of Genes and Genomes (KEGG) functional enrichment analyses were performed for these DEGs using Goatools (https://github.com/tanghaibao/Goatools) and KOBAS (http://kobas.cbi.pku.edu.cn/home.do), respectively.

4.10 Correlation analysis mining anti-inflammatory compounds and genes

Based on the KEGG pathway analysis (https://www.kegg.jp/kegg/pathway.html), genes related to the synthesis of anti-inflammatory compounds were screened. The key genes were identified by Spearman correlation analysis using the GraphPad Prism 8 software.

4.11 Validation of RNA–seq data by qRT–PCR

Total RNA was reverse transcribed using the reverse transcription kit. Then, qPCR amplification was performed on the qTOWER3G qPCR instrument. The primer sequences are shown in Table S1.

4.12 Statistical analysis

Statistical significance analysis was performed using one-way ANOVA or t-test and computed using GraphPad Prism software. A value of $P < 0.05$ was statistically significant.

5 Discussion

In this study, we compared the fruit quality differences of capers from different districts in Xinjiang through metabolome and transcriptome analysis and detected their anti-inflammatory activity *in vitro* and *in vivo*. The fruits from Ili were significantly different from Turpan and Karamay in metabolism and transcription levels. In addition, fruits from all three different districts inhibited the expression of pro-inflammatory cytokines, but ethanol extract of caper from Ili significantly inhibited the expression of CD86 on DCs induced by LPS. There were significant differences in the different districts, morphology, metabolites, gene expression level, and anti-inflammatory activity of capers from the three districts.

C. spinosa fruit extract rich in flavonoids, indoles, and phenolic acids, effectively inhibited carrageenan-induced paw edema in mice (Zhou et al., 2010). *C. spinosa* fruit ethanol extracts significantly inhibited the secretions of IL-12p40, IL-6, IL-1β, and TNF-α in LPS-induced DC (Azeguli et al., 2017). *C. spinosa* leaf alcoholic extract significantly decreased immune cell infiltration, vasodilatation, and dermis thickness in the inflammatory site by inhibiting cytokine gene expression, including IFN-γ, IL-17, and IL-4 in the contact hypersensitivity mice. The extract contained saponins, flavonoids, and alkaloids (Azhary et al., 2017). 70% alcohol extract of *C. spinosa* aerial parts significantly reduced the levels of TNF-α, COX-2, IL-1β, and IL-6 in the LPS-induced inflammation in microglia (Rahimi et al., 2020). Pro-inflammatory cytokines IL-6, TNF-α, and IL-1 played an important pathogenic role in inflammatory processes such as RA (Kaneshiro et al., 2019). The results of this study also confirmed that *C. spinosa* extract could treat inflammation by inhibiting the expression of pro-inflammatory cytokines both *in vitro* and *in vivo*. Thus, fruits from all three districts can be used in the treatment of inflammatory diseases.

At present, most studies on the anti-inflammatory effects and mechanisms of *C. spinosa* fruit are based on experimental animal models. However, it remains uncertain whether comparable positive effects can be achieved in the treatment of human diseases. We will further verify the anti-inflammatory effect of *C. spinosa* fruit on human cells. These results will lay the foundation for clinical trials of the fruit for the treatment of inflammatory diseases.

However, different geographical locations greatly influence the accumulation of active compounds and their function in *C. spinosa*. In this study, we found that the content of secondary metabolites of *C. spinosa* fruits from three different districts was significantly different. Consistently, the analysis of different samples from various regions of Sardinia (Italy) revealed qualitative and quantitative differences in the content of flavonoids, glucosinolates, anthocyanins, and phenolic acids (Maldini et al., 2016). The *C. spinosa* bud samples of Morocco, Turkey, and Italy were analyzed, and the results showed that the content of phenol in the Morocco sample was the highest, and that of rutin in the Italian decoction was the highest. Significantly, the highest acetylcholinesterase inhibitory activity was observed in Turkish and Moroccan samples, and the best butyrylcholinesterase inhibitory effects were detected in the Italian samples (Stefanucci et al., 2018). Therefore, the chemical composition of *C. spinosa* with different geographical distributions changed significantly, which endowed them with various biological activities. Among the anti-inflammatory compounds, the flavonoids in fruits from Turpan were the highest, while those in fruits from Ili were the lowest. The biosynthesis and accumulation of flavonoids were related to drought stress (Nakabayashi et al., 2014; Yang et al., 2020). The humid climate in the Ili region was not conducive to the accumulation of flavonoids.

The extracts from all three districts reduced TNF-α and IL-6 both *in vitro* and *in vivo*. However, only a few authors reported the inhibition of TNF-α and IL-6 by flavonoids (Peluso et al., 2015). DCs are professional antigen-presenting cells, link innate and adaptive immune responses. They regulate T cell homeostasis and inflammatory response by expressing costimulatory molecules and releasing cytokines (Waisman et al., 2017). However, ethanol extract of caper from Ili had the best inhibitory effect on the expression of DC surface molecule CD86. Therefore, flavonoids may not be the main component of *C. spinosa* fruits in inhibiting DC maturation. Our experimental results showed that diosmetin had no anti-inflammatory activity at the concentration of 4 mM, which supported the above conclusions.

The contents of stachydrine were higher in 15 anti-inflammatory compounds, and there was little difference in the contents among the three districts. But stachydrine also had no anti-inflammatory activity. Therefore, the anti-inflammatory components in capers need to be further verified by subsequent experiments. Ferulic acid reduced TNF-α, IL-1β, IL-6, IL-23, and MMP9, and increased TGF-β in inflammatory conditions (Doss et al., 2018; Ganesan and Rasool, 2019; Yin et al., 2019; Zhu et al., 2020). On the other hand, 6-gingerol inhibited COX-2, IL-17, IL-6, IL-1β, IL-8, and TNF-α, and increased IL-10 to treat inflammation (Kim et al., 2005; Saha et al., 2016; Zhang and Zheng, 2018; Zhang et al., 2018; Liu et al., 2020; Sheng et al., 2020). 3,4-Dihydroxybenzaldehyde was a phenolic compound with high content in capers. Our results showed that it significantly inhibited DCs maturation and secretion of pro-inflammatory cytokines. These studies suggested that phenols had good anti-inflammatory activity.

Plants respond to environmental changes by regulating gene expression and thus affect metabolic processes. *Cistanche deserticola* was investigated and the 12 key genes involved in PhGs biosynthesis were found to be differentially expressed among three ecotypes (Sun et al., 2020). The content of starting compound phenylalanine was the highest in group C. However, due to the down-regulated expression of most genes in the synthetic pathway, there was no difference in the content of the final product 6-gingerol among the three groups. As an intermediate product, ferulic acid did not accumulate in the three groups. According to the content of compounds, the biosynthetic pathway of 3,4-dihydroxybenzaldehyde played a dominant role.

6 Conclusion

In this study, we found there were significant differences in the morphology, metabolites, gene expression level, and anti-inflammatory activity of capers from the three different districts. All the 95% ethanol extracts from the three districts showed

remarkable anti-inflammatory effects, but the anti-inflammatory effects of *Capparis spinosa* L. vary by origin. The extract from Ili significantly inhibited the expression levels of CD86 on DCs induced by LPS. Phenols were the main compounds that inhibited DCs maturation and secretion of pro-inflammatory cytokines in capers. The gene of REF1 (Cluster-22225.7764) might be the key gene promoting ferulic acid biosynthesis in *C. spinosa*.

Data availability statement

The metabolomics data presented in the study are deposited in the OMIX repository, accession number OMIX004470. The transcript data presented in the study are deposited in the NCBI repository, accession number PRJNA778809.

Ethics statement

The animal study was reviewed and approved by Ethics Committee of Xinjiang University, Xinjiang University (XJUAE-2019-017).

Author contributions

XL, AA, XW, and JL designed the research and analyzed the data. XL, AA, YD, PH, and LM performed the experiments. JL, XW, and XL wrote the manuscript. All authors contributed to the article and approved the submitted version.

Funding

This work was supported by the National Natural Science Foundation of China (31760260), Key research and development program in Xinjiang Uygur Autonomous Region (2022B03002-2), and the Young Qihuang Scholars Project of National Administration of Traditional Chinese Medicine ([2021] No. 200).

Acknowledgments

We thank Professor Jianjun Yang (College of Ecology and Environment, Xinjiang University) for providing the data on habitat climate, Researcher Chunhui Ge (Xinjiang Academy of Agricultural Sciences) for providing the data on edaphic factor, Professor Liqiong Xie (College of Life Science and Technology, Xinjiang University) for providing the proposal of writing.

Conflict of interest

The authors declare that the research was conducted in the absence of any commercial or financial relationships that could be construed as a potential conflict of interest.

Publisher's note

All claims expressed in this article are solely those of the authors and do not necessarily represent those of their affiliated organizations, or those of the publisher, the editors and the reviewers. Any product that may be evaluated in this article, or claim that may be made by its manufacturer, is not guaranteed or endorsed by the publisher.

Supplementary material

The Supplementary Material for this article can be found online at: https://www.frontiersin.org/articles/10.3389/fpls.2023.1224073/full#supplementary-material

References

Aipire, A., Li, J. Y., Yuan, P. F., He, J., Hu, Y. L., Liu, L., et al. (2017). *Glycyrrhiza uralensis* water extract enhances dendritic cell maturation and antitumor efficacy of HPV dendritic cell-based vaccine. *Sci. Rep.* 7, 43796. doi: 10.1038/srep43796

Azeguli, H., Li, J., Zhou, F., Adila, A., Ma, J., Yang, J., et al. (2017). *Capparis spinosa* fruit ethanol extracts exert different effects on the maturation of dendritic cells. *Molecules* 22 (1), 97. doi: 10.3390/molecules22010097

Azhary, K. E., Jouti, N. T., Khachibi, M. E., Moutia, M., Tabyaoui, I., Hou, A. E., et al. (2017). Anti-inflammatory potential of capparis spinosa l. *in vivo* in mice through inhibition of cell infiltration and cytokine gene expression. *BMC Complement. Altern. Med.* 17 (1), 81. doi: 10.1186/s12906-017-1569-7

Bai, H. Y., Bao, F., Fan, X. R., Han, S., Zheng, W. H., Sun, L. L., et al. (2020). Metabolomics study of different parts of licorice from different geographical origins and their anti-inflammatory activities. *J. Separation Sci.* 43 (8), 1593–1602. doi: 10.1002/jssc.201901013

Cao, Y. L., Li, X., and Zheng, M. (2010). *Capparis spinosa* protects against oxidative stress in systemic sclerosis dermal fibroblasts. *Arch. Dermatol. Res.* 302, 349–355. doi: 10.1007/s00403-009-0998-7

Doss, H. M., Samarpita, S., Ganesan, R., and Rasool, M. (2018). Ferulic acid, a dietary polyphenol suppresses osteoclast differentiation and bone erosion *via* the inhibition of rankl dependent NF-κB signalling pathway. *Life Sci.* 207, 284–295. doi: 10.1016/j.lfs.2018.06.013

Editorial Committee of Flora of China and Chinese Academy of Sciences (1999). *Flora of China* Vol. 32, 495 (Beijing: Science Press).

Editorial Committee of Flora of Xinjiang. (1995). *Flora of Xinjiang (Volume 2, Part 2)*. (Urumqi: Xinjiang Science Technology and Health Press) 1995, 36.

El Zayat, M. A. S., Ali, M. E. S., and Amar, M. H. (2020). A systematic revision of capparaceae and cleomaceae in egypt: an evaluation of the generic delimitations of capparis and cleome using ecological and genetic diversity. *J. Genet. Eng. Biotechnol.* 18, 58. doi: 10.1186/s43141-020-00069-z

Fici, S. (2001). Intraspecific variation and evolutionary trends in *capparis spinosa* l. (capparaceae). *Plant Syst. Evol.* 228, 123–141. doi: 10.1007/s006060170024

Francesca, N., Barbera, M., Martorana, A., Saiano, F., Gaglio, R., Aponte, M., et al. (2016). Optimised method for the analysis of phenolic compounds from caper (*capparis spinosa* l.) berries and monitoring of their changes during fermentation. *Food Chem.* 196, 1172–1179. doi: 10.1016/j.foodchem.2015.10.045

Ganesan, R., and Rasool, M. (2019). Ferulic acid inhibits interleukin 17-dependent expression of nodal pathogenic mediators in fibroblast-like synoviocytes of rheumatoid arthritis. *J. Cell. Biochem.* 120, 1878–1893. doi: 10.1002/jcb.27502

Inocencio, C., Cowan, R. S., Alcaraz, F., Rivera, D., and Fay, M. F. (2005). AFLP fingerprinting in *capparis* subgenus *capparis* related to the commercial sources of capers. *Genet. Resour. Crop Evol.* 52 (2), 137–144. doi: 10.1007/s10722-003-4432-2

Jalali, M. T., Mohammadtaghvaei, N., and Larky, D. (2016). Investigating the effects of *capparis spinosa* on hepatic gluconeogenesis and lipid content in streptozotocin-induced diabetic rats. *Biomed. Pharmacother.* 84, 1243–1248. doi: 10.1016/j.biopha.2016.10.061

Ji, Y. B., and Yu, L. (2015). *In vitro* analysis of the role of the mitochondrial apoptosis pathway in csbe therapy against human gastric cancer. *Exp. Ther. Med.* 10, 24.3–2409. doi: 10.3892/etm.2015.2779

Kalantari, H., Foruozandeh, H., Khodayar, M. J., Siahpoosh, A., Saki, N., and Kheradmand, P. (2018). Antioxidant and hepatoprotective effects of capparis spinosa l. fractions and quercetin on tert-butyl hydroperoxide- induced acute liver damage in mice. *J. Traditional Complement. Med.* 8, 120–127. doi: 10.1016/j.jtcme.2017.04.010

Kaneshiro, K., Sakai, Y., Suzuki, K., Uchida, K., Tateishi, K., Terashima, Y., et al. (2019). Interleukin-6 and tumour necrosis factor-α cooperatively promote cell cycle regulators and proliferate rheumatoid arthritis fibroblast-like synovial cells. *Scandinavian J. Rheumatol.* 0, 1–9. doi: 10.1080/03009742.2019.1602164

Khatib, M., Pieraccini, G., Innocenti, M., Melani, F., and Mulinacci, N. (2016). An insight on the alkaloid content of *Capparis spinosa* l. root by HPLC-DAD-MS, MS/MS and ^{1}H qNMR. *J. Pharm. Biomed. Anal.* 123, 53–62. doi: 10.1016/j.jpba.2016.01.063

Khavasi, N., Somi, M. H., Khadem, E., Faramarzi, E., Ayati, M. H., Fazljou, S. M. B., et al. (2017). Effect of daily caper fruit pickle consumption on disease regression in patients with non-alcoholic fatty liver disease: a double-blinded randomized clinical trial. *Advanced Pharm. Bull.* 7 (4), 645–650. doi: 10.15171/apb.2017.077

Kim, S. O., Kundu, J. K., Shin, Y. K., Park, J. H., Cho, M. H., Kim, T. Y., et al. (2005). [6]-gingerol inhibits cox-2 expression by blocking the activation of p38 map kinase and nf-kappab in phorbol ester-stimulated mouse skin. *Oncogene* 24, 2558–2567. doi: 10.1038/sj.onc.1208446

Liu, Y., Deng, S. J., Zhang, Z., Gu, Y., Xia, S. N., Bao, X. Y., et al. (2020). 6-gingerol attenuates microglia-mediated neuroinflammation and ischemic brain injuries through akt-mtor-stat3 signaling pathway. *Eur. J. Pharmacol.* 883, 173294. doi: 10.1016/j.ejphar.2020.173294

Maldini, M., Foddai, M., Natella, F., Addis, R., Chessa, M., Petretto, G. L., et al. (2016). Metabolomic study of wild and cultivated caper (*capparis spinosa* l.) from different areas of sardinia and their comparative evaluation. *J. Mass Spectrom. Jms.* 51 (9): 716–728. doi: 10.1002/jms.3830

Mohebali, N., Fazeli, S., Ghafoori, H., Farahmand, Z., and Sanati, M. H. (2016). Effect of flavonoids rich extract of capparis spinosa on inflammatory involved genes in amyloid-beta peptide injected rat model of alzheimer's disease. *Nutr. Neuroence* 21 (2), 1–8. doi: 10.1080/1028415X.2016.1238026

Nakabayashi, R., Yonekura-Sakakibara, K., Urano, K., Suzuki, M., Yamada, Y., Nishizawa, T., et al. (2014). Enhancement of oxidative and drought tolerance in arabidopsis by overaccumulation of antioxidant flavonoids. *Plant J.* 77, 367–379. doi: 10.1111/tpj.12388

Peluso, I., Miglio, C., Morabito, G., Ioannone, F., and Serafini, M. (2015). Flavonoids and immune function in human: a systematic review. *Crit. Rev. Food Sci. Nutr.* 55, 383–395. doi: 10.1080/10408398.2012.656770

Rahimi, V. B., Rajabian, A., Rajabi, H., Vosough, E. M., Mirkarimi, H. R., Hasanpour, M., et al. (2020). The effects of hydro-ethanolic extract of *Capparis spinosa* (*C. spinosa*) on lipopolysaccharide (LPS)-induced inflammation and cognitive impairment: Evidence from *in vivo* and *in vitro* studies. *J. Ethnopharmacol.* 256, 112706. doi: 10.1016/j.jep.2020.112706

Saha, P., Katarkar, A., Das, B., Bhattacharyya, A., and Chaudhuri, K. (2016). 6-gingerol inhibits vibrio cholerae-induced proinflammatory cytokines in intestinal epithelial cells *via* modulation of NF-κB. *Pharm. Biol.* 54 (9), 1606–1615. doi: 10.3109/13880209.2015.1110598

Sheng, Y. Y., Wu, T. L., Dai, Y. Y., Xu, L. L., Zhong, Y., Xue, Y. H., et al. (2020). 6-gingerol alleviates inflammatory injury in DSS-induced ulcerative colitis mice by regulating NF-κB signaling. *Ann. Palliative Med.* 9 (4), 1944–1952. doi: 10.21037/apm-20-903

Stefanucci, A., Zengin, G., Locatelli, M., Macedonio, G., and Mollica, A. (2018). Impact of different geographical locations on varying profile of bioactives and associated functionalities of caper (*capparis spinosa* l.). *Food Chem. Toxicol. Int. J. Published Br. Ind. Biol. Res. Assoc.* 118, 181. doi: 10.1016/j.fct.2018.05.003

Sun, X., Li, L., Pei, J., Liu, C., and Huang, L. F. (2020). Metabolome and transcriptome profiling reveals quality variation and underlying regulation of three ecotypes for *cistanche deserticola*. *Plant Mol. Biol.* 102, 253–269. doi: 10.1007/s11103-019-00944-5

Tlili, N., Mejri, H., Anouer, F., Saadaoui, E., Khaldi, A., and Nasri, N. (2015). Phenolic profile and antioxidant activity of *capparis spinosa* seeds harvested from different wild habitats. *Ind. Crops Products* 76, 930–935. doi: 10.1016/j.indcrop.2015.07.040

Trombetta, D., Occhiuto, F., Perri, D., Puglia, C., Santagati, N. A., Pasquale, A. D., et al. (2005). Antiallergic and antihistaminic effect of two extracts of *capparis spinosa* l. flowering buds. *Phytother. Res.* 19, 29–33. doi: 10.1002/ptr.1591

Waisman, A., Lukas, D., Clausen, B. E., and Yogev, N. (2017). Dendritic cells as gatekeepers of tolerance. *Semin. Immunopathol.* 39, 153–163. doi: 10.1007/s00281-016-0583-z

Yang, L. L., Yang, L., Yang, X., Zhang, T., Lan, Y. M., Zhao, Y., et al. (2020). Drought stress induces biosynthesis of flavonoids in leaves and saikosaponins in roots of *Bupleurum chinense* DC. *Phytochemistry* 177, 112434. doi: 10.1016/j.phytochem.2020.112434

Yin, P., Zhang, Z. C., Li, J. D., Shi, Y. R., Jin, N., Zou, W. S., et al. (2019). Ferulic acid inhibits bovine endometrial epithelial cells against LPS-induced inflammation *via* suppressing NF-κB and MAPK pathway. *Res. Vet. Sci.* 126, 164–169. doi: 10.1016/j.rvsc.2019.08.018

Zhan, Z. L., Fang, W. T., Ma, X. H., Chen, T., Cui, G. H., Ma, Y., et al. (2019). Metabolome and transcriptome analyses reveal quality change in the orange-rooted salvia miltiorrhiza (Danshen) from cultivated field. *Chin. Med.* 14, 42. doi: 10.1186/s13020-019-0265-6

Zhang, F., Zhang, J. G., Wei, Y., Pu, X., Xiao, Y. L., and Zhang, H. T. (2018). 6-gingerol attenuates LPS-induced neuroinflammation and cognitive impairment partially *via* suppressing astrocyte overactivation. *Biomed. Pharmacother.* 107, 1523–1529. doi: 10.1016/j.biopha.2018.08.136

Zhang, H., and Zheng, M. (2018). Phytochemical and pharmacological properties of capparis spinosa as a medicinal plant. *Nutrients* 10 (2), 116. doi: 10.3390/nu10020116

Zhou, H. F., Jian, R. J., Kang, J., Huang, X. L., Li, Y., Zhuang, C. L., et al. (2010). Anti-inflammatory effects of caper (*capparis spinosa* l.) fruit aqueous extract and the isolation of main phytochemicals. *J. Agric. Food Chem.* 58 (24), 12717–12721. doi: 10.1021/jf1034114

Zhu, L. J., Zhang, Z. S., Xia, N. N., Zhang, W. F., Wei, Y. L., Huang, J. S., et al. (2020). Anti–arthritic activity of ferulic acid in complete freund's adjuvant (CFA)–induced arthritis in rats: JAK2 inhibition. *Inflammopharmacology* 28 (2), 463–473. doi: 10.1007/s10787-019-00642-0

frontiers | Frontiers in Plant Science

TYPE Original Research
PUBLISHED 27 July 2023
DOI 10.3389/fpls.2023.1208724

OPEN ACCESS

EDITED BY
Hosam O. Elansary,
King Saud University, Saudi Arabia

REVIEWED BY
Amit Srivastava,
University of Jyväskylä, Finland
Jianhua Fan,
East China University of Science and Technology, China

*CORRESPONDENCE
Maryam Abidizadegan
Maryam.abidizadegan@helsinki.fi

RECEIVED 19 April 2023
ACCEPTED 07 July 2023
PUBLISHED 27 July 2023

CITATION
Abidizadegan M, Blomster J and Peltomaa E (2023) Effect of micronutrient iron on bioactive compounds isolated from cryptophytes.
Front. Plant Sci. 14:1208724.
doi: 10.3389/fpls.2023.1208724

Effect of micronutrient iron on bioactive compounds isolated from cryptophytes

Maryam Abidizadegan[1]*, Jaanika Blomster[2] and Elina Peltomaa[3]

[1]Ecosystem and Environment Research Program, Faculty of Biological and Environmental Sciences, University of Helsinki, Lahti, Finland, [2]Ecosystem and Environment Research Program, Faculty of Biological and Environmental Sciences, University of Helsinki, Helsinki, Finland, [3]Department of Forest Sciences, University of Helsinki, Helsinki, Finland

Iron is one of the important micronutrients affecting algal growth due to its fundamental role in the physiological processes, including photosynthetic electron transport, respiration, and nitrogen fixation. In this study, the effect of different iron levels on growth and the production of bioactive compounds (phycoerythrin (PE), extracellular polymeric substances (EPS), and phenolic compounds (PCs)) of five cryptophyte strains were investigated. Also, the antioxidant capacity of the bioactive compounds was explored. The results showed species-specific responses to the impact of iron on growth of cryptophytes and accumulation of bioactive compounds. The growth rates of *C. pyrenoidifera* and *Cryptomonas* sp. varied significantly at different iron levels, and a reduction in the PE content was observed for several cryptophytes cultured at the highest iron level. However, no significant differences were detected in EPS content at different iron levels. Differences in PC contents of *C. pyrenoidifera* and *Cryptomonas* sp. at medium iron level were statistically significant compared with the other two treatments. The results also revealed species-specific differences in antioxidant activity at different iron levels; each studied strain followed its own pattern in response to change in iron level, and each bioactive compound had a different antioxidant activity. Overall, however, PCs demonstrated higher antioxidant activity than PE and EPS. In summary, iron has an impact on growth, bioactive compound accumulation, and antioxidant activity. However, the species-specific responses to changes in iron level should not be ignored when modifying culture conditions for optimal harvest of bioactive compounds.

KEYWORDS

antioxidant activity, bioactive compounds, cryptophytes, extracellular polymeric substances, iron, phenolic compounds, phycobiliprotein

1 Introduction

The effect of macronutrients, including nitrogen and phosphorous, on microalgal growth and their bioactive compounds has been extensively researched. However, micronutrients, such as iron, also play a fundamental role in the growth of microalgae. Iron has a crucial function in algal metabolic processes, involving photosynthetic electron

transport, nitrogen fixation process, and respiration (Liu et al., 2018). The function of iron in phytoplankton cells has been explained as iron directly affecting the various methanolic pathways by its catalytic role in enzymes and indirectly contributing to energy production by high energy-carrier molecules, including NADPH and ATP (Schoffman et al., 2016).

Although the effect of iron on algal growth has been established, little research has focused on the impact of iron on the accumulation of bioactive compounds. Growth rates of certain microalgal species, such as the green algae *Raphidocelis subcapitata*, *Dunaliella salina*, *Desmodesmus subspicatus*, *Parachlorella kessleri*, *Chlorella vulgaris*, and *Haematococcus pluvialis*, the cryptomonad *Cryptomonas* sp., and the dinoflagellate *Prorocentrum micans*, have been enhanced by increasing the iron concentration of the culture media (Weng et al., 2007; Liu et al., 2008; Padrova et al., 2015; Rastar et al., 2018). On the other hand, a study where *Chlorella* sp. was cultured at different iron levels demonstrated that it grew well at the lowest iron level (0.35 mg L^{-1}) (Iriani et al., 2011).

It can be deduced from previous studies that the effect of iron on algal growth rate depends largely on algal species. Therefore, the investigation of the impact of iron on other algal groups is essential for identifying optimal culture conditions to produce high-quantity/quality bioactive compounds applicable in various industries. One of the main groups of microalgae is cryptophytes found in such diverse aquatic habitats as marine, freshwater, and brackish waters (Clay, 2015). The absence of a recalcitrant cell wall is one important feature of cryptophytes, making biomass processing and cell breaking simpler when extracting biomolecules. This benefit leads to the higher ratio of usable total biomass with biological active compounds. In fact, the lack of a heavy cell wall in cryptophytes enhances the possibility of harvesting biomass with high-quantity biomolecules instead of increasing only the biomass weight of the useless part (Mercier et al., 2022). Furthermore, cryptophytes produce several valuable bioactive compounds such as phycobiliproteins (PBPs), extracellular polymeric substances (EPS), and omega-3 polyunsaturated fatty acids, including eicosapentaenoic acid (EPA) and docosahexaenoic acid (DHA) (Giroldo et al., 2005; Peltomaa et al., 2018; Abidizadegan et al., 2022; Mercier et al., 2022). Nonetheless, the biotechnological potential and applications of cryptophytes have not been thoroughly investigated. Hence, in addition to exploring the bioactive compounds of cryptophytes and their potential, studying the optimum cultural conditions to derive bioactive compounds of high quantity and quality is necessary.

In this study, the effect of iron on biomolecules of cryptophytes, including PBPs, EPS, and phenolic compounds (PCs), is explored. Contrary to red algae and cyanobacteria, cryptophyte strains only contain one type of PBP, either phycocyanin or phycoerythrin (Hill and Rowan, 1989). This removes the necessity of isolating different PBPs from each other, and accordingly, makes the protein purification simpler in the production process of PBPs (Mercier et al., 2022). Additionally, due to the lower molecular weight, cryptophyte PBPs are more practical as labels in fluorescence medical diagnostics than cyanobacterial and red algal PBPs (Telford et al., 2001; Roman et al., 2002). The cryptophytes in this study contain phycoerythrin (PE), which is used to make natural colorant of food, cosmetics, drugs, fluorescent probes for immunoassays, and flow cytometry (Garcia et al., 2021; Chen et al., 2022). The EPS – a mixture of biopolymers, including polysaccharides, proteins, nucleic acids, and lipids – with physiochemical properties are applied in food and pharmacy as preservatives, gelling agents, and thickeners (Tiwari et al., 2020). EPS can also be used as an emulsion stabilizer in food and as a hydrating agent in pharmaceuticals and cosmetics (Xiao and Zheng, 2016). Moreover, permeability properties of EPS make them advantageous as plant biostimulants to promote sustainable agriculture (Rachidi et al., 2020). The PCs are considered to be natural antioxidants applicable in pharmaceutical, cosmetic, and food industries with health-promoting effects to prevent such diseases as cancer and inflammatory disorders (Cory et al., 2018). Although there are several studies on the antioxidant activity of algal PE, EPS, and PCs (Kim et al., 2018; Punampalam et al., 2018; Frazzini et al., 2022; Mousavian et al., 2022; Wang et al., 2022), cryptophyte algae have not yet been explored in terms of antioxidant activity of bioactive compounds.

Several studies have presented the effect of different iron levels on the above-mentioned bioactive compounds of certain algae. For example, the highest PBP content of the red macroalga *Gracilaria tenuistipitata* has been reported with high iron content in tissue (549 µg dw^{-1}) (Liu et al., 2000). Contrary to this, cyanobacterium *Arthrospira platenis* has shown a negative correlation with iron concentration (Akbarnezhad et al., 2016). Additionally, the highest total PC content of the green alga *Chlorella* sp. after a 14-day cultivation occurred at the highest iron level (13.99 mg L^{-1}), while after 21 days it was high at the lowest iron level (0.35 mg L^{-1}) (Iriani et al., 2011). The aim of this investigation is to better understand the relationship between culture conditions at different iron levels and the accumulation of bioactive compounds, such as PBP, EPS, and PCs, of cryptophyte algae. Growth and biomass productivity changes of cryptophyte algae under different iron levels, and the antioxidant activity of studied bioactive compounds were explored. Finally, promising cryptophyte strains for producing high amounts of bioactive compounds were identified.

2 Materials and methods

2.1 Algae and growth conditions

Five cryptophyte strains (Table 1) were grown in culture media with three different iron levels. Culture media used for the marine strain *Rhodomonas salina* was F/2 and for freshwater *Cryptomonas* strains MWC (Guillard and Ryther, 1962; Guillard and Lorenzen, 1972). The iron source in both applied media was $FeCl_3$ at a concentration of 3.15 mg L^{-1} (control and medium level). By manipulating the media, two other iron treatments contained 1.75 mg L^{-1} (low level) and 6.3 mg L^{-1} (high level). The changes in iron content of the algal biomass caused by the treatments were confirmed by iron analysis (see Supplemental Table 1). The experiment was conducted in four replicates, and in 2 L glass bottles, which were randomly arranged in growth cabinets (Friocell

TABLE 1 Cryptophyte strains, culture collection codes, and habitats of each strain.

Strain	Code in culture collection	Habitat
Rhodomonas salina	CCMP 757	Marine
Cryptomonas pyrenoidifera	CCAP 979/61	Freshwater
Cryptomonas curvata	CCAP 979/63	Freshwater
Cryptomonas ozolinii	UTEX LB 2782	Freshwater
Cryptomonas sp.	CPCC 336	Freshwater

Evo 404, MMM Group, Germany) for ten days. Strains were kept at 20°C, under a 16 h: 8h light/dark cycle at a light level of 100 µmol photons m^{-2} s^{-1}, and 2% (v/v) CO_2 level.

2.2 Growth rates and biomass yield

Algal growth rate was determined by measuring optical density at 750 nm (OD_{750}) five times (day 0, 1, 3, 6, and 9) during the experiment with a SHIMADZU UV-2401 PC spectrophotometer. The specific growth rate (μ_{exp}; d^{-1}) was estimated using Equation (1):

$$\mu_{exp} = \ln(\alpha_f/\alpha_i)/(t_f - t_i) \quad (1)$$

where α_f and α_i are the absorbance reading at the end and the beginning of the exponential growth phase, at initial time (t_i) and final time (t_f), respectively.

Whatman filter papers (GF/C, 47 mm diameter, ca 1.2 µm pore size) were used in dry weight determinations. The filter papers were dried at 105°C overnight and weighed. Of the cultures, 20 mL was filtered using a vacuum filter, and then the filters were dried overnight at 105°C again and reweighed.

2.3 Extraction and measurement of bioactive compounds

For PBPs, 40 mL of cultures were centrifuged at 4000 × g for 10 min (Heraeus Multifuge 1 S-R, Kendro Laboratory Products, Germany) to obtain pellets. The pellets were dissolved in 5 mL of 0.1 M phosphate buffer and kept at -20°C to break the cells and release the PBPs. The samples were thawed at 5°C overnight and then centrifuged at 4000 × g for 15 min to remove cell debris. Harvested supernatants were used for PBP analysis by measuring the absorption spectra. Absorbance of extracts was measured from 280 to 750 nm using spectrophotometry (Shimadzu UV-2401 PC spectrophotometer, Shimadzu Corporation, Japan) and 1 cm cuvettes against phosphate buffer as a blank sample. Finally, the PBP concentrations (µg L^{-1}) were calculated using Equation (2) (Lawrenz et al., 2011; Cunningham et al., 2019):

$$c = \frac{A}{\varepsilon d} \times MW \times \frac{V_{buffer}}{V_{sample}} \times 10^6 \quad (2)$$

where A = subtracting the absorbance at 750 nm from the absorbance maximum of the phycoerythrin peak (548 nm for marine strain and 565 nm for freshwater strains), ε = the molar extinction coefficient for cryptophyceae PE (5.67×10^5 L $mol^{-1}cm^{-1}$), MW = the molecular weight of cryptophyceae PE (45000 g mol^{-1}), and V_{buffer} and V_{sample} = the volume of the buffer and sample, respectively.

For EPS, freeze-dried biomass was dissolved in 5 mL of deionized water and shaken for 20 min. After centrifuging of samples at 4000 × g for 15 min, pellets were mixed in 5 mL of 0.05% NaCl solution and placed in an overhead shaker at 60°C for one hour. After sonication of samples for 10 min at 100 W and 20° C, the suspensions were centrifuged for 15 min at 4000 × g. Finally, supernatants were lyophilized for 48 h at -60°C and 0.6 mbar and the weight of EPS was determined gravimetrically (Chang et al., 2019; Strieth et al., 2020).

For PCs, the mixture of dry biomass and methanol as solvent was sonicated at 50 Hz and 37°C for 15 min. Samples were incubated at room temperature and after one hour were centrifuged at 4000 × g for 15 min (Irondi et al., 2012; Korzeniowska et al., 2020). The Folin-Ciocalteu (FC) procedure was used to measure PCs. Folin-Ciocalteu reagent (1.5 mL) and 7.5% Na_2CO_3 solution (1.2 mL) were added to the sample extract (300 µL). After incubation of samples in the dark for 30 min, the absorbance was read at 765 nm. PC contents (C) were measured in milligrams gallic acid equivalent (GAE) per gram of algae dry weight using the calibration curve in mg ml^{-1} (Y= 0.014 x + 0.15, R^2 = 0.9898) (Irondi et al., 2012; Korzeniowska et al., 2020).

2.4 Antioxidant capacity of bioactive compounds

To determine antioxidant capacity, DPPH (2,2-diphenyl-1-picrylhydrazyl) solution (0.1mM) was used. Extracts of bioactive compounds (0.5 mL) were mixed with 3 mL of DPPH solution. After incubating the mixture in the dark for 30 min, the absorbance (A) was read at 517 nm. The results were expressed as antioxidant capacity equivalent ascorbic acid (AEAA) using Equation (3) (Leong and Shui, 2002):

$$\begin{aligned}&\textbf{AEAA (mg AA g}^{-1}\textbf{bioactive compounds)}\\&= ((\mathbf{A_{control}} - \mathbf{A_{sample}})/(\mathbf{A_{control}} - \mathbf{A_{AA}}))\\&\quad \times \textbf{conc. AA(mg mL}^{-1}\textbf{)}\\&\quad \times \textbf{vol extract (mL)/used bioactive compounds (g)}\end{aligned} \quad (3)$$

where $A_{control}$ is the absorbance of the methanolic DPPH solution in the presence of the extract.

2.5 Statistical analyses

The differences between the growth rates, biomass productivity, and bioactive compounds content between the studied cryptophytes were analyzed with ANOVA and Tukey *post-hoc* test's honestly significant difference (HSD) *post hoc* test. The significance level was set to $p< 0.05$. All statistical analyses were performed using IBM SPSS 26 Statistical package (SPSS Inc., Chicago, IL, USA).

3 Results

3.1 Specific growth and biomass productivity

Each studied strain had a specific growth pattern at different iron levels. *C. pyrenoidifera*, *C. ozolinii*, and *Cryptomonas* sp. continued to grow steadily over the experiment. However, the growth of *R. salina* at low iron level and *C. curvata* at low and control (medium) iron levels decreased after day 6 (Figures 1A–E). In *C. pyrenoidifera* and *Cryptomonas* sp., a significant difference emerged between the growth rates at different iron levels: the highest growth rate of these two cryptophyte strains was at high iron level ($p > 0.05$). Overall, the highest and lowest growth rates were observed in freshwater cryptophyte *C. pyrenoidifera* (~0.3 day^{-1}) and marine cryptophyte *R. salina* (~0.1 day^{-1}), respectively (Figure 2).

There was a significant difference between biomass productivity of the studied cryptophytes cultured at different iron levels ($p< 0.05$), except *C. curvata*. The highest biomass production was at high iron level for most of the strains. Biomass production of *R. salina* increased gradually with rising iron levels, as biomass productivity at high iron level was ~ 55% and 95% higher than at control and low iron levels, respectively. However, biomass production of *C. pyrenoidifera*, *C. ozolinii*, and *Cryptomonas* sp. decreased at control (medium) iron level and was lower than at low or high iron level treatments. Biomass productivity of *C. pyrenoidifera* at low and high iron levels was ~110% and 240% higher than at control iron level, respectively. Regarding to *C. ozolinii*, biomass productivity at low and high iron levels was ~116% and 83% higher than at control iron level, respectively. Although the highest biomass yield of *C. ozolinii* was at low iron level, it made no significant difference to the biomass yield of *C. ozolinii* at high iron level ($p< 0.05$; Figure 3). Additionally, *Cryptomonas* sp. demonstrated that biomass productivity at low

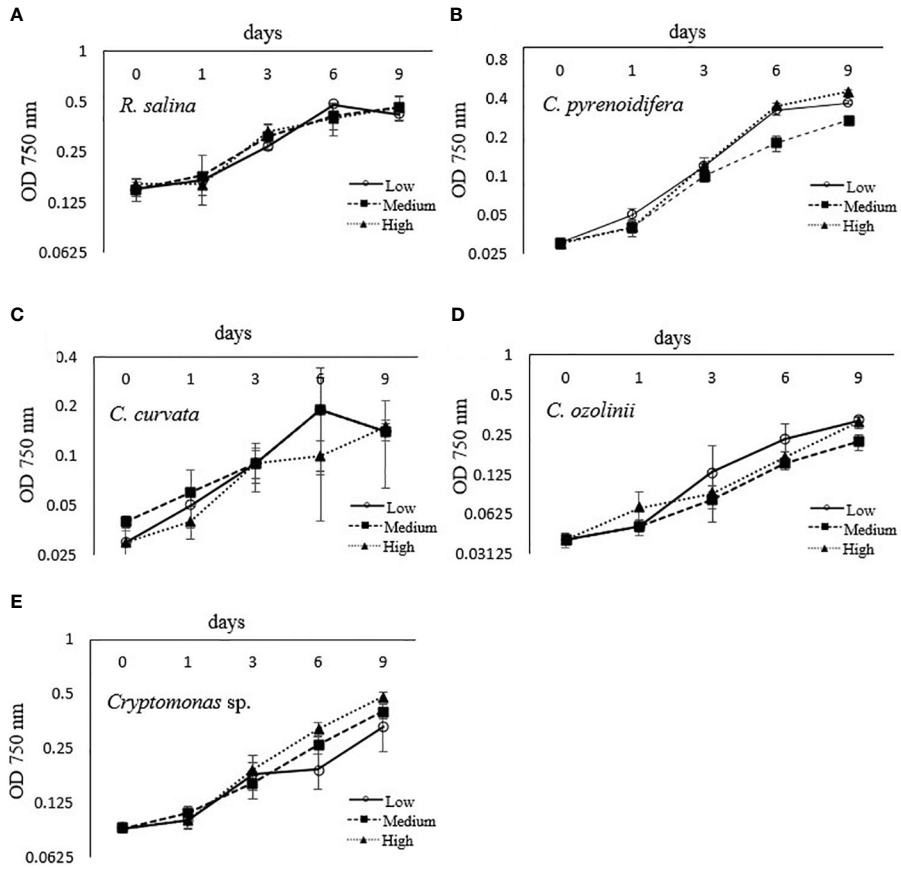

FIGURE 1
Growth curve of studied cryptophyte strains [**(A)** *R. salina*, **(B)** *C. pyrenoidifera*, **(C)** *C.* 685 *curvata*, **(D)** *C. ozolinii*, **(E)** *Cryptomonas* sp.] at different iron levels (Low:—○—, Medium:- -■- -, High:···▲···) measured at 750 nm.

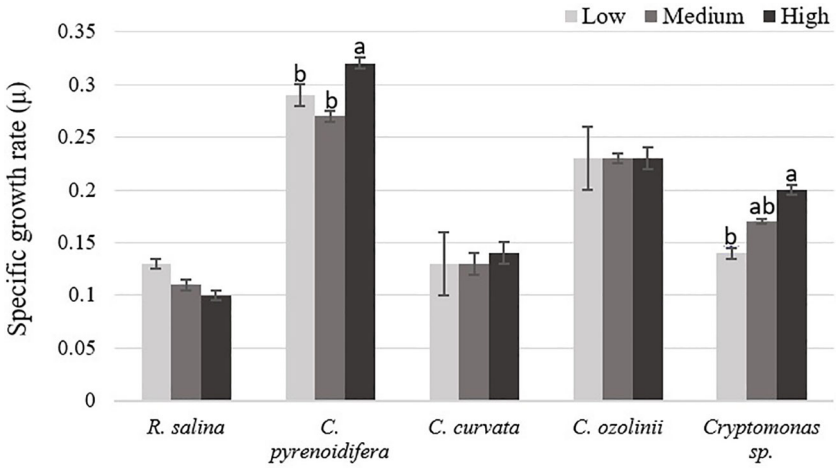

FIGURE 2
Specific growth rate (μ) of studied cryptophytes species at different iron levels. Significant differences between samples are indicated with different letters as determined by ANOVA comparison (p< 0.05).

and high iron levels was ~75% and 150% higher than at control iron level, respectively.

3.2 Bioactive compounds

3.2.1 Phycobiliprotein

Phycobiliprotein content isolated from each strain grown at different iron levels showed a significant difference ($p< 0.05$), excluding *R. salina* and *C. curvata*. The highest PE content of *R. salina* and *C. curvata* was at low iron level, but without significant difference compared with other treatments ($p > 0.05$). However, for *C. pyrenoidifera*, *C. ozolinii*, and *Cryptomonas* sp. the medium iron level was the most favorable condition for PE production (Figure 4).

Antioxidant capacity of PE had significant differences at different iron levels in *R. salina*, *C. pyrenoidifera*, and *C. curvata* ($p< 0.05$). There was a significant difference between antioxidant activities of PE at medium iron level with two other iron levels in *C. pyrenoidifera*. Additionally, in *R. salina* and *C. curvata*, a difference was observed between medium and low iron levels ($p< 0.05$). The highest antioxidant capacity of PE was at medium iron level for all studied cryptophyte strains, except *Cryptomonas* sp. (Figure 5). The PE of *C. ozolinii* contained the highest antioxidant capacity among the studied cryptophytes ($p< 0.05$).

3.2.2 Extracellular polymeric substances

There was no significant difference among EPS isolated at different iron levels for the studied strains ($p > 0.05$; Figure 6). Whereas *R. salina*, *C. pyrenoidifera*, and *Cryptomonas* sp. produced the highest EPS content at low iron level, the highest quantity of derived EPS for *C. pyrenoidifera* and *C. ozolinii* was at control iron

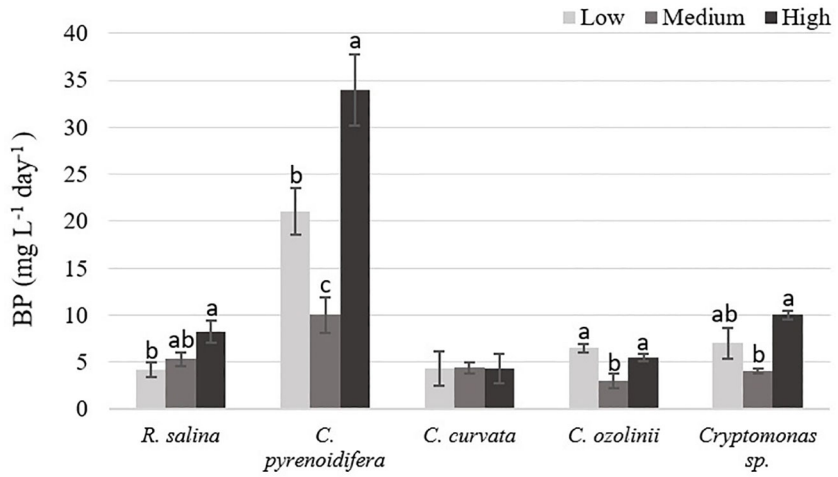

FIGURE 3
Biomass productivity (BP: mg L^{-1} day^{-1}) of studied cryptophytes species at different iron levels. Significant differences between samples are indicated with different letters as determined by ANOVA comparison (p< 0.05).

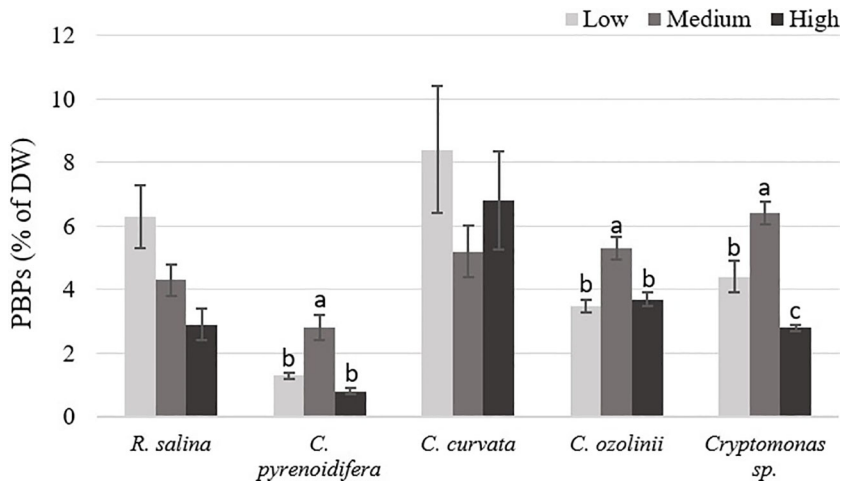

FIGURE 4
Phycobiliproteins (PBPs) content of studied cryptophytes species expressed as percentage of dry weight at different iron levels. Significant differences between samples are indicated with different letters as determined by ANOVA comparison ($p < 0.05$).

level. Among the studied cryptophyte strains, *R. salina* produced the highest EPS with ~50% dry biomass.

In *C. pyrenoidifera* and *C. curvata*, antioxidant activity of EPS was significantly different between the high iron level and the other two iron levels ($p < 0.05$). Although the highest antioxidant activity of EPS for *C. pyrenoidifera* was at low iron level, *C. curvata* grown under high iron level showed the highest antioxidant activity of EPS. However, there was no significant difference between antioxidant activity of EPS for *R. salina, C. ozolinii*, and *Cryptomonas* sp. cultured at different iron levels ($p > 0.05$; Figure 7). The highest and lowest antioxidant activity of EPS was observed in *Cryptomonas* sp. and *R. salina*, respectively.

3.2.3 Phenolic compounds

Phenolic compound contents differed significantly at different iron levels in *R. salina*, *C. pyrenoidifera*, and *Cryptomonas* sp. ($p < 0.05$; Figure 8). The highest PC content of *R. salina* and *C. ozolinii* was at low and high iron levels, respectively, whereas *C. pyrenoidifera*, *C. curvata*, and *Cryptomonas* sp. produced the highest PC content at medium iron level (Figure 8). Overall, among the studied strains, *C. pyrenoidifera* and *C. ozolinii* grown at medium iron level produced the highest quantity of PCs with almost 32% PCs of dry biomass (Figure 8).

Except for *R. salina* and *C. curvata*, other studied cryptophytes showed significant differences in antioxidant activities of PCs at different iron levels ($p < 0.05$). Although *Cryptomonas* sp. contained the highest antioxidant capacity of PCs at low iron level, PCs extracted from *R. salina* and *C. pyrenoidifera* had the maximum antioxidant activity at high iron level. Moreover, *C. ozolinii* showed the highest antioxidant activity of PCs at medium iron level (Figure 9). The PCs of *C. curvata* contained the highest antioxidant capacity among the studied cryptophytes ($p < 0.05$).

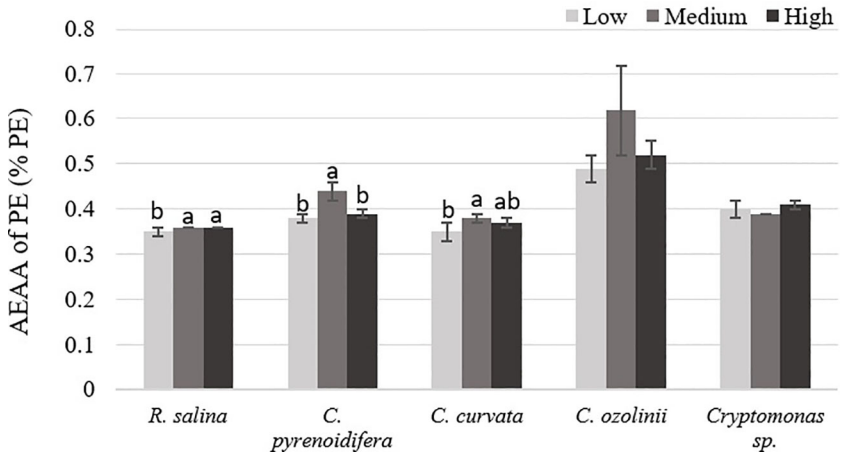

FIGURE 5
Antioxidant capacity (AEAA) of PE (% PE) derived from the studied cryptophytes cultured at different iron levels. Significant differences between samples are indicated with different letters as determined by ANOVA comparison ($p < 0.05$).

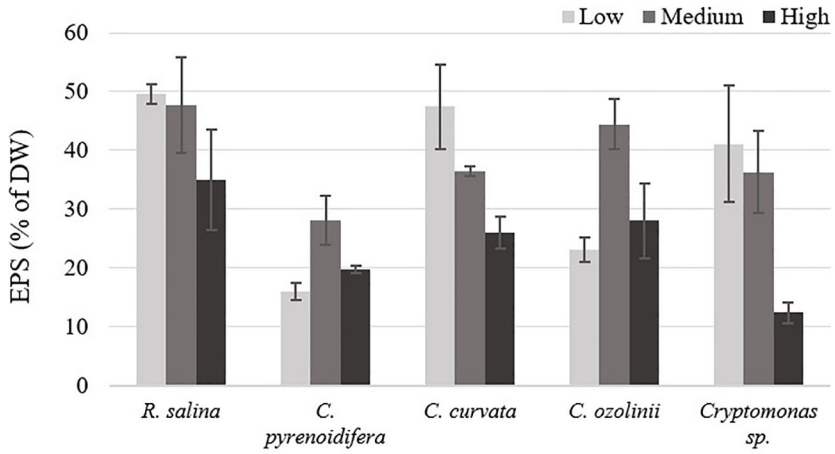

FIGURE 6
Extracellular polymeric substances (EPS) content of studied cryptophytes species expressed as percentage of dry weight at different iron levels.

4 Discussion

Here, we studied the relationship between culture conditions at different iron levels and growth as well as accumulation of bioactive compounds such as PBP, EPS, and PCs of cryptophyte algae. A significant difference emerged in growth rate of *C. pyrenoidifera* and *Cryptomonas* sp. at different iron levels. Similarly, some other studies have shown a higher growth rate with increased iron levels, e.g. the green alga *C. vulgaris* and flagellate *Gonyostomum semen* cultures grew better at high iron levels (Liu et al., 2008; Munzner et al., 2021). By contrast, the eustigmatophyte *Nannochloropsis salina*, haptophyte *Pleurochrysis carterae*, and *Chlamydomonas* sp. showed their highest growth rate at low iron levels (Tiamiyu, 2011; Munzner et al., 2021). Furthermore, Weng et al., 2008 found that iron deprivation could lead to slower growth rate in *Cryptomonas* sp. because iron deficiency causes misalignment of chloroplast lamellae, metamorphosis, and twisted thylakoids. It may also weaken algal photosynthesis and general metabolism.

Nevertheless, our practical outcomes indicate that the change in iron level did not have a noticeable impact on the growth rate of the studied cryptophytes, particularly *R. salina*, *C. curvata*, and *C. ozolinii*. Thus, the lowest iron level in our study appears adequate to fulfill the iron requirements for growth of cryptophytes. Consistent with this, Isani et al., 2022 reported no significant difference in growth of *Arthrospira platensis* cultivated at different iron levels (0.84, 3.44, and 6.90 mg L^{-1}). In addition, levels of iron ranging from 1.9 to 10 mg L^{-1} showed no significant effect on the growth of *A. platensis* (Ismaiel et al., 2018). Iron uptake by microalgae depends on the iron demand of the cell and the iron uptake rate, both of which are controlled by cell size. Species with smaller cell size achieve faster iron uptake rate per cell volume than

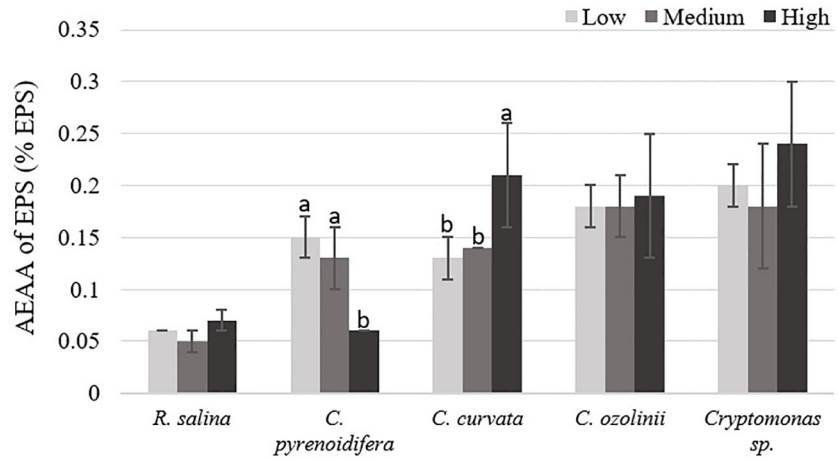

FIGURE 7
Antioxidant capacity (AEAA) of EPS (% EPS) derived from the studied cryptophytes cultured at different iron levels. Significant differences between samples are indicated with different letters as determined by ANOVA comparison ($p < 0.05$).

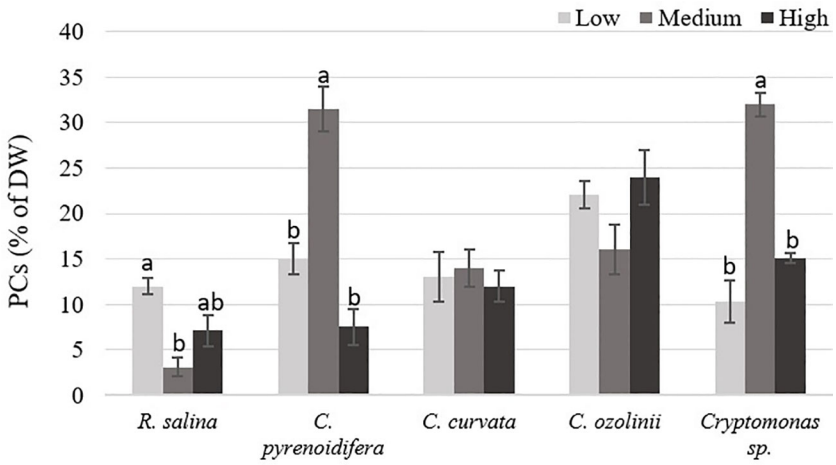

FIGURE 8
phenolic compounds (PCs) content of studied cryptophytes species expressed as percentage of dry weight at different iron levels. Significant differences between samples are indicated with different letters as determined by ANOVA comparison ($p < 0.05$).

those with larger cells and are thus better at fulfilling the iron demand for growth (Marchetti and Maldonado, 2016). Our results support these findings, showing that iron uptake and consequently the growth rate and biomass productivity of *R. salina* with an extremely small cell size [5 µm, with 0.02% dry weight iron content (Supplemental Table 1)] are similar to *C. curvata* with a large cell size (up to 50 µm, with 0.01% dry weight iron content) under low iron level. Moreover, *C. pyrenoidifera* [15–25 × 10–13.5 × 9–12 µm, 0.01% dry weight iron content (Supplemental Table 1)] and *C. ozolinii* [17–29 × 9–13 × 6–9 µm, 0.03% dry weight iron content (Supplemental Table 1)] with smaller cell size than *C. curvata* (35–44 × 18–20 × 17–19 µm) have a higher growth rate and biomass productivity specifically under low iron level. Overall, species with small cell size can cope better with low iron concentration than species with large size (Marchetti and Maldonado, 2016).

In terms of biomass productivity, high iron level resulted in higher biomass productivity in *R. salina*, *C. pyrenoidifera*, and *Cryptomonas* sp. Previous studies on *Chlorella vulgaris* and *Scenedesmus obliquus* demonstrated an increase in biomass production at high iron level (Liu et al., 2008; Abd El Baky et al., 2012). Marine species *R. salina* shows an increasing trend in biomass production with increased iron concentration, while biomass production of *C. curvata* is unaffected by changes in iron level. Hence, the physiological differences of species influence the response to changes of iron concentration. Another reason for lower biomass in iron deficiency is related to the biochemical processes of iron. At the level of iron deficiency, iron ions are released from the functional enzyme aconitase. However, this enzyme cannot catalyze citric acid into isocitric acid, which is an essential chemical reaction in tricarboxylic acid cycle to transform saccharide into ATP (Berg and Tymo, 2002).

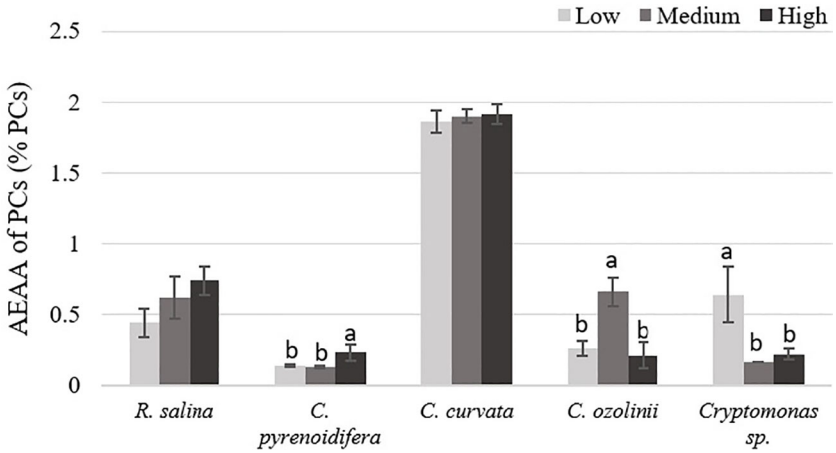

FIGURE 9
Antioxidant capacity (AEAA) of PCs (% PCs) derived from the studied cryptophytes cultured at different iron levels. Significant differences between samples are indicated with different letters as determined by ANOVA comparison ($p < 0.05$).

An increase in iron levels led to the reduction of phycobiliprotein in some of the studied strains. The cultures of *R. salina* showed that by increasing the iron level, the accumulation of phycobiliproteins decreased. This is similar to the results of a study on the cyanobacterium *Arthrospira platensis* (Akbarnezhad et al., 2016). Moreover, phycobiliprotein content at control level was higher than at low and high iron level for *C. pyrenoidifera*, *C. ovata*, and *C. curvata*. Iron is a fundamental micronutrient in phycobiliprotein pigment biosynthesis and a component of the photosynthetic system (Geider and La Roche, 1994). Therefore, its concentration can directly affect the accumulation of phycobiliproteins in microalgae. On the other hand, the location of phycobiliproteins has a significant impact on the absorption of trace elements, particularly iron. In red algae, phycobiliproteins are placed in phycobilisomes, which are anchored to thylakoid membranes (from the stromal or cytosolic side), and phycoerythrin is located in the peripheral areas of the phycobilisomes (Talarico, 1996; Gould et al., 2007). However, in cryptophytes, due to the lack of phycobilisomes and a cell wall, phycobiliproteins are situated in lumenal side of thylakoid membrane, and consequently, their sensitivity to trace elements, including iron, is increased (Kiran and Thanasekaran, 2011; Green, 2019; Spangler et al., 2022).

Although no significant difference existed among EPS at different iron levels due to high deviations between the replicates, visual inspection of the results suggests that high iron level could have a negative effect on EPS accumulation. No reports are available on the effects of iron on EPS production. However, there are a few reports of the effect of iron on its constituent compounds containing protein, lipid, and carbohydrates. Increasing the iron concentration led to lipid accumulation in the green alga *Chlorella vulgaris* (Liu et al., 2008), suggesting that iron can have an effect on enhancing the lipid content in microalgae (Rana and Prajapati, 2021). Interestingly, the green alga *Chlamydomonas reinhardtii* produced the highest lipid content under severe iron deficiency (Devadasu and Subramanyam, 2021). In addition, iron had a negative impact on protein and carbohydrate accumulation, as low iron concentration resulted in high protein content in *Chlorella* sp. and high carbohydrate production in *C. reinhardtii* (Iriani et al., 2011; Devadasu and Subramanyam, 2021). However, a study of the effect of iron on biochemical content derived from a mix culture of microalgae revealed a positive correlation between iron concentration and protein content (Ermis et al., 2020). These different reactions of constituent compounds of EPS to changes in iron concentration make it difficult to understand EPS variation with iron changes in cultures.

The changes of PC content at different iron levels can arise from iron stress and this critical condition can be variable for each species. While the highest PC content of *C. pyrenoidifera*, *C. curvata*, and *Cryptomonas* sp. was at medium iron level (iron stress), *R. salina* and *C. ozolinii* produced the highest PC content at low and high iron levels (iron stress), respectively.

The study by Lopez et al., 2015 showed that by increasing iron level the quantity of total PCs of *Dunaliella tertiolecta* diminished. When the alga was under iron stress, the growth and production of biomass decreased, while the quantity of polyphenols increased (Lopez et al., 2015). This is consistent with our results for *R. salina*, *C. pyrenoidifera*, and *Cryptomonas* sp. On the other hand, the PC content of the diatom *Phaeodactylum tricornutum* under high iron level has been shown to be higher (Rico et al., 2012), similar to our study of *C. ozolinii*. This can be due to the role of PCs in controlling osmotic stress. Under osmotic stress, by binding polyphenols to metal ion, polyphenols act as chelate towards metals, protecting cells from metal toxicity and oxidative damage (Jung et al., 2003). According to Isani et al., 2022, there was no significant difference in PC content of *A. platensis* at different iron levels, similar to our results for *C. ozolinii* and *C. curvata*.

Overall, the quantity of PCs and iron concentration in the cell have a negative relationship (Lopez et al., 2015). A high concentration of PCs prevents excessive entrance of iron to cells. The effect of PCs as organic ligands to form a complex with Fe^{3+} and to reduce Fe^{3+} to bioavailable Fe^{2+} has been proven (Rose and Waite, 2003). Thus, at low Fe^{2+} concentration the biomass production declines steeply (Khamoushi et al., 2020). Outcomes of this study for *R. salina*, *C. pyrenoidifera*, and *Cryptomonas* sp. confirm this connection. Although there is limited literature on the effect of different iron concentrations on PC content of microalgae, especially cryptophytes, based on physiological characteristics of each species, they can have a distinct response to iron changes in cultures. Besides the impact of iron levels on PC production, physiological characteristics of each species can be effective in producing PCs under different iron concentrations. Excessively low or high concentrations of iron induce stress, which can inhibit the metabolism of the species (Xing et al., 2007). However, the limits for excessively low and high iron concentrations are different for each species and could have a distinct effect on growth and biochemical accumulation in each species.

According to Iriani et al., 2011, in addition to iron level, culturing time can affect PC production. In the study by Iriani et al., 2011, on *Chlorella* sp. after 7 days of incubation under different iron levels (0.35, 4.89, 9.44, and 13.99 mg L^{-1}), the highest PC content was at 0.35, followed by 9.44 mg L^{-1} iron concentrations, consistent with our results not showing a direct correlation between iron level and PC content. However, after 14 days, the highest PC content of *Chlorella* sp. was at high iron level (13.99 mg L^{-1}), and after 21 days, the highest PC content was at a lower iron level (0.35 mg L^{-1}; Iriani et al., 2011). In summary, variation in culturing time can have an effect on PC production. However, this correlation has not been explored in the present study.

The results of this research indicate that the antioxidant activity of studied bioactive compounds depends on two factors. First, the antioxidant activity of each biochemical is different. Overall, PCs have higher antioxidant activity than PE and particularly EPS. Second, there are also species-specific differences; no regular pattern exists for changing the antioxidant activity at different iron levels, and each studied strain follows its own specific pattern under different culture conditions. Other studies have found that different strains of the same taxa show different antioxidant capacity; e.g. *Cryptomonas pyrenoidifera* ACOI 1847

contains higher antioxidant capacity than *C. pyrenoidifera* ACOI 1850 (Assuncao et al., 2017).

Few reports have examined the effect of iron on the antioxidant activity of microalgae and their biomolecules. However, iron plays a key role in the production of reactive oxygen species (ROS) *via* the Harber-Weiss mechanism, the Fenton reaction, and the electron transport chain (Gauthier et al., 2020). High iron concentration induces oxidative stress, and accordingly, microalga produce antioxidants as a defensive mechanism (Gauthier et al., 2020). The results of their study are confirmed by our findings of antioxidant activity of bioactive compounds. By contrast, the biomass of *Arthrospira platensis* cultivated at the lowest iron level was noted in another study to contain the highest antioxidant activity (Spangler et al., 2022). However, in their study, the antioxidant activity of the whole biomass was reported, not the antioxidant activity of specific biochemicals, which have been demonstrated as in our study.

Based on our previous study, the antioxidant activities of the investigated compounds were high (IC50< 50 µl mL-1) (Abidizadegan et al., 2022). In the present study, we also show that the quantity of antioxidants is considerable; PE derived from *C. ozolinii* is capable of producing ~6 mg EAA g^{-1} PE, EPS of Cryptomonas sp. can produce ~2.5 mg EAA g^{-1} EPS, and high antioxidant quantity is observed in PCs extracted from *C. curvata*, with ~19 mg EAA g^{-1} PCs. The results obtained for antioxidant capacity in this study are difficult to compare with those of other studies due to differences in methods and representation of data, e.g. antioxidant capacity can be presented as Trolox equivalent antioxidant capacity, ferric-reducing antioxidant power, or IC50. Additionally, unlike our study showing antioxidant activity of different algal compounds, other published studies have only evaluated the total antioxidant activity. The highest total antioxidant activities measured in microalgae are for the marine diatom *Navicula clavata* and the green microalgae *Chlorella marina* and *Dunaliella salina*, which have shown total antioxidant activity of ~0.6, 1.0, and 0.9 mg EAA g^{-1} dry weight, respectively (Hemalatha et al., 2013). A study by Haoujar et al., 2022 showed total antioxidant capacity of ~0.40 mg EAA g^{-1} dry weight for the green microalgae *Nannochloropsis gaditana* and *Tetraselmis suecica* and for the marine diatom *Phaeodactylum tricornutum*. Therefore, since antioxidant activity of PE, EPS, and PCs derived from cryptophyte algae combined is more than the total antioxidant activity of other studied microalgal species, cryptophyte algae could be a potential source of natural antioxidants for the food, cosmetic, and nutraceutical industries.

4.1 Commercial potential

For thousands of years, humans have been benefitting from microalgae (Koyande et al., 2019), and over the last five decades the field of microalgal biotechnology has grown and expanded significantly. However, despite recent advancements, the range of algal products available for commercial use is still relatively limited. Although progress has been made in applying microalgae to produce a wide range of bioproducts, only a small number of the vast species of microalgae has been examined. Cryptophytes are one of the promising microalgae with high nutritional value, including a rich polyunsaturated fatty acid (PUFA) profile, high protein content, and antioxidant pigments, warranting more attention in academic and industry research.

According to the results of the present study and our previous report (Abidizadegan et al., 2022), cryptophyte species are able to produce PBP pigment content of about 1-35% dry weight. Additionally, a study by Latsos et al., 2021 showed that *Rhodomonas* sp. can produce phycoerythrin content ~28% of dry weight. In comparison to well-known phycoerythrin producing strains, including *Spirulina* sp. (~1.4% DW), *Oscillatoria* sp. (1.8% DW), and *Porphyridium purpureum* (12.58% DW), cryptophytes have capability to produce higher phycoerythrin content (Ji et al., 2023). Compared with other PBP producers, including cyanobacteria and red algae, cryptophytes produce only one type of PBP by each strain, simplifying the production process of PBP. Additionally, cryptophytes possess PBP with lower molecular weight, making them practical in terms of fluorescent labeling application. The lack of a strong cell wall in cryptophytes is another advantage of this algal group to facilitate biomass processing and PBP extraction. Thus, cryptophytes could be considered a reliable source of PBP to be applied as natural color in food and cosmetic industries and as fluorescent probes and analytical reagents in biomedical science (Garcia et al., 2021; Mercier et al., 2022). Furthermore, phycoerythrin has shown pharmacological and biological properties including anti-inflammation and anti-tumor effects, as well as preventing Alzheimer disease and liver cancer (Ji et al., 2023).

High microalgal EPS productivity is essential for cost-effective global EPS production. Identifying new microalgae with high EPS yield is a priority to facilitate its industrial development. The EPS-producing capability of cryptophytes in this study is remarkable, as the amount of EPS secreted from R. salina is about 50% dry weight. Therefore, compared with the microalgal species studied to date, cryptophytes would be a rich source of beneficial EPS in industries associated with the production of paper, paint, food, textile, and drugs, among others, due to having thickening, stabilizing, and gelling capacities (Tiwari et al., 2020).

Phenolic compounds are promising substances with health-giving properties that are valuable to many industries. Cryptophyte algae produce PC content of about 30% dry weight (*C. pyrenoidifera* and *Cryptomonas* sp.) and are capable of being additional or alternative natural sources of PCs in food, pharmaceutical industries, and healthcare products (Cory et al., 2018).

Data derived from this study demonstrate that cryptophytes could be considered a natural antioxidant source. For example, phycoerythrin derived from *C. ozolinii* contains ~0.6% antioxidant capacity. The highest antioxidant content of EPS is in *Cryptomonas* sp., at ~0.2%. Phenolic compounds of cryptophytes indicate the highest antioxidant capacity, which PCs extracted from *C. curvata* involves ~2% antioxidant capacity.

5 Conclusion

This study investigated the effect of iron on bioactive compound accumulation and antioxidant activity of these bioactive compounds isolated from different cryptophyte strains. In addition to iron impact, each strain has a specific response to change in iron level. Based on our results, cryptophytes could be a natural source of phenolic compounds and particularly extracellular polysaccharides, in addition to the phycoerythrin pigment. The antioxidant capacity of the investigated cryptophytes was also significant. The future of cryptophytes thus looks bright and their potential in various applications should be considered. Improving the growth rate of cryptophytes will be a challenge, but it can be addressed through a better understanding of their physiology and optimizing the culture conditions and procedures, including photobioreactors.

Data availability statement

The raw data supporting the conclusions of this article will be made available by the authors, to any qualified researcher with reasonable request.

Author contributions

MA performed the research, analyzed the data, and wrote the manuscript. EP and JB contributed to the study design and manuscript revisions. All authors have reviewed, discussed and agreed to the authorship and submission of the manuscript.

Funding

This research was funded by Jenny and Antti Wihuri Foundation, grant number 00200005.

Acknowledgments

The authors gratefully thank the Language Center of the University of Helsinki for editing the English of this paper.

Conflict of interest

The authors declare that the research was conducted in the absence of any commercial or financial relationships that could be construed as a potential conflict of interest.

Publisher's note

All claims expressed in this article are solely those of the authors and do not necessarily represent those of their affiliated organizations, or those of the publisher, the editors and the reviewers. Any product that may be evaluated in this article, or claim that may be made by its manufacturer, is not guaranteed or endorsed by the publisher.

Supplementary material

The Supplementary Material for this article can be found online at: https://www.frontiersin.org/articles/10.3389/fpls.2023.1208724/full#supplementary-material

References

Abd El Baky, H. H., El-Baroty, G. S., Bouaid, A., Martinez, M., and Aracil, J. (2012). Enhancement of lipid accumulation in *Scenedesmus obliquus* by Optimizing CO2 and Fe^{3+} levels for biodiesel production. *Bioresour. Technol.* 119, 429–432. doi: 10.1016/j.biortech.2012.05.104

Abidizadegan, M., Blomster, J., Fewer, D., and Peltomaa, E. (2022). Promising biomolecules with high antioxidant capacity derived from cryptophyte algae grown under different light conditions. *J. Biol.* 11, 8. doi: 10.3390/biology11081112

Akbarnezhad, M., Mehrgan, M. S., Kamali, A., and Baboli, M. (2016). Bioaccumulation of Fe2+ and its effects on growth and pigment content of Spirulina (*Arthrospira platensis*). *Aquac Aquarium Conserv. Legis.* 9, 227–238. doi: 10.22092/ijfs.2019.120614

Assuncao, M. F. G., Amaral, R., Martins, C. B., Ferreira, J. D., Ressurreicao, S., Santos, S. D., et al. (2017). Screening microalgae as potential sources of antioxidants. *Appl. Phycol.* 29, 865–877. doi: 10.1007/s10811-016-0980-7

Berg, J. M., and Tymo, J. L. (2002). *Biochemistry* (New York: Freeman and Company).

Chang, S. P., Sheu, H. L., and Lee, Y. C. (2019). Comparison of EPS extraction efficiencies from *Spirogyra fluviatilis* by chemical and physical extraction methods. *Int. J. Biosci. Biochem. Bioinform.* 9, 4. doi: 10.17706/ijbbb.2019.9.4.202-209

Chen, C., Tang, T., Shi, Q., Zhou, Z., and Fan, J. (2022). The potential and challenge of microalgae as promising future food source. *Trends Food Sci. Technol.* 126, 99–112. doi: 10.1016/j.tifs.2022.06.016

Clay, B. L. (2015). "Cryptomonads," in *Freshwater algae of North America: ecology and classification*. Eds. J. D. Wehr, R. G. Sheath and P. Kociolek (London, UK: Elsevier), 809–850.

Cory, H., Passarelli, S., Szeto, J., Tamez, M., and Mattei, J. (2018). The role of polyphenols in human health and food system. *Front. Nutr.* 5. doi: 10.3389/fnut.2018.00087

Cunningham, B. R., Greenwold, M. J., Lachenmyer, E. M., Heidenreich, K. M., Davis, A. C., Dudycha, J. L., et al. (2019). Light capture and pigment diversity in marine and freshwater cryptophytes. *J. Phycol.* 55, 3. doi: 10.1111/jpy.12816

Devadasu, E., and Subramanyam, R. (2021). Enhanced lipid production in *Chlamydomonas reinhardtii* caused by severe Iron deficiency. *Front. Plant Sci.* 12. doi: 10.3389/fpls.2021.615577

Ermis, H., Guven-Gulhan, U., Cakir, T., and Altinbas, M. (2020). Effect of iron and magnesium addition on population dynamics and high value product of microalgae grown in anaerobic liquid digestate. *Sci. Rep.* 10, 3510. doi: 10.1038/s41598-020-60622-1

Frazzini, S., Scaglia, E., Dell'Anno, M., Reggi, S., Panseri, S., Giromini, C., et al. (2022). Antioxidant and antimicrobial activity of algal and cyanobacterial extracts: an *in vitro* study. *Antioxidants* 11, 992. doi: 10.3390/antiox11050992

Garcia, A. B., Longo, E., Murillo, M. C., and Bermejo, R. (2021). Using a B-phycoerythrin extract as a natural colorant: application in milk-based products. *Molecules* 26, 297 doi: 10.3390/molecules26020297

Gauthier, M. R., Senhorinho, G. N. A., and Scott, J. A. (2020). Microalgae under environmental stress as a source of antioxidant. *Algal Res.* 52, 102104. doi: 10.1016/j.algal.2020.102104

Geider, R. J., and La Roche, J. (1994). The role of iron in phytoplankton photosynthesis, and the potential for iron-limitation of primary productivity in the sea. *Photosynth. Res.* 39, 275–301. doi: 10.1007/BF00014588

Giroldo, D., Vieira, A., and Paulsen, B. S. (2005). Extracellular polysaccharides produced by a tropical cryptophyte as a carbon source for natural bacterial populations. *Eur. J. Phycol.* 40, 241–249. doi: 10.1080/09670260500192810

Gould, S. B., Fan, E., Hempel, F., Maier, U. G., and Klosgen, R. B. (2007). Translocation of phycoerythrin α subunit across five biological membranes. *J. Biol. Chem.* 282, 41. doi: 10.1074/jbc.M701869200

Green, B. R. (2019). What happened to the phycobilisome. *Biomolecules* 9, 11. doi: 10.3390/biom9110748

Guillard, R. R. L., and Lorenzen, C. J. (1972). Yellow green algae with chlorophyllide. *J. Phycol.* 8, 1. doi: 10.1111/j.1529-8817.1972.tb03995.x

Guillard, R. R. L., and Ryther, J. H. (1962). Studies of marine planktonic diatoms. I. *Cyclotella nana* hustedt and *Detonula confervacea* Cleve. *Can. J. Microbiol.* 8, 2. doi: 10.1139/m62-029

Haoujar, I., Cacciola, F., Chairi, H., Altemimi, A., Essafi, A., Abrini, J., et al. (2022). Evaluation of the antioxidant properties of microalgae naturally isolated from Mediterranean Morocco. *Egypt. J. Aquat. Biol. Fish.* 26, 4. doi: 10.21608/EJABF.2022.249822

Hemalatha, A., Girija, K., Parthiban, C., Saranya, C., and Anantharaman, P. (2013). Antioxidant properties and total phenolic content of a marine diatom, *Navicula clavata* and green microalgae, *Chlorella marina* and *Dunaliella salina*. *Adv. Appl. Sci. Res.* 4, 151–157.

Hill, D. R. A., and Rowan, K. S. (1989). The biliproteins of the cryptophyceae. *Phycologia* 28, 4. doi: 10.2216/i0031-8884-28-4-455.1

Iriani, D., Suriyaphan, O., and Chaiyanate, N. (2011). Effect of iron concentration on growth, protein content and total phenolic content of Chlorella sp. cultured in basal medium. *Sains Malays.* 40, 353–358.

Irondi, A. E., Oboh, G., and Akinrunde, J. K. (2012). Comparative and synergistic antioxidant properties of *Carica papaya* and *Azadarichta indica* leaves. *Int. J. Pharm. Sci. Res.* 3, 4773–4779.

Isani, G., Niccolai, A., Andreani, G., Dalmonte, T., Bellei, E., Bertocchi, M., et al. (2022). Iron speciation and iron binding proteins in *Arthrospira platensis* grown in media containing different iron concentrations. *Int J Mol Sci.* 23, 6283. doi: 10.3390/ijms23116283

Ismaiel, M. M. S., Piercey-Normore, M. D., and Rampitsch, C. (2018). Proteomic analyses of the cyanobacterium *Arthrospira* (*Spirulina*) *platensis* under iron and salinity stress. *J. Exp. Bot.* 147, 15. doi: 10.1016/j.envexpbot.2017.11.013

Ji, L., Qiu, S., Wang, Z., Zhao, C., Tang, B., Gao, Z., et al. (2023). Phycobiliproteins from algae: Current updates in sustainable production and applications in food and health. *Food Res. Int.* 167, 112737. doi: 10.1016/j.foodres.2023.112737

Jung, C., Maeder, V., Funk, F., Frey, B., Sticher, H., and Frossard, E. (2003). Release of phenols from *Lupinus albus* L. roots exposed to Cu and their possible role in Cu detoxification. *Plant Soil.* 252, 301–312. doi: 10.1023/A:1024775803759

Khamoushi, A., Tafakori, V., Zahed, M. A., Eghrari Gayglou, S., and Angaji, S. A. (2020). Augmenting the expression of accD and rbcL genes using optimized iron concentration to achieve higher biomass and biodiesel in *Chlorella vulgaris*. *Biotechnol. Lett.* 42, 12. doi: 10.1007/s10529-020-02973-3

Kim, E. Y., Choi, Y. H., and Nam, T. J. (2018). Identification and antioxidant activity of synthetic peptides from phycobiliproteins of *Pyropia yezoensis*. *Int. J. Mol. Med.* 42, 2. doi: 10.3892/ijmm.2018.3650

Kiran, B., and Thanasekaran, K. (2011). Metal tolerance of an indigenous cyanobacterial strain, *Lyngbya putealis*. *Int. Biodeterior. Biodegrad.* 65, 8. doi: 10.1016/j.ibiod.2011.08.011

Korzeniowska, K., Leska, B., and Wieczorek, P. P. (2020). Isolation and determination of phenolic compounds from freshwater *Cladophora glomerata*. *Algal Res.* 48, 101912. doi: 10.1016/j.algal.2020.101912

Koyande, A. K., Chew, K. W., Rambabu, K., Tao, Y., Chu, D., and Show, P. (2019). Microalgae: A potential alternative to health supplementation for humans. *Food. Sci. Hum. Wellness.* 8, 1. doi: 10.1016/j.fshw.2019.03.001

Lawrenz, E., Fedewa, E. J., and Richardson, T. L. (2011). Extraction protocols for the quantification of phycobilins in aqueous phytoplankton extracts. *J. Appl. Phycol.* 23, 5. doi: 10.1007/s10811-010-9600-0

Latsos, C., van Houcke, J., Blommaert, L., Verbeeke, G.P., Kromkamp, J., and Timmermans, K.R. (2021). Effect of light quality and quantity on productivity and phycoerythrin concentration in the cryptophyte Rhodomonas sp. *J. Appl. Phycol.* 33, 729–741. doi: org/10.1007/s10811-020-02338-3

Leong, L. P., and Shui, G. (2002). An investigation of antioxidant capacity of fruits in Singapore markets. *Food Chem.* 76, 1. doi: 10.1016/S0308-8146(01)00251-5

Liu, J., Dong, S., Liu, X., and Ma, S. (2000). Responses of the macroalga *Gracilaria tenuistipitata* var. liui (Rhodophyta) to iron stress. *J. Appl. Phycol.* 12, 605–612. doi: 10.1023/A:1026523213818

Liu, J., Tan, K., He, L., Qiu, Y., Tan, W., Guo, Y., et al. (2018). Effect of limitation of iron and manganese on microalgae growth in fresh water. *Microbiol. (Reading).* 164, 12. doi: 10.1099/mic.0.000735

Liu, Z. Y., Wang, G. C., and Zhou, B. C. (2008). Effect of iron on growth and lipid accumulation in *Chlorella vulgaris*. *Bioresour Technol.* 99, 11. doi: 10.1016/j.biortech.2007.09.073

Lopez, A., Rico, M., Santana-Casiano, J. M., Gonzalez, A. G., and Gonzalez-Davila, M. (2015). Phenolic profile of *Dunaliella tertiolecta* growing under high levels of copper and iron. *Envirn. Sci. pollut. Res.* 22, 19. doi: 10.1007/s11356-015-4717-y

Marchetti, A., and Maldonado, M. T. (2016). "Iron," in *The Physiology of Microalgae*. Eds. J. Beardall and J. A. Raven (New York, US: Springer), 233–279.

Mercier, L., Peltomaa, E., and Ojala, A. (2022). Comparative analysis of phycoerythrin production in cryptophytes. *J. Appl. Phycol.* 34, 789–797. doi: 10.1007/s10811-021-02657-z

Mousavian, Z., Safavi, M., Azizmohseni, F., Hadizadeh, M., and Mirdamadi, S. (2022). Characterization, antioxidant and anticoagulant properties of exopolysaccharide from marine microlage. *AMB Express.* 12, 27. doi: 10.1186/s13568-022-01365-2

Munzner, K., Gollnisch, R., Rengefors, K., Koreiviene, J., and Lindstrom, E. S. (2021). High iron requirements for growth in the nuisance alga *Gonyostomum semen* (Raphidophyceae). *J. Phycol.* 57, 4. doi: 10.1111/jpy.13170

Padrova, K., Lukavsky, J., Nedbalova, L., Cejkova, A., Cajthaml, T., Sigler, K., et al. (2015). Trace concentrations of iron nanoparticles cause overproduction of biomass and lipids during cultivation of cyanobacteria and microalgae. *J. Appl. Phycol.* 27, 4. doi: 10.1007/s10811-014-0477-1

Peltomaa, E., Johnson, M. D., and Taipale, S. J. (2018). Marine cryptophytes are great source of EPA and DHA. *Mar. Drugs* 16, 1. doi: 10.3390/md16010003

Punampalam, R., Khoo, K. S., and Nw, S. (2018). Evaluation of antioxidant properties of phycobiliproteins and phenolic compounds extracted form *Bangia atropurpurea*. Mal. *J. Fund. Appl. Sci.* 14, 2. doi: 10.11113/mjfas.v14n2.1096

Rachidi, F., Benhima, R., Sbabou, L., and El Arroussi, H. (2020). Microalgae polysaccharides bio-stimulating effect on tomato plants: growth and metabolic distribution. *Biotechnol. Rep.* 25, e00426. doi: 10.1016/j.btre.2020.e00426

Rana, M. S., and Prajapati, S. K. (2021). Resolving the dilemma of iron bioavailability to microalgae for commercial sustenance. *Algal Res.* 59, 102458. doi: 10.1016/j.algal.2021.102458

Rastar, M., Hosseini Shekarabi, S. P., Shamsaie Mehrgan, M., and Sabz, S. (2018). Effects of iron and zinc concentrations on growth performance and biochemical composition of *Haematococcus pluvialis*: A comparison between nanoparticles and their corresponding metals bulks. *J. Algal Biomass Util.* 9, 59–67.

Rico, M., Lopez, A., Santana-Casiano, J. M., Gonzalez, A. G., and Gonzalez-Davila, M. (2012). Variability of the phenolic profile in the diatom *Phaeodactylum tricornutum* growing under copper and iron stress. *Limnol. Oceanogr.* 58, 1. doi: 10.4319/lo.2013.58.1.0144

Roman, R. B., Alvarez-Pez, J. M., Acien Fernandez, F. G., and Grima, E. M. (2002). Recovery of pure B-phycoerythrin from the microalga *Porphyridium cruentum*. *J. Biotechnol.* 93, 1. doi: 10.1016/S0168-1656(01)00385-6

Rose, A. L., and Waite, T. D. (2003). Kinetics of iron complexation by dissolved natural organic matter in coastal water. *Mar. Chem.* 84, 1–2. doi: 10.1016/S0304-4203(03)00113-0

Schoffman, H., Li, H., Shaked, Y., and Keren, N. (2016). Iron-nutrient interactions within phytoplankton. *Front. Plant Sci.* 7. doi: 10.3389/fpls.2016.01223

Spangler, L. C., Yu, M., Jeffrey, P. D., and Scholes, G. D. (2022). Controllable phycobilin modification: an alternative photoacclimation response in cryptophyte algae. *ACS Cent. Sci.* 8, 3. doi: 10.1021/acscentsci.1c01209

Strieth, D., Stiefelmaier, J., Wrabl, B., Schwing, J., Schmeckebier, A., Nonno, S. D., et al. (2020). A new strategy for a combined isolation of EPS and pigments from cyanobacteria. *J. Appl. Phycol.* 32, 1729–1740. doi: 10.1007/s10811-020-02063-x

Talarico, L. (1996). Phycobiliproteins and phycobilisomes in red algae: adaptive responses to light. *Sci. Mar.* 60, 205–222.

Telford, W. G., Moss, M. W., Morseman, J. P., and Allnutt, F. C. (2001). Cyanobacterial stabilized phycobilisomes as fluorochromes for extracellular antigen detection by flow cytometry. *J. Immunol. Methods* 254, 1–2. doi: 10.1016/s0022-1759(01)00367-2

Tiamiyu, G. A. (2011). *Effect of nitrogen, iron and temperature on yield and composition of microalgae* (Oklahoma: Oklahoma State University). dissertation/master's thesis.

Tiwari, O. N., Sasmal, S., Kataria, A. K., and Devi, I. (2020). Application of microbial extracellular carbohydrate polymeric substances in food and allied industries. *3 Biotech.* 10, 5. doi: 10.1007/s13205-020-02200-w

Wang, N., Dai, L., Chen, Z., Li, T., Wu, J., Wu, H., et al. (2022). Extraction optimization, physiochemical characterization, and antioxidant activity of polysaccharides from Rhodosorus sp. SCSIO-45730. *J. Appl. Phycol.* 34, 285–299. doi: 10.1007/s10811-021-02646-2

Weng, H. X., Qin, Y. C., Sun, X. W., and Chen, J. F. (2008). Limitation and combined effects of iron and phosphorus on the growth of *Prorocentrum micans* Ehrenberg (Dinophyceae) and Cryptomonas sp. (Cryptophyceae). *Environ. Geol.* 55, 1431–1436. doi: 10.1007/s00254-007-1093-z

Weng, H. X., Sun, X. W., Qin, Y. C., and Chen, J. F. (2007). Effect of irradiance on Fe and P uptake by Cryptomonas sp. *Geochimica* 73, 3–4. doi: 10.1016/j.ecss.2007.02.002

Xiao, R., and Zheng, Y. (2016). Overview of microalgal extracellular polymeric substances (EPS) and their applications. *Biotechnol* 34, 7. doi: 10.1016/j.biotechadv.2016.08.004

Xing, W., Huang, W., Li, D., and Liu, Y. (2007). Effects of iron on growth, pigment content, photosystem II efficiency, and siderphores production of *Microcystis aeruginosa* and *Microcystis wesenbergii*. *Curr. Microbiol.* 55, 2. doi: 10.1007/s00284-006-0470-2

frontiers | Frontiers in Plant Science

TYPE Original Research
PUBLISHED 29 September 2023
DOI 10.3389/fpls.2023.1265018

OPEN ACCESS

EDITED BY
Eman A. Mahmoud,
Damietta University, Egypt

REVIEWED BY
Ilkay Erdogan Orhan,
Gazi University, Türkiye
Tlili Imen,
Carthage University, Tunisia

*CORRESPONDENCE
Qunxian Deng
dqxlwj@sina.com.cn

†These authors have contributed equally to this work

RECEIVED 21 July 2023
ACCEPTED 13 September 2023
PUBLISHED 29 September 2023

CITATION
Zhang H, Wang M, Yu G, Pu J, Tian K, Tang X, Du Y, Wu H, Hu J, Luo X, Lin L and Deng Q (2023) Comparative analysis of the phenolic contents and antioxidant activities of different parts of two pomegranate (*Punica granatum* L.) Cultivars: 'Tunisia' and 'Qingpi'. *Front. Plant Sci.* 14:1265018. doi: 10.3389/fpls.2023.1265018

Comparative analysis of the phenolic contents and antioxidant activities of different parts of two pomegranate (*Punica granatum* L.) Cultivars: 'Tunisia' and 'Qingpi'

Huifen Zhang[1†], Miao Wang[1†], Guoqiang Yu[1], Jing Pu[1], Kun Tian[1], Xiaofu Tang[1], Ying Du[1], Hongxia Wu[2], Jiong Hu[3], Xian Luo[1], Lijin Lin[1] and Qunxian Deng[1*]

[1]College of Horticulture, Sichuan Agricultural University, ChengDu, Sichuan, China, [2]Rural Professional Technology Association of Huili, Huili, Sichuan, China, [3]Science and Technology Association of Huili, Huili, Sichuan, China

Pomegranate (*Punica granatum* L.), with its abundant phenolic substances and strong antioxidant activity, holds significant research and utilization potential across various organs. However, there have been few studies on the phenolic content and antioxidant activity of different parts of pomegranate, especially the placenta. This study investigated the phenolic content and antioxidant activity of fruits, flowers, and leaves of two pomegranate varieties, 'Tunisia' and 'Qingpi', throughout their growth and development. Results indicated significant variations in phenolic content among different organs, with petals exhibiting the highest total polyphenol content (TPC, 49.40 mg GAE/g FW) and total anthocyanin content (TMAC, 1938.54 nmol/g FW). Placenta contained the highest levels of total flavonoids (TFC, 173.58 mg RE/g FW) and punicalagin (109.30 mg/g FW). The peel had the highest content of total flavanols (TFAC, 19.42 mg CE/g FW). Over the course of pomegranate development, total polyphenols, total flavonoids, total flavanols, punicalagin, and antioxidant activity declined in different organs. Antioxidant activity followed the order: fruit > flower > leaf, with the placenta exhibiting the highest antioxidant activity among fruits. Antioxidant activity showed a significant positive correlation with total polyphenols (R^2 = 0.77-1.00), total flavonoids (R^2 = 0.71-0.99, except tegmens), and punicalagin (R^2 = 0.71-1.00). This study provides a comparative analysis of the phenolic content and antioxidant activity in different organs of pomegranate, highlighting the placenta as the primary source of punicalagin. This study provides a theoretical basis for the development and utilization of pomegranate phenolic compounds.

KEYWORDS

***Punica granatum* L., phenolic contents, antioxidant activity, different parts, cultivars**

1 Introduction

Pomegranate (*Punica granatum* L.) is a small arbor or shrub belonging to the family Lythraceae. It is used for both food and medicinal purposes (Zhao and Yuan, 2021; Wang et al., 2023). Pomegranate is known for its strong antioxidant properties due to its abundant phenolic compounds, and it has been traditionally used for preventing and treating various diseases, such as heart disease and diabetes (Asgary et al., 2014; Bahmani et al., 2014; Asgharpour and Alirezaei, 2021). Natural extracts from pomegranate are also widely used in food products as antioxidants and antimicrobial agents (Shaygannia et al., 2016; Martínez et al., 2019; Essid et al., 2020; Parafati et al., 2021), thus promoting greater research attention on antioxidants and application of pomegranates.

The antioxidant activity of pomegranate is attributed to its phenolic substances, including polyphenols, flavonoids, flavanols, and anthocyanins (Gözlekçi et al., 2011; Ávila-Gálvez et al., 2019; Yuan et al., 2022). Flavonoids scavenge oxygen free radicals, prevent cell degradation, and possess anti-aging properties (Hostetler et al., 2017; Ganai et al., 2021). Flavanols exhibit antioxidant, anti-tumor, anti-inflammatory, and antimicrobial effects (Kopustinskiene et al., 2020; Chagas et al., 2022). Anthocyanins, on the other hand, are edible polyphenolic pigments with strong free radical scavenging ability and anti-cancer properties (Silva et al., 2017; Wang et al., 2023). Indicators such as total polyphenol content (TPC), total flavonoid content (TFC), total flavanol content (TFAC), and total anthocyanin content (TMAC) are often used to assess the antioxidant properties of plants. Pomegranate peel, tegmen, juice, flower, and leaf are rich sources of phenolic substances (Marcelino et al., 2023). Man et al. (2022). identified 64 phenolic compounds in the pomegranate peel. Pomegranate flowers contain polyphenols, flavonoids, and triterpenes (Liu and Seeram, 2018; Niknam et al., 2021; Yisimayili and Chao, 2022), while pomegranate leaves have been found to contain various compounds such as flavonoids, quercetin, tannic acid, ursolic acid, and ellagic tannins (Hussein et al., 1997). Punicalagin is the most abundant polyphenol in pomegranate (Seeram et al., 2005), and it is found in pomegranate fruit as well as in the leaves of *Terminalia chebula* Retz. and *Terminalia catappa* L. (Chen et al., 2009; Mo et al., 2019). Gull et al. (2021) found that the punicalagin content was related to the antioxidant capacity.

Pomegranates are commercially cultivated in over 30 countries, including India, Iran, Spain, China, and the United States (Jaime et al., 2013; Derakhshan et al., 2018). China is one of the largest pomegranate producers, with cultivation dating back over 2000 years (Zhao et al., 2015). Huili is a major pomegranate-producing area in China, with regions such as Huili, Kaifeng, Xingyang, Yicheng, Huaiyuan, Lintong, Mengzi, and Yecheng being the primary distribution areas (Peng et al., 2020). However, there is a lack of studies on the nutritional and functional substances of the main pomegranate varieties in Huili, as well as product development. Although some studies have investigated changes in phenolic content and antioxidant activity during the development of pomegranate fruits, flowers, and leaves (Gözlekçi et al., 2011; Bekir et al., 2013a; Bekir et al., 2013b), there is limited research on the phenolic content and antioxidant activity in different parts of pomegranate. In particular, there is a lack of understanding of phenolic content in placenta. Therefore, this study aims to explore the changes in phenolic content and antioxidant activity during the development of different parts of pomegranate fruits, flowers, and leaves using the 'Tunisia' and 'Qingpi' pomegranate cultivars, which are prevalent in Huili. The findings of this study can provide valuable insights for the utilization and processing of pomegranate.

2 Materials and methods

2.1 Plant material

The materials used in this study were 7-year-old 'Qingpi' (identified by Pomegranate Research Institute, Huili city, Sichuan Province, China) pomegranate trees and 6-year-old 'Tunisia' (identified by Zhongfu Liu, Henan Provincial Economic Forestry and Tree Seedling Workstation, Henan Province, China) trees grafted onto 'Qingpi'. These trees were located in Zhangguan Town, Huili City, Sichuan Province (26° 51′ N, 102° 29′ E, altitude 1780 m). Leaf samples without obvious pests and diseases in the middle of the branches were collected at three different stages: young leaf expansion (T1, March 21, 2021), turning green (T2, April 5, 2021), and mature (T3, April 21, 2021). For flower samples, both normal and abnormal flowers without diseases or insect pests were collected (April 23, 2021) during the bud period and full-blossom period. The calyx, petals, stamens, and ovaries were sampled separately. The peel, placenta, septum, tegmen, and testa (Juice source) of fruits were sampled 7 times (Samples have been taken every 15 days starting May 28, 2021) from the young fruit stage to the mature fruit stage, including at different stages: 30, 45, 60, 75, 90, 105, and 120 days after flowering (DAF) (S1, S2, S3, S4, S5, S6, and S7, respectively). More than thirty leaves, flowers and fruits of both pomegranate varieties were collected with three biological replicates. Samples were immediately transported to the laboratory, pre-cooled with liquid nitrogen, and stored at -80°C for further analysis.

2.2 Extraction and determination of phenolic compounds

2.2.1 Extraction of phenolic compounds

TPC, TFC, and TFAC extraction followed the method by Ozgen et al. (2008). The extraction solution consisted of 70% methanol, 28% anhydrous ethanol, and 2% formic acid (*v/v*). A 0.2 g sample was ground with liquid nitrogen and placed in a centrifuge tube. Subsequently, 5 mL of the extraction solution was added, followed by 30 min of ultrasonic extraction. After shaking at 250 rpm at 30°C for 2 h, the extract was centrifuged at 8000 rpm for 10 min at 4°C. The supernatant was then filtered through a 0.45 μm needle tube filter for analysis of TPC, TFC, TFAC, DPPH, and FRAP. All procedures were conducted in the dark.

2.2.2 Determination of total polyphenol content

The TPC was determined using the Folin-Ciocalteu method (García-Ruiz et al., 2011). For the analysis, 100 µL of the extract was mixed with 1.5 mL of distilled water and 0.1 mL of Folin-Ciocalteu reagent in a centrifuge tube. After shaking well, 1.5 mL of a 20% saturated Na_2CO_3 solution was added, and the mixture was shaken again and left to react away from light for 2 h. The absorbance was measured at 765 nm using a spectrophotometer (UV-1800PC, MAPADA Instrument Co., LTD., Shanghai, China). The TPC content was calculated using Gallic Acid Equivalents (GAE) as the standard (50–1000 mg/L).

2.2.3 Determination of total flavonoid content

The TFC was assessed as described by Park et al. (2008). A 200 µL sample extract was mixed with 1.3 mL of methanol, followed by the addition of 100 µL $NaNO_2$ (0.5 M) and 100 µL $AlCl_3$ (0.3 M). After 5 min of incubation, 500 µL NaOH (1 M) was added. The extraction solvent was used as the control, with the absorbance being measured by a spectrophotometer (UV-1800PC, MAPADA Instrument Co., LTD., Shanghai, China) at 510 nm wavelength, and the content was calculated with rutin (Rutin Equivalents, RE) as the standard (20–100 mg/L).

2.2.4 Determination of total flavanol content

The TFAC was measured following Zhang et al.'s method (Zhang et al., 2023). The extract (100 µL) was sequentially mixed with distilled water (1.5 mL) and 1% p-DMACA solution (1 mL). After 10 min of shaking, the absorbance was measured at 640 nm wavelength using a spectrophotometer (UV-1800PC, MAPADA Instrument Co., LTD., Shanghai, China), with the extraction solvent as the control. The content was determined using catechin as the standard (6.25-200 mg/L) and expressed as catechin equivalents (CE).

2.2.5 Determination of total anthocyanin content

The method by Zhang et al. (2022) was modified to determine TMAC. For this, 0.2 g of the sample or 0.2 mL of fruit juice was added to a centrifuge tube containing 5 mL of a 1% hydrochloric acid-methanol solution. The mixture was shaken and then incubated at 4°C in the dark for 20 h. Ultrasonic extraction was performed for 30 min, followed by centrifugation at 8000 rpm and 4°C for 5 min. The resulting supernatant was collected, and the optical density (OD) was measured at 530 nm, 620 nm, and 650 nm using a microplate reader (Varioskan LUX, Thermo Fisher Scientific, MA, USA). The ODλ value of anthocyanin was calculated as $OD\lambda = (OD_{530} - OD_{620}) - 0.1(OD_{650} - OD_{620})$. Finally, TMAC was calculated using the following formula:

$$TMAC(nmol/g) = (OD\lambda \times V \times 10^6) / (\epsilon\lambda \times m)$$

V: the total volume of the extract (mL);

$\epsilon\lambda$: molar extinction coefficient of anthocyanin;

m: the amount of sample taken (g or mL)

2.2.6 Determination of punicalagin content

The punicalagin content was quantitatively determined using the high-performance liquid chromatography (HPLC) method described by Zhao et al. (2015). A 0.2 g sample was ground and mixed with 5 mL of extraction solution (methanol: water *v/v* = 84:16) in a centrifuge tube. The tube was shaken and then subjected to ultrasonication for 30 min at room temperature. The mixture was further shaken at 30°C and 250 rpm for 2 h. After centrifugation at 8000 rpm for 15 min at 4°C, the supernatant was filtered through a 0.22 µm microporous filter membrane.

The analysis was performed using an Agilent 1260 series HPLC system (Agilent Technologies, USA) equipped with a Comatex C18 column (5 µm, 46 mm * 250 mm). The column temperature was maintained at 30°C, and 20 µL of the sample was injected. The mobile phase comprised ultrapure water with 0.1% formic acid (A) and acetonitrile chromatographic pure solution with 0.1% formic acid (B). The gradient elution method was used with a flow rate of 1 mL/min. The elution program wa: 0–24 min, 91.8% A, 8.2% B; 25–30 min, 80.3% A, 19.7% B; 30–35 min, 91.8% A, 8.2% B. Detection was performed at 280 nm and 320 nm. A standard curve was constructed using different gradient standard solutions of HPLC-grade punicalagin (Yuanye Bio-Technology Co., Ltd, Shanghai, China).

2.3 Antioxidant activity determinations

The DPPH radical scavenging was assessed following Williams et al.'s method (Williams et al., 1995). A 100 µL sample extract was added to a 2 mL of methanol solution of DPPH (6.25×10^{-5} M). After incubating the mixture in darkness for 20 min, the absorbance was measured at 517 nm using a spectrophotometer (UV-1800PC, MAPADA Instrument Co., LTD., Shanghai, China). The results were reported as µM Trolox equivalent antioxidant capacity (TEAC).

The FRAP reduction ability was determined based on Benzie et al.'s approach (Benzie and Strain, 1999). The TPTZ solution was prepared by combining 300 mM acetate buffer, 10 mM TPTZ solution (40 mM hydrochloric acid solution), and 20 mM ferric chloride solution at a volume ratio of 10:1:1. A 100 µL sample extract was sequentially mixed with 1 mL of distilled water and 1.8 mL of TPTZ solution. The reaction was conducted in a 37°C water bath for 10 min, and the absorbance was measured at 593 nm. The result was expressed as µM Trolox equivalent antioxidant capacity (TEAC).

2.4 Statistical analysis

Each experiment was performed in triplicates, and the results are reported as the mean ± standard deviation (SD). Data variance was analyzed using IBM SPSS Statistics 26 (SPSS Inc., Chicago, IL, USA) and the significance of differences was determined using the LSD method. The significance level was set at $p < 0.05$. GraphPad Prism 8 (GraphPad Software Llc., San Diego, CA, USA) and chiplot

online (https://www.chiplot.online) were utilized for data visualization.

3 Results

3.1 Analysis of phenolic accumulation and antioxidant activity in pomegranate leaves

The color of pomegranate leaves transitions from tender red to tender green and then to deep green (Supplementary Figure 1). During leaf growth, TPC, TFC, TMAC, and punicalagin content in both pomegranate varieties exhibited a decreasing trend (Table 1). However, TFAC showed an increasing trend compared to other phenols. The TPC, TFC, and TFAC in leaves were 33.28–41.57 mg GAE/g FW (GAE, Gallic acid equivalent; FW, Fresh weight), 47.65–84.23 mg RE/g FW (RE, Rutin Equivalents), and 1.83–4.07 mg CE/g FW (CE, Catechin Equivalents), respectively. TMAC correlated with leaf color, when leaves were red at T1, TMAC was highest, with 'Qingpi' (694.71 nmol/g FW) significantly surpassing 'Tunisia' (647.98 nmol/g FW). As leaves matured, TMAC significantly decreased, reaching its lowest at T3 (4.91–6.05 nmol/g FW). Punicalagin content also decreased during leaf development, with the highest levels (10.88–11.25 mg/g FW) in young red leaves and the lowest levels (3.45–3.62 mg/g FW) in mature functional leaves. Antioxidant capacity of leaves, as determined by the DPPH method, was (395.25–545.25 μmol/g Trolox FW), and as determined by the FRAP method, it was (754.68–1349.58 μmol/g Trolox FW). Antioxidant capacity, TPC, TFC, and TMAC exhibited a consistent downward trend. Young leaves showed the highest antioxidant activity, while mature leaves displayed the lowest.

3.2 Analysis of phenolic accumulation and antioxidant activity in pomegranate flowers

The pomegranate flowers exhibit normal vase-shaped and abnormal bell-shaped structures (Figure 1). The phenolic substance content and antioxidant activity were analyzed in different parts of the pomegranate floral bud and fully blossomed flowers (Table 2). The TPC ranges in the calyx, petals, stamens, and ovary were 15.07–26.86 mg GAE/g FW, 18.86–50.15 mg GAE/g FW, 19.05–31.99 mg GAE/g FW, and 16.03–25.24 mg GAE/g FW, respectively. There were no significant differences in TPC between normal and abnormal flowers. The TPC decreased in the calyx, petal, and ovary during flower development, with significantly higher levels in the floral bud period compared to the full-blossom period. In contrast, the stamens showed an opposite trend, with lower TPC during the floral bud period than in the full-blossom period. The TPC in the petals was the highest, significantly higher than those in the calyx, stamen, and ovary.

The TFC ranges in the calyx, petal, stamen, and ovary were 35.14–84.34 mg RE/g FW, 45.86–117.60 mg RE/g FW, 59.39–105.97 mg RE/g FW, and 46.77–87.89 mg RE/g FW, respectively. During flower development, the TFC significantly decreased in the calyx, petal, and ovary, while increasing in the stamens. The order of TFC during the floral bud period was petal > ovary > stamen > calyx, while during the full-blossom period, it was stamens > ovary > petals > calyx. Among normal flowers, the petals exhibited the highest TFC, while in abnormal flowers, the calyx and stamens showed the highest levels. The 'Tunisia' variety had significantly higher TFC than 'Qingpi'.

Table 2 demonstrates that the TFAC in the calyx, petal, stamen, and ovary were 0.37–0.58 mg CE/g FW, 0.33–0.88 mg CE/g FW,

TABLE 1 Analysis of phenolic accumulation and antioxidant activity in pomegranate leaves throughout growth and development.

Parameter	Cultivar	T1	T2	T3
Total polyphenols (mg GAE/g FW)	Tunisia	40.74 ± 0.73 ab	38.45 ± 0.62 c	33.28 ± 0.39 d
	Qingpi	41.57 ± 0.42 a	38.86 ± 1.16 bc	33.78 ± 0.58 d
Total flavonoids (mg RE/g FW)	Tunisia	84.23 ± 0.63 a	79.44 ± 0.99 b	50.71 ± 0.95 d
	Qingpi	80.46 ± 0.55 b	65.56 ± 0.41 c	47.65 ± 0.70 e
Total flavanols (mg CE/g FW)	Tunisia	2.05 ± 0.08 c	2.15 ± 0.07 c	3.68 ± 0.12 b
	Qingpi	1.99 ± 0.09 c	1.83 ± 0.02 c	4.07 ± 0.25 a
Total anthocyanins (nmol/g FW)	Tunisia	647.98 ± 8.79 b	32.90 ± 0.50 c	4.91 ± 0.67 d
	Qingpi	694.71 ± 8.25 a	28.92 ± 0.43 c	6.05 ± 1.54 d
Punicalagin (mg/g FW)	Tunisia	10.88 ± 0.34 a	8.33 ± 0.06 b	3.62 ± 0.41 c
	Qingpi	11.25 ± 0.24 a	7.74 ± 0.26 b	3.45 ± 0.30 c
DPPH (μmol/g Trolox FW)	Tunisia	545.25 ± 6.12 a	481.28 ± 14.57 b	395.25 ± 4.31 c
	Qingpi	530.15 ± 9.12 a	482.13 ± 23.40 b	397.95 ± 3.11 c
FRAP (μmol/g Trolox FW)	Tunisia	1349.58 ± 2.40 a	1082.22 ± 8.53 b	758.61 ± 21.62 c
	Qingpi	1324.81 ± 12.42 a	1046.57 ± 9.02 b	754.68 ± 11.90 c

The values are expressed as the means ± SD. The leaves are categorized as T1 (red young leaves), T2 (tender green leaves), and T3 (deep green leaves). Different lowercase letters (a–c) indicate significant differences between sampling dates for each treatment, determined using Duncan's multiple range test ($p < 0.05$).

10.3389/fpls.2023.1265018

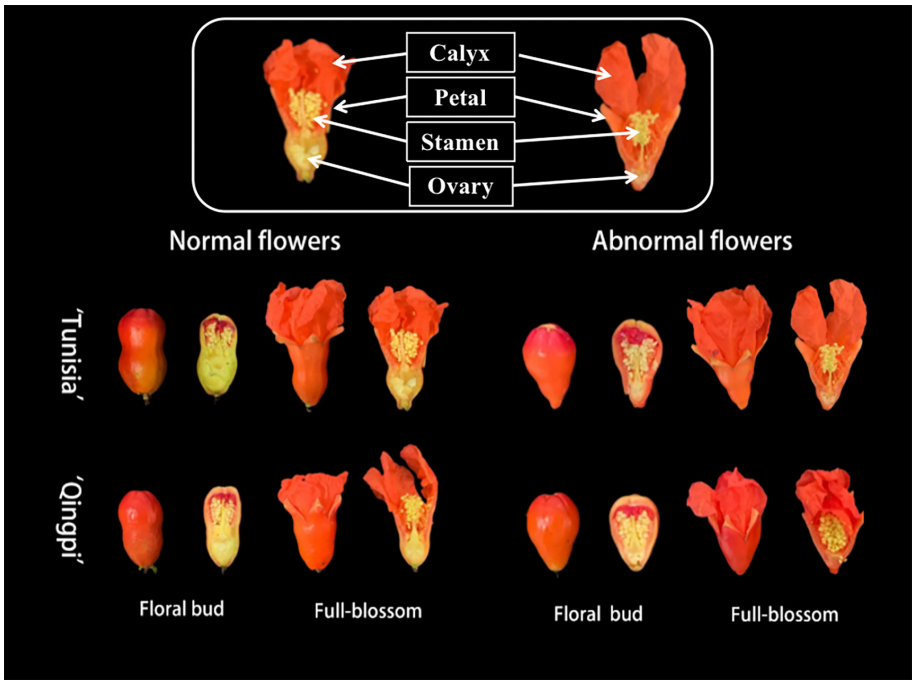

FIGURE 1
Different developmental stages of pomegranate flowers, highlighting the flower with the longitudinal profile. The flowers contain calyx, petal, stamen, and ovary.

TABLE 2 Phenolic accumulation analysis in pomegranate flowers throughout their growth and development.

Parameter	Part	Cultivar	Normal flower		Abnormal flower	
			Floral bud period	Full-blossom period	Floral bud period	Full-blossom period
Total polyphenols (mg GAE/g FW)	Calyx	Tunisia	26.33 ± 2.46 a	15.79 ± 0.91 b	26.86 ± 1.25 a	15.07 ± 0.96 b
		Qingpi	22.86 ± 0.81 a	16.86 ± 0.83 b	23.03 ± 2.40 a	16.86 ± 1.49 b
	Petal	Tunisia	49.40 ± 1.09 a	25.78 ± 1.43 c	50.15 ± 1.13 a	24.82 ± 1.41 c
		Qingpi	44.46 ± 0.29 b	18.86 ± 1.80 d	45.95 ± 0.85 ab	18.74 ± 2.75 d
	Stamen	Tunisia	22.83 ± 1.88 bc	31.99 ± 1.46 a	22.66 ± 1.72 bc	31.17 ± 0.57 a
		Qingpi	19.53 ± 0.37 c	26.39 ± 0.73 b	19.05 ± 1.49 c	26.05 ± 0.75 b
	Ovary	Tunisia	24.86 ± 0.90 a	17.28 ± 1.38 b	24.15 ± 0.70 a	17.90 ± 3.87 b
		Qingpi	25.24 ± 2.69 a	16.03 ± 1.22 b	25.08 ± 0.45 a	16.65 ± 1.95 b
Total flavonoids (mg RE/g FW)	Calyx	Tunisia	67.13 ± 1.24 b	44.63 ± 0.66 d	84.34 ± 1.16 a	45.16 ± 1.20 d
		Qingpi	55.44 ± 1.12 c	36.94 ± 0.92 e	66.45 ± 1.33 b	35.14 ± 0.80 e
	Petal	Tunisia	117.60 ± 1.24 a	56.93 ± 2.96 d	102.92 ± 2.51 b	49.05 ± 1.48 e
		Qingpi	98.69 ± 1.89 b	50.95 ± 3.46 de	82.11 ± 2.42 c	45.86 ± 1.35 e
	Stamen	Tunisia	74.19 ± 1.40 e	105.97 ± 0.78 a	83.33 ± 1.00 cd	88.11 ± 1.14 c
		Qingpi	59.39 ± 1.84 f	99.10 ± 2.58 b	75.02 ± 2.64 e	81.77 ± 1.91 d
	Ovary	Tunisia	87.89 ± 1.87 a	67.61 ± 1.96 c	84.57 ± 3.07 a	51.31 ± 1.56 e
		Qingpi	74.14 ± 0.97 b	60.16 ± 0.57 d	68.75 ± 2.28 bc	46.77 ± 0.54 e

(Continued)

TABLE 2 Continued

Parameter	Part	Cultivar	Normal flower		Abnormal flower	
			Floral bud period	Full-blossom period	Floral bud period	Full-blossom period
Total flavanols (mg CE/g FW)	Calyx	Tunisia	0.37 ± 0.02 c	0.32 ± 0.01 c	0.58 ± 0.05 a	0.32 ± 0.01 c
		Qingpi	0.56 ± 0.01 ab	0.52 ± 0.02 b	0.58 ± 0.01a	0.35 ± 0.02 c
	Petal	Tunisia	0.71 ± 0.02 b	0.33 ± 0.02 c	0.70 ± 0.03 b	0.42 ± 0.02 c
		Qingpi	0.88 ± 0.06 a	0.35 ± 0.03 c	0.77 ± 0.03 b	0.39 ± 0.02 c
	Stamen	Tunisia	0.92 ± 0.03 e	1.10 ± 0.04 d	1.06 ± 0.01 de	1.26 ± 0.04 c
		Qingpi	1.04 ± 0.02 de	2.07 ± 0.04 a	1.70 ± 0.08 b	1.78 ± 0.04 b
	Ovary	Tunisia	0.56 ± 0.02 d	0.41 ± 0.01 d	0.93 ± 0.02 c	0.85 ± 0.05 c
		Qingpi	1.60 ± 0.23 b	1.38 ± 0.02 b	2.24 ± 0.09 a	2.08 ± 0.07 a
Total anthocyanins (nmol/g FW)	Calyx	Tunisia	163.94 ± 1.28 d	183.27 ± 3.58 c	114.95 ± 2.54 e	180.65 ± 2.19 c
		Qingpi	176.13 ± 5.83 c	227.91 ± 3.91 a	177.79 ± 2.16 c	217.65 ± 2.03 b
	Petal	Tunisia	1938.54 ± 1.60 a	1899.99 ± 6.15 b	1951.30 ± 3.29 a	1873.10 ± 11.05 b
		Qingpi	1929.43 ± 2.84 a	1792.47 ± 14.49 c	1938.39 ± 2.53 a	1780.47 ± 20.37 c
	Stamen	Tunisia	161.57 ± 6.19 f	272.95 ± 5.40 d	196.68 ± 8.28 e	459.51 ± 10.65 a
		Qingpi	151.37 ± 4.19 f	298.67 ± 5.20 c	158.66 ± 1.75 f	380.09 ± 4.96 b
	Ovary	Tunisia	49.47 ± 1.03 f	85.37 ± 1.20 d	167.91 ± 2.21 b	168.16 ± 0.90 b
		Qingpi	55.03 ± 1.97 e	129.82 ± 0.99 c	209.23 ± 3.48 a	211.31 ± 3.57 a
Punicalagin (mg/g FW)	Calyx	Tunisia	7.20 ± 0.07 b	6.48 ± 0.28 bc	3.98 ± 0.10 d	3.60 ± 0.02 d
		Qingpi	8.49 ± 0.04 a	5.83 ± 0.34 c	8.79 ± 0.16 a	6.84 ± 0.74 b
	Petal	Tunisia	45.58 ± 2.88 b	16.68 ± 0.13 e	55.50 ± 2.44 a	22.83 ± 0.17 d
		Qingpi	31.71 ± 1.41 c	13.78 ± 0.26 e	30.29 ± 2.19 c	16.28 ± 0.05 e
	Stamen	Tunisia	5.48 ± 0.10 c	6.21 ± 0.12 a	5.07 ± 0.07 d	5.54 ± 0.02 c
		Qingpi	4.92 ± 0.14 d	5.50 ± 0.14 c	5.40 ± 0.08 c	5.88 ± 0.11 b
	Ovary	Tunisia	13.13 ± 0.38 cd	10.12 ± 0.09 f	12.35 ± 0.03 de	8.66 ± 0.53 g
		Qingpi	16.53 ± 0.19 a	13.89 ± 0.34 c	14.88 ± 0.16 b	11.76 ± 0.26 e

Values (mean ± SD) of three replicates. Lowercase letters (a-c) in the table indicate significant differences between sampling dates for each treatment ($p < 0.05$) using Duncan's multiple range test.

0.92–1.70 mg CE/g FW, and 0.56–2.24 mg CE/g FW, respectively. Similar to TPC and TFC changes, TFAC in the calyx, petal, and ovary was higher during the floral bud period, while TFAC in the stamen increased during the full-blossom period. The TFAC in stamens of the 'Tunisia' variety was the highest (0.92–1.26 mg CE/g FW), whereas the calyx had the lowest levels (0.32–0.58 mg CE/g FW). The TFAC in the ovary of the 'Qingpi' variety was the highest (1.38–2.24 mg CE/g FW), while the calyx content was the lowest (0.34–0.58 mg CE/g FW). The 'Qingpi' variety flowers had higher TFAC than 'Tunisia'.

The TMAC ranges in the calyx, petal, stamen, and ovary were 114.95–227.91 nmol/g FW, 1780.47–1951.30 nmol/g FW, 151.37–459.51 nmol/g FW, and 49.47–211.31 nmol/g FW, respectively. Stamens, calyxes, and ovaries had higher TMAC in full-blossom flowers, whereas it was higher for petals during the floral bud period. Moreover, the TMAC of abnormal flowers exceeded that of normal flowers.

The punicalagin contents in the calyx, petal, stamen, and ovary were 3.60–8.79 mg/g, 13.78– 55.50 mg/g, 4.92–6.21 mg/g, and 8.66–16.53 mg/g, respectively. Among different developmental stages, petals exhibited the highest punicalagin content, followed by ovaries, while calyxes and stamens had the lowest content. Notably, the punicalagin content in the petals of abnormal flowers from the 'Tunisia' pomegranate was significantly higher (55.50 mg/g) than that of normal flowers (45.58 mg/g). However, there was no significant difference in the punicalagin content between abnormal and normal flowers of the 'Qingpi' pomegranate, although it was significantly lower than that of the 'Tunisia' variety.

The antioxidant activity of 'Tunisia' and 'Qingpi' flower organs was determined using the DPPH and FRAP methods (Table 3). Both methods yielded consistent results. The antioxidant activity of petals, calyxes, and ovaries decreased as the flowers developed, whereas the antioxidant activity of stamens increased. No

10.3389/fpls.2023.1265018

significant difference in antioxidant activity was observed between normal and abnormal flowers. During the floral bud period, petals and ovaries exhibited the highest antioxidant activity, while stamens demonstrated the highest antioxidant capacity during the full-blossom period.

3.3 Analysis of phenolic accumulation and antioxidant activity during pomegranate fruit development

The developmental stages of pomegranate fruit are shown in Figure 2. The pomegranate fruit peel color changes from red to green and then back to red. 'Tunisia' fruit pulp begins coloring at S2, while 'Qingpi' starts at S4. The TPC decreases during fruit development (Figures 3A1, A2). The TPC of peel, placenta, and septum decreases rapidly from S2 to S3. The TPC of tegmens and juice decrease gradually, and are significantly lower than the other parts. Initially, the TPC order was placenta > peel > septum > tegmen ≈ juice. In the middle and late stages, there's no significant difference among peel, placenta, and septum, but they're significantly higher than juice and tegmen. 'Tunisia' has higher TPC than 'Qingpi'.

During pomegranate development, the TFC initially increases, then decreases, and finally increases slowly (Figures 3B1, B2). In the early stage, the TFC in peel, placenta, and septum were higher. At S2 stage, the TFC was highest in peel, placenta, and septum (55.42–140.02 mg RE/g FW, 23.75–173.98 mg RE/g FW, 18.33–92.61 mg RE/g FW, respectively). The TFC in tegmens was highest during fruit ripening ('Tunisia', 14.97 mg RE/g FW; 'Qingpi', 17.09 mg RE/g FW). Placenta has the highest TFC in the early stage, while peel has the highest in the late stage. Juice and tegmens have significantly lower TFC than other parts at the same stage.

Figures 3C1, C2 show the distribution of TFAC in different parts of the pomegranate fruit during development. The TFAC was mainly found in peels and tegmens. Peel TFAC increases, peaks in the S3 period, then decreases. Tegmens exhibit significant changes, with the highest TFAC at fruit maturity.

The TMAC is mainly distributed in peel, tegmen, and juice. The TMAC increases during development and peaks at fruit maturity (Figures 3D1, D2). 'Tunisia' has the fastest TMAC accumulation from S4 to S5, while 'Qingpi' accumulates fastest from S6 to S7. TMAC during the mature period was 3–57 times higher than the early stage. The order of TMAC concentration was juice > peel > tegmen > placenta ≈ septum. 'Tunisia' has a higher TMAC than 'Qingpi'.

Punicalagin is primarily found in the placenta, peel, and septum of the pomegranate fruit, with lower contents in their juice and tegmen. The punicalagin content in peel, placenta, and septum initially increases, reached the peak at the S2-stage, then declines, and was the lowest in the mature period (S7). In the premiddle-stage, the order of punicalagin concentration was placenta > peel > septum > tegmen ≈ juice. In the mature stage, it was peel > placenta > septum > tegmen > juice.

The antioxidant activity of pomegranate during development was evaluated using DPPH (Figure 3F) and FRAP methods

TABLE 3 Antioxidant activity analysis in pomegranate flowers during growth and development.

Parameter	Part	Cultivar	Normal flower		Abnormal flower	
			Floral bud period	Full-blossom period	Floral bud period	Full-blossom period
DPPH (μmol/g Trolox FW)	Calyx	Tunisia	449.89 ± 6.03 ab	355.60 ± 4.51 c	458.59 ± 1.37 a	354.91 ± 7.44 cd
		Qingpi	431.09 ± 8.45 b	337.60 ± 4.87 cd	437.60 ± 4.48 b	334.12 ± 7.93 d
	Petal	Tunisia	509.27 ± 5.84 a	331.96 ± 4.61 b	522.99 ± 11.79 a	328.61 ± 8.61 b
		Qingpi	518.43 ± 2.13 a	342.37 ± 3.97 b	526.15 ± 11.65 a	340.19 ± 3.36 b
	Stamen	Tunisia	432.02 ± 2.79 c	489.16 ± 7.68 ab	428.77 ± 5.65 c	472.90 ± 2.46 b
		Qingpi	424.92 ± 5.67 c	494.60 ± 1.35 a	415.05 ± 7.45 c	477.09 ± 9.15 ab
	Ovary	Tunisia	522.61 ± 0.81 a	419.76 ± 4.08 e	516.10 ± 2.82 a	411.58 ± 4.43 e
		Qingpi	492.88 ± 6.25 b	476.15 ± 1.23 c	488.93 ± 4.49 bc	442.71 ± 6.70 d
FRAP (μmol/g Trolox FW)	Calyx	Tunisia	930.55 ± 6.83 a	576.89 ± 1.70 c	934.35 ± 5.50 a	575.22 ± 11.87 c
		Qingpi	832.63 ± 3.69 b	544.55 ± 15.34 d	842.50 ± 9.51 b	541.15 ± 3.43 d
	Petal	Tunisia	1500.76 ± 3.04 a	677.52 ± 3.32 d	1505.78 ± 10.63 a	670.22 ± 3.66 d
		Qingpi	1310.70 ± 22.40 c	620.78 ± 11.04 e	1375.41 ± 1.85 b	609.66 ± 7.23 e
	Stamen	Tunisia	804.53 ± 2.65 c	981.64 ± 7.89 a	802.72 ± 16.39 c	970.04 ± 16.85 a
		Qingpi	730.78 ± 4.79 d	963.18 ± 18.25 ab	717.03 ± 6.49 d	930.78 ± 5.30 b
	Ovary	Tunisia	962.81 ± 30.71 a	647.37 ± 9.31 c	964.25 ± 5.15 a	628.55 ± 9.34 c
		Qingpi	846.52 ± 6.75 b	570.22 ± 14.83 d	838.74 ± 7.11 b	571.56 ± 4.83 d

Values of three replicates are expressed as the means ± SD. Different lowercase letters (a-c) in the table indicate significant differences between sampling dates for each treatment ($p < 0.05$) using Duncan's multiple range test.

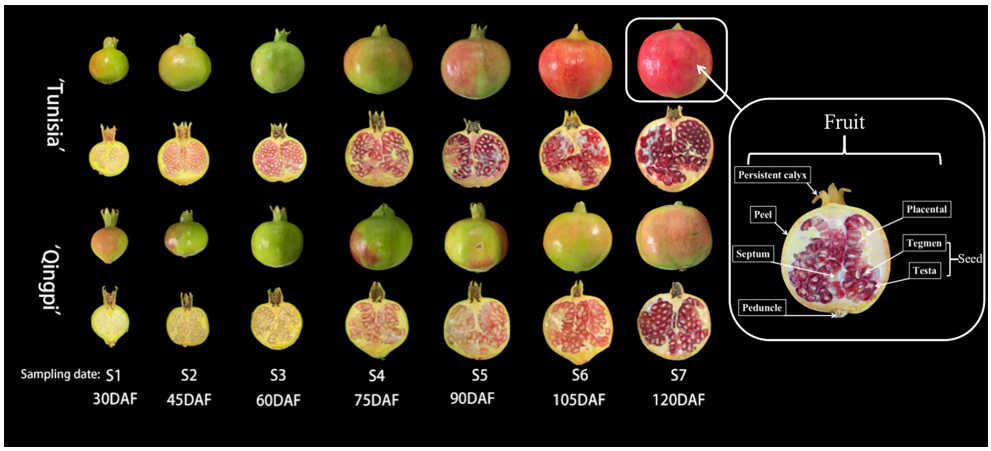

FIGURE 2
Pomegranate fruit undergoes various developmental stages, comprising the inner and outer parts. It includes the persistent calyx, peduncle, peel, placenta, septum, and seed. The seed consists of tegmen and testa, with the fleshy part serving as the juice source.

(Figure 3G). Overall, the fruit exhibited a decreasing trend in antioxidant activity. Notably, the peel, placenta, and septum demonstrated higher antioxidant activities, while the tegmens and juice showed significantly lower levels. Initially, the placenta exhibited the highest antioxidant activity, followed by the peel and septum. However, starting from stage S4, the placenta's antioxidant activity rapidly declined, and the peel had the highest activity, followed by the placenta and septum. Throughout all stages, the tegmens and juice consistently displayed the lowest antioxidant activity.

3.4 Comparison of antioxidant activity and phenolic content in different parts of pomegranate during development

During pomegranate development, phenolic substances and antioxidant activity were compared across different parts (Figure 4), and values were assigned on a scale of 1 to 10 based on concentration. Results revealed that the placenta had the highest contents of TFC and punicalagin, the peel had the highest TFAC, and the petals had the highest TPC and TMAC. The order of antioxidant activity was placenta > peel >petals ≈ leaves. The fruit's edible part was primarily protected by the high phenolic content and strong antioxidant activity of the placenta, peel, and septum. Anthocyanin, along with total flavanols, plays a significant role in pomegranate juice as the main pigment and antioxidant.

3.5 Correlation analysis between antioxidant activity and phenolic content in different organs of pomegranate during development

The antioxidant activity showed a significant positive correlation with phenolic content in various organs of pomegranate (Figure 5). The correlation coefficient between DPPH and FRAP (Figures 5A, C) and FRAP (Figures 5B, D) was 0.94–1.00. Furthermore, the antioxidant activity of pomegranate organs was positively correlated with TPC, punicalagin, and TFC. Except for the fruit's tegmen, the antioxidant activity in different organs showed a significant positive correlation with TFC, with correlation coefficients being 0.71–0.99. The correlation coefficients between antioxidant activity and TPC and punicalagin were 0.77–1.00 and 0.71–1.00, respectively. The relationship between antioxidant activity and TFAC and TMAC varied across different parts. The TFAC showed significant positive correlations with the antioxidant activity of placenta, tegmen, petal, stamen, calyx, and leaf, and the correlation coefficient were respectively 0.84 ~ 0.99 (Positive correlation, P), -0.92 ~ -0.73 (Negative correlation, N), 0.97 ~ 0.98 (P), 0.64 ~ 0.76 (P), 0.73 ~ 0.76 (P) and -0.94 ~ -0.85(N). The TMAC showed significant correlations with the antioxidant activity of peel, juice, petal, stamen, calyx, and leaf, while other parts of the pomegranate did not show significance. The antioxidant activity of the petal showed a particularly high correlation coefficient of 1 with TMAC.

4 Discussion

Pomegranate was widely utilized in food production and processing. Its edible part, the testa, can be consumed fresh or used to make fruit juice. Pomegranate juice was a significant source of anthocyanins, which possess health benefits due to their antioxidant properties (Gardeli et al., 2019). Besides the fruit juice, other parts of the pomegranate, such as the peel, leaves, and flowers, are abundant in phenols (Tzulker et al., 2007; Legua et al., 2012; Bekir et al., 2013a). These parts exhibit high antioxidant activity and hold great value for development and utilization.

Pomegranate leaves are rich in bioactive compounds and serve as a natural source of pigments and antioxidants. Yu et al. (2021) characterized the phenolic composition and antioxidant activity of

10.3389/fpls.2023.1265018

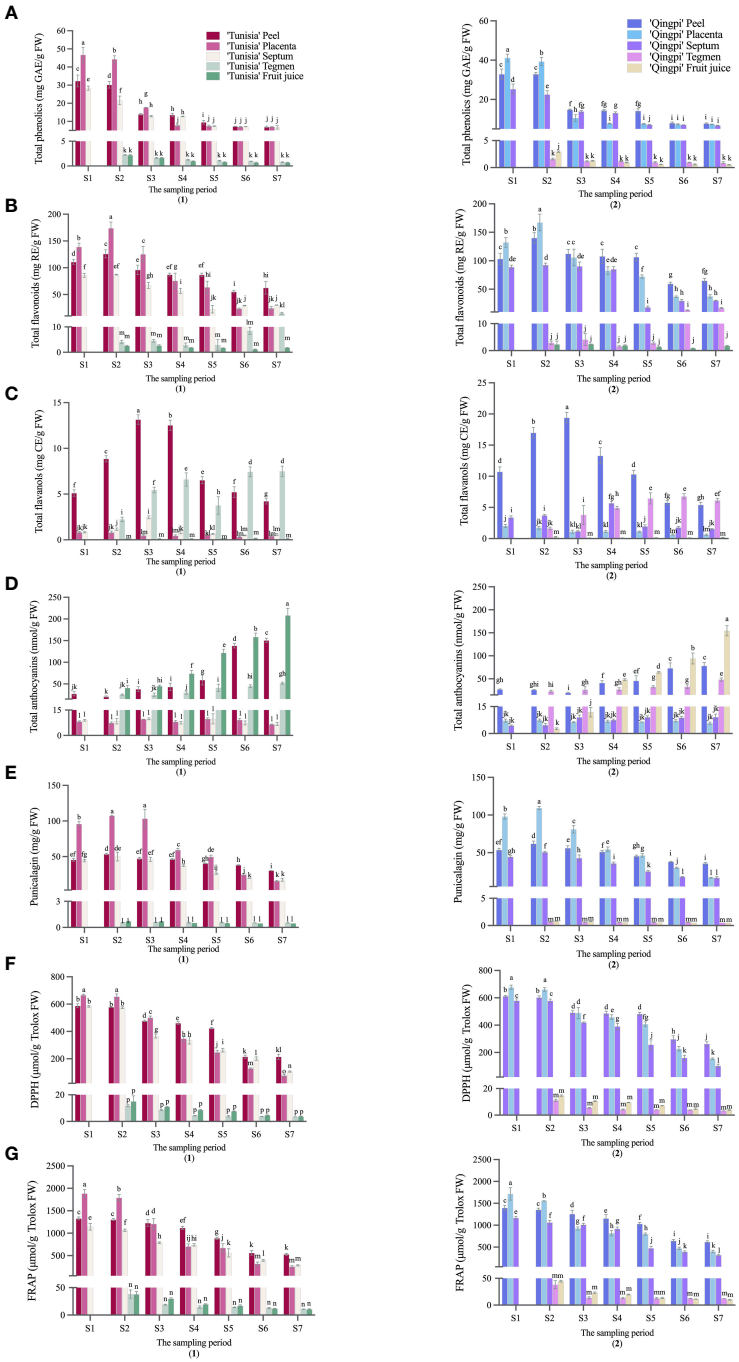

FIGURE 3
Phenolic accumulation and antioxidant activity analysis in pomegranate fruit during growth and development was conducted. The parameters measured were TPC **(A)**, TFC **(B)**, TFAC **(C)**, TMAC **(D)**, Punicalagin **(E)**, DPPH **(F)**, and FRAP **(G)** for 'Tunisia' (1) and 'Qingpi' (2). Mean ± standard deviation (n = 3) was presented in each column, and a *t*-test was performed at the 0.05 significance level ($p < 0.05$). Different letters (a-p) indicate significant differences, while the same letter indicates no significant difference.

several medicinal and food plants, finding that pomegranate leaves have the highest TFC (199.26 mg GAE/g DW, DW, Dry Weight) and antioxidant activity compared to other varieties. The leaves can be used as a substitute for tea, extract development, and synthetic antioxidants (Wang et al., 2013; Mansour et al., 2022). Pomegranate leaf tea contains more phenolic substances (41.01-83.43 mg/100 g) than green tea (Legua et al., 2012), which is lower than the TPC (33.28-41.57 mg/g FW) measured in the leaves of this study. Our study shows that the phenolic substances and antioxidant activity of pomegranate leaves are highest when they are red (T1), which is similar to the study by Zhang et al. (2010). Therefore, for tea or other beverages made from pomegranate leaves, the nutritional

10.3389/fpls.2023.1265018

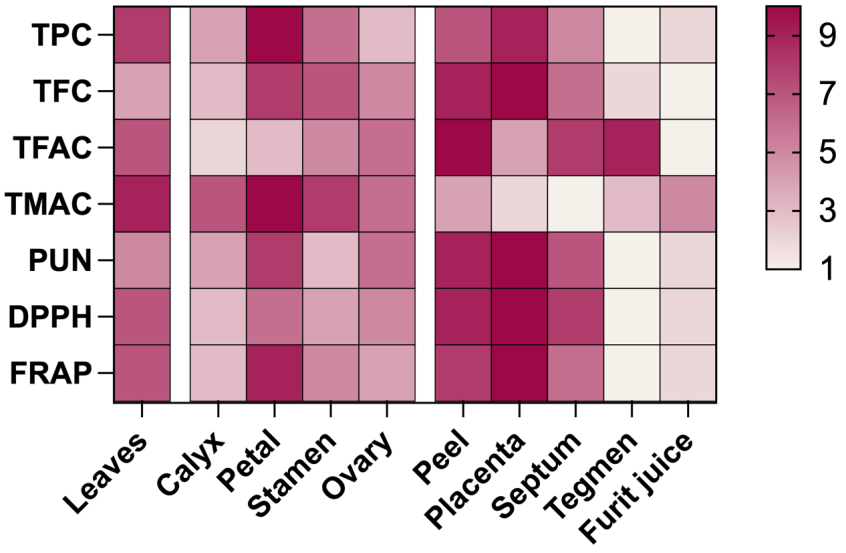

FIGURE 4
Comparing antioxidant activity and phenolic content in various parts of developing pomegranates. Color depth represents concentration, with red indicating high and white indicating low. Values range from 1 to 10. TPC, Total polyphenols; TFC, total flavonoids; TFAC, total flavanols; TMAC, total anthocyanins; PUN, punicalagin.

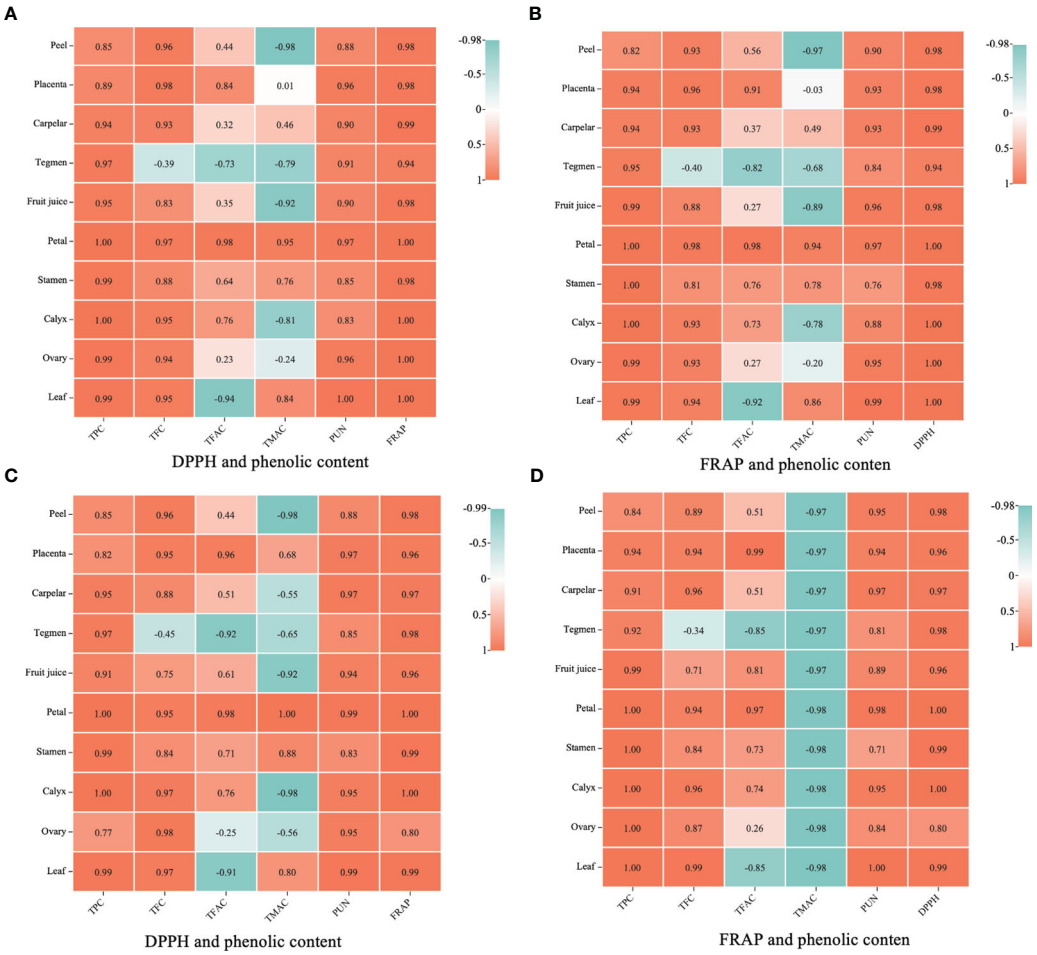

FIGURE 5
Correlation analysis between antioxidant activity and phenolic content in different tissues and organs of *Punica granatum*. The concentration was expressed by the color depth, orange means high, blue means low, and the value from low to high was 1–10. **(A, B)**: 'Tunisia'; **(C, D)**: 'Qingpi'; TPC, Total polyphenols; TFC, total flavonoids; TFAC, total flavanols; TMAC, total anthocyanins; PUN, punicalagin.

value was higher when young leaves are harvested compared to mature leaves.

Edible flowers have gained popularity in recent years due to their unique flavors and nutritional content. Flowers from peach (Li and Wang, 2011), broccoli (Lou et al., 2023), chrysanthemum (Wei et al., 2023), and *Osmanthus fragrans* (Wang et al., 2022) are used as a good source for food products. Pomegranate flowers, with their vibrant colors and high phenolic content, surpass white roses, chrysanthemums, and other edible flowers, making them desirable in the consumer market (Teniente et al., 2023). Bekir et al. (2013b) measured the highest TPC, TFC, TMAC in various pomegranate dry flowers as 330.9 mg GAE/g DW, 29.5 mg QE/g DW (QE, quercetin equivalent), and 0.70 mg CGE/g DW (CGE, cyanidin-3-glucoside equivalent), respectively. In our study, the highest TPC, TFC, and TMAC in pomegranate fresh flowers were 50.15 mg GAE/g FW, 117.6 mg RE/g FW, and 1938 nmol/g FW, respectively, significantly surpassing the levels in fruit juice. Interestingly, studies have shown that the proportion of abnormal flowers (bell-shaped flowers) in the total flowers can reach 60–94.88%, with abnormal flowers being good for pollination but not for fruit yield (Chen et al., 2017). This study found that abnormal flowers are rich in phenolic substances similar to normal flowers. Although abnormal flowers are typically discarded as bio-waste, their long harvesting period highlights their potential as a local specialty food and as raw materials for phenolic substance extraction and processing, thereby enhancing the economic benefits of pomegranate.

Pomegranate products, including juice, wine, vinegar, and others, are widely accepted by consumers globally (Kalaycıoğlu and Erim, 2017). Pomegranate juice, constituting 78% (*w/w*) (Singh et al., 2022) of fresh food products, exhibits three times higher antioxidant activity compared to wine and green tea (Arantino et al., 2023). In this study, the TPC, TFC and TMAC of 'Tunisia' and 'Qingpi' fruit juice were respectively 0.53-2.95 mg GAE/g, 0.84-2.55 mg RE/g, and 2.67-208.35 nmol/g, which were lower than 'Wonderful' pomegranate juice (Arantino et al., 2023). El Kar et al. (2011) reported TPC, TFC, and TMAC in juice of 'Tunisia' and 'Gabsi' as 458-3299 mg GAE/L, 135-636 mg QE/L, and 11-178 mg CGE/L, respectively, and their ranges were also higher than those in this experiment. Except for the edible part, the pomegranate peel comprising 40–50% of the total fruit weight was considered a rich source for the extraction of bioactive substances due to its abundant phenolic content (El Kar et al., 2011; Akhtar et al., 2015). Despite its high phenolic content, the utilization of pomegranate peel as a by-product remains limited, leading to wastage (Lampakis et al., 2021; Montefusco et al., 2021). Liu et al. (2022) discovered that punicalagin content was highest in the peel. Additionally, Derakhshan et al. (2018) showed that pomegranate peel exhibits higher antioxidant activity and phenolic content than fruit juice and tegmens, with a positive correlation between phenolic content and antioxidant activity, these are consistent with the results of this study. In addition, in our study, the fruit placenta exhibited the highest TPC, TFC, punicalagin contents, and antioxidant activity during the premiddle period of fruit development.

The TPC, TFC, TFAC, and antioxidant activity of pomegranate flowers and fruits peaked in the early growth stage. As different organs develop, the content of phenolic compounds and antioxidant activity gradually decrease, which was consistent with the study of Mirdehghan and Rahemi (2007). Conversely, the TFC of pomegranate fruit tegmens and pomegranate flower stamens increased with fruit development, suggesting variations in flavonoid accumulation among different organs. Punicalagin, a specific component of pomegranate, exhibits therapeutic effects on cervical cancer (Teniente et al., 2023). Punicalagin content was the highest in pomegranate peel, and the granatine content decreased gradually with the growth and development of pomegranate (Bekir et al., 2013a). This study detected punicalagin in different parts of pomegranate the placenta contained the highest punicalagin (109.30 mg/g FW).

The antioxidant activity of various pomegranate organs correlates with changes in phenolic substances. Initially, during early fruit development, different organs exhibited higher phenol content and stronger antioxidant activity. However, as the pomegranate matured, the DPPH and FRAP levels in pomegranate leaf, flower, and fruit decreased progressively as the fruit ripened, consistent with findings in *Rosa rugosa* (Zeng and Peng, 2007) and apple leaves and fruit (Wojdyło and Oszmiański, 2020). Montefusco et al. (2021) demonstrated a positive correlation between TFC and antioxidant activity during pomegranate growth. Similarly, Gil et al. (2000) determined that punicalagin contributed to 50% of the antioxidant activity in pomegranate juice, supporting the present study's results. The antioxidant activity of both pomegranate varieties positively correlated with TPC, TFC, and punicalagin, indicating that these compounds primarily contribute to pomegranate's high antioxidant capacity. Derakhshan et al. (2018) reported that phenolic content and antioxidant activity in pomegranate fruit follow the order: peel > seed > juice. However, the analysis of various pomegranate fruit parts revealed a different order of the concentration of phenolic content and antioxidant activity: placenta > peel, septum > tegmen > juice.

5 Conclusion

This study revealed that pomegranate leaves, flowers, and fruits exhibit high TPC and are abundant in TFC, TMAC, and punicalagin. These components offer various health benefits, making pomegranate a valuable source of phenols. Notably, the pomegranate placenta highlighted the highest TPC, TFC, punicalagin content, and antioxidant activity compared to other fruit parts like juice and tegmens. As a widely cultivated fruit tree globally, pomegranate serves as an excellent raw material for food processing. To enhance utilization rates and reduce costs, priority should be given to developing and utilizing phenols from floral bud flowers, young leaves, and young thinning fruits. Mature fruit peel, juice, and full-bloom flowers are suitable for anthocyanin development and utilization. The placenta and peel of young fruits can be utilized for punicalagin extraction. This study contributes new insights into processing and utilizing pomegranate leaves, flowers, and fruits, particularly their non-edible parts.

Data availability statement

The original contributions presented in the study are included in the article/Supplementary Material. Further inquiries can be directed to the corresponding author.

Author contributions

HZ: Investigation, Conceptualization, Funding acquisition, Writing – review & editing. MW: Data curation, Formal Analysis, Methodology, Software, Writing – original draft. GY: Conceptualization, Investigation, Methodology, Writing – original draft. JP: Writing – review & editing. KT: Writing – review & editing. XT: Writing – review & editing. YD: Writing – review & editing. HW: Writing – original draft, Resources. JH: Writing – original draft, Resources. XL: Writing – review & editing, Methodology. LL: Writing – review & editing, Methodology. QD: Funding acquisition, Writing – review & editing, Conceptualization.

Funding

The authors declare financial support was received for the research, authorship, and/or publication of this article. The research was supported by the Natural Science Foundation on Sichuan Province (2022NSFSC0092), the Technology Innovation Research and Development Project of Chengdu (2022-YF05-01144-SN) and the Open Bidding for Selecting the Best Candidates Project of Sichuan Tianfu New District Rural Revitalization Research Institute (XZY1-06).

Conflict of interest

The authors declare that the research was conducted in the absence of any commercial or financial relationships that could be construed as a potential conflict of interest.

Publisher's note

All claims expressed in this article are solely those of the authors and do not necessarily represent those of their affiliated organizations, or those of the publisher, the editors and the reviewers. Any product that may be evaluated in this article, or claim that may be made by its manufacturer, is not guaranteed or endorsed by the publisher.

Supplementary material

The Supplementary Material for this article can be found online at: https://www.frontiersin.org/articles/10.3389/fpls.2023.1265018/full#supplementary-material

References

Akhtar, S., Ismail, T., Fraternale, D., and Sestili, P. (2015). Pomegranate peel and peel extracts: Chemistry and food features. *Food Chem.* 174, 417–425. doi: 10.1016/j.foodchem.2014.11.035

Arantino, A., Disciglio, G., Frabboni, L., and Lopriore, G. (2023). Organo mineral fertilizers increases vegetative growth and yield and quality parameters of pomegranate cv. Wonderful fruits. *Horticulturae* 9 (2), 164. doi: 10.3390/horticulturae9020164

Asgary, S., Sahebkar, A., Afshani, M. R., Keshvari, M., Haghjooyjavanmard, S., and Rafieian-Kopaei, M. (2014). Clinical evaluation of blood pressure lowering, endothelial function improving, hypolipidemic and anti-inflammatory effects of pomegranate juice in hypertensive subjects. *Phytotherapy Res.* 28 (2), 193–199. doi: 10.1002/ptr.4977

Asgharpour, M., and Alirezaei, A. (2021). Herbal antioxidants in dialysis patients: a review of potential mechanisms and medical implications. *Renal Failure* 43 (1), 351–361. doi: 10.1080/0886022X.2021.1880939

Ávila-Gálvez, MÁ., García-Villalba, R., Martínez-Díaz, F., Ocaña-Castillo, B., Monedero-Saiz, T., Torrecillas-Sánchez, A., et al. (2019). Metabolic profiling of dietary polyphenols and methylxanthines in normal and Malignant mammary tissues from breast cancer patients. *Mol. Nutr. Food Res.* 63 (9), e1801239. doi: 10.1002/mnfr.201801239

Bahmani, M., Rafieian-Kopaei, M., Jeloudari, M., Eftekhari, Z., Delfan, B., Zargaran, A., et al. (2014). A review of the health effects and uses of drugs of plant licorice (*Glycyrrhiza glabra* L.) in Iran. *Asian Pacific J. Trop. Dis.* 4 (2), 847–849. doi: 10.1016/S2222-1808(14)60742-8

Bekir, J., Mars, M., Souchard, J. P., and Bouajila, J. (2013a). Assessment of antioxidant, anti-inflammatory, anti-cholinesterase and cytotoxic activities of pomegranate (*Punica granatum*) leaves. *Food Chem. Toxicol.* 55, 470–475. doi: 10.1016/j.fct.2013.01.036

Bekir, J., Mars, M., Vicendo, P., Fterrich, A., and Bouajila, J. (2013b). Chemical composition and antioxidant, anti-inflammatory, and antiproliferation activities of pomegranate (*Punica granatum*) flowers. *J. Medicinal Food* 16 (6), 544–550. doi: 10.1089/jmf.2012.0275

Benzie, I. F., and Strain, J. J. (1999). Ferric reducing/antioxidant power assay: direct measure of total antioxidant activity of biological fluids and modified version for simultaneous measurement of total antioxidant power and ascorbic acid concentration. *Methods In Enzymology* 299, 15–27. doi: 10.1016/s0076-6879(99)99005-5

Chagas, M. D. S. S., Behrens, M. D., Moragas-Tellis, C. J., Penedo, G. X. M., Silva, A. R., and Gonçalves-de-Albuquerque, C. F. (2022). Flavonols and flavones as potential anti-inflammatory, antioxidant, and antibacterial compounds. *Oxid. Med. Cell. Longevity* 2022, 9966750. doi: 10.1155/2022/9966750

Chen, L. G., Huang, W. T., Lee, L. T., and Wang, C. C. (2009). Ellagitannins from *Terminalia calamansanai* induced apoptosis in HL-60 cells. *Toxicol. In Vitro* 23 (4), 603–609. doi: 10.1016/j.tiv.2009.01.020

Chen, L., Zhang, J., Li, H., Niu, J., Xue, H., Liu, B., et al. (2017). Transcriptomic analysis reveals candidate genes for female sterility in pomegranate flowers. *Front. Plant Sci.* 8. doi: 10.3389/fpls.2017.01430

Derakhshan, Z., Ferrante, M., Tadi, M., Ansari, F., Heydari, A., Hosseini, M. S., et al. (2018). Antioxidant activity and total phenolic content of ethanolic extract of pomegranate peels, juice and seeds. *Food Chem. Toxicol.* 114, 108–111. doi: 10.1016/j.fct.2018.02.023

El Kar, C., Ferchichi, A., Attia, F., and Bouajila, J. (2011). Pomegranate (*Punica granatum*) juices: chemical composition, micronutrient cations, and antioxidant capacity. *J. Food Sci.* 76 (6), C795–C800. doi: 10.1111/j.1750-3841.2011.02211.x

Essid, I., Tajine, S., Gharbi, S., and Bellagha, S. (2020). Use of pomegranate peel and artichoke leaf extracts to improve the quality of marinated sardine (*Sardinella aurita*) fillets. *J. Food Sci. Technol.* 57 (2), 713–722. doi: 10.1007/s13197-019-04104-x

Ganai, S. A., Sheikh, F. A., and Baba, Z. A. (2021). Plant flavone Chrysin as an emerging histone deacetylase inhibitor for prosperous epigenetic-based anticancer therapy. *Phytotherapy Res.* 35 (2), 823–834. doi: 10.1002/ptr.6869

García-Ruiz, A., González-Rompinelli, E. M., Bartolomé, B., and Moreno-Arribas, M. V. (2011). Potential of wine-associated lactic acid bacteria to degrade biogenic amines. *Int. J. Of Food Microbiol.* 148 (2), 115–120. doi: 10.1016/j.ijfoodmicro.2011.05.009

Gardeli, C., Varela, K., Krokida, E., and Mallouchos, A. (2019). Investigation of anthocyanins stability from pomegranate juice (*Punica Granatum* L. Cv Ermioni) under a simulated digestion process. *Medicines (Basel)* 6 (3), 90. doi: 10.3390/medicines6030090

Gil, M. I., Tomás-Barberán, F. A., Hess-Pierce, B., Holcroft, D. M., and Kader, A. A. (2000). Antioxidant activity of pomegranate juice and its relationship with phenolic composition and processing. *J. Agric. Food Chem.* 48 (10), 4581–4589. doi: 10.1021/jf000404a

Gözlekçi, S., Saraçoğlu, O., Onursal, E., and Ozgen, M. (2011). Total phenolic distribution of juice, peel, and seed extracts of four pomegranate cultivars. *Pharmacognosy Magazine* 7 (26), 161–164. doi: 10.4103/0973-1296.80681

Gull, A., Bhat, N., Wani, S. M., Masoodi, F. A., Amin, T., and Ganai, S. A. (2021). Shelf life extension of apricot fruit by application of nanochitosan emulsion coatings containing pomegranate peel extract. *Food Chem.* 349, 129149. doi: 10.1016/j.foodchem.2021.129149

Hostetler, G. L., Ralston, R. A., and Schwartz, S. J. (2017). Flavones: Food sources, bioavailability, metabolism, and bioactivity. *Adv. Nutr.* 8 (3), 423–435. doi: 10.3945/an.116.012948

Hussein, S. A. M., Barakat, H. H., Merfort, I., and Nawwar, M. A. M. (1997). Tannins from the leaves of *Punica granatum*. *Phytochemistry* 45 (4), 819–823. doi: 10.1016/S0031-9422(96)00888-6

Jaime, A., Teixeira, D. S., Tikam, S. R., Diganta, N., Nidhi, V., Deodas, T. M., et al. (2013). Pomegranate biology and biotechnology: A review. *Scientia Hortic.* 160, 85–107. doi: 10.1016/j.scienta.2013.05.017

Kalaycıoğlu, Z., and Erim, F. B. (2017). Total phenolic contents, antioxidant activities, and bioactive ingredients of juices from pomegranate cultivars worldwide. *Food Chem.* 221, 496–507. doi: 10.1016/j.foodchem.2016.10.084

Kopustinskiene, D. M., Jakstas, V., Savickas, A., and Bernatoniene, J. (2020). Flavonoids as anticancer agents. *Nutrients* 12 (2), 457. doi: 10.3390/nu12020457

Lampakis, D., Skenderidis, P., and Leontopoulos, S. (2021). Technologies and extraction methods of polyphenolic compounds derived from pomegranate (*Punica granatum*) peels. A Mini Review. *Processes* 9, 236. doi: 10.3390/pr9020236

Legua, P., Melgarejo, P., Abdelmajid, H., Martínez, J. J., Martínez, R., Ilham, H., et al. (2012). Total phenols and antioxidant capacity in 10 Moroccan pomegranate varieties. *J. Of Food Sci.* 77 (1), 115–120. doi: 10.1111/j.1750-3841.2011.02516.x

Li, C., and Wang, M. (2011). Antioxidant activity of peach blossom extracts. *J. Korean Soc. Appl. Biol. Chem.* 54, 46–53. doi: 10.3839/jksabc.2011.006

Liu, Y., Kong, K., Wu, D., Liu, H., Li, H., Zhang, J., et al. (2022). Pomegranate peel-derived punicalagin: Ultrasonic-assisted extraction, purification, and its α-glucosidase inhibitory mechanism. *Food Chem.* 374, 131635. doi: 10.1016/j.foodchem.2021.131635

Liu, Y., and Seeram, N. P. (2018). Liquid chromatography coupled with time-of-flight tandem mass spectrometry for comprehensive phenolic characterization of pomegranate fruit and flower extracts used as ingredients in botanical dietary supplements. *J. Separation Sci.* 41 (15), 3022–3033. doi: 10.1002/jssc.201800480

Lou, J., Wu, C., Wang, H., Cao, S., Wei, Y., Chen, Y., et al. (2023). Melatonin treatment delays postharvest senescence of broccoli with regulation of carotenoid metabolism. *Food Chem.* 408, 135185. doi: 10.1016/j.foodchem.2022.135185

Man, G., Xu, L., Wang, Y., Liao, X., and Xu, Z. (2022). Profiling phenolic composition in pomegranate peel from nine selected cultivars using UHPLC-QTOF-MS and UPLC-QQQ-MS. *Front. In Nutr.* 8. doi: 10.3389/fnut.2021.807447

Mansour, H. M. M., El-Sohaimy, S. A., Zeitoun, A. M., and Abdo, E. M. (2022). Effect of natural antioxidants from fruit leaves on the oxidative stability of soybean oil during accelerated storage. *Antioxidants (Basel)* 11 (9), 1691. doi: 10.3390/antiox11091691

Marcelino, S., Mandim, F., Taofiq, O., Pires, T. C. S. P., Finimundy, T. C., Prieto, M. A., et al. (2023). Valorization of *Punica granatum* L. leaves extracts as a source of bioactive molecules. *Pharm. (Basel)* 16, 342. doi: 10.3390/ph16030342

Martínez, L., Castillo, J., Ros, G., and Nieto, G. (2019). Antioxidant and antimicrobial activity of rosemary, pomegranate and olive extracts in fish patties. *Antioxidants (Basel)* 8 (4), 86. doi: 10.3390/antiox8040086

Mirdehghan, H. S., and Rahemi, M. (2007). Seasonal changes of mineral nutrients and phenolics in pomegranate (*Punica granatum* L.) fruit. *Scientia Hortic.* 111 (2), 120–127. doi: 10.1016/j.scienta.2006.10.001

Mo, F., Lv, B., An, T., Miao, J., Liu, J., Zhang, J., et al. (2019). Protective mechanism of punicalagin against endoplasmic reticulum stress in the liver of mice with type 2 diabetes mellitus. *J. Funct. Foods* 56, 57–64. doi: 10.1016/J.JFF.2019.03.006

Montefusco, A., Durante, M., Migoni, D., De Caroli, M., Ilahy, R., Pék, Z., et al. (2021). Analysis of the phytochemical composition of pomegranate fruit juices, peels and kernels: a comparative study on four cultivars grown in southern Italy. *Plants* 10 (11), 2521. doi: 10.3390/plants10112521

Niknam, S., Tofighi, Z., Faramarzi, M. A., Abdollahifar, M. A., Sajadi, E., Dinarvand, R., et al. (2021). Polyherbal combination for wound healing: *Matricaria chamomilla* L. and *Punica granatum* L. *J. Pharm. Sci.* 29 (1), 133–145. doi: 10.1007/s40199-021-00392-x

Ozgen, M., Durgaç, C., Serçe, S., and Kaya, C. (2008). Chemical and antioxidant properties of pomegranate cultivars grown in the Mediterranean region of Turkey. *Food Chem.* 111 (3), 703–706. doi: 10.1016/J.FOODCHEM.2008.04.043

Parafati, L., Pesce, F., Siracusa, L., Fallico, B., Restuccia, C., and Palmeri, R. (2021). Pomegranate byproduct extracts as ingredients for producing experimental cheese with enhanced microbiological, functional, and physical characteristics. *Foods* 10 (11), 2669. doi: 10.3390/foods10112669

Park, Y., Jung, S. T., Kang, S., Heo, B. G., Arancibia-Avila, P., Toledo, F., et al. (2008). Antioxidants and proteins in ethylene-treated kiwifruits. *Food Chem.* 107 (2), 640–648. doi: 10.1016/J.FOODCHEM.2007.08.070

Peng, Y., Wang, G., Cao, F., and Fu, F. (2020). Collection and evaluation of thirty-seven pomegranate germplasm resources. *Appl. Biol. Chem.* 63, 15. doi: 10.1186/s13765-020-00497-y

Seeram, N. P., Lee, R., Hardy, M. L., and Heber, D. (2005). Rapid large scale purification of ellagitannins from pomegranate husk, a by-product of the commercial juice industry. *Separation Purification Technol.* 41 (1), 49–55. doi: 10.1016/J.SEPPUR.2004.04.003

Shaygannia, E., Bahmani, M., Zamanzad, B., and Rafieian-Kopaei, M. (2016). A review study on *Punica granatum* L. *J. Evidence-Based complementary Altern. Med.* 21 (3), 221–227. doi: 10.1177/2156587215598039

Silva, S., Costa, E. M., Calhau, C., Morais, R. M., and Pintado, M. E. (2017). Anthocyanin extraction from plant tissues: A review. *Crit. Rev. Food Sci. Nutr.* 57 (14), 3072–3083. doi: 10.1080/10408398.2015.1087963

Singh, J., Pareek, S., Maurya, V. K., Sagar, N. A., Kumar, Y., Badgujar, P. C., et al. (2022). Application of *Aloe vera* gel coating enriched with cinnamon and rosehip oils to maintain quality and extend shelf life of pomegranate arils. *Foods* 11 (16), 2497. doi: 10.3390/foods11162497

Teniente, S. L., Flores-Gallegos, A. C., Esparza-González, S. C., Campos-Múzquiz, L. G., Nery-Flores, S. D., and Rodríguez-Herrera, R. (2023). Anticancer effect of pomegranate peel polyphenols against cervical cancer. *Antioxidants (Basel)* 12 (1), 127. doi: 10.3390/antiox12010127

Tzulker, R., Glazer, I., Bar-Ilan, I., Holland, D., Aviram, M., and Amir, R. (2007). Antioxidant activity, polyphenol content, and related compounds in different fruit juices and homogenates prepared from 29 different pomegranate accessions. *J. Agric. Food Chem.* 55 (23), 9559–9570. doi: 10.1021/jf071413n

Wang, B., Luan, F., Bao, Y., Peng, X., Rao, Z., Tang, Q., et al. (2022). Traditional uses, phytochemical constituents and pharmacological properties of *Osmanthus fragrans*: A review. *J. Ethnopharmacology* 293, 115273. doi: 10.1016/j.jep.2022.115273

Wang, C., Shi, L., Fan, L., Ding, Y., Zhao, S., Liu, Y., et al. (2013). Optimization of extraction and enrichment of phenolics from pomegranate (*Punica granatum* L.) leaves. *Ind. Crops Products* 42, 587–594. doi: 10.1016/J.INDCROP.2012.06.031

Wang, Q., Yuan, T., Zhu, X., Song, G., Wang, D., Li, L., et al. (2023). The phenolics, antioxidant activity and in *vitro* digestion of pomegranate (*Punica granatum* L.) peels: an investigation of steam explosion pre-treatment. *Front. In Nutr.* 10. doi: 10.3389/fnut.2023.1161970

Wei, D., Sun, W., Huang, M., Zeng, X., Chen, Y., and Yuan, Z. (2023). Phenolic characterization and antioxidant activity of *Chrysanthemum indicum* and *Opisthopappus* shih during different growth stages. *Chem. Biodiversity* 20(7), e202300370. doi: 10.1002/cbdv.202300370

Williams, W. B., Cuvelier, M. E., and Berset, C. (1995). Use of a free radical method to evaluate antioxidant activity. *Food Sci. Technol.* 28 (1), 25–30. doi: 10.1016/S0023-6438(95)80008-5

Wojdyło, A., and Oszmiański, J. (2020). Antioxidant activity modulated by polyphenol contents in apple and leaves during fruit development and ripening. *Antioxidants (Basel)* 9 (7), 567. doi: 10.3390/antiox9070567

Yisimayili, Z., and Chao, Z. (2022). A review on phytochemicals, metabolic profiles and pharmacokinetics studies of the different parts (juice, seeds, peel, flowers, leaves and bark) of pomegranate (*Punica granatum* L.). *Food Chem.* 395, 133600. doi: 10.1016/j.foodchem.2022.133600

Yu, M., Gouvinhas, I., Rocha, J., and Barros, A.I.R.N.A. (2021). Phytochemical and antioxidant analysis of medicinal and food plants towards bioactive food and pharmaceutical resources. *Sci. Rep.* 11 (1), 10041. doi: 10.1038/s41598-021-89437-4

Yuan, L., Yun, Y., Tian, J., Gao, Z., Xu, Z., Liao, X., et al. (2022). Transcription profile analysis for biosynthesis of flavor volatiles of Tunisian soft-seed pomegranate arils. *Food Res. Int.* 156, 111304. doi: 10.1016/j.foodres.2022.111304

Zeng, Y., and Peng, Y. (2007). Changes in antioxidant activity in *Rosa rugosa* flowers at different stages of development. *New Z. J. Crop Hortic. Sci.* 35, 397–401. doi: 10.1080/01140670709510207

Zhang, L., Gao, Y., Zhang, Y., Liu, J., and Yu, J. (2010). Changes in bioactive compounds and antioxidant activities in pomegranate leaves. *Scientia Hortic.* 123 (4), 543–546. doi: 10.1016/j.scienta.2009.11.008

Zhang, H., Pu, J., Liu, H., Wang, M., Du, Y., Tang, X., et al. (2023). Effects of L-Cysteine and γ-aminobutyric acid treatment on postharvest quality and antioxidant activity of loquat fruit during storage. *Int. J. Mol. Sci.* 24 (13), 10541. doi: 10.3390/ijms241310541

Zhang, H., Pu, J., Tang, Y., Wang, M., Tian, K., Wang, Y., et al. (2022). Changes in phenolic compounds and antioxidant activity during development of 'Qiangcuili' and 'Cuihongli' fruit. *Foods* 11, 3198. doi: 10.3390/foods11203198

Zhao, X., and Yuan, Z. (2021). Anthocyanins from pomegranate (*Punica granatum* L.) and their role in antioxidant capacities in *Vitro*. *Chem. Biodiversity* 18 (10), e2100399. doi: 10.1002/cbdv.202100399

Zhao, X., Zhang, W., Yin, X., Su, M., Sun, C., Li, X., et al. (2015). Phenolic composition and antioxidant properties of different peach [*Prunus persica* (L.) Batsch] cultivars in China. *Int. J. Mol. Sci.* 16 (3), 5762–5778. doi: 10.3390/ijms16035762

frontiers | Frontiers in Plant Science

TYPE Original Research
PUBLISHED 11 October 2023
DOI 10.3389/fpls.2023.1252196

OPEN ACCESS

EDITED BY
Eman A. Mahmoud,
Damietta University, Egypt

REVIEWED BY
Marina Russo,
University of Messina, Italy
Antonio Giovino,
Council for Agricultural and Economics Research (CREA), Italy

*CORRESPONDENCE
Sonia Piacente
piacente@unisa.it

†These authors have contributed equally to this work and share first authorship

RECEIVED 03 July 2023
ACCEPTED 13 September 2023
PUBLISHED 11 October 2023

CITATION
Cerulli A, Napolitano A, Olas B, Masullo M and Piacente S (2023) *Corylus avellana* "Nocciola Piemonte": metabolomics focused on polar lipids and phenolic compounds in fresh and roasted hazelnuts. *Front. Plant Sci.* 14:1252196. doi: 10.3389/fpls.2023.1252196

Corylus avellana "Nocciola Piemonte": metabolomics focused on polar lipids and phenolic compounds in fresh and roasted hazelnuts

Antonietta Cerulli[1†], Assunta Napolitano[1†], Beata Olas[2], Milena Masullo[1] and Sonia Piacente[1,3*]

[1]Department of Pharmacy, University of Salerno, Fisciano, SA, Italy, [2]Department of General Biochemistry, Institute of Biochemistry, Faculty of Biology and Environmental Protection, University of Lodz, Lodz, Poland, [3]National Biodiversity Future Center (NBFC), Palermo, Italy

The common hazel plant (*Corylus avellana* L., Betulaceae) is one of the most popular tree nuts widespread in Europe and Asia. In Italy, there are different cultivars among which the cultivar affording the valuable hazelnut "Tonda Gentile Trilobata," also known as "Tonda Gentile delle Langhe," covered by the Protected Geographical Indication (PGI) label "Nocciola Piemonte" (NP), known for its sweetness, cooked-bread aroma, and the low intensity of the burnt aroma. In order to obtain a detailed and in-depth characterization of the polar fraction of fresh (NPF) and roasted (NPR) kernels of NP the analysis of the *n*-butanol extracts by liquid chromatography coupled to electrospray ionization and high-resolution mass spectrometry (LC-ESI/HRMS) was carried out. Moreover, to evaluate the quantitative distribution of the most representative polar lipids in NPF and NPR, the analysis by liquid chromatography combined with tandem mass spectrometry (LC-MS/MS) was performed. To unambiguously identify the phenolic compounds highlighted by the LC-ESI/HRMS profiles, they were isolated from the *n*-butanol extract and characterized by Nuclear Magnetic Resonance (NMR) experiments. Finally, the ability of the isolated compounds to exert radical scavenging activity and to inhibit the lipid peroxidation induced by H_2O_2 or H_2O_2/Fe^{2+} was tested by Trolox Equivalent Antioxidant Capacity (TEAC) and thiobarbituric acid reactive substances (TBARS) assays, respectively. The LC-ESI/HRMS allowed to ascertain the presence of phenolic compounds and multiple classes of polar lipids including phospholipids, glycolipids, sphingolipids, and oxylipins. The quantitative analysis highlighted in NPR fraction a lipid content three times higher than in NPF, evidencing lyso-phospholipids and phospholipids as the most represented lipid classes in both NPF and NPR, together accounting for 94 and 97% of the considered lipids, respectively. Furthermore, phytochemical analysis permitted to identify flavonoid and diarylheptanoid derivatives. In particular, quercetin 3-O-β-D-galactopyranosyl-(1→2)-β-D-glucopyranoside and myricetin-3-O-α-L-rhamnopyranoside showed the highest antioxidant activity, exhibiting TEAC values similar to that of quercetin, used as reference compound (2.00 ± 0.03 and 2.06 ± 0.03 mM vs 2.03 ± 0.03 mM, respectively). Moreover, most of the tested compounds were found to reduce lipid peroxidation induced by H_2O_2 and

H_2O_2/Fe^{2+} more than curcumin used as positive control, with myricetin-3-O-α-L-rhamnopyranoside determining 44.4 % and 34.1 % inhibition percentage, respectively.

KEYWORDS

Corylus avellana, "Nocciola Piemonte" PGI, fresh and roasted hazelnut, polar lipids, phenolic compounds, LC-ESI/LTQOrbitrap/MS/MS^n, antioxidant activity

Introduction

The common hazel plant (*Corylus avellana* L., Betulaceae) is one of the most popular tree nuts, widespread in Europe and Asia. It grows in mild climates such as Turkey, Spain, and Italy. Turkey represents the leader country in the production and exportation of hazelnuts, accounting for more than 70% of the world crop, followed by Italy (15%–20%) and the United States (less than 5%) (Caligiani et al., 2014).

Currently, in Italy, there are two hazelnut varieties registered by the European Union with the Protected Geographical Indication (PGI) label, that is, "Nocciola di Giffoni" and "Nocciola Piemonte" (also known as "Tonda Gentile Trilobata" or "Tonda Gentile delle Langhe"). Both are widely recognized as excellent hazelnuts for industrial processing into roasted kernels (Caligiani et al., 2014).

Our previous investigations focused the attention on the leaves, flowers, shells, green leafy involucres, and kernel of *C. avellana* cultivar "Tonda di Giffoni," leading to the isolation of natural compounds belonging to the class of flavonoids, caffeic acids, cyclic diarylheptanoids, and cyclic diaryletherheptanoids, named giffonins A–X (Masullo et al., 2015a; Masullo et al., 2015b; Masullo et al., 2016; Cerulli et al., 2017; Masullo et al., 2017; Cerulli et al., 2018b; Cerulli et al., 2018c; Napolitano et al., 2018; Bottone et al., 2019; Masullo et al., 2021b; Masullo et al., 2022).

The edible part of hazelnuts is kernel, a food abundantly consumed raw or roasted, appreciated for flavor and texture. As the dry heat treatment of kernels leads to the development of the flavor, color, and crunchy texture (Slatnar et al., 2014; Binello et al., 2018), confectionary industry prefers roasted hazelnuts to produce chocolates, ice creams, and a wide variety of desserts (Jiang et al., 2021; Cristofori et al., 2022).Several research groups have reported the benefits of the inclusion of nuts in the human diet. Among nut species, US Food and Drug Administration (FDA) has recognized hazelnuts as "heart-healthy" foods by virtue of their nutritional and nutraceutical properties (Alasalvar and Pelvan, 2011).

The beneficial effects of hazelnuts on human health are related to the content of monounsaturated (MUFA) and polyunsaturated fatty acids (PUFAs), proteins, carbohydrates, dietary fibers, phytosterols (mainly β-sitosterol), vitamins (vitamin E), antioxidant phenolics, and minerals. MUFA and PUFA are responsible for health benefits including the lowering of plasma oxidized Low Density Lipoprotein (LDL) levels (Sun et al., 2022) and the prevention of cardiovascular diseases, diabetes, cancer, Alzheimer's disease, and dementia (Rincón-Cervera et al., 2022), while tocopherols of hazelnuts are reported to exert positive effects in preventing heart disease and various types of cancer by inhibiting tumor growth and enhancing the human immune system (Dietrich et al., 2006; Bacchetta et al., 2013). Hazelnuts also contain several phytosterols; they constitute their cell membranes, stabilizing the phospholipid bilayer. In the human gut, due to their high hydrophobicity, phytosterols interfere with cholesterol absorption, consequently contributing to the control of cholesterol levels (Rondanelli et al, 2023, Ostlund, 2002; Sabaté and Salas-Salvadó, 2006).

Studies on *C. avellana* "Nocciola Piemonte" focused the attention mainly on volatile organic compounds present in hazelnuts (Ortega-Gavilán et al., 2023) and on the investigation of hazelnut primary metabolome, with particular attention to monounsaturated and polyunsaturated fatty acids (Caligiani et al., 2014; Granata et al., 2017; Cialiè Rosso et al., 2021). Moreover, their phenolic compound profile was also investigated, highlighting changes caused by different storage conditions (Ghirardello et al., 2016).

Noteworthy, our investigation on "Nocciola di Giffoni" hazelnuts highlighted the occurrence of polar lipids belonging to the class of phospholipids, glycolipids, sphingolipids, and oxylipins, reported in the literature for their biological activity (Cerulli et al., 2021). Oxylipins are involved in *in-vivo* inflammatory cascades, pain perception, and skin barrier integrity, whereas, phospholipids counter the declining of memory, prevent the development of nonalcoholic fatty liver disease, and are involved in the mechanism of angiogenesis, inflammation, cancer, and diabetes (Inoue et al., 2011; Kihara et al., 2015; Napolitano et al., 2018). Glycolipids have been reported to display antiviral, antitumor, and anti-inflammatory activities (Napolitano et al., 2007; Napolitano et al., 2018). Based on the interesting activity reported for these polar lipids (Cannavacciuolo et al., 2022), and considering that, in literature, there was no comprehensive information about the polar lipid composition of "Nocciola Piemonte" hazelnuts, an in-depth investigation on polar metabolites occurring in "Nocciola Piemonte" kernels was carried out, with a special focus on phenolics and polar lipids, to fill the gap existing in "Nocciola Piemonte" literature on the latter metabolites. Considering that hazelnuts are generally consumed roasted, and there is evidence that the roasting process could influence their chemical composition (Locatelli et al., 2015), both fresh (NPF) and roasted (NPR) "Nocciola Piemonte" kernels (without skin) were considered. Thereby, by following an analytical approach based

on high-performance liquid chromatography coupled to linear ion-trap, allowing multiple levels of fragmentation, and orbitrap high-resolution mass spectrometry with both negative and positive electrospray ionization [LC-(±)ESI/LTQOrbitrap/MS/MS^n], exhaustive and thorough profiles of the *n*-butanol extract of both NPF and NPR were achieved. In particular, the presence of several lipid classes including phospholipids, glycolipids, sphingolipids, and oxylipins, along with different phenolic derivatives was ascertained. Subsequently, with the aim to obtain a quantitative distribution of the main polar lipid classes both in NPF and NPR, LC-ESI/QTrap/MS/MS analysis by Multiple Reaction Monitoring (MRM) experiments was carried out on the *n*-butanol extracts.

Moreover, to obtain an unequivocal structural characterization of phenolics highlighted by LC-ESI/HRMS analysis, the *n*-butanol extract of NPR kernel was investigated, leading to the isolation and structural identification, by 1D- and 2D-NMR experiments, of metabolites belonging to flavonoid and diarylheptanoid classes.

Finally, in order to evaluate the isolated compounds for their antioxidant activity and inhibitory effects on human plasma lipid peroxidation induced by H_2O_2 and H_2O_2/Fe^{2+}, a spectrophotometric Trolox Equivalent Antioxidant Capacity (TEAC) assay determining the radical-scavenging activity and a test measuring the concentration of thiobarbituric acid reactive substances (TBARS) were performed, respectively.

Material and methods

Chemicals and reagents

Chloroform, *n*-hexane, methanol (MeOH), and *n*-butanol were purchased from VWR (Milan, Italy). Water, acetonitrile (ACN), 2-propanol (IPA), and formic acid used for LC-MS were of Merck brand and were bought from Deltek (Naples, Italy); methanol-d_4 (99.95%) was bought by Sigma-Aldrich (Milan, Italy).

The following polar lipids of Avanti Polar Lipids brand (bought from Merck, Darmstadt, Germany) were used as internal reference standards: phosphatidylglycerol PG (8:0;8:0), 10 µg/ml; phosphat idylcholine PC (8:0;8:0), 30 µg/ml; phosphatidylethanolamine PE (8:0;8:0), 60 µg/ml; phosphatidic acid PA (14:0;14:0), 20 µg/ml; phosphatidylserine PS (14:0;14:0), 2.5 µg/ml; sulfoquinovo syldiacylglycerol SQDG (18:3;16:0), 20 µg/ml; monogalactosyl diacylglycerol MGDG (18:3;18:3), 50 µg/ml. Dimethylsulfoxide (DMSO), thiobarbituric acid (TBA), and H_2O_2 were purchased from Sigma-Aldrich (St. Louis, MO., USA).

Samples

Corylus avellana L. hazelnuts ("Nocciola Piemonte") were obtained from la Gentile s.r.l. (N:44°34'38.6", E:8°11'42.7"). Hazelnuts (size in the range of 17 mm–21 mm) were collected in August 2021. A voucher specimen was deposited in Department of Pharmacy, University of Salerno, Italy.

Extraction workflow

C. avellana kernels were crushed by a knife and stored at room temperature for 3 days. Hazelnuts (220 g), after removal of the skin, were submitted to defatting with *n*-hexane and chloroform, and successively extracted with MeOH, each time using 4.5 L of solvent. The extractions were repeated, every 3 days, until, for each solvent, the last recovery was less than 10%. The MeOH extract was filtered and dried under vacuum, then, in order to remove oily compounds (e.g., triglycerides), it was partitioned using *n*-hexane and MeOH. Finally, with the aim to remove the free sugars that interfere with the identification of primary and specialized metabolites, the derived MeOH extract underwent to *n*-butanol/water partition, thus obtaining 8.0 g of *n*-butanol extract. Hazelnut kernels without skin (250 g) were roasted as previously reported by Napolitano et al. (Cerulli et al., 2018c; Napolitano et al., 2018) and extracted in the same way of fresh hazelnuts to obtain 9.1 g of *n*-butanol extract.

LC-ESI/HRMS/MS^n qualitative analysis

The analysis of both NPF and NPR *n*-butanol extracts was performed using LC-ESI/HRMS instrument, parameters, and conditions described by Napolitano et al. (Napolitano et al., 2018). Xcalibur software version 2.1 was used for instrument control, data acquisition, and data analysis. For each sample, three replicates were performed.

LC-ESI/MS/MS quantitative analysis

The analysis was performed using a LC-ESI/QTrap/MS System consisting of a Shimadzu Nexera X2 UPLC system in line with a Linear Ion Trap Quadrupole mass spectrometer (QTRAP 6500) (ABSciex, Foster City, CA, USA) in negative ionization mode. A Kinetex EVO C18 column (Phenomenex, 100 mm × 2.1 mm i.d., 1.7 µm), kept at 40°C, and a combination of A (60:40 water:ACN, v/v) and B (85:10:5 IPA:ACN:water, v/v), both containing 0.1% (v/v) formic acid, as mobile phase, were employed for the chromatographic separation. A linear gradient from 15% to 60% B in 9.33 min, to 90% B in 10 min, to 100% B in 4.67 min, held to 100% B for 6 min, back to 15% in 1.3 min, and a flow rate of 0.3 mL/min were used. Six microliter of each extract (0.5 mg/mL) added of internal reference standard lipids was injected. For Ion-Spray operation, the following experimental conditions were used: curtain gas (CUR) = 40; Ion-Spray voltage (IS) = −4500; source temperature (TEM) = 350°C; ion source gas 1 (GS1) = 25; ion source gas 2 (GS2) = 25.

The eluate from the chromatographic column was monitored by MS/MS in MRM mode, by using lipid-class specific values for declustering potential, focusing potential, entrance potential, collision energy, and collision cell exit potential. Three replicates of each sample were performed. The chromatographic peak areas of

detected lipids in each sample, contained in the data set generated by the software supplied by the manufacturer (Analyst 1.6.2), were used as quantitative response. Normalization of the data was performed, calculating the ratio between the peak area of each lipid and that of the corresponding internal reference standard (López-Bascón et al., 2020).

Recovery experiments were performed by adding reference standard solutions at low-, medium-, and high-concentration range in a known amount of both NPF and NPR samples and subsequently extracted as above described and analyzed by LC-ESI/QTrap/MS/MS. Good recovery values (%) in the range of 92% and 108% were obtained.

Isolation of phenolics and NMR analysis

Three grams of *n*-butanol extract of roasted hazelnuts were fractionated on a Sephadex LH-20 (Pharmacia) column (100 cm × 5 cm), using 100% MeOH as mobile phase. In this way, 52 fractions were obtained and monitored by thin-layer chromatography (TLC). To isolate pure compounds, some fractions were chromatographed by semipreparative isocratic RP-HPLC on a Waters 590 system (Waters R401 refractive index detector) a Rheodyne injector, and a Waters XTerra Prep MSC18 column (300 mm × 7.8 mm i.d.), using MeOH-H_2O (2:3) as mobile phase; a flow rate of 2.5 mL/min was used.

By this way, fractions 20–27 (31.0 mg) yielded compounds **4** (2.1 mg, R_t = 9.2 min), **8** (1.6 mg, R_t = 18.2 min), and **11** (1.3 mg, R_t = 21.6 min); fractions 28–33 (21.4 mg) yielded compound **5** (2.3 mg, R_t = 24.0 min); fractions 34–38 (27.5 mg) yielded compound 3 (1.9 mg, R_t = 14.3 min); fractions 39–44 (30.1 mg) yielded compounds **10** (3.4 mg, R_t = 20.8 min) and **9** (2.1 mg, R_t = 24.2 min); fractions 45–47 (8.5 mg) yielded compound **6** (2.1 mg, R_t = 24.2 min). Fraction 50 corresponded to compound **7** (2.3 mg). The purity of these compounds (>99%) was determined by HPLC analysis (Masullo et al., 2015a; Masullo et al., 2015b; Masullo et al., 2016; Masullo et al., 2017).

NMR experiments were acquired in methanol-d_4 on a Bruker DRX-600 spectrometer (Bruker BioSpin GmBH, Rheinstetten, Germany) equipped with a Bruker 5-mm TCI CryoProbe at 300 K. Data processing was carried out with Topspin 3.2 software.

TEAC assays

Radical-scavenging activity was determined by spectrophotometric TEAC assay according to previously described procedures(Maldini et al., 2011; Cerulli et al., 2018a). In particular, in the TEAC assay, the antioxidant activity of isolated compounds (range of 0.3 mM–1.5 mM) was expressed as TEAC value in comparison with the TEAC activity of the reference compound quercetin. The TEAC value is defined as the concentration of a standard Trolox solution with the same antioxidant activity of a 1 mM concentration of the tested compound (calibration equation for Trolox: y = 31.863× + 52.550, R_2 = 1.00).

Lipid peroxidation measurement

Lipid peroxidation was quantified by measuring the concentration of TBARS. Stock solutions of each compound were prepared in 50% DMSO. The final concentration of DMSO in the samples was lower than 0.05%. Fresh human plasma was obtained from medication-free, regular donors at the blood bank (Lodz, Poland). Samples of human plasma were incubated with phenolic compounds and curcumin at the final concentrations of 0.1 μM–100 μM (30 min, at 37°C) alone and plus 2 mM H_2O_2 (30 min, at 37°C) and at the final concentration of 10 μM plus 4.7 mM H_2O_2/3.8 mM Fe_2SO_4/2.5 mM EDTA. Pure compounds were tested by using the TBARS assay as previously reported (Masullo et al., 2015b; Masullo et al., 2016; Cerulli et al., 2017). Three independent experiments were carried out.

Statistical analysis

The statistical analysis was done by several tests. The Q-Dixon test was performed to eliminate uncertain data. All the values in this study were expressed as mean ± standard deviation (SD). The statistical was carried out with one-way analysis of variance for repeated measurements. The statistically significant differences were also evaluated by applying the paired Student's t-test. The significance level used was $p < 0.05$ unless otherwise indicated. Microsoft Excel 2016 was used for statistical analyses.

Results and discussion

LC-ESI/HRMS/MS^n analysis of "Nocciola Piemonte" hazelnuts

With the aim to define the chemical profile of the *n*-butanol extract of both fresh and roasted "Nocciola Piemonte" kernels, an analytical approach based on LC-ESI/LTQOrbitrap/MS/MS^n was carried out. In particular, both negative and positive electrospray ionizations were used considering that lipid classes differ in their ionization capacity, depending on structure and polarity. Furthermore, in addition to an RP-C18 column, an RP-C4 column was used to reduce the strong interactions with the stationary phase of high molecular weight molecules such as phospholipids (Napolitano et al., 2018; Cannavacciuolo et al., 2022).

The careful analysis of accurate masses, characteristic fragmentation patterns, chromatographic behavior, and literature data allowed to putatively ascertain the occurrence, in both NPF and NPR extracts, of polar lipids belonging to oxylipins, phospholipids, sphingolipids, and glycolipids, as well as of phenolic derivatives mainly belonging to flavonoid and diarylheptanoid classes (Tables 1, 2).

10.3389/fpls.2023.1252196

TABLE 1 Polar lipids and phenolic compounds putatively identified in fresh and roasted "Nocciola Piemonte" extracts by using a RP-C18 column for the chromatographic separation.

n°	Compound	R_t (min)	Molecular Formula	$[M-H]^-$	$[(M+FA)-H]^-$	$[M+H]^+$	Error (ppm)	Characteristic product ions	NPR	NPF
1	sucrose	1.94[a]	$C_{12}H_{22}O_{11}$		387.1149		3.61	179, 143	+	+
2	glycerophosphorylinositol	2.13[b]	$C_9H_{19}O_{11}P$	333.0592			3.23	259, 241, 153	+	+
3	quercetin 3-*O*-β-D-galactopyranosyl-(1→2)-β-D-glucopyranoside*	5.74[a]	$C_{27}H_{30}O_{17}$	625.1399			0.04	463, 343, 301	+	+
4	giffonin P	6.13[a]	$C_{19}H_{22}O_7$	361.1286			0.45	343, 301, 271, 241	+	-
5	kaempferol 3-*O*-β-D-glucopyranosyl-(1→2)-β-D-glucopyranoside*	6.25[a]	$C_{27}H_{30}O_{16}$	609.1448			-0.28	447, 327, 285	+	-
6	myricetin-3-*O*-α-L-rhamnopyranoside*	6.54[a]	$C_{21}H_{20}O_{12}$	463.0870			0.07	317	+	–
7	quercetin 3-*O*-β-D-glucopyranoside*	6.70[a]	$C_{21}H_{20}O_{12}$	463.0867			0.64	343, 301	+	+
8	giffonin L	6.74[a]	$C_{19}H_{22}O_6$	345.1331			-0.14	327	+	–
9	kaempferol -3-*O*-β-D-glucopyranoside*	7.40[a]	$C_{21}H_{20}O_{11}$	447.0923			0.06	327, 285	+	+
10	carpinontriol B	8.08[a]	$C_{19}H_{20}O_6$	343.1181			0.48	325, 283, 269	+	+
11	giffonin V	9.65[a]	$C_{19}H_{20}O_5$	327.1233			0.65	309, 283, 253	+	–
12	9,12,13-TriHOME (10)	10.34[b]	$C_{18}H_{34}O_5$	329.2326			1.18	311, 293, 291, 229, 211, 199, 197, 171	+	+
13	l-PC (18:2-1O)	11.20[a]	$C_{26}H_{50}O_8NP$		580.3245		-0.29	520, 431, 295, 242	+	–
14	l-PC (18:2-1O)	11.36[a]	$C_{26}H_{50}O_8NP$		580.3245		-0.29	520, 431, 295, 242	+	–
15	DGMG (18:3)	13.44[b]	$C_{33}H_{56}O_{14}$	675.3593[b]	721.3649		0.68[b]	415, 397, 323, 235	+	+
16	DGMG (18:2)	14.38[b]	$C_{33}H_{58}O_{14}$	677.3755[b]	723.3801		1.27[b]	415, 397, 279, 235	+	+
17	l-PC (16:1)	14.46[a]	$C_{24}H_{48}O_7NP$		538.3138		-0.31	478, 253, 242	+	–
18	l-PC (16:1)	14.74[a]	$C_{24}H_{48}O_7NP$		538.3141		0.38	478, 389, 253, 242	+	+
19	12,13-DiHOME (9)	15.12[b]	$C_{18}H_{34}O_4$	313.2378			1.64	295, 277, 213, 183	+	+
20	DGMG (18:2)	15.13[b]	$C_{33}H_{58}O_{14}$	677.3740[b]	723.3798		-0.26[b]	415, 397, 323, 279, 235	+	+
21	l-PE (18:2)	15.15[b]	$C_{23}H_{44}O_7NP$	476.2771			-0.20	415, 279, 214, 196, 153	+	+
22	l-PC (18:2)	15.23[a]	$C_{26}H_{50}O_7NP$		564.3298[a]	520.3362[d]	0.43[a]	504, 415, 279, 242, 224	+	+
23	9,10-DiHOME (12)	15.47[b]	$C_{18}H_{34}O_4$	313.2381			2.44	295, 277, 269, 245, 201, 183, 171	–	+
24	DGMG (16:0)	15.66[b]	$C_{31}H_{58}O_{14}$	653.3732[b]	699.3799		-1.11[b]	415, 397, 235	+	+
25	l-PE (18:2)	15.78[b]	$C_{23}H_{44}O_7NP$	476.2778			1.27	415, 279, 214, 196, 153	+	+
26	l-PC (18:2)	15.85[a]	$C_{26}H_{50}O_7NP$		564.3299[a]	520.3369[d]	0.54[a]	504, 415, 279, 242, 224	+	+
27	l-PE (16:0)	16.63[b]	$C_{21}H_{44}O_7NP$	452.2772			0.19	391, 255, 214, 196, 153	+	+
28	DGMG (16:0)	16.67[b]	$C_{31}H_{58}O_{14}$	653.3745[b]	699.3798		0.23[b]	415, 397, 255, 235	+	+

(Continued)

10.3389/fpls.2023.1252196

TABLE 1 Continued

n°	Compound	R_t (min)	Molecular Formula	[M-H]$^-$	[(M+FA)-H]$^-$	[M+H]$^+$	Error (ppm)	Characteristic product ions	NPR	NPF
29	9,10-DHSA	16.76[b]	$C_{18}H_{36}O_4$	315.2535			1.76	297, 279, 201, 187, 171	+	+
30	l-PC (16:0)	16.79[a]	$C_{24}H_{50}O_7NP$		540.3290		-1.03	480, 391, 255, 242, 224	+	+
31	DGMG (18:1)	17.11[b]	$C_{33}H_{60}O_{14}$	679.3888[b]	725.3954		-1.08[b]	415, 397, 281, 235	+	+
32	l-PE (16:0)	17.57[b]	$C_{21}H_{44}O_7NP$	452.2773			0.32	391, 255, 214, 196, 153	+	+
33	l-PC (16:0)	17.77[a]	$C_{24}H_{50}O_7NP$		540.3288		-1.47	480, 391, 255, 242, 224	+	+
34	9,10-DHSA	17.98[b]	$C_{18}H_{36}O_4$	315.2536			2.04	297,279, 201, 187, 171	+	+
35	DGMG (18:1)	18.24[b]	$C_{33}H_{60}O_{14}$	679.3911[b]	725.3958		1.18[b]	415, 397, 323, 281, 235	+	+
36	l-PE (18:1)	18.39[b]	$C_{23}H_{46}O_7NP$	478.2933			0.95	417, 281, 214, 196, 153	+	+
37	l-PC (18:1)	18.50[a]	$C_{26}H_{52}O_7NP$		566.3454[a]	522.3538[d]	0.27[a]	506, 417, 281 242, 224	+	+
38	l-PE (18:1)	19.36[b]	$C_{23}H_{46}O_7NP$	478.2935			1.47	417, 281, 214, 196, 153	+	+
39	l-PC (18:1)	19.53[a]	$C_{26}H_{52}O_7NP$		566.3458[a]	522.3538[d]	1.03[a]	506, 417, 281, 242, 224	+	+
40	9-HODE (10, 12)	22.28[b]	$C_{18}H_{32}O_3$	295.2271			1.35	277, 171	+	+
41	acyldiglycoside (18:1)	21.65[b]	$C_{30}H_{54}O_{12}$	605.3537[b]	651.3589		0.55[b]	341, 323, 281	+	+
42	acyldiglycoside (18:1)	22.08[b]	$C_{30}H_{54}O_{12}$	605.3532[b]	651.3590		0.06[b]	341, 323, 281	+	+
43	l-PS (18:2)	22.30[b]	$C_{24}H_{44}O_9NP$	520.2676			0.89	502, 433, 415, 279, 153	+	+
44	acyldiglycoside (18:1)	22.88[b]	$C_{30}H_{54}O_{12}$	605.3533[b]	651.3589		0.12[b]	341, 323, 281	–	+
45	l-PI (16:1)	23.55[b]	$C_{25}H_{47}O_{12}P$	569.2725			0.56	389, 315, 253, 241, 223	–	+
46	DGMG (18:0)	23.93[b]	$C_{33}H_{62}O_{14}$	681.4067[b]	727.4115		1.09[b]	415, 397, 323, 235	–	+
47	l-PE (18:0)	23.94[b]	$C_{23}H_{48}O_7NP$	480.3089			0.97	419, 283, 214, 196, 153	+	+
48	l-PI (16:1)	24.32[b]	$C_{25}H_{47}O_{12}P$	569.2721			-0.09	389, 315, 253, 241, 223	–	+
49	acyldiglycoside (18:1)	24.45[b]	$C_{30}H_{54}O_{12}$	605.3544[b]	651.3594		1.22[b]	281	+	+
50	l-PC (18:0)	25.24[b]	$C_{26}H_{54}O_7NP$		568.3611		0.45	508, 283, 242, 224	+	+
51	l-PI (18:2)	25.57[b]	$C_{27}H_{49}O_{12}P$	595.2880			0.29	415, 333, 315, 279, 241, 223, 171	+	+
52	l-PE (18:0)	25.62[b]	$C_{23}H_{48}O_7NP$	480.3089			0.97	419, 283, 214, 196, 153	–	+
53	l-PS (18:1)	26.10[b]	$C_{24}H_{46}O_9NP$	522.2822			-0.91	504, 435, 417, 283, 153	+	+
54	l-PC (18:0)	27.04[b]	$C_{26}H_{54}O_7NP$		568.3612		0.55	508, 419, 283, 242, 224	+	+
55	l-PI (18:2)	27.61[b]	$C_{27}H_{49}O_{12}P$	595.2882			0.71	415, 333, 315, 279, 241, 223, 171	+	+

(Continued)

TABLE 1 Continued

n°	Compound	R_t (min)	Molecular Formula	[M-H]$^-$	[(M+FA)-H]$^-$	[M+H]$^+$	Error (ppm)	Characteristic product ions	NPR	NPF
56	NA-GPE (18:2)	27.71[b]	$C_{23}H_{44}O_7NP$	476.2772[b]			0.05[b]	402, 384, 278, 214, 171, 153	+	+
					478.2944[d]	3.25[d]	460, 324, 306, 280	+	+	
57	l-PS (18:1)	29.13[b]	$C_{24}H_{46}O_9NP$	522.2830			0.60	504, 435, 417, 281, 153	–	+
58	l-PI (16:0)	29.34[b]	$C_{25}H_{49}O_{12}P$	571.2876			-0.33	409, 391, 333, 315, 255, 241, 223, 171	+	+
59	l-PI (16:0)	32.22[b]	$C_{25}H_{49}O_{12}P$	571.2880			0.40	409, 391, 333, 315, 255, 241, 223, 171	+	+
60	SQMG (18:2)	33.45[b]	$C_{27}H_{48}O_{11}S$	579.2839			0.88	317, 299, 279, 225, 207	+	+
61	l-PI (18:1)	34.29[b]	$C_{27}H_{51}O_{12}P$	597.3049			2.39	435, 417, 333, 315, 281, 241, 223, 171	+	+
62	SQMG (18:2)	35.28[b]	$C_{27}H_{48}O_{11}S$	579.2837			0.67	317, 299, 279, 225, 207	+	+
63	l-PI (18:1)	37.21[b]	$C_{27}H_{51}O_{12}P$	597.3043			1.47	435, 417, 333, 315, 281, 241, 223, 171	+	+
64	NA-GPE (18:1)	37.25[b]	$C_{23}H_{46}O_7NP$	478.2934[b]			1.28[b]	404, 386, 280, 214, 171, 153	+	+
					480.3085[d]	0.07[d]	462, 326, 308, 282	+	+	
65	SQMG (16:0)	39.43[b]	$C_{25}H_{48}O_{11}S$	555.2835			0.27	317, 299, 255, 225, 207	+	+
66	SQMG (16:0)	42.29[b]	$C_{25}H_{48}O_{11}S$	555.2838			0.81	317, 299, 255, 225, 207	+	+
67	MAG (16:0)	46.56[c]	$C_{19}H_{38}O_4$			331.2835	-2.25	313, 281, 257, 239	+	+
68	MAG (18:1)	48.99[c]	$C_{21}H_{40}O_4$			357.2987	-3.49	339, 283, 265	+	+
69	SQMG (18:1)	50.51[b]	$C_{27}H_{50}O_{11}S$	581.2994			0.64	317, 299, 281, 225, 207	+	+
70	MAG (18:0)	54.35[c]	$C_{21}H_{42}O_4$			359.3145	-2.99	341, 285, 267, 239	+	+
71	MAG (18:0)	55.59[c]	$C_{21}H_{42}O_4$			359.3147	-2.47	341, 285, 267, 239	+	+

[a]derived by LC-HRMS analysis of NPR on Atlantis T3 column in negative ion mode; [b]derived by LC-HRMS analysis of NPF on Atlantis T3 column in negative ion mode, [c]derived by LC-HRMS analysis of NPR on Atlantis T3 column in positive ion mode, [d]derived by -MS analysis of NPF on Atlantis T3 column in positive ion mode.
The 18-carbon hydroxylated acyl chain is abbreviated as 18:2-1O to indicate two double bond equivalent and one oxygen atom beyond the carbonyl group.
*Compounds characterized by NMR.
+: metabolites present in the extract; -: metabolites absent in the extract.

Oxylipins identification

The analysis of LC-(-)ESI/HRMS profiles allowed to detect both in NPF and in NPR extracts the compounds **12**, **19**, **23**, **29**, **34**, and **40** (Table 1) ascribable to oxylipins, which are hydroxyl fatty acids having different unsaturation degree and number of hydroxyl groups, and mainly deriving from the oxidative metabolism of essential PUFA, such as α-linolenic acid (ALA) (18:3-3) and linoleic acid (LA) (18:2-6) (Masullo et al., 2021a). The analysis of their tandem mass spectra highlighted the occurrence of characteristic product ions and diagnostic neutral losses generated by molecular rearrangements involving the head and the end of the acyl chain that, according to literature data, allowed to putatively assign the position on the fatty acyl chain of both hydroxyl groups and double bonds (Richardson et al., 2017; Napolitano et al., 2018). By this way, the finding of the diagnostic product ion at *m/z* 171 (originated by the rearrangement to aldehyde of the hydroxyl function at C9, that caused the subsequent cleavage of the C9–C10 bond and the consequent shortening of the acyl chain, retaining the head-carboxyl group as COO^-), allowed the structural assignment of oxylipins **12**, **19**, **23**, **29**, **34**, and **40** (Table 1) (Levandi et al., 2009). Analogously, the detection in the tandem mass spectrum of the diagnostic peak at *m/z* 183 (corresponding to a molecule of hydroxylated heptanal deriving from the end-part of the acyl chain by breakdown of the C11 and C12 bond, subsequent to the typical CHOH→CHO rearrangement involving the hydroxyl group at C12 guided the identification of oxylipin 19 (Napolitano et al., 2018).

10.3389/fpls.2023.1252196

TABLE 2 Polar lipids putatively identified in fresh and roasted "Nocciola Piemonte" extracts by using a RP-C4 column for the chromatographic separation.

n°	Compound	R_t (min)	Molecular Formula	$[M-H]^-$	$[(M+FA)-H]^-$	Error (ppm)	Characteristic product ions	NPR	NPF
72	l-PG (16:0)	12.57[b]	$C_{22}H_{45}O_9P$	483.2722		-1.29	391, 255, 245, 227, 153	–	+
73	l-PA (18:2)	12.88[b]	$C_{21}H_{39}O_7P$	433.2349		-0.11	415, 279, 153, 135	+	+
74	l-PG (16:0)	12.93[b]	$C_{22}H_{45}O_9P$	483.2722		0.86	391, 255, 245, 227, 153	+	+
75	l-PG (18:1)	13.29[b]	$C_{24}H_{47}O_9P$	509.2874		-0.03	417, 281, 245, 227, 153	+	+
76	l-PG (18:1)	13.54[b]	$C_{24}H_{47}O_9P$	509.2870		-0.86	417, 281, 245, 227, 153	+	+
77	l-PA (18:2)	13.59[b]	$C_{21}H_{39}O_7P$	433.2350		0.12	415, 279, 153, 135	+	+
78	l-PA (18:1)	13.75[b]	$C_{21}H_{41}O_7P$	435.2500		-1.42	417, 281, 153, 135	–	+
79	l-PA (16:0)	14.06[b]	$C_{19}H_{39}O_7P$	409.2359		2.21	391, 255, 153	–	+
80	l-PA (18:1)	14.67[b]	$C_{21}H_{41}O_7P$	435.2504		-0.43	417, 281, 153, 135	–	+
81	PI (18:2-1O;16:0)	19.78[a]	$C_{43}H_{79}O_{14}P$	849.5112		-1.34	831, 687, 593, 553, 431, 391, 315, 295, 255, 241	+	-
82	PI (18:2-1O;18:1)	20.50[a]	$C_{45}H_{81}O_{14}P$	875.5273		-0.84	857, 713, 611, 593, 579, 431, 417, 315, 295, 281	+	–
83	PI (18:1;18:2-1O)	22.29[a]	$C_{45}H_{81}O_{14}P$	875.5299		2.16	713, 611, 593, 579, 431, 417, 315, 297, 295, 281	+	–
84	PI (18:2;16:1)	23.67[a]	$C_{43}H_{77}O_{13}P$	831.5022		0.49[a]	577, 569, 551, 389, 297, 279, 253, 241	+	+
85	PI (18:3; 16:0)	23.73[a]	$C_{43}H_{77}O_{13}P$	831.5030		1.46	575, 389, 277, 255, 241	+	+
86	PI (18:2;18:2)	24.34[a]	$C_{45}H_{79}O_{13}P$	857.5177		0.26	595, 577, 433, 415, 315, 297, 279, 241	+	+
87	GlcCer (d18:2; h16:0)	24.76[a]	$C_{40}H_{75}O_9N$	712.5353		-0.74	550, 532, 271, 225; MS^3(550): 532, 314, 312, 296, 271, 270, 253, 235, 225	+	+
88	PI (16:0;18:2)	25.48[a]	$C_{43}H_{79}O_{13}P$	833.5174		-0.09	595, 577, 571, 553, 415, 391, 315, 297, 279, 255, 241	+	+
89	PI (18:1;18:2)	26.63[a]	$C_{45}H_{81}O_{13}P$	859.5334		0.35	597, 595, 579, 577, 435, 417, 315, 297, 281, 279, 241	+	+
90	PI (16:0;18:1)	28.08[a]	$C_{43}H_{81}O_{13}P$	835.5334		0.41	673, 579, 571, 553, 417, 391, 315, 297, 281, 255, 241	+	+
91	GlcCer (d18:2; h18:0)	28.86[a]	$C_{42}H_{79}O_9N$	740.5677		0.86	578, 560; MS^3(578): 560, 530, 342, 340, 324, 299, 298, 281, 253	+	+
92	PI (18:1;18:1)	29.48[a]	$C_{45}H_{83}O_{13}P$	861.5492		0.53	699, 597, 579, 435, 417, 315, 297, 281, 241	+	+
93	PE (18:2; 18:2)	29.85[a]	$C_{41}H_{74}O_8NP$	738.5078		1.36	476, 458, 279	+	+
94	SQDG (16:0; 18:1)	30.83[a]	$C_{43}H_{80}O_{12}S$	819.5277		-1.18	563, 555, 537, 281, 255; MS^3(563): 545, 519, 299, 225	+	+
95	SQDG (18:1; 18:1)	32.33[a]	$C_{45}H_{82}O_{12}S$	845.5431		-1.46	581, 563, 281; MS^3(563): 299, 225	+	+
96	PG (16:0;18:2)	31.35[a]	$C_{40}H_{75}O_{10}P$	745.5005		-1.15	671, 507, 489, 483, 465, 415, 391, 279, 255, 227	+	+
97	PE (16:0; 18:2)	31.81[a]	$C_{39}H_{74}O_8NP$	714.5075		0,92	476, 458, 452, 434, 279, 255	+	+
98	PG (18:1;18:2)	32.80[a]	$C_{42}H_{77}O_{10}P$	771.5182		1.42	697, 509, 507, 491, 489, 417, 415, 281, 279, 245	+	+
99	PI (18:0;18:1)	32.90[a]	$C_{45}H_{85}O_{13}P$	863.5647		0,36	599, 581, 437, 419, 315, 297, 283, 281, 241	+	+
100	PE (18:2; 18:1)	33.11[a]	$C_{41}H_{76}O_8NP$	740.5232		0,99	478, 476, 460, 458, 281, 279	+	+
101	PC (18:2;18:2)	34.24[a]	$C_{44}H_{80}O_8NP$		826.5597	0.52	766, 504, 279	+	+
102	PG (16:0;18:1)	34.76[a]	$C_{40}H_{77}O_{10}P$	747.5176		0.69	673, 509, 491, 483, 465, 417, 391, 281, 255, 245, 227	+	+

(Continued)

10.3389/fpls.2023.1252196

TABLE 2 Continued

n°	Compound	R_t (min)	Molecular Formula	[M-H]$^-$	[(M+FA)-H]$^-$	Error (ppm)	Characteristic product ions	NPR	NPF
103	PE (16:0; 18:1)	35.18[a]	$C_{39}H_{76}O_8NP$	716.5234		1,25	452, 434, 391, 281, 255	+	+
104	SQDG (18:0; 18:1)	35.95[a]	$C_{45}H_{84}O_{12}S$	847.5591		-0.98	565, 563, 283, 281; MS^3(563): 225	+	+
105	PG (18:1;18:1)	36.31[a]	$C_{42}H_{79}O_{10}P$	773.5339		1.50	699, 509, 491, 435, 417, 281, 227	+	+
106	PC (16:0;18:2)	36.57[a]	$C_{42}H_{80}O_8NP$		802.5600	0.92	742, 504, 480, 279, 255	+	+
107	PE (18:1; 18:1)	36.68[a]	$C_{41}H_{78}O_8NP$	742.5391		1,33	486, 478, 460, 281	+	+
108	PA (18:2;18:2)	37.96[b]	$C_{39}H_{69}O_8P$	695.4647		0.13	433, 415, 279	–	+
109	PC (18:2;18:1)	37.98[a]	$C_{44}H_{82}O_8NP$		828.5746	-0.39	768, 506, 504, 488, 486, 281, 279	+	+
110	PA (18:1;18:2)	40.45[b]	$C_{39}H_{71}O_8P$	697.4814		1.57	435, 433, 417, 415, 281, 279	+	+
111	PA (16:0;18:2)	40.82[b]	$C_{37}H_{69}O_8P$	671.4647		0.04	433, 415, 409, 391, 279, 255	-	+
112	PC (16:0;18:1)	40.99[a]	$C_{42}H_{82}O_8NP$		804.5750	0.12	744, 488, 480, 462, 281, 255	+	+
113	PC (18:1;18:1)	42.55[a]	$C_{44}H_{84}O_8NP$		830.5911	0.60	770, 506, 488, 281	+	+
114	PA (16:0;18:1)	45.71[b]	$C_{37}H_{71}O_8P$	673.4810		1.01	435, 417, 409, 391, 281, 255	+	+
115	PA (18:1;18:1)	46.84[b]	$C_{39}H_{73}O_8P$	699.4966		1.01	435, 417, 281	+	+
116	PA (18:1;20:2)	49.31[b]	$C_{41}H_{75}O_8P$	725.5107		-0.84	461, 443, 417, 307, 281	–	+
117	PC (18:1;18:0)	49.59[a]	$C_{44}H_{86}O_8NP$		832.6050	-1.41	772, 508, 283	+	+
118	PA (18:1;18:0)	50.82[b]	$C_{39}H_{75}O_8P$	701.5110		-0.59	437, 419, 417, 283, 281	–	+
119	PA (18:1;20:1)	52.42[b]	$C_{41}H_{77}O_8P$	727.5267		-0.56	463, 445, 417, 309, 281	–	+

[a]derived by LC-HRMS analysis of NPR on Symmetry C4 column in negative ion mode; [b]derived by LC-HRMS analysis of NPF on Symmetry C4 column in negative ion mode.
In GlcCer nomenclature, the 2-hydroxylated fatty acids are indicated by the letter "h" added to their lipid number (i.e., h16:0).
+: metabolites present in the extract; -: metabolites absent in the extract. The 18-carbon hydroxylated acyl chain is abbreviated as 18:2-1O to indicate two double bond equivalent and one oxygen atom beyond the carbonyl group.

Phospholipids and N-acylglycerophosphatidylethanolamines identification

The analysis of mass spectrometric data of both NPF and NPR extracts allowed the identification of several compounds ascribable to different classes of phospholipids and their lyso-forms, in which only one of the *sn-1*/*sn-2* positions of the glycerol unit was fatty acylated.

In MS/MS experiments, the different classes of phospholipids are characterized by the production of typical class-featured fragmentation patterns, promptly allowing to distinguish them. By this way, the occurrence of several compounds identifiable as lyso-phosphatidylinositols (l-PI) (45, 48, 51, 55, 58, 59, 61, and 63) and phosphatidylinositols (PI) (81–86, 88–90, 92>, and 99) (Tables 1, 2) could be ascertained by the occurrence in their tandem mass spectrum of the diagnostic product ion at *m/z* 241, corresponding to the mono-dehydrated form of the inositol hydrophilic head residue linked to the phosphate group. Peaks originated by neutral loss of the polar head group alone, the [(M-162)-H]$^-$ and [(M-180)-H]$^-$ ions, respectively) (Tables 1, 2) could be observed. The product ions yielded from each [M-H]$^-$ on by neutral loss of one (in l-PI case) or two fatty acyl moieties (in PI case), along with the R_xCOO^- carboxylate anions allowed to assign the nature of the fatty acids and, in the case of PI, their regiospecificity, by considering that the fatty acid removed from the *sn-1* position yielded a more intense R_1COO^- anion than that removed from the *sn-2* position (Tables 1, 2) (Geng et al., 2015).

The analysis of the MS data of **21**, **25**, **27**, **32**, **36**, **38**, **47**, and **52** allowed to assign these compounds to the lyso-phosphatidylethanolamine (l-PE) class on the basis both of their molecular formula, containing a common NO_7P heteroatom composition, and of the presence of diagnostic product ions at *m/z* 214 and 196, composed of the head group of this lipid class and the glycerophosphatidyl unit, as whole or in the mono-dehydrated form (Table 1). The nature of the fatty acid could be inferred from the observation of a main R_xCOO^- product ion (Table 1) (Geng et al., 2015). The MS^2 spectra of PE species (**93**, **97**, **100**, **103**, and **107**) were instead characterized by the occurrence of minor [(M-R_xCOOH)-H]$^-$ and [(M-R_x=CO)-H] $^-$ product ions along with abundant carboxylate anions originated by neutral loss of 197 Da (corresponding to the mono-dehydrated form of glycero-phosphatidylamine) from the [(M-R_x=CO)-H]$^-$ ion (Table 2). Their acylation position on the glycerol unit could be deduced from their relative intensity ratio with the fatty acid at *sn-2* position generating a more intense anion than that at *sn-1* position ($R_2COO^- > R_1COO^-$) (Napolitano et al., 2018).

Compounds **56** and **64** (Table 1), occurring both in fresh and roasted kernels, were identified as N-acylglycerophosphatidyle thanolamines (NA-GPE) molecules (Klockmann et al., 2016; Napolitano et al., 2018), that is, lipid compounds in which the fatty

acid is involved in an amide linkage with the amino head group of glycerophosphoethanolamine (Tsuboi et al., 2011).

The analysis of mass spectrometric data acquired in negative ion mode allowed to identify, both in NPR and NPF extracts, a good number of metabolites (**13**, **14**, **17**–**18**, **22**, **26**, **30**, **33**, **37**, **39**, **50**, **54**, **101**, **106**, **109**, **112**–**113**, and **117**) belonging to another class of phospholipids, characterized by a heteroatom composition including an atom of nitrogen and another of phosphorous and by an MS/MS spectrum displaying a main peak originated by neutral loss of 60 Da from the pseudomolecular anion (Tables 1, 2,his product ion represents the typical anion formed from PC derivatives when subjected to CID under negative ionization conditions. In the (⁻)ESI mode the pseudomolecular anion of this phospholipid species is obtained as adduct with formic acid, that, in MS/MS experiment, is promptly removed as methyl formate (60 Da), generating the diagnostic $[M\text{-}15]^-$ ion from which any other product ion derives (Tables 1, 2) (Geng et al., 2015; Napolitano et al., 2018). The occurrence in the (-)ESI/MSMS spectrum of the product ion obtained by neutral loss of a dimethylaminoethanol unit (89 Da) from the $[M\text{-}15]^-$ ion confirmed this assignment, along with the occurrence of two minor product ions, at *m/z* 241 and 224, corresponding to the glycerol-phosphatidyldimethylethanolamine as whole or mono-dehydrated anion, respectively (Table 1).

Moreover, the analysis of the mass spectra acquired for chromatographic peaks yielded by NPF and NPR investigation on RP-C18 column allowed to ascertain the occurrence in both hazelnut extracts of some lyso-phosphatidylserines (l-PS) (**43**, **53**, and **57**) by observing the relative tandem mass spectra characterized by major product ions formed by neutral loss of 105 Da and 87 Da, corresponding to the serine headgroup removed as whole or mono-dehydrated unit (Table 1).

The occurrence of lyso-phosphatidylglycerol (l-PG) (**72** and **74**–**76**) and PG (**96**, **98**, **102**, and **105**) species both in NPR and NPF extracts could be ascertained by analyzing in the tandem mass spectra diagnostic product ions at *m/z* 245 and 227, corresponding to the whole and mono-dehydrated glycerophosphoglycerol anions, respectively, along with the product ion originated by neutral loss of 92 Da corresponding to a glycerol unit (Table 2) (Cerulli et al., 2021).

Finally, the occurrence in both NPR and NPF of phospholipids belonging to the lyso-phosphatidic acid (l-PA)/PA class (Table 2) could be highlighted by the finding of a main peak at *m/z* 153 in MSMS spectra of l-PA (**73** and **77**–**80**) and of a main peak obtained by neutral loss of 154 Da from the $[(M\text{-}H)\text{-}R_xC{=}O]^-$ anion in MSMS spectra of PA (**108**, **110**–**111**, **114**–**116**, and **118**–**119**).

Glycolipids, monoacylglycerols, and sphingolipids identification

The analysis of MS data obtained by using the RP-C18 column for the chromatographic separation allowed to putatively identify in both NPR and NPF extracts digalactosylmonoacylglycerol (DGMG) species (**15**–**16**, **20**, **24**, **28**, **31**, **35**, and **46**), differing for the unsaturation degree and/or regiospecificity of the acyl group (Table 1). Particularly diagnostic for the class-assignment were the product ions occurring in the tandem mass spectrum at *m/z* 415 and 397, corresponding to the digalactosylglycerol as whole or as mono-dehydrated anion, respectively, and at *m/z* 235, relative to the mono-dehydrated galactosylglycerol anion (Table 1) (Napolitano et al., 2018; D'Urso et al., 2020).

Sulfoquinovosylmonoacylglycerols (SQMGs) (**60**, **62**, **65**–**66**, and **69**) could be identified by the occurrence of the typical product ions at *m/z* 299 and 225, referable to the mono-dehydrated glycerosulfoquinovose anion and to the sulphured sugar anion rearranged after removal from the glycerol unit (Table 1) (Zianni et al., 2013; Fu et al., 2018). In both fresh and roasted hazelnut extracts, by using the RP-C4 column, sulfoquinovosylglycerols in which both *sn*-1 and *sn*-2 glycerol positions were acylated (SQDG) (**94**–**95** and **104**) (Table 2) were detectable. For these compounds the regiochemical characterization could be established on the basis of the intensities of the $[(M\text{-}R_xCOOH)\text{-}H]^-$ anions produced in MS/MS spectra according to literature reports (Zianni et al., 2013; Napolitano et al., 2018)

Derivatives of octadecenoic acids esterified with two glycosyl units (**41**–**42**, **44**, and **49**) were detectable in LC-(-)ESI/HRMS profiles acquired for both NPR and NPF extracts by using the RP-C18 column (Table 1). In particular, the tandem mass spectrum of these acyldiglycosides was characterized by the occurrence of product ions at *m/z* 341 and 323, corresponding to the diglycosyl anion as whole or in mono-dehydrated form (Rahman and Akhtar, 2016; Sultana et al., 2018).

In agreement with literature data, both molecular formula and fragmentation pattern of peaks **67**–**68**, **70**, and **71** concurred to define them as MAG. Their tandem mass spectrum, acquired in positive ion mode, was typically characterized by the occurrence of product ions formed by neutral loss of 92 and 74 Da, and corresponding to $[R = CO{+}H]^+$ and $[RCOOH{+}H]^+$ cations, respectively (Table 1) (Della Corte et al., 2015; Napolitano et al., 2018).

Finally, the LC-(-)ESI/HRMS profiles obtained by using the RP-C4 column highlighted the occurrence in both "Nocciola Piemonte" extracts of two peaks (87 and 91) yielding MS^2 spectra characterized by abundant $[(M\text{-}162)\text{-}H]^-$ and $[(M\text{-}180)\text{-}H]^-$ ions (Table 2) corresponding to ceramides (Table 1). These compounds are lipids structurally made up of a long-chain base, in plant usually consisting of an 18-carbon atom backbone supporting hydroxyl groups at C1 and C3 and an amine group at C2, linked by *N*-acylation to a fatty acid generally made up of 14–26 carbon atoms and usually hydroxylated at C-2. The comparison with literature data permitted to identify compounds **87** and **91** as glycosylceramides (GlcCers) (Alasalvar and Pelvan, 2011).

Compositional distribution of polar lipids

The knowledge of the mechanism of lipids fragmentation was used to design an analytical strategy that, by monitoring the characteristic transitions for each lipid class in MRM experiments, allowed to obtain a quantitative distribution, in relative terms, of the main polar lipid families occurring in both NPR and NPF, that is, phosho- and glycolipids.

The pie chart in Figure 1 clearly indicates that NPR was about threefolds richer in lipids than NPF, which could be explained by a

better extractability following the destruction of hazelnut tissues by roasting, in agreement with previous works carried out on different matrices such as safflower, rice germ, argan, pumpkin, and mustard seeds (Belcadi-Haloui et al., 2018). The bar histograms shown in Figure 1A indicate that the relationship existing between the two main lipid families present in NPR and NPF was basically the same, highlighting in both roasted and fresh kernels the clear prevalence in relative terms of the phospholipids family versus that of glycolipids, with the latter being even less represented in NPR with respect to the first one. In particular, both in NPR and in NPF the lyso-phospholipid class resulted to be the most represented lipid class in relative terms, followed by those of phospholipids, digalactosylmonoacylglicerols, and sulfoquinovosyl species (Figure 1B).

The analysis of the quantitative distribution in relative terms of the single classes of lyso-phospholipids allowed to affirm that in both NPF and NPR extracts l-PC was the most represented lyso-phospholipid class, followed in the order by l-PA and l-PE, l-PI, l-PG, and l-PS (Figure 2A).

Notwithstanding this, some peculiar differences could be noted between the two extracts. In particular, the kernel roasting seemed to have a positive effect on the level of l-PC, l-PE, l-PI, and l-PG, that showed an increase in relative terms (more consistent and significative for the first than for the other three classes) with respect to the same classes in NPF, and a contemporary negative effect on the level of l-PA and l-PS, characterized by an evident decrease with respect to the NPF (Figure 2A). It is noteworthy that in NPR the l-PC class was fivefold and 21-fold more represented than l-PA and l-PS, respectively, while the relationship of l-PC with the other lyso-phospholipid classes remained substantially unvaried with respect to that observed between the same classes in NPF. Differing from the distribution trend observed for lyso-phospholipids, among the considered phospholipid classes, PI resulted the most represented, both in NPF and in NPR, followed by PA, PC, PE, and PG (Figure 2B). Once again, the roasting process seemed to have effects on phospholipid relative quantitative profile yielding to, analogously to what observed in the case of lyso-phospholipids, an increase of the level of PI, PC, and PG, and a decrease of PA and PE, much more relevant for the first than for the second (Figure 2B). So, our results led us to consider that probably the used roasting conditions could have determined the destruction of membrane structures of hazelnut oil bodies causing the release of phospholipids such as l-PI, l-PC, l-PG, PI, PC, and PG leading to their increase in the NPR extract, and the contemporary thermal degradation of more susceptible phospholipids such as l-PA, l-PS, PAs, and PEs, in agreement with literature data available for matrices other than hazelnut (Kim et al., 2002; Zhang et al., 2021; Zhang et al., 2022).

Finally, by considering the glycolipid family, both in NPF and in NPR the DGMG resulted to be the most represented glycolipid class in relative terms, with the SQMG class being the most represented between the two considered sulfoquinovosyl classes (Figure 2C). In this case, the analysis of the relationships existing between the different glycolipid classes in NPR highlighted an evident roasting effect determining the decrease of the DGMG level in favor of the increase of the level of both SGMG and SQDG (Figure 2C).

Phenolic derivatives

The analysis of the LC-(-)ESI/HRMS profile obtained by using the RP-C18 column highlighted some peaks that, on the basis of their molecular formula and fragmentation pattern, could be identified as mono- and diglycosylated flavonoids (Table 1). In particular, tandem mass spectra of compounds **6**, **7**, and **9** allowed to promptly identify them as mono-glycosylated flavonoids showing as aglycone myricetin, quercetin, and kaempferol, respectively (Table 1). The

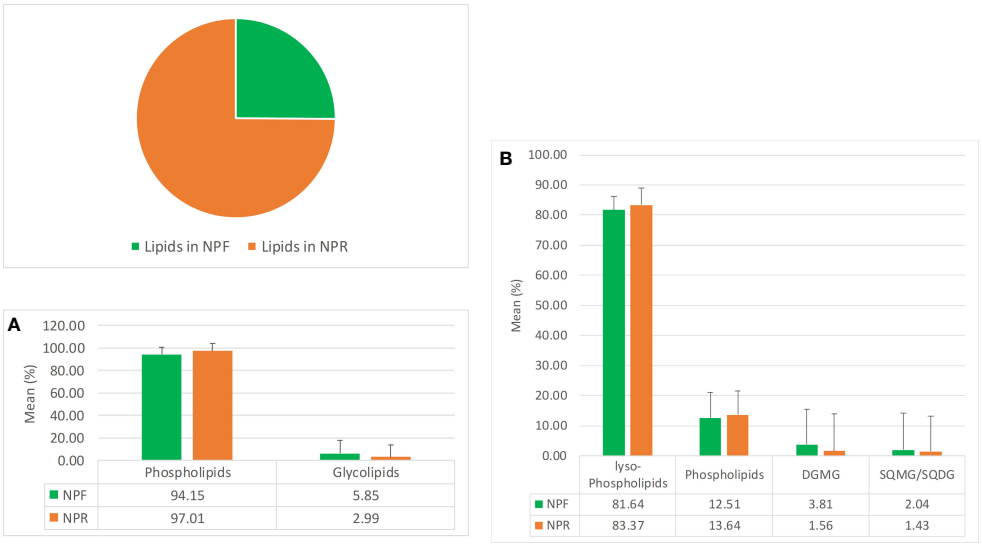

FIGURE 1
Mean quantitative responses and relative standard deviation, expressed as percentage, of total lipids (pie chart), **(A)** phosho- and glycolipids families, and **(B)** phosho- and glycolipids classes occurring in NPR and NPF.

FIGURE 2
Mean quantitative responses and relative standard deviation, expressed as percentage, of **(A)** lyso-phospholipids classes, **(B)** phosholipids classes, and **(C)** glycolipids classes identified in NPR and NPF.

analysis of MSMS spectrum of compounds **3** and **5** allowed instead to define them as diglycosylated flavonols, showing as main peak the aglycone ions at *m/z* 301 and *m/z* 285 corresponding to quercetin and kaempferol, respectively, and as minor product ions those originated from the $[M\text{-}H]^-$ ion by neutral loss of one mono-dehydrated hexose unit and from the $[(M\text{-}H)\text{-}162]^-$ ion by neutral loss of 120 Da via internal breakdown of the second hexose unit (Table 1). In agreement with literature data, this fragmentation pattern suggested that the 3-*O* position of the aglycone core had to be involved in the glycosylation with the two hexose units, that in turn had to be each other linked via a (1→2)-interglycosidic linkage (Masullo et al., 2016; Cerulli et al., 2020; Loizzo et al., 2021). Noteworthy, compounds **3**, **7**, and **9** could be detected in both NPR and NPF extracts, while compounds **5** and **6** were evident only in NPR extract.

Moreover, the analysis of mass spectrometric data acquired by carrying out the chromatographic separation on RP-C18 column allowed to ascertain the occurrence of four phenolic compounds (**4**, **8**, **10**, and **11**) ascribable to diarylheptanoid derivatives (Table 1) (Masullo et al., 2017; Cerulli et al., 2018c). In particular, they were more evident in NPR than in NPF extract, which showed only compound 10.

Isolation and NMR structural elucidation of phenolic derivatives

With the aim to complete and unequivocally characterize the molecular structure of flavonoid and diarylheptanoids derivatives detected in LC-ESI/HRMS profile, the NPR *n*-butanol extract was fractionated on Sephadex LH-20 and the obtained fractions were purified by RP-RI/HPLC. The comparison of NMR data acquired for isolated compounds with those reported in literature allowed to identify the diarylheptanoids as: giffonin P (**4**), giffonin L (**8**), carpinontriol B (**10**), and giffonin V (**11**), and the flavonoids as: quercetin 3-*O*-β-D-galactopyranosyl-(**1→2**)-β-D-glucopyranoside (**3**), kaempferol 3-*O*-β-D-glucopyranosyl-(**1→2**)-β-D-glucopyranoside (**5**), myricetin-3-*O*-α-L-rhamnopyranoside (**6**), quercetin 3-*O*-β-D-glucopyranoside (**7**), and kaempferol-3-*O*-β-D-glucopyranoside (**9**) (Figure 3 and Table 1) (Masullo et al., 2015a; Masullo et al., 2016; Cerulli et al., 2017).

TEAC assay of "Nocciola Piemonte" extracts and phenolic compounds

TEAC assay was used to evaluate the antioxidant ability of isolated specialized metabolites (**3**–**11**). TEAC value is expressed as the concentration of Trolox solution with antioxidant potential equivalent to a 1 mM concentration of the test sample. Among the tested compounds, flavonoid glycosides showed a good antioxidant activity; in particular, compounds **3** and **6** displayed a radical-scavenging activity similar to that of quercetin (reference compound) (TEAC value 2.03 mM). The diarylheptanoids (**4**, **8**, **10**, and **11**), characterized by the presence at least of two phenolic groups, showed a moderate radical-scavenging capacity (Table 3).

Biological evaluation of phenolic compounds in TBARS assay

On the basis of the antioxidant activity reported for phenolic compounds and more specifically for giffonins isolated from *C.*

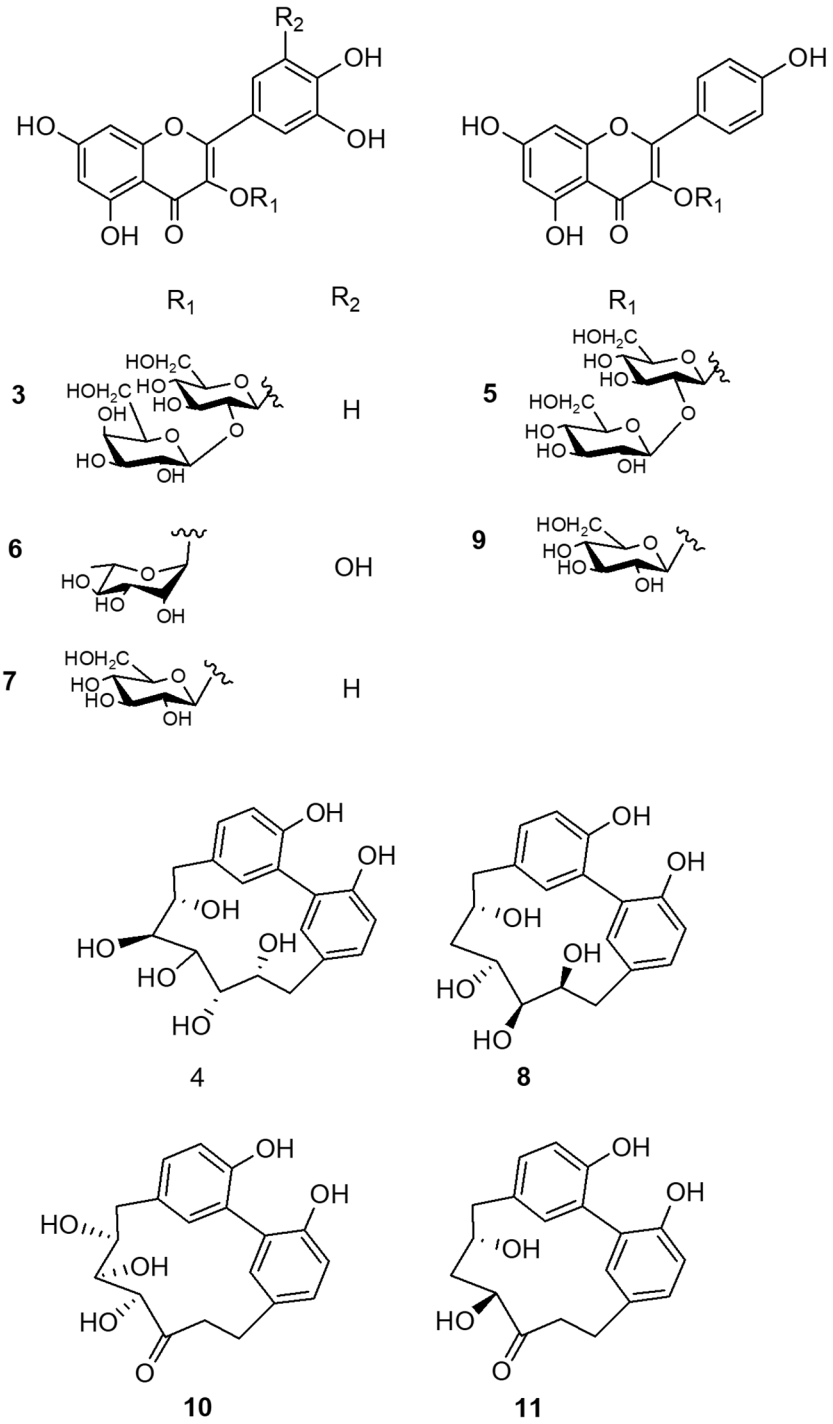

FIGURE 3
Compounds isolated from "Nocciola Piemonte" roasted hazelnut.

avellana byproducts, the phenolic compounds isolated from the extract of roasted "Nocciola Piemonte" were evaluated by measuring the concentration of TBARS (Kolodziejczyk et al., 2009; Masullo et al., 2015b; Masullo et al., 2016; Cerulli et al., 2017).

This assay highlighted that the tested compounds protected plasma against lipid peroxidation induced by H_2O_2 and H_2O_2/Fe^{2+}. In detail, phenolic compounds and curcumin (reference compound) were assayed at different concentrations (0.1 μM–100 μM; 30 min, at 37°C). All tested compounds and reference compound did not exhibit effect on auto-peroxidation of human plasma (data not shown).

Most of the tested compounds at concentration of 10 μM were able to reduce H_2O_2 and H_2O_2/Fe^{2+} induced lipid peroxidation more than curcumin (Table 3). Among the nine tested compounds, the highest activity was displayed by compound **6** which inhibited lipid peroxidation induced by H_2O_2 and H_2O_2/Fe^{2+} by 44.4% and

10.3389/fpls.2023.1252196

TABLE 3 Free radical scavenging activities by TEAC assay and inhibitory effects on plasma lipid peroxidation induced by H_2O_2 or H_2O_2/Fe^{2+} measured for compounds 3–11.

compound	TEAC value (mM)	Inhibition of lipid peroxidation induced by H_2O_2 (%)	Inhibition of lipid peroxidation induced by H_2O_2/Fe^{2+} (%)
3	2.00 ± 0.03	19.9 ± 2.6	18.8 ± 3.1
4	0.99 ± 0.01	33.6 ± 3.2	11.4 ± 2.2
5	1.65 ± 0.02	35.4 ± 3.6*	14.2 ± 2.1
6	2.06 ± 0.03	44.4 ± 4.2	34.1 ± 3.4
7	1.98 ± 0.03	23.1 ± 2.8	19.9 ± 2.0
8	0.75 ± 0.01	33.3 ± 3.3	14.4 ± 1.9
9	1.55 ± 0.02	5.7 ± 1.6	20.1 ± 3.6
10	0.87 ± 0.01	32.0 ± 3.4	24.4 ± 3.3
11	0.60 ± 0.01	–	7.0 ± 2.3
quercetin[a]	2.03 ± 0.03	–	–
curcumin[b]		20.6 ± 4.1	23.2 ± 2.4

[a]reference compound used for TEAC assay; [b]reference compound used for TBARS assay. *$p < 0.01$. -, Quercetin was used as reference standard only for TEAC assay.

34.1%, respectively. These data are in agreement with the antioxidant activity reported for diarylheptanoids and flavonoids isolated from *C. avellana* cultivar Tonda di Giffoni (Masullo et al., 2015b; Masullo et al., 2016; Cerulli et al., 2017).

Conclusions

In conclusion, the results obtained in this study allowed to define "Nocciola Piemonte" hazelnut as a good source of polar lipids. In particular, the analysis of the LC-MS profiles of NPF and NPR *n*-butanol extracts allowed to ascertain the occurrence of phospholipids, glycolipids, sphingolipids, and oxylipins, highlighting only small qualitative differences in the metabolite composition between fresh and roasted "Nocciola Piemonte" kernels. Noteworthy was the absence of some l-PA/PA species in NPR and the lack of hydroxylated species of l-PC and PI in NPF, in agreement with that already observed for "Tonda di Giffoni" hazelnut. This finding could be traced back to degradation and oxidation processes caused by the high roasting temperature (Napolitano et al., 2018). This latter seemed to be responsible also for the results obtained by the semiquantitative analysis carried out on the most representative NPR and NPF lipid families, that is, phospholipids and glycolipids, that evidenced the NPR extract as the extract richest in lipids. Indeed, even though lyso- and phospholipids resulted to be the most represented lipid classes in relative terms in both NPR and NPF (with lyso-phospholipids being the prevalent one), the increased levels of the l-PI/PI, l-PC/PC, and l-PG/PG, along with the marked decrease of the l-PA/PA and l-PS levels, both detectable in NPR, could be interpreted as an effect of the roasting temperature. These results are interesting by considering that scientific literature attributes to this lipid classes beneficial effects on human health (Inoue et al., 2011; Napolitano et al., 2018). In particular, PC-rich foods represent good nutrients to improve memory and prevent liver disease in rats, and PI are described as able to give protection in hyperlipidemic deseases and to promote transport, excretion, metabolism, and absorption of the cholesterol in rabbits. For their part, lysoglycerophospholipids are not only structural components of cellular membranes and precursors for the synthesis of glycerolipids but also an essential lipid class as signaling mediators in physiological and pathological processes (Lee et al., 2016; Tan et al., 2020; Hachem and Nacir, 2022).

Furthermore, the phytochemical isolation of phenolics occurring in "Nocciola Piemonte" kernels allowed to unambiguously ascertain, in particular in NPR, the occurrence of flavonoids and giffonins—diarylheptanoids detected in different "Tonda di Giffoni" byproducts and kernels—interestingly highlighting the presence of giffonin L (8) and giffonin V (11), not detected in "Tonda di Giffoni" kernels. These specialized metabolites are known in literature for the antioxidant activity (Bottone et al., 2019; Masullo et al., 2022). In addition, diarylheptanoids from *C. avellana* are reported for their inhibitory activity on human plasma protein carbonylation and oxidation of thiol groups. These results are interesting by considering that protein carbonyl content is used as marker of protein oxidation, which could be responsible for oxidative damage to cells (Masullo et al., 2021b).

In conclusion, the consideration of the synergistic effect of phenolic compounds and bioactive and healthy lipids occurring in the polar fraction of fresh and roasted kernels of "Nocciola Piemonte" concurred to confirm this variety as a precious and beneficial food.

Data availability statement

The raw data supporting the conclusions of this article will be made available by the authors, without undue reservation.

Author contributions

SP contributed toward conceptualization, writing, review and editing of the manuscript, supervision, project administration, and

funding acquisition. AC, AN, BO, and MM contributed to the methodology, data curation, formal analysis, and writing – original draft preparation. AC and AN contributed to investigation. SP contributed to resources. All authors contributed to the article and approved the submitted version.

Funding

This research was carried out within the National Biodiversity Future Center S.c.a.r.l., Piazza Marina 61 (c/o Palazzo Steri) Palermo, Italy, and received funding from the European Union Next-Generation EU (PIANO NAZIONALE DI RIPRESA E RESILIENZA (PNRR)—MISSIONE 4 COMPONENTE 2, INVESTIMENTO 1.4, C.I. CN00000033); CUP UNISA D43C22001260001.

Acknowledgments

The authors would like to thank la Gentile s.r.l. (Cortemilia, Cuneo) for providing as a kind gift hazelnuts "Nocciola Piemonte". The authors would like to thank Bogdan Kontek and Monika Sikora (University of Lodz, Department of General Biochemistry, Faculty of Biology and Environmental Protection, Lodz, Poland) for contributing to TBARS analysis.

Conflict of interest

The authors declare that the research was conducted in the absence of any commercial or financial relationships that could be construed as a potential conflict of interest.

Publisher's note

References

Alasalvar, C., and Pelvan, E. (2011). Fat-soluble bioactives in nuts. *Eur. J. Lipid Sci. Technol.* 113, 943–949. doi: 10.1002/ejlt.201100066

Bacchetta, L., Aramini, M., Zini, A., Di Giammatteo, V., Spera, D., Drogoudi, P., et al. (2013). Fatty acids and alpha-tocopherol composition in hazelnut (*Corylus avellana* L.): a chemometric approach to emphasize the quality of European germplasm. *Euphytica* 191, 57–73. doi: 10.1007/s10681-013-0861-y

Belcadi-Haloui, R., Zekhnini, A., El-Alem, Y., and Hatimi, A. (2018). Effects of roasting temperature and time on the chemical composition of argan oil. *Int. J. Food Sci.* 4, 1–8, 7683041. doi: 10.1155/2018/7683041

Binello, A., Giorgis, M., Cena, C., Cravotto, G., Rotolo, L., Oliveri, P., et al. (2018). Chemical modifications of Tonda Gentile Trilobata hazelnut and derived processing products under different infrared and hot-air roasting conditions: a combined analytical study. *J. Sci. Food Agric.* 98, 4561–4569. doi: 10.1002/jsfa.8984

Bottone, A., Cerulli, A., D'Urso, G., Masullo, M., Montoro, P., Napolitano, A., et al. (2019). Plant specialized metabolites in hazelnut (*Corylus avellana*) kernel and byproducts: an update on chemistry, biological activity, and analytical aspects. *85* 840doi: 10.1055/a-0947-5725

Caligiani, A., Coisson, J. D., Travaglia, F., Acquotti, D., Palla, G., Palla, L., et al. (2014). Application of ^{1}H NMR for the characterisation and authentication of "Tonda Gentile Trilobata". *hazelnuts Piedmont (Italy)Food Chem.* 148, 77–85. doi: 10.1016/j.foodchem.2013.10.001

Cannavacciuolo, C., Napolitano, A., Heiss, E. H., Dirsch, V. M., and Piacente, S. (2022). *Portulaca oleracea*, a rich source of polar lipids: Chemical profile by LC-ESI/LTQOrbitrap/MS/MS^{n} and in *vitro* preliminary anti-inflammatory activity. *Food Chem.* 388, 132968. doi: 10.1016/j.foodchem.2022.132968

Cerulli, A., Lauro, G., Masullo, M., Cantone, V., Olas, B., Kontek, B., et al. (2017). Cyclic diarylheptanoids from *corylus avellana* green leafy covers: determination of their absolute configurations and evaluation of their antioxidant and antimicrobial activities. *J. Nat. Prod.* 80, 1703–1713. doi: 10.1021/acs.jnatprod.6b00703

Cerulli, A., Masullo, M., Mari, A., Balato, A., Filosa, R., Lembo, S., et al. (2018a). Phenolics from *Castanea sativa* leaves and their effects on UVB-induced damage. *Nat. Prod. Res.* 32, 1170–1175. doi: 10.1080/14786419.2017.1331225

Cerulli, A., Masullo, M., Montoro, P., Hosek, J., Pizza, C., and Piacente, S. (2018b). Metabolite profiling of "green" extracts of *Corylus avellana* leaves by 1H NMR spectroscopy and multivariate statistical analysis. *J. Pharm. Biomed. Anal.* 160, 168–178. doi: 10.1016/j.jpba.2018.07.046

Cerulli, A., Napolitano, A., Hošek, J., Masullo, M., Pizza, C., and Piacente, S. (2021). Antioxidant and *In Vitro* preliminary anti-inflammatory activity of *Castanea sativa* (italian cultivar "marrone di roccadaspide" PGI) burs, leaves, and chestnuts extracts and their metabolite profiles by LC-ESI/LTQOrbitrap/MS/MS. *Antioxidants* 10, 278. doi: 10.3390/antiox10020278

Cerulli, A., Napolitano, A., Masullo, M., Hošek, J., Pizza, C., and Piacente, S. (2020). Chestnut shells (Italian cultivar "Marrone di Roccadaspide" PGI): Antioxidant activity and chemical investigation with in depth LC-HRMS/MS^{n} rationalization of tannins. *Food Res. Int.* 129, 108787. doi: 10.1016/j.foodres.2019.108787

Cerulli, A., Napolitano, A., Masullo, M., Pizza, C., and Piacente, S. (2018c). LC-ESI/LTQOrbitrap/MS/MS^{n} Analysis Reveals Diarylheptanoids and Flavonol O-glycosides in Fresh and Roasted Hazelnut (*Corylus avellana* cultivar "Tonda di Giffoni"). *Nat. Prod. Commun.* 13, 1934578X1801300906. doi: 10.1177/1934578x1801300906

Cialiè Rosso, M., Stilo, F., Bicchi, C., Charron, M., Rosso, G., Menta, R., et al. (2021). Combined untargeted and targeted fingerprinting by comprehensive two-dimensional gas chromatography to track compositional changes on hazelnut primary metabolome during roasting. *Appl. Sci.* 11, 1–18. doi: 10.3390/app11020525

Cristofori, V., Botta, R., Rovira, M., Molnar, T. J., and Mehlenbacher, S. A. (2022). Editorial: Recent advances in hazelnut (*Corylus* spp.). *Front. Plant Sci.* 13. doi: 10.3389/fpls.2022.1120595

Della Corte, A., Chitarrini, G., Di Gangi, I. M., Masuero, D., Soini, E., Mattivi, F., et al. (2015). A rapid LC–MS/MS method for quantitative profiling of fatty acids, sterols, glycerolipids, glycerophospholipids and sphingolipids in grapes. *Talanta* 140, 52–61. doi: 10.1016/j.talanta.2015.03.003

Dietrich, M., Traber, M. G., Jacques, P. F., Cross, C. E., Hu, Y., and Block, G. (2006). Does gamma-tocopherol play a role in the primary prevention of heart disease and cancer? A review. *J. Am. Coll. Nutr.* 25, 292–299. doi: 10.1080/07315724.2006.10719538

D'Urso, G., Napolitano, A., Cannavacciuolo, C., Masullo, M., and Piacente, S. (2020). Okra fruit: LC-ESI/LTQOrbitrap/MS/MSn based deep insight on polar lipids and specialized metabolites with evaluation of anti-oxidant and anti-hyperglycemic activity. *Food Funct.* 11, 7856–7865. doi: 10.1039/D0FO00867B

Fu, L.-L., Ding, H., Han, L.-F., Jia, L., Yang, W.-Z., Zhang, C., et al (2018). Simultaneously targeted and untargeted multicomponent characterization of Erzhi Pill by offline two-dimensional liquid chromatography/quadrupole-Orbitrap mass spectrometry. *J. Chromatogr. A.* 1584, 87–96. doi: 10.1016/j.chroma.2018.11.024

Geng, P., Harnly, J. M., and Chen, P. (2015). Differentiation of whole grain from refined wheat (*T. aestivum*) flour using lipid profile of wheat bran, germ, and endosperm with UHPLC-HRAM mass spectrometry. *J. Agric. Food Chem.* 63, 6189–6211. doi: 10.1021/acs.jafc.5b01599

Ghirardello, D., Bertolino, M., Belviso, S., Dal Bello, B., Giordano, M., Rolle, L., et al. (2016). Phenolic composition, antioxidant capacity and hexanal content of hazelnuts (*Corylus avellana* L.) as affected by different storage conditions. *Postharvest Biol. Technol.* 112, 95–104. doi: 10.1016/j.postharvbio.2015.09.039

Granata, M. U., Bracco, F., Gratani, L., Catoni, R., Corana, F., Manucci, B., et al. (2017). Fatty acid content profile and main constituents of *Corylus avellana* kernel in wild type and cultivars growing in Italy. *Natural Product Res.* 31, 204–209. doi: 10.1080/14786419.2016.1217204

Hachem, M., and Nacir, H. (2022). Emerging role of phospholipids and lysophospholipids for improving brain docosahexaenoic acid as potential preventive and therapeutic strategies for neurological diseases. *Int. J. Mol. Sci.* 23, 1–27. doi: 10.3390/ijms23073969

Inoue, M., Adachi, M., Shimizu, Y., Tsutsumi, T., and Tokumura, A. (2011). Comparison of lysophospholipid levels in rat feces with those in a standard chow. *J. Agric. Food Chem.* 59, 7062–7067. doi: 10.1021/jf200986k

Jiang, J., Liang, L., and Q.and Zhao, T. (2021). Kernel nutrient composition and antioxidant ability of corylus spp. in China. *Front. Plant Sci.* 12. doi: 10.3389/fpls.2021.690966

Kihara, Y., Mizuno, H., and Chun, J. (2015). Lysophospholipid receptors in drug discovery. *Exp. Cell Res.* 333, 171–177. doi: 10.1016/j.yexcr.2014.11.020

Kim, I.-H., Kim, C.-J., You, J.-M., Lee, K.-W., Kim, C.-T., Chung, S. H., et al. (2002). Effect of roasting temperature and time on the chemical composition of rice germ oil. *JAOCS* 79, 413–418. doi: 10.1007/s11746-002-0498-2

Klockmann, S., Reiner, E., Bachmann, R., and T.and Fischer, M. (2016). Food fingerprinting: metabolomic approaches for geographical origin discrimination of hazelnuts (Corylus avellana) by UPLC-QTOF-MS. *J. Agric. Food Chem.* 64, 9253–9262. doi: 10.1021/acs.jafc.6b04433

Kolodziejczyk, J., Masullo, M., Olas, B., and S.and Wachowicz, B. (2009). Effects of garcinol and guttiferone K isolated from *Garcinia cambogia* on oxidative/nitrative modifications in blood platelets and plasma. *Platelets* 20, 487–492. doi: 10.3109/09537100903165182

Lee, B. H., Choi, S. H., Kim, H. J., Jung, S. W., Kim, H. K., and Nah, S. Y. (2016). Plant lysophosphatidic acids: A rich source for bioactive lysophosphatidic acids and their pharmacological applications. *Biol. Pharm. Bull.* 39, 156–162. doi: 10.1248/bpb.b15-00575

Levandi, T., Puessa, T., Vaher, M., Toomik, P., and Kaljurand, M. (2009). Oxidation products of free polyunsaturated fatty acids in wheat varieties. *Eur. J. Lipid Sci. Technol.* 111, 715–722. doi: 10.1002/ejlt.200800286

Locatelli, M., Coisson, J. D., Travaglia, F., Bordiga, M., and Arlorio, M. (2015). Impact of roasting on identification of hazelnut (*Corylus avellana* L.) origin: A chemometric approach. *J. Agric. Food Chem.* 63, 7294–7303. doi: 10.1021/acs.jafc.5b03201

Loizzo, M. A. O., Napolitano, A., Bruno, M., Geraci, A., Schicchi, R., Leporini, M., et al. (2021). LC-ESI/HRMS analysis of glucosinolates, oxylipins and phenols in Italian rocket salad (*Diplotaxis erucoides* subsp. *erucoides* (L.) DC.) and evaluation of its healthy potential. *J. Sci. Food Agric.* 101, 5872–5879. doi: 10.1002/jsfa.11239

López-Bascón, M. A., Calderón-Santiago, M., Díaz-Lozano, A., Camargo, A., López-Miranda, J., and Priego-Capote, L. (2020). Development of a qualitative/quantitative strategy for comprehensive determination of polar lipids by LC–MS/MS in human plasma. *Anal. Bioanal. Chem.* 412, 489–498. doi: 10.1007/s00216-019-02261-8

Maldini, M., Montoro, P., Hamed, A. I., Mahalel, U. A., Oleszek, W., StochmaL, A., et al. (2011). Strong antioxidant phenolics from *Acacia nilotica*: Profiling by ESI-MS and qualitative–quantitative determination by LC–ESI-MS. *J. Pharm. BioMed. Anal.* 56, 228–239. doi: 10.1016/j.jpba.2011.05.019

Masullo, M., Cantone, V., Cerulli, A., Lauro, G., Messano, F., and Giffonins, J. P. (2015a). highly hydroxylated cyclized diarylheptanoids from the leaves of Corylus avellana cultivar "Tonda di Giffoni". *J. Nat. Prod.* 78, 2975–2982. doi: 10.1021/acs.jnatprod.5b00695

Masullo, M., Cerulli, A., and C., and Piacente, S. (2021a). *Pouteria lucuma* pulp and skin: in depth chemical profile and evaluation of antioxidant activity. *Molecules* 26, 1–13. doi: 10.3390/molecules26175236

Masullo, M., Cerulli, A., Mari, A., De Souza Santos, C. C., Pizza, C., and Piacente, S. (2017). LC-MS profiling highlights hazelnut (Nocciola di Giffoni PGI) shells as a byproduct rich in antioxidant phenolics. *Food Res. Int.* 101, 180–187. doi: 10.1016/j.foodres.2017.08.063

Masullo, M., Cerulli, A., Olas, B., and C.and Piacente, S. (2015b). Antioxidant Cyclized Diarylheptanoids from the Leaves of the Hazelnut Tree (*Corylus avellana*), Source of the Italian PGI Product "Nocciola di Giffoni". *J. Nat. Prod.* 78, 17–25. doi: 10.1021/np5004966

Masullo, M., Lauro, G., Cerulli, A., and G.and Piacente, S. (2022). *Corylus avellana*: A Source of Diarylheptanoids With α-Glucosidase Inhibitory Activity Evaluated by in *vitro* and in silico Studies. *Front. Plant Sci.* 13. doi: 10.3389/fpls.2022.805660

Masullo, M., Lauro, G., Cerulli, A., Kontek, B., Olas, B., Bifulco, G., et al. (2021b). Giffonins, antioxidant diarylheptanoids from *corylus avellana*, and their ability to prevent oxidative changes in human plasma proteins. *J. Nat. Prod.* 84, 646–653. doi: 10.1021/acs.jnatprod.0c01251

Masullo, M., Mari, A., Cerulli, A., Bottone, A., Kontek, B., Olas, B., et al. (2016). Quali-quantitative analysis of the phenolic fraction of the flowers of *Corylus avellana*, source of the Italian PGI product "Nocciola di Giffoni": Isolation of antioxidant diarylheptanoids. *Phytochemistry* 130, 273–281. doi: 10.1016/j.phytochem.2016.06.007

Napolitano, A., Carbone, V., Saggese, P., Takagaki, K., and Pizza, C. (2007). Novel galactolipids from the leaves of *ipomoea batatas* L.: characterization by liquid chromatography coupled with electrospray ionization–quadrupole time-of-flight tandem mass spectrometry. *J. Agric. Food Chem.* 55, 10289–10297. doi: 10.1021/jf071331z

Napolitano, A., Cerulli, A., and Pizza Piacente, C.S. (2018). Multi-class polar lipid profiling in fresh and roasted hazelnut (*Corylus avellana* cultivar "Tonda di Giffoni") by LC-ESI/LTQOrbitrap/MS/MS<sup<n</sup&gt. *Food Chem.* 269, 125–135. doi: 10.1016/j.foodchem.2018.06.121

Ortega-Gavilán, F., Squara, S., Cordero, C., Cuadros-Rodríguez, L., and Bagur-González, M. G. (2023). Application of chemometric tools combined with instrument-agnostic GC-fingerprinting for hazelnut quality assessment. *J. Food Composition Anal.* 115, 104904. doi: 10.1016/j.jfca.2022.104904

Ostlund, R. E. (2002). Phytosterols in human nutrition. *Annu. Rev. Nutr.* 22, 533–549. doi: 10.1146/annurev.nutr.22.020702.075220

Rahman, M. A., and Akhtar, ,. J. (2016). A new linoleiyl arabinopyranoside from the bark of *Bauhinia racemosa* Lam and a new flavonoidal glycoside from the leaves of Cordia dichotoma Linn. *Nat. Prod. Res.* 30, 2265–2273. doi: 10.1080/14786419.2016.1163694

Richardson, C. E., Hennebelle, M., Otoki, Y., Zamora, D., Yang, J., Hammock, B. D., et al. (2017). Lipidomic analysis of oxidized fatty acids in plant and algae oils. *J. Agric. Food Chem.* 65, 1941–1951. doi: 10.1021/acs.jafc.6b05559

Rincón-Cervera, M.Á., Bravo-Sagua, R., Manólio Soares Freitas, R. A., and S.and De Camargo, A. C. (2022). "Chapter 8 - Monounsaturated and polyunsaturated fatty acids: structure, food sources, biological functions, and their preventive role against noncommunicable diseases," in *Bioactive food components activity in mechanistic approach*. Eds. C. B. B. Cazarin, J. L. Bicas, G. M. Pastore and M. R. Marostica Junior (Campinas, Brazil: Academic Press).

Rondanelli, M., Nichetti, M., Martin, V., Barrile, G. C., Riva, A., Petrangolini, G., et al. (2023). Phytoextracts for human health from raw and roasted hazelnuts and from hazelnut skin and oil: A narrative review. *Nutrients* 15, 1–19. doi: 10.3390/nu15112421

Sabaté, J., and Salas-Salvadó, J. (2006). Nuts: nutrition and health outcomes. *Br. J. Nutr.* 96, S1–S2. doi: 10.1017/BJN20061857

Slatnar, A., Mikulic-Petkovsek, M., Stampar, F., Veberic, R., and Solar, A. (2014). HPLC-MS^n identification and quantification of phenolic compounds in hazelnut kernels, oil and bagasse pellets. *Food Res. Int.* 64, 783–789. doi: 10.1016/j.foodres.2014.08.009

Sultana, S., Zaman, K., and M.and Mir, S. R. (2018). Chemical constituents from the stem bark of *Bauhinia racemosa* lam. and leaves of *Machilus bombycina* king ex hook. F. *Eur. J. Biomed. Pharm.* 5, 714–721.

Sun, J., Hu, P., Lyu, C., Tian, J., Meng, X., Tan, H., et al. (2022). Comprehensive lipidomics analysis of the lipids in hazelnut oil during storage. *Food Chem.* 378, 132050. doi: 10.1016/j.foodchem.2022.132050

Tan, S. T., Ramesh, T., Toh, X. R., and Nguyen, L. N. (2020). Emerging roles of lysophospholipids in health and disease. *Prog. Lipid Res.* 80, 101068. doi: 10.1016/j.plipres.2020.101068

Tsuboi, K., Okamoto, Y., Ikematsu, N., Inoue, M., Shimizu, Y., Uyama, T., et al. (2011). Enzymatic formation of N-acylethanolamines from N-acylethanolamine plasmalogen through N-acylphosphatidylethanolamine-hydrolyzing phospholipase D-dependent and -independent pathways. *Biochim. Biophys. Acta* 1811, 565–577. doi: 10.1016/j.bbalip.2011.07.009

Zhang, D., Guo, X., Wang, Q., Zhao, L., Sun, Q., Duan, X., et al. (2022). Investigation on lipid profile of peanut oil and changes during roasting by lipidomic approach. *LWT* 154, 112594. doi: 10.1016/j.lwt.2021.112594

Zhang, D., Li, X., Duan, X., and H.and Cao, Y. (2021). Lipidomics reveals the changes in lipid profile of flaxseed oil affected by roasting. *Food Chem.* 364, 130431. doi: 10.1016/j.foodchem.2021.130431

Zianni, R., Bianco, G., Lelario, F., Losito, I., Palmisano, F., Cataldi, T. R. I., et al. (2013). Fatty acid neutral losses observed in tandem mass spectrometry with collision-induced dissociation allows regiochemical assignment of sulfoquinovosyl-diacylglycerols. *J. Mass Spectrom.* 48, 205–215. doi: 10.1002/jms.3149

frontiers | Frontiers in Plant Science

TYPE Original Research
PUBLISHED 01 November 2023
DOI 10.3389/fpls.2023.1268043

OPEN ACCESS

EDITED BY
Eman. A. Mahmoud,
Damietta University, Egypt

REVIEWED BY
Mohammad Mukarram,
Technical University of Zvolen, Slovakia
Kollipara P. M. S. V. Padmasree,
University of Hyderabad, India

*CORRESPONDENCE
Fikadu N. Biru
fikadu.negese@ju.edu.et;
f.biru@westernsydney.edu.au

RECEIVED 27 July 2023
ACCEPTED 17 October 2023
PUBLISHED 01 November 2023

CITATION
Biru FN, Cazzonelli CI, Elbaum R and Johnson SN (2023) Silicon-mediated herbivore defence in a pasture grass under reduced and Anthropocene levels of CO_2. *Front. Plant Sci.* 14:1268043. doi: 10.3389/fpls.2023.1268043

Silicon-mediated herbivore defence in a pasture grass under reduced and Anthropocene levels of CO_2

Fikadu N. Biru[1,2]*, Christopher I. Cazzonelli[2], Rivka Elbaum[3] and Scott N. Johnson[2]

[1]College of Agriculture and Veterinary Medicine, Jimma University, Jimma, Ethiopia, [2]Hawkesbury Institute for the Environment, Western Sydney University, Penrith, NSW, Australia, [3]R H Smith Institute of Plant Sciences and Genetics in Agriculture, The Hebrew University of Jerusalem, Rehovot, Israel

The uptake and accumulation of silicon (Si) in grass plants play a crucial role in alleviating both biotic and abiotic stresses. Si supplementation has been reported to increase activity of defence-related antioxidant enzyme, which helps to reduce oxidative stress caused by reactive oxygen species (ROS) following herbivore attack. Atmospheric CO_2 levels are known to affect Si accumulation in grasses; reduced CO_2 concentrations increase Si accumulation whereas elevated CO_2 concentrations often decrease Si accumulation. This can potentially affect antioxidant enzyme activity and subsequently insect herbivory, but this remains untested. We examined the effects of Si supplementation and herbivory by *Helicoverpa armigera* on antioxidant enzyme (catalase, CAT; superoxide dismutase, SOD; and ascorbate peroxidase, APX) activity in tall fescue grass (*Festuca arundinacea*) grown under CO_2 concentrations of 200, 410, and 640 ppm representing reduced, ambient, and elevated CO_2 levels, respectively. We also quantified foliar Si, carbon (C), and nitrogen (N) concentrations and determined how changes in enzymes and elemental chemistry affected *H. armigera* relative growth rates and plant consumption. Rising CO_2 concentrations increased plant mass and foliar C but decreased foliar N and Si. Si supplementation enhanced APX and SOD activity under the ranging CO_2 regimes. Si accumulation and antioxidant enzyme activity were at their highest level under reduced CO_2 conditions and their lowest level under future levels of CO_2. The latter corresponded with increased herbivore growth rates and plant consumption, suggesting that some grasses could become more susceptible to herbivory under projected CO_2 conditions.

KEYWORDS

antioxidant enzyme, carbon, carbon dioxide, herbivore, physical defences, plant defences, silicon

Introduction

Most grasses are silicon (Si) accumulators, which can account for up to 10% of their dry mass (Epstein, 1994). Si uptake and accumulation are a functional trait with multiple implications for plant biology and ecology (Epstein, 2009). Si is taken up as silicic acid [$Si(OH)_4$] via the roots and, after being transported into plant tissues, is deposited within and between plant cells, the cell wall, and silicified structures such as trichomes or other phytoliths (Perry et al., 1984; Kumar et al., 2017). Although the role of Si in protecting plants against multiple biotic (e.g., herbivores and pathogens) and abiotic (e.g., drought and salinity) stresses has been widely reported (Cooke and Leishman, 2011; Debona et al., 2017), an understanding of the exact mechanisms underpinning such protection remains incomplete (Coskun et al., 2019). However, the consensus is that Si supplementation enhances plant physical defences and integrates with the regulation of secondary metabolite defences (Reynolds et al., 2016; Alhousari and Greger, 2018; Hall et al., 2019; Waterman et al., 2020).

In terms of physical defences, it is well established that Si confers plant resistance and reduces plant damage caused by both vertebrate and invertebrate herbivores (Massey and Hartley, 2009; Hartley et al., 2015; Alhousari and Greger, 2018). Si deposition within and around plant cells makes plant tissues tougher and abrasive, causing wear on herbivore mouthparts, damages digestive organs, inhibits movement, and reduces the feeding efficiency of insect herbivores (Massey et al., 2006; Reynolds et al., 2009). Moreover, Si is known to alter grass physical defences such as macrohairs, silica cells, and prickle cells, which are linked to reduced feeding by insect herbivores (Hartley et al., 2015; Hall et al., 2020; Biru et al., 2021). Si uptake and accumulation have also been shown to be induced following herbivory (Massey et al., 2007; Islam et al., 2020; Biru et al., 2022).

In addition to direct physical defences, Si potentially protects plants against herbivores by influencing production of plant biochemical defences (Reynolds et al., 2016; Yang et al., 2017), although there is much uncertainty about this since Si has limited chemical reactivity within the plant. Herbivore attack is associated with the induction of oxidative stress in plants, resulting from overproduction of reactive oxygen species (ROS) (Bi and Felton, 1995; Kerchev et al., 2012). For instance, insect herbivore attacks can induce various ROS such as hydrogen peroxide (H_2O_2), superoxide ($O_2\bullet-$), singlet oxygen ($^1O_2$), or hydroxyl radicals ($\bullet OH$) in cells (Sharma et al., 2012; Das and Roychoudhury, 2014). While ROS have signalling roles under physiological setup (Hasanuzzaman et al., 2020), (biotic) stress-induced ROS overproduction damages cell structures and functionality (Tripathy and Oelmüller, 2012; Das and Roychoudhury, 2014; Fichman and Mittler, 2020). In order to reduce excessive ROS content caused by the imbalance between free radical formation and the capability of cells to detoxify them (Pizzino et al., 2017), plants have developed efficient antioxidant enzymatic machinery to scavenge ROS (Tripathy and Oelmüller, 2012). The antioxidant defence system in the plant cell includes both enzyme constituents such as superoxide dismutase (SOD), catalase (CAT), ascorbate peroxidase (APX), glutathione reductase (GR), and non-enzyme constituents like cysteine (Cys), reduced glutathione (GSH), and ascorbic acid (AsA) (Farooq et al., 2013; Kim et al., 2017). Plants possess either constitutive or induced antioxidants (Sudhakar et al., 2001) and the increased activities of these enzymes in plant cells appear to better control oxidative stress (Das and Roychoudhury, 2014; Huang et al., 2019).

Exogenous Si application has been linked to enhanced activity of antioxidant enzyme defences such as CAT, APX, and SOD (Kim et al., 2016; Hasanuzzaman et al., 2018; Ahanger et al., 2020). However, the mode of action by which Si regulates antioxidant capacities is poorly understood. Previous work has shown that Si enhances SOD, CAT, APX, and peroxidase activities in rice (*Oryza sativa*) (Han et al., 2016), wheat (*Triticum aestivum* L.) (Gong et al., 2005), and maize (*Zea mays* L.) (Moussa, 2006). Si-mediated regulation of antioxidant defences, therefore, reduces the harmful effects of herbivore-induced oxidative stress (Ahanger et al., 2020; Acevedo et al., 2021).

Atmospheric concentrations of carbon dioxide (CO_2) have emerged as an important environmental driver of Si accumulation (Johnson and Hartley, 2018). In general, several studies report that elevated CO_2 concentrations (eCO_2) decrease Si accumulation (Ryalls et al., 2017; Johnson and Hartley, 2018; Johnson et al., 2023), but see Frew et al. (2017) and Fulweiler et al. (2014). In contrast, reduced levels of atmospheric CO_2 can lead to increased Si accumulation (Biru et al., 2020; Biru et al., 2021). These effects are likely due to carbon (C) being either more available under eCO_2 (Johnson and Hartley, 2018; Johnson et al., 2022) or less available under reduced CO_2 conditions (Biru et al., 2020). Si accumulation is often negatively correlated with C potentially due to stoichiometric dilution or Si substitution for C-based structural or defensive compounds (Raven, 1983; Hodson et al., 2005).

Given CO_2 is such an important driver of Si accumulation, which has been shown to influence enzymatic responses (e.g., Kim et al., 2016; Ahanger et al., 2020; Acevedo et al., 2021), CO_2 may also affect production of plant biochemical defences (i.e., antioxidant enzyme), potentially via enhanced plant susceptibility to herbivore-induced oxidative stress. To our knowledge, no studies have yet investigated the effects of variable rates of Si accumulation on antioxidant enzyme activity and regulation of herbivore-induced oxidative stress under different CO_2 concentrations. Using tall fescue (*Festuca arundinacea*) and the generalist insect herbivore, cotton bollworm [*Helicoverpa armigera* (Hübner)], we investigated the effect of Si treatments on antioxidant enzyme activities and foliar chemistry of plants grown under three CO_2 concentrations (200, 410, and 640 ppm) and the consequences for insect herbivory. The objective of this study was to determine how Si treatments (+Si or −Si) under different CO_2 concentrations affect antioxidant enzyme activity and foliar chemistry (e.g., C, N) in tall fescue and the consequences for insect herbivore growth rate and feeding efficiency. We hypothesised that (1) +Si and reduced CO_2 decrease shoot C concentrations but increase shoot N concentration, i.e., decreasing shoot C-to-N ratio, and (2) +Si together with reduced CO_2 treatments increases antioxidant enzyme activity, whereas −Si together with elevated CO_2 would decrease antioxidant enzyme activity.

Materials and methods

Plant material and growth conditions

Tall fescue (*Festuca arundinacea*) is a common pasture grass and a high Si accumulator (Hodson et al., 2005). Seeds of tall fescue (accession T 9627), obtained from Margot Forde Germplasm Centre (Palmerston North, New Zealand), were sterilised in a solution of 0.9% sodium hypochlorite and 0.1% Triton X-100 for 30 min, followed by washing several times with water before being inserted into perlite irrigated with water. Seeds were stratified at 4°C for 3 days, and plants were grown in the glasshouse for 2 weeks using a rectangular plastic tray to achieve uniform seedling growth. Two weeks after germination, individual plants were transferred to hydroponics cups. The hydroponics setup consisted of two nested disposable plastic cups as per Hall et al. (2019). Each cup was filled with approximately 350 mL of full-strength standard hydroponic solutions following the protocol of Jung et al. (2015). Seedlings were grown in three plant growth chambers (TPG-1260TH, Thermoline Scientific, NSW, Australia), maintained at a reduced CO_2 of 200 ppm, an ambient CO_2 of 410 ppm, and an elevated CO_2 of 640 ppm CO_2 concentrations; the latter CO_2 concentration predicted for 2100 under the RCP6.0 scenario outlined by the IPCC (2014). Chambers were illuminated with five 400-W Sunmaster Dual Spectrum High-Pressure Sodium globes at 350 μmol m^{-2} s^{-1} at the plant canopy level. Daytime air temperature was regulated at 26°C and fell to 18°C at night on a 15L:9D photoperiod cycle. Humidity was controlled at 50% (± 6%). Carbon dioxide within the chambers was monitored by a Li-Cor LI-820 CO_2 gas analyser, with CO_2 (food grade, Air Liquide, NSW, Australia) injected from pressurised cylinders through solenoid valves. For reduced CO_2 treatment in the chamber, the computer controller constantly monitors CO_2 and powers fans to direct chamber air through the scrubbers filled with Sodasorb® (W.R. Grace & Co, Chicago, USA).

Experimental design

The experimental design consisted of 252 hydroponically grown tall fescue plants. The experiment comprised a factorial combination of CO_2 concentrations (200, 410, or 640 ppm), Si (+Si or −Si), and herbivore (herbivory, +H; no herbivory, −H) treatments (see Figure 1). Si treatments (+Si) used liquid potassium silicate (K_2SiO_3) (Agsil32, PQ Australia, SA, Australia) at a concentration equivalent to 2 mM SiO_2. Chemically, silicic acid polymerises to form silica gel when the concentration of silicic acid exceeds 2 mM (Ma and Yamaji, 2006). Potassium chloride was added to the control (−Si) cups to balance additional K^+ ions in +Si treatments. The pH of both +Si and −Si solutions was adjusted to 5.6 using hydrochloric acid to reduce silicate polymerisation (Ma and Yamaji, 2006). Solutions were replaced weekly for the first 2 weeks and then three times a week afterwards. Cups were rotated and chambers were swapped weekly to minimise chamber effects and pseudo-replication as previously described by Johnson et al. (2018). Plants were grown hydroponically for a further 6 weeks (42 days, Figure 1) before insect inoculation.

Herbivore performance

To assess the impacts of different CO_2 concentrations and Si supplementation on the growth of *H. armigera* larvae, a feeding performance assay was conducted. *Helicoverpa armigera* third instar larvae supplied by CSIRO Agriculture & Food, Narrabri, Australia, reared on an artificial diet (Teakle and Jensen, 1985), were used for feeding assays. Initially, larvae were starved for 24 h and weighed, and a single larva was either applied for each plant shoot [herbivory (+H)]) or kept control [no herbivory (−H)] (see Figure 1 for details). Each plant was then caged with transparent Perspex sheaths and herbivores were allowed to feed on shoot parts of the plants for 6 days, after which they were removed and starved for a further 24 h to allow the frass to pass, before being reweighed. All frass were collected, dried, and weighed. Frass production was used as a surrogate for plant consumption. RGR was calculated according to Massey and Hartley (2009). RGR estimates the change in larval fresh mass relative to initial mass and was calculated as mass gained (mg)/initial mass (mg)/time (days).

Antioxidant enzyme activity assays

Immediately after herbivore removal, plants from all treatment groups were harvested into liquid nitrogen and stored at −80°C until analysis. For the measurement of enzymatic activities, ca. 0.05 g of leaf tissue was ground in liquid N and homogenised in 3 mL of ice-cold 100 mM K-phosphate buffer (pH 6.8) containing 0.1 mM EDTA. The homogenate was centrifuged at 16,000 *g* for 15 min and the supernatant was used as the source of crude extracts. The supernatant was utilised to measure the activity of antioxidant enzyme such as CAT, APX, and SOD.

CAT activity was measured spectrophotometrically following the method of Fimognari et al. (2020) and Maksimović and Živanović (2012). Reaction mixture consists of 50 mM potassium phosphate buffer, pH 7.0, 20 mM H_2O_2, and crude extract. Absorbance at 240 nm was recorded for 130s using CLARIOstar® plate reader (BMG Labtech, Ortenberg, Germany) in 96-well plates (96-well Flat Bottom Plate, Greiner Bio-one, Australia). For control reactions, H_2O_2 was omitted. Enzyme activity was calculated using the molar extinction coefficient 36×10^3 mM^{-1} m^{-1} and expressed as μmol H_2O_2 oxidised g^{-1} FW min^{-1}.

APX activity was assayed according to Hartmann and Asch (2019). The reaction mixture consists of 50 mM potassium phosphate buffer, pH 7.0, 0.2 mM ascorbate, 0.2 mM H_2O_2 and crude extract. Absorbance at 290 nm was recorded for 130 s using CLARIOstar® in 96-well plates. APX activity was calculated according to Hartmann and Asch (2019); one unit of APX is defined as the amount of enzyme required to oxidise 1 μmol of ascorbic acid per minute.

SOD activity was estimated following the inhibition of photochemical reduction of nitroblue tetrazolium (NBT) by the enzyme according to Hartmann and Asch (2019). The reaction mixture contained 0.05 M sodium carbonate, 13.3 mM methionine, 1.3 μM riboflavin, 21 μM NBT, and plant extract (Hartmann and Asch, 2019). The reaction took place in a chamber under

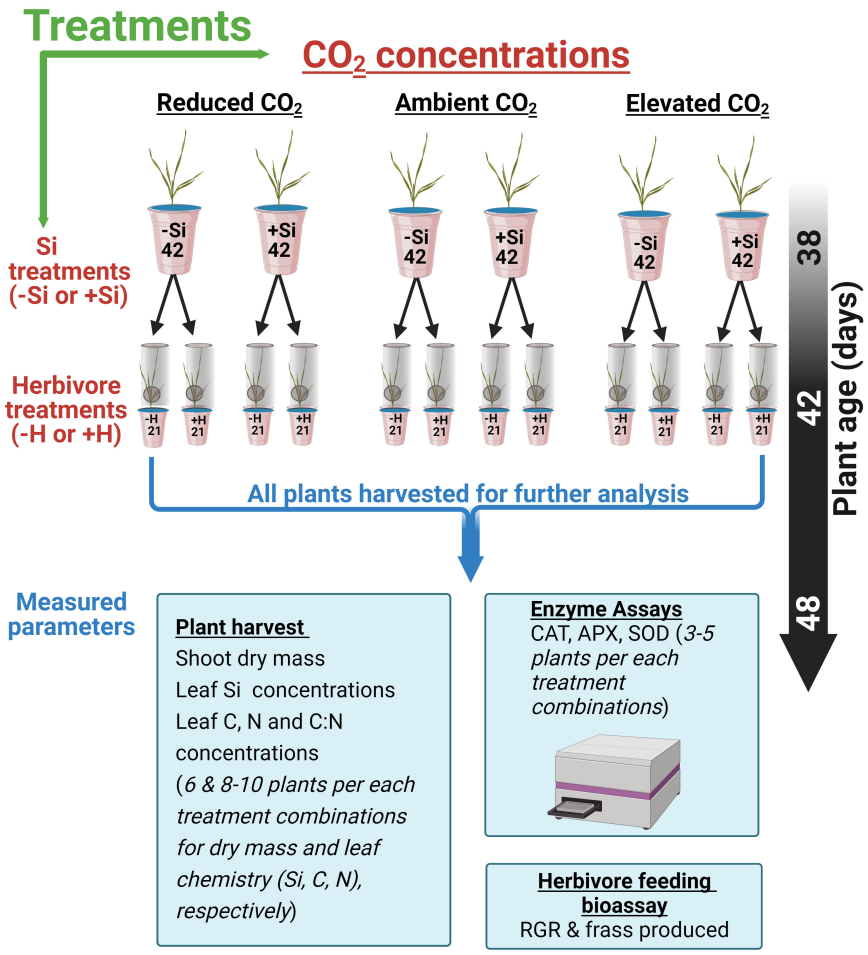

FIGURE 1
Schematic showing 252 (42*6) fescue grass grown under three CO_2 concentrations and Si treatments (–Si or +Si). Six weeks after transplant, plants were either inoculated with herbivore, (+H) or kept in control (–H). The specific arrangement of the cup within each chamber was randomised and swiped within the chambers every 2 weeks.

illumination of a 30-W fluorescent lamp at 25°C. The reaction was started by turning the fluorescent lamp on and stopped 5 min later by turning it off. The blue formazan produced by NBT photoreduction was measured as increase in absorbance at 560 nm. The blank solution had the same complete reaction mixture but was kept in the dark. One SOD unit was defined as the amount of enzyme required to inhibit 50% of the NBT photoreduction in comparison with wells lacking the plant extract and expressed as units of enzyme activity g^{-1} FW min^{-1} (Cavalcanti et al., 2004).

Analyses of foliar chemistry

Harvested sample leaves were oven-dried for 3 days at 60°C and ball milled for further analysis (see sample size from Figure 1). For foliar Si analysis, roughly 80 mg of ground leaf material was analysed using x-ray fluorescence spectrometry (Epsilon 3^x, PANalytical, EA Almelo, The Netherlands) as per Reidinger et al. (2012). Si measurements were calibrated against a certified plant reference material of known Si concentrations (Hiltpold et al., 2017). For foliar C and N concentration, approximately 7 mg of ground leaf material was analysed using Elementar Vario EL Cube, CHNOS elemental analyser (Elementar Analysensysteme GmbH, Hanau, Germany), at a combustion temperature of 950°C.

Statistical analysis

All data were analysed using SPSS (version 27) statistical software. Before analysis, all data were checked for assumptions of normality for residuals according to inspection of quantile–quantile plots. Plant dry mass was analysed on square-root transformed data whereas CAT, C:N ratio, and RGR were analysed on log10 transformed data, as they did not meet the assumptions of normality. Foliar Si was analysed using two-way analysis of variance (ANOVA) type = II, comparing CO_2, and herbivory (larval fed vs. undamaged controls) as treatments and their interaction. For foliar Si analyses, control (–Si) plants were omitted since –Si plants had Si concentrations lower than the machine detection limits (Reidinger et al., 2012). Plant dry mass,

antioxidant enzyme activities (CAT, APX, and SOD), foliar C, N, and C-to-N ratio concentrations were all analysed using three-way ANOVA type = II, comparing CO_2, Si (Si-supplemented vs. non-Si-supplemented plants) and herbivory as treatments and their interaction. Additionally, we tested the independent effects of CO_2 on antioxidant enzyme using a one-way ANCOVA, with CO_2 levels as a fixed factor and foliar Si concentration fitted as a covariate. For herbivore RGR and frass produced, three insects escaped, so data were analysed using type = III ANOVAs due to the unbalanced design. Bonferroni *post hoc* test (Aslam and Albassam, 2020) was applied for pairwise multiple comparisons when interaction terms were statistically significant. Potential relationships between foliar Si and herbivore RGR, frass produced, CAT, APX, and SOD enzymes activity were investigated using Spearman's rank correlation test.

Results

Plant dry mass and foliar chemistry

Averaged across CO_2 treatments, Si supply increased plant dry mass by 160% relative to those grown without Si supply, whereas elevated CO_2 increased plant dry mass by twofold and threefold compared to reduced CO_2 and ambient CO_2, respectively (Figure 2A; Table 1). Furthermore, herbivory decreased plant dry mass in Si-free (control) plants by 1.5-, 2-, and 2-fold under reduced, ambient, and elevated CO_2, respectively, compared to Si-supplemented plants (Figure 2A). Si supplementation decreased foliar C concentrations under all CO_2 regimes. This effect was reversed when herbivores were present and foliar C concentrations increased to levels observed in Si-free plants (Figure 2B; Table 1). Si supply decreased foliar C by 149%, 177%, and 107% under reduced, ambient, and elevated CO_2, respectively, regardless of herbivore treatments (Figure 2B). Reduced CO_2 significantly decreased foliar C (Figure 2B; Table 1). Si supply decreased foliar N under all CO_2 regimes. However, there was also an effect of CO_2 whereby reduced CO_2 increased foliar N by twofold and threefold compared to ambient and elevated CO_2, respectively, irrespective of herbivore treatments (Figure 2C; Table 1). In addition to variations in C and N concentrations, there was also an effect on their ratio. Si supply increased foliar C:N ratio especially when plants were damaged by herbivores or in herbivore-free plants only under elevated CO_2 (Figure 2D; Table 1). While herbivory increased foliar C:N ratio regardless of CO_2 levels, reduced CO_2 decreased foliar C:N ratio relative to elevated CO_2 (Figure 2D; Table 1). Foliar Si accumulation [% dry weight (DW)] was significantly higher under reduced CO_2 relative to ambient and elevated CO_2 (Figure 3; Table 1).

Antioxidant enzyme activity was enhanced by Si uptake and reduced CO_2

CAT activity increased in response to Si supply and herbivore damage overall, although this was only apparent under reduced CO_2 concentrations (Table 1; Figure 4A). The significant interaction between Si and CO_2 reflects that Si impacts were only apparent under reduced CO_2 concentrations (Table 1). In contrast, Si supply increased APX enzymes activity under all CO_2 regimes and SOD enzyme activity under reduced and ambient CO_2 (Table 1; Figures 4B, C). Herbivory caused higher APX activity specifically in Si-supplemented plants (Table 1; Figure 4B); however, it had no significant effect on SOD enzyme activity (Table 1; Figure 4C). Overall, antioxidant enzyme activity (CAT, APX, and SOD) declined with increasing CO_2 concentrations (Table 1;

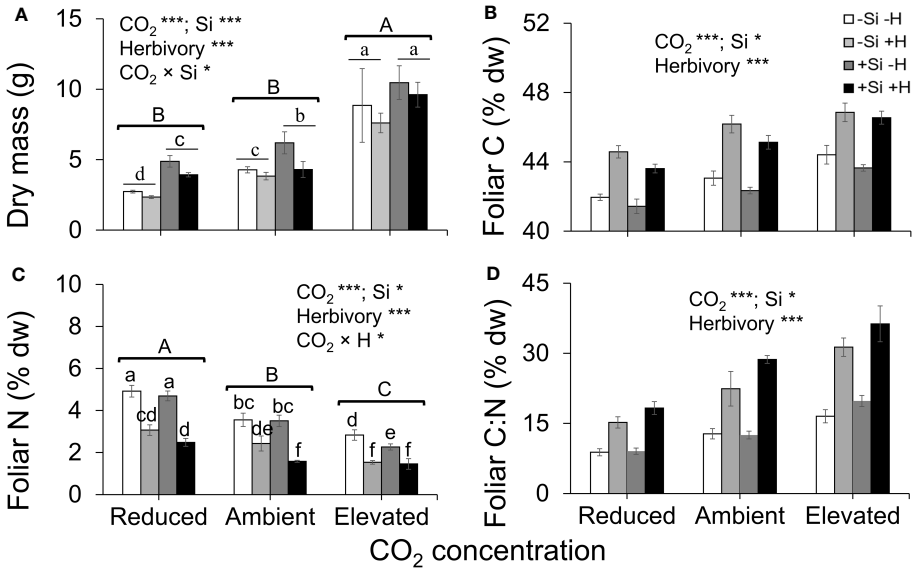

FIGURE 2
Effects of Si supply (+Si or −Si) and herbivory treatments (+H or −H) on **(A)** plant dry mass, **(B)** foliar C, **(C)** foliar N, and **(D)** foliar C:N of tall fescue grass grown under reduced, ambient, and elevated CO_2 concentration. Means ± SE shown. N = 6–8. Uppercase letters represent differences between CO_2 concentrations whereas lowercase letters indicate differences between Si treatments (Panel 1A) and herbivore treatments (Panel 1C). Statistically significant effects are indicated *p < 0.05, and ***p < 0.001.

TABLE 1 Results of ANOVA for plant biomass, foliar chemistry, and antioxidant enzyme as affected by CO_2 levels, Si treatment, and herbivore presence and their interactive effects.

Response variables	Figures	Factors						
		CO_2	Si	Herbivory	CO_2 × Si	CO_2 × Herbivory	Si × Herbivory	CO_2 × Si × Herbivory
Biomass and foliar chemistry								
Biomass[z]	**1A**	$F_{2,60} = 153.1$ $p < \mathbf{0.001}$	$F_{1,60} = 44.61$ $p < \mathbf{0.001}$	$F_{1,60} = 14.23$ $p < \mathbf{0.001}$	$F_{2,60} = 5.761$ $p = \mathbf{0.005}$	$F_{2,54} = 0.545$ $p = 0.582$	$F_{1,60} = 0.489$ $p = 0.487$	$F_{2,60} = 1.043$ $p = 0.359$
C[x]	**1B**	$F_{2,84} = 41.34$ $p < \mathbf{0.001}$	$F_{1,84} = 10.54$ $p = \mathbf{0.002}$	$F_{1,84} = 145.5$ $p < \mathbf{0.001}$	$F_{2,84} = 0.211$ $p = 0.801$	$F_{2,84} = 0.515$ $p = 0.599$	$F_{1,84} = 0.062$ $p = 0.804$	$F_{2,84} = 0.409$ $p = 0.666$
N[x]	**1C**	$F_{2,84} = 54.73$ $p < \mathbf{0.001}$	$F_{1,84} = 7.973$ $p = \mathbf{0.006}$	$F_{1,84} = 123.1$ $p < \mathbf{0.001}$	$F_{2,84} = 0.072$ $p = 0.930$	$F_{2,84} = 4.151$ $p = \mathbf{0.019}$	$F_{1,84} = 0.645$ $p = 0.424$	$F_{2,84} = 1.856$ $p = 0.163$
C:N[z]	**1D**	$F_{2,84} = 62.33$ $p < \mathbf{0.001}$	$F_{1,84} = 7.512$ $p = \mathbf{0.007}$	$F_{1,84} = 154.7$ $p < \mathbf{0.001}$	$F_{2,84} = 0.102$ $p = 0.903$	$F_{2,84} = 0.146$ $p = 0.864$	$F_{1,84} = 1.818$ $p = 0.181$	$F_{2,84} = 1.462$ $p = 0.237$
Si[a]	**2**	$F_{2,54} = 19.31$ $p < \mathbf{0.001}$	———	$F_{1,54} = 4.267$ $p = \mathbf{0.044}$	———	$F_{2,54} = 0.949$ $p = 0.393$	———	———
Antioxidant enzyme activity								
CAT[y]	**3A**	$F_{2,45} = 19.19$ $p < \mathbf{0.001}$	$F_{1,45} = 5.672$ $p = \mathbf{0.022}$	$F_{1,45} = 4.290$ $p = \mathbf{0.044}$	$F_{2,45} = 3.843$ $p = \mathbf{0.029}$	$F_{2,45} = 0.649$ $p = 0.528$	$F_{1,45} = 0.000$ $p = 0.989$	$F_{2,45} = 0.007$ $p = 0.993$
APX[x]	**3B**	$F_{2,34} = 13.69$ $p < \mathbf{0.001}$	$F_{1,34} = 33.36$ $p < \mathbf{0.001}$	$F_{1,34} = 20.57$ $p < \mathbf{0.001}$	$F_{2,34} = 1.218$ $p = 0.308$	$F_{2,34} = 0.199$ $p = 0.820$	$F_{1,34} = 0.054$ $p = 0.818$	$F_{2,34} = 0.066$ $p = 0.936$
SOD[x]	**3C**	$F_{2,45} = 7.489$ $p = \mathbf{0.002}$	$F_{1,45} = 8.781$ $p = \mathbf{0.005}$	$F_{1,45} = 2.047$ $p = 0.159$	$F_{2,45} = 0.061$ $p = 0.941$	$F_{2,45} = 0.018$ $p = 0.983$	$F_{1,45} = 0.109$ $p = 0.743$	$F_{2,45} = 0.094$ $p = 0.910$
Herbivore performance								
RGR[a]	**5A**	$F_{2,39} = 6.067$ $p = \mathbf{0.005}$	$F_{1,39} = 10.03$ $p = \mathbf{0.003}$	———	$F_{2,39} = 0.224$ $p = 0.801$	———	———	———
Frass[a]	**5B**	$F_{2,39} = 2.510$ $p = 0.094$	$F_{1,39} = 4.825$ $p = \mathbf{0.034}$	———	$F_{2,39} = 0.635$ $p = 0.536$	———	———	———

[a]Analysed using a two-way ANOVA.
[x]Analysed using a three-way ANOVA.
[y]Analysed using a three-way ANOVA on square-root transformed data.
[z]Analysed using a three-way ANOVA on log10 transformed data.
Statistically significant factors at *p*-values <0.05 are indicated in bold.

Figures 3A–C). Including foliar Si as a covariate in ANCOVA indicated that the changes in antioxidant enzyme activity were linked to CO_2 levels, which fully explained the observed changes in CAT ($F_{1,53} = 11.67$, $p = 0.001$) and APX ($F_{1,42} = 5.79$, $p = 0.021$) but not in SOD ($F_{1,53} = 1.130$, $p = 0.258$). There was a positive correlation between foliar Si concentrations and concentration of CAT under reduced CO_2, and concentration of APX under elevated CO_2 (Figures 5A, B). Interestingly, frass produced was negatively correlated with SOD ($r = -0.310$, $p = 0.038$), but had marginally non-significant negative correlation with APX ($r = -0.286$, $p = 0.057$). However, there was no such relationship observed between CAT and frass produced ($r = -0.191$, $p = 0.208$) (data not shown).

Si supply and low CO_2 environment suppressed herbivore RGR and feeding efficiency

Si supplementation decreased RGR under all CO_2 regimes; RGR was significantly lower under reduced CO_2 compared to elevated CO_2 (Table 1; Figure 6A). Si supply decreased the amount of frass produced by caterpillars (indicative of feeding efficiency) under all CO_2 levels; CO_2 had no significant effect on frass production, although there was a large increase in production in Si-free plants grown under elevated CO_2 (Table 1; Figure 6B). While herbivore RGR and frass produced were negatively correlated with foliar Si under ambient CO_2, there was no such relationship observed under the other two CO_2 regimes (Figures 6C, D). Here, the correlation between rate of herbivore feeding on foliar tissues of tall fescue grown under different CO_2 concentrations potentially indicates a new perspective towards mitigating challenges of CO_2 enriched environment on plant defences.

Discussion

We demonstrated that reduced levels of atmospheric CO_2 caused plants to accumulate more Si and produce higher levels of antioxidant enzyme relative to future levels of atmospheric CO_2. These increased levels of Si and antioxidant enzyme concentrations

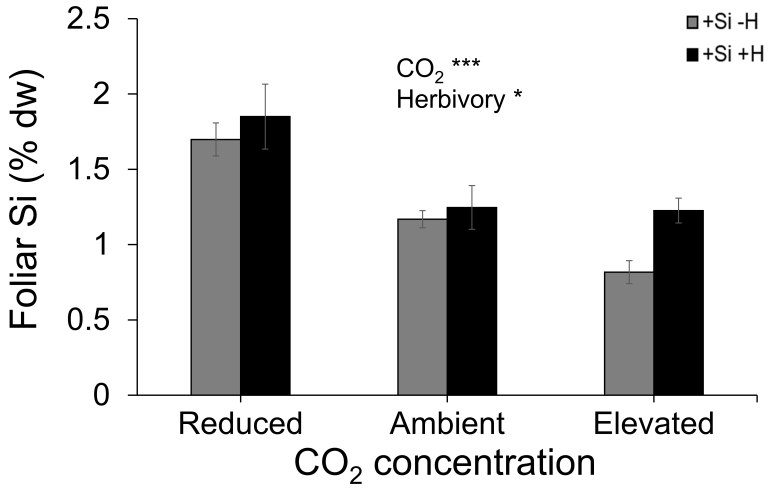

FIGURE 3
Effects of Si supply and herbivory (+H or −H) on foliar Si concentration of tall fescue grass grown under reduced, ambient, and elevated CO_2 concentration. Means ± SE shown. *N* = 10. Statistically significant effects are indicated *p < 0.05, and ***p < 0.001.

under reduced levels of CO_2 were associated with reduced insect herbivore performance. In contrast, herbivore performance and plant consumption (frass production as proxy) were highest under elevated atmospheric CO_2 conditions, which typically had the lowest levels of Si and antioxidant enzyme. To our knowledge, this is the first study to address the relationship between Si defences and antioxidant enzyme production in the context of variable atmospheric CO_2 conditions, which we summarise in Figure 7.

Direct and Si-mediated impacts of CO_2 on the activity of antioxidant enzyme

The effects of CO_2 in this study on Si concentrations are broadly similar to the few studies exploring this, whereby elevated CO_2 leads to decreased Si accumulation (Ryalls et al., 2017; Johnson and Hartley, 2018; Biru et al., 2022; Johnson et al., 2022; Johnson et al., 2023), whereas reduced CO_2 leads to increased Si accumulation. To

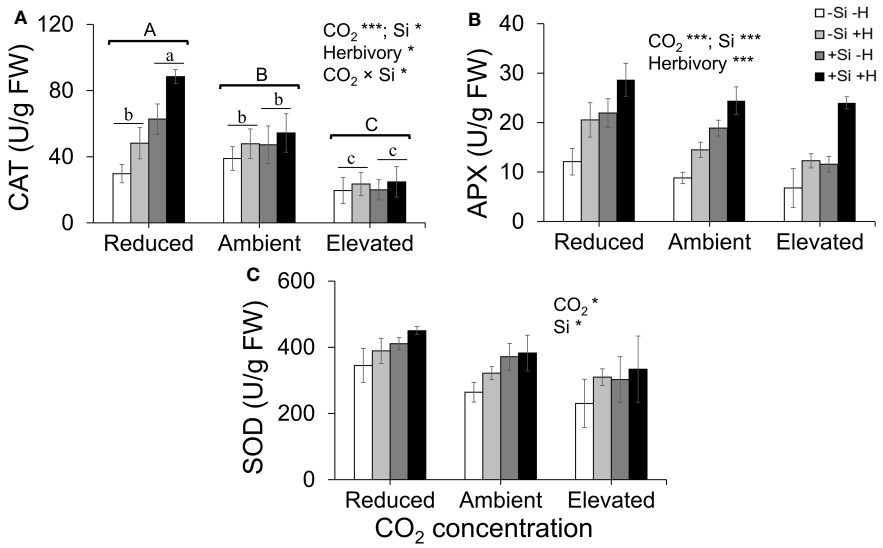

FIGURE 4
Effects of Si supply (+Si or −Si) and herbivory (+H or −H) on **(A)** CAT, **(B)** APX, and **(C)** SOD enzyme activity of tall fescue grass grown under reduced, ambient, and elevated CO_2 concentration. Means ± SE shown. *N* = 3–5. Uppercase letters represent differences between CO_2 concentrations whereas lowercase letters indicate differences between Si treatments (Panel 1A). Statistically significant effects are indicated *p < 0.05, and ***p < 0.001

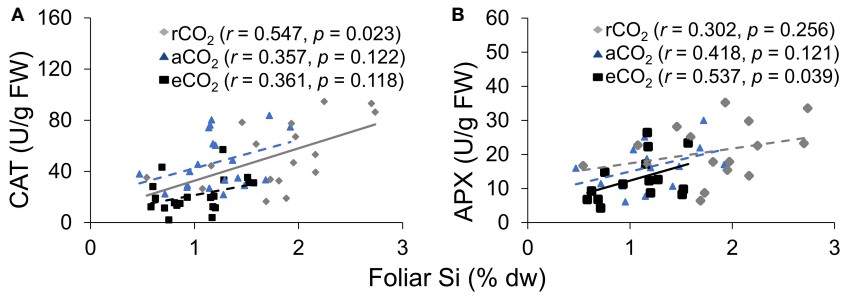

FIGURE 5
The relationship between **(A)** CAT and foliar Si, and **(B)** APX and foliar Si. The solid line represents linear regression through all data points and dashed lines indicate that no significant relationship was observed.

the best of our knowledge, the current study is only the third study to investigate the latter (Biru et al., 2020; Biru et al., 2021). Si has been hypothesised to act as a structural substitute for C at a lower metabolic cost, particularly when CO_2 concentrations were lower in the Miocene (Craine, 2009).

Exogenous application of Si has been shown to increase antioxidant enzyme including CAT, APX, and SOD (Kim et al., 2016; Hasanuzzaman et al., 2018; Ahanger et al., 2020). It seems likely that changes in Si in response to CO_2 growing conditions influenced activity of antioxidant enzyme in the current study. Additionally, the ANCOVA results indicated that CO_2 affects antioxidant enzyme activity (e.g., CAT and APX), which were mostly explained by the direct impacts of CO_2 levels on antioxidant enzyme. However, the observed positive correlation of leaf Si with CAT and APX under reduced CO_2 and elevated CO_2, respectively, suggests that CAT defence response may be linked to higher levels of Si under reduced CO_2, whereas APX defence response may be associated with increased induction of defence responses following herbivore attack under elevated CO_2. Overall, our results demonstrated significant augmentation of antioxidant enzyme responses via increased Si uptake under reduced CO_2 as well as by the direct effect of CO_2 levels (see Figure 7). In contrast, previous studies have reported that elevated CO_2 increases activity of antioxidant enzyme in different plants (Wang et al., 2003; Moghimifam et al., 2020). For example, Moghimifam et al. (2020) found that elevated CO_2 enhances CAT, polyphenol oxidase (PPO), SOD, and proline activity in algae (*Dunaliella* sp.). Our result may reflect that reduced CO_2 often increases photorespiration (Moroney et al., 2013; Voss et al., 2013) and since photorespiration is the key source for ROS production (Voss et al., 2013), reduced CO_2 may cause increased antioxidant enzyme activity in order to scavenge excessive ROS produced. However, these studies did not address whether Si played a role in these changes, while our findings suggest Si as an important influencer of the activity of these enzymes.

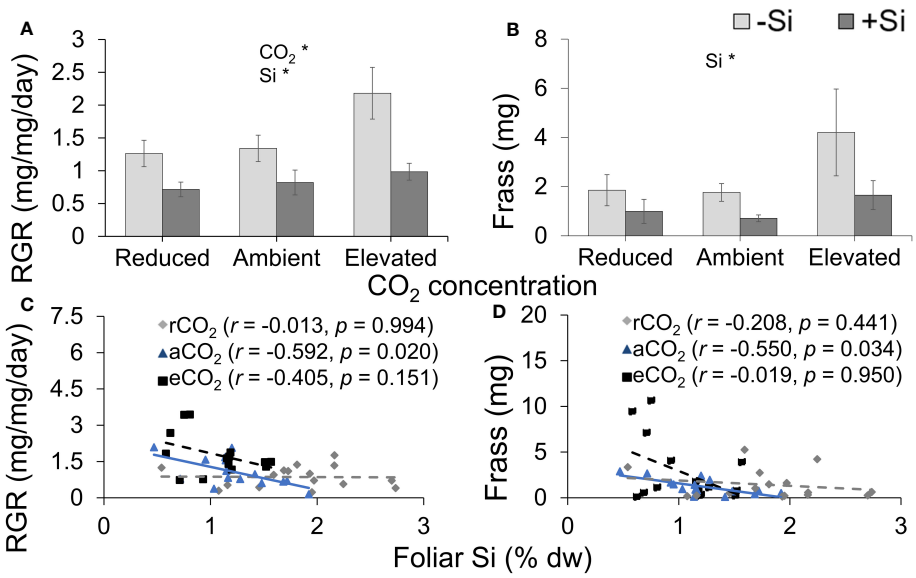

FIGURE 6
Effects of Si supply (+Si or −Si) and CO_2 level on **(A)** relative growth rate (RGR) of *Helicoverpa armigera* fed on tall fescue grass, **(B)** frass produced, and the relationship between foliar Si concentrations and **(C)** RGR and **(D)** frass produced. Means ± SE shown. *N* = 7–8. For **(C)** and **(D)**, the solid line represents linear regression through all data points and dashed lines indicate that no significant relationship was observed. Statistically significant effects are indicated *p < 0.05.

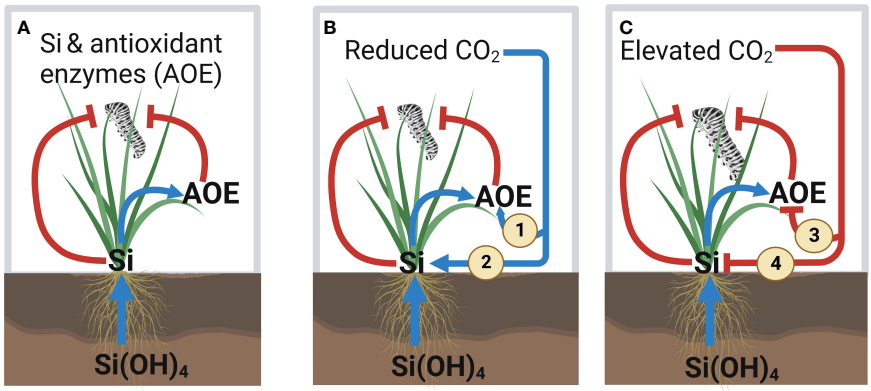

FIGURE 7
Summary of the effect of silicon (Si) and variable atmospheric CO_2 concentrations on the Si and antioxidant enzyme defences against herbivory. **(A)** Current knowledge of the interaction effect between Si and antioxidant enzyme (AOE) activity on insect herbivory. Our key results from this study are indicated in panels **(B, C). (B)** Reduced CO_2 enhances AOE defences by (1) directly enhancing AOE activity and (2) indirectly increasing Si uptake, which leads to reduced herbivore performance. **(C)** Elevated CO_2 reduces AOE defences by (3) directly reducing AOE activity and (4) indirectly decreasing Si uptake, which leads to increased herbivore performance. Positive and negative effects for both plants and insects are indicated by blue arrows and red lines, respectively.

Herbivory and Si enhanced antioxidant enzyme activity

In addition to CO_2 having direct and Si-mediated impacts on antioxidant enzyme activity, it is also possible that the amount of herbivore damage played a role in antioxidant enzyme activity. Herbivores induced higher activity of CAT and APX, so these enzymes activity is at least associated with the levels of damage done to the plant, which has been similarly reported in previous studies (Leitner et al., 2005; Yang et al., 2017). Increased levels of antioxidant enzyme under reduced CO_2 may reflect the fact that insects were doing less damage to the plant under these conditions and, therefore, there was less ROS oxidative stress that may have persisted in plant tissues to react with higher levels of antioxidant enzyme. Results from the ANCOVA and correlation tests also revealed that CO_2 directly changed antioxidant enzyme activity and altered feeding efficiency (leaf consumption), which eventually reduced the growth rate of herbivores.

Diminishing Si defence with rising CO_2

The recent finding by Biru et al. (2021) showed that *H. armigera* RGR was lowest when fed on the model grass *Brachypodium distachyon* grown under reduced CO_2 due to these plants having higher levels of Si defences compared to plants grown under ambient and elevated CO_2 concentrations. In the current study, we observed that tall fescue had the highest concentrations of foliar N when grown under reduced CO_2, which, in theory, could have promoted herbivore RGR because N is frequently the limiting factor in insect herbivore diets (Mattson, 1980; Huberty and Denno, 2006). The lower production of frass under reduced CO_2, which we used as a proxy for plant consumption, suggests that herbivores were deterred from feeding; thus, they would have not been able to access these N resources.

Understanding the diminishing levels of Si-based plant defences against herbivores under future elevated atmospheric CO_2 concentrations has received limited attention. Previous studies have shown that elevated CO_2 concentrations decrease Si accumulation in different Poaceae genera (e.g., grass species and wheat) (Johnson and Hartley, 2018; Biru et al., 2022; Johnson et al., 2022), and this was associated with reduced Si defences while increasing herbivore performance; however, this effect is not always reproducible (Frew et al., 2017). The impact of elevated CO_2 on Si defences reflects that plants switch from Si defences to C-based defences due to higher C availability under this scenario (Johnson and Hartley, 2018; Johnson et al., 2022). Although not examined in the context of Si defences, previous studies have demonstrated that elevated atmospheric CO_2 increased consumption and growth rate of the generalist (*Pseudaletia unipuncta*) and specialist (*Spodoptera frugiperda*) insect herbivores when fed on C_3 grass relative to lower atmospheric CO_2 conditions (Barbehenn et al., 2004). Johnson et al. (2020) also reported that *H. armigera* RGR increased under elevated CO_2 as a result of lower plant defence signalling and minimal reductions in the nutritional quality of lucerne (*Medicago sativa*).

Conclusions

The present study provides further evidence that CO_2 concentrations are strong drivers of Si accumulation in an important plant species, not previously reported on. We found strong evidence that reduced CO_2 increased foliar Si concentration and antioxidant enzyme levels, which potentially linked to suppressed insect herbivore performance. This suggests that the negative effects of silicification, whether via physical or biochemical mechanisms, are stronger under reduced CO_2. We showed a strong linkage between Si supplementation and activity of antioxidant enzyme, which may help in alleviating the harmful effects of

herbivore-induced oxidative stress on plant defence responses. Although Si defences are minimal under elevated atmospheric CO_2 conditions, many agricultural soils can become deficient in bioavailable Si (Haynes, 2017), which points to the importance of maintaining Si levels in soils under future projected atmospheric CO_2 conditions.

Data availability statement

The raw data supporting the conclusions of this article will be made available by the authors, without undue reservation.

Author contributions

FB: Conceptualization, Data curation, Formal Analysis, Methodology, Validation, Writing – original draft. CC: Supervision, Writing – review & editing. RE: Supervision, Writing – review & editing. SJ: Conceptualization, Supervision, Writing – review & editing.

Funding

The author(s) declare financial support was received for the research, authorship, and/or publication of this article. FB is the holder of a scholarship as part of an Australian Research Council Future Fellowship (grant no. FT170100342) awarded to SJ.

Acknowledgments

Special thank you to Tarikul Islam for assisting with larvae inoculation. We thank Ximena Cibils-Stewart for providing the *F. arundinacea* seeds. We also express sincere thanks to Andrew Gherlenda for the technical assistance with this work.

Conflict of interest

The authors declare that the research was conducted in the absence of any commercial or financial relationships that could be construed as a potential conflict of interest.

Publisher's note

References

Acevedo, F. E., Peiffer, M., Ray, S., Tan, C.-W., and Felton, G. W. (2021). Silicon-mediated enhancement of herbivore resistance in agricultural crops. *Front. Plant Sci.* 12, 631824. doi: 10.3389/fpls.2021.631824

Ahanger, M. A., Bhat, J. A., Siddiqui, M. H., Rinklebe, J., and Ahmad, P. (2020). Integration of silicon and secondary metabolites in plants: a significant association in stress tolerance. *J. Exp. Bot.* 71, 6758–6774. doi: 10.1093/jxb/eraa291

Alhousari, F., and Greger, M. (2018). Silicon and mechanisms of plant resistance to insect pests. *Plants-Basel* 7, 33. doi: 10.3390/plants7020033

Aslam, M., and Albassam, M. (2020). Presenting *post hoc* multiple comparison tests under neutrosophic statistics. *J. King Saud Univ. Sci.* 32, 2728–2732. doi: 10.1016/j.jksus.2020.06.008

Barbehenn, R. V., Karowe, D. N., and Spickard, A. (2004). Effects of elevated atmospheric CO_2 on the nutritional ecology of C_3 and C_4 grass-feeding caterpillars. *Oecologia* 140, 86–95. doi: 10.1007/s00442-004-1572-9

Bi, J. L., and Felton, G. W. (1995). Foliar oxidative stress and insect herbivory: primary compounds, secondary metabolites, and reactive oxygen species as components of induced resistance. *J. Chem. Ecol.* 21, 1511–1530. doi: 10.1007/bf02035149

Biru, F. N., Cazzonelli, C. I., Elbaum, R., and Johnson, S. N. (2020). Contrasting effects of Miocene and Anthropocene levels of atmospheric CO_2 on silicon accumulation in a model grass. *Biol. Lett.* 16, 20200608. doi: 10.1098/rsbl.2020.0608

Biru, F. N., Cazzonelli, C. I., Elbaum, R., and Johnson, S. N. (2022). Contrasting impacts of herbivore induction and elevated atmospheric CO_2 on silicon defences and consequences for subsequent herbivores. *Entomol. Exp. Appl.* 170, 681–688. doi: 10.1111/eea.13168

Biru, F. N., Islam, T., Cibils-Stewart, X., Cazzonelli, C. I., Elbaum, R., and Johnson, S. N. (2021). Anti-herbivore silicon defences in a model grass are greatest under Miocene levels of atmospheric CO_2. *Glob. Change Biol.* 27, 2959–2969. doi: 10.1111/gcb.15619

Cavalcanti, F. R., Oliveira, J. T. A., Martins-Miranda, A. S., Viégas, R. A., and Silveira, J. A. G. (2004). Superoxide dismutase, catalase and peroxidase activities do not confer protection against oxidative damage in salt-stressed cowpea leaves. *New Phytol.* 163, 563–571. doi: 10.1111/gcb.15619

Cooke, J., and Leishman, M. R. (2011). Is plant ecology more siliceous than we realise? *Trends Plant Sci.* 16, 61–68. doi: 10.1016/j.tplants.2010.10.003

Coskun, D., Deshmukh, R., Sonah, H., Menzies, J., Reynolds, O., Kronzucker,, et al. (2019). The controversies of silicon's role in plant biology. *New Phytol.* 221, 1340–1357. doi: 10.1111/nph.15343

Craine, J. M. (2009). *Resource strategies of wild plants* (Princeton, NJ, USA: Princeton University Press). doi: 10.1515/9781400830640

Das, K., and Roychoudhury, A. (2014). Reactive oxygen species (ROS) and response of antioxidants as ROS-scavengers during environmental stress in plants. *Front. Environ. Sci.* 2, 53. doi: 10.3389/fenvs.2014.00053

Debona, D., Rodrigues, F., and Datnoff, L. (2017). Silicon's role in abiotic and biotic plant stresses. *Annu. Rev. Phytopathol.* 55, 85–107. doi: 10.1146/annurev-phyto-080516-035312

Epstein, E. (1994). The anomaly of silicon in plant biology. *PNAS.* 91, 11–17. doi: 10.1073/pnas.91.1.11

Epstein, E. (2009). Silicon: its manifold roles in plants. *Ann. Appl. Biol.* 155, 155–160. doi: 10.1111/j.1744-7348.2009.00343.x

Farooq, M. A., Ali, S., Hameed, A., Ishaque, W., Mahmood, K., and Iqbal, Z. (2013). Alleviation of cadmium toxicity by silicon is related to elevated photosynthesis, antioxidant enzymes; suppressed cadmium uptake and oxidative stress in cotton. *Ecotoxicol. Environ. Saf.* 96, 242–249. doi: 10.1016/j.ecoenv.2013.07.006

Fichman, Y., and Mittler, R. (2020). Rapid systemic signaling during abiotic and biotic stresses: is the ROS wave master of all trades? *TPJ.* 102, 887–896. doi: 10.1111/tpj.14685

Fimognari, L., Dölker, R., Kaselyte, G., Jensen, C. N. G., Akhtar, S. S., Großkinsky, D. K., et al. (2020). Simple semi-high throughput determination of activity signatures of key antioxidant enzymes for physiological phenotyping. *Plant Methods* 16, 42. doi: 10.1186/s13007-020-00583-8

Frew, A., Allsopp, P. G., Gherlenda, A. N., and Johnson, S. N. (2017). Increased root herbivory under elevated atmospheric carbon dioxide concentrations is reversed by silicon-based plant defences. *J. Appl. Ecol.* 54, 1310–1319. doi: 10.1111/1365-2664.12822

Fulweiler, R. W., Maguire, T. J., Carey, J. C., and Finzi, A. C. (2014). Does elevated CO_2 alter silica uptake in trees? *Front. Plant Sci.* 5, 793. doi: 10.3389/fpls.2014.00793

Gong, H. J., Zhu, X. Y., Chen, K. M., Wang, S. M., and Zhang, C. L. (2005). Silicon alleviates oxidative damage of wheat plants in pots under drought. *Plant Sci.* 169, 313–321. doi: 10.1016/j.plantsci.2005.02.023

Hall, C. R., Dagg, V., Waterman, J. M., and Johnson, S. N. (2020). Silicon alters leaf surface morphology and suppresses insect herbivory in a model grass species. *Plants* 9, 643. doi: 10.3390/plants9050643

Hall, C. R., Waterman, J. M., Vandegeer, R. K., Hartley, S. E., and Johnson, S. N. (2019). The role of silicon in antiherbivore phytohormonal signalling. *Front. Plant Sci.* 10, 1132. doi: 10.3389/fpls.2019.01132

Han, Y., Li, P., Gong, S., Yang, L., Wen, L., and Hou, M. (2016). Defense responses in rice induced by silicon amendment against infestation by the leaf folder *Cnaphalocrocis medinalis*. *PloS One* 11, e0153918. doi: 10.1371/journal.pone.0153918

Hartley, S. E., Fitt, R. N., McLarnon, E. L., and Wade, R. N. (2015). Defending the leaf surface: intra- and inter-specific differences in silicon deposition in grasses in response to damage and silicon supply. *Front. Plant Sci.* 6, 35. doi: 10.3389/fpls.2015.00035

Hartmann, J., and Asch, F. (2019). Extraction, storage duration, and storage temperature affect the activity of ascorbate peroxidase, glutathione reductase, and superoxide dismutase in rice tissue. *Biology* 8, 70. doi: 10.3390/biology8040070

Hasanuzzaman, M., Bhuyan, M. H. M. B., Zulfiqar, F., Raza, A., Mohsin, S. M., Mahmud, J. A., et al. (2020). Reactive oxygen species and antioxidant defense in plants under abiotic stress: revisiting the crucial role of a universal defense regulator. *Antioxidants* 9, 681. doi: 10.3390/antiox9080681

Hasanuzzaman, M., Nahar, K., Anee, T. I., Khan, M. I. R., and Fujita, M. (2018). Silicon-mediated regulation of antioxidant defense and glyoxalase systems confers drought stress tolerance in *Brassica napus L. S. Afr. J. Bot.* 115, 50–57. doi: 10.1016/j.sajb.2017.12.006

Haynes, R. J. (2017). Chapter 3: Significance and role of Si in crop production. *Adv. Agron.* 146, 83–166. doi: 10.1016/bs.agron.2017.06.001

Hiltpold, I., Demarta, L., Johnson, S. N., Moore, B. D., Power, S. A., Mitchell, C., et al. (2017). "Silicon and other essential element composition in roots using X-ray fluorescence spectroscopy: A high throughput approach," in *Invertebrate ecology of Australasian grasslands*. Ed. S. N. Johnson (Western Sydney University, Hawkesbury, NSW, Australia:Proceedings of the Ninth ACGIE. Western Sydney University), 191–196).

Hodson, M. J., White, P. J., Mead, A., and Broadley, M. R. (2005). Phylogenetic variation in the silicon composition of plants. *Ann. Bot.* 96, 1027–1046. doi: 10.1093/aob/mci255

Huang, H., Ullah, F., Zhou, D.-X., Yi, M., and Zhao, Y. (2019). Mechanisms of ROS regulation of plant development and stress responses. *Front. Plant Sci.* 10, 800. doi: 10.3389/fpls.2019.00800

Huberty, A. F., and Denno, R. F. (2006). Consequences of nitrogen and phosphorus limitation for the performance of two planthoppers with divergent life-history strategies. *Oecologia* 149, 444–455. doi: 10.1007/s00442-006-0462-8

IPCC (2014). *Climate Change 2014: Impacts, Adaptation, and Vulnerability. Part A: Global and sectoral aspects. Contribution of working group II to the fifth assessment report of the intergovernmental panel on climate change*. Eds. C. B. Field, V. R. Baros, D. J. Dokken, K. J. Mach, M. D. Mastrandrea, T. E. Bilir, M. Chatterjee, K. L. Ebi, Y. O. Estrada, R. C. Genova, B. Girma, E. S. Kissel, A. N. Levy, S. MacCracken, P. R. Mastrandrea and L. L. White (Cambridge, UK and New York, NY: Cambridge University Press).

Islam, T., Ben D, M., and S Cott N, J. (2020). Novel evidence for systemic induction of silicon defences in cucumber following attack by a global insect herbivore. *Ecol. Entomol.* 45, 1373–1381. doi: 10.1111/een.12922

Johnson, S. N., Barton, C. V. M., Biru, F. N., Islam, T., Mace, W. J., Rowe, R. C., et al. (2023). Elevated atmospheric CO_2 suppresses silicon accumulation and exacerbates endophyte reductions in plant phosphorus. *Funct. Ecol.* 37, 1567–1579. doi: 10.1111/1365-2435.14342

Johnson, S. N., Cibils-Stewart, X., Waterman, J. M., Biru, F. N., Rowe, R. C., and Hartley, S. E. (2022). Elevated atmospheric CO_2 changes defence allocation in wheat but herbivore resistance persists. *Proc. R. Soc B: Biol. Sci.* 289, 20212536. doi: 10.1098/rspb.2021.2536

Johnson, S. N., and Hartley, S. E. (2018). Elevated carbon dioxide and warming impact silicon and phenolic-based defences differently in native and exotic grasses. *Glob. Change Biol.* 102, 3886–3896. doi: 10.1002/ecy.3250

Johnson, S. N., Ryalls, J. M. W., Gherlenda, A. N., Frew, A., and Hartley, S. E. (2018). Benefits from below: silicon supplementation maintains legume productivity under predicted climate change scenarios. *Front. Plant Sci.* 9, 202. doi: 10.3389/fpls.2018.00202

Johnson, S. N., Waterman, J. M., and Hall, C. R. (2020). Increased insect herbivore performance under elevated CO_2 is associated with lower plant defence signalling and minimal declines in nutritional quality. *Sci. Rep.* 10, 14553. doi: 10.1038/s41598-020-70823-3

Jung, H.-I., Yan, J., Zhai, Z., and Vatamaniuk, O. (2015). Gene functional analysis using protoplast transient assays. In: Alonso, J., Stepanova, A. (eds) *Plant Functional Genomics. Methods in Molecular Biology*, vol 1284. Humana Press, New York, NY

Kerchev, P. I., Fenton, B., Foyer, C. H., and Hancock, R. D. (2012). Plant responses to insect herbivory: interactions between photosynthesis, reactive oxygen species and hormonal signalling pathways. *Plant, Cell Environ.* 35, 441–453. doi: 10.1111/j.1365-3040.2011.02399.x

Kim, Y.-H., Khan, A., Waqas, M., and Lee, I.-J. (2017). Silicon regulates antioxidant activities of crop plants under abiotic-induced oxidative stress: a review. *Front. Plant Sci.* 8, 510. doi: 10.3389/fpls.2017.00510

Kim, Y. H., Khan, A. L., Waqas, M., Shahzad, R., and Lee, I. J. (2016). Silicon-mediated mitigation of wounding stress acts by up-regulating the rice antioxidant system. *Cereal Res. Commun.* 44, 111–121. doi: 10.1556/0806.43.2015.031

Kumar, S., Soukup, M., and Elbaum, R. (2017). Silicification in grasses: variation between different cell types. *Front. Plant Sci.* 8, 438. doi: 10.3389/fpls.2017.00438

Leitner, M., Boland, W., and Mithöfer, A. (2005). Direct and indirect defences induced by piercing-sucking and chewing herbivores in *Medicago truncatula*. *New Phytol.* 167, 597–606. doi: 10.1111/j.1469-8137.2005.01426.x

Ma, J. F., and Yamaji, N. (2006). Silicon uptake and accumulation in higher plants. *Trends Plant Sci.* 11, 392–397. doi: 10.1016/j.tplants.2006.06.007

Maksimović, J. J. D., and Živanović, B. D. (2012). Quantification of the antioxidant activity in salt-stressed tissues. *Methods Mol. Biol.* 913, 237–250. doi: 10.1007/978-1-61779-986-0_16

Massey, F. P., Ennos, A. R., and Hartley, S. E. (2006). Silica in grasses as a defence against insect herbivores: contrasting effects on folivores and a phloem feeder. *J. Anim. Ecol.* 75, 595–603. doi: 10.1111/j.1365-2656.2006.01082.x

Massey, F. P., and Hartley, S. E. (2009). Physical defences wear you down: progressive and irreversible impacts of silica on insect herbivores. *J. Anim. Ecol.* 78, 281–291. doi: 10.1111/j.1365-2656.2008.01472.x

Massey, F. P., Roland Ennos, A., and Hartley, S. E. (2007). Herbivore specific induction of silica-based plant defences. *Oecologia* 152, 677–683. doi: 10.1007/s00442-007-0703-5

Mattson, W. J. (1980). Herbivory in relation to plant nitrogen content. *Annu. Rev. Evol. Syst.* 11, 119–161. doi: 10.1146/annurev.es.11.110180.001003

Moghimifam, R., Niknam, V., Ebrahimzadeh, H., and Hejazi, M. A. (2020). The influence of different CO_2 concentrations on the biochemical and molecular response of two isolates of *Dunaliella* sp. (ABRIINW-CH2 and ABRIINW-SH33). *J. Appl. Phycol.* 32, 175–187. doi: 10.1007/s10811-019-01914-6

Moroney, J. V., Jungnick, N., DiMario, R. J., and Longstreth, D. J. (2013). Photorespiration and carbon concentrating mechanisms: two adaptations to high O_2, low CO_2 conditions. *Photosynth. Res.* 117, 121–131. doi: 10.1007/s11120-013-9865-7

Moussa, H. (2006). Influence of exogenous application of silicon on physiological response of salt-stressed maize (*Zea mays* L.). *Int. J. Agric. Biol.* 8, 293–297. doi: 10.1007/s12633-015-9372-x

Perry, C. C., Mann, S., and Williams, R. J. P. (1984). Structural and analytical studies of the silicified macrohairs from the lemma of the grass *Phalaris canariensis* L. *Proc. R. Soc B.* 222, 427–438. doi: 10.1098/rspb.1984.0075

Pizzino, G., Irrera, N., Cucinotta, M., Pallio, G., Mannino, F., Arcoraci, V., et al. (2017). Oxidative stress: harms and benefits for human health. *Oxid. Med. Cell. Longev.* 2017, 8416763. doi: 10.1155/2017/8416763

Raven, J. A. (1983). The transport and function of silicon in plants. *Biol. Rev.* 58, 179–207. doi: 10.1111/j.1469-185x.1983.tb00385.x

Reidinger, S., Ramsey, M. H., and Hartley, S. E. (2012). Rapid and accurate analyses of silicon and phosphorus in plants using a portable X-ray fluorescence spectrometer. *New Phytol.* 195, 699–706. doi: 10.1111/j.1469-8137.2012.04179.x

Reynolds, O. L., Keeping, M. G., and Meyer, J. H. (2009). Silicon-augmented resistance of plants to herbivorous insects: a review. *Ann. Appl. Biol.* 155, 171–186. doi: 10.1111/j.1744-7348.2009.00348.x

Reynolds, O. L., Padula, M. P., Zeng, R. S., and Gurr, G. M. (2016). Silicon: potential to promote direct and indirect effects on plant defense against arthropod pests in agriculture. *Front. Plant Sci.* 7, 744. doi: 10.3389/fpls.2016.00744

Ryalls, J. M. W., Hartley, S. E., and Johnson, S. N. (2017). Impacts of silicon-based grass defences across trophic levels under both current and future atmospheric CO_2 scenarios. *Biol. Lett.* 13, 20160912. doi: 10.1098/rsbl.2016.0912

Sharma, P., Jha, A. B., Dubey, R. S., and Pessarakli, M. (2012). Reactive oxygen species, oxidative damage, and antioxidative defense mechanism in plants under stressful conditions. *J. Bot.* 2012, 1–26. doi: 10.1155/2012/217037

Sudhakar, C., Lakshmi, A., and Giridarakumar, S. (2001). Changes in the antioxidant enzyme efficacy in two high yielding genotypes of mulberry (*Morus alba* L.) under NaCl salinity. *Plant Sci.* 161, 613–619. doi: 10.1016/s0168-9452(01)00450-2

Teakle, R., and Jensen, J. (1985). "Heliothis punctiger," in *Handbook of insect rearing*. Eds. P. Singh and R. F. Moore (Amsterdam, The Netherlands: Elsevier), 313–322.

Tripathy, B. C., and Oelmüller, R. (2012). Reactive oxygen species generation and signaling in plants. *Plant Signal. Behav.* 7, 1621–1633. doi: 10.4161/psb.22455

Voss, I., Sunil, B., Scheibe, R., and Raghavendra, A. S. (2013). Emerging concept for the role of photorespiration as an important part of abiotic stress response. *Plant Biol.* 15, 713–722. doi: 10.1111/j.1438-8677.2012.00710.x

Wang, S. Y., Bunce, J. A., and Maas, J. L. (2003). Elevated carbon dioxide increases contents of antioxidant compounds in field-grown strawberries. *J. Agric. Food Chem.* 51, 4315–4320. doi: 10.1021/jf021172d

Waterman, J. M., Hall, C. R., Mikhael, M., Cazzonelli, C. I., Hartley, S. E., and Johnson, S. N. (2020). Short-term resistance that persists: rapidly induced silicon anti-herbivore defence affects carbon-based plant defences. *Funct. Ecol.* 35, 82–92. doi: 10.1111/1365-2435.13702

Yang, L., Han, Y., Li, P., Li, F., Ali, S., and Hou, M. (2017). Silicon amendment is involved in the induction of plant defense responses to a phloem feeder. *Sci. Rep.* 7, 4232. doi: 10.1038/s41598-017-04571-2

frontiers | Frontiers in Plant Science

TYPE Original Research
PUBLISHED 10 November 2023
DOI 10.3389/fpls.2023.1229994

OPEN ACCESS

EDITED BY
Eman A. Mahmoud,
Damietta University, Egypt

REVIEWED BY
Tlili Imen,
Carthage University, Tunisia
Ilahy Riadh,
Institut National de la Recherche Agronomique de Tunisie (INRAT), Tunisia
Vishwas Anant Bapat,
Shivaji University, India

*CORRESPONDENCE
Lahcen Hssaini
lahcen.hssaini@inra.ma;
hssaiini@gmail.com

†These authors have contributed equally to this work

RECEIVED 27 May 2023
ACCEPTED 11 October 2023
PUBLISHED 10 November 2023

CITATION
Irchad A, Ouaabou R, Aboutayeb R, Razouk R, Houmanat K and Hssaini L (2023) Lipidomic profiling reveals phenotypic diversity and nutritional benefits in *Ficus carica* L. (Fig.) seed cultivars. *Front. Plant Sci.* 14:1229994. doi: 10.3389/fpls.2023.1229994

Lipidomic profiling reveals phenotypic diversity and nutritional benefits in *Ficus carica* L. (Fig.) seed cultivars

Ahmed Irchad[1,2†], Rachida Ouaabou[3], Rachid Aboutayeb[4], Rachid Razouk[4], Karim Houmanat[4] and Lahcen Hssaini[4*†]

[1]Faculty of Sciences and Techniques, University of Comoros, Moroni, Comoros, [2]Hygiene and Food Safety Department, National Research Institute for Agriculture, Fisheries and Environment (INRAPE), Ex CEFADER, M'dé, Ngazidja, Moroni, Comoros, [3]Environmental Technologies, Biotechnology and Valorization of Bio-Resources Team, Faculty of Sciences and Techniques Al-Hoceïma, Abdelmalek Essâadi University, Al-Hoceïma, Morocco, [4]Agro-Food Technology and Quality Laboratory, Regional Center of Agricultural Research of Meknes, National Institute of Agricultural Research, Rabat, Morocco

Introduction: *Ficus carica* L. seeds are a substantial source of minor oil with high unsaturation levels and potent antioxidant properties. The study aims to evaluate the mineral composition, lipodomic profile, and vibrational fingerprints of 22 fig genotypes utilizing FTIR-ATR techniques and chemometrics.

Methods: FTIR-ATR spectroscopy and chemometric techniques were employed to examine the phenotypic diversity of fig seeds. The investigation was performed in detail. The research analyzed twenty-two fig genotypes to assess their nutritional properties, genetic relationships, and potential applications.

Results: The results demonstrate substantial nutritional benefits related to fig seeds, which could serve as genetic resources for selection programs for extracting vegetable oil and functional ingredients. Additionally, a detailed lipodomic profile analysis led to the categorization of the genotypes into four unique clusters. The study uncovered new insights regarding the nutritional composition of the samples, while also highlighting significant similarities and differences. The findings showcased the phenotypic diversity within the studied fig germplasm, which is likely attributed to underlying genetic factors. These accessions offer a valuable gene pool for future breeding programs and diverse applications involving fig seeds.

Discussion: This work contributes to the selection of potential genotypes for scientific and industrial purposes. Furthermore, the application of FTIR and chemometrics revealed a noteworthy diversity of patterns, emphasizing the previously underestimated significance of this aspect in evaluating the chemodiversity of the species.

KEYWORDS

chemometrics, *Ficus carica* L, ionomic analysis, nutritional quality, seeds, vibrational spectroscopy

Highlights

- Phenotypic diversity of seeds and fig seed oils were described for the first time.
- This first exploratory study screened 22 cultivars of fig seeds based on their proteins and mineral content and lipid properties using a combination of FTIR-ATR spectroscopic analysis and multivariate analysis.
- Lipochemical-based fingerprinting of fig seeds revealed the phenotypic diversity within the germplasm of the fig tree.
- The findings revealed the substantial nutritional benefits of fig seeds as a nutritious source of lipids, minerals and proteins, and their potentialities in genetic material selection programs.
- Results introduce FTIR-ATR spectroscopy combined with multivariate analysis as a convenient highly sensitive method and effective in fig seed cultivars discrimination and classification.

1 Introduction

Figs (*Ficus carica* L.) are commonly consumed fruits which are known for their sweet and flavorful taste, but the seeds contained within the fruits often go unnoticed (Hssaini et al., 2021a). These seeds, which vary in number and size, play a crucial role in determining the flavor and taste of figs, as well as their nutritional composition. These aspects are influenced by several factors, including the genotype of the fig, its ripening stage, and the mutualistic relationship between the fig and its pollinator wasp, which is known as caprification (Solomon et al., 2006; Gaaliche et al., 2011; Rosianski et al., 2016; Hssaini et al., 2022). Despite their contribution to the nutritional composition of figs, there have been very few studies on fig seeds (Hssaini et al., 2020; Hssaini et al., 2021a). Previous research has shown that fig seed oil is generally pale yellow in color and yields can vary significantly based on the genotype, with some genotypes yielding up to 30% oil content (Hssaini et al., 2020). The macro-qualitative components of fig seeds, including oil yield and lipochemical composition, are influenced by both genetic differences between seeds and geographical variations (Raihana et al., 2015; Górnaś and Rudzińska, 2016) as well as the pollination system (Hssaini et al., 2022). Compared to other fruit seeds, fig seeds have an oil yield that is similar to pumpkin (27.83%) (Alfawaz, 2004), honeydew (25%) (Yanty et al., 2008), and mangosteen (21.18%) (Ajayi et al., 2007), and higher than those of durian seeds (1.8%) (Berry, 1980), Opuntia ficus indica seeds (5.4 to 9.9%) (Taoufik et al., 2015), and guava (16%) (Prasad and Azeemoddin, 1994). With such high oil yields, fig seeds have the potential to be used for industrial purposes, much like other fruit seeds. Despite this, fig seeds have been relatively unstudied, and many questions remain unanswered, particularly regarding the large-scale impact of genotype on the nutritional components and oil yield of fig seeds.

The mineral composition of fig (*Ficus carica* L.) seeds has received limited attention, and there is a notable gap in the literature when it comes to investigating seeds from a wide range of genotypes. While several studies have estimated the concentration of mineral elements in different parts of the *Ficus carica* L. plant, including its leaves, aerial roots, and bark (Khan, 2011), the majority of research has predominantly focused on the entire fruit, particularly dried figs (Aljane and Ferchichi, 2007; Aljane and Ferchichi, 2009; Khan, 2011; Sadia et al., 2014; Lo Turco et al., 2020). To date, there have been very few studies dedicated to exploring the mineral composition of fig seeds, despite their importance in providing essential nutrients that cannot be synthesized by the human body and must be obtained through dietary sources or supplements to meet daily nutritional requirements (Chongtham et al., 2020). Scientific evidence suggests that a diet rich in minerals can play a crucial role in preventing and treating various diseases, such as diabetes, heart disease, stroke, and cancer (Tolonen, 1990; Branco et al., 2016). Macro-elements, including calcium, phosphorus, sodium, magnesium, and potassium, are involved in vital cellular transmission and signaling processes. Additionally, micro-elements, such as copper, iron, manganese, selenium, and zinc, serve as essential structural components of numerous enzymes (Gharibzahedi and Jafari, 2017). Given the potential health implications and the significance of mineral elements in the human diet, the scarcity of studies investigating the mineral composition of fig seeds is noteworthy. As such, the present study aims to address this gap in the literature by comprehensively evaluating the mineral content of Ficus carica L. seeds from various fig genotypes. By conducting such a study, we aim to shed light on the nutritional importance and potential health benefits associated with the consumption of fig seeds. The findings from this research may provide valuable insights into the unique mineral profiles of different fig genotypes, thus contributing to a deeper understanding of the overall nutritional composition of the fig tree and its potential applications in promoting human health.

Recently, phenotypic diversity of seeds and fig seed oils has been reported for only four genotypes (Hssaini et al., 2020; Hssaini et al., 2021a). This study represents the first exploratory work that screens 22 genotypes of fig seeds based on their proteins and mineral content and lipid properties using a combination of FTIR-ATR spectroscopic analysis and multivariate analysis. This study is crucial in providing information that could be useful in genetic improvement and identifying desirable traits for this atypical oilseed source. By conducting the genotypes under similar experimental conditions, our study overcomes the problem of environmental variability and captures the chemodiversity potentially linked to genetic factors. Using highly sensitive vibrational methods, such as FTIR-ATR spectroscopy, has been already effective in fig genotypes discrimination and classification (Hssaini et al., 2021a; Hssaini et al., 2021b; Hssaini et al., 2022). This novel study will contribute to the improvement and expansion of the scientific knowledge of fig seeds and will be of utmost importance since the chemical composition of fig seeds has

10.3389/fpls.2023.1229994

received very little attention and no previous study has screened such a wide range of genotypes.

2 Materials and methods

2.1 Plant material and experimental design

Plant material used in this study involves 22 genotypes of fig trees from an ex-situ collection located in the Sais plain in Morocco and managed by the National Institute for Agricultural Research (INRA Morocco). The collection is 14 years old, trained to a cup shape, and planted in a randomized complete block design with three trees per genotype and a spacing of 5x3 meters. The collection comprised a diverse range of both exotic and locally sourced genotypes, as detailed in Table 1.

2.2 Fruit sampling method

Fig fruits were harvested at their full ripening stage in the summer. The genotypes were carefully selected based on the quantity and size of seeds in their fruits. To determine full ripeness, the figs were evaluated for a reddish-purple coloration that covered three-quarters of the receptacle and ensured that the fruit could be easily separated from the twig. The fruits were randomly picked from various positions around the canopy at a height of 160 cm, ensuring that the sample was representative of the entire tree.

2.3 Extraction of seeds and oil

Manually peeling figs, the seeds were separated from the pulp through a technical ethanol solution (10%). The mixture was stirred for about 10 minutes, then allowed to settle until the seeds separated and floated to the surface. The yellow, round-shaped seeds were collected, thoroughly washed with distilled water, and left to dry at room temperature for 24 hours. For each sample, the extracted seeds were ground into a fine powder using an IKA A11 Basic type grinder. The fig seed oil was then extracted chemically using a Soxhlet apparatus. To extract the oil, 20g of the powder was mixed with 150ml of 99% pure n-hexane using cellulose cartridges. The extraction process took up to 4 hours, after which the solvent was evaporated using a Buchi rotavapor R-200 at 40°C. The oil weight was determined through the relationship provided by Chougui et al. (2013):

$$\text{Oil yield}(\%) = [(M_1 - M_0)/M_2] \times 100$$

Where M_0 refers to empty flask weight (g), M_1 is the flask weight after solvent evaporation (g), and M_2 is the seed powder weight (g). At the same time, the average oilcake weight was determined, and extracted oils were stored in dark glass bottles at 4°C until analysis.

TABLE 1 List of exotic and local genotypes of fig (*Ficus carica* L.) trees used in this study.

Exotic genotypes	Local genotypes
Breval Blanca 2736	Ahra 2870
Grosse Dame Blanche 2953	Aicha Moussa 2208
Melissosyki 3074	EL Qoti Lezreq 2883
White Adriatic 102	Embar El Khal 2247
Lerida 2280	Hafer Jmel 2253
Bourjassate Noire	Nabout 2893
Rhoult 2216	INRA 2105
Adroulaniki 3073	INRA 2603
Kamalata 3075	INRA 2802
Bourqui 2210	
Hayoul 2265	
Amtalaa Arch 2210	
Breba Blanca	

2.4 Ionomic analysis

The Total Nitrogen (NT) content was quantified using the Kjeldahl method (Buchi, Switzerland). The Nitrate content was measured by complexing with chromotropic acid and analyzing the absorbance in a spectrophotometer (Spectronics, USA) set at 410 nm (Hadjidemetriou, 1982). The protein content was calculated based on the Nitrogen content, using the formula P = 6.25 * NT. The Phosphorus (P) content was determined using the yellow color method with NaOH to neutralize excessive acidity, measured using a spectrophotometer (Shimadzu, China) (Gupta et al., 1993). Other elements (K, Na, Ca, Mg, Fe, Cu, Zn, and Mn) were analyzed through a dry incineration method carried out at 50°C for 48 hours in an oven. The macroelements (K, Na, Ca, and Mg) were evaluated using a flame photometer (Model CL 378, Elico, India) after extraction with nitric acid from 250mg of dry samples (Knudsen et al., 1982). The microelements (Fe, Cu, Zn, and Mn) were evaluated by atomic absorption spectrometry (AAS) (Perkin Elmer Analyst 300, USA) (Estefan et al., 2013). Three measurements were taken for each sample to ensure the reliability of the analysis.

2.5 Spectral analyzes

2.5.1 Mid-infrared spectroscopic measurements

The Fourier Transform Infrared (FTIR) spectra of the seeds were collected using a Bruker FTIR spectrometer Vertex 70 equipped with a diamond ATR attachment (Bruker Optics Inc., Ettlingen, Germany). The spectra were taken in the wavenumber range of 4000 to 450 cm^{-1}, with a spectral resolution of 4 cm^{-1}. At room temperature, 100mg of each sample was analyzed and the resulting spectrum was the mean of multiple replicates, each of which was an accumulation of 128 scans. The germanium crystal was in contact with the samples after applying the standard pressure

setting. Before the sample evaluation, a background spectrum was collected and matched with the infrared spectrum of the empty germanium crystal surface, which was then automatically subtracted from the sample spectrum. The crystal cell was cleaned between spectral collections using technical ethanol and hot water, and then carefully dried with paper towels.

2.5.2 Spectra processing

Prior to data analysis, the Standard Normal Variable (SNV) and Multiplicative Scattering Correction (MSC) procedure, a basic correction method, were performed to correct multiplicative interferences (Shen et al., 2018). An Attenuated Total Reflectance (ATR) correction procedure was applied using the following processing parameters: angle of incidence = 45°, ATR reflection number = 1, average refractive index of the sample = 1.5, maximum interaction = 50, and 1.8mm for the crystal surface. The important feature of ATR is the evanescent field, which occurs when infrared light reflects at the interface between a high refractive index material (ATR crystal) and a low refractive index material (sample) (De Nardo et al., 2009). The peaks in each spectrum, which indicate the presence of certain vibrational regions corresponding to the functional groups of the sample, including the integrated areas, were calculated using Essential FTIR software (version 3.50.183). The corrected spectra and peaks absorbance were plotted using OriginLab Pro v2019 software (OriginLab Corporation Inc.).

2.6 Statistical processing and chemometrics

To validate the results of our chemometric analysis, we first checked the normality and homogeneity of variance in our data. Next, we used IBM SPSS Statistics v22 software to conduct a one-way ANOVA to determine significant differences ($P<0.05$) between fig seed samples. The ionomic and FTIR data were then subjected to a principal component analysis (PCA) to uncover variables and spectral signatures that best explain the phenotypic diversity between samples. The PCA was performed using OriginLab Pro v2019 and 2D scatterplots were created to illustrate the classification patterns based on genetic seed variability. The PCA was significant because it reduced the dimensionality of the data set and allowed us to identify the signatures that reflect shared variance within the data set. Pearson's correlation coefficient (r) was used to evaluate the associations between traits. Lastly, we performed a hierarchical cluster analysis (HCA) using Ward's method based on Euclidean distance to cluster fig seed genotypes based on mineral composition and protein content. The results were displayed using a tree diagram (dendrogram) after standardizing the data.

3 Results and discussion

3.1 Seed yield per fruit and oil yield

Fig seeds are typically round and yellow in appearance. According to Hssaini et al. (2020), the average weight of a thousand seeds is around 1.14 ± 0.01g. However, as shown in Table 2, the weight of seeds per fig fruit can vary significantly based on the genotype. There were differences ranging from a minimum of 1.14 g/fruit for the "Grosse Dame Blanche" genotype to a maximum of 2.45 g/fruit for the "El Qoti Lezreq" genotype. On the other hand, few studies have evaluated the oil yield from fig seeds. Yarosh and Umarov (1971) found that the extraction produced 29.4% oil, while seeds from various regions in Turkey had oil yields ranging from 23.06 to 23.67% for the "Sarilop" cultivar (Nakilcioğlu-Tas, 2019). Joseph and Raj (2011) reported that the dried fig seeds had a fixed oil content of 30%. Hssaini et al. (2020) found that the oil content of four different fig seed cultivars from Morocco ranged from 21.54 to 29.65% and was characterized by a high content of linolenic acid. This high yield compared to the oil from other fruits makes fig seed oil a valuable component of the human diet and its commercial production should be encouraged due to its health benefits (Hssaini et al., 2020; Hssaini et al., 2021a). Despite these benefits, there are limited studies on fig seeds and the impact of cultivar on oil yield has not received much attention. However, our results are in line with previous studies. As seen in Table 2, the oil yield from fig seeds can vary greatly based on the cultivar, with the highest yields recorded by the "Bourqui" (39.68%)

TABLE 2 Fig (*Ficus carica* L.) seeds yield (g/fruit) and oil content (%) of studied genotypes (mean values of three repetitions).

Genotypes	Seeds yield (g/fruit)	Oil yield (%)
Bourqui 2210	1,39 ±0,54	39,68 ±3,3
Melissosyki 3074	1,97 ±0,48	23,88 ±0,5
Embar El Khal 2247	2,09 ±0,75	34,13 ±0,4
Kamalata 3075	2,09 ±0,14	30,14 ±5,2
Adroulaniki 3073	1,94 ±0,48	28,72 ±4,5
Amtalaa Arch 2210	2,08 ±0,12	35,18 ±2,5
Lerida 2280	2,24 ±0,38	32,44 ±4,3
Breba Blanca	2,29 ±0,18	25,99 ±4,9
Hayoul 2265	2,17 ±0,87	26,55 ±4,2
INRA 2802	1,79 ±0,8	16,66 ±1,4
Bourjassate Noire	1,99 ±0,51	38,44 ±0,1
Breval Blanca 2736	2,04 ±0,3	35,28 ±5,3
Aicha Moussa 2208	1,39 ±0,89	34,2 ±3,6
Nabout 2893	2,44 ±0,6	32,58 ±4,2
Grosse Dame Blanche 2953	1,14 ±0,35	29,75 ±4,6
EL Qoti Lezreq 2883	2,45 ±0,02	28,19 ±2,6
Hafer Jmel 2253	2,23 ±0,4	30,39 ±1
Rhoult 2216	2,07 ±0,78	32,06 ±2,4
White Adriatic 102	2,27 ±0,93	23,05 ±3,3
INRA 2603	1,98 ±0,15	25,29 ±3,1
INRA 2105	1,96 ±0,09	15,06 ±2,1
Ahra 2870	2,24 ±0,05	34,93 ±5,2

and "Bourjassate Noire" (38.44%) genotypes, while the genotypes "INRA 2105" and "INRA 2802" had lower yields of 15.06 and 16.66% respectively. These results suggest that the variability in yield can be attributed to the genetic diversity of the cultivars. Further research is necessary to fully understand the impact of cultivar diversity on the chemical composition and other qualities of this oil.

3.2 Proteins and mineral content

Richness of fig seeds in proteins and mineral elements has already been reported (Duman et al., 2018; Nakilcioğlu-Tas, 2019; Bölek, 2020); also, the effect of pollination on their content (Hssaini et al., 2022). Ustun-Argon et al. (2021) report that Potassium, Magnesium and Calcium were the main mineral compounds in the dried fig seeds. Our investigation showed similar results. Nevertheless, identification of genetic material that combines both agronomic performance and good nutritional quality is a major objective of genetic improvement programs for agricultural organisms and nurseries. During the past ten years, biofortification has gained prominence as a way of enhancing the nutritional profile of food crops (Jha and Warkentin, 2020). This is how this investigation was initiated, which remains to the best of our knowledge the first to highlight the genotypically effect of fig seeds diversity on the protein composition and mineral elements. A potential effect of biotic and abiotic factors, as well as essential chemical inputs, on fruit and seed cultivation and quality exists. To this end, genotypes were methodologically cultured under similar experimental conditions to circumvent environmental variability, and the discrimination collected is potentially linked to the genetic factor of the matrix. Thus, analysis of results presented here, first, joined the previous investigations on the presence in figs seeds ten mineral elements including Nitrogen (N), Phosphorus (P), Potassium (K), Calcium (Ca), Sodium (Na), Iron (Iron), Zinc (Zn), Manganese (Mn), Copper (Cu) and Magnesium (Mg), which showed as expected statistically significant ($P<0.05$) and non-significant differences between genotypes. Among macro-elements (P, K, Na, Ca and Mg) analyzed, calcium and potassium were the most abundant elements in the figs seeds genotypes studied (Figure 1). As the visual representation alone did not provide a comprehensive understanding of the phenotypic diversity, we recognized the need to supplement it with numerical data. In order to achieve a more thorough analysis, we included Tables 3A, B which presents the experimental data for the nutritional elements found in fig seeds, combined with the ANOVA results for fig samples mineral composition. This additional data not only supports our findings, but also offers a more detailed perspective on the observed phenotypic diversity.

According to the data presented in Table 3A, it's evident that the Ca content in the different fig seed genotypes varied significantly. The highest concentration of Ca was observed in the "Aicha Moussa" genotype, with a value of 32.18 ± 0.50 (g/kg), whereas the lowest concentration was found in the "Nabout" genotype, with a value of 7.28 ± 0.08 (g/kg). Similarly, Potassium was present in significant amounts in all the sampled genotypes, with values ranging from 1.84 ± 0.00 (g/kg) in the "INRA 2105" genotype to 5.8 ± 0.28 (g/kg) in the "Melissosyki" genotype. In addition to the macro-elements, the results from the study also revealed that the sampled genotypes had a substantial content of

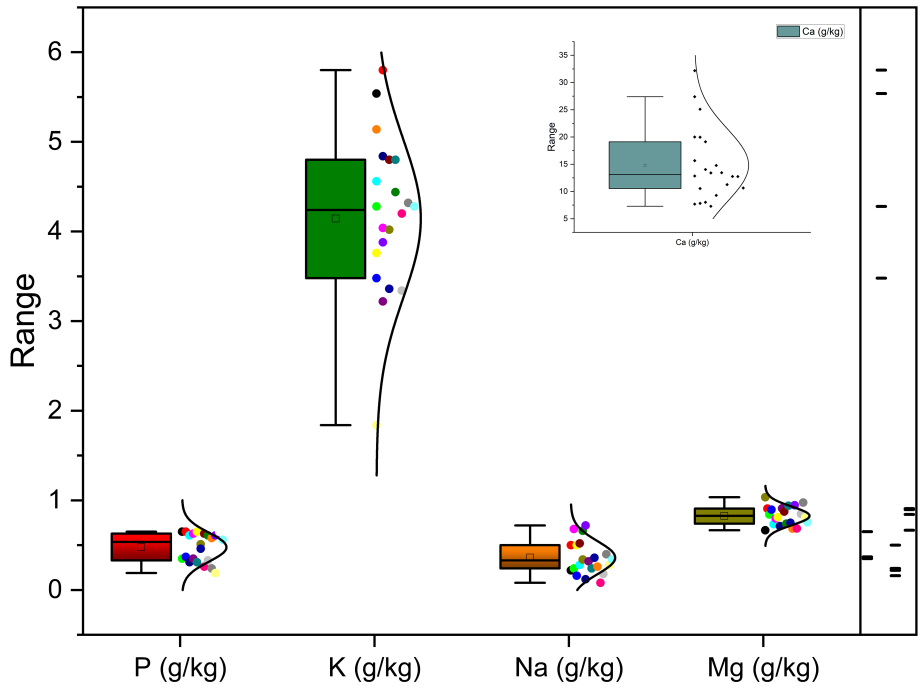

FIGURE 1
Diversity in macro-elements (P, K, NA, Ca and Mg) across investigated fig seed cultivars.

10.3389/fpls.2023.1229994

TABLE 3A Statistical analysis of the nutritional elements of fig (*Ficus carica* L.) seeds.

Fig seed samples	NT (%)	Proteins (%)	P (g/kg)	K (g/kg)	Ca (g/kg)	Na (g/kg)	Mg (g/kg)	Fe (mg/kg)	Zn (mg/kg)	Mn (mg/kg)	Cu (mg/kg)
Bourqui 2210	3.56 ± 0.06	22.27 ± 0.3	0.65 ± 0.05	5.54 ± 0.02	12.84 ± 0.04	0.22 ± 0.10	0.667 ± 0.00	94.5 ± 3.85	20.45 ± 0.80	15.48 ± 0.08	27.43 ± 0.48
Melissosyki 3074	2.83 ± 0.14	17.68 ± 0.88	0.65 ± 0.00	5.8 ± 0.28	15.66 ± 0.02	0.5 ± 0.02	0.909 ± 2.50	145.15 ± 1.00	36.95 ± 4.80	16.28 ± 0.33	24 ± 0.05
Embar El Khal 2247	2 ± 0.04	12.51 ± 0.26	0.35 ± 0.02	4.28 ± 0.40	10.54 ± 0.46	0.24 ± 0.04	0.842 ± 1.40	98.23 ± 4.27	26.13 ± 3.33	17.65 ± 0.60	31.28 ± 0.03
Kamalata 3075	2.74 ± 0.02	17.11 ± 0.13	0.37 ± 0.00	3.48 ± 0.00	14.04 ± 2.20	0.16 ± 0.00	0.896 ± 25.00	230.78 ± 10.18	20.18 ± 4.03	17.48 ± 1.68	34.73 ± 1.43
Adroulaniki 3073	2.55 ± 0.01	15.93 ± 0.09	0.61 ± 0.00	4.56 ± 0.04	13.4 ± 0.20	0.28 ± 0.08	0.734 ± 8.00	105.13 ± 0.68	16.35 ± 2.25	17.9 ± 0.45	23.53 ± 0.12
Amtalaa Arch 2210	3.29 ± 0.15	20.56 ± 0.96	0.63 ± 0.02	4.04 ± 0.00	7.68 ± 0.32	0.68 ± 0.24	0.797 ± 0.00	120.13 ± 3.43	37.53 ± 0.38	19.88 ± 0.28	27.18 ± 0.53
Lerida 2280	3.21 ± 0.04	20.04 ± 0.26	0.65 ± 0.00	3.76 ± 0.12	7.82 ± 0.70	0.5 ± 0.02	0.812 ± 13.75	108.98 ± 6.02	19.18 ± 1.93	16.23 ± 0.07	27.5 ± 1.10
Breba Blanca	2.39 ± 0.04	14.92 ± 0.22	0.51 ± 0.00	4.02 ± 0.14	20 ± 0.12	0.34 ± 0.10	1.036 ± 4.25	94.3 ± 2.90	125.9 ± 41.40	10.13 ± 0.42	19.83 ± 0.28
Hayoul 2265	2.68 ± 0.01	16.76 ± 0.04	0.31 ± 0.02	4.84 ± 0.20	27.4 ± 1.04	0.12 ± 0.04	0.713 ± 1.75	281.25 ± 13.40	33.78 ± 2.68	12.83 ± 0.13	34.28 ± 0.42
INRA 2802	1.46 ± 0.01	9.1 ± 0.09	0.35 ± 0.02	3.22 ± 0.14	19.96 ± 0.52	0.32 ± 0.00	0.91 ± 18.75	51.73 ± 4.08	18.7 ± 1.05	8.28 ± 1.13	19.33 ± 0.88
Bourjassate Noire	3.12 ± 0.06	19.51 ± 0.35	0.63 ± 0.02	4.8 ± 0.16	14.78 ± 0.22	0.52 ± 0.32	0.875 ± 11.75	106.5 ± 10.05	29.58 ± 4.08	15.25 ± 1.10	25.83 ± 0.78
Breval Blanca 2736	2.86 ± 0.05	17.89 ± 0.31	0.61 ± 0.05	4.44 ± 0.12	8.02 ± 0.66	0.66 ± 0.18	0.74 ± 2.75	165.68 ± 0.78	16.08 ± 0.53	16.05 ± 0.25	30.23 ± 0.13
Aicha Moussa 2208	2.7 ± 0.01	16.89 ± 0.09	0.31 ± 0.02	4.8 ± 0.16	32.18 ± 0.50	0.24 ± 0.08	0.94 ± 9.00	332.58 ± 16.88	25.58 ± 1.38	13.05 ± 0.15	33.55 ± 0.30
Nabout 2893	2.07 ± 0.01	12.91 ± 0.04	0.46 ± 0.00	3.36 ± 0.00	7.28 ± 0.08	0.36 ± 0.04	0.75 ± 6.75	120.5 ± 10.70	20.38 ± 2.23	9.95 ± 0.50	23.93 ± 0.13
Grosse Dame Blanche 2953	2.85 ± 0.04	17.81 ± 0.22	0.58 ± 0.02	5.14 ± 0.10	13.44 ± 0.20	0.26 ± 0.02	0.685 ± 0.50	83.45 ± 3.05	28.98 ± 1.28	15.33 ± 0.28	25.2 ± 0.70
EL Qoti Lezreq 2883	2.87 ± 0.06	17.94 ± 0.35	0.61 ± 0.00	3.88 ± 0.00	9.28 ± 0.16	0.72 ± 0.04	0.945 ± 3.00	91.38 ± 0.93	32.88 ± 9.93	14.7 ± 0.10	24.38 ± 0.07
Hafer Jmel 2253	2.28 ± 0.03	14.22 ± 0.22	0.26 ± 0.02	4.2 ± 0.08	25.1 ± 0.82	0.08 ± 0.04	0.686 ± 0.00	87.93 ± 24.93	11.93 ± 2.88	15.33 ± 0.33	25.48 ± 0.73
Rhoult 2216	3.86 ± 0.37	24.11 ± 2.32	0.65 ± 0.05	3.24 ± 0.08	11.26 ± 0.54	0.54 ± 0.06	0.867 ± 2.75	155.88 ± 8.83	28.53 ± 1.08	20.08 ± 0.23	25.68 ± 0.63
White Adriatic 102	2.09 ± 0.04	13.08 ± 0.22	0.33 ± 0.00	3.34 ± 0.06	12.76 ± 0.24	0.18 ± 0.02	0.848 ± 63.25	72.13 ± 23.58	12.23 ± 6.93	17.33 ± 1.58	27.55 ± 0.45
INRA 2603	2.13 ± 0.06	13.3 ± 0.35	0.24 ± 0.00	4.32 ± 0.04	12.74 ± 0.74	0.4 ± 0.12	0.975 ± 18.50	115.1 ± 0.45	25.4 ± 1.10	23.58 ± 0.57	28.4 ± 0.60
INRA 2105	0.97 ± 0.01	6.08 ± 0.04	0.19 ± 0.00	1.84 ± 0.00	19.12 ± 0.52	0.28 ± 0.04	0.811 ± 96.00	38.98 ± 6.33	4.55 ± 2.35	6.03 ± 1.33	23.45 ± 1.55
Ahra 2870	3.22 ± 0.00	20.13 ± 0.00	0.56 ± 0.00	4.28 ± 0.00	10.64 ± 0.24	0.34 ± 0.10	0.755 ± 2.25	117.9 ± 2.50	26.55 ± 1.90	9.38 ± 0.82	18.38 ± 0.32

NT, Total Nitrogen; P, Phosphorus; K, Potassium; Ca, Calcium; Na, Sodium; Mg, Magnesium; Fe, Iron; Zn, Zinc; Mn, Manganese; Cu, Copper.

10.3389/fpls.2023.1229994

TABLE 3B Results of the Analysis of Variance (ANOVA).

	Sum of Squares	df	Mean Square	F	Sig.
NT (%)	30.230	25	1.209	134.519	0.000
Proteins (%)	1180.863	25	47.235	134.519	0.000
P (g/kg)	1.941	25	0.078	160.060	0.000
K (g/kg)	70.165	25	2.807	157.779	0.000
Ca (g/kg)	3174.203	25	126.968	285.853	0.000
Na (g/kg)	3.297	25	0.132	11.020	0.000
Mg (g/kg)	777727.635	25	31109.105	50.343	0.000
Fe (mg/kg)	368579.086	25	14743.163	117.277	0.000
Zn (mg/kg)	35424.697	25	1416.988	16.802	0.000
Mn (mg/kg)	1570.680	25	62.827	66.204	0.000
Cu (mg/kg)	1292.888	25	51.716	71.766	0.000

ANOVA, Analyze of variance; Sig., Significance of ANOVA.

Iron compared to other micro-elements (as depicted in Figure 2). The Iron content ranged from a minimum of 38.98 ± 6.33 mg/kg observed in the "INRA 2105" genotype to a maximum of 332.58 ± 16.88 mg/kg recorded in the "Aicha Moussa" genotype.

Furthermore, Nakilcioğlu-Tas (2019) reported the protein content of fig seeds between 14.74-15.07%, and Ustun-Argon et al. (2021) found 14.65%. Whereas, in our investigation, protein content varied between a minimum of 6.08 ± 0.04% recorded in the "INRA 2105" genotype and a maximum of 24.11 ± 2.32% recorded in the "Rhoul" genotype. As a comparison with the content of other fruit seeds, protein content of mangosteen seeds is 6.57%, 7.6% for guava, 12.4% for rambutan, 25.0% for honeydew, 25.63% for papaya, 25.2 to 37% for watermelon and 39.25% for pumpkin (Raihana et al., 2015). Moreover, between nitrogen and proteins, proteins are logically the most abundant in the fig seed genotypes studied (Figure 3). In agreement with the finding of Hssaini et al. (2022), it seems that minerals and proteins content of fig seeds depends on pollination and then on the source of pollen, which requires further studies able to investigate the qualitative performance of female genotypes sampled by compared to crossing with any caprifig tree. Since fig seeds have not received particular attention until now compared to the other parts of the species, results reported here constitute a solid base which will allow the orientation of new investigations.

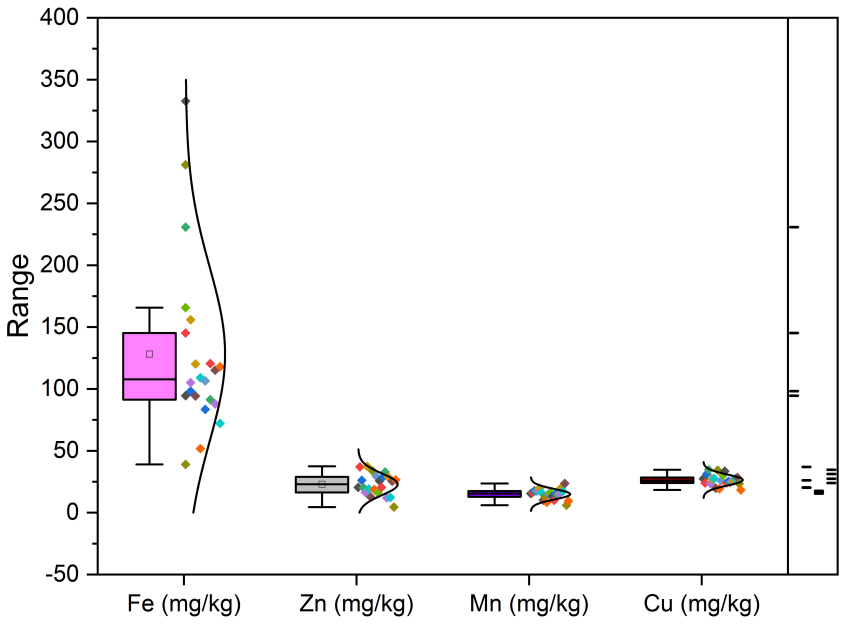

FIGURE 2
Variability of micro-elements (Fe, Zn, Mn and Cu) in fig seed genotypes.

10.3389/fpls.2023.1229994

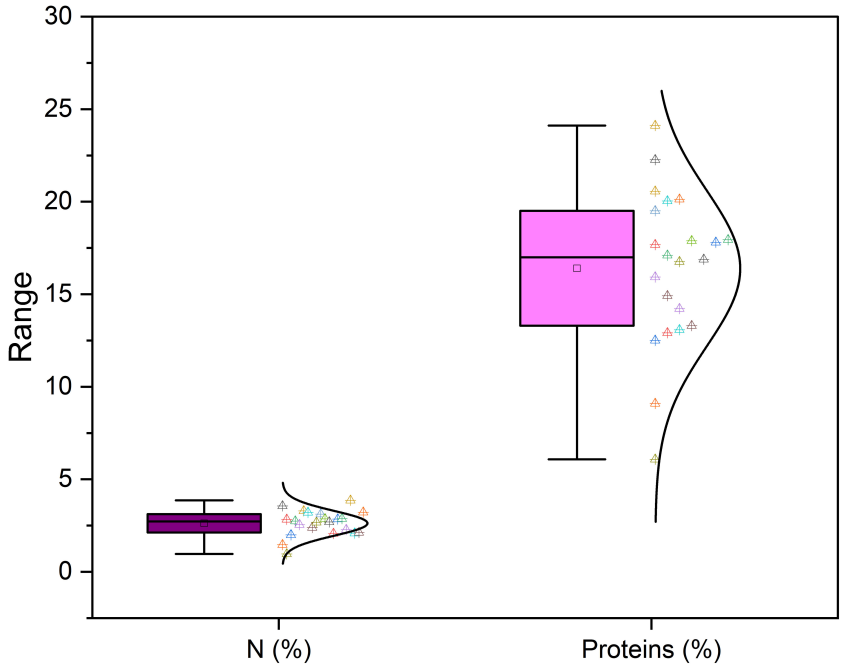

FIGURE 3
Variation in nitrogen and protein content among studied fig seed cultivars.

3.3 Pairwise correlations between nutritional elements on fig seeds genotypes

To explore potential connections between protein content and mineral levels in fig seeds, we conducted a pairwise correlation analysis using the Pearson coefficient and presented the results in Figure 4. Weak correlations between the variables are represented by a low color intensity, while strong correlations are indicated by a high color intensity. Only correlations that were statistically significant at the 0.001 level with correlation coefficients greater than or equal to |0.5| were considered noteworthy. The matrix heatmap generated from the correlation analysis revealed a highly significant positive correlation between protein content and

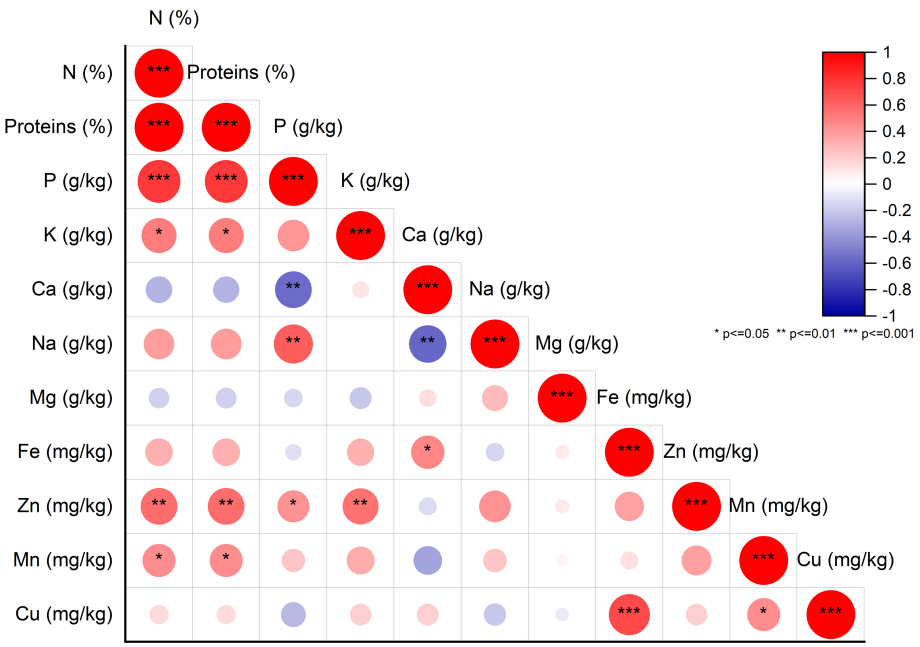

FIGURE 4
Pearson Pairwise correlation analysis of nutritional element content. Positive correlations (+) displayed in red and negative correlations (-) in blue. Color intensity corresponds to correlation coefficient magnitude. Color legend depicts correlation coefficients and respective colors.

phosphorus content. We also observed a significant positive correlation between copper and iron levels. Additionally, bivariate correlations of the variables showed positive weakly correlated associations between manganese and protein as well as potassium. However, a highly significant negative correlation was detected between the calcium content and both phosphorus and sodium levels. Interestingly, our results differ from those of previous studies that found a significant positive correlation between iron and zinc concentrations in lentil seeds (Choukri et al., 2020). No such correlation was observed in the analyzed fig seed genotypes. Our findings align with those of other researchers, such as Kumar et al. (2014) and Darai et al. (2020), who reported similar observations of no correlation between iron and zinc levels. These results hold significant implications for future fig seed breeding programs, as they can serve as biomarkers to predict the level of significance, strength, and direction of associations between different variables. Examining potential correlations in the data set provides valuable insights into the most critical factors for evaluating and classifying fig seed genotypes.

3.4 Two-dimensional clustered heatmap analysis

The hierarchically clustered heatmap is a useful tool for analyzing complex biological data without reducing the dimensionality. This technique displays network connections in a symmetric adjacency matrix, providing a two-dimensional color-coded heatmap (Clark and Ma'ayan, 2011). The heatmap was formed with two groupings using the Euclidean distance and the Ward's method. The first grouping was oriented for fig seed genotypes, while the second was for mineral elements and proteins, with a color indicating numerical differences in the correlation coefficient (Figure 5). The heatmap showed that Calcium and Iron had the highest scores in the data set, meaning they had the greatest impact on genotype clustering. However, other variables also showed an impact, although they were less important than these two elements. The combined dendrogram in Figure 5 differentiated the fig seed genotypes into four main clusters. The first cluster included two genotypes; "Hayoul" and "Aicha Moussa", which were particularly very rich in Ca, Fe and Cu, and moderately rich in Zn, K, proteins and poor in P and Na. The second cluster included nine genotypes composed of "INRA 2105", "INRA 2802", "Breba Blanca", "Kamalata", "Nabout", "Hafer Jmel", "INRA 2603", "White Adriatic" and "Embar El Khal", which were rich in Mg, Cu and poor in proteins, P and Na. The third cluster consisted of genotypes including "Ahra", "Rhoul", "Amtalaa Arch", "Breval Blanca", "Lerida", "El Qoti Lezreq", "Bourjassate Noire" and "Melissosyki", which were grouped based on their poverty in Ca compared to other clusters but were rich in proteins, P, Na, and Zn compared to other clusters. The last cluster included the genotypes "Grosse Dame Blanche", "Adroulaniki" and "Bourqui", which were mainly grouped by their richness in proteins, P, K and moderate values of Zn, Mn, Ca, and Fe but poor in Na and Mg. Finally, the heatmap combined to PCA (Principal Component Analysis) below allowed a better understanding of the relationship between the variables and the resulting clusters. The heatmap was a supervised variable construction method, while the PCA was an unsupervised method.

3.5 PCA of minerals and protein content

Based on the correlation coefficient, a principal component analysis (PCA) was performed to determine the discriminating variables in the data set. This analysis aimed to define the main

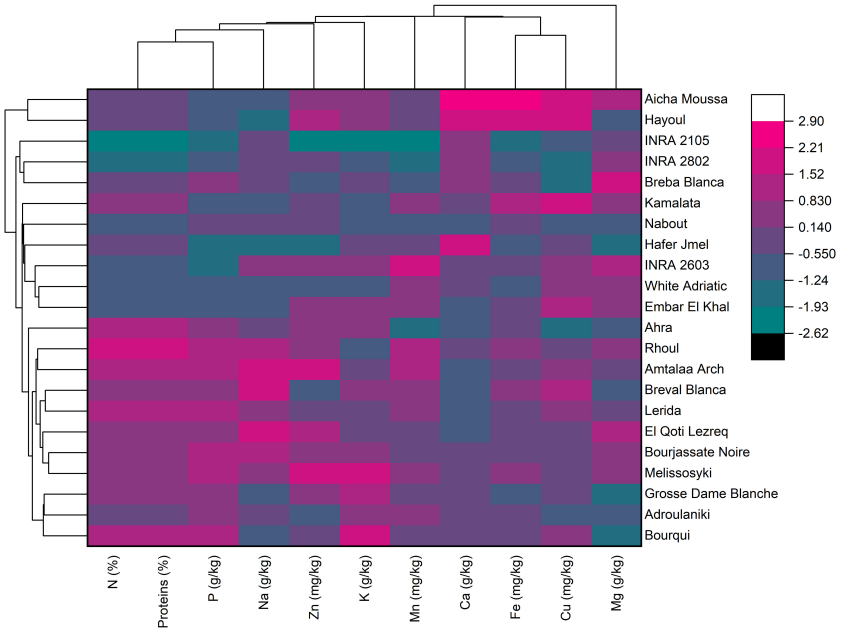

FIGURE 5
Two-dimensional hierarchical clustering heatmap based on the correlation matrix of nutrient elements and proteins in fig seed genotypes.

factors that contribute to the discrimination of fig seeds. In our study, only a principal component loading of more than |0.35| was considered as being significant for each factor. The analysis of nutritional data using PCA revealed valuable insights into the minerals and protein content of fig seed cultivars. The results showed that three principal components were enough to explain 73.44% of the total variance, with the first component accounting for the majority at 38.69% (Figure 6). With reference to Table 4, the first component (PC1) consisted of the variables, N, P and Zn, for which the scores were respectively 0.45075, 0.39814 and 0.35065. It explained about 38.69% of the total variance observed, which means that these attributes had the highest impact on the discrimination. The second component (PC2) accounted for about 22.60% of the total variance and was defined by Fe, Cu and Ca, for which the respective scores were 0.53085, 0.49685 and 0.43542. The third component (PC3) represented 12.15% of the total inertia and was mainly correlated with the amount of Mg (0.7528) and Na (0.39577). This information reported here could be used to inform on the distribution of these compositions between all genotypes studied, and could serve as a starting point for further research into the relationships between fig seed phenotypic attributes and nutritional properties.

3.6 Characteristics of FTIR-ATR signatures

For evaluation of fig seeds chemotypic properties, FTIR-ATR fingerprinting has proven to be a powerful and interesting approach for screening and discriminating the characteristic signatures present in the analyzed samples (Hssaini et al., 2021a). Also, this technique has provided in previous studies satisfactory results with a high-throughput screening framework providing numerous biomolecules in several food samples (De la Mata et al., 2012; Anjos et al., 2015; Cassani et al., 2017). In this sense, FTIR spectroscopy coupled with an ATR was used in this work to assess relevance of chemotypic discrimination, and to identify the characteristic molecular signatures of biochemical substances present in fig seeds in order to study their sensitivity to phenotypic diversity. Therefore, seeds samples were directly scanned in the wavenumber range of 4000 to 450 cm^{-1} with a spectral resolution of 4 cm^{-1}. Figure 7 illustrates spectra of the 22 fig seeds cultivars. Obviously, as expected for all seeds, all the spectra are similar. However, using chemometric tools, analysis of these spectra reveals important differences, particularly by evaluating their integrated intensities for each major vibrational region. These differences, even if sometimes considered minor, indicate molecular dissimilarities between samples. Overall, the peaks of each spectrum were identified at different wavenumbers, assigned to specific functional groups (Koch et al., 2014) and summarized in Table 5. The latter reports the detailed attributions of the bands, which reveal fifteen identifiable footprints in Figure 8. Indeed, Figure 8 represents a unitary case for the genotype "El Qoti Lezreq", which perfectly shows values of the wavelengths from 4000 to 450 cm^{-1} of the large vibratory regions with their corresponding peaks.

The first FTIR fingerprint appeared around 3417.51 cm^{-1} which would be assigned to O–H stretching vibration, most likely attributed

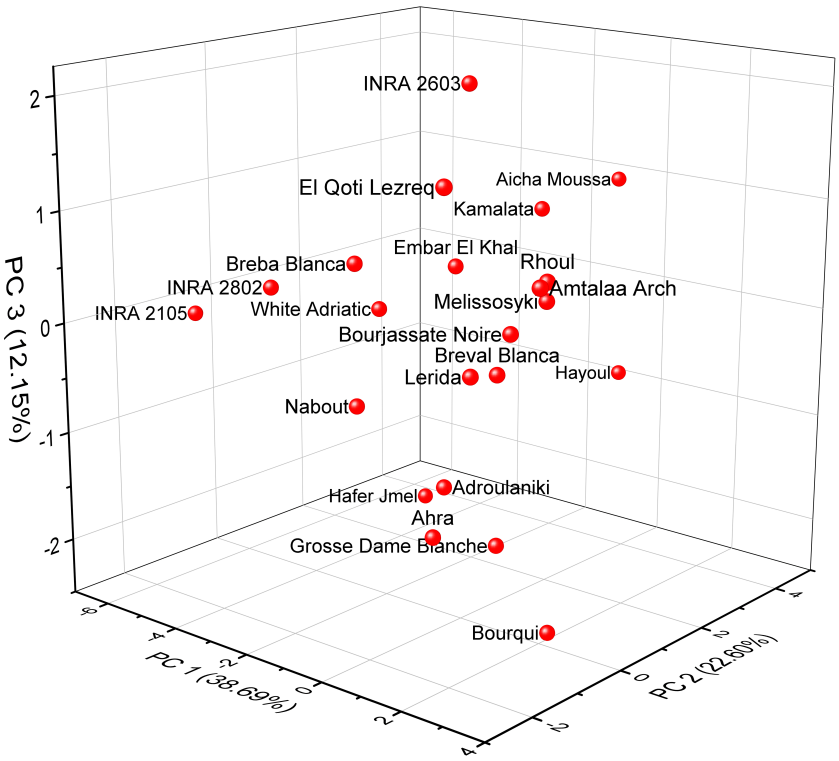

FIGURE 6
Principal component analysis (PCA) score plots derived from three components of mineral and protein content dataset.

10.3389/fpls.2023.1229994

TABLE 4 Eigenvectors of principal component axes from PCA analysis.

	Coefficients of PC1	Coefficients of PC2	Coefficients of PC3
N (%)	0.45075	0.04115	-0.12927
Proteins (%)	0.45079	0.04168	-0.12954
P (g/kg)	0.39814	-0.27596	-0.14759
K (g/kg)	0.29419	0.23866	-0.25989
Ca (g/kg)	-0.21076	0.43542	-0.05608
Na (g/kg)	0.27295	-0.34175	0.39577
Mg (g/kg)	-0.05464	-0.02922	0.7528
Fe (mg/kg)	0.12815	0.53085	0.15065
Zn (mg/kg)	0.35065	0.12292	0.19788
Mn (mg/kg)	0.28236	0.11153	0.24865
Cu (mg/kg)	0.08685	0.49685	0.16435

to fibers, which have been reported to be present in large quantities in fig seeds (Bölek, 2020). This flattened peak appeared in the vibrational region from 3750 to 3100 cm^{-1} associated with intramolecular hydrogen bonding in cellulose between C(3)OH•••O(5) and C(6)O•••O(2)H according to Schwanninger et al. (2004); Oh et al. (2005) and Cassani et al. (2017). A second vibration can be detected between 3250 and 3000 cm^{-1}. This occurred around 3071.26 cm^{-1}, which is most likely attributed to C–H stretching of olefinic double bonds bonded to long carbon chains containing a relatively high number of unsaturated fatty acid CH_2 groups (Oh et al., 2005; Bouafif et al., 2008; Gopalakrishnan and Raghu, 2014; Niu et al., 2017). Absorbance in the vibrational region from 3100 to 2950 cm^{-1} has been attributed to symmetric and asymmetric stretching of C–H, O–H and NH_3. The peak appears around 3012.70 cm^{-1}, which is probably typical for carboxylic acids, carbohydrates and phenolic compounds (Oh et al., 2005; Bouafif et al., 2008). Peaks in the range of 2950 to 2800 cm^{-1} are identified as absorbances related to asymmetric and symmetric stretching of aliphatic C–H in the $–CH_2$ and terminal $–CH_3$ groups, respectively (Niu et al., 2017; Tulukcu et al., 2019). A first sharp and distinct peak is at 2929.11 cm^{-1} and a second occurred at 2860.06 cm^{-1}. Bands in the range of 1775 to 1725 cm^{-1} are attributed to stretching of ester carbonyl groups of triglycerides (Tulukcu et al., 2019). This absorbance region is related to C=O elongation of carboxylic ester type (Ahmed et al., 2005; Vlachos et al., 2006). At 1746.56 cm^{-1}, a sharp peak was identified, and is probably due to C=O stretching vibration of carbonyl groups belonging to triacylglycerols. It's probably associated with lipids and fatty acids contained in seeds (Oh et al., 2005; De la Mata et al., 2012). Nevertheless, several authors report that this peak could be attributed to proteins (Cai and Singh, 2004; Cocchi et al., 2004; Cocchi et al., 2006; Terpugov et al., 2016).

Amide I and Amide II bonds usually resulting from protein-bound structures. Vibrations in the wavenumber range of 1700 to 1550 cm^{-1} shows two peaks appeared at 1648.75 cm^{-1} and 1544.32 cm^{-1} which have been assigned to the Amide I and Amide II bands respectively (Ellepola et al., 2005; Tulukcu et al., 2019). According to

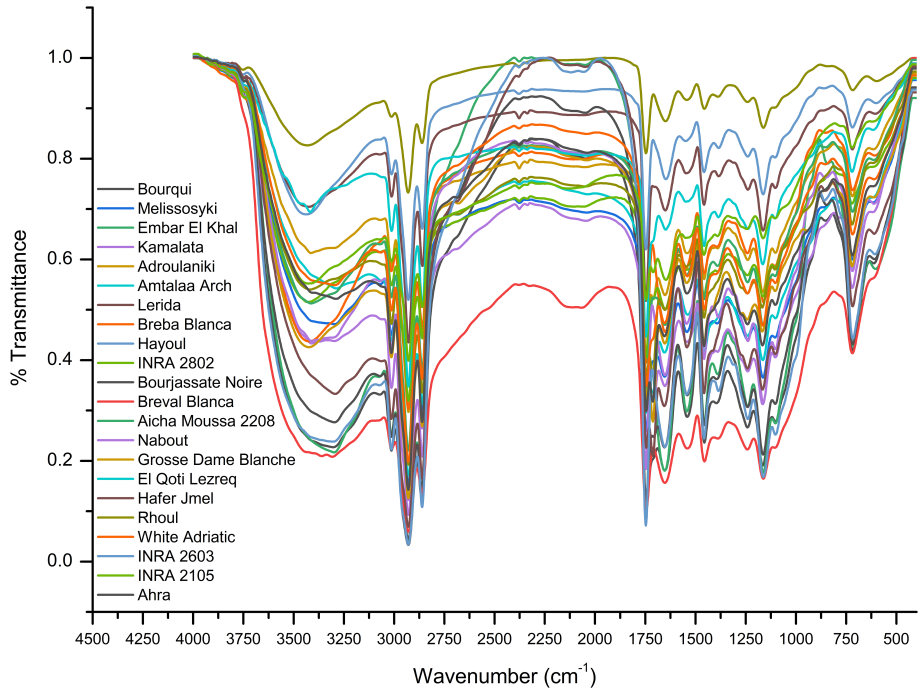

FIGURE 7
FTIR-ATR spectroscopy data of fig seeds in the wavenumber range from 4000 to 450 cm^{-1}.

TABLE 5 FTIR peaks assignments for functional groups found in fig (*Ficus carica* L.) seeds spectrum.

Wavenumber (cm^{-1})	Functional groups	Modes of vibration	Assignments	References
3417.51	δ(O–H)	Stretching vibration	Intramolecular hydrogen bond between C (3)OH• • •O(5) and C(6)O• • •O(2)H (fibers)	Schwanninger et al. (2004); Oh et al. (2005) and Cassani et al. (2017)
3071.26	ν(=C–H)	Bending vibration	Unsaturated fatty acids	Oh et al. (2005); Bouafif et al. (2008); Gopalakrishnan and Raghu (2014) and Niu et al. (2017)
3012.70	δ(C–H), δ(O–H), δ(N–H)	Stretching vibration	Carboxylic acids, carbohydrates and phenolic compounds	Oh et al. (2005) and Bouafif et al. (2008)
2929.11 2860.06	δ(C–H), δ(–CH2–), δ(–CH3)	Stretching vibration	Methylene and methyl groups (lipids)	Niu et al. (2017) and Tulukcu et al. (2019)
1746.56	δ(COH), δ(OCH)	Stretching vibration	Ester carbonyl functional group of the triglycerides and fatty acids	Ahmed et al. (2005); Oh et al. (2005); Vlachos et al. (2006); De la Mata et al. (2012) and Tulukcu et al. (2019)
1648.75	δ(COH), δ(CCH), δ(OCH), ν(C–O)	Stretching and bending vibration	β-Sheet of amide I	Ellepola et al. (2005) and Tulukcu et al. (2019)
1544.32	δ(N–H), ν(C–N)	Stretching and bending vibrations	Amide II (α-Helix)	Ellepola et al. (2005) and Tulukcu et al. (2019)
1458.15	δ(C–H), ν(C–H)	Stretching and bending vibrations	Lipids, protein and cholesterol esters	Ahmed et al. (2005); Vlachos et al. (2006) and Liu et al. (2021)
1386.02 1239.31	ν(C–H), δ(C–O),	Stretching and bending vibrations	Esters	Sylverstein et al. (1991); Guillén and Cabo (1997); Ahmed et al. (2005) and Niu et al. (2017)
1165.91	δ(C–O), ν(C–C)	Bending vibration	Esters	Ahmed et al. (2005) and Niu et al. (2017)
1102.25	δ(C–O)	Stretching vibration	Unsaturated esters and esters derived from secondary alcohols	Guillén and Cabo (1997)
721.19	ν(–HC=CH– (*cis*-) and (*trans*-)	Bending vibration out of plane	Aromatic hydrocarbons	Guillén and Cabo (1997); Gopalakrishnan and Raghu (2014)
611.93	ν(–$(CH2)_n$–),δ(–HC=CH–(*cis*-))	Bending vibration (rocking)	Disubstituted olefinic *cis*-alkenes	Van de Voort et al. (1995); Vlachos et al. (2006)

several studies, this band between 1500 and 1100 cm^{-1} are the result of several weak peaks wouldn't be differentiated in the analyzed samples, which would correspond to mixed vibrations resulting from bending modes of groups $>CH_2$ and $–CH_3$ in proteins, fatty acids and phosphate bearing compounds (Tulukcu et al., 2019). The spectral band at 1458.15 cm^{-1} could probably be associated with CH_2 bending and methylene deformation of lipids, proteins or cholesterol esters (Ahmed et al., 2005; Vlachos et al., 2006; Liu et al., 2021). Vibrations occurred around 1386.02 and 1239.31 cm^{-1} could probably be assigned to CH_2 shearing and C–O stretching vibrations attributed to esters (Ahmed et al., 2005). Indeed, absorptions of certain bending vibrations of the methylene group occur between 1350 and 1150 cm^{-1} (Guillén and Cabo, 1997). On the other hand, C–O bond stretching vibrations of esters are composed of two coupled asymmetric vibrations C–C(=O)–O and O–C–C, whose the former being larger (Sylverstein et al., 1991); these bands occur in the region between 1300 and 1000 cm^{-1}. The C–C(=O)–O band of saturated esters appears between 1240 and 1163 cm^{-1}, and in unsaturated esters, the vibration is produced at lower frequencies (Guillén and Cabo, 1997). Thus, the band appearing around 1165.91 cm^{-1} can be assigned to bending vibration of C–O ester group (Ahmed et al., 2005; Niu et al., 2017). However, O–C–C band of esters derived from primary alcohols appears in the range between 1064 and 1031 cm^{-1}, whereas for those derived from secondary alcohols, the band appears at approximately 1100 cm^{-1}; what can probably correspond to vibration appeared around 1102.25 cm^{-1} (Guillén and Cabo, 1997). Vibrational region ranging from 850 to 700 cm^{-1} is marked by a sharp peak appearing at 721.19 cm^{-1} which would probably be assigned to C–H deformation in aromatic hydrocarbons (Guillén and Cabo, 1997; Gopalakrishnan and Raghu, 2014). The last vibrational region ranging from 700 to 400

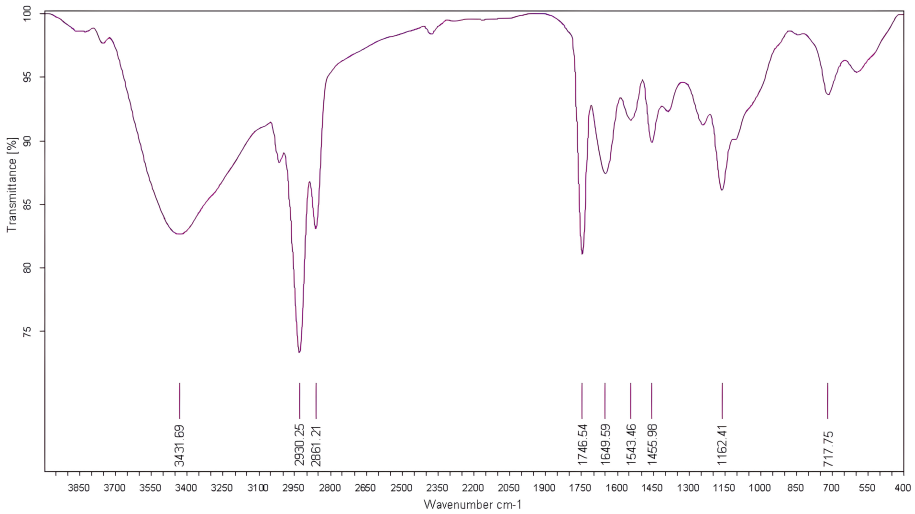

FIGURE 8
FTIR spectra of the local clone 'El Qoti Lezreq' fig seeds highlighting key peaks in the wavenumber range of 4000 to 450 cm^{-1}.

cm^{-1} shows a peak around 611.93 cm^{-1} attributed to overlap of bending vibrations of methylene $-CH_2$ and out-of-plane vibrations of C–H bonds of disubstituted olefinic cis-alkenes (Van de Voort et al., 1995; Vlachos et al., 2006). As expected, although the fig seeds spectra appear to be similar and generally overlap in Figure 7, they show differences in integrated intensity of their bands as well as in the exact frequency at which maximum absorbance is produced in each case; probably because of genotypically differences in nature and composition.

The marginal boxplot chart in Figure 9 provides a clear visualization of the phenotypic differences between the seed cultivars based on their vibrational intensities in the 3500-1000 cm^{-1} range. The chart displays the distribution of integrated intensities for each genotype, as well as the median, interquartile range, and outliers. The one-way analysis of variance conducted on the data revealed statistically significant differences in the integrated intensities of major peaks among the sampled fig seeds. For instance, the "Hafer Jmel" genotype had an integrated area of approximately 2250, while the "White Adriatic" genotype had an integrated area of around 2500. Interestingly, the "Breval Blanca" genotype had the lowest integrated area of about 1500, making it unique among the cultivars studied. These findings highlight the significant impact of genotype on the molecular signatures of fig seed cultivars. Although the differences may seem minor, they are crucial in determining the distribution of nutritional composition among the various genotypes. This is consistent with previous studies that have demonstrated a similar pattern of phenotypic effect on fig seed quality, including nutritional composition. Overall, the results suggest that FTIR-ATR spectroscopy could be an effective and non-destructive method for rapid analysis of the structural characteristics and functional properties of various genotypes of fig seeds. This could have important implications for improving breeding programs and enhancing the nutritional value of fig seeds for human consumption.

3.7 Multivariate analysis of FTIR-ATR spectra

Infrared spectroscopy or FTIR is a powerful analytical tool that has been widely used with chemometric methods such as PCA. By using PCA, the complexity of multi-wavelength FTIR data can be reduced to a limited number of parameters, with minimal loss of total variance. This process results in the creation of a scatterplot, which reveals the resolution of the classification of fig seed samples based on their phenotypic diversity. This unsupervised variable construction method was applied to spectra to unveil the resolution of fig seed classification based on phenotypic diversity. This technique was also employed to evaluate if spectra data could produce a discrimination pattern similar to that of nutritional composition. Figure 10 presents FTIR data in the 4000-450 cm^{-1} wavenumber range, exhibiting a total variance of 91.62%. The first component (PC1) accounted for 64.09% of the variance, while the second component (PC2) contributed 27.53% to the total variance. The PCA plot displayed a high level of discrimination resolution, clustering cultivars with similar FTIR profiles, as spectra are a qualitative method that precisely measures functional groups.

The scatter plot of the PCA model reveals four main clusters, with clear classification of the "Breval Blanca" genotype, which showed the lowest vibration intensities among all cultivars studied. These four groups were differentiated based on the total intensity area in the entire vibration range. This result is in line with previous studies that used FTIR spectra and chemometric approaches to distinguish several fruit seeds, including apples and grapes. Previous studies using FTIR spectra coupled with chemometric approaches have demonstrated the excellent discrimination capacity of this method in differentiating various fruit seeds, such as apples (Anang et al., 2019) and grape (Lucarini et al., 2019). The results suggest that FTIR spectroscopy is a useful tool for the screening and

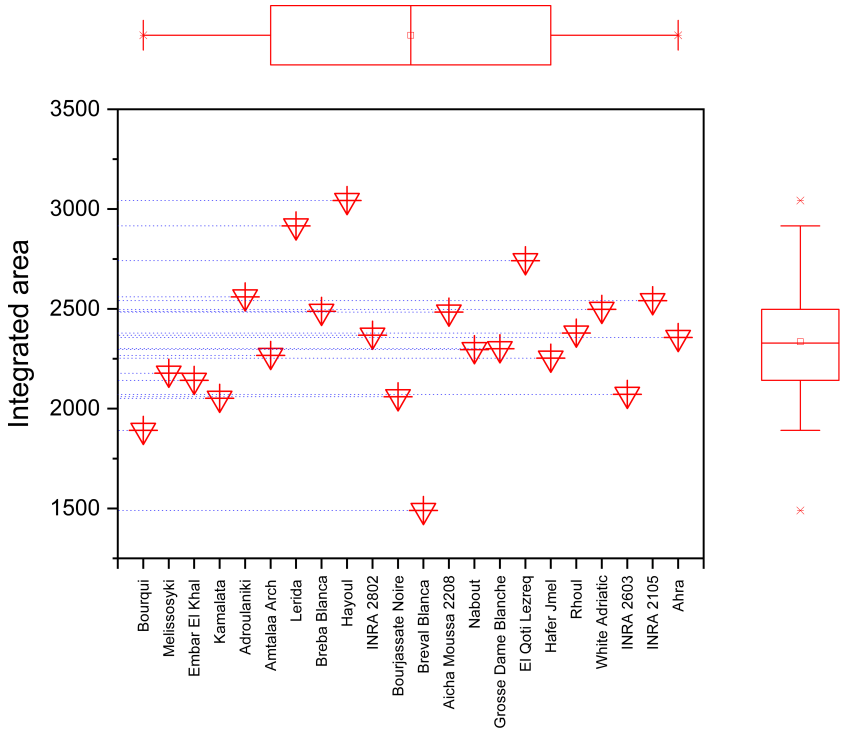

FIGURE 9
Marginal boxplot chart illustrating the total integrated area of the entire infrared (IR) spectrum for each fig seed cultivar.

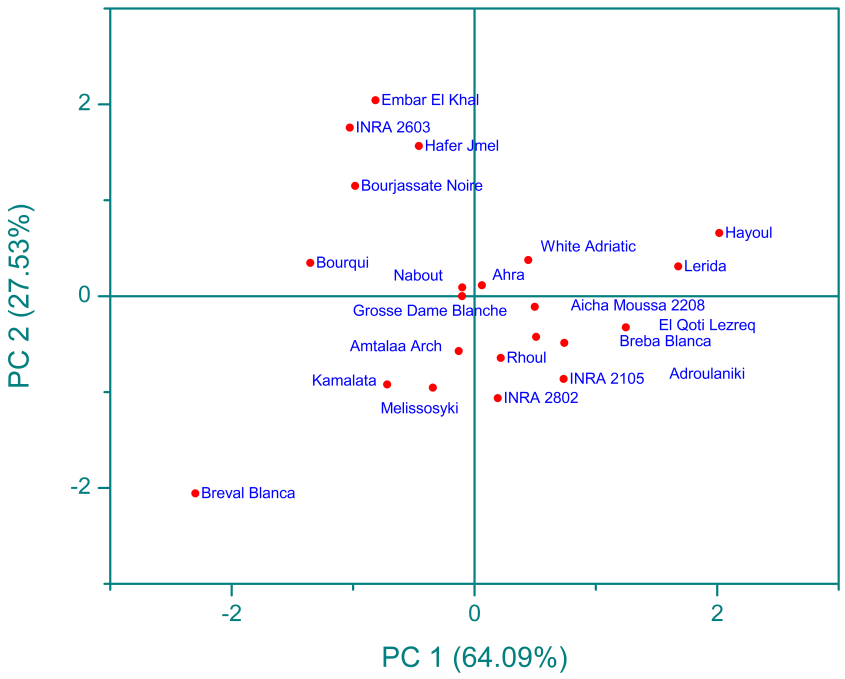

FIGURE 10
Principal component analysis (pca) score plot (pc1 x pc2) for ftir-atr spectra in the wavenumber range of 4000-450 cm^{-1}.

discrimination of a large sample of fig seeds based on chemotypic attributes. It's an accurate, rapid, inexpensive, and environmentally friendly technology that requires minimal sample preparation, making it a valuable tool for the management of fig seed diversity and for use in breeding and industrial development programs. This study is the first of its kind to assess the chemotypic attributes of a wide range of fig seed genotypes and has important implications for maintaining the longevity and genetic diversity of the species.

4 Conclusion

The findings of this study underscore the considerable potential of fig seeds as a rich source of lipids, proteins, and minerals. The results reveal substantial variations in the content of these essential nutrients among different fig genotypes, emphasizing the significance of exploring the phenotypic diversity of fig seeds. The two-dimensional clustered heatmap differentiated the fig seed genotypes into four distinct clusters based on their lipochemical profiles. Furthermore, the utilization of multivariate analysis for FTIR data proved effective in classifying the genotypes and providing insights into their chemotypic variability. This study contributes to the selection of potential fig seed cultivars for both scientific and industrial purposes, promoting the utilization of the chemotypic properties of fig seeds and unlocking their complete nutritional potential. The extracted oil from fig seeds holds promise as a food supplement or ingredient in various food products. However, to fully leverage the potential of fig seeds, further research is required, such as investigating techniques to increase oil yield and improve lipochemical properties by exploring environmental conditions like heat and salt stress. Additionally, assessing the bioavailability and bioaccessibility of nutrients present in fig seeds is crucial. Ultimately, this work represents a significant contribution to the selection of highly discriminant variables for optimizing the agronomic performance of fig seed genotypes. The findings also hold important implications for fig collection management, ensuring the preservation of species longevity and diversity, and facilitating its utilization in breeding programs.

Data availability statement

The original contributions presented in the study are included in the article/supplementary material. Further inquiries can be directed to the corresponding author.

Author contributions

LH conceived and performed the project; AI and LH conducted species identification and collected samples; LH designed and managed the experiments; LH, AI, RO, and RA performed the analyses and collected data; LH analyzed data and performed the chemometrics analysis; AI assisted with data analyses, interpreted and discussed the data and drafted the manuscript; RR and KH contributed to the data curation and visualization; LH revised the manuscript; All authors contributed to the article and approved the submitted version.

Conflict of interest

The authors declare that the research was conducted in the absence of any commercial or financial relationships that could be construed as a potential conflict of interest.

Publisher's note

References

Ahmed, M. K., Daun, J. K., and Przybylski, R. (2005). FT-IR based methodology for quantitation of total tocopherols, tocotrienols and plastochromanol-8 in vegetable oils. *J. Food Compos. Anal.* 18 (5), 359–364. doi: 10.1016/j.jfca.2003.12.008

Ajayi, I. A., Oderinde, R. A., Ogunkoya, B. O., Egunyomi, A., and Taiwo, V. O. (2007). Chemical analysis and preliminary toxicological evaluation of *Garcinia mangostana* seeds and seed oil. *Food Chem.* 101 (3), 999–1004. doi: 10.1016/j.foodchem.2006.02.053

Alfawaz, M. A. (2004). Chemical composition and oil characteristics of pumpkin (*Cucurbita maxima*) seed kernels. *Food Sci. Agric.* 2 (1), 5–18.

Aljane, F., and Ferchichi, A. (2007). Morphological, chemical and sensory characterization of Tunisian fig (*Ficus carica* L.) cultivars based on dried fruits. *Acta Hortic.* 741, 81–86. doi: 10.17660/ActaHortic.2007.741.10

Aljane, F., and Ferchichi, A. (2009). Postharvest chemical properties and mineral contents of some fig (*Ficus carica* L.) cultivars in Tunisia. *J. Food Agric. Environ.* 7 (2), 209–212.

Anang, M. A., Oteng-Peprah, M., and Opoku-Boadu, K. (2019). Extraction and characterisation of african star apple (*Chrysophyllum albidum*) seed oil and the adsorptive properties of the fruit shell in Ghana. *Int. J. Food Sci.* 1–8. doi: 10.1155/2019/4959586

Anjos, O., Campos, M. G., Ruiz, P. C., and Antunes, P. (2015). Application of FTIR-ATR spectroscopy to the quantification of sugar in honey. *Food Chem.* 169, 218–223. doi: 10.1016/j.foodchem.2014.07.138

Berry, S. K. (1980). Cyclopropene fatty acids in some Malaysian edible seeds and nuts: I. Durian (*Durio zibethinus* Murr.). *Lipids* 15 (6), 452–455. doi: 10.1007/bf02534071

Bölek, S. (2020). Effects of waste fig seed powder on quality as an innovative ingredient in biscuit formulation. *J. Food Sci.*, 1750–3841.15548. doi: 10.1111/1750-3841.15548

Bouafif, H., Koubaa, A., Perré, P., Cloutier, A., and Riedl, B. (2008). Analysis of among-species variability in wood fiber surface using DRIFTS and XPS: effects on esterification efficiency. *J. Wood Chem. Technol.* 28 (4), 296–315. doi: 10.1080/02773810802485139

Branco, A. F., Ferreira, A., Simoes, R. F., Magalhães- Novais, S., Zehowski, C., Cope, E., et al. (2016). Ketogenic diets: from cancer to mitochondrial diseases and beyond. *Eur. J. Clin. Invest.* 46 (3), 285–298. doi: 10.1111/eci.12591

Cai, S., and Singh, B. R. (2004). A distinct utility of the amide III infrared band for secondary structure estimation of aqueous protein solutions using partial least squares methods. *Biochemistry* 43 (9), 2541–2549. doi: 10.1021/bi030149y

Cassani, L., Santos, M., Gerbino, E., Del Rosario Moreira, M., and Gómez-Zavaglia, A. (2017). A combined approach of infrared spectroscopy and multivariate analysis for the simultaneous determination of sugars and fructans in strawberry juices during storage. *J. Food Sci.* 83 (3), 631–638. doi: 10.1111/1750-3841.13994

Chongtham, N., Bisht, M. S., Bajwa, H. K., Santosh, O., and Indira, A. (2020). Mineral elements in Bamboo shoots and Potential role in Food Fortification. *J. Food Compos. Anal.*, 103662. doi: 10.1016/j.jfca.2020.103662

Chougui, N., Tamendjari, A., Hamidj, W., Hallal, S., Barras, A., Richard, T., et al. (2013). Oil composition and characterisation of phenolic compounds of Opuntia ficus-indica seeds. *Food Chem.* 139 (1-4), 796–803. doi: 10.1016/j.foodchem.2013.01.054

Choukri, H., Hejjaoui, K., El-Baouchi, A., El haddad, N., Smouni, A., Maalouf, F., et al. (2020). Heat and drought stress impact on phenology, grain yield, and nutritional quality of lentil (*Lens culinaris* medikus). *Front. Nutr.* 7. doi: 10.3389/fnut.2020.596307

Clark, N. R., and Ma'ayan, A. (2011). Introduction to statistical methods to analyze large data sets: principal components analysis. *Sci. Signal* 4 (190), tr3–tr3. doi: 10.1126/scisignal.2001967

Cocchi, M., Durante, C., Foca, G., Marchetti, A., Tassi, L., and Ulrici, A. (2006). Durum wheat adulteration detection by NIR spectroscopy multivariate calibration. *Talanta* 68 (5), 0–1511. doi: 10.1016/j.talanta.2005.08.005

Cocchi, M., Lucisano, M., Marchetti, A., Pagani, M. A., Tassi, L., and Ulrici, A. (2004). Classification of cereal flours by chemometric analysis of MIR spectra. *J. Agric. Food Chem.* 52 (5), 1062–1067. doi: 10.1021/jf034441o

Darai, R., Sarker, A., Pandey, M., Dhakal, K., Kumar, S., and Sah, R. (2020). Genetic variability and genotype X environment interactions effect on grain iron (Fe) and zinc (Zn) concentration in lentils and their characterization under Terai environments of Nepal. *Adv. Nutr. Food Sci.* 5, 1–12. doi: 10.33140/ANFS.05.01.01

De la Mata, P., Dominguez-Vidal, A., Bosque-Sendra, J. M., Ruiz-Medina, A., Cuadros Rodríguez, L., and Ayora-Cañada, M. J. (2012). Olive oil assessment in edible oil blends by means of ATR-FTIR and chemometrics. *Food Control* 23 (2), 449–455. doi: 10.1016/j.foodcont.2011.08.013

De Nardo, T., Shiroma-Kian, C., Halim, Y., Francis, D., and Rodriguez-Saona, L. E. (2009). Rapid and simultaneous determination of lycopene and β-carotene contents in tomato juice by infrared spectroscopy. *J. Agric. Food Chem.* 57 (4), 1105–1112. doi: 10.1021/jf802920z

Duman, E., Şimşek, M., and Özcan, M. M. (2018). Monitoring of composition and antimicrobial activity of fig (*Ficus carica* L.) fruit and seed oil. *J. Agroaliment. Proc. Technol.* 24 (2), 75–80.

Ellepola, S. W., Siu, M. C., and Ma, C. Y. (2005). Conformational study of globulin from rice (*Oryza sativa*) seeds by Fourier transform infrared spectroscopy. *Int. J. Biol. Macromol.* 37(1–2), 12–20. doi: 10.1016/j.ijbiomac.2005.07.008

Estefan, G., Sommer, R., and Ryan, J. (2013). *Methods of Soil, Plant, and Water Analysis: A manual for the West Asia and North Africa region. 3rd Edition* (Lebanon: International Center for Agricultural Research in the Dry Areas (ICARDA). 244p.

Gaaliche, B., Trad, M., and Mars, M. (2011). Effect of pollination intensity, frequency and pollen source on fig (*Ficus carica* L.) productivity and fruit quality. *Scientia Hortic.* 130 (4), 737–742. doi: 10.1016/j.scienta.2011.08.032

Gharibzahedi, S. M. T., and Jafari, S. M. (2017). The importance of minerals in human nutrition: Bioavailability, food fortification, processing effects and nanoencapsulation. *Trends Food Sci. Technol.* 62, 119–132. doi: 10.1016/j.tifs.2017.02.017

Gopalakrishnan, R., and Raghu, K. (2014). Biosynthesis and characterization of gold and silver nanoparticles using milk thistle (*Silybum marianum*) seed extract. *J. Nanosci.* 2014. Article ID 905404, 8 pages. doi: 10.1155/2014/905404

Górnaś, P., and Rudzińska, M. (2016). Seeds recovered from industry by-products of nine fruit species with a high potential utility as a source of unconventional oil for biodiesel and cosmetic and pharmaceutical sectors. *Ind. Crops Prod.* 83, 329–338. doi: 10.1016/j.indcrop.2016.01.021

Guillén, M. D., and Cabo, N. (1997). Infrared spectroscopy in the study of edible oils and fats. *J. Sci. Food Agric.* 75 (1), 1–11. doi: 10.1002/(sici)1097-0010(199709)75:1<1::aid-jsfa842>3.0.co;2-r

Gupta, A. P., Neue, H. U., and Singh, V. P. (1993). Phosphorus determination in rice plants containing variable manganese content by the phospho-molybdo-vanadate (yellow) and phosphomolybdate (blue) colorimetric methods. *Commun. Soil Sci. Plant Anal.* 24 (11-12), 1309–1318. doi: 10.1080/00103629309368878

Hadjidemetriou, D. G. (1982). Comparative study of the determination of nitrates in calcareous soils by the ion-selective electrode, chromotropic acid and phenoldisulphonic acid methods. *Anal.* 107 (1270), 25. doi: 10.1039/an9820700025

Hssaini, L., Elfazazi, K., Razouk, R., Ouaabou, R., Hernandez, F., Hanine, H., et al. (2021b). Combined effect of cultivar and peel chromaticity on figs' Primary and secondary metabolites: preliminary study using biochemical and FTIR fingerprinting coupled to chemometrics. *Biology* 10 (7), 573. doi: 10.3390/biology10070573

Hssaini, L., Hanine, H., Charafi, J., Razouk, R., Elantari, A., Ennahli, S., et al. (2020). First report on fatty acids composition, total phenolics and antioxidant activity in seeds oil of four fig cultivars (*Ficus carica* L.) grown in Morocco. *Oilseeds fats Crops Lipids* 27, 8. doi: 10.1051/ocl/2020003

Hssaini, L., Razouk, R., Charafi, J., Houmanat, K., and Hanine, H. (2021a). Fig seeds: Combined approach of lipochemical assessment using gas chromatography and FTIR-ATR spectroscopy using chemometrics. *Vibration. Spectrosc.* 114, 103251. doi: 10.1016/j.vibspec.2021.103251

Hssaini, L., Razouk, L., Irchad, A., Aboutayeb, R., and Ouaabou, R. (2022). Do pollination and pollen sources affect fig seed set and quality? First attempt using chemical and vibrational fingerprints coupled with chemometrics. *J. Chem.* 2022. doi: 10.1155/2022/3969165. Article ID 3969165, 13 pages, 2022.

Jha, A. B., and Warkentin, T. D. (2020).Biofortification of pulse crops: Status and future perspectives. *Plants* 9 (1), 73.

Joseph, B., and Raj, S. J. (2011). Pharmacognostic and phytochemical properties of *Ficus carica* Linn–An overview. *Int. J. pharmtech Res.* 3 (1), 8–12.

Khan, Y. (2011). Element content analysis of plants of genus *Ficus* using atomic absorption spectrometer. *Afr. J. Pharm. Pharmacol.* 5 (3). doi: 10.5897/ajpp10.339

Knudsen, D., Peterson, G. A., and Pratt, P. F. (1982). "Lithium, sodium and potassium," in *Methods of soil analysis. Part 2 Chemical and microbiological properties, 2nd edition*. Eds. A. L. Page, R. H. Miller and D. R. Keeney (Madison, WI, USA: American Society of Agronomy Inc.), 225–246.

Koch, C., Posch, A. E., Goicoechea, H. C., Herwig, C., and Lendl, B. (2014). Multi-analyte quantification in bioprocesses by Fourier-transform-infrared spectroscopy by partial least squares regression and multivariate curve resolution. *Anal. Chimica Acta* 807, 103–110. doi: 10.1016/j.aca.2013.10.042

Kumar, H., Dikshit, H. K., Singh, A., Jain, N., Kumari, J., Singh, A. M., et al. (2014). Characterization of grain iron and zinc in lentil (*Lens culinaris* Medikus *culinaris*) and analysis of their genetic diversity using SSR markers. *Aust. J. Crop Sci.* 8, 1005–1012.

Liu, X., Renard, C. M. G. C., Bureau, S., and Le Bourvellec, C. (2021). Revisiting the contribution of ATR-FTIR spectroscopy to characterize plant cell wall polysaccharides. *Carbohydr. Polymers* 262, 117935. doi: 10.1016/j.carbpol.2021.117935

Lo Turco, V., Potortì, A. G., Tropea, A., Dugo, G., and Di Bella, G. (2020). Element analysis of dried figs (*Ficus carica* L.) from the Mediterranean areas. *J. Food Compos. Anal.* 90, 103503. doi: 10.1016/j.jfca.2020.103503

Lucarini, M., Durazzo, A., Kiefer, J., Santini, A., Lombardi-Boccia, G., Souto, E. B., et al. (2019). Grape seeds: chromatographic profile of fatty acids and phenolic compounds and qualitative analysis by FTIR-ATR spectroscopy. *Foods* 9 (1), 10. doi: 10.3390/foods9010010

Nakilcioğlu-Tas, E. (2019). Biochemical characterization of fig (*Ficus carica* L.) seeds. *J. Agric. Sci.* 25 (2), 232–237.

Niu, S., Zhou, Y., Yu, H., Lu, C., and Han, K. (2017). Investigation on thermal degradation properties of oleic acid and its methyl and ethyl esters through TG-FTIR. *Energy Conver. Manage.* 149, 495–504. doi: 10.1016/j.enconman.2017.07.053

Oh, S. Y., Yoo, D. I., Shin, Y., and Seo, G. (2005). FTIR analysis of cellulose treated with sodium hydroxide and carbon dioxide. *Carbohydr. Res.* 340 (3), 417–428. doi: 10.1016/j.carres.2004.11.027

Prasad, N. B. L., and Azeemoddin, G. (1994). Characteristics and composition of guava (*Psidium guajava* L.) seed and oil. *J. Am. Oil Chemists' Soc.* 71 (4), 457–458. doi: 10.1007/BF02540531

Raihana, A. R. N., Marikkar, J. M. N., Amin, I., and Shuhaimi, M. (2015). A review on food values of selected tropical fruits' Seeds. *Int. J. Food Properties* 18 (11), 2380–2392. doi: 10.1080/10942912.2014.980946

Rosianski, Y., Freiman, Z. E., Cochavi, S. M., Yablovitz, Z., Kerem, Z., and Flaishman, M. A. (2016). Advanced analysis of developmental and ripening characteristics of pollinated common-type fig (*Ficus carica* L.). *Scientia Hortic.* 198, 98–106. doi: 10.1016/j.scienta.2015.11.027

Sadia, H., Ahmad, M., Sultana, S., Abdullah, A. Z., Teong, L., Zafar, M., et al. (2014). Nutrient and mineral assessment of edible wild fig and mulberry fruits. *Fruits* 69 (2), 159–166. doi: 10.1051/fruits/2014006

Schwanninger, M., Rodrigues, J. C., Pereira, H., and Hinterstoisser, B. (2004). Effects of short-time vibratory ball milling on the shape of FT-IR spectra of wood and cellulose. *Vibration. Spectrosc.* 36 (1), 23–40. doi: 10.1016/j.vibspec.2004.02.003

Shen, J., Huang, G., An, C., Xin, X., Huang, C., and Rosendahl, S. (2018). Removal of Tetrabromobisphenol A by adsorption on pinecone-derived activated charcoals: Synchrotron FTIR, kinetics and surface functionality analyses. *Biores. Technol.* 247, 812–820. doi: 10.1016/j.biortech.2017.09.177

Solomon, A., Golubowicz, S., Yablowicz, Z., Grossman, S., Bergman, M., Gottlieb, H. E., et al. (2006). Antioxidant activities and anthocyanin content of fresh fruits of common fig (*Ficus carica* L.). *J. Agric. Food Chem.* 54 (20), 7717–7723. doi: 10.1021/jf060497h

Sylverstein, R. M., Bassler, G. C., and Morrill, T. C. (1991). *Spectrophotometric Identification of Organic Compounds. 5th edn* (New York, USA: Wiley).

Taoufik, F., Zine, S., El Hadek, M., Idrissi Hassani, L., Gharby, S., Harhar, H., et al. (2015). Oil content and main constituents of cactus seed oils *Opuntia Ficus Indica* of different origin in Morocco. *Mediterr. J. Nutr. Metab.* 8, 85–92. doi: 10.3233/MNM-150036

Terpugov, E. L., Degtyareva, O. V., and Savransky, V. V. (2016). Possibility of light-induced mid-IR emission in situ analysis of plants. *J. Russian Laser Res.* 37 (5), 507–510. doi: 10.1007/s10946-016-9602-8

Tolonen, M. (1990). *Vitamins and Minerals in Health and Nutrition* (Elsevier).

Tulukcu, E., Cebi, N., and Sagdic, O. (2019). Chemical fingerprinting of seeds of some *salvia* species in Turkey by using GC-MS and FTIR. *Foods* 8 (4), 1–12. doi: 10.3390/foods8040118

Ustun-Argon, Z., Sari, Z., Gokyer, A., and Buyukhelvacigil-Ozturk, S. (2021). Phytochemical evaluation of *ficus carica* seeds and their cold pressed oil. *J. Pharm. Res.* 20 (4), 71–79. doi: 10.18579/jopcr/v20i4.2

Van de Voort, F. R., Ismail, A. A., and Sedman, J. (1995). A rapid automated method for the determination of *cis* and *trans* content of fats and oils by Fourier transform infrared spectroscopy. *J. Am. Oil Chemists' Soc.* 72 (8), 873–880. doi: 10.1007/bf02542063

Vlachos, N., Skopelitis, Y., Psaroudaki, M., Konstantinidou, V., Chatzilazarou, A., and Tegou, E. (2006). Applications of Fourier transform-infrared spectroscopy to edible oils. *Anal. Chimica Acta* 573–574, 459–465. doi: 10.1016/j.aca.2006.05.034

Yanty, N. A. M., Lai, O. M., Osman, A., Long, K., and Ghazali, H. M. (2008). Physicochemical properties of Cucumis melo Var. Inodorus (*Honeydew Melon*) seed and seed oil. *J. Food Lipids* 15 (1), 42–55. doi: 10.1111/j.1745-4522.2007.00101.x

Yarosh, É.A., and Umarov, A. U. (1971). A study of the oil of the seeds of Ficus carica. *Chem. Natural Compounds* 7 (1), 99–99. doi: 10.1007/bf01032037

frontiers | Frontiers in Plant Science

TYPE Original Research
PUBLISHED 21 December 2023
DOI 10.3389/fpls.2023.1274700

OPEN ACCESS

EDITED BY
Hosam O. Elansary,
King Saud University, Saudi Arabia

REVIEWED BY
Anna Kulma,
University of Wrocław, Poland
Challa Surekha,
Gandhi Institute of Technology and Management, India

*CORRESPONDENCE
Jingle Zhu
zhujingle@caf.ac.cn

†These authors have contributed equally to this work

RECEIVED 08 August 2023
ACCEPTED 04 December 2023
PUBLISHED 21 December 2023

CITATION
Yang Y, Chen M, Zhang W, Zhu H, Li H, Niu X, Zhou Z, Hou X and Zhu J (2023) Metabolome combined with transcriptome profiling reveals the dynamic changes in flavonoids in red and green leaves of *Populus* × *euramericana* 'Zhonghuahongye'.
Front. Plant Sci. 14:1274700.
doi: 10.3389/fpls.2023.1274700

Metabolome combined with transcriptome profiling reveals the dynamic changes in flavonoids in red and green leaves of *Populus* × *euramericana* 'Zhonghuahongye'

Yun Yang[1,2†], Mengjiao Chen[3†], Wan Zhang[1,4], Haiyang Zhu[1,4], Hui Li[1,5], Xinjiang Niu[1], Zongshun Zhou[6], Xiaoya Hou[4] and Jingle Zhu[1,2*]

[1]Research Institute of Non-Timber Forestry, Chinese Academy of Forestry, Zhengzhou, Henan, China, [2]Key Laboratory of Non-timber Forest Germplasm Enhancement and Utilization of National Forestry and Grassland Administration, Zhengzhou, Henan, China, [3]Research Institute of Tropical Forestry, Chinese Academy of Forestry, Guangzhou, Guangdong, China, [4]College of Forestry, Henan Agricultural University, Zhengzhou, Henan, China, [5]Institute of Gene Science and Industrialization for Bamboo and Rattan Resources, International Center for Bamboo and Rattan, Beijing, China, [6]China Experimental Centre of Subtropical Forestry, Chinese Academy of Forestry, Xinyu, Jiangxi, China

Flavonoids are secondary metabolites that have economic value and are essential for health. Poplar is a model perennial woody tree that is often used to study the regulatory mechanisms of flavonoid synthesis. We used a poplar bud mutant, the red leaf poplar variety 2025 (*Populus* × *euramericana* 'Zhonghuahongye'), and green leaves as study materials and selected three stages of leaf color changes for evaluation. Phenotypic and biochemical analyses showed that the total flavonoid, polyphenol, and anthocyanin contents of red leaves were higher than those of green leaves in the first stage, and the young and tender leaves of the red leaf variety had higher antioxidant activity. The analyses of widely targeted metabolites identified a total of 273 flavonoid metabolites (114 flavones, 41 flavonols, 34 flavonoids, 25 flavanones, 21 anthocyanins, 18 polyphenols, 15 isoflavones, and 5 proanthocyanidins). The greatest difference among the metabolites was found in the first stage. Most flavonoids accumulated in red leaves, and eight anthocyanin compounds contributed to red leaf coloration. A comprehensive metabolomic analysis based on RNA-seq showed that most genes in the flavonoid and anthocyanin biosynthetic pathways were differentially expressed in the two types of leaves. The flavonoid synthesis genes *CHS* (chalcone synthase gene), *FLS* (flavonol synthase gene), *ANS* (anthocyanidin synthase gene), and proanthocyanidin synthesis gene *LAR* (leucoanthocyanidin reductase gene) might play key roles in the differences in flavonoid metabolism. A correlation analysis of core metabolites and genes revealed several candidate regulators of flavonoid and anthocyanin biosynthesis, including five MYB (MYB domain), three bHLH (basic helix-

loop-helix), and HY5 (elongated hypocotyl 5) transcription factors. This study provides a reference for the identification and utilization of flavonoid bioactive components in red-leaf poplar and improves the understanding of the differences in metabolism and gene expression between red and green leaves at different developmental stages.

KEYWORDS

Populus × *euramericana* 'Zhonghuahongye', flavonoids, anthocyanin, metabolome, RNA-seq

1 Introduction

Poplars (*Populus*, *Salicaceae*) have strong regeneration ability and wide-ranging economic and ecological benefits (Koes et al., 2005; Felix et al., 2008). There are 35 tree species of the genus *Populus*, including *P. alba*, *P.* × *canescens*, *P. nigra*, *P. tremula*, *P. tremuloides*, and *P. deltoides*. Poplar is a rich source of phytocompounds, including proteins, vitamins, mineral elements, phenolic compounds, and terpenoids, flavonoids (Devappa et al., 2015). Research on poplars has mainly focused on the cultivation of new varieties and the development of planting technologies (Biselli et al., 2022), while research on the utilization of poplars as phytochemical resources is limited. The potential applications of poplar extract might provide new opportunities in the pharmaceutical industry (Guleria et al., 2022). In addition, with the development of feed processing technology, research on poplar leaves as feed additives has increased (McAvoy et al., 2020). As early as 1980, Canadian scientists assumed the cultivation of a ruminant-type animal that feeds on poplar leaves. Recent studies have shown that the use of poplar leaves in appropriate amounts as feed additives can reduce methane emissions and improve the antioxidant activity of blood in buffalo (*Bubalus bubalis*) calves (Dey et al., 2021; Kumar et al., 2022).

Chemical extraction and isolation of metabolites from poplars are performed mainly by chromatographic separation and structural elucidation techniques, including high-performance liquid chromatography (HPLC), nuclear magnetic resonance (NMR), and liquid chromatography tandem mass spectrometry (LC–MS) (Guleria et al., 2022). Over 155 specific metabolites, including 27 phenolic acids and their derivatives, 32 phenolic glycosides, 53 flavonoids, and 44 terpenoids, have been characterized from poplar plants (Kis et al., 2020). Among all bioactive ingredients, flavonoids have antioxidant, anti-inflammatory, antibiotic, and anticarcinogenic potential (Panche et al., 2016). Flavones, flavonols, flavanones, flavanonols, isoflavones, catechins, anthocyanins, and proanthocyanidins are subgroups of flavonoids (Panche et al., 2016). The anthocyanins and flavonoids separated from *Delonix regia* flowers inhibited the activity of pathogenic bacteria *in vitro* (Ebada et al., 2023). *Morus alba* L. leaf extracts were studied for clinical treatment of diabetes and obesity because they are rich in isoquercitrin, kaempferol, quercetin, rutin, chlorogenic acid, and gallic acid (Zhang et al., 2022). Bud extracts of *P. nigra*, with the bioactive ingredients caffeic and p-coumaric acids, have high antioxidant potential (Dudonné et al., 2011). Therefore, it is important to accurately identify the flavonoid metabolites in poplars to effectively use these resources.

Plant flavonoid metabolites and their distribution are important subjects and hot topics for research (Shen et al., 2022b). Although flavonoid biosynthesis pathways are dependent on plant species and environmental conditions, the development of plant or microbial cell engineering and genetic engineering provides the possibility of industrial biosynthesis of specific flavonoids (Shen et al., 2022a). Flavonoid regulation has the same upstream chemical process as proanthocyanidin and anthocyanin biosynthesis (Falcone Ferreyra et al., 2012; Liu et al., 2021). MYB, basic helix-loop-helix (bHLH), and WD40 transcription factors (TFs) play an important role in regulating flavonoid synthesis (LaFountain and Yuan, 2021). TFs can promote or suppress flavonoid synthesis by recognizing and binding specific sequences of structural gene promoters (An et al., 2012; Zhu et al., 2015). There are many TFs in poplar that might be related to flavonoids, and these await further exploration.

Populus × *euramericana* 'Zhonghuahongye' is a bud mutant that was selected from *Populus nigra* L2025 (green leaves) (Chen et al., 2022a). This variety is widely planted commercially for landscaping. The color of *Populus* × *euramericana* 'Zhonghuahongye' leaves varies from bright red to reddish brown with age. Flavonoid and anthocyanin metabolites are differentially expressed as the color changes (Chen et al., 2023). Another study showed that in *Populus deltoides* varieties with red leaves, the contents of quercetin, rhamnetin, isorhamnetin, and kaempferol were higher than those in the green leaves of *Populus* sp. Linn. '2025' (Tian et al., 2021). Red poplar varieties have higher feeding value than common poplar varieties because of the flavonoid content (Ayers et al., 1996). There is currently no comprehensive and detailed description of whether the contents of these flavonoids vary among different growth stages of red poplar. What are the differences in flavonoids between red leaves and green leaves of *Populus nigra* over time? Which metabolic pathways and putative genes contribute to these differences? In this study, *Populus* × *euramericana* 'Zhonghuahongye' leaves (red) and green leaves

from three developmental stages were taken as the research material. Anthocyanins, flavanones, flavones, flavonoids, flavonols, isoflavones, polyphenols, and proanthocyanidins were identified. A comprehensive analysis was performed, and dynamic flavonoid accumulation in red leaves was observed. Structural gene expression and TF regulation provide the foundation for studying flavonoid biosynthesis. Our results provide insights into flavonoid metabolism in *Populus nigra* at different developmental stages and will be beneficial for the utilization of its leaf resources.

2 Materials and methods

2.1 Plant materials and sampling

The *Populus* × *euramericana* 'Zhonghuahongye' variety is a bud mutant of the Poplar L2025 clone. The *Populus* × *euramericana* 'Zhonghuahongye' variety is a highly valuable ornamental tree that exhibits red leaves throughout the growth cycle. From spring to early summer, all the plant leaves, especially newly sprouted leaves, are a beautiful rose-red color. In the middle stage of growth, the leaves are bright purplish-red, and the mature leaves turn red –green. The studied plants were kept at the state-owned Mengzhou exploratory site (north latitude 32°06'; east longitude 118°06'). However, several branches with green leaves were found on the red-leaved trees. Thus, green leaves and red leaves of 3-year-old trees were collected for the experiment. Red leaves were collected at three stages: R1 (1 April 2019), R2 (6 April 2019), and R3 (11 April 2019). Green leaves were collected on the same dates and referred to as the G1, G2, and G3 samples (Figure 1A). Three trees were selected as biological replicates. For each sample, leaves with similar positions and colors on the branches were selected. The sampling procedures are shown in Figure S1.

2.2 Leaf color measurement and determination of physiological indexes

Leaf color was measured according to the International Commission on Illumination (CII) color standard. L^*, a^*, and b^* values were determined using a CR2500 chromatic aberration meter (Minolta, Japan). Ten points were randomly selected on each blade, chromatic aberration timing was used to avoid the leaf veins, and the average value for each blade was used for analysis (not transparent when measuring). The measured a^*, b^*, and L^* values could be used to calculate chromaticity (C^*) and light color values (Tian et al., 2021; Yang et al., 2021). The photosynthetic pigment contents of the R1, R2, R3, G1, G2, and G3 samples were determined. The chlorophyll a (C_a), chlorophyll b (C_b), total chlorophyll (C_T), carotenoid (C_{car}), and anthocyanin (C_A) contents were determined by ultraviolet spectrophotometry (JINGHUA Instruments 752), and 3 biological replicates were analyzed per sample. The experiment was performed according to a published paper (Chen et al., 2022a). The data were analyzed by SPSS 17.0 software.

The leaves were dried to a constant weight. Then, the samples were precisely weighed to 0.5000 g, extracted with 25 mL of boiling water for 5 min, heated in a 25°C water bath for 30 min, and centrifuged at 10,000 r · min $^{-1}$ for 10 min, after which the precipitate was discarded. The supernatant was used for further analysis. The total flavonoid content was determined by the $AlCl_3$ - (HAc - NaAc) chromogenic method (Han et al., 2014). Rutin was used as the standard, and the absorbance was measured at 400 nm. The total phenol content was determined spectrophotometrically by the Folin-Ciocalteu method (Han et al., 2015). Gallic acid was used as the standard, and the absorbance was measured at 765 nm. In addition, the extraction method used for fresh samples was the same as that used for dry samples. The DPPH assay and $ABTS^+$ assay for studying free radical scavenging activity were performed using fresh samples. DPPH solution exhibits maximum absorption at 517 nm. The procedure was as follows: 1 mL of DPPH solution (0.05 g · mL^{-1}) was prepared, 500 µL of sample solution was added, and the mixture was reacted at room temperature for 30 min before measurement. $ABTS^+$ solution exhibits maximum absorption at 734 nm. In the assay, 300 µL of sample solution and 1.2 mL of $ABTS^+$ application solution was mixed evenly. The mixture was allowed to stand in the dark for 6 min and then measured. Trolox was used as a standard solution to quantify the antioxidant capacity.

2.3 Metabolite data analysis

Sample pretreatment and metabolite detection and quantification were accomplished at Wuhan MetWare Biotechnology Co., Ltd. (www.metware.cn) according to a standard procedure. Leaf metabolites were extracted from 100 mg powdered samples in 70% aqueous methanol (1.0 mL) for 24 h at 4°C. Following centrifugation at 10,000 × g for 10 min, the extracts were absorbed (CNWBOND Carbon-GCB SPE Cartridge, 250 mg, 3 mL; ANPEL, Shanghai, China) and filtered (SCAA-104, 0.22 µm pore size; ANPEL, Shanghai, China) before LC-MS analysis.

The sample extracts were analyzed using an LC-ESI-MS/MS system (HPLC, Shim-pack UFLC SHIMADZU CBM30A system, MS; Applied Biosystems 4500 Q TRAP). The analytical conditions were described in Table S1. The effluent was alternatively directed to an ESI-triple quadrupole-linear ion trap (Q TRAP)-MS. LIT and triple quadrupole (QQQ) scans were acquired on a triple quadrupole-linear ion trap mass spectrometer (Q TRAP), an API 4500 Q TRAP LC/MS/MS System, equipped with an ESI Turbo Ion-Spray interface, operating in positive ion mode and controlled by Analyst 1.6.3 software (AB Sciex). The ESI-Q TRAP-MS/MS parameter is displayed in Table S2. A specific set of multiple reaction monitoring (MRM) transitions was monitored for each period according to the metabolites eluted within this period.

Analyst 1.6.3 software was used to process the mass spectral data. Based on the self-built database MWDB and the metabolite information public database, qualitative analysis of the primary and secondary mass spectral data was performed. The mass spectral peaks detected in different samples for each metabolite were corrected to ensure qualitative and quantitative accuracy (Fraga et al., 2010). Quality control (QC) of mixed samples was performed after every 10 samples prior to data analysis to monitor the

10.3389/fpls.2023.1274700

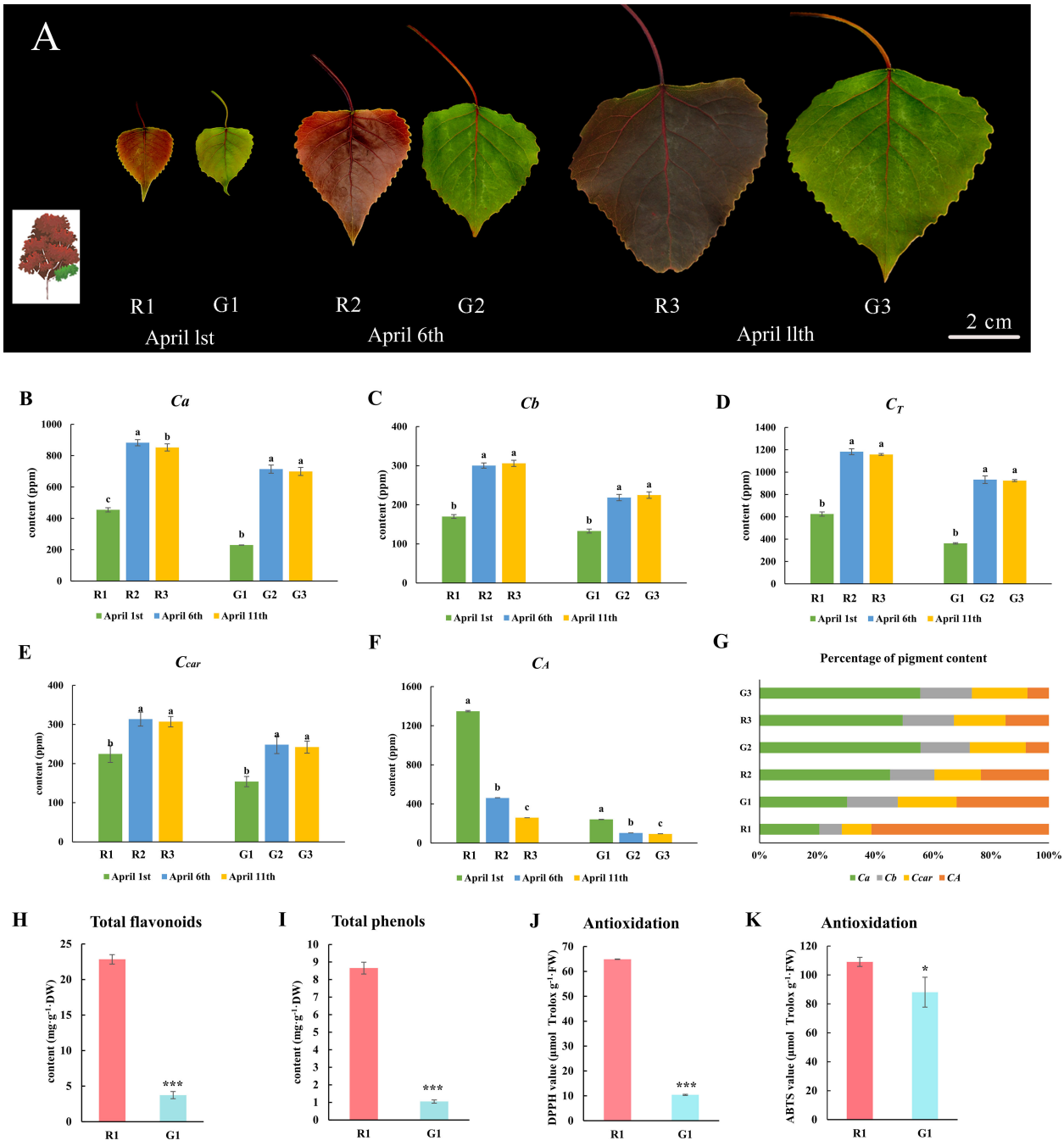

FIGURE 1
Morphology, pigment content, total flavonoid content and polyphenol content, and antioxidant ability of green and red poplar leaves. **(A)** Morphological observations of red and green leaves on 1 April 2019, 6 April 2019, and 11 April 2019; **(B)** chlorophyll a content; **(C)** chlorophyll b content; **(D)** total chlorophyll content; **(E)** carotenoid content; **(F)** anthocyanin content; **(G)** percentage of pigment content in each sample. These data were analyzed using Duncan's multiple range test (p-value ≤ 0.05) and are expressed as the means ± standard deviations (SDs) of triplicates. **(H)** Total flavonoid content; **(I)** total polyphenol content; **(J)** DPPH values; **(K)** ABTS values. These data of R1 and G1 leaves were analyzed by the T-test method. *** indicates a significant p value ≤ 0.001, and * indicates a p value ≤ 0.05. The small letters represent significant differences at three different developmental stages.

reproducibility of the analytical process. QC samples were prepared using mixed sample extracts.

Orthogonal partial least squares discriminant analysis (OPLS-DA) and principal component analysis (PCA) were conducted to analyze and verify the differences and reliability of metabolites in the samples. The metabolite content data were normalized by the range method, and the accumulation mode of metabolites among different samples was analyzed by heatmap cluster analysis (hierarchical cluster analysis, HCA) through R software (www.r-project.org/). PLS-DA analysis was applied to calculate the corresponding variable importance in projection (VIP) value. Metabolites with VIP≥ 1 and fold change ≥2 or fold change ≤ 0.5 were considered differentially expressed metabolites (DEMs). Then, the differentially abundant metabolites were mapped to the Kyoto Encyclopedia of

Genes and Genomes (KEGG) database for significant enrichment analysis, and major enriched pathways were identified.

2.4 Transcriptomics

Eighteen sample libraries representing 2 leaf colors and 3 developmental stages were constructed for RNA-seq. The procedures for high-throughput sequencing were reported in previous studies (Chen et al., 2022a). An Illumina HiSeq instrument was used for sequencing. The *Populus trichocarpa* genome was selected as the reference (Tuskan et al., 2006). To quantify transcription or gene expression levels, fragments per kilobase of exon model per million mapped fragments (FPKM) values were used. To identify differentially expressed genes (DEGs), DESeq2 software and the Benjamini–Hochberg method were used (Love et al., 2014; Varet et al., 2016). The DEGs met the criteria $|\log_2\text{Fold Change}| \geq 1$ and false discovery rate (FDR) < 0.05. DEG enrichment was assessed based on comparison with Gene Ontology (GO) and KEGG data. The transcriptome data are available in the NCBI database (https://www.ncbi.nlm.nih.gov/) under BioProject PRJNA881405 and PRJNA934137. qRT–PCR (real-time fluorescence quantitative PCR) was used to confirm the gene expression results. As targets for analysis, 11 structural and regulatory genes related to the anthocyanin pathway were selected. Total RNA from green and red leaf tissues at three developmental stages was extracted and then employed to synthesize cDNA. The primer sequences employed are shown in Table S3, and β-actin was used as an internal reference gene. qRT–PCR was conducted on a LightCyclerR480 system (Roche, Switzerland) as described in a previous article (Chen et al., 2022a).

TFs were annotated with iTAK software and then subjected to BLAST searches with PlnTFDB and PlantTFDB. Based on the measured gene expression levels and metabolite contents, a network of TFs, structural genes, and metabolites was constructed. The selected genes and metabolites are listed in Table S4. The correlation network was constructed in the MetWare Cloud (https://cloud.metware.cn/) according to the following settings: the correlation analysis method was Pearson, the numerical conversion method was log2, the correlation analysis threshold was 0.8, and the *P* value threshold for the significant difference was 0.05. The network was visualized in a concentric circle diagram using Cytoscape software (v3.8.2) and was distributed using the degree algorithm. Phylogenetic trees of MYB and bHLH amino acid sequences were constructed and downloaded from the NCBI database. The phylogenetic tree was drawn with MEGA software (v6.0) using the neighbor-joining method. Correlation analysis of the transcriptome and metabolome data was carried out based on published methods (Yang et al., 2021). The genes and metabolites related to the flavonoid pathway (k00941) and anthocyanin pathway (k00942) are displayed.

Weighted gene coexpression network analysis (WGCNA) is used to find co-expressed gene modules and explore the association between gene networks and phenotypes (Langfelder & Horvath, 2008). The module is defined as a group of genes with similar expression profiles. If certain genes always show similar expression changes during a physiological process, it is reasonable to consider these genes to be functionally related; they can be defined as a module (Liu et al., 2020). First, the gene expression data are processed. The correlation coefficient between any two genes is calculated using the weighted correlation method. In the second step, a hierarchical clustering tree is constructed from the correlation coefficients between genes. Genes are classified according to their expression patterns, and genes with similar patterns are grouped into a module. In this way, tens of thousands of genes can be divided into dozens of modules according to their expression patterns. The corresponding modules are merged into the same module. The final merged modules are used for subsequent analyses. In the third step, the modules associated with the traits were identified. The correlation coefficients between gene modules and phenotypes were calculated using the Pearson correlation algorithm. The trait must be a numerical trait. In this study, WGCNA was used to analyze the correlation between the gene network and the total anthocyanin content. Bioinformatic analysis was performed using OECloud tools at https://cloud.oebiotech.cn according to the following settings: the power value was 30, the threshold value for standard deviation filtering was 0.5, and the threshold value for module merging was 0.25.

3 Results

3.1 Variations in phenotypes and biochemical analyses during leaf development

There are three distinct stages (R1, R2, and R3) of color transition in red leaves, and there are three corresponding developmental stages (G1, G2, and G3) in green leaves (Figure 1A). The green leaves remain green to the naked eye, regardless of the changes in red leaves. The chlorophyll a (Figure 1B), chlorophyll b (Figure 1C), total chlorophyll (Figure 1D), and carotenoid contents (Figure 1E) of the red leaves at different stages were much higher than those of the green leaves. However, the total anthocyanin content in the red leaves was higher than that in the green leaves in all three stages (Figure 1F). In the first stage, the anthocyanin content accounted for a high proportion of all pigments compared to the other two stages (Figure 1G). Moreover, the contents of flavonoids and polyphenols in red leaves at the first stage were considerably greater than those in green leaves. The total flavonoid content in R1 was 6.46 times that in G1 (Figure 1H), and the total polyphenol content in R1 was 8.25 times that in G1 (Figure 1I). DPPH and $ABTS^+$ assays were performed to measure the total antioxidant ability. The DPPH and ABTS values in R1 were significantly higher than those in G1 (Figures 1J, K). It could be preliminarily inferred that polyphenols, flavonoids, and anthocyanins were the principal differentially abundant metabolites between red and green leaves.

3.2 Analysis of bioactive flavonoids in green and red leaves of *Populus* × *euramericana* 'Zhonghuahongye'

Flavonoid metabolites were analyzed in the three periods of leaf color change in red leaf material (R1, R2, and R3) and green leaf

material (G1, G2, and G3). A total of 273 flavonoid metabolites were identified (Table S5), which were mainly divided into eight categories, among which flavones and flavonols were the most numerous (114 and 41, respectively), followed by flavonoids (34), flavanones (25), anthocyanins (21), polyphenols (18), isoflavones (15), and proanthocyanidins (5) (Figure 2A). PCA showed large differences in the metabolite composition in different developmental stages of red leaves and green leaves (Figure 2B). The PCA results showed a clear clustering of metabolic profiles based on leaf color and developmental period. The 1st, 2nd, and 3rd principal components accounted for 27.49%, 24.02%, and 12.18% of the total variability, respectively (Figure S2). In the OPLS-DA model, the Q^2 values of pairwise comparisons exceeded 0.9 (Figure S3). The cluster diagram of all samples showed that the metabolites from R1, R2, and G1 had similar expression patterns. There were obvious differences between the R3 and the R1 and R2 stages. The metabolites of R2 and G2 had significant differences and were assigned to two branches of the cluster (Figure 2C). These results provide a basis for further analysis of metabolite differences in the samples.

The flavonoids in *Populus* × *euramericana* 'Zhonghuahongye' leaves were analyzed. In the flavonoid category, the bioactive ingredients isoquercitroside, liquiritin, and the rare narcissoside were identified. In the flavonol category, the valuable components quercetin, kaempferol, quercetin 3-*O*-rutinoside (rutin), kaempferol 7-*O*-rhamnoside, kaempferol 3-*O*-rutinoside (nicotiflorin), kumatakenin, dihydroquercetin (taxifolin), and isorhamnetin were found. In the flavone class, baicalein-7-*O*-glucuronide was identified. In the bioactive ingredient isoflavone class, daidzein, genistein, galycosin, and prunetin were identified. In the medicinal polyphenol class, catechin, L-epicatechin, epicatechin gallate (ECG), and theaflavin were identified. The procyanidin components A3, A1, A2, B2, and B3 were detected. Furthermore, in the anthocyanin class, cyanidin 3-*O*-galactoside, cyanidin 3,5-*O*-diglucoside, peonidin *O*-hexoside, cyanidin *O*-syringic acid, delphinidin 3-*O*-rutinoside, delphinidin *O*-malonyl-malonylhexoside, and peonidin 3-*O*-glucoside chloride were identified. These representative compounds have been proven to have antioxidant and anti-inflammatory properties *in vitro*, and most of them showed relatively high abundances in red leaves of the

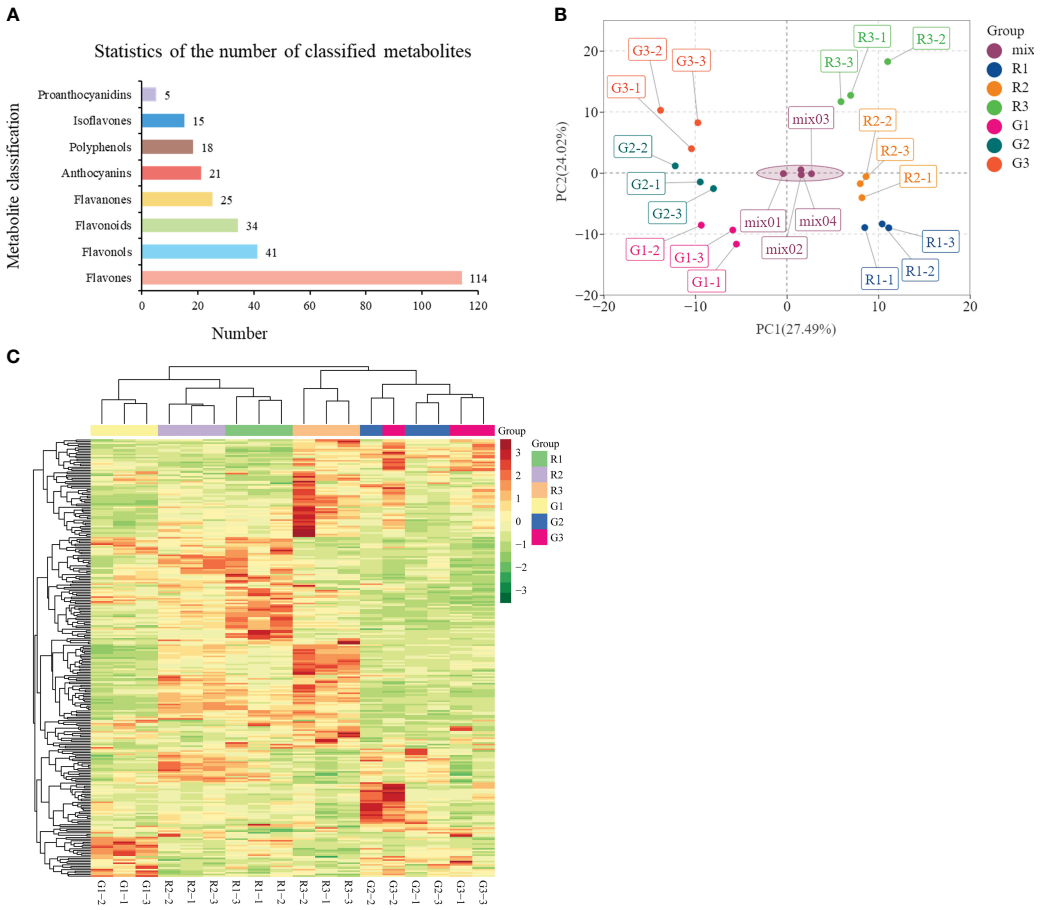

FIGURE 2
Analysis of flavonoid metabolites in green and red leaves. **(A)** Statistics of the number of classified metabolites. **(B)** Principal component analysis (PCA) of the samples from three developmental stages and quality control samples (mix). The x-axis represents the first principal component, and the y-axis represents the second principal component. **(C)** Cluster heatmap of all samples.

R1 and R2 stages (Figure S4). Other phytochemical components are listed in Table S5 for further analysis.

3.3 Analysis of differentially abundant flavonoid metabolites between red and green leaves and their KEGG classification

To reveal the accumulation patterns of flavonoids in the red and green leaves of *Populus* × *euramericana* 'Zhonghuahongye' poplar, pairwise comparisons of G1 vs. R1, G2 vs. R2, and G3 vs. R3 were conducted. Seventy-four significant DEMs were identified between G1 and R1 (63 increased and 11 decreased) (Figure 3A). In addition, 62 significant DEMs were identified in G2 vs. R2 (53 increased and 9 decreased) (Figure 3B), and 71 significant DEMs were identified in G3 vs. R3 (66 increased and 5 decreased) (Figure 3C). Most flavonoid metabolites accumulate in large quantities in red leaves. Venn diagram analysis showed that 33 significant DEMs were shared by the G1 vs. R1, G2 vs. R2, and G3 vs. R3 comparison groups (Figure S5). These flavonoids were considered the 'core metabolite group' in poplar leaves (Table S6). The hierarchical clustering analysis showed that most of the 'core metabolites' were upregulated in the red leaves compared with the green leaves, other than silibinin and cyanidin 3,5-*O*-diglucoside (Figure 3D). This implies that the 31 'core metabolites' of flavonoids (7 flavones, 6 flavonols, 5 flavonoids, 4 flavanones, 7 anthocyanins, and 2 polyphenols) were enriched in red poplar leaves.

The KEGG classification results showed that the significant DEMs of G1 vs. R1 were mainly involved in the isoflavonoid biosynthesis, flavonoid biosynthesis, flavone and flavonol biosynthesis, and anthocyanin biosynthesis pathways (Figure S6A). The significant DEMs of G2 vs. R2 were mainly enriched in flavonoid biosynthesis, anthocyanin biosynthesis, and isoflavonoid biosynthesis (Figure S6B). The significant DEMs of G3 vs. R3 were mainly related to flavonoid biosynthesis, anthocyanin biosynthesis, flavone and flavonol biosynthesis, and isoflavonoid biosynthesis, with the *P* value of anthocyanin biosynthesis being the smallest among the four pathways (Figure S6C). The KEGG enrichment classification histograms are shown in Figure S4D. The results indicated that leaf color presentation may be influenced by anthocyanin biosynthesis and flavonoid biosynthesis. Thereafter, the significant DEMs of the anthocyanin class in G1 vs. R1, G2 vs. R2, and G3 vs. R3 were analyzed (Table 1). Nine anthocyanins, including peonidin *O*-hexoside, delphinidin *O*-malonyl-malonylhexoside, cyanidin *O*-syringic acid, malvidin 3-*O*-galactoside, malvidin 3-*O*-glucoside, delphinidin 3-*O*-rutinoside, cyanidin, cyanidin 3-*O*-galactoside, and peonidin 3-*O*-glucoside chloride, were upregulated in R1 compared with G1. In addition to the anthocyanins mentioned above, cyanidin 3-*O*-glucoside showed upregulated expression in R2

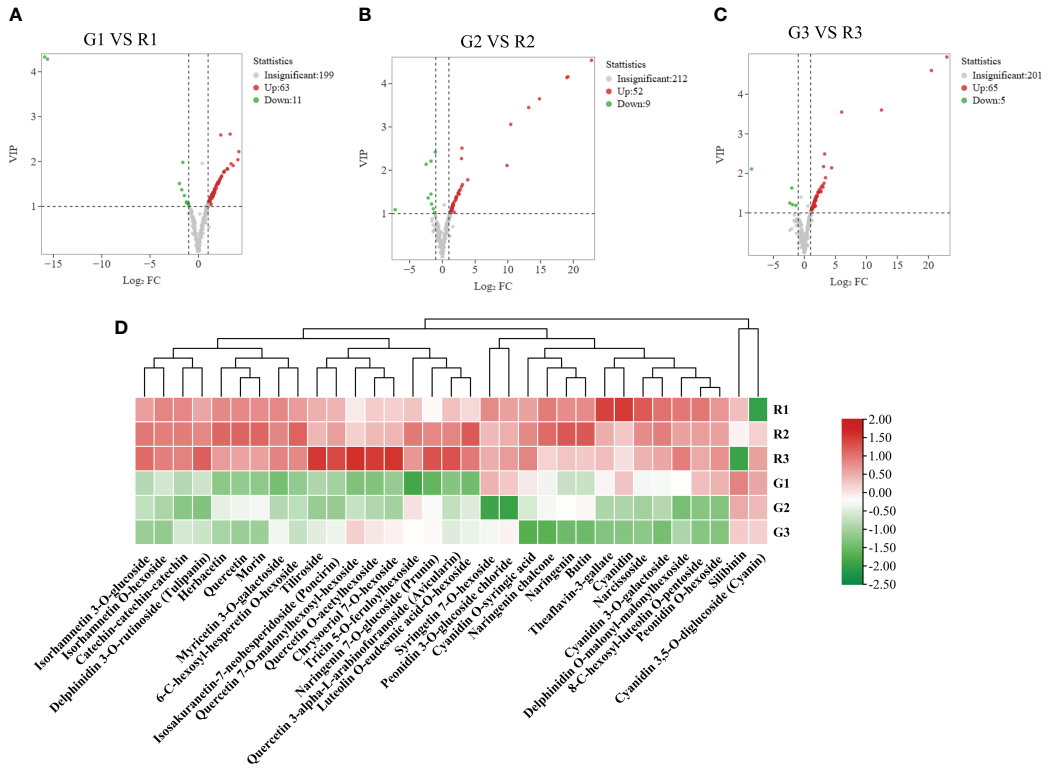

FIGURE 3
Differentially abundant metabolite screening. **(A)** Volcano plot of differentially abundant metabolite clustering for the G1 vs. R1 comparison. **(B)** Volcano plot of DEMs for the G2 vs. R2 comparison; **(C)** volcano plot of DEMs for the G3 vs. R3 comparison; **(D)** metabolites with significant differences in three developmental stages of poplar green (G1, G2, and G3) and red (R1, R2, and R3) leaves. The volcano plot map reflects the differences in metabolite expression levels in the two samples. The vertical coordinates represent the VIPs of the OPLS-DA model, and the horizontal coordinate values are the log2 (fold changes). Each point in the graph represents a detected metabolite. The legend of the volcano plot indicates the number of significant DEMs.

10.3389/fpls.2023.1274700

TABLE 1 Anthocyanin accumulation in different periods.

Anthocyanins	G1 vs R1[a]		G2 vs R2[b]		G3 vs R3[c]	
	Log_2FC[d]	KEGG[e]	Log_2FC	KEGG	Log_2FC	KEGG
Peonidin O-hexoside	2.63	Nd	19.19	Nd	20.49	Nd
Rosinidin O-hexoside	-1.45	Nd	-1.73	Nd	NS	NS
Delphinidin O-malonyl-malonylhexoside	1.42	Nd	2.43	Nd	2.22	Nd
Cyanidin O-syringic acid	1.09	Nd	2.41	Nd	4.38	Nd
Malvidin 3-O-galactoside	3.60	Nd	14.82	Nd	NS	NS
Malvidin 3-O-glucoside	4.09	ko00942	1.47	ko00942	NS	NS
Cyanidin 3,5-O-diglucoside	-15.61	ko00942	-1.07	ko00942	2.39	ko00942
Malvidin 3,5-diglucoside	-1.72	Nd	NS	NS	NS	NS
Delphinidin 3-O-rutinoside	1.22	ko00942	2.15	ko00942	1.85	ko00942
Cyanidin	2.71	ko00941 ko00942	2.72	ko00941 ko00942	3.01	ko00941 ko00942
Cyanidin 3-O-galactoside	2.20	Nd	3.07	Nd	3.40	Nd
Peonidin 3-O-glucoside chloride	2.64	Nd	19.02	Nd	6.00	Nd
Cyanidin 3-O-glucoside	NS	NS	22.77	ko00942	22.99	ko00942
Delphinidin	NS	NS	NS	NS	2.20	ko00941 ko00942
Malvidin 3-acetyl-5-diglucoside	NS	NS	NS	NS	1.96	Nd

[a] G1 vs R1 refers to the content of metabolites in the R1 group of red leaves compared with that in the G1 group of green leaves. The G1 is the control group in this comparison. [b] G2 vs R2 refers to the content of metabolites in the R2 group of red leaves compared with that in the G2 group of green leaves. The G2 is the control group in this comparison. [c] G3 vs R3 refers to the content of metabolites in the R3 group of red leaves compared with that in the G3 group of green leaves. The G3 is the control group in this comparison. [d] Log_2FC is Log_2 (fold change). [e] KEGG refers to metabolites are annotated to the pathway of KEGG database. 'ND' indicates this metabolite was not found in the KEGG enrichment pathway. 'NS' indicates that there is no significant difference in comparison group.

compared with G2, and cyanidin 3-*O*-glucoside, delphinidin, and malvidin 3-acetyl-5-diglucoside were significantly upregulated in R3 compared with G3. Notably, the majority of anthocyanins, especially peonidin *O*-hexoside, malvidin 3-*O*-galactoside, peonidin 3-*O*-glucoside chloride, and cyanidin 3-*O*-glucoside, were more abundant in all three developmental stages of red leaves than in green leaves. Thus, these results suggest that the differences in the anthocyanin compositions are responsible for the differences in the leaves of *Populus* × *euramericana* 'Zhonghuahongye'.

3.4 Analysis of the transcriptome and DEGs of green leaves and red leaves

RNA-Seq was used for genome-wide gene expression profiling in the red leaves and green leaves of *Populus* × *euramericana* 'Zhonghuahongye'. A total of 134.1 Gb of clean data was generated, with an average GC content of 44.10% (Table S7). The matching rate of each sample was 81.12-85.19% (Table S8). A total of 34,200 genes were identified, among which 15,019 DEGs were identified by taking green leaves as the control group and red leaves as the experimental group. Then, hierarchical clustering of DEGs across all samples revealed the transcriptomic profiles of normal red leaf and green leaf tissues during leaf development in *Populus* × *Euramerica* 'Zhonghuahongye' (Figure 4A). The DEGs of normal red leaves and green leaves (G1 vs. R1, G2 vs. R2, G3 vs. R3) in different developmental stages were analyzed. A total of 1014 DEGs were obtained from the G1 vs. R1 group, among which 295 genes (29.09%) showed upregulated expression, and 719 genes (70.91%) showed downregulated expression, indicating that the difference in leaf color was mainly regulated by genes with downregulated expression in the first stage (Figure 4B). However, the highest number of DEGs (2383) was obtained in G2 vs. R2, and the lowest number of 500 DEGs was obtained in G3 vs. R3. The genes with upregulated expression accounted for 52.20% of all DEGs in the second stage and 53.76% in the third stage. Next, a Venn diagram was generated to show the distribution of DEGs in different developmental stages (Figure S7). There were 609 unique DEGs in the G1 vs. R1 group, 1875 unique DEGs in the G2 vs. R2 group, and 217 DEGs in the G3 vs. R3 group. Seventy-six common DEGs were screened in these three comparison groups. Taken together, these results suggest that differential gene expression in the first and second stages plays a crucial role in leaf color differences.

To understand the functions of the DEGs, GO and KEGG enrichment analyses were performed. The GO enrichment results showed that the DEGs of the G1 vs. R1 group were significantly enriched in biological processes such as photosynthesis, carbohydrate biosynthesis, hormone metabolism, apoplast, and other biological processes (Figure 4C). The DEGs of G2 vs. R2 were enriched in the carbohydrate biosynthesis process, cell cycle process, cytoskeleton, and other cellular components, as well as in UDP glycosyltransferase activity

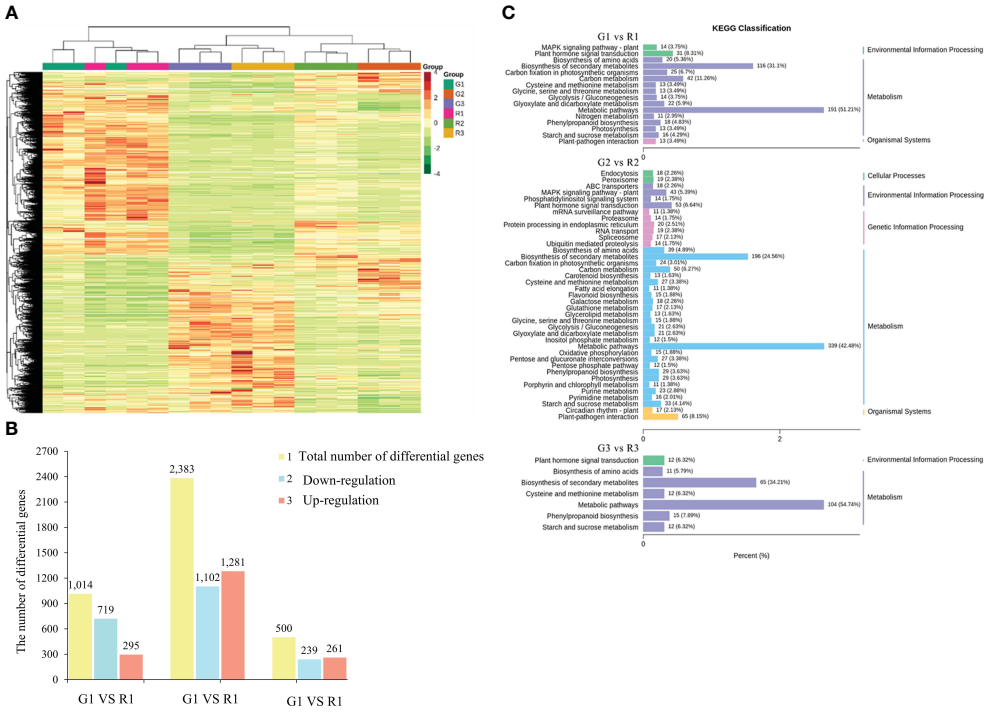

FIGURE 4
Differential gene expression. **(A)** Heatmap of differentially expressed gene clusters. **(B)** The number of genes with differences in the comparison of red leaves and green leaves. **(C)** Column chart of KEGG classification of DEGs between red and green leaves. The abscissa represents the ratio of annotated genes to the total number of genes annotated, and the ordinate represents the name of the KEGG pathway. The labels on the right side of the graph represent the category to which the KEGG pathway belongs.

and other molecular functions. The DEGs of G3 vs. R3 were enriched in pigment metabolism, isoprenoid metabolism, terpene metabolism, and UDP glycosyltransferase activity. The KEGG enrichment results showed that the 1016 DEGs of the G1 vs. R1 group were annotated into 116 metabolic pathways. Among these pathways, the carbon metabolism (42 DEGs, 11.26%), plant hormone signal transduction (31 DEGs, 8.31%), and phenylpropanoid biosynthesis (18 DEGs, 4.83%) pathways were significantly enriched (Figure 4C). The 2383 DEGs of G2 vs. R2 were enriched in 122 metabolic pathways. In addition to the abovementioned pathways identified in G1 vs. R1, the starch and sucrose metabolism (33 DEGs, 4.14%), glycolysis-related metabolism, ABC transporters (18 DEGs, 2.26%), glutathione metabolism (17 DEGs, 2.13%), and flavonoid biosynthesis (15 DEGs, 1.88%) pathways were annotated in this group (Figure 4C). The DEGs of G3 vs. R3 were enriched in 95 metabolic pathways. In general, the numbers of KEGG pathways and their types in G2 vs. R2 were significantly higher than those in the other two groups, indicating that more complex biological activities were carried out in leaves in the second stage.

3.5 Construction of the gene coexpression network during leaf coloration based on WGCNA

To explore the genetic regulatory networks of anthocyanin biosynthesis in green and red leaves, WGCNA was conducted based on all genes and the total anthocyanin content. All the filtered genes of green and red leaves were analyzed by WGCNA. The modules were classified according to the hierarchical clustering tree, and a total of 12 merged dynamic modules were generated (Figure S8A). The genes in a module have similar expression profiles. The midnightblue module contained the most genes (4826), while the bisque4 module contained the fewest (51) (Figure S8B). In the midnightblue module, the Pearson correlation coefficient of genes and total anthocyanins in R1 was 0.67, which was higher than that in G1 (0.48). The red color of R1 and G1 in the heatmap shows that the high expression of genes and high total anthocyanin content in the first stage was strongly and positively correlated. The redder the color was, the stronger the correlation. The Pearson correlation coefficient in R3 was -0.45. The blue color of R3 in the heatmap indicates that those genes in the third stage were negatively correlated with the total anthocyanin content. The results of anthocyanin determination indicate that the content was higher in red leaves than in green leaves at each time point. The changes in the Pearson correlation coefficient among the midnightblue module were consistent with the anthocyanin content. The Eigengene expression histogram shows the distribution of gene expression variables in each sample in the module (Figure S8C). The Eigengene expression histogram is a different method for visualization of the obtained results. Thus, the results suggested that the genes in the midnightblue module might be associated with the anthocyanin content. Therefore, the midnightblue module was selected for further analysis.

The GO enrichment analysis of genes revealed high enrichment of BP (biological process) terms, CC (cellular component) terms, and MF (molecular function) terms. The genes in the midnightblue modules

were highly enriched in BP terms (Figure S9A; Table S9), including signaling (GO:0023052), response to hormone (GO:0009725) and response to abscisic acid (GO:0009737), and CC terms, including nucleus (GO:0005634), endomembrane system (GO:0012505), and vacuole (GO:0005773). The top 20 enriched KEGG pathways were mainly related to starch and sucrose metabolism, plant hormone signal transduction, glycolysis/gluconeogenesis, and the MAPK signaling pathway (Figure S9B; Table S10). Phenylpropanoid biosynthesis and photosynthesis-related pathways were also enriched. In the starch and sucrose metabolism pathways, the *HXK* (hexokinase) gene (*POPTR_001G190400v3*) and beta-glucosidase genes (*POPTR_002G114000v3* and *POPTR_004G019800v3*) were identified. In the plant hormone signal transduction pathways, auxin-responsive *GH3* genes (*POPTR_001G298300v3* and *POPTR_003G161300v3*) and *SAUR* genes (*POPTR_002G000600v3* and *POPTR_002G024500v3*) were annotated. The *SnRK2* (serine/threonine-protein kinase SRK2) gene (POPTR_002G099700v3) is related to the ABA signaling pathway. Flavonoid and anthocyanin biosynthesis genes, including four *HCT* genes (*POPTR_005G028200v3*, *POPTR_005G052200v3*, *POPTR_008G034100v3*, *POPTR_019G001400v3*), *CHS* (POPTR_012G138800v3), and *ANS* (*POPTR_016G117100v3*), were differentially expressed. The above genes might play important roles in the higher anthocyanin content in red leaves.

3.6 TFs related to flavonoid and anthocyanin dynamics in *Populus* × *euramericana* 'Zhonghuahongye' leaves

TFs are important regulators in the regulatory network of flavonoid biosynthesis. A total of 278 DEGs encoding TFs were identified in the G1 vs. R1, G2 vs. R2, and G3 vs. R3 comparisons (Table S11). The top 20 TFs were identified, and the top 5 categories were bHLH (27), MYB (25), AP2 superfamily/ERF (23), MYB related (25), and C2H2 (13) (Figure 5A). The network results showed that MYB TFs, bHLH TFs, and bZIP (basic leucine zipper) family HY5 (elongated hypocotyl 5) TFs may mediate flavonoid and anthocyanin metabolism (Figure 5B). The phylogenetic analysis results showed that the MYB TF (POPTR_002G198100v3) clustered with the flavonol induction TFs AtPFG1 and AtPFG2. POPTR_017G125800v3_MYB90 and POPTR_017G125600v3_MYB113 clustered with anthocyanin-promoting MYB TFs (Figure 5C). The phylogenetic results for bHLH TFs showed that three candidate bHLHs presented high homology with the known bHLH sequence regulating flavonoids (Figure 5D). In particular, the translated POPTR_001G103600v3_GLABRA3 amino acid sequence was similar to the LcbHLH3 sequence of *Litchi chinensis* Sonn., which interacts with LcMYB1 to enhance anthocyanin accumulation (Lai et al., 2016). Expression pattern analysis showed that five MYB TFs, three bHLH TFs, and two HY5 TFs were significantly differentially expressed (Figure 5E). The putative flavonol accumulation-related TFs POPTR_002G198100v3_MYB and POPTR_002G198100v3_MYB showed higher expression in the R1, R2, and G1 stages, consistent with the accumulation pattern of flavonoid metabolites. The assumed anthocyanin synthesis promoters POPTR_017G125800v3_MYB90 and POPTR_017G125700v3_MYB113 showed upregulated expression in the R1 and R2 stages. In contrast, POPTR_016G083900v3_MYB_like showed downregulated expression in the R stage, which might have inhibited flavonoid synthesis. The bHLH TF POPTR_ 001G103600v3_ GLABRA3 showed upregulated expression, especially in the R1 stage. In addition, two HY5 TFs showed upregulated expression in the R1 and R2 stages of red leaves compared with green leaves (Figure 5E). These MYB, bHLH, and HY5 TFs played key roles in flavonoid and anthocyanin synthesis in *Populus* × *euramericana* 'Zhonghuahongye'.

3.7 Relationships between flavonoid biosynthesis and metabolites

The correlation between metabolites and RNA-seq data was analyzed. A 9-quadrant diagram based on correlation analysis showed that the metabolite and gene expression patterns were consistent in the third and seventh quadrants (Figure S10). Among these, 20 genes associated with 9 metabolites were enriched in the flavonoid and anthocyanidin pathways. Two *CHI* genes and 4,2',4',6'-tetrahydroxy chalcone were identified as related. Four HCT genes, two *CHI* genes, an *ANR* gene, and dihydromyricetin were identified as related. Three *HCT* genes, four *FLS* (flavonol synthase) genes, an *ANS* gene, and naringenin 7-*O*-glucoside were identified as positively related. In addition, an *HCT* gene and delphinidin were identified as related. The *HCT* gene *CYP75B1* and luteolin were identified as related (Figure S11). To further confirm the reliability of the RNA-Seq results, the 11 candidate genes mentioned above were selected for verification. The RT–qPCR results showed that these gene expression patterns were consistent with the RNA-Seq results (Figure S12).

The combination analysis indicated that the expression of genes related to flavonoid synthesis in red leaves was higher than that in green leaves in the same developmental stage, including the *HCT* (shikimate O-hydroxycinnamoyl-transferase gene), *CHS*, *DFR*, and *ANS* genes (Figure 6). Under the action of DFR, dihydromyricetin and dihydroquercetin are transformed into leucoanthocyanin. Leucoanthocyanins are generated as anthocyanins under the action of ANS, so anthocyanins (such as delphinidin and cyanidin) accumulate in young red leaves (R1). With the development of red leaves, the *CHS*, *DFR*, and *ANS* genes were continuously downregulated in the subsequent developmental stages (R2 and R3). In contrast, *FLS* showed continuous upregulation, which promoted the synthesis of flavonol. The high expression of *LAR* (leucoanthocyanin reductase gene) and *ANR* (anthocyanidin reductase gene) led to the conversion of leucoanthocyanin and anthocyanin to proanthocyanidin A1. The substrate of anthocyanin synthesis in red leaves was consumed, which may be an important reason for the color change in red leaves. Similarly, the high expression of *FLS* in green leaves resulted in the inability to synthesize anthocyanins in green leaves. The continuous downregulation of naringin, dihydromyricetin, cyanidin, and malvidin 3-*O*-glucoside might be responsible for the color change in red leaves of *Populus* × *euramericana* 'Zhonghuahongye' from the R1 to R3 stages. However, in the green leaf developmental period, the contents of cyanidin 3,5-*O*-diglucoside, peonidin O-hexoside, and malvidin 3-*O*-galactoside decreased significantly. Compared with green leaves, delphinidin 3-*O*-rutinoside, malvidin 3-*O*-glucoside,

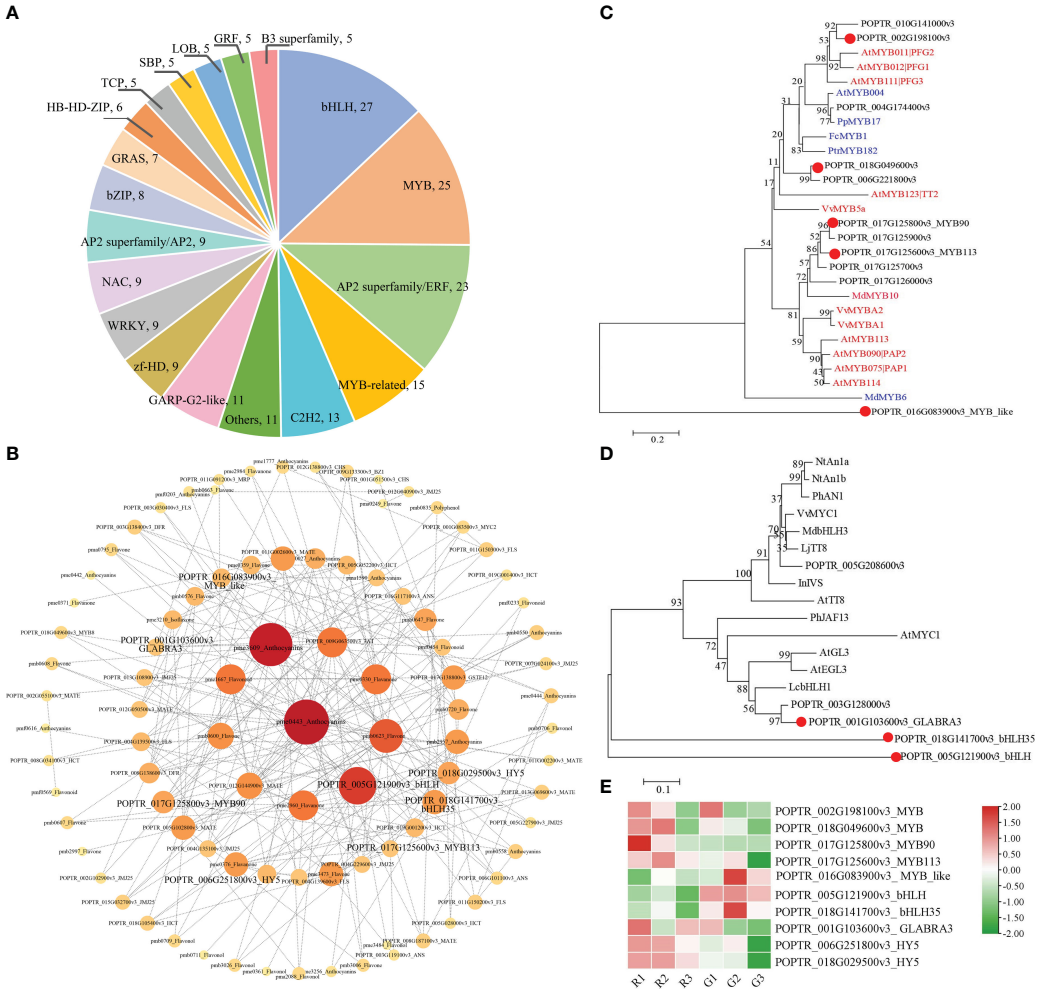

FIGURE 5
Identification of TFs involved in the biosynthesis of flavonoids and anthocyanins **(A)** Classifications and proportions of TFs. Each section shows the names and numbers of TF families. **(B)** Network among structural genes, transporter genes, TFs, and metabolites involved in the flavonoid and anthocyanin pathways. **(C)** Phylogeny of putative MYBs in *Populus* × *euramericana* 'Zhonghuahongye' and other known MYBs related to flavonol, flavonoids, proanthocyanidins, and anthocyanins in other species. In these phylogenetic relationships, the red ID represents a TF that promotes synthesis, and the blue ID is a TF that inhibits synthesis. **(D)** Phylogeny of putative bHLHs and other known bHLHs related to anthocyanins in other species. The GenBank IDs and annotations of MYB and bHLH TFs are listed in Table S12. The distance scale represents the unit length of the difference value between sequences. The bootstrap value is used to evaluate the credibility of the branch. **(E)** The expression patterns of 10 genes encoding TFs. The FPKM values were normalized by the Z score method in TBtools software.

malvidin 3-*O*-galactoside, and peonidin *O*-hexoside showed the most significant increases in red leaves during the three stages.

4 Discussion

4.1 Insight into the potential utility of *Populus* × *euramericana* 'Zhonghuahongye'

Populus extract has high therapeutic potential because of its antioxidant, anti-inflammatory, hepatoprotective, antitumor, and antimicrobial properties. More than 100 compounds have been isolated from *Populus nigra* extract, including phenolic compounds, terpenoids, flavonoids, flavanone, caffeic and p-coumaric acids, and nearly 50 molecules from the essential oil of its buds (Tebbi & Debbache-Benaida, 2022). To date, several studies have focused on the chemical composition of *Populus* red leaves (Tian et al., 2021; Chen et al., 2023), whereas no further analysis has been conducted on the difference in the composition between red and green leaves throughout the lifecycle. In this study, we profiled the flavonoid compositions of the red and green leaves of *Populus* × *euramericana* 'Zhonghuahongye' at three stages. A total of 273 flavonoid metabolites were identified in the three stages of leaf development. Among these metabolites, flavones, and flavonols accounted for the largest proportion, and 21 kinds of anthocyanins were identified. In the first stage, compared to green leaves, red leaves exhibited higher levels of total flavonoids, total phenols, and antioxidant activity. The metabolite results indicate that at each stage of red leaf development, the contents of most flavonoid metabolites in red leaves were higher than those in green leaves. Sixty-three significant DEMs were upregulated, while eleven DEMs were downregulated in R1 compared with G1. In addition, fifty-two significant DEMs were upregulated, while

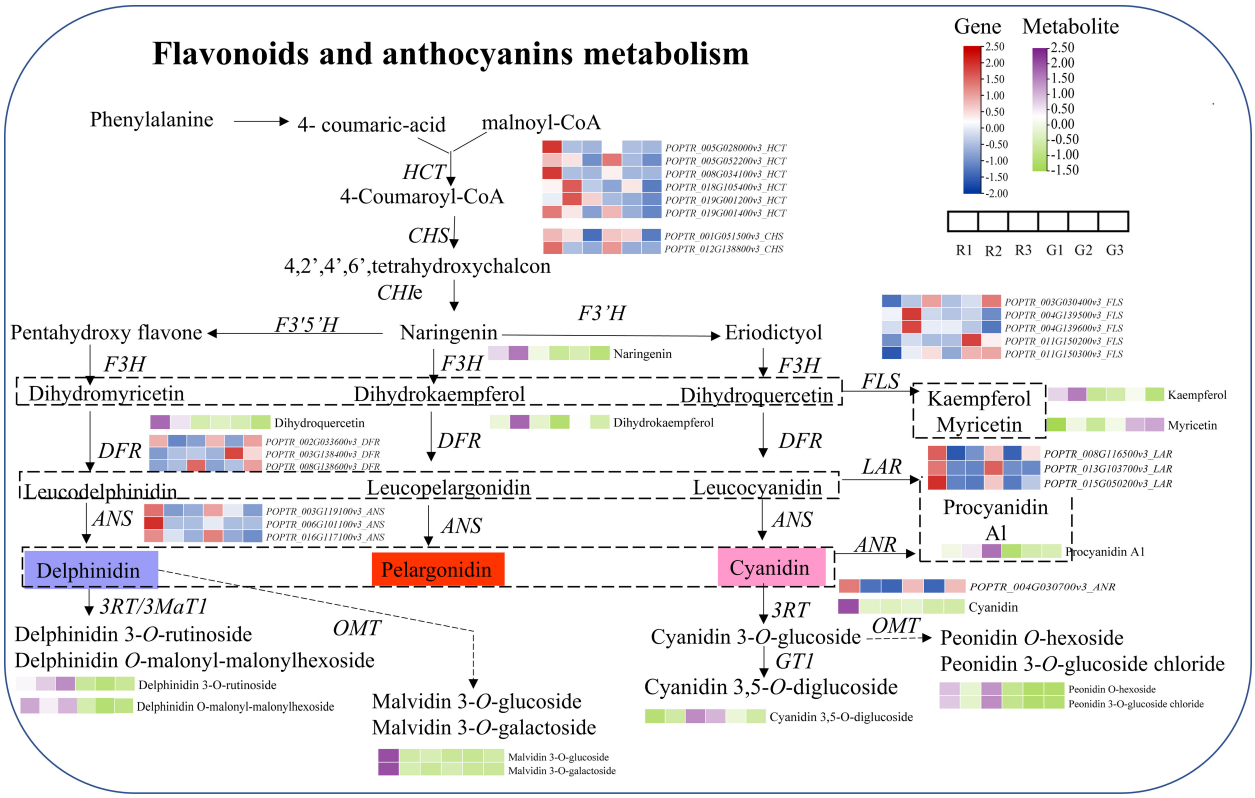

FIGURE 6
Combined analysis of metabolites and genes involved in flavonoid and anthocyanin biosynthesis. The purple and yellow–green heatmaps indicate the accumulation of metabolites. Blue and red heatmaps show gene expression. HCT, Hydroxycinnamoyl CoA: shikimate hydroxycinnamoyl transferase; PAL, phenylalanine ammonia-lyase; C4H, cinnamic acid 4-hydroxylase; 4CL, 4-coumaric acid: CoA-ligase; CHS, chalcone synthase; CHI, chalcone isomerase; F3H, flavanone 3-hydroxylase; F3′,5′H, flavonoid 3′,5′-hydroxylase) or F3′H, flavonoid 3′-hydroxylase; DFR, dihydroflavonol 4-reductase; ANS, anthocyanidin synthase; FLS, flavonoid synthase; LAR, Leucoanthocyantin reductase; ANR, Anthocyanidin reductase; RT, glycosyltransferase; 3MaT1, anthocyanin 3-*O*-glucoside-6''-*O*-malonyltransferase; and OMT, *O*-methyltransferase.

nine DEMs were downregulated, in R2 compared with G2. In addition, sixty-six significant DEMs were upregulated, while five DEMs were downregulated, in R3 compared with G3. In the various developmental stages of *Populus* × *euramericana* 'Zhonghuahongye', most of the 31 core flavonoid metabolites exhibited relatively high contents in red leaves at the three developmental stages, including 7 flavonoids, 6 flavonoids, 5 flavonoids, 4 flavonoids, 7 anthocyanins, and 2 polyphenols. In Tian's study, only 210 flavonoid metabolites were identified in two red-leaf poplar cultivars (*Populus* sp. bright red leaf and completely red leaf varieties) based on a widely targeted metabolomic analysis on the HPLC –ESI–MS/MS platform (Tian et al., 2021). In this study, more metabolites were detected, which may be due to the selection of multiple leaf developmental stages. Compared with the green leaf variety of *Populus* sp. Linn. '2025' collected in September 2018, 48 and 8 flavonoids were more and less abundant, respectively, in *Populus deltoides* varieties with bright red leaves, whereas 51 and 9 flavonoids were more and less abundant, respectively, in *Populus deltoides* varieties with completely red leaves (Tian et al., 2021). In Chen's study, at three stages of leaf development (R1, R2, and R3) of *Populus* × *euramericana* 'Zhonghuahongye', 81 differentially abundant metabolites were detected in the R1 vs. R3 comparison, 45 were detected in the R1 vs. R2 comparison, and 75 were detected in the R2 vs. R3 comparison. Ten metabolites showed significant differences in all comparisons, which were mostly flavonoid metabolites (Chen et al., 2023). Unlike previous reports, our study observed leaves from the tender stage to the mature stage of *Populus* × *euramericana* 'Zhonghuahongye'. More types of metabolites were identified in the metabolome, and more DEMs between the two leaves were identified. Among the 31 metabolites, naringenin, Butin, myricetin 3-O-galactoside, quercetin, cyanidin, and other compounds were highly expressed in red leaves. The antioxidant activity of the red leaf extract was higher due to the presence of flavonoids, polyphenols, and anthocyanins. Poplar leaves have been used as feed for ruminants, especially for goats and buffaloes (Ayers et al., 1996; Kumar et al., 2022). Thus, *Populus* × *euramericana* 'Zhonghuahongye', which is rich in flavonoids, has a higher feeding value than common green leaves. There is potential to develop the use of bioactive compounds from poplar red leaves.

4.2 Flavonoid metabolism is responsible for the difference between red and green leaves of *Populus* × *euramericana* 'Zhonghuahongye'

Flavonoids have been studied in depth for more than a century (Koes et al., 2005). It is critical to further clarify the molecular basis of flavonoid biosynthesis (Chen et al., 2022b; Kundan et al., 2022). Poplar is recognized as a model perennial woody plant. Thus, this study aimed

to elucidate the process of flavonoid formation in red leaves and green leaves of the *Populus* × *euramericana* 'Zhonghuahongye' variety. First, 4-coumaric acid and malonyl-CoA were found to be regulated by high expression of HCT genes in the R1 and R2 stages, followed by the CHS gene. The relative content of naringenin in R1 and R2 was approximately three times that in the G1 and G2 stages. Then, dihydroquercetin and kaempferol also exhibited increased levels in the R1 and R2 stages. Dihydrokaempferol was only upregulated in the R2 and G2 stages, while myricetin was abundant in the green leaves of the G2 and G3 stages. Naringenin, dihydroquercetin, kaempferol, dihydrokaempferol, and procyanidin A1 accumulated at higher levels in red leaves than in green leaves. In fig (*Ficus carica* L.) fruit, a very significant accumulation of the colorless flavonoids procyanidin B1, luteolin-3,7-di-*O*-glucoside, epicatechin, and quercetin-3-*O*-rhamnoside was observed in the mature "Purple Peel" compared to "Green Peel" (Wang et al., 2017). In *Actinidia arguta*, seven flavonoid compounds were closely associated with the pigmentation of red- and green-fleshed cultivars (Yu et al., 2020). The flavonoid profiles visualized by hierarchical cluster analysis indicated that *Populus* has a different flavonoid composition from *Ficus carica* L. and *Actinidia arguta*. Moreover, the flavonoid composition and contents vary among poplar species and clones (Donaldson et al., 2006; Pobłocka-Olech et al., 2021; Mazurek et al., 2022). Thus, we propose that red poplar varieties may be useful as models for studying flavonoids in trees.

Anthocyanins are responsible for coloration in most leaves, flowers, fruits, and seeds. This important feature has long attracted breeders and consumers. In chokecherry (*Padus virginiana*), the accumulation of malvidin 3-*O*-glucoside (violet) and pelargonidin 3-*O*-glucoside (orange–red) significantly correlated with the leaf color change from green to purple–red (Li et al., 2021). Tian et al. examined the following 8 anthocyanins, which did not exist in green leaves of L2025, in two red poplar varieties: cyanidin 3-*O*-glucoside, cyanidin 3-*O*-rutinoside, cyanidin 3,5-*O*-diglucoside, malvidin 3-*O*-galactoside, malvidin 3-*O*-glucoside, pelargonin, delphinidin 3-*O*-glucoside, and delphinidin 3,5-*O*-glucoside (Tian et al., 2021). However, in this study, the 8 anthocyanins had significant discrepancies in green leaves and red leaves among the three stages: cyanidin, cyanidin 3-*O*-galactoside, cyanidin *O*-syringic acid, cyanidin 3,5-*O*-diglucoside, delphinidin 3-*O*-rutinoside, delphinidin *O*-malonyl-malonylhexoside, peonidin *O*-hexoside, and peonidin 3-*O*-glucoside chloride. Interestingly, more peonidin anthocyanins associated with the leaf color difference were detected. In addition, while there was a difference in pelargonin abundance, it was not significant. In addition, centaverin 3-*O*-glucoside exhibited the highest expression in the three stages of red leaves. Therefore, these main anthocyanin compounds are responsible for the variance in leaf color of *Populus* × *euramericana* 'Zhonghuahongye'.

4.3 A possible transcriptional activation network affects flavonoid and anthocyanin synthesis in *Populus* × *euramericana* 'Zhonghuahongye'

Populus, as model plants, are considered excellent materials for studying flavonoid synthesis in woody plants. The biosynthesis of flavonoids/anthocyanin metabolites is also regulated by MYB and bHLH TFs (Yan et al., 2021). According to our data, five MYB TFs (POPTR_002G198100v3_MYB, POPTR_018G049600v3_MYB, MYB_like, MYB90, and MYB113) and three bHLH TFs (GLABRA3, bHLH, and bHLH35) may be key TFs that regulate the contents of flavonoids and anthocyanins in *Populus* × *euramericana* 'Zhonghuahongye'. In previous studies, *PtrMYB117* gene overexpression led to the accumulation of anthocyanins, proanthocyanidins, and flavonols through the upregulation of the flavonoid 3',5'-hydroxylase gene (Ma et al., 2021). Obvious upregulation of the R2R3-MYB gene was observed in red poplar varieties with bright red leaves and completely red leaves (Tian et al., 2021). The R3 domain may contain the motif [D/E]Lx2[R/K]x3Lx6Lx3R, which is responsible for the interaction with an R-like bHLH protein. In addition, coexpression of the *PalbHLH1* and *PalMYB90* genes in *Populus alba* increased flavonoid levels to strengthen pathogen resistance (Bai et al., 2019).

The bZIP TF HY5 plays a critical role in controlling flavonoid and anthocyanin accumulation in response to light (Shin et al., 2007; Zhang et al., 2011; Xian et al., 2023). Overexpression of *CtHY5* initially promoted *CtCHS1* expression and flavonoid content in *Carthamus tinctorius* L. protoplasts (Xian et al., 2023). Previous studies have also emphasized that three TFs (HY5, HYH, and TTG2) may directly participate in the regulation of anthocyanin synthesis in two varieties, 'Quanhong' and 'Xuanhong' (Chen et al., 2021). The promotion of anthocyanin accumulation by FvbHLH9 depends on the HY5-bHLH heterodimer in *Fragaria ananassa* Duch. (Li et al., 2020). This study showed that two HY5 TFs (POPTR_006G251800v3_HY5 and POPTR_018G029500v3_HY5) were highly expressed in young, fresh red leaves, and the expression level gradually decreased as the leaves turned red–green. Therefore, we speculate that the high expression of the HY5 gene promotes the synthesis of flavonoids and anthocyanins in R1 (when the leaves are bright red), resulting in red leaves in the R2 stage. With the development of leaves, the downregulation of the HY5 gene may reduce flavonoid and anthocyanin synthesis, resulting in red–green leaves. CHS, as a key gene in the biosynthesis pathway of flavonoids, was upregulated in the R1 and R2 stages. ANS gene products transformed the accumulated metabolites into key anthocyanins (delphinidin and cyanidin) in the young red leaves of *Populus* × *euramericana* 'Zhonghuahongye' compared with green leaves. This paper shows that the high activity of TFs (MYB-bHLH-HY5) and structural genes (*CHS* and *ANS*) triggered the early accumulation of molecules of the flavonoid and anthocyanin biosynthesis pathways in young, bright red leaves.

5 Conclusion

In this study, we focused on the diversity of flavonoids in the red and green leaves of *Populus* × *euramericana* 'Zhonghuahongye' in three developmental stages, combined with phenotypic observations, physiological determinations, and gene expression profiles. Young red leaves have higher anthocyanin, total flavonoid and polyphenol contents, and antioxidant ability. A total of 273 flavonoids with various modifications were detected

using widely targeted metabolomics. Most of these flavonoids exhibited higher levels of accumulation in the young leaves of poplars compared with the green leaves in the same stage. In particular, peonidin *O*-hexoside, malvidin 3-*O*-galactoside, peonidin 3-*O*-glucoside chloride, cyanidin 3-*O*-glucoside chloride, and cyanidin 3-*O*-glucoside might be responsible for the differences between green and red leaves. RNA-seq analysis showed that the downregulated expression of the flavonoid biosynthesis genes *CHS*, *DFR*, and *ANS* in poplar resulted in decreased red color in red leaves. The profile also revealed differential expression of several flavonoid and anthocyanin regulators, five MYB, three bHLH, and two HY5 genes. These findings provide new insights into the utilization of bioactive flavonoids in red poplar leaves, as well as the existence of green leaves from the perspective of gene transcription and flavonoid metabolism.

Data availability statement

The datasets presented in this study can be found in online repositories. The names of the repository/repositories and accession number(s) can be found below: BioProject PRJNA881405 and PRJNA934137.

Author contributions

YY: Data curation, Visualization, Writing – original draft, Writing – review & editing. MC: Conceptualization, Data curation, Formal analysis, Investigation, Methodology, Software, Validation, Writing – original draft, Writing – review & editing. HL: Investigation, Methodology, Validation, Writing – original draft. WZ: Data curation, Investigation, Methodology, Writing – original draft. HZ: Investigation, Validation, Writing – original draft. XN: Writing – review & editing. ZZ: Investigation, Validation, Writing – original draft. XH: Methodology, Validation, Writing – original draft. JZ: Investigation, Project administration, Resources, Supervision, Validation, Writing – review & editing.

Funding

The author(s) declare financial support was received for the research, authorship, and/or publication of this article. This work was funded by the Opening Project of the State Key Laboratory of Tree Genetics and Breeding with grant number K2022201.

Acknowledgments

The authors sincerely thank laboratory colleague Weijuan Han for providing technical support in the determination of physiological indexes. The authors wish to thank the editor and reviewers for their helpful comments and suggestions on the manuscript.

Conflict of interest

The authors declare that the research was conducted in the absence of any commercial or financial relationships that could be construed as a potential conflict of interest.

Publisher's note

Supplementary material

The Supplementary Material for this article can be found online at: https://www.frontiersin.org/articles/10.3389/fpls.2023.1274700/full#supplementary-material

SUPPLEMENTARY FIGURE 1
The sampling operations.

SUPPLEMENTARY FIGURE 2
PCA results show a clear clustering of metabolic profiles based on leaf color and developmental period.

SUPPLEMENTARY FIGURE 3
Metabolomic data were analyzed based on the OPLS-DA model.

SUPPLEMENTARY FIGURE 4
Representative bioactive flavonoids. The heatmap was generated based on the relative contents of metabolites. Red represents high abundance in these samples, and green represents low abundance.

SUPPLEMENTARY FIGURE 5
Venn diagram showing the number of DEMs identified in the pairwise comparisons and the common DEMs.

SUPPLEMENTARY FIGURE 6
KEGG enrichment bubble plots for DEMs in G1 vs. R1, G2 vs. R2, and G3 vs. R3.

SUPPLEMENTARY FIGURE 7
Venn diagrams of differentially expressed genes in red leaves and green leaves.

SUPPLEMENTARY FIGURE 8
WGCNA of filter genes and the total anthocyanin content.

SUPPLEMENTARY FIGURE 9
The GO and KEGG enrichment of genes in the midnightblue modules.

SUPPLEMENTARY FIGURE 10
A 9-quadrant diagram based on correlation analysis of metabolites and genes in the G1 vs. R1, G2 vs. R2, and G3 vs. R3 comparisons.

SUPPLEMENTARY FIGURE 11
The 20 genes associated with 9 metabolites were enriched in the flavonoid and anthocyanin pathways.

SUPPLEMENTARY FIGURE 12
qRT–PCR results of 11 candidate genes. β-Actin was used as an internal reference gene.

References

An, X.-H., Tian, Y., Chen, K.-Q., Wang, X.-F., and Hao, Y.-J. (2012). The apple WD40 protein MdTTG1 interacts with bHLH but not MYB proteins to regulate anthocyanin accumulation. *J. Plant Physiol.* 169, 710–717. doi: 10.1016/j.jplph.2012.01.015

Ayers, A. C., Barrett, R. P., and Cheeke, P. R. (1996). Feeding value of tree leaves (hybrid poplar and black locust) evaluated with sheep, goats and rabbits. *Anim. Feed Sci. Technol.* 57, 51–62. doi: 10.1016/0377-8401(95)00845-4

Bai, Q., Duan, B., Ma, J., Fen, Y., Sun, S., Long, Q., et al. (2019). Coexpression of *palbHLH1* and *palMYB90* genes from *Populus alba* enhances pathogen resistance in poplar by increasing the flavonoid content. *Front. Plant Sci.* 10. doi: 10.3389/fpls.2019.01772

Biselli, C., Vietto, L., Rosso, L., Cattivelli, L., Nervo, G., and Fricano, A. (2022). Advanced breeding for biotic stress resistance in poplar. *Plants* 11, 2032. doi: 10.3390/plants11152032

Chen, M., Chang, C., Li, H., Huang, L., Zhou, Z., Zhu, J., et al. (2023). Metabolome analysis reveals flavonoid changes during the leaf color transition in *Populus* × *euramericana* 'Zhonghuahongye'. *Front. Plant Sci.* 14. doi: 10.3389/fpls.2023.1162893

Chen, M., Li, H., Zhang, W., Huang, L., and Zhu, J. (2022a). Transcriptomic Analysis of the Differences in Leaf Color Formation during Stage Transitions in *Populus* × *euramericana* 'Zhonghuahongye'. *Agronomy* 12, 2396. doi: 10.3390/agronomy12102396

Chen, Q., Li, Y., Han, H., Ma, Y., Xie, X., Feng, Y., et al. (2022b). Transcriptome and metabolite profiling analyses reveal the molecular mechanism underlying the characteristic accumulation of anthocyanins and flavonols in *Fritillaria unibracteata* and F. *delavayi. Ind. Crops Prod.* 186, 115183. doi: 10.1016/j.indcrop.2022.115183

Chen, X., Liu, H., Wang, S., Zhang, C., Liu, L., Yang, M., et al. (2021). Combined transcriptome and proteome analysis provides insights into anthocyanin accumulation in the leaves of red-leaved poplars. *Plant Mol. Biol.* 106, 491–503. doi: 10.1007/s11103-021-01166-4

Devappa, R. K., Rakshit, S. K., and Dekker, R. F. H. (2015). Forest biorefinery: Potential of poplar phytochemicals as value-added co-products. *Biotechnol. Adv.* 33, 681–716. doi: 10.1016/j.bioteChadv.2015.02.012

Dey, A., Attri, K., Dahiya, S. S., and Paul, S. S. (2021). Influence of dietary phytogenic feed additives on lactation performance, methane emissions and health status of *Murrah buffaloes* (Bubalus bubalis). *J. Sci. Food Agric.* 101, 4390–4397. doi: 10.1002/jsfa.11080

Donaldson, J. R., Stevens, M. T., Barnhill, H. R., and Lindroth, R. L. (2006). Age-related shifts in leaf chemistry of clonal aspen (Populus tremuloides). *J. Chem. Ecol.* 32, 1415–1429. doi: 10.1007/s10886-006-9059-2

Dudonné, S., Poupard, P., Coutière, P., Woillez, M., Richard, T., Mérillon, J. M., et al. (2011). Phenolic composition and antioxidant properties of poplar bud (*Populus nigra*) extract: individual antioxidant contribution of phenolics and transcriptional effect on skin aging. *J. Agric. Food Chem.* 59, 4527–4536. doi: 10.1021/jf104791t

Ebada, D., Hefnawy, H. T., Gomaa, A., Alghamdi, A. M., Alharbi, A. A., Almuhayawi, M. S., et al. (2023). Characterization of *Delonix regia* flowers' Pigment and polysaccharides: evaluating their antibacterial, anticancer, and antioxidant activities and their application as a natural colorant and sweetener in beverages. *Molecules* 28, 3243. doi: 10.3390/molecules28073243

Falcone Ferreyra, M. L., Rius, S., and Casati, P. (2012). Flavonoids: biosynthesis, biological functions, and biotechnological applications. *Front. Plant Sci.* 3. doi: 10.3389/fpls.2012.00222

Felix, E., Tilley, D., Felton, G., and Flamino, E. (2008). Biomass production of hybrid poplar (*Populus* sp.) grown on deep-trenched municipal biosolids. *Ecol. Eng.* 33, 8–14. doi: 10.1016/j.ecoleng.2007.10.009

Fraga, C. G., Clowers, B. H., Moore, R. J., and Zink, E. M. (2010). Signature discovery approach for sample matching of a nerve-agent precursor using liquid chromatography-mass spectrometry, XCMS, and chemometrics. *Anal. Chem.* 82, 4165–4173. doi: 10.1021/ac1003568

Guleria, I., Kumari, A., Lacaille-Dubois, M.-A., Kumar, V., AK, S., Dhatwalia, J., et al. (2022). A review on the genus *Populus*: a potential source of biologically active compounds. *Phytochem. Rev.* 21, 987–1046. doi: 10.1007/s11101-021-09772-2

Han, W J LYQ, Sun, P., Li, J. R., and Fu, J. M. (2015). Optimizing of Folin ciocalteu method for the determination of total polyphenol content in leaves of Diospyros and the determination of leaf total polyphenol of some species (varieties). *Comput. andApplied Chem.* 32, 6. doi: 10.11719/com.app.chem20150705

Han, W. J. L. Y. Q., Zhang, J. J., and Fu, J. M. (2014). Review on thequantitative analysis methods of polyphenols and flavonoids inthe leaf of persimmon. *Chin. Agric. Sci. Bull.* 30, 52–56. doi: 10.11924/j.issn.1000-6850.2014-1527

Kis, B., Avram, S., Pavel, I. Z., Lombrea, A., Buda, V., Dehelean, C. A., et al. (2020). Recent advances regarding the phytochemical and therapeutic uses of *Populus nigra* L. *Buds. Plants.* 9, 1464. doi: 10.3390/plants9111464

Koes, R., Verweij, W., and Quattrocchio, F. (2005). Flavonoids: a colorful model for the regulation and evolution of biochemical pathways. *Trends Plant Sci.* 10, 236–242. doi: 10.1016/j.tplants.2005.03.002

Kumar, K., Dey, A., Rose, M. K., and Dahiya, S. S. (2022). Impact of dietary phytogenic composite feed additives on immune response, antioxidant status, methane production, growth performance and nutrient utilization of buffalo (*Bubalus bubalis*) calves. *Antioxid. (Basel)* 11, 325. doi: 10.3390/antiox11020325

Kundan, M., Gani, U., Fayaz, M., Angmo, T., Kesari, R., Rahul, V. P., et al. (2022). Two R2R3-MYB transcription factors, CsMYB33 and CsMYB78 are involved in the regulation of anthocyanin biosynthesis in *Cannabis sativa* L. *Ind. Crops Prod.* 188, 115546. doi: 10.1016/j.indcrop.2022.115546

LaFountain, A. M., and Yuan, Y. W. (2021). Repressors of anthocyanin biosynthesis. *New Phytol.* 231, 933–949. doi: 10.1111/nph.17397

Lai, B., Du, L. N., Liu, R., Hu, B., Su, W. B., Qin, Y. H., et al. (2016). Two lcbHLH transcription factors interacting with lcMYB1 in regulating late structural genes of anthocyanin biosynthesis in *Nicotiana* and *Litchi chinensis* during anthocyanin accumulation. *Front. Plant Sci.* 7. doi: 10.3389/fpls.2016.00166

Langfelder, P., and Horvath, S. (2008). WGCNA: an R package for weighted correlation network analysis. *BMC Bioinf.* 9, 559. doi: 10.1186/1471-2105-9-559

Li, X., Li, Y., Zhao, M., Hu, Y., Meng, F., Song, X., et al. (2021). Molecular and Metabolic Insights into Anthocyanin Biosynthesis for Leaf Color Change in Chokecherry (Padus virginiana). *Int. J. Mol. Sci.* 22, 10697. doi: 10.3390/ijms221910697

Li, Y., Pengbo, X., Chen, G., Wu, J., Liu, Z., and Lian, H.-L. (2020). FvbHLH9 functions as a positive regulator of anthocyanin biosynthesis by forming a HY5-bHLH9 transcription complex in strawberry fruits. *Plant Cell Physiol.* 61, 826–837. doi: 10.1093/pcp/pcaa010

Liu, W., Feng, Y., Yu, S., Fan, Z., Li, X., Li, J., et al. (2021). The flavonoid biosynthesis network in plants. *Int. J. Mol. Sci.* 22, 12824. doi: 10.3390/ijms222312824

Liu, Y., Lv, J., Liu, Z., Wang, J., Yang, B., Chen, W., et al. (2020). Integrative analysis of metabolome and transcriptome reveals the mechanism of color formation in pepper fruit (Capsicum annuum L.). *Food Chem.* 306, 125629. doi: 10.1016/j.foodchem.2019.125629

Love, M. I., Huber, W., and Anders, S. (2014). Moderated estimation of fold change and dispersion for RNA-seq data with DESeq2. *Genome Biol.* 15, 550. doi: 10.1186/s13059-014-0550-8

Ma, D., Tang, H., Reichelt, M., Piirtola, E. M., Salminen, J. P., Gershenzon, J., et al. (2021). Poplar MYB117 promotes anthocyanin synthesis and enhances flavonoid B-ring hydroxylation by up-regulating the flavonoid 3',5'-hydroxylase gene. *J. Exp. Bot.* 72, 3864–3880. doi: 10.1093/jxb/erab116

Mazurek, S., Włodarczyk, M., Pielorz, S., Okińczyc, P., Kuś, P. M., Długosz, G., et al. (2022). Quantification of salicylates and flavonoids in poplar bark and leaves based on IR, NIR, and raman spectra. *Molecules* 27, 3954. doi: 10.3390/molecules27123954

McAvoy, D. J., Burritt, B., and Villalba, J. J. (2020). Use of biochar by sheep: impacts on diet selection, digestibility, and performance. *J. Anim. Sci.* 98, 380. doi: 10.1093/jas/skaa380

Panche, A. N., Diwan, A. D., and Chandra, S. R. (2016). Flavonoids: an overview. *J. Nutr. Sci.* 5, e47. doi: 10.1017/jns.2016.41

Pobłocka-Olech, L., Głód, D., Jesionek, A., Łuczkiewicz, M., and Krauze-Baranowska, M. (2021). Studies on the polyphenolic composition and the antioxidant properties of the leaves of poplar (Populus spp.) various species and hybrids. *Chem. Biodiversity.* 18, e2100227. doi: 10.1002/cbdv.202100227

Shen, N., Wang, T., Gan, Q., Liu, S., Wang, L., and Jin, B. (2022). Plant flavonoids: Classification, distribution, biosynthesis, and antioxidant activity. *Food Chem.* 383, 132531. doi: 10.1016/j.foodchem.2022.132531

Shin, J., Park, E., and Choi, G. (2007). PIF3 regulates anthocyanin biosynthesis in an HY5-dependent manner with both factors directly binding anthocyanin biosynthetic gene promoters in *Arabidopsis. Plant J.* 49, 981–994. doi: 10.1111/j.1365-313X.2006.03021.x

Tebbi, S. O., and Debbache-Benaida, N. (2022). Phytochemistry, chemical composition and therapeutic uses of *Populus nigra* L. aerial parts from 1991-2021 onwards: An overview. *Sustain. Chem. Pharmacy.* 30, 100880. doi: 10.1016/j.scp.2022.100880

Tian, Y., Li, Q., Rao, S., Wang, A., Zhang, H., Wang, L., et al. (2021). Metabolic profiling and gene expression analysis provides insights into flavonoid and anthocyanin metabolism in poplar. *Tree Physiol.* 41, 1046–1064. doi: 10.1093/treephys/tpaa152

Tuskan, G. A., DiFazio, S., Jansson, S., Bohlmann, J., Grigoriev, I., Hellsten, U., et al. (2006). The genome of black cottonwood, *Populus trichocarpa* (Torr. & Gray). *Science* 313, 1596–1604. doi: 10.1126/science.1128691

Varet, H., Brillet-Guéguen, L., Coppée, J.-Y., and Dillies, M.-A. (2016). SARTools: A DESeq2- and edgeR-based R pipeline for comprehensive differential analysis of RNA-Seq data. *PloS One* 11, e0157022. doi: 10.1371/journal.pone.0157022

Wang, Z., Cui, Y., Vainstein, A., Chen, S., and Ma, H. (2017). Regulation of fig (Ficus carica L.) fruit color: metabolomic and transcriptomic analyses of the flavonoid biosynthetic pathway. *Front. Plant Sci.* 8. doi: 10.3389/fpls.2017.01990

Xian, B., Chen, C., Wang, J., Chen, J., Wu, Q., Ren, C., et al. (2023). Cloning and expression analysis of HY5 transcription factor gene of safflower in response to light signal. *Biotechnol. Appl. Biochem.* 70, 509–517. doi: 10.1002/bab.2373

Yan, H., Pei, X., Zhang, H., Li, X., Zhang, X., Zhao, M., et al. (2021). MYB-mediated regulation of anthocyanin biosynthesis. *Int. J. Mol. Sci.* 22, 3103. doi: 10.3390/ijms22063103

Yang, Y., Chen, M., Liu, Y., Ding, H., Du, H., Sun, Z., et al. (2021). Metabolome and transcriptome analyses reveal different flavonoid biosynthesis and chlorophyll metabolism profiles between red leaf and green leaf of *Eucommia ulmoides*. *Forests* 12, 1260. doi: 10.3390/f12091260

Yu, M., Man, Y.-p., Lei, R., Lu, X., and Wang, Y. (2020). Metabolomics Study of Flavonoids and Anthocyanin-Related Gene Analysis in Kiwifruit (Actinidia chinensis) and Kiwiberry (Actinidia arguta). *Plant Mol. Biol. Reporter.* 38, 353–369. doi: 10.1007/s11105-020-01200-7

Zhang, R., Zhang, Q., Zhu, S., Liu, B., Liu, F., and Xu, Y. (2022). Mulberry leaf (Morus alba L.): A review of its potential influences in mechanisms of action on metabolic diseases. *Pharmacol. Res.* 175, 106029. doi: 10.1016/j.phrs.2021.106029

Zhang, Y., Zheng, S., Liu, Z., Wang, L., and Bi, Y. (2011). Both HY5 and HYH are necessary regulators for low temperature-induced anthocyanin accumulation in *Arabidopsis* seedlings. *J. Plant Physiol.* 168, 367–374. doi: 10.1016/j.jplph.2010.07.025

Zhu, Z., Wang, H., Wang, Y., Guan, S., Wang, F., Tang, J., et al. (2015). Characterization of the cis elements in the proximal promoter regions of the anthocyanin pathway genes reveals a common regulatory logic that governs pathway regulation. *J. Exp. Bot.* 66, 3775–3789. doi: 10.1093/jxb/erv173

Frontiers in
Plant Science

Cultivates the science of plant biology and its applications

The most cited plant science journal, which advances our understanding of plant biology for sustainable food security, functional ecosystems and human health.

Discover the latest Research Topics

See more →

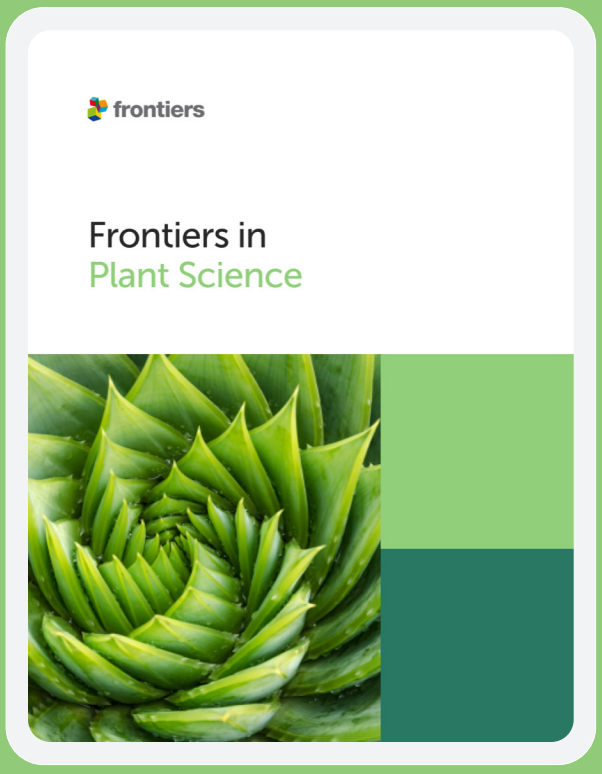

Frontiers

Avenue du Tribunal-Fédéral 34
1005 Lausanne, Switzerland
frontiersin.org

Contact us

+41 (0)21 510 17 00
frontiersin.org/about/contact